Multicomponent and Supramolecular Self-Assemblies as Functional Biomaterials

A dissertation presented to the faculty of the School of Engineering and Applied Science

University of Virginia

In partial fulfillment of the requirements for the degree of Doctor of Philosophy in Chemical Engineering

By

James D. Tang

July 2019

ABSTRACT

There is a pressing need to develop bioactive matrices that promote cellular interactions and elicit desirable regenerative behavior *in vivo*. This is particularly important in the context of ischemic stroke where a focal lesion forms forestalling the regrowth of brain tissue. We can develop and synthesize these matrices utilizing peptide-based molecules as building blocks to create supramolecular structures that emulate the properties of the native healthy extracellular matrix (ECM) within the central nervous system (CNS). In order to facilitate the regeneration of lost and/or damaged tissue, we propose using peptidic biomaterials that have the ability to emulate the properties of the native healthy extracellular matrix (ECM) within the CNS. The work completed in this thesis focuses on employing a combinatorial strategy involving computational modeling and experimental approaches to design and synthesize stimuli-responsive, self-assembling biomaterial systems that mimic many of the biochemical and mechanical properties, such as the viscoelastic properties, bioactive motifs, etc. found in the ECM. Additionally, we leveraged the power of atomistic molecular dynamics simulations to examine the dynamical effects of systematically perturbing the pentapeptide sequence motif. This enables us to screen for a myriad of design candidates *in silico,* and promising leads that exhibit higher order self-assembling behavior will later be experimentally produced.

ACKNOWLEDGEMENTS

I would like to first acknowledge my undergraduate adviser Dr. Lisa Bullard and undergraduate research adviser Dr. Robert Kelly for their time, direction, and patience throughout my undergraduate career. I definitely would not have decided to pursue a graduate degree, let alone an academic career, if it had not been for your help and guidance. I would also like to thank my graduate adviser Dr. Kyle Lampe, who has been a great adviser and mentor during my graduate career, and who has provided significant career advice. The scientific training I have received has thus prepared me for a career in research and academia.

I would like to thank all the members of my committee for all their time, input, and resources: Dr. Stephen Caliari, Dr. Bryan Berger, Dr. Nina Solenski, and Dr. Rachel Letteri, who have all provided me valuable career advice and technical guidance.

I would also like to thank all the past and present members of the Lampe Lab. In particular, Chelsea Harris for showing me the ropes, the other graduate students during my time- Edi Meco, Nick Murphy, Dr. Lauren Russell, Deniz Unal, and Zhiqi Zhang. To all of my wonderful undergrads- Isabella Zecchini, Maryam Ansari, Jonas Bowman, Emily Roloson, and Connor Amelung, with the latter two for directly contributing to the data included in my dissertation- thank you for all your hard work.

Finally, I would like to thank all of the friends I have made here in Charlottesville. Without your support and encouragement, I would not have made it through this last year in one piece. A special thanks to the greatest group of people I could ever ask for: Melissa Deschamp, Natalia Diaz, Evan Eckersley, Preston Fuks, Stephanie Guthrie, Erica Hui, Dr. James Kammert, Tracy Kuper, Madison Mann, Dr. Holly Mayton, Rachel Mazur, Nick Murphy, Costanza Preziosi, and Nate Sallada. I am especially grateful for all of the times we have laughed, cried, sang, yelled, ate, drank, jammed out, and passed out together. Thank you for all of the love and support over the years.

Table of Contents

Table of Figures

Index of Tables

1 Introduction and Background

1.1 Neural stem cell therapies and ECM biomimicry for 3D culture in a stroke injury environment

The complex interconnectivity of cells, including neurons, astrocytes, and oligodendrocytes, within the central nervous system (CNS) provides a formidable challenge for tissue engineers aiming to recapitulate the extracellular environment. These native microenvironments often serve as a guidance cue for initiating neural tissue regeneration following injury. For instance, the design of suitable microenvironments to improve the regenerative capacity of injured neurons is often complicated by the composition of the native CNS extracellular milieu, followed by the replacement of cells lost to apoptosis after a stroke. A stroke lesion is characterized by a region of necrotic cell death, in particular neuronal cells, which have a limited ability to regenerate once mature. Drug therapeutics targeting regenerative pathways have the ability to attenuate inhibitory molecules or accelerate the production of endogenous neurotrophins but are usually non-specific, thereby restricting the utility of such applications. A promising approach in stroke therapy is a combinatorial approach of controlled drug delivery and cell transplantation in a matrix that maintains appropriate cell-matrix interactions mimicking the native neural tissue environment. In a stroke environment, this often necessitates tissue replacement via encapsulation of neural stem cells in a hydrogel biomaterial that is directly injected to the infarct.

The native neural microenvironment includes extracellular matrix (ECM) molecules, myelin-associated glycoproteins, trophic factors and signaling pathways that modulate a neuron's intrinsic axonal growth capacity (readers are referred to excellent recent reviews on this topic by Lutz *et al.* [1] and Lau *et al.*[2]). On a cellular level, engineers must also account for various cellular components such as astrocytes and/or oligodendrocytes in the CNS that play a major role in nervous system repair and regeneration[3-4]. We now know that astrocytes can regulate neurotransmitter and ionic homeostasis, metabolic support of neurons, and guidance of neuronal migration and immune function[5]. These cellular constituents, as well as others, require appropriate morphogenic cues and mechanotransduction pathways from the ECM to trigger a cascade of cellular and biochemical events that can stimulate endogenous neurogenesis within the brain[2, 6]. However, in order to properly investigate these cell-cell signaling and cell-matrix interactions, it is important to

decouple the synergistic effects of both the hierarchical microstructures and signaling cues that initiate and/or propagate neural regeneration processes. This thesis presents several strategies that aim to overcome these limitations through engineered biomaterial scaffolds. Additionally, I discuss conventional approaches to the design of suitable microenvironments to stimulate neural tissue regeneration and repair in stroke injury environments.

Stroke is the second leading cause of disease mortality worldwide, resulting in close to 6,200,000 deaths annually[7], and the third most common cause of disability[8]. It is estimated that more than 130 million incidences of stroke (that do not result in death) occur in people younger than 75 years per year, with most of the burden found in low-income and middle-income countries[9-10]. The pathogenesis of ischemic brain injury from cerebral vessel occlusion involves two sequential processes: 1) the reduction or impairment of blood flow as a result of vascular occlusions and 2) alteration of normal cellular function resulting in necrosis of neurons, glia, and other supporting cells, and subsequent disruption of the blood-brain barrier (BBB)[11-12]. A rapidly evolving area in stroke research involves targeting specific inhibitory molecular and cellular pathways in tissue regeneration, and inflammation associated with cerebral ischemia. Promising therapeutic treatments prevent further damage and restore some cellular function by reestablishing perfusion to the ischemic brain, such as the administration of tissue plasminogen activator (tPA) that is used to break down clots[13-14]. However, these types of treatments are only effective when administered in a narrow therapeutic time window and the side effects of such treatments can potentially be more destructive than their beneficial thrombolytic activity[15].

Recently, there has been growing interest in transplanting different types of stem cells to restore neurological functions and improve behavioral recovery following an ischemic insult. Several well-documented studies show that transplanted stem cells can ameliorate ischemic stroke by reducing cortical infarct size and increasing blood vessel density[16-17]. However, cell transplantation strategies often suffer from poor cell survival due to the toxicity of the surrounding environment at the injury site[18-19]. This can potentially be addressed by encapsulating cells in suitable microenvironments (e.g. hydrogels) that protect cells during and after delivery and support cell survival and growth. Cleverly designed materials can influence the subsequent fate of either transplanted or endogenous stem cells by directing their differentiation.

For this thesis, we will present recent studies that use central nervous system (CNS) relevant biomaterials to promote cell survival and discuss their potential applications to stem cell therapy in the treatment of stroke. In many cases, administering these materials alone may have beneficial therapeutic effects in a transplant-free treatment strategy. For example, salmon fibrin has also been used in the treatment of spinal cord injuries. Salmon-derived fibrin gels were implanted into the lesion site after a dorsal hemisection in rat models, with no alteration in the degree of glial scar formation versus untreated controls, which were elevated in human fibrin-treated animals. Rats treated with salmon fibrin saw increased serotonergic fibers caudal to the injury site[20]. Similarly, the Shoichet group injected epidermal growth factor (EGF) and fibroblast growth factor 2 (FGF-2) impregnated collagen gel solutions to spinal cord injury sites of Sprague-Dawley rats and observed significantly greater ependymal cell proliferation in injured animals compared to controls[21]. Neural progenitor cells (NPCs) derived from bone marrow stromal cells (MSCs) transplanted with collagen sponges and basic fibroblast growth factor (bFGF) releasing gelatin microspheres into rat stroke models saw increased cell survival and neovascularization around the transplanted region[22]. The synergistic effect of bFGF releasing microspheres and NS-MSCs suggests that, when properly utilized, these biomaterials can provide appropriate scaffolding to ameliorate functional recovery in stroke or neurodegenerative diseases.

As discussed above, biomaterials have been engineered to mimic the physical and mechanical characteristics of the native extracellular matrix (ECM). Recent studies have focused on improving structural and functional recovery after stroke by enhancing endogenous neuronal regeneration through the incorporation of scaffolds that promote neuroblast migration into lesion sites[23-24]. Cell-based therapies have also received noticeable attention, and these notable preclinical and clinical trials include intravenous autologous mesenchymal stem cell (MSC) transplantation in the subacute phase, or 6 months after onset of stroke[25-26]. While the transplantation was deemed safe for stroke patients, there have been conflicting reports regarding the efficacy of the treatment[27], underscoring the need to improve cell survival in a long-term transplantation and promote host tissue integration.

1.2 Pathophysiology of ischemic stroke

Brain damage from ischemic insult involves a cascade of neurochemical events leading to cerebrovascular dysfunction and cell death. The interruption of local blood circulation reduces the supply of oxygen (hypoxia) and glucose, which prevents the brain from generating sufficient ATP to maintain cellular homeostasis[28]. Cell death occurs rapidly in areas with the most dramatic reduction in blood flow (ischemic core)[29-30]. For less severe areas of ischemia (ischemic penumbra), a cascade of cellular and molecular events trigger the disruption of cellular homeostasis, leading to slow cell death and accumulation of necrotic tissue[11]. Within the penumbra, depolarization of neurons and glia results in the activation of voltage-gated calcium channels and an increase in intracellular Ca^{2+} concentration, activating proteases, mitochondrial dysfunction, and oxidative and nitrosative stress (i.e. the result of excess production of reactive oxygen species (ROS), ultimately leading to cell death[31-32]. Production of such reactive oxygen species (ROS) can trigger the coagulation cascade, leading to further deleterious effects resulting from activated inflammatory mediators surrounding the injury site[33-34]. Post-ischemic oxidative and nitrosative stress have been closely linked to the pathophysiology of ischemic stroke as reviewed in depth elsewhere[35-36]. Recent studies have also implicated ROS in the activation of a host of matrix metalloproteinases (MMPs) that can significantly degrade the extracellular matrix (ECM) and BBB[37]. Thus, designing biomaterials that are able to sequester these ROS would be an ideal therapeutic strategy to improve patient outcomes.

It has been well established that post-ischemic inflammation triggers a molecular cascade involving a multimodal and multicellular series of downstream mechanisms. Various proinflammatory cytokines produced by complement, platelet, and endothelial cells play an important role in cell-ECM remodeling[38]. The intravascular compartment is immediately exposed to ischemic insult, leading to the accumulation of fibrin-trapping platelets and leukocyte infiltration into the brain parenchyma[39]. Neutrophils, followed by monocytes and lymphocytes are also recruited into the brain and accumulate in the microvessels of the penumbra. Endothelial cells in post-ischemic brain tissue express cell adhesion molecules (ICAM-1/VCAM-1) and upregulate E- and P-selectin, which provides a platform for leukocyte binding through their β2 integrins CD11a/CD18 and CD11b/CD18 (LFA-1 and MAC-1, respectively)[38, 40]. This then leads to leukocyte accumulation along the vascular wall, and accelerates cell death through the production

of free radicals and cytokines. These infiltrating inflammatory mediators take part in both cell and ECM remodeling and influence neural plasticity and relay circuit function[41-42].

Astrocytes play an important role in cerebral inflammation, as they are able to produce anti-inflammatory cytokines that downregulate inflammation, such as TGF-β1 and IL-10[38, 43]. Microglia and macrophages upregulate TGF-β1 in ischemic stroke[44-45], which has a neuroprotective role by promoting regulatory T lymphocyte development, and has also been implicated in dampening the immune response by suppressing T cell effector activity[46-48]. Additionally, astrocytes can express proteoglycans that are released into the ECM compartment. Following an injury, TGF-β1 can also regulate astrogliosis, facilitating glial scar formation by increasing cellular GFAP expression and upregulating inhibitory ECM molecules (e.g. chondroitin sulfate proteoglycans)[49]. Consequently, the modulation of NPC differentiation should be considered, especially in the design of biomaterial scaffolds that reduce astroglial activation or differentiation and promote differentiation into neuronal and oligodendroglial lineages.

Despite advancement in the understanding of the pathophysiology of stroke, many clinical trials have failed regardless of their success at the preclinical stage. A number of external factors such as, the animal model used and monitoring of physiological conditions may play a role in failure rates of proposed therapeutic strategies. Remaining challenges faced by tissue engineers in targeting stroke therapies is the ability to design biomaterials that 1) are also low cost and simple to synthesize and 2) are able to regulate and support cell function as a substitute for their normal physiological microenvironment. Thus, there is a critical need to establish a biomimicry strategy to enable stimuli-responsive and multifunctional biomaterials that can deliver and allow precise control of stem cell behavior for neural tissue regeneration applications.

1.3 Limitations of therapeutic potential in current preclinical and experimental studies

The acute management of ischemic stroke includes the administration of intravenous recombinant tPA[50], which is the first, and only, U.S. Food and Drug Administration (FDA) approved drug for the treatment of ischemic stroke. However, it was reported that tPA was more effective in patients with small to moderate-sized strokes, but was not as beneficial to patients with large-vessel

occlusions[51]. Later studies show that tPA regulates several molecular signaling pathways that activate matrix metalloproteinase-9, leading to the degradation of the extracellular matrix (ECM) and disruption of the BBB[37, 52]. This can have severe pathological consequences that can exacerbate brain injury and contribute to cognitive impairment. Additionally, the increased paracellular permeability results in hemorrhagic transformation and ultimately increased mortality.

With current advances in understanding the effects of introducing stem cells and their therapeutic potential, stem cell transplantation has caught on to be a promising alternative therapy in the treatment of stroke[16, 53-54]. However, there are several critical limitations of cell transplant therapies that plague the efficacy and success of preclinical and clinical trials. Namely, there is 1) a limited source of engraftable stem cells, 2) the narrow therapeutic window for stem cell therapies, and 3) possible transplanted cell mediated adverse effects, such as unregulated stem cell proliferation (i.e. tumor formation), or even stroke as a result of clotting from cells trapped with circulatory vessels. Moreover, stem cells themselves may have inherited limitations in terms of growth, trophic support, and differentiation potentials[55]. Additionally, the functional activity of stem/progenitor cells might be decreased due to disturbances of the cell secretome, and altered interactions with its microenvironment[56].

More recently, antioxidants and free radical scavengers have been explored for treatment of central nervous system (CNS) injury[57-59]. Free radicals are continuously generated by the use of oxygen in mitochondria to supply the energy needs of the brain, and studies have demonstrated that overproduction of these free radicals and related ROS modulate a host of cellular and molecular processes that promote neuronal degeneration[60-62]. Several compounds such as ebselen[63], edaravone[64], tirilazad[65], and NXY-059[66] have been developed to remove or degrade free radicals, or inhibiting their production. Administration of these drugs has proven to be effective in experimental stroke injury models, however, with the exception of NXY-059, no clear evidence for the efficacy of these drugs in the treatment of human stroke patients was obtained[67]. More recently, polymeric nanoparticles have been used to encapsulate or incorporate small drugs to more efficiently deliver its payload. Jin *et al*. used a methoxypoly (ethylene glycol)-*b*-poly (D,L-lactic acid) (PEG-PLA) polymeric micelle to encapsulate edaravone (EDV-AM), seeking to eradicate ROS produced by infiltrated inflammatory cells. It was shown that the EDV-AM nanoparticle had

a higher uptake in brain ischemia versus free EDV, resulting in rapid infarct volume reduction, and reduced behavioral deficits in ischemic stroke models[68]. The use of such a delivery vehicle could subsequently improve BBB permeability and be used to treat the majority of ischemic stroke patients who miss the time-window of tPA treatment.

Many therapeutics, while effective in animal injury models, completely fail in clinical trials. One reason for the high failure rate is because the therapeutic time window for effective reperfusion appears to be extremely short (< 4.5 h), and that the long 'door-to-needle' time (i.e. the time from emergency arrival to administration of tPA) limits the efficacy of the drug. Existing strategies also target a specific pathway of acute ischemic stroke. As mentioned above, the pathophysiology of stroke is extremely complex involving an assortment of chemical and biological processes and signaling pathways. A combinatorial approach in the treatment of stroke, i.e. combining neuroregenerative agents that target multiple pathways of the ischemic cascade, may be necessary to improve patient outcomes following an ischemic insult. Alternatively, rebuilding the tissue lost to ischemic degradation may supplement efforts to limit injury severity.

Recently, biomaterials-based approaches have garnered considerable interest in the field of neural tissue regeneration as a promising alternative for stroke repair[24, 69-71]. These biomaterial scaffolds can A) provide integration of a highly biocompatible three-dimensional microenvironment with the host tissue that promotes neural tissue regeneration and B) act as a drug delivery vehicle releasing neuroprotective agents in a spatiotemporally controlled manner. Implantations of these scaffolds at an injury site may not only reduce stroke mortality, but restore lost neurological functions through the regeneration of neural tissue. For example, a recent publication demonstrated that sericin-based hydrogels were neuroprotective, and could promote axonal extension and branching of primary cortical neurons. When transplanted *in vivo*, these hydrogels promoted cell survival and proliferation, suggesting that their neuroprotective and neurotrophic properties are suitable for ischemic stroke repair and de novo tissue formation[72]. Additionally, an effective hydrogel biomaterial for stroke treatment should meet several requirements: First, clinical application to the infarct cavity must be achieved via simple injection, a minimally invasive patient delivery. Second, the hydrogel must not swell during or after gelation to prevent further damage to the brain. Finally, these hydrogels must allow for the precise control of stem cell behavior to

promote neural tissue regeneration. Thus, in the next chapter, we will focus on recent findings describing micro- to nano-scale hierarchical constructs that have been designed to mimic native ECM. We will describe key biological and mechanical properties that a biomaterial should possess that can modulate both cell proliferation and differentiation. The high biocompatibility, ease of functionalization, and precise control over the sequence and structural elements make proteinaceous biomaterials excellent candidates for neural regeneration applications.

2 Design and fabrication techniques of amino acid containing biomaterials

Protein and peptidic biomaterials have typically been modeled after structural elements found within the ECM. This includes fibrous scaffolds and hydrogel matrices that are designed to mimic *in vivo* 3D microenvironments associated with native tissue. These biomaterials are often designed with several criteria in mind: 1) their components and gelation process must be cytocompatible in order to be considered useful in applications for tissue engineering, 2) and they should recapitulate the cell-matrix interactions found *in vivo*. Selecting or designing these peptide or protein-based materials typically requires parsing of known cell-binding or assembly epitopes or intuiting novel domains/designs that could be useful. Furthermore, the format and structure of the subsequent hydrogel biomaterial greatly impacts cellular interactions, and thus the fabrication strategies can dramatically impact a material's ability to replicate qualities of native, healthy, CNS tissue.

Advancements in genetic engineering and molecular biology now allow for the design and engineering of biosynthetic proteins with precise control over their sequences, length, secondary structure, and intermolecular interactions (e.g. hydrogen bonding, electrostatic interactions, π- π stacking)[73]. Protein engineering has been a staple in the biological sciences for decades and has gained traction in biomaterials research for multidisciplinary applications in engineering, medicine, and material sciences. Researchers are able to create a vast array of designer protein systems with desired properties that either function as biomimetics of native proteins, or contain novel structural and biofunctional moieties[74-75]. These proteins have been used in a variety of applications related to CNS regeneration, where they often serve as 3D scaffolds and/or depots for

release of neurotrophins or growth factors[76-77]. Protein-based materials may also play a role in mediating the host immune response[78]. Molecular biology has opened up new avenues to allow for the development of recombinant elastomeric proteins, such as keratin, silk, and collagen, as well as designer peptides and proteins which may be suitable biocompatible scaffolds for tissue engineering applications.

In the early 1960s, Merrifield developed a novel approach to the chemical synthesis of polypeptides involving the stepwise addition of protected amino acids to a growing peptide chain[79]. Since its conception there have been significant improvements and refinements to the solid-phase methodology, most notably the introduction of the 9-fluorenylmethoxycarbonyl (Fmoc) group for N^{α} protection[80], resulting in greater peptide yields and reduction in side reactions during cleavage. Solid-phase peptide synthesis (SPPS) has enabled the successful preparation of tailor-made peptide sequences without the use of complex and often impracticable purification steps of naturally occuring proteins, while simultaneously maintaining similar biological activity as its native analog. The most advantageous property of peptides is that they are chemically defined; SPPS provides exceptional control over the peptide's chemical identity, giving researchers the freedom to synthesize almost any protein sequence they desire without concerns regarding troublesome contaminants that often accompany proteins expressed in bacterial or mammalian cultures. Through the use of SPPS, tissue engineers are now able to easily synthesize a whole host of *de novo* peptides with unique structural and biofunctional properties, including but not limited to proteolytic susceptibility[81-83], cell surface and/or matrix binding[84-86], growth factor binding[87-89], and self-assembly[90-95]. The use of designer peptides capable of self-assembling into matrices that act as ECM mimics have seen momentous growth in regenerative medicine[96-98]. The self-assembling propensities of these oligopeptides have been shown to fold into higher ordered tertiary and quaternary structures. The use of external stimuli to induce spontaneous gel formation is also unique in this class of biomaterials, in that *monomeric* peptides (rather than a composite, or two component system in polypeptide systems) are able to self-assemble in aqueous solutions without the addition of chemical crosslinks or other proteinaceous materials.

2.1 Molecular-based design of biomolecular assemblies

The macroscopic (and/or bulk) properties of proteinaceous biomaterials can be controlled by fine tuning the underlying conformational space and associative interactions between amino acid building blocks. The supramolecular structure (i.e. specific, directional, tunable, reversible, non-covalent molecular recognition motifs that exploit hydrogen bonding, hydrophobic interactions, π-π interactions, and/or van der Waals interactions[99-102]) can be designed in such a way that it adheres to the hierarchical architecture that is present in native tissue. As such, the exploitation and fundamental understanding of nano- to microscale interactions within biological structures allows researchers to design novel biomaterials capable of maximizing biological function and biocompatibility. Several recent techniques provide a rational approach to the design and synthesis of biomaterials with applications in CNS regeneration.

Multiscale modeling of complex biological systems are now possible, including a comprehensive analysis of the microarchitecture found within biomaterials. However, few groups have taken advantage of the powerful computational methods available to accelerate and improve the materials design process. In theory, the hierarchical architecture of biological materials can be simplified to fundamental (bio)physical properties of self-assembling systems. By modeling the basic building blocks (i.e. atoms in an amino acid residue) and their intra- and intermolecular interactions, it is possible to observe and predict trajectory-derived conformations of these systems that can describe the material's properties[103]. A combinatorial strategy utilizing both computational and experimental approaches will allow researchers to rationally design new molecules with desired structural and functional properties. This design strategy could transform current approaches to biomaterials development and address the particular challenges of characterizing the dynamical processes that occur in biological matrices.

2.1.1 Molecular Dynamics

All-atom molecular dynamics (MD) simulations are utilized to predict the spatiotemporal dynamics in the folding pathway of proteins, formation of secondary structures, and protein association via specific binding sites[104-112]. More recently, MD simulations have been applied to the design of biomaterials in order to predict the occurrence of complex molecular interactions at

a microscopic scale. Several examples use simulations of elastin-like polypeptides (ELPs) [104, 112-116] as well as laminin-mimetic fusion proteins[117] to predict the conformational changes and kinetics associated with the known phase transition behavior of ELPs. Other notable studies involve the analysis of secondary structures within spider silk[118-119], self-assembly of peptides[120-123], and dynamics of micelle and fibril formation[124-128]. The motivation behind using MD simulations is manifold; understanding the atomic contacts (via non-covalent interactions) that mediate the folding pathway of nano- to microscopic structures gives researchers the ability to finely tune protein sequences that could lead to desirable bulk material properties, later verified experimentally. The exponentially large combinatorial space of biomolecule design, in general, are intrinsically complex and resource-intensive to disseminate. Therefore, MD-based simulations allow access to such dynamics on a characteristic timescale (~femtosecond to microsecond) essentially inaccessible via experimental approaches.

In classical MD simulations, the movement of atoms of a biomolecule can be described according to the Newtonian equations of motion. For an all-atom MD simulation, one assumes that every atom experiences a force that accounts for the interaction of that atom with the rest of the system, such that

$$\vec{F}(\vec{x}) = \vec{M} \odot \vec{f}(\vec{x}) \tag{2.1-1}$$

where $\vec{M}$ is the vector of masses of each degree of freedom in the system ($[m_1, m_1, m_2, m_3, \ldots]$, since the degrees of freedom are the *x, y,* and *z* coordinates for each atom), $\vec{f}(\vec{x})$ is some function of the position of all the particles in the system, and $\odot$ indicates element-wise multiplication of the two vectors. Given the positions $\vec{x}(t)$, velocities $\vec{v}(t)$, and accelerations $\vec{a}(t)$ of every atom in the system (for each degree of freedom, with a *x, y,* and *z* coordinate at time *t*), one can write the equations for the *Verlet integrator*[108]

$$\vec{v}\left(t + \frac{1}{2}\Delta t\right) = \vec{v}(t) + \frac{1}{2}\vec{a}(t)\Delta t \tag{2.1-2}$$

$$\vec{x}(t + \Delta t) = \vec{x}(t) + \vec{v}(t + \frac{1}{2}\Delta t) \tag{2.1-3}$$

$$\vec{a}(t+\Delta t) = \vec{f}(\vec{x}(t+\Delta t)) \tag{2.1-4}$$

$$\vec{v}(t+\Delta t) = \vec{v}\left(t+\frac{1}{2}\Delta t\right) + \frac{1}{2}\vec{a}(t+\Delta t)\Delta t \tag{2.1-5}$$

Summarily, the force $\vec{F}(\vec{x})$ is in turn calculated from the system's potential energy $U(\vec{x})$

$$\vec{F}(\vec{x}) = -\nabla U(\vec{x}) \tag{2.1-6}$$

defined through the MD "force field" which represents the interactions between atoms. These interactions are specified by a model force field that describes the stretching, bending, and torsional bonded interactions as well as nonbonded interactions which correspond to the van der Waal's forces (approximated by a Lennard-Jones 6-12 potential) and electrostatic interactions,

$$U(\vec{x}) = U_{bond} + U_{angle} + U_{dihedral} + U_{vdW} + U_{Coulomb} \tag{2.1-7}$$

Subsequently, the potential energy function has the following contributions:

$$U_{bond} = \sum_{bonds,i} k_i^{bond}\,(r_i - r_{0,i})^2 \tag{2.1-8}$$

$$U_{angle} = \sum_{angles,i} k_i^{angle}\,(\theta_i - \theta_{0,i})^2 \tag{2.1-9}$$

$$U_{dihedral} = \sum_{dihedral,i} k_i^{dihe}\,[1 + \cos(n_i\phi_i - \gamma_i)] \tag{2.1-10}$$

$$U_{vdW} = \sum_i \sum_{j>i} 4\varepsilon_{ij}\left[\left(\frac{\sigma_{ij}}{r_{ij}}\right)^{12} - \left(\frac{\sigma_{ij}}{r_{ij}}\right)^{6}\right] \tag{2.1-11}$$

$$U_{Coulomb} = \sum_i \sum_{j>i} \frac{q_i q_j}{4\pi\varepsilon_0 r_{ij}} \tag{2.1-12}$$

The bond stretching term is usually represented with a harmonic potential where for (2.1-8) *bonds* is the total number of bonds in the system, $k_{bond,i}$ is a Hooke's law spring constant, r_i is the current length of that bond (the distance between the relevant atomic nuclei in $\vec{x}$), i.e. the value of the bond length when all other terms in the potential energy function are zero, and $r_{0,i}$ is the equilibrium length for bond *i.* For (2.1-9) the terms are analogous to (2.1-8) such that $k_{angle,i}$ is the strength of

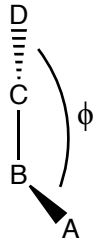

Figure 2-1. Torsional angle definition

the angle, modeled as a Hookean spring, and θ_i is the angle between the atoms in angle *i*. In (2.1-10), the *dihedral* describes atom pairs separated by exactly three covalent bonds with the central bond subject to the torsion angle ϕ_i (depicted below). The dihedral term attempts to capture some of the steric and electrostatic nonbonded interactions between two atoms **A** and **D** connected through an intermediate bond **B-C (Figure 2-2).** The γ_i term is the offset for the dihedral potential, and n_i is the periodicity of the potential, e.g. for a molecule like ethylene, rotation about the C=C bond must be periodic by 180°, so only even terms n = 2, 4, … can occur, whereas n would be 3, 6, … for an ethane molecule rotating along its H-C-C-H dihedral. The van der Waals energy arises from the interactions between electron clouds around two nonbonded atoms. The attraction is due to electron correlation which results in "dispersion" or "London" forces (instantaneous multipole / induced multipole). At intermediate to long ranges, the attraction is proportional to 1 / R^6, and can be estimated by the Lennard-Jones potential (2.1-11). The term iterates over all pairs of atoms (*i, j*), ε_{ij} is the strength of the interaction between atoms *i* and *j*. σ_{ij} is the distrance at which dispersion and steric clash exactly cancel out, and r_{ij} is the distance between atoms *i* and *j*. Finally, the electrostatic terms describe the Coulomb interaction between atoms *i* and *j* with partial charges q_i and q_j, respectively. ε_0 is an effective dialectric constant (or vacuum permittivity) and r_{ij} is the distance between atoms *i* and *j*. The actual values of the fixed parameters, such as $k_{bond,i,}$ ε_{ij}, etc. are called the *force field*.

The version of NAMD[108] being used in this work was compiled by Dr. Charles McAnany (Mura lab, Chemistry) specifically for the high-performance computing cluster, Rivanna. In particular, the simulations are carried out in periodic boundary conditions, such that a biomolecule can freely diffuse in an infinite periodic bath. These modeling conditions are effective in eliminating surface interactions of the water molecules and creates a more faithful representation of the *in vivo* environment, but also significantly complicates the evaluation of electrostatic interactions[129]. Additionally, the simulations are performed in the isothermal-isobaric (NPT) ensemble. The energy, pressure, and enthalpy of the system fluctuate via the introduction of stochastic collisions that affect the momentum of one particle at a time. The effect of each stochastic collision is used to replace the momentum of the affected particle by the new value chosen from the correlated Boltzmann distribution[130].

2.1.2 Reaching biological timescales with MD simulations

Molecular dynamics (MD) simulations[103] offer a powerful approach to examine the conformational and structural dynamics of peptides and proteins. MD uses a simple physics-based model for interatomic interactions, and integrates the classical equations of motion to yield a trajectory that consists of the positions of each atom in a system, with picosecond resolution. Virtually any imaginable property can be computed from a trajectory, giving predictions that can help understand assembly as a function of the peptide sequence. From MD simulations, one can study a system's phase behavior (by comparing results at different pH values), aggregation propensity (by simulating multiple peptides together), and other thermodynamic and structural information. Notable studies involve the analysis of peptide self-assembly[120-123], and dynamics of micelle and fibril formation[124-128]. Yet few examples exist of using computational approaches to design functional peptide scaffolds for tissue regeneration applications. In addition to aiding in the design and engineering of novel peptides (such as those proposed here), MD simulations can reveal experimentally-inaccessible information about the dynamic behavior of aggregation. Simulations can illuminate the assembly *process*, not just the final assembled state. When modeling the behavior of peptides that exhibit higher-order secondary structures, MD should be viewed as a hypothesis-generating tool and, as for any method, its results should not be blindly trusted. Note that our proposed use of MD is in close linkage with suitable experimental studies: we used MD to examine peptide sequences that have desired properties, and then experimentally characterize

additional sequences that calculations suggest to be promising. In studying the assembly process more generally, a model derived from MD data can provide experimentally-testable hypotheses regarding inter-residue distances, shifts in secondary structure content, thermodynamics of structural rearrangements, etc.

Yet, it should be noted that there are certain limitations that restrict the usage of MD simulations to small biomolecules and/or short timescales that do not necessarily correlate with experimental measurements. The time it takes to perform one step in a simulation on a system containing N particles is proportional to $N * \log(N)$ [103]. Typically, the timestep using the *Verlet integrator* cannot be much larger than 2 femtoseconds, and so, simulating a system for a single nanosecond requires 500,000 integration steps (a typical simulation today is on the order of 500 nanoseconds[131]), while many important biological processes occur on the microsecond timescale and beyond. However, many local perturbations in the protein backbone and sidechain moieties occur on the picosecond to nanosecond timescale, and that the formation of *β-sheets* typically occur on timescales extending from tens of nanoseconds to a few milliseconds[132]. We are able to observe these localized biological phenomena in our simulations in the subsequent chapters. *It is also important to point out that we do not claim that the resulting equations of motion generate phase-space trajectories that are* ***ergodic****.* Given the system size and timescales of the simulations performed in this thesis, it is difficult (if not impossible) to verify that a true, equilibrium structural ensemble were being thoroughly sampled in all of our simulations. Moreover, strictly speaking, biomolecules are many-body systems with nonlinear, chaotic dynamics, and all MD trajectories will, as a matter of principle, suffer from Lyapunov instability—meaning they will never capture, with perfect accuracy, the true underlying dynamics of the system (see, e.g., Frenkel, Eur. Phys. J. (2013) 128: 10. doi:10.1140/epjp/i2013-13010-8). In more practical terms, at the timescales that are currently feasible (computationally) via all-atom MD simulations, for systems of large sizes (e.g., >160,000 particles for the solvated fusion system in our current work), it is unfortunately impossible to comprehensively explore such a vast conformational space. This inherent convergence problem is exacerbated when simulating protein sequences that are likely to exhibit intrinsically less order. It should also be noted that the above 'issues' are almost entirely generic—i.e., they are not problems that are specific to our system or study, and are equally applicable to any simulation study.

2.1.3 Coarse-grained MD simulations

Coarse-graining (CG) allows researchers to model biomaterials on a mesoscale that overcomes the expensive computational demands that often plague MD simulations. In CG, the number of atomic particles and the corresponding degrees of freedom are reduced compared to atomistic MD simulations, while retaining similar molecular interactions between the CG particles. The broad range of spatiotemporal scales available in CG due to simplified atomistic models allows researchers to conduct simulations of large and highly complex biologically relevant systems. Several groups have used CG to design novel stimuli-responsive biomaterials[133-135] as well as self-assembly of polymeric materials[120, 134, 136]. For instance, researchers have been recently been interested in designing self-assembling nanostructures that can gelate (sol-gel transition) at higher concentrations. However, the design space and detail of such systems limits the robustness and scalability of such an approach, especially in the wet lab. As such, researchers used CG to investigate the molecular self-assembly of 8,000 tripeptide sequences to determine a predictive model of self-assembly propensity, which would not have been economically feasible through experimental approaches[136].

2.2 Fabrication techniques for building structure in biomaterials

The synthesis of complex 3D heterogenous microstructures is often limited by the dimensionality and structural resolution of existing manufacturing techniques. As noted above, biomimetic tissue constructs should not only be able to recapitulate biological functions in native cell-cell and cell-matrix interactions, they must also reproduce the complex microarchitectures of ECM components that propels dynamic signaling cues to initiate cellular attachment, migration, growth, and differentiation. This can be accomplished by replicating individual cellular and extracellular components of a tissue or organ, such as the nano- to microscale branching patterns of the capillary in complex organs like the brain, heart, kidney, liver, and lungs.

Electrospinning allows engineers to fabricate biomaterial scaffolds with micro to nanoscale fiber topography that can mimic key features of the ECM. Electrospinning is a process where a polymer solution is extruded through a charged needle [137-138]. The inherently high surface to volume ratio

of these electrospun fibers plays an integral role in enchanced cell attachment, proliferation, and migration. A variety of protein polymers have been succesfully electrospun into fibers, including BSA[139-140], collagen[141-143], fibrinogen[144-145], gelatin[146-147], elastin[148-150], silk[151-153], and self-assembling peptides[154]. Electrospun scaffolds have been used in tissue engineering applications[155-156], drug delivery[157-158], wound healing[138, 159], as well as biosensors[160-161]. The nanotopographical cues that can be generated using electrospinning methods have important implications in neuronal cell growth and differentiation[162-164]. These biophysical cues serve as stimuli (i.e. nanotopographical stimulation of mechanotransduction[165]) to guide neurite extension, can mediate NSC differentation, and can improve the therapeutic efficacy of stem cells in treating CNS diseases and injuries.

In recent years, 3D bioprinting has become a powerful fabrication technique that gives researchers the ability to generate intricate 3D microstructures that can mimic native microenvironments using a bottom-up approach. In 3D bioprinting, a computer-aided design software is used to control the placement of materials in a syringe, or print head, onto a substrate, enabling layer-by-layer deposition of material. Bioprinters have been used to print a variety of biocompatible materials, from 3D microconstructs encapsulating individual mammalian cells[166] to 3D organs[167-168]. Pioneering work by Atala *et al.* used inkjet printing technology to generate 3D heterogeneous tissue constructs using alginate-collagen composites containing multiple cell types that were able to form vascular networks upon implantation *in vivo*[169]. Additionally, the Burdick group have produced multimaterial structures comprised of shear-thinning hydrogel "bioinks" printed directly into self-healing hydrogels based on supramolecular assembly through guest-host interactions[170]. 3D bioprinting has also seen extensive use in replicating 3D microenvironments in native neural ECM. Examples include printing of hNSCs in alginate/chitosan constructs[171], construction of brain-like structures using RGD (fibronectin-derived cell adhesion site)-modified gellan gum[172], and guiding NSC differentiation through the use of stereolithography based 3D printing of gelatin methacrylamide hydrogels[173].

In the last decade or so, photolithography has gained immense popularity in the biomedical sciences, owing to lower production costs and increased access to fabrication tools. Photolithography is a powerful technique that enables formation of precise and complex 3D

structures at the micro and nanoscale using light to transfer intricate patterns on to a substrate. Novel work by DeForest *et al.* uses multiphoton laser-scanning lithography to immobilize peptides and full-length proteins in discrete patterns within polymeric hydrogels[174-175]. Another approach involves mask-based photolithography, and as the name suggests, uses a patterned mask where only regions exposed to UV light polymerize and cure to form a network of 3D structures[176-177]. This fabrication technique allows for the precise control of the cell-material interface and patterning of ligands and biomacromolecules on a variety of substrates. Recent work by Timashev *et al.* described a two-photon polymerization technique to fabricate polymeric ceramic composite scaffolds that support primary hippocampal neurons. These scaffolds induced the formation of neuronal networks from dissociated hippocampal cultures and demonstrated their functional calcium activity[178]. All of these patterning techniques have applications in CNS tissue reconstruction and may be utilized in the context of various different proteinaceous materials discussed in more detail below.

While native protein-based biomaterials can exhibit many unique biochemical and mechanical properties, they also display some shortcomings. These protein constituents are more prone to degradability and often have unwanted contaminants that are co-purified, which can lead to undesirable immunological responses in the human body. As an example, the insolubility of elastic microfibrils has made isolation, purification, and characterization of native elastin difficult, and has not been as widely used as a biomaterial. However, its synthetic component known as elastin-like polypeptides (ELPs), which are artificial repetitive polypeptides derived from mammalian elastin, have been useful for a wide variety of biomedical applications. ELPs consist of a pentapeptide repeat, (-Val-Pro-Gly-Xaa-Gly-), where Xaa is any guest amino acid residue, except proline. ELPs are unique in that they exhibit lower critical solution temperature (LCST) transition behavior; above a certain transition temperature, the disruption of ordered water molecules surrounding the polymeric backbone leads to the collapse of the polymer, giving rise to self-assembly and temperature-dependent gelation behavior[117, 179-180]. The transition temperature is completely tunable by the molecular weight and length of the sequence, as well as the guest residue, which can impart different folding pathways following the phase transition, and can be made susceptible to pH and ionization changes[181-182].

Incorporation of ionizable guest residues (e.g. lysine) allows ELPs to be chemically crosslinked resulting in the formation of hydrogels. Straley *et al.* used ELPs as substrates adsorbed onto glass coverslips and demonstrated that PC12 cells cultured on adsorbed protein surfaces had a high level of cell-surface biocompatibility and similar cellular morphology to those seen on collagen positive-control surfaces[183]. Shortly after, experiments using ELPs crosslinked by disuccinimidyl suberate showed that the resulting protein hydrogel could be used to modulate differentiation and neurite outgrowth of PC12 cells by tuning the RGD and degradable ELP densities[184]. Chung et al. used tetrakis (hydroxylmethyl) phosphonium chloride (THPC) as an amine reactive crosslinker[185] in lysine-containing ELPs. Later studies done by Lampe *et al.* used these crosslinked protein hydrogels to encapsulate chick DRGs[186]. DRG growth was dependent on mechanical and RGD ligand density, and maximized neurite outgrowth was seen in hydrogels where matrix stiffness was similar to that of the native neural ECM. The enhanced neurite outgrowth within tunable 3-D microenvironments suggests that these ELP hydrogels may be useful in developing therapeutic nerve guidance channels to enhance stroke recovery, as they provide independent control of tailored integrin-binding density as well as tunable biomechanical stiffness and stability. A more recent publication by the Heilshorn group functionalized the same RGD-ELP sequence to crosslink via bio-orthogonal strain-promoted azide-alkyne cycloaddition (SPAAC) reactions[187]. mNPCs encapsulated in SPAAC-ELP hydrogels showed high viability, and maintained their ability to differentiate into both neurons and astrocytes following treatment with differentiation medium for a week.

Additionally, neurotrophin-ELP-based fusion proteins have been used as stimuli-responsive nanoparticles that can deliver NGF and BDNF. PC12 cells with recombinant fusions saw substantial increases in neurite extension versus soluble neurotrophins, indicating that ELPs are able to interact with the cell without being quickly diffused throughout the system[188]. Likewise, silk-elastin-like proteins have been used as thin films to culture primary cortical neurons, where more surface adhesion and growth were observed in silk-elastin composites versus elastin and silk controls[189]. The appearance of a tightly connected neuronal network was seen, as cells formed clusters indicative of strong cell-matrix interactions within the protein alloy. Additionally, hNSCs encapsulated in IKVAV-modified silk fibroin hydrogels had increased β III-tubulin and MAP-2-

positive cells compared to unmodified silk fibroin hydrogels after 1 week in differentiation culture[190].

Biosynthetic polypeptide sequences also have the capacity to self-assemble into various nano- to microscale structures, ranging from α-helical fibrils to β-sheet rich hydrogels. Banwell *et al.* have developed a two-component peptide system based on the coiled-coil heptad sequence repeat, ***abcdefg***, where ***a*** and ***d*** are usually occupied by hydrophobic amino acids, and charged residues are found in positions ***e*** and ***g***[191]. The α-helical peptide hydrogel was shown to support PC12 cell growth and differentiation. Another example of such a self-assembling material is a triblock protein composed a polyelectrolyte domain flanked by two amphiphilic leucine zipper sequences. NSCs proliferated on adhesive substrates (incorporation of RGDs into the polyelectrolyte region) or aggregated as neurospheres on non-adhesive substrates. It was demonstrated that proliferation of NSCs can be modulated through control of RGD surface density[192]. Similarly, the Heilshorn group designed two-component protein engineered hydrogels composed of two protein association domains – a WW domain and a proline-rich domain[193]. Upon mixing of the two components, formation of a hydrogel occurs due to physical crosslinking that takes place between the two associative domains. NSCs, as well as PC12 and HUVEC cells were encapsulated in the hydrogels, where the former were able to differentiate, and the hydrogel supported growth and proliferation of all cell types. The resulting hydrogels demonstrate complete self-healing after shear-thinning, making them suitable as injectable materials for clinical use.

Early work by Holmes *et al.* looked at designing self-assembling peptide scaffolds that could support neuronal cell attachment and differentiation[194]. Now known as RADA16 peptides, the $(\text{-Arg-Ala-Asp-Ala-})_{16}$ sequence is capable of spontaneous assembly into β-sheet-rich hydrogels, and has been used extensively as a substitute for Matrigel. Recently, Koutsopoulos *et al.* used RADA16 hydrogels to study NSC differentiation. Cell survival was highest in peptide nanofiber hydrogels containing the SKPPGTSS functional motif (neuronal apoptosis inhibitor) after 3 months compared to tissue cultures in Matrigel and collagen type I[195]. In functionalized hydrogels, a majority of encapsulated NSCs enter neuronal lineage, and one week post-encapsulation showed ~62% of the neuron Tuj1^+ cells were monopolar, ~23% bipolar, and 15% multipolar, suggesting that these RADA16 were suitable 3D environments for neural tissue cultures. Additionally,

treatment with RADA16 hydrogels improved the survival of implanted donor NSCs *in* vivo. Nissl stains confirmed that damaged lesions saw significant regeneration following RADA16-IKVAV/NSCs implantation after 6 weeks compared to controls[196]. Furthermore, RADA16 hydrogels have also been shown to promote angiogenesis in a chick embryo[197]. RADA16 hydrogels (RAD/KLT) functionalized with a VEGF-mimicking peptide (KLTWQELYQLKYKGI) supported the highest endothelial cell sprout formation and average sprout length versus RADA16. The angiogenic properties of these hydrogel systems could potentially support endogenous recovery mechanisms in the recovering penumbra following stroke.

Peptide amphiphiles (PAs) have the ability to self-assemble in aqueous solution, driven by the sequence's hydrophobic aliphatic tail and a hydrophilic peptide domain. Seminal work done by the Stupp group demonstrated that PAs functionalized with the laminin epitope IKVAV was shown to induce rapid differentiation of encapsulated NPCs into neurons, and subsequently reducing astrocyte formation[198]. In other experiments, PA-IKVAVs were injected 24 h after SCI, and was shown to suppress astroglial differentiation. At 5 weeks and 11 weeks after SCI, there was a significant reduction in astrogliosis in PA-IKVAV treated groups, and 80% of all labeled corticospinal axons in the PA-IKVAV group were able to traverse through the area of injury[199]. Later studies by the same group reported increased serotonergic fibers in the caudal SC, with improved functional recovery at 10 weeks post injury[200]. Other peptides include amphiphilic diblock copolypeptides (DCHs), which can readily self-assemble into hydrogels under physiological conditions[201]. Histological characterizations indicated that DCH formulations did not induce any inflammatory or immune response upon injection. It was later shown that DCH deposits were densely vascularized, and contained microglia, astrocytes, and NG2 cells by 8 weeks *in vivo*. Researchers have also used amyloid-based self-assembling hydrogels to facilitate the attachment and neuronal differentiation of mesenchymal stem cells (MSCs)[202]. The high expression levels of ENO and TUBB3 and low levels of GFAP indicated that the amyloid hydrogel promoted hMSC differentiation toward the neuronal lineage. Additionally, $K_2(QL)_6K_2$ self-assembling hydrogels demonstrated that the cystic cavity in damaged spinal cords can be reduced by $K_2(QL)_6K_2$ or a combined $K_2(QL)_6K_2$ and NPC injection[203]. Furthermore, animals treated with $K_2(QL)_6K_2$ and NPCs showed a marked improvement in both grip strength, while vehicle-treated and NPC-treated groups reached a recovery plateau at 12 weeks.

2.3 Objectives of this work

A core problem in biomaterials—with both fundamental significance and technological relevance—concerns the rational design of bioactive microenvironments. As the unique microenvironment plays a role in determining encapsulated cell fate, we aimed to design a new family of peptides that can self-assemble, under cytocompatible conditions, into an ECM with structure and bioactivity that drive NSC differentiation. To pursue this goal, we utilized an integrated computational and experimental approach to the design of protein-based ECM mimetics for tissue regeneration applications. Computational approaches allow us to develop an atomic-resolution, quantitative understanding of the 3D structure and conformational dynamics of our peptide design; in this way, we were able to assess the suitability of our construct as a general-purpose scaffold for our longer-term goals (hydrogels to mimic ECMs of neural tissues). We examined the dynamical effects of systematically perturbing the pentapeptide sequence motif, Lys-Tyr-Phe-Ile-Leu-NH2 (KYFIL) that has been experimentally shown to self-assemble into a hydrogel.

In our earlier work, we proposed the use of a novel self-assembling peptide hydrogels to encapsulate neural cell types to drive tissue regeneration. Hydrogels are a promising class of biomaterials composed of water-swollen polymeric networks that mimic several biological and mechanical properties of the naturally compliant human brain tissue. In particular, peptide-based hydrogel materials are generally cytocompatible[97], and are inherently more physiologically relevant as they allow for cellular remodeling and can promote cell viability[96]. However, hydrogels must meet several criteria in order to be effective delivery vehicles for stem cell transplantation into the brain following an ischemic stroke. First, clinical application to the infarct cavity must be achieved via simple injection, a minimally invasive patient delivery. Second, the hydrogel must not swell during or after gelation to prevent further damage to the brain. Finally, these hydrogels must allow for the precise control of stem cell behavior to promote neural tissue regeneration. More broadly, the goal of this thesis was to design and create biomaterials that have properties (e.g. stiffness, self-healing, biological cues, etc.) compatible with neural tissue to elicit a desirable regenerative effect. The specific objectives are outlined below:

1. Model pentapeptide assembly via atomistic molecular dynamics simulations

2. Synthesize pentapeptide hydrogels and characterize biophysical properties
3. Assess the cytocompatibility of pentapeptide hydrogels
4. Identify and synthesize cell-responsive hydrogels via incorporation of cell-matrix interactive domains.

References

1. Lutz, A. B.; Barres, B. A., Contrasting the Glial Response to Axon Injury in the Central and Peripheral Nervous Systems. *Dev Cell* **2014,** *28* (1), 7-17.
2. Lau, L. W.; Cua, R.; Keough, M. B.; Haylock-Jacobs, S.; Yong, V. W., OPINION Pathophysiology of the brain extracellular matrix: a new target for remyelination. *Nat Rev Neurosci* **2013,** *14* (10), 722-729.
3. Allen, N. J.; Barres, B. A., NEUROSCIENCE Glia - more than just brain glue. *Nature* **2009,** *457* (7230), 675-677.
4. Russell, L. N.; Lampe, K. J., Engineering Biomaterials to Influence Oligodendroglial Growth, Maturation, and Myelin Production. *Cells Tissues Organs* **2016,** *202* (1-2), 85-101.
5. Sofroniew, M. V.; Vinters, H. V., Astrocytes: biology and pathology. *Acta Neuropathol* **2010,** *119* (1), 7-35.
6. Zimmermann, D. R.; Dours-Zimmermann, M. T., Extracellular matrix of the central nervous system: from neglect to challenge. *Histochem Cell Biol* **2008,** *130* (4), 635-653.
7. World Health Organization, Global Health Estimates 2015: Deaths by Cause, Age, Sex, by Country and by Region, 2000-2015. **2016**.
8. Murray, C. J. L.; Vos, T.; Lozano, R., Disability-adjusted life years (DALYs) for 291 diseases and injuries in 21 regions, 1990-2010: a systematic analysis for the Global Burden of Disease Study 2010 (vol 380, pg 2197, 2012). *Lancet* **2014,** *384* (9943), 582-582.
9. Krishnamurthi, R. V.; deVeber, G.; Feigin, V. L.; Barker-Collo, S.; Fullerton, H.; Mackay, M. T.; O'Callahan, F.; Lindsay, M. P.; Kolk, A.; Lo, W.; Shah, P.; Linds, A.; Jones, K.; Parmar, P.; Taylor, S.; Norrving, B.; Mensah, G. A.; Moran, A. E.; Naghavi, M.; Forouzanfar, M. H.; Nguyen, G.; Johnson, C. O.; Vos, T.; Murray, C. J. L.; Roth, G. A.; Grp, G. S. P. E., Stroke Prevalence, Mortality and Disability-Adjusted Life Years in Children and Youth Aged 0-19 Years: Data from the Global and Regional Burden of Stroke 2013. *Neuroepidemiology* **2015,** *45* (3), 177-189.
10. Feigin, V. L.; Forouzanfar, M. H.; Krishnamurthi, R.; Mensah, G. A.; Connor, M.; Bennett, D. A.; Moran, A. E.; Sacco, R. L.; Anderson, L.; Truelsen, T.; O'Donnell, M.; Venketasubramanian, N.; Barker-Collo, S.; Lawes, C. M. M.; Wang, W. Z.; Shinohara, Y.; Witt, E.; Ezzati, M.; Naghavi, M.; Murray, C.; Fa, G. B. D. I. R.; Grp, G. S. E., Global and regional burden of stroke during 1990-2010: findings from the Global Burden of Disease Study 2010. *Lancet* **2014,** *383* (9913), 245-255.
11. Moskowitz, M. A.; Lo, E. H.; Iadecola, C., The Science of Stroke: Mechanisms in Search of Treatments. *Neuron* **2010,** *67* (2), 181-198.
12. Mitsios, N.; Gaffney, J.; Kumar, P.; Krupinski, J.; Kumar, S.; Slevin, M., Pathophysiology of acute ischaemic stroke: An analysis of common signalling mechanisms and identification of new molecular targets. *Pathobiology* **2006,** *73* (4), 159-175.
13. Zhang, L.; Chopp, M.; Liu, X. S.; Teng, H.; Tang, T.; Kassis, H.; Zhang, Z. G., Combination Therapy With VELCADE and Tissue Plasminogen Activator Is Neuroprotective in Aged Rats After Stroke and Targets MicroRNA-146a and the Toll-Like Receptor Signaling Pathway. *Arterioscl Throm Vas* **2012,** *32* (8), 1856-U336.
14. Peerschke, E. I.; Yin, W.; Ghebrehiwet, B., Complement activation on platelets: Implications for vascular inflammation and thrombosis. *Mol Immunol* **2010,** *47* (13), 2170-2175.
15. Wechsler, L. R.; Jovin, T. G., Intravenous Recombinant Tissue-Type Plasminogen Activator in the Extended Time Window and the US Food and Drug Administration Confused About the Time. *Stroke* **2012,** *43* (9), 2517-2519.
16. Wechsler, L.; Steindler, D.; Borlongan, C.; Chopp, M.; Savitz, S.; Deans, R.; Caplan, L.; Hess, D.; Mays, R. W.; Participants, S., Stem Cell Therapies as an Emerging Paradigm in Stroke (STEPS) Bridging Basic and Clinical Science for Cellular and Neurogenic Factor Therapy in Treating Stroke. *Stroke* **2009,** *40* (2), 510-515.
17. Savitz, S. I.; Chopp, M.; Deans, R.; Carmichael, S. T.; Phinney, D.; Wechsler, L., Stem Cell Therapy as an Emerging Paradigm for Stroke (STEPS) II. *Stroke* **2011,** *42* (3), 825-829.
18. Cooke, M. J.; Zahir, T.; Phillips, S. R.; Shah, D. S. H.; Athey, D.; Lakey, J. H.; Shoichet, M. S.; Przyborski, S. A., Neural differentiation regulated by biomimetic surfaces presenting motifs of extracellular matrix proteins. *J Biomed Mater Res A* **2010,** *93a* (3), 824-832.
19. Kubinova, S.; Sykova, E., Nanotechnology for treatment of stroke and spinal cord injury. *Nanomedicine-Uk* **2010,** *5* (1), 99-108.
20. Sharp, K. G.; Dickson, A. R.; Marchenko, S. A.; Yee, K. M.; Emery, P. N.; Laidmae, I.; Uibo, R.; Sawyer, E. S.; Steward, O.; Flanagan, L. A., Salmon fibrin treatment of spinal cord injury promotes functional recovery and density of serotonergic innervation. *Exp Neurol* **2012,** *235* (1), 345-56.
21. Hamann, M. C. J.; Tator, C. H.; Shoichet, M. S., Injectable intrathecal delivery system for localized administration of EGF and FGF-2 to the injured rat spinal cord. *Exp Neurol* **2005,** *194* (1), 106-119.
22. Matsuse, D.; Kitada, M.; Ogura, F.; Wakao, S.; Kohama, M.; Kira, J.; Tabata, Y.; Dezawa, M., Combined Transplantation of Bone Marrow Stromal Cell-Derived Neural Progenitor Cells with a Collagen Sponge and Basic Fibroblast Growth Factor Releasing Microspheres Enhances Recovery After Cerebral Ischemia in Rats. *Tissue Eng Pt A* **2011,** *17* (15-16), 1993-2004.
23. Ajioka, I.; Jinnou, H.; Okada, K.; Sawada, M.; Saitoh, S.; Sawamoto, K., Enhancement of Neuroblast Migration into the Injured Cerebral Cortex Using Laminin-Containing Porous Sponge. *Tissue Eng Pt A* **2015,** *21* (1-2), 193-201.
24. Oshikawa, M.; Okada, K.; Kaneko, N.; Sawamoto, K.; Ajioka, I., Affinity-Immobilization of VEGF on Laminin Porous Sponge Enhances Angiogenesis in the Ischemic Brain. *Adv Healthc Mater* **2017,** *6* (11).
25. Hess, D. C.; Auchus, A. P.; Uchino, K.; Sila, C.; Clark, W. M.; Chiu, D.; Wechsler, L. R.; Mays, R. W.; Investigators, B.-. Final Results of the B01-02 Phase 2 Trial Testing the Safety and Efficacy of MultiStem(R) in Treatment of Ischemic Stroke. *Stroke* **2016,** *47*.
26. Friedrich, M. A. G.; Martins, M. P.; Araujo, M. D.; Klamt, C.; Vedolin, L.; Garicochea, B.; Raupp, E. F.; El Ammar, J. S.; Machado, D. C.; da Costa, J. C.; Nogueira, R. G.; Rosado-de-Castro, P. H.; Mendez-Otero, R.; de Freitas, G. R., Intra-Arterial Infusion of Autologous Bone Marrow Mononuclear Cells in Patients With Moderate to Severe Middle Cerebral Artery Acute Ischemic Stroke. *Cell Transplant* **2012,** *21*, S13-S21.
27. Bang, O. Y., Clinical Trials of Adult Stem Cell Therapy in Patients with Ischemic Stroke. *J Clin Neurol* **2016,** *12* (1), 14-20.

28. Burnstock, G., Purinergic signalling and disorders of the central nervous system. *Nat Rev Drug Discov* **2008,** *7* (7), 575-590.
29. Broughton, B. R. S.; Reutens, D. C.; Sobey, C. G., Apoptotic Mechanisms After Cerebral Ischemia. *Stroke* **2009,** *40* (5), E331-E339.
30. Unal-Cevik, I.; Kilinc, M.; Can, A.; Gursoy-Ozdemir, Y.; Dalkara, T., Apoptotic and necrotic death mechanisms are concomitantly activated in the same cell after cerebral ischemia. *Stroke* **2004,** *35* (9), 2189-2194.
31. Fabricius, M.; Fuhr, S.; Bhatia, R.; Boutelle, M.; Hashemi, P.; Strong, A. J.; Lauritzen, M., Cortical spreading depression and peri-infarct depolarization in acutely injured human cerebral cortex. *Brain* **2006,** *129*, 778-790.
32. Mattson, M. P.; Culmsee, C.; Yu, Z. F., Apoptotic and antiapoptotic mechanisms in stroke. *Cell Tissue Res* **2000,** *301* (1), 173-187.
33. Chukanova, E. I.; Khozhamzharov, B. E.; Chukanova, A. S., Current possibilities of the correction of oxidative stress in acute brain ischemia. *Zh Nevrol Psikhiatr* **2012,** *112* (11), 79-82.
34. Dobrotvorskaya, I. S.; Fedorova, T. N.; Dobrota, D.; Berezov, T. T., Characteristics of Oxidative Stress in Experimental Rat Brain Ischemia Aggravated by Homocysteic Acid. *Neurochem J+* **2011,** *5* (1), 42-46.
35. Dirnagl, U.; Iadecola, C.; Moskowitz, M. A., Pathobiology of ischaemic stroke: an integrated view. *Trends Neurosci* **1999,** *22* (9), 391-397.
36. Sims, N. R.; Anderson, M. F., Mitochondrial contributions to tissue damage in stroke. *Neurochem Int* **2002,** *40* (6), 511-526.
37. Lakhan, S. E.; Kirchgessner, A.; Tepper, D.; Leonard, A., Matrix metalloproteinases and blood-brain barrier disruption in acute ischemic stroke. *Front Neurol* **2013,** *4*.
38. Iadecola, C.; Anrather, J., The immunology of stroke: from mechanisms to translation. *Nat Med* **2011,** *17* (7), 796-808.
39. Hyman, M. C.; Petrovic-Djergovic, D.; Visovatti, S. H.; Liao, H.; Yanamadala, S.; Bouis, D.; Su, E. M. J.; Lawrence, D. A.; Broekman, M. J.; Marcus, A. J.; Pinsky, D. J., Self-regulation of inflammatory cell trafficking in mice by the leukocyte surface apyrase CD39. *J Clin Invest* **2009,** *119* (5), 1136-1149.
40. Zhang, R. L.; Chopp, M.; Zhang, Z. G.; Jiang, N.; Powers, C., The expression of P- and E-selectins in three models of middle cerebral artery occlusion. *Brain Res* **1998,** *785* (2), 207-214.
41. Stephan, A. H.; Barres, B. A.; Stevens, B., The Complement System: An Unexpected Role in Synaptic Pruning During Development and Disease. *Annual Review of Neuroscience, Vol 35* **2012,** *35*, 369-389.
42. Rosenberg, G. A., Extracellular matrix inflammation in vascular cognitive impairment and dementia. *Clin Sci* **2017,** *131* (6), 425-437.
43. Cekanaviciute, E.; Fathali, N.; Doyle, K. P.; Williams, A. M.; Han, J.; Buckwalter, M. S., Astrocytic Transforming Growth Factor-Beta Signaling Reduces Subacute Neuroinflammation After Stroke in Mice. *Glia* **2014,** *62* (8), 1227-1240.
44. Arnold, L.; Henry, A.; Poron, F.; Baba-Amer, Y.; van Rooijen, N.; Plonquet, A.; Gherardi, R. K.; Chazaud, B., Inflammatory monocytes recruited after skeletal muscle injury switch into antiinflammatory macrophages to support myogenesis. *J Exp Med* **2007,** *204* (5), 1057-1069.
45. Nathan, C.; Ding, A. H., Nonresolving Inflammation. *Cell* **2010,** *140* (6), 871-882.
46. Liesz, A.; Suri-Payer, E.; Veltkamp, C.; Doerr, H.; Sommer, C.; Rivest, S.; Giese, T.; Veltkamp, R., Regulatory T cells are key cerebroprotective immunomodulators in acute experimental stroke. *Nat Med* **2009,** *15* (2), 192-199.
47. Veltkamp, R.; Suri-Payer, E.; Veltkamp, C.; Sommer, C.; Rivest, S.; Liesz, A., Endogenous immunomodulation after experimental focal ischemia: multitargeted cerebroprotection by regulatory T cells is the key. *J Cerebr Blood F Met* **2009,** *29*, S508-S509.
48. Gliem, M.; Krammes, K.; Liaw, L.; van Rooijen, N.; Hartung, H. P.; Jander, S., Macrophage-Derived Osteopontin Induces Reactive Astrocyte Polarization and Promotes Re-Establishment of the Blood Brain Barrier After Ischemic Stroke. *Glia* **2015,** *63* (12), 2198-2207.
49. Wiese, S.; Karus, M.; Faissner, A., Astrocytes as a source for extracellular matrix molecules and cytokines. *Front Pharmacol* **2012,** *3*.
50. Marler, J. R.; Brott, T.; Broderick, J.; Kothari, R.; Odonoghue, M.; Barsan, W.; Tomsick, T.; Spilker, J.; Miller, R.; Sauerbeck, L.; Jarrell, J.; Kelly, J.; Perkins, T.; Mcdonald, T.; Rorick, M.; Hickey, C.; Armitage, J.; Perry, C.; Thalinger, K.; Rhude, R.; Schill, J.; Becker, P. S.; Heath, R. S.; Adams, D.; Reed, R.; Klei, M.; Hughes, S.; Anthony, J.; Baudendistel, D.; Zadicoff, C.; Rymer, M.; Bettinger, I.; Laubinger, P.; Schmerler, M.; Meirose, G.; Lyden, P.; Rapp, K.; Babcock, T.; Daum, P.; Persona, D.; Brody, M.; Jackson, C.; Lewis, S.; Liss, J.; Mahdavi, Z.; Rothrock, J.; Tom, T.; Zweifler, R.; Dunford, J.; Zivin, J.; Kobayashi, R.; Kunin, J.; Licht, J.; Rowen, R.; Stein, D.; Grisolia, J.; Martin, F.; Chaplin, E.; Kaplitz, N.; Nelson, J.; Neuren, A.; Silver, D.; Chippendale, T.; Diamond, E.; Lobatz, M.; Murphy, D.; Rosenberg, D.; Ruel, T.; Sadoff, M.; Schim, J.; Schleimer, J.; Atkinson, R.; Wentworth, D.; Cummings, R.; Frink, R.; Heublein, P.; Grotta, J. C.; Degraba, T.; Fisher, M.; Ramirez, A.; Hanson, S.; Morgenstern, L.; Sills, C.; Pasteur, W.; Yatsu, F.; Andrews, K.; Villarcordova, C.; Pepe, P.; Bratina, P.; Greenberg, L.; Rozek, S.; Simmons, K.; Kwiatkowski, T. G.; Horowitz, S. H.; Libman, R.; Kanner, R.; Silverman, R.; Lamantia, J.; Mealie, C.; Duarte, R.; Donnarumma, R.; Okola, M.; Cullin, V.; Mitchell, E.; Levine, S. R.; Lewandowski, C. A.; Tokarski, G.; Ramadan, N. M.; Mitsias, P.; Gorman, M.; Zarowitz, B.; Kokkinos, J.; Dayno, J.; Verro, P.; Gymnopoulos, C.; Dafer, R.; Dolhaberriague, L.; Sawaya, K.; Daley, S.; Mitchell, M.; Frankel, M.; Mackay, B.; Barch, C.; Braimah, J.; Faherty, B.; Macdonald, J.; Sailor, S.; Cook, A.; Karp, H.; Nguyen, B.; Washington, J.; Weissman, J.; Williams, M.; Williamson, T.; Kozinn, M.; Hellwick, L.; Haley, E. C.; Bleck, T. P.; Cail, W. S.; Lindbeck, G. H.; Granner, M. A.; Wolf, S. S.; Gwynn, M. W.; Mettetal, R. W.; Chang, C. W. J.; Solenski, N. J.; Brock, D. G.; Ford, G. F.; Kongable, G. L.; Parks, K. N.; Wilkinson, S. S.; Davis, M. K.; Sheppard, G. L.; Zontine, D. W.; Gustin, K. H.; Crowe, N. M.; Massey, S. L.; Meyer, M.; Gaines, K.; Payne, A.; Bales, C.; Malcolm, J.; Barlow, R.; Wilson, M.; Cape, C.; Bertorini, T.; Misulis, K.; Paulsen, W.; Shepard, D.; Tilley, B. C.; Welch, K. M. A.; Fagan, S. C.; Lu, M.; Patel, S.; Masha, E.; Verter, J.; Boura, J.; Main, J.; Gordon, L.; Maddy, N.; Chociemski, T.; Windham, J.; Zadeh, H. S.; Alves, W.; Keller, M. F.; Wenzel, J. R.; Raman, N.; Cantwell, L.; Warren, A.; Smith, K.; Bailey, E.; Welch, K. M. A.; Tilley, B. C.; Froehlich, J.; Breed, J.; Easton, J. D.; Hallenbeck, J. F.; Lan, G.; Marsh, J. D.; Walker, M. D., Tissue-Plasminogen Activator for Acute Ischemic Stroke. *New Engl J Med* **1995,** *333* (24), 1581-1587.
51. Frey, J. L., Recombinant tissue plasminogen activator (rtPA) for stroke - The perspective at 8 years. *Neurologist* **2005,** *11* (2), 123-133.

52. Heo, J. H.; Kim, S. H.; Lee, K. Y.; Kim, E. H.; Chu, C. K.; Nam, J. M., Increase in plasma matrix metalloproteinase-9 in acute stroke patients with thrombolysis failure. *Stroke* **2003,** *34* (6), E48-E50.
53. Zhu, J. X.; Xiao, Y. L.; Li, Z. M.; Han, F. B.; Xiao, T. W.; Zhang, Z. T.; Geng, F. Y., Efficacy of Surgery Combined with Autologous Bone Marrow Stromal Cell Transplantation for Treatment of Intracerebral Hemorrhage. *Stem Cells Int* **2015**.
54. Yoo, J.; Seo, J. J.; Eom, J. H.; Hwang, D. Y., Enhanced Recovery From Chronic Ischemic Injury by Bone Marrow Cells in a Rat Model of Ischemic Stroke. *Cell Transplant* **2015,** *24* (2), 167-182.
55. Chen, J. L.; Ye, X. C.; Yan, T.; Zhang, C. L.; Yang, X. P.; Cui, X.; Cui, Y. S.; Zacharek, A.; Roberts, C.; Liu, X. F.; Dai, X. G.; Lu, M.; Chopp, M., Adverse Effects of Bone Marrow Stromal Cell Treatment of Stroke in Diabetic Rats. *Stroke* **2011,** *42* (12), 3551-3558.
56. Efimenko, A. Y.; Kochegura, T. N.; Akopyan, Z. A.; Parfyonova, Y. V., Autologous Stem Cell Therapy: How Aging and Chronic Diseases Affect Stem and Progenitor Cells. *Bioresearch Open Acc* **2015,** *4* (1), 26-38.
57. Davis, S. M.; Pennypacker, K. R., Targeting antioxidant enzyme expression as a therapeutic strategy for ischemic stroke. *Neurochem Int* **2017,** *107*, 23-32.
58. Ghezzi, P.; Jaquet, V.; Marcucci, F.; Schmidt, H. H. H. W., The oxidative stress theory of disease: levels of evidence and epistemological aspects. *Brit J Pharmacol* **2017,** *174* (12), 1784-1796.
59. Petro, M.; Jaffer, H.; Yang, J.; Kabu, S.; Morris, V. B.; Labhasetwar, V., Tissue plasminogen activator followed by antioxidant-loaded nanoparticle delivery promotes activation/mobilization of progenitor cells in infarcted rat brain. *Biomaterials* **2016,** *81*, 169-180.
60. Isik, M.; Beydemir, S.; Yilmaz, A.; Naldan, M. E.; Aslan, H. E.; Gulcin, I., Oxidative stress and mRNA expression of acetylcholinesterase in the leukocytes of ischemic patients. *Biomed Pharmacother* **2017,** *87*, 561-567.
61. Kaur, C.; Rathnasamy, G.; Ling, E. A., Antioxidants and Neuroprotection in the Brain and Retina. *Front Med Chem* **2015,** *7*, 3-33.
62. Papapetrou, A.; Moris, D.; Patelis, N.; Kouvelos, G. N.; Bakogiannis, C.; Klonaris, C.; Georgopoulos, S., Oxidative Stress and Total Antioxidant Status During Internal Carotid Artery Clamping with or without Shunting: An Experimental Pilot Study. *Med Sci Monit Basic* **2015,** *21*, 200-205.
63. Imai, H.; Masayasu, H.; Dewar, D.; Graham, D. I.; Macrae, I. M., Ebselen protects both gray model of focal and white matter in a rodent cerebral ischemia. *Stroke* **2001,** *32* (9), 2149-2156.
64. Noor, J. I.; Ikeda, T.; Mishima, K.; Aoo, N.; Ohta, S.; Egashira, N.; Iwasaki, K.; Fujiwara, M.; Ikenoue, T., Short-term administration of a new free radical scavenger, edaravone, is more effective than its long-term administration for the treatment of neonatal hypoxic-ischemic encephalopathy. *Stroke* **2005,** *36* (11), 2468-2474.
65. Schmid-Elsaesser, R.; Zausinger, S.; Hungerhuber, E.; Baethmann, A.; Reulen, H. J., Neuroprotective effects of combination therapy with tirilazad and magnesium in rats subjected to reversible focal cerebral ischemia. *Neurosurgery* **1999,** *44* (1), 163-171.
66. Maples, K. R.; Ma, F.; Zhang, Y. K., Comparison of the radical trapping ability of PBN, S-PBN and NXY-059. *Free Radical Res* **2001,** *34* (4), 417-426.
67. Green, A. R.; Shuaib, A., Therapeutic strategies for the treatment of stroke. *Drug Discov Today* **2006,** *11* (15-16), 681-693.
68. Jin, Q.; Cai, Y.; Li, S.; Liu, H. R.; Zhou, X. Y.; Lu, C. Q.; Gao, X. H.; Qian, J.; Zhang, J.; Ju, S. H.; Li, C., Edaravone-Encapsulated Agonistic Micelles Rescue Ischemic Brain Tissue by Tuning Blood-Brain Barrier Permeability. *Theranostics* **2017,** *7* (4), 884-898.
69. Zheng, S. Y.; Bai, Y. Y.; Liu, Y. K.; Gao, X. H.; Li, Y.; Changyi, Y. Z.; Wang, Y. C.; Chang, D.; Ju, S. H.; Li, C., Salvaging brain ischemia by increasing neuroprotectant uptake via nanoagonist mediated blood brain barrier permeability enhancement. *Biomaterials* **2015,** *66*, 9-20.
70. Massensini, A. R.; Ghuman, H.; Saldin, L. T.; Medberry, C. J.; Keane, T. J.; Nicholls, F. J.; Velankar, S. S.; Badylak, S. F.; Modo, M., Concentration-dependent rheological properties of ECM hydrogel for intracerebral delivery to a stroke cavity. *Acta Biomaterialia* **2015,** *27*, 116-130.
71. Boisserand, L. S. B.; Kodama, T.; Papassin, J.; Auzely, R.; Moisan, A.; Rome, C.; Detante, O., Biomaterial Applications in Cell-Based Therapy in Experimental Stroke. *Stem Cells Int* **2016**.
72. Wang, Z.; Wang, J.; Jin, Y.; Luo, Z.; Yang, W.; Xie, H. J.; Huang, K.; Wang, L., A Neuroprotective Sericin Hydrogel As an Effective Neuronal Cell Carrier for the Repair of Ischemic Stroke. *Acs Appl Mater Inter* **2015,** *7* (44), 24629-24640.
73. Lampe, K. J.; Heilshorn, S. C., Building stem cell niches from the molecule up through engineered peptide materials. *Neuroscience Letters* **2012,** *519* (2), 138-146.
74. Harris, J. P.; Struzyna, L. A.; Murphy, P. L.; Adewole, D. O.; Kuo, E.; Cullen, D. K., Advanced biomaterial strategies to transplant preformed micro-tissue engineered neural networks into the brain. *J Neural Eng* **2016,** *13* (1).
75. Mehdizadeh, H.; Bayrak, E. S.; Lu, C.; Somo, S. I.; Akar, B.; Brey, E. M.; Cinar, A., Agent-based modeling of porous scaffold degradation and vascularization: Optimal scaffold design based on architecture and degradation dynamics. *Acta Biomaterialia* **2015,** *27*, 167-178.
76. Manning, C. N.; Schwartz, A. G.; Liu, W.; Xie, J.; Havlioglu, N.; Sakiyama-Elbert, S. E.; Silva, M. J.; Xia, Y.; Gelberman, R. H.; Thomopoulos, S., Controlled delivery of mesenchymal stem cells and growth factors using a nanofiber scaffold for tendon repair. *Acta Biomaterialia* **2013,** *9* (6), 6905-6914.
77. Ju, R. K.; Wen, Y. J.; Gou, R. B.; Wang, Y.; Xu, Q. Y., The Experimental Therapy on Brain Ischemia by Improvement of Local Angiogenesis With Tissue Engineering in the Mouse. *Cell Transplant* **2014,** *23*, S83-S95.
78. Pace, L. A.; Plate, J. F.; Smith, T. L.; Van Dyke, M. E., The effect of human hair keratin hydrogel on early cellular response to sciatic nerve injury in a rat model. *Biomaterials* **2013,** *34* (24), 5907-5914.
79. Merrifield, R. B., Solid Phase Peptide Synthesis. I. The Synthesis of a Tetrapeptide. *J Am Chem Soc* **1963,** *85* (14), 2149-2154.
80. Carpino, L. A.; Han, G. Y., 9-Fluorenylmethoxycarbonyl Function, a New Base-Sensitive Amino-Protecting Group. *J Am Chem Soc* **1970,** *92* (19), 5748-&.
81. Lutolf, M. P.; Lauer-Fields, J. L.; Schmoekel, H. G.; Metters, A. T.; Weber, F. E.; Fields, G. B.; Hubbell, J. A., Synthetic matrix metalloproteinase-sensitive hydrogels for the conduction of tissue regeneration: Engineering cell-invasion characteristics. *P Natl Acad Sci USA* **2003,** *100* (9), 5413-5418.

82. Patterson, J.; Hubbell, J. A., Enhanced proteolytic degradation of molecularly engineered PEG hydrogels in response to MMP-1 and MMP-2. *Biomaterials* **2010,** *31* (30), 7836-7845.
83. Tokatlian, T.; Shrum, C. T.; Kadoya, W. M.; Segura, T., Protease degradable tethers for controlled and cell-mediated release of nanoparticles in 2-and 3-dimensions. *Biomaterials* **2010,** *31* (31), 8072-8080.
84. Bellis, S. L., Advantages of RGD peptides for directing cell association with biomaterials. *Biomaterials* **2011,** *32* (18), 4205-4210.
85. Wang, A. Y.; Leong, S.; Liang, Y. C.; Huang, R. C. C.; Chen, C. S.; Yu, S. M., Immobilization of Growth Factors on Collagen Scaffolds Mediated by Polyanionic Collagen Mimetic Peptides and Its Effect on Endothelial Cell Morphogenesis. *Biomacromolecules* **2008,** *9* (10), 2929-2936.
86. Rothenfluh, D. A.; Bermudez, H.; O'Neil, C. P.; Hubbell, J. A., Biofunctional polymer nanoparticles for intra-articular targeting and retention in cartilage. *Nat Mater* **2008,** *7* (3), 248-254.
87. Chen, T. T.; Luque, A.; Lee, S.; Anderson, S. M.; Segura, T.; Iruela-Arispe, M. L., Anchorage of VEGF to the extracellular matrix conveys differential signaling responses to endothelial cells. *J Cell Biol* **2010,** *188* (4), 595-609.
88. Lesauteur, L.; Wei, L.; Gibbs, B. F.; Saragovi, H. U., Small Peptide Mimics of Nerve Growth-Factor Bind Trka Receptors and Affect Biological Responses. *J Biol Chem* **1995,** *270* (12), 6564-6569.
89. Martino, M. M.; Hubbell, J. A., The 12th-14th type III repeats of fibronectin function as a highly promiscuous growth factor-binding domain. *Faseb J* **2010,** *24* (12), 4711-4721.
90. Zhang, S. G.; Holmes, T.; Lockshin, C.; Rich, A., SPONTANEOUS ASSEMBLY OF A SELF-COMPLEMENTARY OLIGOPEPTIDE TO FORM A STABLE MACROSCOPIC MEMBRANE. *P Natl Acad Sci USA* **1993,** *90* (8), 3334-3338.
91. Schneider, J. P., Responsive hydrogels from the intramolecular folding and self-assembly of a designed peptide. *Abstr Pap Am Chem S* **2003,** *225*, U321-U321.
92. Rajagopal, K.; Ozbas, B.; Pochan, D. J.; Schneider, J. P., Self-assembly of beta hairpin peptides to hydrogels and tuning of material properties by design of turn sequence. *Abstr Pap Am Chem S* **2004,** *228*, U68-U68.
93. Ozbas, B.; Kretsinger, J.; Rajagopal, K.; Schneider, J. P.; Pochan, D. J., Salt-triggered peptide folding and consequent self-assembly into hydrogels with tunable modulus. *Macromolecules* **2004,** *37* (19), 7331-7337.
94. Dong, H.; Paramonov, S. E.; Aulisa, L.; Bakota, E. L.; Hartgerink, J. D., Self-assembly of multidomain peptides: Balancing molecular frustration controls conformation and nanostructure. *J Am Chem Soc* **2007,** *129* (41), 12468-12472.
95. Webber, M. J.; Tongers, J.; Newcomb, C. J.; Marquardt, K. T.; Bauersachs, J.; Losordo, D. W.; Stupp, S. I., Supramolecular nanostructures that mimic VEGF as a strategy for ischemic tissue repair. *P Natl Acad Sci USA* **2011,** *108* (33), 13438-13443.
96. Perez, C. M. R.; Stephanopoulos, N.; Sur, S.; Lee, S. S.; Newcomb, C.; Stupp, S. I., The Powerful Functions of Peptide-Based Bioactive Matrices for Regenerative Medicine. *Ann Biomed Eng* **2015,** *43* (3), 501-514.
97. Stephanopoulos, N.; Ortony, J. H.; Stupp, S. I., Self-assembly for the synthesis of functional biomaterials. *Acta Mater* **2013,** *61* (3), 912-930.
98. Tavakol, S.; Musavi, S. M. M.; Tavakol, B.; Hoveizi, E.; Ai, J.; Rezayat, S. M., Noggin Along with a Self-Assembling Peptide Nanofiber Containing Long Motif of Laminin Induces Tyrosine Hydroxylase Gene Expression. *Mol Neurobiol* **2017,** *54* (6), 4609-4616.
99. Fleming, S.; Ulijn, R. V., Design of nanostructures based on aromatic peptide amphiphiles. *Chem Soc Rev* **2014,** *43* (23), 8150-8177.
100. Pappas, C. G.; Shafi, R.; Sasselli, I. R.; Siccardi, H.; Wang, T.; Narang, V.; Abzalimov, R.; Wijerathne, N.; Ulijn, R. V., Dynamic peptide libraries for the discovery of supramolecular nanomaterials. *Nat Nanotechnol* **2016,** *11* (11), 960-967.
101. Zhou, J.; Li, J.; Du, X. W.; Xu, B., Supramolecular biofunctional materials. *Biomaterials* **2017,** *129*, 1-27.
102. Webber, M. J.; Appel, E. A.; Meijer, E. W.; Langer, R., Supramolecular biomaterials. *Nat Mater* **2016,** *15* (1), 13-26.
103. Mura, C.; McAnany, C. E., An introduction to biomolecular simulations and docking. *Molecular Simulation* **2014,** *40* (10-11), 732-764.
104. Chang, D. K.; Urry, D. W., Molecular-Dynamics Calculations on Relaxed and Extended States of the Polypentapeptide of Elastin. *Chem Phys Lett* **1988,** *147* (4), 395-400.
105. Leech, J.; Prins, J. F.; Hermans, J., SMD: Visual steering of molecular dynamics for protein design. *Ieee Comput Sci Eng* **1996,** *3* (4), 38-45.
106. MacKerell, A. D.; Bashford, D.; Bellott, M.; Dunbrack, R. L.; Evanseck, J. D.; Field, M. J.; Fischer, S.; Gao, J.; Guo, H.; Ha, S.; Joseph-McCarthy, D.; Kuchnir, L.; Kuczera, K.; Lau, F. T. K.; Mattos, C.; Michnick, S.; Ngo, T.; Nguyen, D. T.; Prodhom, B.; Reiher, W. E.; Roux, B.; Schlenkrich, M.; Smith, J. C.; Stote, R.; Straub, J.; Watanabe, M.; Wiorkiewicz-Kuczera, J.; Yin, D.; Karplus, M., All-atom empirical potential for molecular modeling and dynamics studies of proteins. *J Phys Chem B* **1998,** *102* (18), 3586-3616.
107. Sreerama, N.; Woody, R. W., Molecular dynamics simulations of polypeptide conformations in water: A comparison of alpha, beta, and poly(Pro)II conformations. *Proteins* **1999,** *36* (4), 400-406.
108. Phillips, J. C.; Braun, R.; Wang, W.; Gumbart, J.; Tajkhorshid, E.; Villa, E.; Chipot, C.; Skeel, R. D.; Kale, L.; Schulten, K., Scalable molecular dynamics with NAMD. *J Comput Chem* **2005,** *26* (16), 1781-1802.
109. Popovych, N.; Sun, S.; Ebright, R. H.; Kalodimos, C. G., Dynamically driven protein allostery. *Nature Structural & Molecular Biology* **2006,** *13* (9), 831-838.
110. Zhao, Y.; Kormos, B. L.; Beveridge, D. L.; Baranger, A. M., Molecular dynamics simulation studies of a protein-RNA complex with a selectively modified binding interface. *Biopolymers* **2006,** *81* (4), 256-269.
111. Frembgen-Kesner, T.; Elcock, A. H., Striking Effects of Hydrodynamic Interactions on the Simulated Diffusion and Folding of Proteins. *J Chem Theory Comput* **2009,** *5* (2), 242-256.
112. Li, N. K.; Quiroz, F. G.; Hall, C. K.; Chilkoti, A.; Yingling, Y. G., Molecular Description of the LCST Behavior of an Elastin-Like Polypeptide. *Biomacromolecules* **2014,** *15* (10), 3522-3530.
113. Li, B.; Alonso, D. O. V.; Daggett, V., The molecular basis for the inverse temperature transition of elastin. *J Mol Biol* **2001,** *305* (3), 581-592.

114. Rousseau, R.; Schreiner, E.; Kohlmeyer, A.; Marx, D., Temperature-dependent conformational transitions and hydrogen-bond dynamics of the elastin-like octapeptide GVG(VPGVG): A molecular-dynamics study. *Biophysical Journal* **2004,** *86* (3), 1393-1407.
115. Zhao, B. W.; Li, N. K.; Yingling, Y. G.; Hall, C. K., LCST Behavior is Manifested in a Single Molecule: Elastin-Like polypeptide (VPGVG)n. *Biomacromolecules* **2016,** *17* (1), 111-118.
116. Tarakanova, A.; Huang, W.; Weiss, A. S.; Kaplan, D. L.; Buehler, M. J., Computational smart polymer design based on elastin protein mutability. *Biomaterials* **2017,** *127*, 49-60.
117. Tang, J. D.; McAnany, C. E.; Mura, C.; Lampe, K. J., Toward a Designable Extracellular Matrix: Molecular Dynamics Simulations of an Engineered Laminin-Mimetic, Elastin-Like Fusion Protein. *Biomacromolecules* **2016,** *17* (10), 3222-3233.
118. Keten, S.; Xu, Z. P.; Ihle, B.; Buehler, M. J., Nanoconfinement controls stiffness, strength and mechanical toughness of beta-sheet crystals in silk. *Nat Mater* **2010,** *9* (4), 359-367.
119. Krishnaji, S. T.; Bratzel, G.; Kinahan, M. E.; Kluge, J. A.; Staii, C.; Wong, J. Y.; Buehler, M. J.; Kaplan, D. L., Sequence-Structure-Property Relationships of Recombinant Spider Silk Proteins: Integration of Biopolymer Design, Processing, and Modeling. *Adv Funct Mater* **2013,** *23* (2), 241-253.
120. Fu, I. W.; Markegard, C. B.; Nguyen, H. D., Solvent Effects on Kinetic Mechanisms of Self-Assembly by Peptide Amphiphiles via Molecular Dynamics Simulations. *Langmuir* **2015,** *31* (1), 315-324.
121. Lee, O. S.; Stupp, S. I.; Schatz, G. C., Atomistic Molecular Dynamics Simulations of Peptide Amphiphile Self-Assembly into Cylindrical Nanofibers. *J Am Chem Soc* **2011,** *133* (10), 3677-3683.
122. Tsonchev, S.; Troisi, A.; Schatz, G. C.; Ratner, M. A., All-atom numerical studies of self-assembly of Zwitterionic peptide amphiphiles. *J Phys Chem B* **2004,** *108* (39), 15278-15284.
123. Raspa, A.; Saracino, G. A. A.; Pugliese, R.; Silva, D.; Cigognini, D.; Vescovi, A.; Gelain, F., Complementary Co-assembling Peptides: From In Silico Studies to In Vivo Application. *Adv Funct Mater* **2014,** *24* (40), 6317-6328.
124. Marrink, S. J.; Tieleman, D. P.; Mark, A. E., Molecular dynamics simulation of the kinetics of spontaneous micelle formation. *J Phys Chem B* **2000,** *104* (51), 12165-12173.
125. Henriques, J.; Cragnell, C.; Skepö, M., Molecular Dynamics Simulations of Intrinsically Disordered Proteins: Force Field Evaluation and Comparison with Experiment. *J Chem Theory Comput* **2015,** *11* (7), 3420-3431.
126. Nguyen, H. D.; Hall, C. K., Molecular dynamics simulations of spontaneous fibril formation by random-coil peptides. *P Natl Acad Sci USA* **2004,** *101* (46), 16180-16185.
127. Bond, P. J.; Sansom, M. S. P., Molecular Dynamics simulations of spontaneous micelle formation around membrane proteins. *Biophysical Journal* **2005,** *88* (1), 356a-356a.
128. Saracino, G. A. A.; Gelain, F., Modelling and analysis of early aggregation events of BMHP1-derived self-assembling peptides. *J Biomol Struct Dyn* **2014,** *32* (5), 759-775.
129. Darden, T.; York, D.; Pedersen, L., Particle Mesh Ewald - an N.Log(N) Method for Ewald Sums in Large Systems. *J Chem Phys* **1993,** *98* (12), 10089-10092.
130. Andersen, H. C., Molecular-Dynamics Simulations at Constant Pressure and-or Temperature. *J Chem Phys* **1980,** *72* (4), 2384-2393.
131. Sborgi, L.; Verma, A.; Piana, S.; Lindorff-Larsen, K.; Cerminara, M.; Santiveri, C. M.; Shaw, D. E.; de Alba, E.; Munoz, V., Interaction Networks in Protein Folding via Atomic-Resolution Experiments and Long-Time-Scale Molecular Dynamics Simulations. *J Am Chem Soc* **2015,** *137* (20), 6506-6516.
132. Bouvignies, G.; Bernado, P.; Meier, S.; Cho, K.; Grzesiek, S.; Bruschweiler, R.; Blackledge, M., Identification of slow correlated motions in proteins using residual dipolar and hydrogen-bond scalar couplings. *P Natl Acad Sci USA* **2005,** *102* (39), 13885-13890.
133. Stanzione, F.; Jayaraman, A., Computational Design of Oligopeptide Containing Poly(ethylene glycol) Brushes for Stimuli-Responsive Drug Delivery. *J Phys Chem B* **2015,** *119* (42), 13309-13320.
134. McCullagh, M.; Prytkova, T.; Tonzani, S.; Winter, N. D.; Schatz, G. C., Modeling self-assembly processes driven by nonbonded interactions in soft materials. *J Phys Chem B* **2008,** *112* (34), 10388-10398.
135. Johnston, K.; Harmandaris, V., Hierarchical simulations of hybrid polymer-solid materials. *Soft Matter* **2013,** *9* (29), 6696-6710.
136. Frederix, P. W. J. M.; Scott, G. G.; Abul-Haija, Y. M.; Kalafatovic, D.; Pappas, C. G.; Javid, N.; Hunt, N. T.; Ulijn, R. V.; Tuttle, T., Exploring the sequence space for (tri-) peptide self-assembly to design and discover. *Nature Chemistry* **2015,** *7* (1), 30-37.
137. Pham, Q. P.; Sharma, U.; Mikos, A. G., Electrospinning of polymeric nanofibers for tissue engineering applications: A review. *Tissue Eng* **2006,** *12* (5), 1197-1211.
138. Abrigo, M.; McArthur, S. L.; Kingshott, P., Electrospun Nanofibers as Dressings for Chronic Wound Care: Advances, Challenges, and Future Prospects. *Macromol Biosci* **2014,** *14* (6), 772-792.
139. Dror, Y.; Ziv, T.; Makarov, V.; Wolf, H.; Admon, A.; Zussman, E., Nanofibers Made of Globular Proteins. *Biomacromolecules* **2008,** *9* (10), 2749-2754.
140. Zhang, Y. Z.; Wang, X.; Feng, Y.; Li, J.; Lim, C. T.; Ramakrishna, S., Coaxial electrospinning of (fluorescein isothiocyanate-conjugated bovine serum albumin)-encapsulated poly(epsilon-caprolactone) nanofibers for sustained release. *Biomacromolecules* **2006,** *7* (4), 1049-1057.
141. Dong, B.; Arnoult, O.; Smith, M. E.; Wnek, G. E., Electrospinning of Collagen Nanofiber Scaffolds from Benign Solvents. *Macromol Rapid Comm* **2009,** *30* (7), 539-542.
142. Fischer, R. L.; McCoy, M. G.; Grant, S. A., Electrospinning collagen and hyaluronic acid nanofiber meshes. *J Mater Sci-Mater M* **2012,** *23* (7), 1645-1654.
143. Rui, C.; Mo, X. M.; Ke, Q. F., Fabrication and characterization of thermoplastic polyurethane/collagen blend nanofiber by electrospinning method. *2007 International Forum on Biomedical Textile Materials, Proceedings* **2007**, 144-150.
144. Wnek, G. E.; Carr, M. E.; Simpson, D. G.; Bowlin, G. L., Electrospinning of nanofiber fibrinogen structures. *Nano Lett* **2003,** *3* (2), 213-216.
145. Carlisle, C. R.; Coulais, C.; Namboothiry, M.; Carroll, D. L.; Hantgan, R. R.; Guthold, M., The mechanical properties of individual, electrospun fibrinogen fibers. *Biomaterials* **2009,** *30* (6), 1205-1213.

146. Casper, C. L.; Yang, W. D.; Farach-Carson, M. C.; Rabolt, J. F., Coating electrospun collagen and gelatin fibers with perlecan domain I for increased growth factor binding. *Biomacromolecules* **2007,** *8* (4), 1116-1123.
147. Li, M. Y.; Guo, Y.; Wei, Y.; MacDiarmid, A. G.; Lelkes, P. I., Electrospinning polyaniline-contained gelatin nanofibers for tissue engineering applications. *Biomaterials* **2006,** *27* (13), 2705-2715.
148. Mascharak, S.; Benitez, P. L.; Proctor, A. C.; Madl, C. M.; Hu, K. H.; Dewi, R. E.; Butte, M. J.; Heilshorn, S. C., YAP-dependent mechanotransduction is required for proliferation and migration on native-like substrate topography. *Biomaterials* **2017,** *115*, 155-166.
149. Liu, Y.; Xu, Y. C.; Wang, Z. H.; Wen, D. Z.; Zhang, W. T.; Schmull, S.; Li, H. Y.; Chen, Y.; Xue, S., Electrospun nanofibrous sheets of collagen/elastin/polycaprolactone improve cardiac repair after myocardial infarction. *Am J Transl Res* **2016,** *8* (4), 1678-+.
150. McClure, M. J.; Sell, S. A.; Simpson, D. G.; Walpoth, B. H.; Bowlin, G. L., A three-layered electrospun matrix to mimic native arterial architecture using polycaprolactone, elastin, and collagen: A preliminary study. *Acta Biomaterialia* **2010,** *6* (7), 2422-2433.
151. Zhang, K. H.; Mo, X. M.; Huang, C.; He, C. L.; Wang, H. S., Electrospun scaffolds from silk fibroin and their cellular compatibility. *J Biomed Mater Res A* **2010,** *93a* (3), 976-983.
152. Kim, U. J.; Park, J.; Kim, H. J.; Wada, M.; Kaplan, D. L., Three-dimensional aqueous-derived biomaterial scaffolds from silk fibroin. *Biomaterials* **2005,** *26* (15), 2775-2785.
153. Zhang, H.; Wang, K. F.; Xing, Y. M.; Yu, Q. Z., Lysine-doped polypyrrole/spider silk protein/poly(L-lactic) acid containing nerve growth factor composite fibers for neural application. *Mat Sci Eng C-Mater* **2015,** *56*, 564-573.
154. Maleki, M.; Natalello, A.; Pugliese, R.; Gelain, F., Fabrication of nanofibrous electrospun scaffolds from a heterogeneous library of co- and self-assembling peptides. *Acta Biomaterialia* **2017,** *51*, 268-278.
155. Rho, K. S.; Jeong, L.; Lee, G.; Seo, B. M.; Park, Y. J.; Hong, S. D.; Roh, S.; Cho, J. J.; Park, W. H.; Min, B. M., Electrospinning of collagen nanofibers: Effects on the behavior of normal human keratinocytes and early-stage wound healing. *Biomaterials* **2006,** *27* (8), 1452-1461.
156. Lee, Y. S.; Arinzeh, T. L., Electrospun Nanofibrous Materials for Neural Tissue Engineering. *Polymers-Basel* **2011,** *3* (1), 413-426.
157. Jing, Z.; Xu, X. Y.; Chen, X. S.; Liang, Q. Z.; Bian, X. C.; Yang, L. X.; Jing, X. B., Biodegradable electrospun fibers for drug delivery. *J Control Release* **2003,** *92* (3), 227-231.
158. Sell, S. A.; McClure, M. J.; Garg, K.; Wolfe, P. S.; Bowlin, G. L., Electrospinning of collagen/biopolymers for regenerative medicine and cardiovascular tissue engineering. *Adv Drug Deliver Rev* **2009,** *61* (12), 1007-1019.
159. Liu, X.; Lin, T.; Fang, J. A.; Yao, G.; Zhao, H. Q.; Dodson, M.; Wang, X. G., In vivo wound healing and antibacterial performances of electrospun nanofibre membranes. *J Biomed Mater Res A* **2010,** *94a* (2), 499-508.
160. Ren, G. L.; Xu, X. H.; Liu, Q.; Cheng, J.; Yuan, X. Y.; Wu, L. L.; Wan, Y. Z., Electrospun poly(vinyl alcohol)/glucose oxidase biocomposite membranes for biosensor applications. *React Funct Polym* **2006,** *66* (12), 1559-1564.
161. El-Moghazy, A. Y.; Soliman, E. A.; Ibrahim, H. Z.; Marty, J. L.; Istamboulie, G.; Noguer, T., Biosensor based on electrospun blended chitosan-poly (vinyl alcohol) nanofibrous enzymatically sensitized membranes for pirimiphosmethyl detection in olive oil. *Talanta* **2016,** *155*, 258-264.
162. Chua, J. S.; Chng, C. P.; Moe, A. A. K.; Tann, J. Y.; Goh, E. L. K.; Chiam, K. H.; Yim, E. K. F., Extending neurites sense the depth of the underlying topography during neuronal differentiation and contact guidance. *Biomaterials* **2014,** *35* (27), 7750-7761.
163. Solanki, A.; Chueng, S. T. D.; Yin, P. T.; Kappera, R.; Chhowalla, M.; Lee, K. B., Axonal Alignment and Enhanced Neuronal Differentiation of Neural Stem Cells on Graphene-Nanoparticle Hybrid Structures. *Adv Mater* **2013,** *25* (38), 5477-5482.
164. Yang, K.; Jung, K.; Ko, E.; Kim, J.; Park, K. I.; Kim, J.; Cho, S. W., Nanotopographical Manipulation of Focal Adhesion Formation for Enhanced Differentiation of Human Neural Stem Cells. *Acs Appl Mater Inter* **2013,** *5* (21), 10529-10540.
165. Dalby, M. J.; Gadegaard, N.; Oreffo, R. O. C., Harnessing nanotopography and integrin-matrix interactions to influence stem cell fate. *Nat Mater* **2014,** *13* (6), 558-569.
166. Xu, T.; Jin, J.; Gregory, C.; Hickman, J. J.; Boland, T., Inkjet printing of viable mammalian cells. *Biomaterials* **2005,** *26* (1), 93-99.
167. Zopf, D. A.; Hollister, S. J.; Nelson, M. E.; Ohye, R. G.; Green, G. E., Bioresorbable Airway Splint Created with a Three-Dimensional Printer. *New Engl J Med* **2013,** *368* (21), 2043-2045.
168. Cui, X. F.; Breitenkamp, K.; Finn, M. G.; Lotz, M.; D'Lima, D. D., Direct Human Cartilage Repair Using Three-Dimensional Bioprinting Technology. *Tissue Eng Pt A* **2012,** *18* (11-12), 1304-1312.
169. Xu, T.; Zhao, W. X.; Zhu, J. M.; Albanna, M. Z.; Yoo, J. J.; Atala, A., Complex heterogeneous tissue constructs containing multiple cell types prepared by inkjet printing technology. *Biomaterials* **2013,** *34* (1), 130-139.
170. Highley, C. B.; Rodell, C. B.; Burdick, J. A., Direct 3D Printing of Shear-Thinning Hydrogels into Self-Healing Hydrogels. *Adv Mater* **2015,** *27* (34), 5075-+.
171. Hsieh, F. Y.; Lin, H. H.; Hsu, S. H., 3D bioprinting of neural stern cell-laden thermoresponsive biodegradable polyurethane hydrogel and potential in central nervous system repair. *Biomaterials* **2015,** *71*, 48-57.
172. Lozano, R.; Stevens, L.; Thompson, B. C.; Gilmore, K. J.; Gorkin, R.; Stewart, E. M.; Panhuis, M. I. H.; Romero-Ortega, M.; Wallace, G. G., 3D printing of layered brain-like structures using peptide modified gellan gum substrates. *Biomaterials* **2015,** *67*, 264-273.
173. Zhu, W.; Harris, B. T.; Zhang, L. J. G., Gelatin Methacrylamide Hydrogel with Graphene Nanoplatelets for Neural Cell-laden 3D Bioprinting. *Ieee Eng Med Bio* **2016**, 4185-4188.
174. DeForest, C. A.; Anseth, K. S., Photoreversible Patterning of Biomolecules within Click-Based Hydrogels. *Angew Chem Int Edit* **2012,** *51* (8), 1816-1819.
175. DeForest, C. A.; Tirrell, D. A., A photoreversible protein-patterning approach for guiding stem cell fate in three-dimensional gels. *Nat Mater* **2015,** *14* (5), 523-531.
176. Marklein, R. A.; Burdick, J. A., Spatially controlled hydrogel mechanics to modulate stem cell interactions. *Soft Matter* **2010,** *6* (1), 136-143.
177. Nichol, J. W.; Koshy, S. T.; Bae, H.; Hwang, C. M.; Yamanlar, S.; Khademhosseini, A., Cell-laden microengineered gelatin methacrylate hydrogels. *Biomaterials* **2010,** *31* (21), 5536-5544.

178. Timashev, P. S.; Vedunova, M. V.; Guseva, D.; Ponimaskin, E.; Deiwick, A.; Mishchenko, T. A.; Mitroshina, E. V.; Koroleva, A. V.; Pimashkin, A. S.; Mukhina, I. V.; Panchenko, V. Y.; Chichkov, B. N.; Bagratashvili, V. N., 3D in vitro platform produced by two-photon polymerization for the analysis of neural network formation and function. *Biomedical Physics & Engineering Express* **2016,** *2* (3), 035001.

179. Dandurand, J.; Samouillan, V.; Lacabanne, C.; Pepe, A.; Bochicchio, B., Water structure and elastin-like peptide aggregation A differential calorimetric approach. *J Therm Anal Calorim* **2015,** *120* (1), 419-426.

180. Li, B.; Alonso, D. O. V.; Bennion, B. J.; Daggett, V., Hydrophobic hydration is an important source of elasticity in elastin-based biopolymers. *J Am Chem Soc* **2001,** *123* (48), 11991-11998.

181. Urry, D. W., Physical chemistry of biological free energy transduction as demonstrated by elastic protein-based polymers. *J Phys Chem B* **1997,** *101* (51), 11007-11028.

182. Reguera, J.; Urry, D. W.; Parker, T. M.; McPherson, D. T.; Rodriguez-Cabello, J. C., Effect of NaCl on the exothermic and endothermic components of the inverse temperature transition of a model elastin-like polymer. *Biomacromolecules* **2007,** *8* (2), 354-358.

183. Straley, K. S.; Heilshorn, S. C., Design and adsorption of modular engineered proteins to prepare customized, neuron-compatible coatings. *Front Neuroengineering* **2009,** *2*, 1-10.

184. Straley, K. S.; Heilshorn, S. C., Independent tuning of multiple biomaterial properties using protein engineering. *Soft Matter* **2009,** *5* (1), 114-124.

185. Chung, C.; Lampe, K. J.; Heilshorn, S. C., Tetrakis(hydroxymethyl) Phosphonium Chloride as a Covalent Cross-Linking Agent for Cell Encapsulation within Protein-Based Hydrogels. *Biomacromolecules* **2012,** *13* (12), 3912-3916.

186. Lampe, K. J.; Antaris, A. L.; Heilshorn, S. C., Design of three-dimensional engineered protein hydrogels for tailored control of neurite growth. *Acta Biomaterialia* **2013,** *9* (3), 5590-5599.

187. Madl, C. M.; Katz, L. M.; Heilshorn, S. C., Bio-Orthogonally Crosslinked, Engineered Protein Hydrogels with Tunable Mechanics and Biochemistry for Cell Encapsulation. *Adv Funct Mater* **2016,** *26* (21), 3612-3620.

188. Johnson, T.; Koria, P., Expression and Purification of Neurotrophin-Elastin-Like Peptide Fusion Proteins for Neural Regeneration. *Biodrugs* **2016,** *30* (2), 117-127.

189. Hu, X.; Tang-Schomer, M. D.; Huang, W. W.; Xia, X. X.; Weiss, A. S.; Kaplan, D. L., Charge-Tunable Autoclaved Silk-Tropoelastin Protein Alloys That Control Neuron Cell Responses. *Adv Funct Mater* **2013,** *23* (31), 3875-3884.

190. Sun, W.; Incitti, T.; Migliaresi, C.; Quattrone, A.; Casarosa, S.; Motta, A., Viability and neuronal differentiation of neural stem cells encapsulated in silk fibroin hydrogel functionalized with an IKVAV peptide. *J Tissue Eng Regen M* **2017,** *11* (5), 1532-1541.

191. Banwell, E. F.; Abelardo, E. S.; Adams, D. J.; Birchall, M. A.; Corrigan, A.; Donald, A. M.; Kirkland, M.; Serpell, L. C.; Butler, M. F.; Woolfson, D. N., Rational design and application of responsive alpha-helical peptide hydrogels. *Nat Mater* **2009,** *8* (7), 596-600.

192. Fischer, S. E.; Liu, X. Y.; Mao, H. Q.; Harden, J. L., Controlling cell adhesion to surfaces via associating bioactive triblock proteins. *Biomaterials* **2007,** *28* (22), 3325-3337.

193. Foo, C. T. S. W. P.; Lee, J. S.; Mulyasasmita, W.; Parisi-Amon, A.; Heilshorn, S. C., Two-component protein-engineered physical hydrogels for cell encapsulation. *P Natl Acad Sci USA* **2009,** *106* (52), 22067-22072.

194. Holmes, T. C.; de Lacalle, S.; Su, X.; Liu, G. S.; Rich, A.; Zhang, S. G., Extensive neurite outgrowth and active synapse formation on self-assembling peptide scaffolds. *P Natl Acad Sci USA* **2000,** *97* (12), 6728-6733.

195. Koutsopoulos, S.; Zhang, S. G., Long-term three-dimensional neural tissue cultures in functionalized self-assembling peptide hydrogels, Matrigel and Collagen I. *Acta Biomaterialia* **2013,** *9* (2), 5162-5169.

196. Cheng, T. Y.; Chen, M. H.; Chang, W. H.; Huang, M. Y.; Wang, T. W., Neural stem cells encapsulated in a functionalized self-assembling peptide hydrogel for brain tissue engineering. *Biomaterials* **2013,** *34* (8), 2005-2016.

197. Liu, X.; Wang, X. M.; Horii, A.; Wang, X. J.; Qiao, L.; Zhang, S. G.; Cui, F. Z., In vivo studies on angiogenic activity of two designer self-assembling peptide scaffold hydrogels in the chicken embryo chorioallantoic membrane. *Nanoscale* **2012,** *4* (8), 2720-2727.

198. Silva, G. A.; Czeisler, C.; Niece, K. L.; Beniash, E.; Harrington, D. A.; Kessler, J. A.; Stupp, S. I., Selective differentiation of neural progenitor cells by high-epitope density nanofibers. *Science* **2004,** *303* (5662), 1352-1355.

199. Tysseling-Mattiace, V. M.; Sahni, V.; Niece, K. L.; Birch, D.; Czeisler, C.; Fehlings, M. G.; Stupp, S. I.; Kessler, J. A., Self-assembling nanofibers inhibit glial scar formation and promote axon elongation after spinal cord injury. *J Neurosci* **2008,** *28* (14), 3814-3823.

200. Tysseling, V. M.; Sahni, V.; Pashuck, E. T.; Birch, D.; Hebert, A.; Czeisler, C.; Stupp, S. I.; Kessler, J. A., Self-Assembling Peptide Amphiphile Promotes Plasticity of Serotonergic Fibers Following Spinal Cord Injury. *J Neurosci Res* **2010,** *88* (14), 3161-3170.

201. Yang, C. Y.; Song, B. B.; Ao, Y.; Nowak, A. P.; Abelowitz, R. B.; Korsak, R. A.; Havton, L. A.; Deming, T. J.; Sofroniew, M. V., Biocompatibility of amphiphilic diblock copolypeptide hydrogels in the central nervous system. *Biomaterials* **2009,** *30* (15), 2881-2898.

202. Das, S.; Zhou, K.; Ghosh, D.; Jha, N. N.; Singh, P. K.; Jacob, R. S.; Bernard, C. C.; Finkelstein, D. I.; Forsythe, J. S.; Maji, S. K., Implantable amyloid hydrogels for promoting stem cell differentiation to neurons. *Npg Asia Mater* **2016,** *8*.

203. Iwasaki, M.; Wilcox, J. T.; Nishimura, Y.; Zweckberger, K.; Suzuki, H.; Wang, J.; Liu, Y.; Karadimas, S. K.; Fehlings, M. G., Synergistic effects of self-assembling peptide and neural stem/progenitor cells to promote tissue repair and forelimb functional recovery in cervical spinal cord injury. *Biomaterials* **2014,** *35* (9), 2617-2629.

3 From *de novo* peptides to native proteins: advancements in biomaterial scaffolds toward acute ischemic stroke repair

Published as: JD Tang, KJ Lampe, "From de novo peptides to native proteins: advancements in biomaterial scaffolds toward acute ischemic stroke repair," Biomedical Materials, 13: 3 (2018)

3.1 Abstract

An active area of research in the field of regenerative medicine involves the development of bioactive matrices that can promote cellular interactions and elicit desirable regenerative behavior *in vivo*. This is particularly important in the context of ischemic stroke where a focal lesion forms forestalling the regrowth of brain tissue. Protein-based molecules have been used as building blocks to create supramolecular structures that emulate the properties of the native healthy extracellular matrix (ECM) within the central nervous system (CNS). In this review, we briefly describe the relevant biological aspect of stroke and the techniques found in molecular biology and biochemical synthesis methodologies used in the design and synthesis of novel biomaterials. Within these biomaterials, researchers are able to incorporate a number of different domains that trigger assembly or promote cell growth and survival and direct transplanted or endogenous stem cell behavior within the 3D scaffolds. Such domains may also yield stimuli-responsive biomaterial scaffolds where the structure of the hydrogel undergoes a change in response to the local environment. These highly modular proteinaceous materials allow incorporation of diverse biofunctional motifs and structural elements comparable to those found in native ECM. We explore CNS relevant biomaterials that promote cell survival and host tissue integration and discuss their applications to stem cell therapy in the treatment of stroke.

3.2 Introduction

Stroke is the second leading cause of disease mortality worldwide, resulting in close to 6,200,000 deaths annually[1], and the third most common cause of disability[2]. It is estimated that more than 130 million incidences of stroke occur in people younger than 75 years per year, with most of the

burden found in low-income and middle-income countries[3-4]. The pathogenesis of ischemic brain injury from cerebral vessel occlusion involves two sequential processes: 1) severely depressed tissue perfusion as a result of vascular occlusions and subsequent reduction or impairment of blood flow, and 2) ischemic-induced alteration of normal cellular function resulting in necrosis of neurons, glia, and other supporting cells, and disruption of the blood-brain barrier (BBB)[5-6]. A rapidly evolving area in stroke research involves targeting specific inhibitory molecular and cellular pathways in tissue regeneration, and inflammation associated with cerebral ischemia. Promising therapeutic treatments prevent further damage and restore some cellular function by reestablishing perfusion to the ischemic brain, such as the administration of tissue plasminogen activator (tPA) that is used to break down clots and delivery of antiselectin antibodies to decrease infarct volume[7-8]. However, these types of treatments are only effective when administered in a narrow therapeutic time window and the side effects of such treatments can potentially be more destructive than their beneficial thrombolytic activity[9].

Recently, there has been growing interest in transplanting different types of stem cells to restore neurological functions and improve behavioral recovery following an ischemic insult. Several well-documented studies show that transplanted stem cells can ameliorate ischemic stroke by reducing cortical infarct size and increasing blood vessel density[10-11]. However, cell transplantation strategies often suffer from poor cell survival due to the toxicity of the surrounding environment at the injury site[12-13]. This can potentially be addressed by encapsulating cells in suitable microenvironments (e.g. hydrogels) that protect cells during and after delivery and support cell survival and growth. Cleverly designed materials can influence the subsequent fate of either transplanted or endogenous stem cells by directing their differentiation.

In this review, we will present recent studies that use central nervous system (CNS) relevant biomaterials to promote cell survival and host tissue integration and discuss their applications to stem cell therapy in the treatment of stroke. In many cases, administering these materials alone may have beneficial therapeutic effects in a transplant-free treatment strategy. Currently, biomaterials have been engineered to mimic the physical and mechanical characteristics of the native extracellular matrix (ECM). Recent studies have focused on improving structural and functional recovery after stroke by enhancing endogenous neuronal regeneration through the

incorporation of scaffolds that promote neuroblast migration into lesion sites[14-15]. Cell-based therapies have also received noticeable attention, and these notable preclinical and clinical trials include intravenous autologous mesenchymal stem cell (MSC) transplantation in the subacute phase of stroke[16-17]. While the transplantation was deemed safe for stroke patients, there have been conflicting reports regarding the efficacy of the treatment[18], underscoring the need to improve cell survival in a long-term transplantation and promote host tissue integration.

3.3 **Pathophysiology of ischemic stroke**

Brain damage from ischemic insult involves a cascade of neurochemical events leading to cerebrovascular dysfunction and cell death. The interruption of local blood circulation reduces the supply of oxygen (hypoxia) and glucose, which prevents the brain from generating sufficient ATP to maintain cellular homeostasis[19]. Cell death occurs rapidly in areas with the most dramatic reduction in blood flow (ischemic core)[20-21]. For less severe areas of ischemia (ischemic penumbra), a cascade of cellular and molecular events trigger the disruption of cellular homeostasis, leading to slow cell death and accumulation of necrotic tissue[5]. Within the penumbra, depolarization of neurons and glia results in the activation of voltage-gated calcium channels and an increase in intracellular Ca^{2+} concentration, activating proteases, mitochondrial dysfunction, and oxidative and nitrosative stress, ultimately leading to cell death[22-23]. Production of such reactive oxygen species (ROS) can trigger the coagulation cascade, leading to further deleterious effects resulting from activated inflammatory mediators surrounding the injury site[24-25]. Post-ischemic oxidative and nitrosative stress have been closely linked to the pathophysiology of ischemic stroke; both have been reviewed in depth elsewhere[26-27]. Recent studies have also implicated ROS in the activation of a host of matrix metalloproteinases (MMPs) that can significantly degrade the extracellular matrix (ECM) and BBB[28].

It has been well established that post-ischemic inflammation triggers a molecular cascade involving a multimodal and multicellular series of downstream mechanisms. Various proinflammatory cytokines produced by complement, platelet, and endothelial cells play an important role in cell-ECM remodeling[29]. The intravascular compartment is immediately exposed to ischemic insult, leading to the accumulation of fibrin-trapping platelets and leukocyte

infiltration into the brain parenchyma[30]. Neutrophils, followed by monocytes and lymphocytes are also recruited into the brain and accumulate in the cerebral microvessels of the penumbra. Endothelial cells in post-ischemic brain tissue express cell adhesion molecules (ICAM-1/VCAM-1) and upregulate E- and P-selectin, which provides a platform for leukocyte binding through their β2 integrins CD11a/CD18 and CD11b/CD18 (LFA-1 and MAC-1, respectively)[29, 31]. This then leads to leukocyte accumulation along the vascular wall, and accelerates cell death through the production of free radicals and cytokines. These infiltrating inflammatory mediators take part in both cell and ECM remodeling and influence neural plasticity and relay circuit function[32-33].

Astrocytes play an important role in cerebral inflammation, as they are able to produce anti-inflammatory cytokines that downregulate inflammation, such as TGF-β1 and IL-10[29, 34]. Microglia and macrophages upregulate TGF-β1 in ischemic stroke[35-36], which has a neuroprotective role by promoting regulatory T lymphocyte development, and has also been implicated in dampening the immune response by suppressing T cell effector activity[37-39]. Additionally, astrocytes can express proteoglycans that are released into the ECM compartment. Following an injury, TGF-β1 can also regulate astrogliosis, facilitating glial scar formation by increasing cellular GFAP expression and upregulating inhibitory ECM molecules (e.g. chondroitin sulfate proteoglycans)[40]. Consequently, the modulation of NPC differentiation should be considered, especially in the design of biomaterial scaffolds that reduce astroglial activation or differentation and promote differentiation into neuronal and oligodendroglial lineages.

3.4 Limitations of therapeutic potential in current preclinical and experimental studies

The acute management of ischemic stroke includes the administration of intravenous recombinant tPA[41], which is the first, and only, U.S. Food and Drug Administration (FDA) approved drug for the treatment of ischemic stroke. However, it was reported that tPA was more effective in patients with small to moderate-sized strokes, but was not as beneficial to patients with large-vessel occlusions[42]. Later studies show that tPA regulates several molecular signaling pathways that activate matrix metalloproteinase-9, leading to the degradation of the extracellular matrix (ECM) and disruption of the BBB[28, 43].

More recently, antioxidants and free radical scavengers have been explored for treatment of central nervous system (CNS) injury[44-46]. Free radicals are continuously generated by the use of oxygen in mitochondria to supply the energy needs of the brain, and studies have demonstrated that overproduction of these free radicals and related ROS modulate a host of cellular and molecular processes that promote neuronal degeneration[47-49]. Several compounds such as ebselen[50], edaravone[51], tirilazad[52], and NXY-059[53] have been developed to remove or degrade free radicals, or inhibiting their production. Administration of these drugs has proven to be slightly effective in experimental stroke injury models, however, with the exception of NXY-059, no clear evidence for the efficacy of these drugs in the treatment of human stroke patients was obtained[54]. More recently, polymeric nanoparticles have been used to encapsulate or incorporate small drugs to more efficiently deliver its payload. Jin *et al*. used a methoxypoly (ethylene glycol)-*b*-poly (D,L-lactic acid) (PEG-PLA) polymeric micelle to encapsulate edaravone (EDV-AM), seeking to eradicate ROS produced by infiltrated inflammatory cells. It was shown that the EDV-AM nanoparticle had a higher uptake in brain ischemia versus free EDV, resulting in rapid infarct volume reduction, and reduced behavioral deficits in ischemic stroke models[55]. The use of such a delivery vehicle could subsequently improve BBB permeability and be used to treat the majority of ischemic stroke patients who miss the time-window of tPA treatment.

Many therapeutics, while effective in animal injury models, completely fail in clinical trials. One reason for the high failure rate is because the therapeutic time window for effective reperfusion appears to be extremely short (< 4.5 h), and that the long 'door-to-needle' time (i.e. the time from emergency arrival to administration of tPA) limits the efficacy of the drug. Existing strategies also target a specific pathway of acute ischemic stroke. As mentioned above, the pathophysiology of stroke is extremely complex involving an assortment of chemical and biological processes and signaling pathways. A combinatorial approach in the treatment of stroke, i.e. combining neuroprotective agents that target multiple pathways of the ischemic cascade, may be necessary to improve patient outcomes following an ischemic insult. For example, implantation of a hyaluronic acid-based hydrogel scaffold combined with controlled growth factor delivery of vascular endothelial growth factor (VEGF) and angiopoietin-1 (Ang1) inhibited tissue inflammation and

promoted angiogenesis following implantation in an ischemic model of mice[56]. Alternatively, rebuilding the tissue lost to ischemic degradation may supplement efforts to limit injury severity.

Recently, biomaterials-based approaches have garnered considerable interest in the field of neural tissue regeneration as a promising alternative for stroke repair. These biomaterial scaffolds can A) provide integration of a highly biocompatible three-dimensional microenvironment with the host tissue that promotes neural tissue regeneration and B) act as a drug delivery vehicle releasing neuroprotective agents in a spatiotemporally controlled manner. Implantations of these scaffolds at an injury site may not only reduce stroke mortality, but restore lost neurological functions through the regeneration of neural tissue. For example, a recent publication demonstrated that sericin-based hydrogels were neuroprotective, and could promote axonal extension and branching of primary cortical neurons. When transplanted *in vivo*, these hydrogels promoted cell survival and proliferation, suggesting that their neuroprotective and neurotrophic properties are suitable for ischemic stroke repair and de novo tissue formation[57]. Thus, this review will focus on recent findings describing micro- to nano-scale hierarchical constructs that have been designed to mimic native ECM. The next section will describe key biological and mechanical properties that a biomaterial should possess that can modulate both cell proliferation and differentiation. The high biocompatibility, ease of functionalization, and precise control over the sequence and structural elements make proteinaceous biomaterials excellent candidates for neural regeneration applications.

3.5 Design and fabrication techniques of novel proteinaceous biomaterials

Protein biomaterials have typically been modeled after structural elements found within the ECM. This includes fibrous scaffolds and hydrogel matrices that are designed to mimic *in vivo* 3D microenvironments associated with native tissue. These biomaterials are often designed with several criteria in mind: 1) their components and gelation process must be cytocompatible in order to be considered useful in applications for tissue engineering, 2) and they should recapitulate the cell-matrix interactions found *in vivo.* Selecting or designing these peptide or protein-based materials typically requires parsing of known cell-binding or assembly epitopes or intuiting novel domains/designs that could be useful. This is made all the more complicated by the limited inquiry

into CNS-specific functionalities. Furthermore, the format and structure of the subsequent hydrogel biomaterial greatly impacts cellular interactions, and thus the fabrication strategies can dramatically impact a material's ability to replicate qualities of native, healthy, CNS tissue.

Advancements in genetic engineering and molecular biology now allow for the design and engineering of biosynthetic proteins with precise control over their sequences, length, secondary structure, and intermolecular interactions (e.g. hydrogen bonding, electrostatic interactions, π- π stacking)[58]. Protein engineering has been a staple in the biological sciences for decades and has gained traction in biomaterials research for multidisciplinary applications in engineering, medicine, and material sciences. Researchers are able to create a vast array of designer protein systems with desired properties that either function as biomimetics of native proteins, or contain novel structural and biofunctional moieties. These proteins have been used in a variety of applications related to CNS regeneration, where they often serve as 3D scaffolds and/or depots for release of neurotrophins or growth factors. Protein-based materials may also play a role in mediating the host immune response. Molecular biology has opened up new avenues to allow for the development of recombinant elastomeric proteins, such as keratin, silk, and collagen, as well as designer peptides and proteins which may be suitable biocompatible scaffolds for tissue engineering applications.

3.6 **Molecular-based design of biomaterials**

The macroscopic (and/or bulk) properties of proteinaceous biomaterials can be controlled by fine tuning the underlying conformational space and associative interactions between amino acid building blocks. The supramolecular structure can be designed in such a way that it adheres to the hierarchical architecture that is present in native tissue. As such, the exploitation and fundamental understanding of nano- to microscale interactions within biological structures allows researchers to design novel biomaterials capable of maximizing biological function and biocompatibility. Several recent techniques provide a rational approach to the design and synthesis of biomaterials with applications in CNS regeneration.

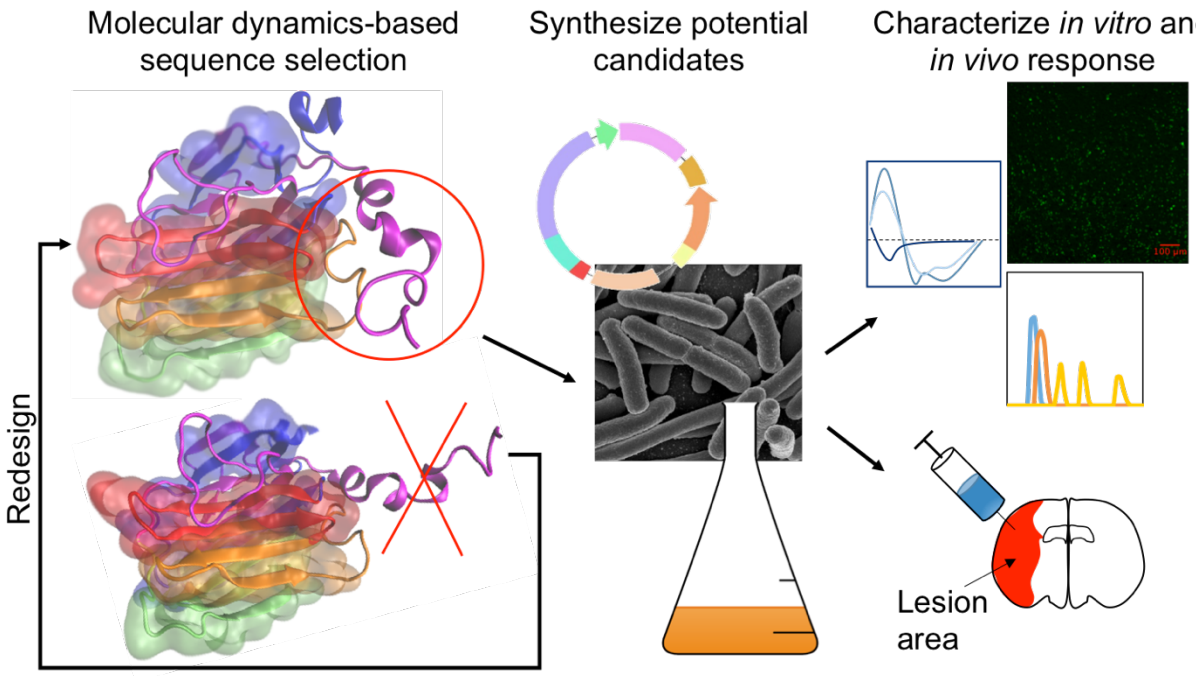

Figure 3-1. A proposed integrated strategy to protein design for suitable 3D microenvironments. This three-stage approach will be the foundation for a powerful design-analyze-test refinement loop: (i) in silico design/analysis, via molecular simulations, for candidate selection with desirable properties, (ii) synthesis of viable candidates utilizing recombinant host expression tools of molecular biology followed by fermentation or other biochemical methods, and (iii) in situ biophysical characterization of promising designs via dynamic light scattering and circular dichroism spectroscopy, as well as in vitro and in vivo analysis of cytocompatability. Lead candidates can be produced experimentally and characterized for their biochemical, biophysical, and cytological properties and this information fed back into new design rules. In this iterative way, knowledge gleaned about the designs, from stages (ii) and (iii), could be used to refine protein designs in subsequent rounds of in silico simulations (stage (i)).

Multiscale modeling of complex biological systems are now possible, including a comprehensive analysis of the microarchitecture found within biomaterials. However, few groups have taken advantage of the powerful computational methods available to accelerate and improve the materials design process. In theory, the hierarchical architecture of biological materials can be simplified to fundamental (bio)physical properties of self-assembling systems. By modeling the basic building blocks (i.e. atoms in an amino acid residue) and their intra- and intermolecular interactions, it is possible to observe and predict trajectory-derived conformations of these systems that can describe the material's properties[59]. A combinatorial strategy utilizing both computational and experimental approaches will allow researchers to rationally design new molecules with desired structural and functional properties (Figure 1). This design strategy could transform current

approaches to biomaterials development and address the particular challenges of characterizing the dynamical processes that occur in biological matrices.

All-atom molecular dynamics (MD) simulations are utilized to predict the spatiotemporal dynamics in the folding pathway of proteins, formation of secondary structures, and protein association via specific binding sites[60-68]. More recently, MD simulations have been applied to the design of biomaterials in order to predict the occurrence of complex molecular interactions at a microscopic scale. Several examples use simulations of elastin-like polypeptides (ELPs) [60, 68-72] as well as laminin-mimetic fusion proteins[73] to predict the conformational changes and kinetics associated with the known phase transition behavior of ELPs. Other notable studies involve the analysis of secondary structures within spider silk[74-75], self-assembly of peptides[76-79], and dynamics of micelle and fibril formation[80-84]. The motivation behind using MD simulations is manifold; understanding the atomic contacts (via non-covalent interactions) that mediate the folding pathway of nano- to microscopic structures gives researchers the ability to finely tune protein sequences that could lead to desirable bulk material properties, later verified experimentally. The exponentially large combinatorial space of biomolecule design, in general, are intrinsically complex and resource-intensive to disseminate. Therefore, MD-based simulations allow access to such dynamics on a characteristic timescale (~femtosecond to microsecond) essentially inaccessible via experimental approaches.

Coarse-graining (CG) allows researchers to model biomaterials on a mesoscale that overcomes the expensive computational demands that often plague MD simulations. In CG, the number of atomic particles and the corresponding degrees of freedom are reduced compared to atomistic MD simulations, while retaining similar molecular interactions between the CG particles. The broad range of spatiotemporal scales available in CG due to simplified atomistic models allows researchers to conduct simulations of large and highly complex biologically relevant systems. Several groups have used CG to design novel stimuli-responsive biomaterials[85-87] as well as self-assembly of polymeric materials[76, 86, 88]. For instance, researchers have been recently been interested in designing self-assembling nanostructures that can gelate (sol-gel transition) at higher concentrations. However, the design space and detail of such systems limits the robustness and scalability of such an approach, especially in the wet lab. As such, researchers used CG to

investigate the molecular self-assembly of 8,000 tripeptide sequences to determine a predictive model of self-assembly propensity, which would not have been economically feasible through experimental approaches[88].

3.7 Fabrication techniques for building structure into biomaterials

The synthesis of complex 3D heterogenous microstructures is often limited by the dimensionality and structural resolution of existing manufacturing techniques. As noted above, biomimetic tissue constructs should not only be able to recapitulate biological functions in native cell-cell and cell-matrix interactions, they must also reproduce the complex microarchitectures of ECM components that propels dynamic signaling cues to initiate cellular attachment, migration, growth, and differentiation. This can be accomplished by replicating individual cellular and extracellular components of a tissue or organ, such as the nano- to microscale branching patterns of the capillary in complex organs like the brain, heart, kidney, liver, and lungs. Several techniques have been developed to more closely mimic native tissue architecture, and will be discussed in this section of the review.

Electrospinning allows engineers to fabricate biomaterial scaffolds with micro to nanoscale fiber topography that can mimic key features of the ECM. The inherently high surface to volume ratio of these electrospun fibers plays an integral role in enchanced cell attachment, proliferation, and migration. A variety of protein polymers have been succesfully electrospun into fibers, including BSA[89-90], collagen[91-93], fibrinogen[94-95], gelatin[96-97], elastin[98-100], silk[101-103], and self-assembling peptides[104]. Electrospun scaffolds have been used in tissue engineering applications[105-106], drug delivery[107-108], wound healing[109-110], as well as biosensors[111-112]. The nanotopographical cues that can be generated using electrospinning methods have important implications in neuronal cell growth and differentiation[113-115]. These biophysical cues serve as stimuli (i.e. nanotopographical stimulation of mechanotransduction[116]) to guide neurite extension, can mediate NSC differentation, and can improve the therapeutic efficacy of stem cells in treating CNS diseases and injuries.

In recent years, 3D printing has become a powerful fabrication technique that gives researchers the ability to generate intricate 3D microstructures that can mimic native microenvironments using a bottom-up approach. Bioprinters have been used to print a variety of biocompatible materials, from 3D microconstructs encapsulating individual mammalian cells[117] to 3D organs[118-119]. Pioneering work by Atala *et al.* used inkjet printing technology to generate 3D heterogeneous tissue constructs using alginate-collagen composites containing multiple cell types that were able to form vascular networks upon implantation *in vivo*[120]. Additionally, the Burdick group have produced multimaterial structures comprised of shear-thinning hydrogel "bioinks" printed directly into self-healing hydrogels based on supramolecular assembly through guest-host interactions[121]. 3D bioprinting has also seen extensive use in replicating 3D microenvironments in native neural ECM. Examples include printing of hNSCs in alginate/chitosan constructs[122], construction of brain-like structures using RGD (fibronectin-derived cell adhesion site)-modified gellan gum[123], and guiding NSC differentiation through the use of stereolithography based 3D printing of gelatin methacrylamide hydrogels[124].

In the last decade or so, photolithography has gained immense popularity in the biomedical sciences, owing to lower production costs and increased access to fabrication tools. Photolithography is a powerful technique that enables formation of precise and complex 3D structures at the micro and nanoscale using light to transfer intricate patterns on to a substrate. Novel work by DeForest *et al.* uses multiphoton laser-scanning lithography to immobilize peptides and full-length proteins in discrete patterns within polymeric hydrogels[125-126]. Another approach involves mask-based photolithography, and as the name suggests, uses a patterned mask where only regions exposed to UV light polymerize and cure to form a network of 3D structures[127-128]. This fabrication technique allows for the precise control of the cell-material interface and patterning of ligands and biomacromolecules on a variety of substrates. Recent work by Timashev *et al.* described a two-photon polymerization technique to fabricate polymeric ceramic composite scaffolds that support primary hippocampal neurons. These scaffolds induced the formation of neuronal networks from dissociated hippocampal cultures and demonstrated their functional calcium activity[129]. All of these patterning techniques have applications in CNS tissue reconstruction and may be utilized in the context of various different proteinaceous materials discussed in more detail below.

3.8 ECM biomimicry for the design of suitable microenvironments to stimulate neural tissue regeneration and repair

The complex interconnectivity of cells, including neurons, astrocytes, and oligodendrocytes, within the CNS provides a formidable challenge for tissue engineers aiming to recapitulate the extracellular environment. These native microenvironments often serve as a guidance cue for initiating neural tissue regeneration following injury. The design of suitable microenvironments to improve the regenerative capacity of injured neurons and replacing cells lost to apoptosis after a stroke is often complicated by the composition of the native CNS extracellular milieu. A stroke lesion is characterized by a region of necrotic cell death, in particular neuronal cells, which have a limited ability to regenerate once mature. Drug therapeutics targeting regenerative pathways have the ability to attenuate inhibitory molecules or accelerate the production of endogenous neurotrophins but are usually non-specific, thereby restricting the utility of such applications. A promising approach in stroke therapy is a combinatorial approach of controlled drug delivery and cell transplantation in a matrix that maintains appropriate cell-matrix interactions mimicking the native neural tissue environment.

The native neural microenvironment includes ECM molecules, myelin-associated glycoproteins, trophic factors and signaling pathways that modulate a neuron's intrinsic axonal growth capacity (readers are referred to excellent recent reviews on this topic by Lutz *et al.* [130] and Lau *et al.*[131]). On a cellular level, engineers must also account for various cellular components such as astrocytes and/or oligodendrocytes in the CNS that play a major role in nervous system repair and regeneration[132-133]. We now know that astrocytes can regulate neurotransmitter and ionic homeostasis, metabolic support of neurons, and guidance of neuronal migration and immune function[134]. These cellular constituents, as well as others, require appropriate morphogenic cues and mechanotransduction pathways from the ECM to trigger a cascade of cellular and biochemical events that can stimulate endogenous neurogenesis within the brain[131, 135]. However, in order to properly investigate these cell-cell signaling and cell-matrix interactions, it is important to decouple the synergistic effects of both the hierarchical microstructures and signaling cues that

initiate and/or propagate neural regeneration processes. We will cover several strategies that aim to overcome these limitations through proteinaceous biomaterial scaffolds.

3.9 Decellularized tissue scaffolds and cell-derived ECMs for use as suitable biomaterials

The complexity of the native ECM that drives cellular behavior such as attachment, differentiation, and proliferation is rarely represented by single component materials (e.g. synthetic polymer[136] or proteins)[137-138]. In order to mimic the unique composition of tissues as closely as possible, researchers have developed several techniques that closely capture the *in vivo* microenvironment by using decellularized tissues or cell-derived ECM proteins. The usage of decellularized tissues and organs have become increasingly frequent in both pre-clinical animal studies and in human clinical applications[139-141]. Decellularization protocols to efficiently remove all cellular and nuclear material include a combination of physical, chemical, and enzymatic approaches, and have been expertly reviewed elsewhere[142]. Often decellularization protocols aim to preserve the native ultrastructure and composition of the ECM (Figure 2). Researchers are able to isolate organs and tissues such as the pancreas[143], the brain[144], peripheral nerve[145-146], heart[140, 147], liver[148], kidney[149-150], and lung[151-152]. Decellularized brain ECM from animal models is reportedly compatible with neural cells, as human induced pluripotent stem cell (hiPSC) derived neurons grow and mature on such scaffolds[144]. In recent work, cortically-derived neuronal networks were more plentiful when seeded within decellularized brain ECM constructs compared to collagen type I and Matrigel controls[153], demonstrating that the inclusion of brain ECM supports more physiologically relevant axon and synapse development. Similarly, biological scaffolds consisting of decellularized brain tissue can supported long-term growth of NSCs[154-156]. The success of these strategies may ultimately depend on our ability to address sample-to-sample variation and develop consistent isolation protocols. In the context of stem cell growth, it is also possible that the age of tissue from which the ECM was harvested will affect encapsulated cell fate as younger animals have more regenerative tissues[157-158].

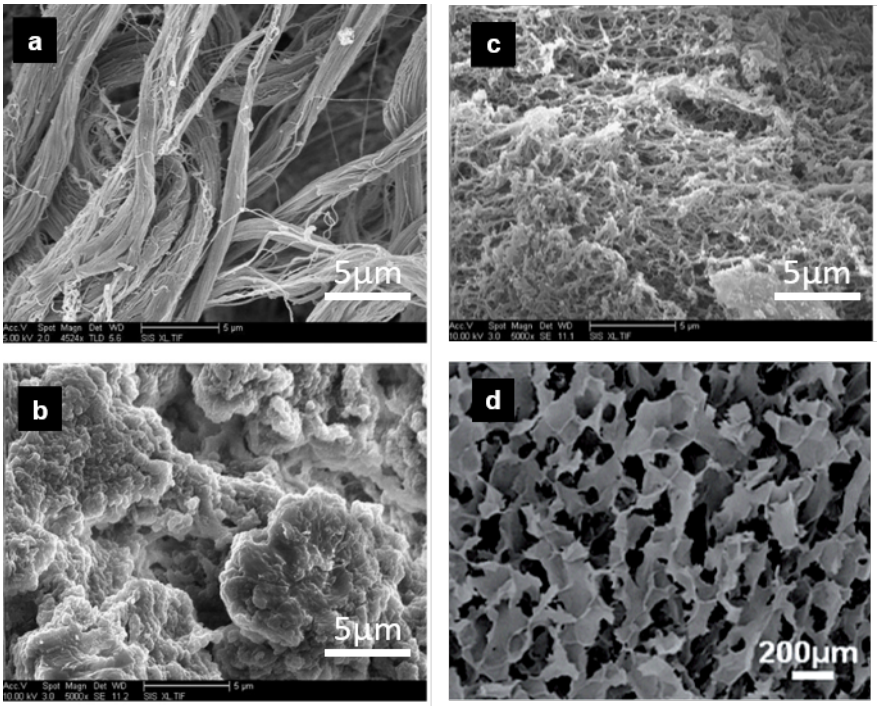

Figure 3-2. SEM analysis of the micromorphologies of (a) decellularized porcine brain matrix gels, (b) native porcine brain tissue, (c) Matrigel gels, and (d) silk fibroin hydrogels. The brain matrix material was able to undergo a sol-gel transition when brought to a physiological pH and injected subcutaneously into C57 mice. Silk solutions prepared from Bombyx mori cocoons were able to self-assemble into nanofiber-based hydrogels, composed of β-sheet structures. These images highlight the series of nanofibrous structures inherently present in both engineered and native brain ECM, and demonstrate that materials can be designed to mimic both the nanostructure and surface topography of the ECM of nerve tissues. SEM images (a - c) are adapted with permission from DeQuach J.A., et al. Decellularized Porcine Brain Matrix for Cell Culture and Tissue Engineering Scaffolds. Tissue Eng Pt A 2011, 17(21-22):2583-2592. Silk fiber images (d) adapted with permission from Bai S.M., et al. Silk nanofiber hydrogels with tunable modulus to regulate nerve stem cell fate. J Mater Chem B 2014, 2(38):6590-6600.

Mammalian cell-derived ECM provides a customizable alternative to decellularized scaffolds, where proteins can be produced by simply modulating the culture system (2D vs 3D structures) and types of cells used to generate specific ECM proteins[159]. A popular method in extracting naturally derived proteins for use as biomaterials is through organic solvent extraction. Keratins, for example, are a group of proteins that can be extracted from both animal and human sources. Their high cysteine content and hydrophobic amino acids in keratin molecules makes them highly insoluble, and so the extraction process primarily involves the breakage of disulfide bonds[160-162].

Keratin-based biomaterials have also been used extensively in peripheral nerve regeneration[163-164], wound dressing[165-166], as well as drug delivery vehicles[167-168]. The application of these ECM proteins as biomaterials in the CNS are further explored later in this review.

3.10 **Naturally-derived protein biomaterials**

Native fibrous proteins such as elastin, collagen, and silk have been proven to have low immunogenicity, minimal toxicity, and are proteolytically degradable. Proteins are synthesized with a high degree of specificity compared to synthetic polymers. The precisely defined primary structures of peptides and proteins instructs the protein folding pathway leading to unique secondary, tertiary, and even quaternary structures that are often not achievable by chemical synthesis methods. Advancements in biomolecular techniques now allow researchers to synthesize protein polymers with uniform chain lengths and precisely defined monomer sequences, and post-translational modification of these proteins to impart unique biological functions is also possible.

Collagen is found in all connective tissues, including bone, skin, and cartilage and can be isolated from animal tissue, or produced in vitro from cultured cells/tissues. Collagen can be isolated through enzymatic or chemical hydrolysis following acid or alkaline pretreatment at a controlled temperature[169-171]. It is a biocompatible material with unique mechanical and biological functions that has been used in wound healing, 3D scaffolds for tissue engineering, and implicated in cellular processes such as cell proliferation, adhesion and migration[172-176].There are four major types of collagen (collagen type I, II, III and IV), however collagen type IV is the most prevalent form in the CNS[177]. Collagen is able to form large fiber bundle networks with high tensile strength and flexibility, which are further stabilized by crosslinks to support stress in tissues. In addition to their structural role, collagens are integral in providing cellular and biochemical functionalities, including the binding and release of cellular mediators such as cytokines and growth factors[178].

Collagens are fabricated in a variety of scaffolds such as tablets, pellets, sponges, films, and hydrogels. Collagen gels implanted in a 6mm gap within the mouse sciatic nerve promoted a noticeable increase in innervation[179]. The Shoichet group injected epidermal growth factor (EGF) and fibroblast growth factor 2 (FGF-2) impregnated collagen gel solutions to spinal cord injury

sites of Sprague-Dawley rats and observed significantly greater ependymal cell proliferation in injured animals compared to controls[180]. Neural progenitor cells (NPCs) derived from bone marrow stromal cells (MSCs) transplanted with collagen sponges and basic fibroblast growth factor (bFGF) releasing gelatin microspheres into rat stroke models saw increased cell survival and neovascularization around the transplanted region[181]. The synergistic effect of bFGF releasing microspheres and NS-MSCs suggests that, when properly utilized, these biomaterials can provide appropriate scaffolding to ameliorate functional recovery in stroke or neurodegenerative diseases. Similarly, transplanted neural stem cells (NSCs) from E14 rats seeded onto a collagen type I scaffold saw increased differentiation and new synapse formation in rats subjected to cerebral ischemia[182]. The Cullen lab have pioneered the use of tissue engineered nerve grafts (TENGs) and micro-tissue engineered neural networks (micro-TENNs) for use as scaffolds for neurodegeneration and neuromodulation (Figure 3). These scaffolds are purposely designed to contain 'stretch-grown' axonal tracts that can facilitate nerve regeneration after CNS degeneration[183]. These scaffolds can subsequently be applied to stroke injury models where highly aligned neurons are desirable, such as for the regeneration of corticospinal tracts, especially for lesions in the primary cortex were the infarct cavity significantly affects white matter.

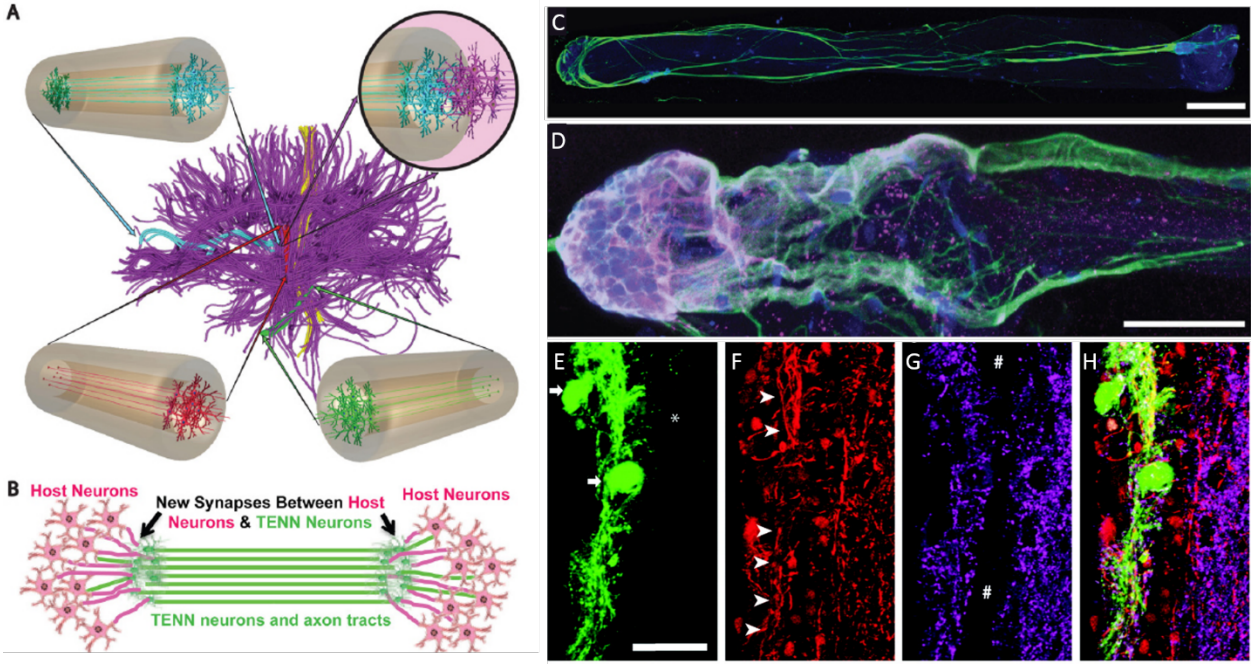

Figure 3-3. Micro-tissue engineered neural network (micro-TENN) hierarchical microstructure comprised of an agarose tubular shell with an inner collagen core. (a)

*Diffusion tensor imaging representation of the human brain highlighting the interconnectivity between functionally distinct regions of the brain. Unidirectional (red, green) micro-TENNs and bi-directional (blue) micro-TENNs can bridge various regions of the brain (blue: corticothalamic pathway, red: nigostriatal pathway, green: entorhinal cortex to hippocampus pathway) and synapse with host axons (purple; top right). (b) Schematic representation of host-tissue integration, where TENN neurons are able to form local synapses with host neurons to reconstruct damaged or lost axonal pathways. (c) Representative confocal reconstruction of a bi-directional micro-TENN consisting of two populations of cortical neurons spanned by long axonal tracts (β III-tubulin, green), and cell nuclei (Hoechst, blue). (d) Confocal reconstruction of a unidirectional micro-TENN stained via immunocytochemistry to denote neuronal somata/dendrites (MAP2, purple), neuronal somata/axons (Tau, green), and cell nuclei (Hoechst, blue) (e) GFP+ cerebral cortical neurons and longitudinal projections [arrow heads in (f)] were observed in transplanted micro-TENNs. GFP+ aligned processes were predominantly axonal (NF200, red) with (g) numerous synapses (synapsin, purple) in both the micro-column hydrogel and bordering host cortical tissue [denoted by * in (e)]; and a overlay of all channels (h). Scale bars are 300 μm in C, and 100 μm in D. (a - d) adapted with permission from Struzyna L.A., et al. Restoring nervous system structure and function using tissue engineered living scaffolds. Neural Regen Res 2015, 10(5):679-685. (e - h) adapted with permission from Struzyna L.A., et al. Rebuilding Brain Circuitry with Living Micro-Tissue Engineered Neural Networks. Tissue Eng Pt A 2015, 21(21-22):2744-2756.*

Elastin is a major structural protein found in the ECM that provides mechanical integrity and elasticity to tissues. The compliancy of native elastin has been exploited in the form of scaffolds for usage as vascular grafts[184-186]. The durability of elastin proved to be more effective in maintaining construct strength and improved viscoelastic properties versus collagen scaffolds. Angiogenesis was seen following implantation of pure elastin tubular scaffolds containing bFGF in subdermal patches in adult rats[187]. The neovascularization and cellular infiltration following an ischemic insult warrants further investigation into the potential benefit of utilizing elastin-based biomaterials in the treatment of stroke. While engineered forms of elastin, termed elastin-like polypeptides (ELPs) will be discussed later, conserved sequences of native elastin can be produced recombinantly. Recombinant tropoelastin (TE), the soluble form of elastin, features an alternating hydrophobic and hydrophilic domain structure. Like elastin, TE exhibits the same mechanical properties, but it also includes key cell signaling and adhesion properties[188-190]. The Weiss group has shown that TE can be enzymatically[191] or chemically crosslinked[192] to form hydrogels.

Silk is produced by a variety of insects, most notably silkworms (e.g. *Bombyx mori)* and orb-weaving spiders. Silks are fibrous proteins known for their mechanical properties, biocompatibility, and controlled proteolytic susceptibility[193]. Silk fibroin, produced by *B. mori* consists of a light chain (~26 kDa) and heavy chain (~390 kDA), which are present in a 1:1 ratio and linked by a disulfide bond. Silk fibroin consists primarily of a highly repetitive hexapaptide sequence of (-Gly-Ala-Gly-Ala-Gly-Xaa) where Xaa is serine, tyrosine, or alanine. Spider silk has been used in the development of artificial nerve conduits as guiding channels for regenerating axons[194].. Partially degummed silk conduits were shown to promote axon regeneration and myelination in both Schwann cells and DRG neurons compared to autologous graft controls[195-196]. These guidance channels have shown to provide a permissive and nonimmunogenic biomaterial to enhance nerve regeneration. Additionally, while these artificial nerve conduits can be composed of various materials, this new technique provides an interesting segue into optimizing neurite extension and bridging long-distance defects of CNS nerves for larger animals, such as humans. Wittmer *et al.* demonstrated that electrospun silk fibroins functionalized with brain derived neurotrophic factor (BDNF) and ciliary neurotrophic factor (CNTF) promoted the survival of retinal ganglion cells (RGC) and growth cones were shown to progress along silk fibers[197]. Recently, work done by Bai *et al.* used self-assembling silk nanofibers to effectively control differentiation of neural stem cells (NSCs) to neurons and inhibited glial differentiation without the addition of growth factors[198]. Similarly, Tang-Schomer *et al.* used silk-protein based scaffolds to fabricate 3D tissue constructs that promoted neuronal connectivity between white matter-like and gray-matter like regions within the scaffold[199-200]. These results demonstrate that these silk biomaterials are suitable as brain models, and therefore *in vitro* stroke injury models, as these scaffolds can fully support the coculturing of astrocytes and endothelial cells that capture BBB permeability changes in various degrees following the induction of ischemic stroke.

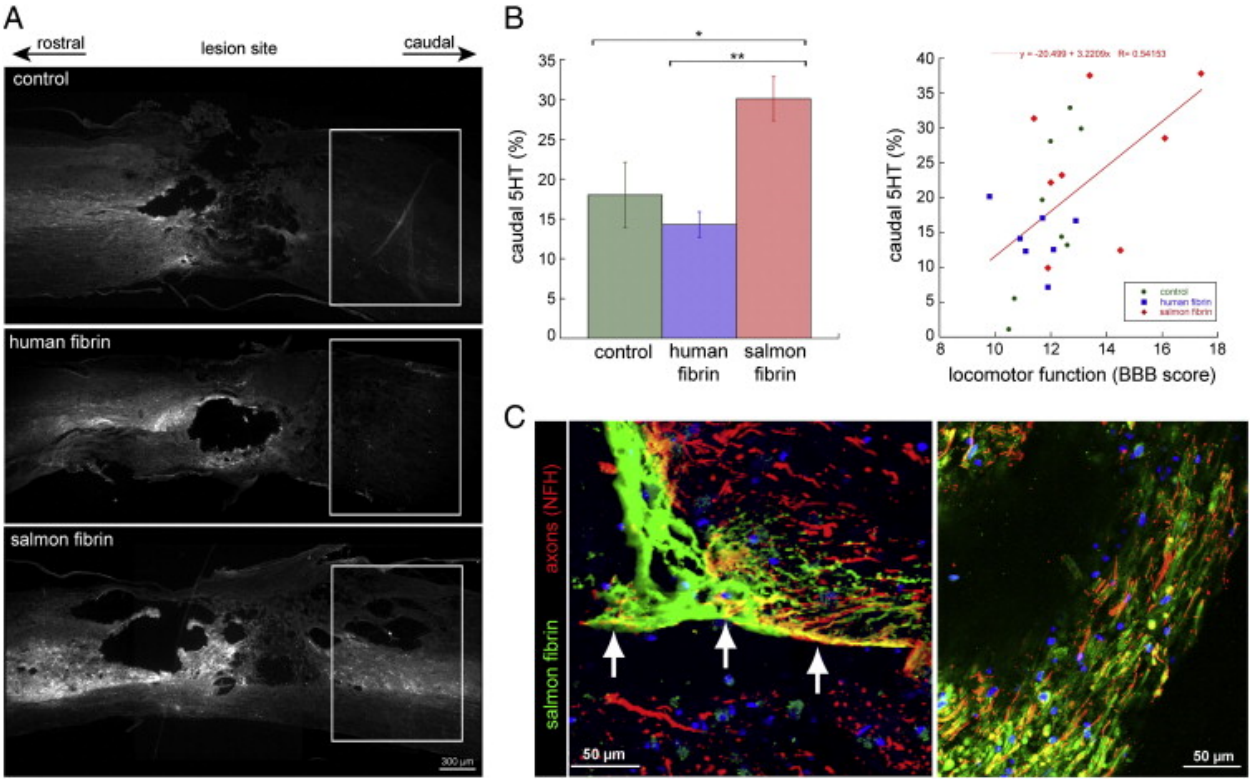

Figure 3-4. Salmon fibrin hydrogels used for treatment of dorsal hemisection SCI. 5 µl of a fribrinogen (3.0 mg/ml) and thrombin (0.15 U/ml) solution in phenol-free EMEM was injected into the lesion site immediately after surgery. (a) A greater density of serotonergic axons caudal to the lesion have more serotonergic fibers present in salmon fibrin treated adult female Sprague-Dawley rats compared with human fibrin and untreated controls (5-hydroxytryptamine, 5-HT immunostaining for serotonin). (b) Salmon-fibrin treated animals had a higher percentage of caudal 5-HT-positive tissue, where they retained ~30% caudal 5-HT innervation compared to human fibrin (~ 14%) and untreated controls (~ 18%). Top right graph indicates that there is a positive correlation between the percentage of caudal serotonergic fibers and locomotor function. (c) Analysis of spinal cord sections at the lesion sites show colocalization of neurofilament (NFH, red)-positive neuronal axons with salmon fibrin (anti-salmon fibrin antibody, green) 2 days after treatment (marked by arrows). Lower right image is a different location of the lesion site. Reprinted with permission from Sharp K.G., et al. Salmon fibrin treatment of spinal cord injury promotes functional recovery and density of serotonergic innervation. Exp Neurol 2012, 235(1):345-356.

Fibrin, a biopolymer of the monomer fibrinogen, has been clinically proven to be an effective hemostatic agent in cardiac and liver surgery. Fibrin is formed after thrombin-mediated cleavage of fibrinopeptide A from the Aα chains and fibrinopeptide B from the Bβ chains[201]. Fibrin hydrogels can serve as potential scaffolds for enhancing neurite extension[202] and promoting

angiogenesis[203], as well as tissue engineering of liver[204], cartilage[205], and bone tissues[206]. The Sakiyama-Elbert group have developed novel fibrin-based scaffolds to treat both CNS and PNS diseases and injuries in the form of 3D hydrogel structures and nerve conduits[207-209]. The incorporation of exogenous heparin-binding peptides into fibrin gels were shown to enhance the degree of neurite extension of embryonic chicken DRGs[210]. It was later shown that fibrin gels containing heparin-binding domains could successfully provide controlled release of neurotrophin-3 (NT-3) and platelet-derived growth factor (PDGF) [211], bFGF[212], and BDNF[213], leading to enhanced nerve regeneration in animal injury models. Subsequently, the tailoring of exogenous heparin-binding growth factors by the incorporation of heparin chains within a 3D scaffold allows the material to spatiotemporally modulate key components of cellular morphogenesis through different signaling pathways and other biomolecular cues. Similarly, growth-factor treatment may be necessary to enhance nerve regeneration during the early stages of injury, as well as providing a basis for more specific cellular responses (e.g., TGF-β versus bFGF mediated collagen type I production). Additionally, salmon fibrin has also been used in the treatment of spinal cord injuries. Salmon-derived fibrin gels were implanted into the lesion site after a dorsal hemisection in rat models, with no alteration in the degree of glial scar formation versus untreated controls, which were elevated in human fibrin-treated animals. Rats treated with salmon fibrin saw increased serotonergic fibers caudal to the injury site[214] (Figure 4). Salmon fibrin also demonstrated enhanced neurite outgrowth in both rat cortical neurons and mouse spinal cord neurons[215] versus fibrin derived from cows or humans. Investigators postulate that the RGD motifs are more accessible for binding to cellular integrins, and may be involved in differential integrin activation. This suggests that salmon fibrin is a potentially useful biomaterial for promoting neurite outgrowth, which may prove beneficial in stroke recovery. While fibrin has largely been used in the spinal cord, continuing work clearly demonstrates it's potential to mimic the biomechanical properties of the CNS, and therefore its potential for engineering brain tissue as well where heparin-binding capabilities are equally important.

3.11 **Molecularly designed, engineered, polypeptide-based biomaterials**

While native protein-based biomaterials can exhibit many unique biochemical and mechanical properties, they also display some shortcomings. These protein constituents are more prone to

degradability and often have unwanted contaminants that are co-purified, which can lead to undesirable immunological responses in the human body. As an example, the insolubility of elastic microfibrils has made isolation, purification, and characterization of native elastin difficult, and has not been as widely used as a biomaterial. However, its synthetic component known as elastin-like polypeptides (ELPs), which are artificial repetitive polypeptides derived from mammalian elastin, have been useful for a wide variety of biomedical applications. ELPs consist of a pentapeptide repeat, (-Val-Pro-Gly-Xaa-Gly-), where Xaa is any guest amino acid residue, except proline. ELPs are unique in that they exhibit lower critical solution temperature (LCST) transition behavior; above a certain transition temperature, the disruption of ordered water molecules surrounding the polymeric backbone leads to the collapse of the polymer, giving rise to self-assembly and temperature-dependent gelation behavior[73, 216-217]. The transition temperature is completely tunable by the molecular weight and length of the sequence, as well as the guest residue, which can impart different folding pathways following the phase transition, and can be made susceptible to pH and ionization changes[218-219].

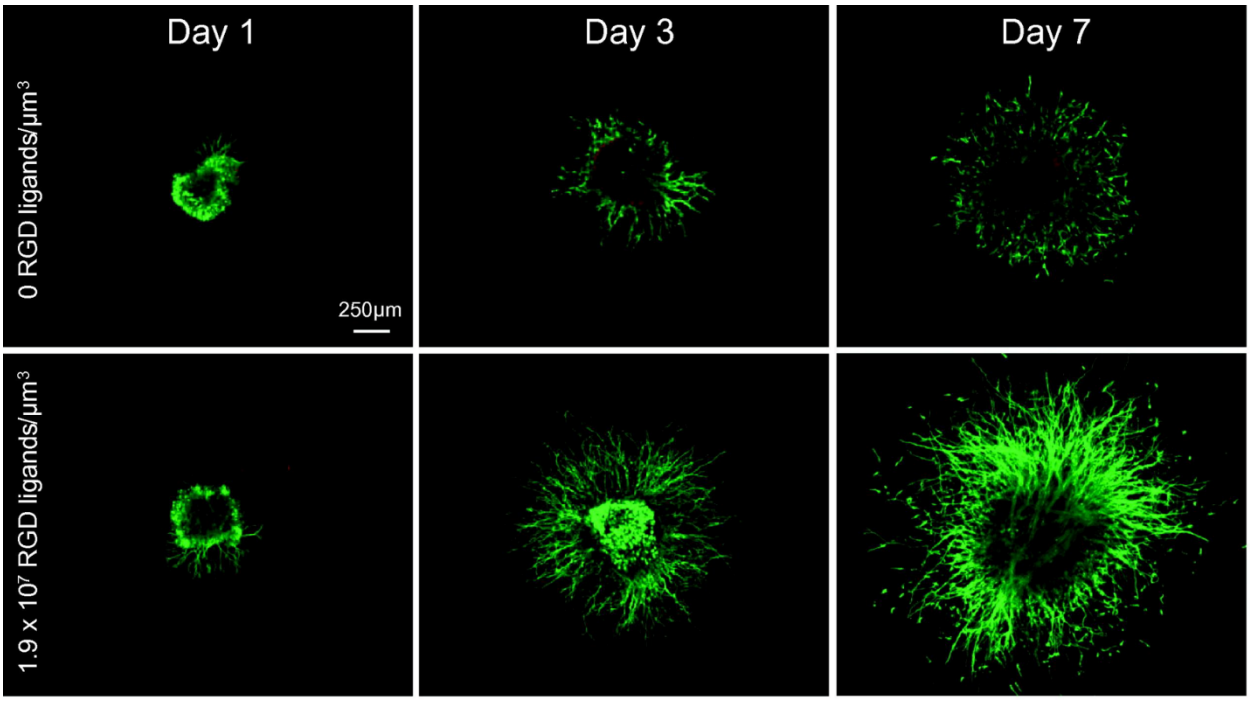

Figure 3-5. Dorsal root ganglia encapsulated in elastin-like protein hydrogels were used to study the effects of RGD (fibronectin derived cell adhesion motif) ligand density on neurite outgrowth. Over the course of 7 days, RGD promoted a statistically significant increase in both neurite outgrowth length and total neurite density in ELP hydrogels with similar mechanical properties. Adapted with permission from Lampe K.J., et al. Design of three-

dimensional engineered protein hydrogels for tailored control of neurite growth. Acta Biomaterialia 2013, 9(3):5590-5599.

Incorporation of ionizable guest residues (e.g. lysine) allows ELPs to be chemically crosslinked resulting in the formation of hydrogels. Straley *et al.* used ELPs as substrates adsorbed onto glass coverslips and demonstrated that PC12 cells cultured on adsorbed protein surfaces had a high level of cell-surface biocompatibility and similar cellular morphology to those seen on collagen positive-control surfaces[220]. Shortly after, experiments using ELPs crosslinked by disuccinimidyl suberate showed that the resulting protein hydrogel could be used to modulate differentiation and neurite outgrowth of PC12 cells by tuning the RGD and degradable ELP densities[221]. Chung et al. used tetrakis (hydroxylmethyl) phosphonium chloride (THPC) as an amine reactive crosslinker[222] in lysine-containing ELPs. Later studies done by Lampe *et al.* used these crosslinked protein hydrogels to encapsulate chick DRGs[223] (Figure 5). DRG growth was dependent on mechanical and RGD ligand density, and maximized neurite outgrowth was seen in hydrogels where matrix stiffness was similar to that of the native neural ECM. The enhanced neurite outgrowth within tunable 3-D microenvironments suggests that these ELP hydrogels may be useful in developing therapeutic nerve guidance channels to enhance stroke recovery, as they provide independent control of tailored integrin-binding density as well as tunable biomechanical stiffness and stability. A more recent publication by the Heilshorn group functionalized the same RGD-ELP sequence to crosslink via bio-orthogonal strain-promoted azide-alkyne cycloaddition (SPAAC) reactions[224]. mNPCs encapsulated in SPAAC-ELP hydrogels showed high viability, and maintained their ability to differentiate into both neurons and astrocytes following treatment with differentiation medium for a week.

Additionally, neurotrophin-ELP-based fusion proteins have been used as stimuli-responsive nanoparticles that can deliver NGF and BDNF. PC12 cells with recombinant fusions saw substantial increases in neurite extension versus soluble neurotrophins, indicating that ELPs are able to interact with the cell without being quickly diffused throughout the system[225]. Likewise, silk-elastin-like proteins have been used as thin films to culture primary cortical neurons, where more surface adhesion and growth were observed in silk-elastin composites versus elastin and silk controls[226]. The appearance of a tightly connected neuronal network was seen, as cells formed clusters indicative of strong cell-matrix interactions within the protein alloy. Additionally, hNSCs encapsulated in IKVAV-modified silk fibroin hydrogels had increased β III-tubulin and MAP-2-

positive cells compared to unmodified silk fibroin hydrogels after 1 week in differentiation culture[227].

Biosynthetic polypeptide sequences also have the capacity to self-assemble into various nano- to microscale structures, ranging from α-helical fibrils to β-sheet rich hydrogels. Banwell *et al.* have developed a two-component peptide system based on the coiled-coil heptad sequence repeat, ***abcdefg***, where ***a*** and ***d*** are usually occupied by hydrophobic amino acids, and charged residues are found in positions ***e*** and ***g***[228]. The α-helical peptide hydrogel was shown to support PC12 cell growth and differentiation. Another example of such a self-assembling material is a triblock protein composed a polyelectrolyte domain flanked by two amphiphilic leucine zipper sequences. NSCs proliferated on adhesive substrates (incorporation of RGDs into the polyelectrolyte region) or aggregated as neurospheres on non-adhesive substrates. It was demonstrated that proliferation of NSCs can be modulated through control of RGD surface density[229]. Similarly, the Heilshorn group designed two-component protein engineered hydrogels composed of two protein association domains – a WW domain and a proline-rich domain[230]. Upon mixing of the two components, formation of a hydrogel occurs due to physical crosslinking that takes place between the two associative domains. NSCs, as well as PC12 and HUVEC cells were encapsulated in the hydrogels, where the former were able to differentiate, and the hydrogel supported growth and proliferation of all cell types. The resulting hydrogels demonstrate complete self-healing after shear-thinning, making them suitable as injectable materials for clinical use.

In the early 1960s, Merrifield developed a novel approach to the chemical synthesis of polypeptides involving the stepwise addition of protected amino acids to a growing peptide chain[231]. Since its conception there have been significant improvements and refinements to the solid-phase methodology, most notably the introduction of the 9-fluorenylmethoxycarbonyl (Fmoc) group for N^{α} protection[232], resulting in greater peptide yields and reduction in side reactions during cleavage. Solid-phase peptide synthesis (SPPS) has enabled the successful preparation of tailor-made peptide sequences without the use of complex and often impracticable purification steps of naturally occuring proteins, while simultaneously maintaining similar biological activity as its native analog. The most advantageous property of peptides is that they are chemically defined; SPPS provides exceptional control over the peptide's chemical identity,

giving researchers the freedom to synthesize almost any protein sequence they desire without concerns regarding troublesome contaminants that often accompany proteins expressed in bacterial or mammalian cultures. Through the use of SPPS, tissue engineers are now able to easily synthesize a whole host of *de novo* peptides with unique structural and biofunctional properties,

including but not limited to proteolytic susceptibility[233-235], cell surface and/or matrix binding[236-238], growth factor binding[239-241], and self-assembly[242-247].

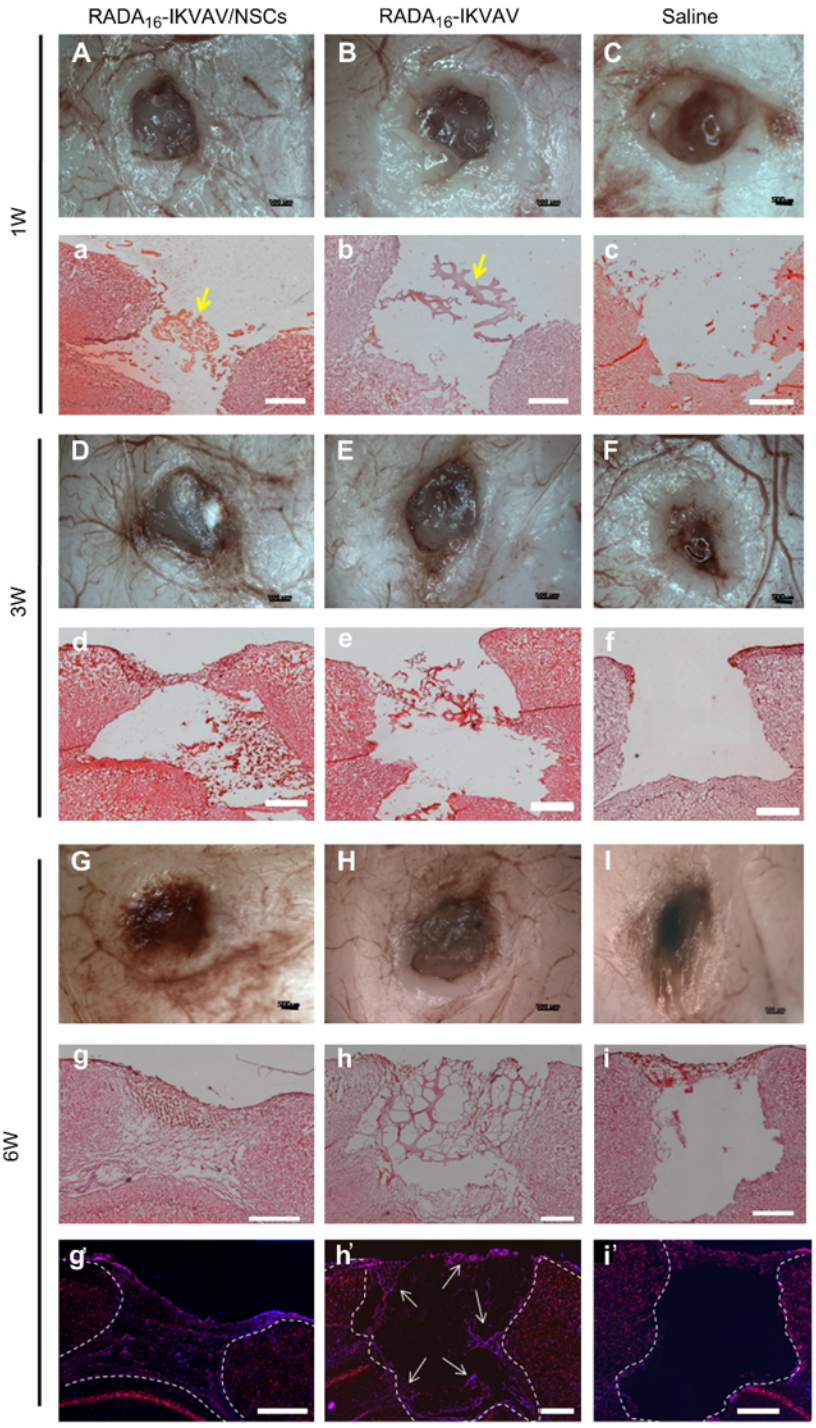

Figure 3-6. Analysis of histological H/E and Nissl/DAPI double staining of brain neural tissue in coronary sections with RADA16-IKVAV/Neural stem cell (NSC) and RADA16-IKVAV treated and non-treated traumatic brain tissue injury models. 12 week old Sprague-Dawley rats were injected with 1% (w/v) of RADA16-IKVAV with or without encapsulated NSCs immediately after surgery. H/E staining shows severe tissue loss and contour distortion of cerebral cortex in the saline control group (c, f, i), and confirmed via Nissl/DAPI double staining (i'). Animals treated with RADA16-IKVAV in combination with NSCs saw significantly enhanced regeneration in neural tissue, demonstrated by the decreasing wound size. At 6 weeks post surgery, the implanted hydrogel scaffolds were mostly degraded and replaced by newly regenerated tissue (g). Surprisingly, the RADA16-IKVAV treated groups saw some endogenous regeneration after 6 weeks (h), suggesting that the scaffold itself could still properly integrate within the damaged cavity and enhance neurogenesis. Reprinted with permission from Cheng T.Y., et al. Neural stem cells encapsulated in a functionalized self-assembling peptide hydrogel for brain tissue engineering. Biomaterials 2013, 34(8):2005-2016.

The use of designer peptides capable of self-assembling into matrices that act as ECM mimics have seen momentous growth in regenerative medicine[248-250]. The self-assembling propensities of these oligopeptides have been shown to fold into higher ordered tertiary and quaternary structures. The use of external stimuli to induce spontaneous gel formation is also unique in this class of biomaterials, in that *monomeric* peptides (rather than a composite, or two component system in polypeptide systems) are able to self-assemble in aqueous solutions without the addition of chemical crosslinks or other proteinaceous materials. Early work by Holmes *et al.* looked at designing self-assembling peptide scaffolds that could support neuronal cell attachment and differentiation[251]. Now known as RADA16 peptides, the $(\text{-Arg-Ala-Asp-Ala-})_{16}$ sequence is capable of spontaneous assembly into β-sheet-rich hydrogels, and has been used extensively as a substitute for Matrigel. Recently, Koutsopoulos *et al.* used RADA16 hydrogels to study NSC differentiation. Cell survival was highest in peptide nanofiber hydrogels containing the SKPPGTSS functional motif (neuronal apoptosis inhibitor) after 3 months compared to tissue cultures in Matrigel and collagen type I[252]. In functionalized hydrogels, a majority of encapsulated NSCs enter neuronal lineage, and one week post-encapsulation showed ~62% of the neuron Tuj1^+ cells were monopolar, ~23% bipolar, and 15% multipolar, suggesting that these RADA16 were suitable 3D environments for neural tissue cultures. Additionally, treatment with RADA16

hydrogels improved the survival of implanted donor NSCs *in* vivo. Nissl stains confirmed that damaged lesions saw significant regeneration following RADA16-IKVAV/NSCs implantation after 6 weeks compared to controls[253] (Figure 6). Furthermore, RADA16 hydrogels have also been shown to promote angiogenesis in a chick embryo[254]. RADA16 hydrogels (RAD/KLT) functionalized with a VEGF-mimicking peptide (KLTWQELYQLKYKGI) supported the highest endothelial cell sprout formation and average sprout length versus RADA16. The angiogenic properties of these hydrogel systems could potentially support endogenous recovery mechanisms in the recovering penumbra following stroke.

Peptide amphiphiles (PAs) have the ability to self-assemble in aqueous solution, driven by the sequence's hydrophobic aliphatic tail and a hydrophilic peptide domain. Seminal work done by the Stupp group demonstrated that PAs functionalized with the laminin epitope IKVAV was shown to induce rapid differentiation of encapsulated NPCs into neurons, and subsequently reducing astrocyte formation[255]. In other experiments, PA-IKVAVs were injected 24 h after SCI, and was shown to suppress astroglial differentiation. At 5 weeks and 11 weeks after SCI, there was a significant reduction in astrogliosis in PA-IKVAV treated groups, and 80% of all labeled corticospinal axons in the PA-IKVAV group were able to traverse through the area of injury[256]. Later studies by the same group reported increased serotonergic fibers in the caudal SC, with improved functional recovery at 10 weeks post injury[257]. Other peptides include amphiphilic diblock copolypeptides (DCHs), which can readily self-assemble into hydrogels under physiological conditions[258]. Histological characterizations indicated that DCH formulations did not induce any inflammatory or immune response upon injection. It was later shown that DCH deposits were densely vascularized, and contained microglia, astrocytes, and NG2 cells by 8 weeks *in vivo*. Researchers have also used amyloid-based self-assembling hydrogels to facilitate the attachment and neuronal differentiation of mesenchymal stem cells (MSCs)[259]. The high expression levels of ENO and TUBB3 and low levels of GFAP indicated that the amyloid hydrogel promoted hMSC differentiation toward the neuronal lineage. Additionally, $K_2(QL)_6K_2$ self-assembling hydrogels demonstrated that the cystic cavity in damaged spinal cords can be reduced by $K_2(QL)_6K_2$ or a combined $K_2(QL)_6K_2$ and NPC injection[260]. Furthermore, animals treated with $K_2(QL)_6K_2$ and NPCs showed a marked improvement in both grip strength, while vehicle-treated and NPC-treated groups reached a recovery plateau at 12 weeks.

3.12 **Composite and hybrid biomaterials**

Combinatorial strategies that incorporate bioactive molecules (e.g. growth factors, proteins, and small molecules), biomaterial scaffolds, and relevant cell types have increasingly been used in recent years to both improve cell survival and support host-tissue integration following cell transplantation for stroke treatment. For example, hybrid biomaterials such as poly(ethylene glycol) (PEG) conjugated to proteins and peptides (i.e. PEGylation), are used in order to improve the solubility of proteins, as a main structural polymeric backbone of a material, and reducing the degradation by proteolytic enzymes[261]. PEG's ability to retain a high volume of water and biocompatibility makes it an ideal substrate for use as a conjugate. For instance, the Seliktar group has conjugated fibrinogen, gelatin, and albumin to PEG. These protein components are used primarily to mediate cell-matrix interactions that would otherwise be absent in PEG-only polymers. In a recent study, they investigated using laser-ablation techniques for generating nerve guidance microchannels in these PEG-conjugated ECM protein hydrogels[262-263]. They observed DRG and glial cell outgrowth was highly dependent on channel dimensions[263], and that channels with a diameter greater than 50 μm supported extensive DRG cell invasion[262]. In the latter study, it was determined that the protein constituents could substantially accelerate DRG invasion; PEG-fibrinogen gels saw rapid propagation of DRG cells inside the channels during the first three days, and tightly packed axon bands were observed in PEG-gelatin gels[262]. Additionally, star-PEG hydrogels functionalized with RGD peptides and heparin were able to improve the survivability of primary fetal midbrain cultures. Incorporation of FGF-2, however, showed a tremendous increase in survival rate. FGF-2 releasing gels were able to induce NSC expansion by maintaining their undifferentiated state[264].

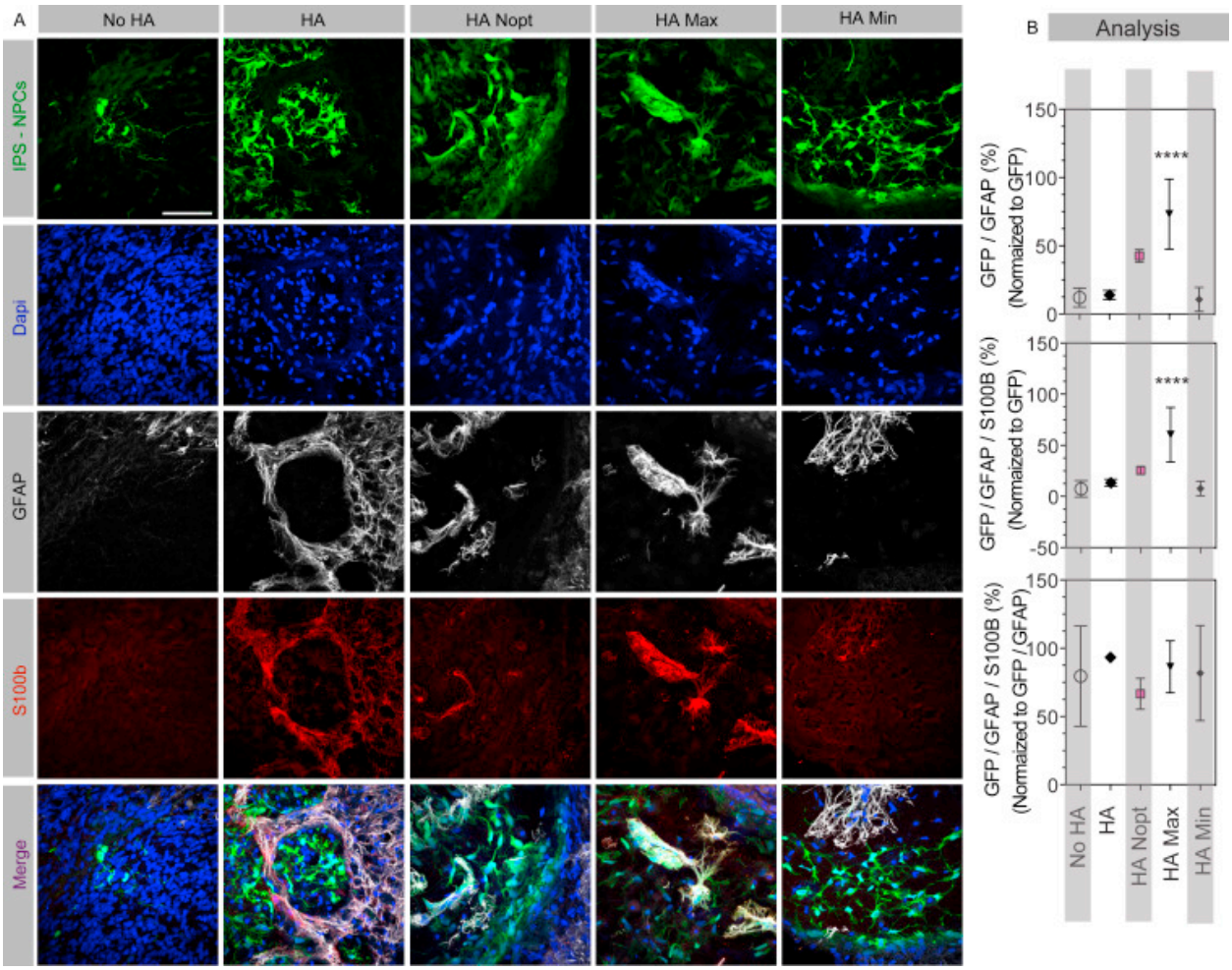

Figure 3-7. Encapsulation of human induced pluripotent neural precursor cells (iPS-NPC) in a HA gel modified with BMP4 and BDNF growth factors transplanted in immunosupressed C57BL/6 mice 7 d post injury. ***(a)*** *1x10^5 cells were transplanted into the stroke cavity and stained for GFP, GFAP, and S100b 6 wk post injury. HA Max gels saw significantly increased astrocytic differentiation compared to other groups.* ***(b)*** *Quantification of GFAP/S100b positive cells. GFP/GFAP as well as GFP/GFAP/S100b positive cells were normalized to the total GFP cells to obtain a percentage cells expressing one or both astrocytic markers. Scale bars, 50 µm. Reprinted from Moshayedi P., et al.* ***Systematic optimization of an engineered hydrogel allows for selective control of human neural stem cell survival and differentiation after transplantation in the stroke brain****. Biomaterials 2016,* ***105****:145-155 (https://doi.org/10.1016/j.biomaterials.2016.07.028) under the terms of the Creative Commons Attribute License (CC BY - https://creativecommons.org/licenses/by-nc-nd/4.0/legalcode)*

Another promising material is hyaluronic acid (HA), a polysaccharide that plays an important role in regulating cell adhesion and motility, and ECM organization[265]. For example,

hyaluronan/methyl cellulose (HAMC) has been used extensively as an injectable hydrogel in stroke treatment. In combination with erythropoietin (EPO), implantation of the HAMC hydrogel reduced stroke cavity size compared to untreated and HAMC controls and significantly increased the number of $NeuN^+$ mature neurons in the injured cortex[266]. Interestingly, EPO delivery in HAMC gels 11 d post-stroke also led to fewer apoptotic cells, demonstrating the effectiveness of neuroprotective properties utilizing this delivery platform in addition to EPO[267]. Similarly, Zhong et al. demonstrated that a hyaluronan-heparin-collagen composite hydrogel was able to improve the survival of NPCs near the injured cortex after stroke[268]. Additionally, there was a significant decrease in activated microglial/macrophages that infiltrated the graft site compared to controls without gels. Work done by Moshayedi et al. demonstrated that a modified HA hydrogel with MMP degradable motifs and heparin bound growth factors (HA Max) provided maximum cell survival both in vitro and in vivo[269]. There was significantly increased proliferation of iPS-NPCs at two weeks compared to unmodified HA gels. Cells that were not encapsulated (no HA) were found to retain higher levels of SOX2 expression compared to cells transplanted within HA gels. Additionally, iPS-NPCs saw significantly increased expression of GFAP and S100b markers, suggesting that HA Max gels promote astrocytic differentiation of iPS-NPCs within the stroke cavity (Figure 7).

Poly(lactic-co-glycolic acid) (PLGA) has also seen extensive use as a biodegradable synthetic polymeric scaffold for tissue engineering applications. Bible *et al.* entrapped VEGF within surface-modified PLGA microparticles which were subsequently administrated into the lesion cavity 2 w post-stroke. It was shown that the particles promoted the recruitment of a substantial number of ECs into the neuroscaffold within the lesion cavity. Additionally, hNSCs initially bound to the surface of PLGA-VEGF particles led to the formation of neurovascular units in stroke regions compared to the surrounding intact host tissue[270], suggesting that the formation of host-derived *de novo* tissue in the lesion cavity is achievable using VEGF-releasing PLGA microspheres seeded with hNSCs. Additionally, PLGA-b-PEG nanoparticles have been used to deliver triiodothyronine as a neuroprotective agent[271]. MCAO mouse stroke models treated with PLGA-b-PEG nanoparticles led to a significant decrease in tissue infarction and >50% decrease in brain edema. This has potentially immense clinical relevance in that rising intracranial pressure due to edema is one of the primary reasons for morality in stroke patients.

Additionally, alginate hydrogels have been used as an ECM mimetic due to its biochemical stability and high biocompatibility[272]. Alginate hydrogels were used to encapsulate VEGF to be delivered to MCAO models. Animals treated with the VEGF gel saw significant improvement in motor asymmetry relative to animals receiving blank alginate gels (42%) and stroke alone (45%)[273]. Histograms demonstrated that animals receiving VEGF gels saw reduction in lesion sizes compared to animals with stroke only and injections of alginate gel. Later studies done by Anderson *et al.* used alginate hydrogels to encapsulate VEGF and insulin-like growth factor-1 (IGF)[274]. These gels were injected into ischemic hind limbs in middle-aged and old-mice, and only treatment from a combination of VEGF and IGF delivery from gels significantly rescued perfusion in both groups. This suggests that VEGF systems could potentially provide a potent neuroprotective benefit across a broad range of CNS diseases following neuronal degeneration.

Alternatively, the functionalization of collagen-based scaffolds have also been of particular interest in the neural tissue engineering field. Collagen conduits modified with neurotrophin-3 (NT-3) were used to assess functional recovery in rats with completely transected spinal cord. It was shown that aligned collagen fibers of the conduit channels significantly enhanced axonal growth within the channels of the conduits[275]. This suggested that the walls of the conduit provided additional topographical guidance to regenerating axons, and that the additional functionalization with NT-3 allowed for the constant release of plasmid, resulting in improved axonal regeneration and functional recovery. Work done by Fan *et al.* demonstrated that a collagen scaffold modified with collagen-binding EGFR antibody successfully inhibits myelin-associated inhibitors in acute spinal cord injury models (SCI). Surprisingly, no lesion cavities were observed in the injury sites, and only a slight glial scar was observed in the modified collagen scaffolds versus controls, suggesting that the EGFR antibody plays an important role in improving neurogenesis in a dose-dependent manner[276]. Similarly, Masand *et al.* conjugated peptide mimetics of human natural killer cells (HNK-1) to collagen type I scaffolds to study the effects that glycans have on motor axons[277]. They showed that the HNK-grafted collagen hydrogels supported motor neuron outgrowth, suggesting that glycomimetics can encourage preferential motor reinnervation within the PNS. Winter *et al.* have shown that neurons co-seeded with astrocytes in cylindrical constructs composed of agarose and collagen type I demonstrated that neurons associated closely with

longitudinally aligned astrocytes. This suggests that these astrocytic bundles could provide a favorable substrate for neurons to grow alongside with, and provides a proof of concept for cell-cell interactions and intrinsic chemotactic interactions between seeded astrocytes[278].

Keratin-based biomaterials have recently attracted attention due to keratin's ability to control cellular attachment and migration[279]. Sierpinski *et al.* developed a keratin-based hydrogel that was used to fill collagen conduit channels, and saw improved histological characteristics such as greater axon density and axon diameter compared to autograft controls in mice with a 4 mm gap in the tibial nerve[280]. The keratin-treated groups also tested significantly better for conduction delay and amplitude of the nerve-motor unit compared to controls. Hill *et al.* injected a keratin hydrogel into the lumen of NeuraGen collagen nerve guides, and saw that nerves that regenerated in empty conduits were ~30% smaller in size than keratin-treated nerves, and even smaller in size than both empty conduit and seral nerve autograft controls.. Electrophysiology testing showed that the conduction delay was significantly improved in the keratin group compared to both empty (>300%) and autograft controls (>700%) in rabbits with a 2-3 cm sciatic nerve break[163]. In a similar study in rats with a 1 cm sciatic nerve defect, keratin hydrogel groups saw significantly increased migration of endogenous Schwann cells, higher myelin debris clearance, and decreased macrophage infiltration compared to autograft controls[281].

3.13 **Future perspectives**

The loss of neuronal cell bodies, axons, and associated glial support is a hallmark of several neurological insults, including ischemic stroke and neurodegenerative disease. Recent attempts at restoring damaged neural tissue involve engineering a 3D microenvironment suitable for regulating neural stem cell behavior. These microenvironments are designed to mimic essential properties of the ECM, including elasticity, proteolytic remodeling, and cell-adhesive sites. However, remaining challenges faced by tissue engineers is the ability to design biomaterials that 1) are also low cost and simple to synthesize, 2) have the ability to gel autonomously to applied stimulus such as pH or temperature changes, and 3) are able to regulate and support cell function as a substitute for their normal physiological microenvironment. Thus, there is a critical need to establish a biomimicry strategy to enable stimuli-responsive and multifunctional biomaterials that

can deliver and allow precise control of stem cell behavior for neural tissue regeneration applications.

Protein-based biomaterials are extremely versatile biopolymers that can be engineered with unique structural and biological properties. The recent developments of making injectable and self-healing hydrogels[227, 230, 282-283] predestine applying this biomaterial clinically to lesion areas near the disease site via simple injection followed by gelation. This enables minimally invasive patient delivery. While it has been demonstrated that cell transplantation strategies using biomaterial scaffolds can potentially improve the neurologic outcome and reduce infarct size, many questions still remain, and the precise cellular and biochemical mechanisms of cell-induced repair remain to be elucidated. For example, are necrotic cells being replaced, or do transplanted cells produce neurotrophic factors that stimulate endogenous repair? What cell type(s) should be used that would promote neurogenesis and/or vasculogenesis? What are the specific cues that initiate cell propagation or differentiation within biomaterials? What intracellular signaling pathways should be considered (i.e. conjugation of growth factors and ECM proteins to biomaterials) that would have the most impact on cell-matrix interactions? What is the optimum therapeutic time window for such biomaterials-based therapy? What key mechanical properties (e.g. topography, matrix stiffness, porosity) of hydrogel biomaterials are most important in improving regeneration? And, most importantly, what types of biomaterials, or combinations thereof, will yield the most therapeutic benefit?

Furthermore, biomaterials development should consider cell-matrix interactions that influence trophic support and differentiation potentials. This includes incorporating degradable sites in the biomaterial to allow for cell secreted protease-induced remodeling of the matrix. Additional molecules from the secretome (i.e. cytokines, chemokines produced through paracrine signaling, and trophic factors) derived from stem cells also play a large role in improving post-stroke angiogenesis and functional recovery[284-286]. Additionally, the interplay between the cell and its microenvironment in the context of modulating the mechanotransduction pathway should be considered. Bulk matrix stiffness and topography are known biomechanical cues in stem cell differentiation[287-288]. However, there is a shortage of methodologies for incorporating anisotropic topographical cues in 3D biomaterial scaffolds to induce cell alignment and migration. Most

cellular alignment studies are conducted using 2D electrospun fibers or patterned grooves and channels, but these cues are confined to the surface of such matrices. The development of magnetic-field induced aligned is a promising method in incorporating anisotropy within a hydrogel[289], and more recent alternatives of using electrical and mechanical stretching have been introduced as a versatile strategy in creating aligned hydrogel microfibers in 3D[290]. These new approaches would allow researchers to more effectively incorporate a wider range of patterning within biomaterial scaffolds to study the effects of anisotropy on cell-matrix interactions.

Therapeutic strategies that include brain protection following stroke involve the delivery of neuroprotective compounds that suppress the deleterious effects of inflammation and prevent cellular degeneration. However, most of these drugs are inactive following systemic administration due to the low permeability of the BBB[291]. From a holistic standpoint, nano-scale delivery systems that can mediate cell-cell and cell surface receptors-ligand levels that are able to permeate through the BBB have yet to be developed. Recently, work done by Nance *et al.* investigated the surface properties of nanoparticles and the influence of PEG coating on brain tissue penetration[292]. It was found that particle sizes in the range of 40 to 100 nm were highly distributed in mouse brains, but only if they were heavily coated with PEG. Additionally, a refined understanding of the crosstalk between endothelial cells and associated astrocytes, as well as the selectivity of the tight junctions from between the two, would be needed to develop effective carriers. Even after the delivery vehicle is able to penetrate into the brain tissue, the surface of the vehicle must be tailored with site-specific ligands to localize the bioavailability to only the affected areas of the brain (i.e. infarct cavity).

Incorporation of vasculature within biomaterial scaffolds, especially in the context of neural regeneration in stroke injury models, still remains a significant challenge in the field. Mimicking the endogenous expansion of blood vessels into vast networks during neurogenesis and concomitantly remodeling of the neovasculature is a highly unexplored area. NSCs and oligodendrocyte progenitor cells are frequently found, and migrate along, small blood vessels. Ultimately, most in the field have opted for developing models that can establish tight junctions between endothelial cells and contacts with pericytes and astrocyte endfeet using induced pluripotent stem cell (iPSC)-derived sources[293-294], however, these models insufficiently describe the vascular tree and cerebral arterial hierarchy inherently present in the CNS. Understanding the

cross-talk between neural and vascular cells and signaling pathways will reveal how a dysfunctional neurovascular unit is remodeled upon injury. The challenge of decoupling the synergistic effects of vascular development and brain development, however, remain to be addressed, although there have been significant efforts in the engineering of vascular constructs[295-296]. Hyaluronic acid-based hydrogels that incorporated salmon fibrin and laminin have been used to study the effects on hNSPC proliferation and differentiation, and subsequently, vasculogenesis of human endothelial colony-forming cell-derived endothelial cells (hECFC-ECs)[297]. hNSPCs secreted angiogenic factors (i.e. VEGF-A and VEGF-B) that promoted sprouting of hECFC-ECs. The co-culturing of hNSPCs and hECFC-ECs demonstrated that hNSPC had a positive effect on vessel formation, where there was an increase in both vessel length and branch points. More recently, the Segura group designed a hydrogel scaffold that is able to promote endothelial cell sprouting and branching through the incorporation of integrin-binding peptides, α3/α5β1. Additionally, VEGF was incorporated into the system and promoted EC sprouting and anastomosis *in vivo*[298]. Similarly, a more recent study used a combination of HA, salmon fibrin, and laminin. Co-culturing of hNSPCs and ECs in the scaffolds showed significantly greater vessel formation versus ECs alone in fibrin scaffolds (Figure 8) [297]. The use of such combination scaffolds warrants further investigation into the effects on vasculogenesis while simultaneously supporting neural cell growth. Such a fibrin/HA/laminin scaffold could potentially increase NSPC survival when transplanted into the infarct core within the stroke environment.

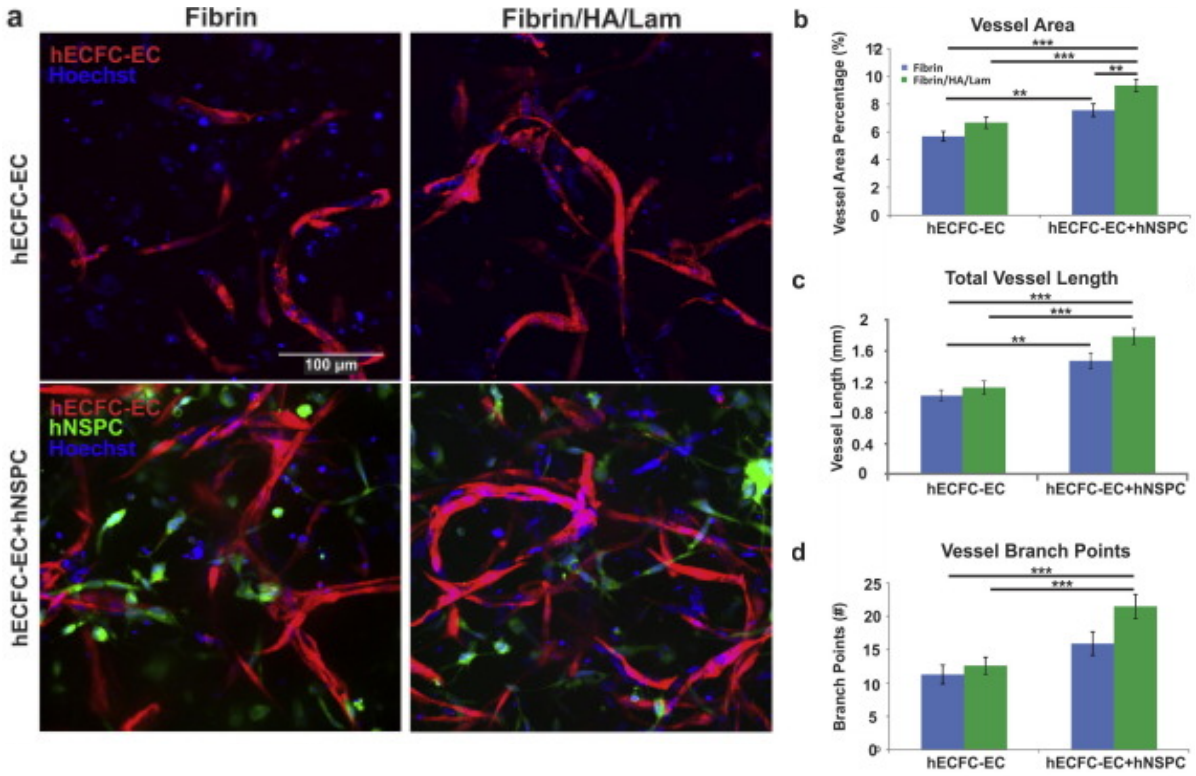

Figure 3-8. Scaffolds of fibrin, HA, and laminin promotes neurovascular unit formation. (a) Human endothelial colony-forming cell-derived endothelial cells (hECFC-ECs) expressing mCherry cultured with human neural stem/progenitor cells (hNSPCs) in the Fibrin/HA/Laminin composite scaffold saw significantly increased vessel formation. (b) Quantitative analysis demonstrating that composite scaffolds contained significantly higher vessel area percentage compared to scaffolds containing fibrin with hECFC-ECs, fibrin with co-cultured hNSPCs and hECFC-ECs, or combination scaffolds with hECFC-ECs only. (c) Total vessel length is also significantly greater in composite scaffolds and is also highest in scaffolds containing both hNSPCs and hECFC-ECs. (d) There is a two fold increase in number of vessel branch points in co-cultures within composite scaffolds compared to the hECFC-ECs cultured alone in fibrin, highlighting the synergistic effect of both HA and laminin with hNSPCs on vascular network complexity. Adapted from Arulmoli J. et al., Combination scaffolds of salmon fibrin, hyaluronic acid, and laminin for human neural stem cell and vascular tissue engineering. Acta Biomaterialia 2016, 43:122-138 (https://doi.org/10.1016/j.actbio.2016.07.043) under the terms of the CC BY NC ND (https://creativecommons.org/licenses/by-nc-nd/4.0/legalcode)

Such results provide guidance on how to support regrowth of vasculature after stroke lesions have formed. However, further research into the mechanisms that mediate spatiotemporal aspects of vascularization is needed, with biomaterials leading the forefront of inducing endogenous vascularization as well as supporting a functional vascular network.

An underlying topic that has not been addressed in this review is the modulation of the immune system in response to ischemia-induced inflammation. Ideally, a reduced inflammatory response

from biomaterials engraftment is a favorable outcome. However, it has become exceedingly clear that activated microglial and perivascular macrophages play an integral role in reestablishing tissue homeostasis in the brain and remodeling of the neurovascular unit. In early stages of recovery, chronically activated microglial produce pro-inflammatory cytokines, toxic amounts of ROS, and MMPs that degrade the BBB. At later stages, phagocytosis of cellular debris along with the production of anti-inflammatory cytokines by the same microglia occurs, consequently attenuating the deleterious effects of inflammation and inhibition of tissue regeneration. Because of the Janus-faced nature of these reactive glia that could play both a destructive and protective role at different time points, therapeutics targeting inflammation in cerebral ischemia should be mindful of temporal considerations that can block deleterious effects within the penumbra and foster post-ischemic anti-inflammation mediators that can contribute to tissue repair. Ultimately transplanted biomaterials will likely serve as a provisional matrix, influencing the injury environment and directing any transplanted cell behavior, until the integrating transplant or host cells can establish de novo tissue. Modulating both the injury, and the immune reaction to it, are underexplored areas ripe for new strategies in CNS regeneration.

3.14 References

1. World Health Organization, Global Health Estimates 2015: Deaths by Cause, Age, Sex, by Country and by Region, 2000-2015. **2016**.
2. Murray, C. J. L.; Vos, T.; Lozano, R., Disability-adjusted life years (DALYs) for 291 diseases and injuries in 21 regions, 1990-2010: a systematic analysis for the Global Burden of Disease Study 2010 (vol 380, pg 2197, 2012). *Lancet* **2014,** *384* (9943), 582-582.
3. Krishnamurthi, R. V.; deVeber, G.; Feigin, V. L.; Barker-Collo, S.; Fullerton, H.; Mackay, M. T.; O'Callahan, F.; Lindsay, M. P.; Kolk, A.; Lo, W.; Shah, P.; Linds, A.; Jones, K.; Parmar, P.; Taylor, S.; Norrving, B.; Mensah, G. A.; Moran, A. E.; Naghavi, M.; Forouzanfar, M. H.; Nguyen, G.; Johnson, C. O.; Vos, T.; Murray, C. J. L.; Roth, G. A.; Grp, G. S. P. E., Stroke Prevalence, Mortality and Disability-Adjusted Life Years in Children and Youth Aged 0-19 Years: Data from the Global and Regional Burden of Stroke 2013. *Neuroepidemiology* **2015,** *45* (3), 177-189.
4. Feigin, V. L.; Forouzanfar, M. H.; Krishnamurthi, R.; Mensah, G. A.; Connor, M.; Bennett, D. A.; Moran, A. E.; Sacco, R. L.; Anderson, L.; Truelsen, T.; O'Donnell, M.; Venketasubramanian, N.; Barker-Collo, S.; Lawes, C. M. M.; Wang, W. Z.; Shinohara, Y.; Witt, E.; Ezzati, M.; Naghavi, M.; Murray, C.; Fa, G. B. D. I. R.; Grp, G. S. E., Global and regional burden of stroke during 1990-2010: findings from the Global Burden of Disease Study 2010. *Lancet* **2014,** *383* (9913), 245-255.
5. Moskowitz, M. A.; Lo, E. H.; Iadecola, C., The Science of Stroke: Mechanisms in Search of Treatments. *Neuron* **2010,** *67* (2), 181-198.
6. Mitsios, N.; Gaffney, J.; Kumar, P.; Krupinski, J.; Kumar, S.; Slevin, M., Pathophysiology of acute ischaemic stroke: An analysis of common signalling mechanisms and identification of new molecular targets. *Pathobiology* **2006,** *73* (4), 159-175.
7. Zhang, L.; Chopp, M.; Liu, X. S.; Teng, H.; Tang, T.; Kassis, H.; Zhang, Z. G., Combination Therapy With VELCADE and Tissue Plasminogen Activator Is Neuroprotective in Aged Rats After Stroke and Targets MicroRNA-146a and the Toll-Like Receptor Signaling Pathway. *Arterioscl Throm Vas* **2012,** *32* (8), 1856-U336.
8. Peerschke, E. I.; Yin, W.; Ghebrehiwet, B., Complement activation on platelets: Implications for vascular inflammation and thrombosis. *Mol Immunol* **2010,** *47* (13), 2170-2175.
9. Wechsler, L. R.; Jovin, T. G., Intravenous Recombinant Tissue-Type Plasminogen Activator in the Extended Time Window and the US Food and Drug Administration Confused About the Time. *Stroke* **2012,** *43* (9), 2517-2519.
10. Wechsler, L.; Steindler, D.; Borlongan, C.; Chopp, M.; Savitz, S.; Deans, R.; Caplan, L.; Hess, D.; Mays, R. W.; Participants, S., Stem Cell Therapies as an Emerging Paradigm in Stroke (STEPS) Bridging Basic and Clinical Science for Cellular and Neurogenic Factor Therapy in Treating Stroke. *Stroke* **2009,** *40* (2), 510-515.
11. Savitz, S. I.; Chopp, M.; Deans, R.; Carmichael, S. T.; Phinney, D.; Wechsler, L., Stem Cell Therapy as an Emerging Paradigm for Stroke (STEPS) II. *Stroke* **2011,** *42* (3), 825-829.

12. Cooke, M. J.; Zahir, T.; Phillips, S. R.; Shah, D. S. H.; Athey, D.; Lakey, J. H.; Shoichet, M. S.; Przyborski, S. A., Neural differentiation regulated by biomimetic surfaces presenting motifs of extracellular matrix proteins. *J Biomed Mater Res A* **2010,** *93a* (3), 824-832.
13. Kubinova, S.; Sykova, E., Nanotechnology for treatment of stroke and spinal cord injury. *Nanomedicine-Uk* **2010,** *5* (1), 99-108.
14. Ajioka, I.; Jinnou, H.; Okada, K.; Sawada, M.; Saitoh, S.; Sawamoto, K., Enhancement of Neuroblast Migration into the Injured Cerebral Cortex Using Laminin-Containing Porous Sponge. *Tissue Eng Pt A* **2015,** *21* (1-2), 193-201.
15. Oshikawa, M.; Okada, K.; Kaneko, N.; Sawamoto, K.; Ajioka, I., Affinity-Immobilization of VEGF on Laminin Porous Sponge Enhances Angiogenesis in the Ischemic Brain. *Adv Healthc Mater* **2017,** *6* (11).
16. Hess, D. C.; Auchus, A. P.; Uchino, K.; Sila, C.; Clark, W. M.; Chiu, D.; Wechsler, L. R.; Mays, R. W.; Investigators, B.-. Final Results of the B01-02 Phase 2 Trial Testing the Safety and Efficacy of MultiStem(R) in Treatment of Ischemic Stroke. *Stroke* **2016,** *47*.
17. Friedrich, M. A. G.; Martins, M. P.; Araujo, M. D.; Klamt, C.; Vedolin, L.; Garicochea, B.; Raupp, E. F.; El Ammar, J. S.; Machado, D. C.; da Costa, J. C.; Nogueira, R. G.; Rosado-de-Castro, P. H.; Mendez-Otero, R.; de Freitas, G. R., Intra-Arterial Infusion of Autologous Bone Marrow Mononuclear Cells in Patients With Moderate to Severe Middle Cerebral Artery Acute Ischemic Stroke. *Cell Transplant* **2012,** *21*, S13-S21.
18. Bang, O. Y., Clinical Trials of Adult Stem Cell Therapy in Patients with Ischemic Stroke. *J Clin Neurol* **2016,** *12* (1), 14-20.
19. Burnstock, G., Purinergic signalling and disorders of the central nervous system. *Nat Rev Drug Discov* **2008,** *7* (7), 575-590.
20. Broughton, B. R. S.; Reutens, D. C.; Sobey, C. G., Apoptotic Mechanisms After Cerebral Ischemia. *Stroke* **2009,** *40* (5), E331-E339.
21. Unal-Cevik, I.; Kilinc, M.; Can, A.; Gursoy-Ozdemir, Y.; Dalkara, T., Apoptotic and necrotic death mechanisms are concomitantly activated in the same cell after cerebral ischemia. *Stroke* **2004,** *35* (9), 2189-2194.
22. Fabricius, M.; Fuhr, S.; Bhatia, R.; Boutelle, M.; Hashemi, P.; Strong, A. J.; Lauritzen, M., Cortical spreading depression and peri-infarct depolarization in acutely injured human cerebral cortex. *Brain* **2006,** *129*, 778-790.
23. Mattson, M. P.; Culmsee, C.; Yu, Z. F., Apoptotic and antiapoptotic mechanisms in stroke. *Cell Tissue Res* **2000,** *301* (1), 173-187.
24. Chukanova, E. I.; Khozhamzharov, B. E.; Chukanova, A. S., Current possibilities of the correction of oxidative stress in acute brain ischemia. *Zh Nevrol Psikhiatr* **2012,** *112* (11), 79-82.
25. Dobrotvorskaya, I. S.; Fedorova, T. N.; Dobrota, D.; Berezov, T. T., Characteristics of Oxidative Stress in Experimental Rat Brain Ischemia Aggravated by Homocysteic Acid. *Neurochem J+* **2011,** *5* (1), 42-46.
26. Dirnagl, U.; Iadecola, C.; Moskowitz, M. A., Pathobiology of ischaemic stroke: an integrated view. *Trends Neurosci* **1999,** *22* (9), 391-397.
27. Sims, N. R.; Anderson, M. F., Mitochondrial contributions to tissue damage in stroke. *Neurochem Int* **2002,** *40* (6), 511-526.
28. Lakhan, S. E.; Kirchgessner, A.; Tepper, D.; Leonard, A., Matrix metalloproteinases and blood-brain barrier disruption in acute ischemic stroke. *Front Neurol* **2013,** *4*.
29. Iadecola, C.; Anrather, J., The immunology of stroke: from mechanisms to translation. *Nat Med* **2011,** *17* (7), 796-808.
30. Hyman, M. C.; Petrovic-Djergovic, D.; Visovatti, S. H.; Liao, H.; Yanamadala, S.; Bouis, D.; Su, E. M. J.; Lawrence, D. A.; Broekman, M. J.; Marcus, A. J.; Pinsky, D. J., Self-regulation of inflammatory cell trafficking in mice by the leukocyte surface apyrase CD39. *J Clin Invest* **2009,** *119* (5), 1136-1149.
31. Zhang, R. L.; Chopp, M.; Zhang, Z. G.; Jiang, N.; Powers, C., The expression of P- and E-selectins in three models of middle cerebral artery occlusion. *Brain Res* **1998,** *785* (2), 207-214.
32. Stephan, A. H.; Barres, B. A.; Stevens, B., The Complement System: An Unexpected Role in Synaptic Pruning During Development and Disease. *Annual Review of Neuroscience, Vol 35* **2012,** *35*, 369-389.
33. Rosenberg, G. A., Extracellular matrix inflammation in vascular cognitive impairment and dementia. *Clin Sci* **2017,** *131* (6), 425-437.
34. Cekanaviciute, E.; Fathali, N.; Doyle, K. P.; Williams, A. M.; Han, J.; Buckwalter, M. S., Astrocytic Transforming Growth Factor-Beta Signaling Reduces Subacute Neuroinflammation After Stroke in Mice. *Glia* **2014,** *62* (8), 1227-1240.
35. Arnold, L.; Henry, A.; Poron, F.; Baba-Amer, Y.; van Rooijen, N.; Plonquet, A.; Gherardi, R. K.; Chazaud, B., Inflammatory monocytes recruited after skeletal muscle injury switch into antiinflammatory macrophages to support myogenesis. *J Exp Med* **2007,** *204* (5), 1057-1069.
36. Nathan, C.; Ding, A. H., Nonresolving Inflammation. *Cell* **2010,** *140* (6), 871-882.
37. Liesz, A.; Suri-Payer, E.; Veltkamp, C.; Doerr, H.; Sommer, C.; Rivest, S.; Giese, T.; Veltkamp, R., Regulatory T cells are key cerebroprotective immunomodulators in acute experimental stroke. *Nat Med* **2009,** *15* (2), 192-199.
38. Veltkamp, R.; Suri-Payer, E.; Veltkamp, C.; Sommer, C.; Rivest, S.; Liesz, A., Endogenous immunomodulation after experimental focal ischemia: multitargeted cerebroprotection by regulatory T cells is the key. *J Cerebr Blood F Met* **2009,** *29*, S508-S509.
39. Gliem, M.; Krammes, K.; Liaw, L.; van Rooijen, N.; Hartung, H. P.; Jander, S., Macrophage-Derived Osteopontin Induces Reactive Astrocyte Polarization and Promotes Re-Establishment of the Blood Brain Barrier After Ischemic Stroke. *Glia* **2015,** *63* (12), 2198-2207.
40. Wiese, S.; Karus, M.; Faissner, A., Astrocytes as a source for extracellular matrix molecules and cytokines. *Front Pharmacol* **2012,** *3*.
41. Marler, J. R.; Brott, T.; Broderick, J.; Kothari, R.; Odonoghue, M.; Barsan, W.; Tomsick, T.; Spilker, J.; Miller, R.; Sauerbeck, L.; Jarrell, J.; Kelly, J.; Perkins, T.; Mcdonald, T.; Rorick, M.; Hickey, C.; Armitage, J.; Perry, C.; Thalinger, K.; Rhude, R.; Schill, J.; Becker, P. S.; Heath, R. S.; Adams, D.; Reed, R.; Klei, M.; Hughes, S.; Anthony, J.; Baudendistel, D.; Zadicoff, C.; Rymer, M.; Bettinger, I.; Laubinger, P.; Schmerler, M.; Meirose, G.; Lyden, P.; Rapp, K.; Babcock, T.; Daum, P.; Persona, D.; Brody, M.; Jackson, C.; Lewis, S.; Liss, J.; Mahdavi, Z.; Rothrock, J.; Tom, T.; Zweifler, R.; Dunford, J.; Zivin, J.; Kobayashi, R.; Kunin, J.; Licht, J.; Rowen, R.; Stein, D.; Grisolia, J.; Martin, F.; Chaplin, E.; Kaplitz, N.; Nelson, J.; Neuren, A.; Silver, D.; Chippendale, T.; Diamond, E.; Lobatz, M.; Murphy, D.; Rosenberg, D.; Ruel, T.; Sadoff, M.; Schim, J.; Schleimer, J.; Atkinson, R.; Wentworth, D.; Cummings, R.; Frink, R.; Heublein, P.;

Grotta, J. C.; Degraba, T.; Fisher, M.; Ramirez, A.; Hanson, S.; Morgenstern, L.; Sills, C.; Pasteur, W.; Yatsu, F.; Andrews, K.; Villarcordova, C.; Pepe, P.; Bratina, P.; Greenberg, L.; Rozek, S.; Simmons, K.; Kwiatkowski, T. G.; Horowitz, S. H.; Libman, R.; Kanner, R.; Silverman, R.; Lamantia, J.; Mealie, C.; Duarte, R.; Donnarumma, R.; Okola, M.; Cullin, V.; Mitchell, E.; Levine, S. R.; Lewandowski, C. A.; Tokarski, G.; Ramadan, N. M.; Mitsias, P.; Gorman, M.; Zarowitz, B.; Kokkinos, J.; Dayno, J.; Verro, P.; Gymnopoulos, C.; Dafer, R.; Dolhaberriague, L.; Sawaya, K.; Daley, S.; Mitchell, M.; Frankel, M.; Mackay, B.; Barch, C.; Braimah, J.; Faherty, B.; Macdonald, J.; Sailor, S.; Cook, A.; Karp, H.; Nguyen, B.; Washington, J.; Weissman, J.; Williams, M.; Williamson, T.; Kozinn, M.; Hellwick, L.; Haley, E. C.; Bleck, T. P.; Cail, W. S.; Lindbeck, G. H.; Granner, M. A.; Wolf, S. S.; Gwynn, M. W.; Mettetal, R. W.; Chang, C. W. J.; Solenski, N. J.; Brock, D. G.; Ford, G. F.; Kongable, G. L.; Parks, K. N.; Wilkinson, S. S.; Davis, M. K.; Sheppard, G. L.; Zontine, D. W.; Gustin, K. H.; Crowe, N. M.; Massey, S. L.; Meyer, M.; Gaines, K.; Payne, A.; Bales, C.; Malcolm, J.; Barlow, R.; Wilson, M.; Cape, C.; Bertorini, T.; Misulis, K.; Paulsen, W.; Shepard, D.; Tilley, B. C.; Welch, K. M. A.; Fagan, S. C.; Lu, M.; Patel, S.; Masha, E.; Verter, J.; Boura, J.; Main, J.; Gordon, L.; Maddy, N.; Chociemski, T.; Windham, J.; Zadeh, H. S.; Alves, W.; Keller, M. F.; Wenzel, J. R.; Raman, N.; Cantwell, L.; Warren, A.; Smith, K.; Bailey, E.; Welch, K. M. A.; Tilley, B. C.; Froehlich, J.; Breed, J.; Easton, J. D.; Hallenbeck, J. F.; Lan, G.; Marsh, J. D.; Walker, M. D., Tissue-Plasminogen Activator for Acute Ischemic Stroke. *New Engl J Med* **1995,** *333* (24), 1581-1587.

42. Frey, J. L., Recombinant tissue plasminogen activator (rtPA) for stroke - The perspective at 8 years. *Neurologist* **2005,** *11* (2), 123-133.

43. Heo, J. H.; Kim, S. H.; Lee, K. Y.; Kim, E. H.; Chu, C. K.; Nam, J. M., Increase in plasma matrix metalloproteinase-9 in acute stroke patients with thrombolysis failure. *Stroke* **2003,** *34* (6), E48-E50.

44. Davis, S. M.; Pennypacker, K. R., Targeting antioxidant enzyme expression as a therapeutic strategy for ischemic stroke. *Neurochem Int* **2017,** *107*, 23-32.

45. Ghezzi, P.; Jaquet, V.; Marcucci, F.; Schmidt, H. H. H. W., The oxidative stress theory of disease: levels of evidence and epistemological aspects. *Brit J Pharmacol* **2017,** *174* (12), 1784-1796.

46. Petro, M.; Jaffer, H.; Yang, J.; Kabu, S.; Morris, V. B.; Labhasetwar, V., Tissue plasminogen activator followed by antioxidant-loaded nanoparticle delivery promotes activation/mobilization of progenitor cells in infarcted rat brain. *Biomaterials* **2016,** *81*, 169-180.

47. Isik, M.; Beydemir, S.; Yilmaz, A.; Naldan, M. E.; Aslan, H. E.; Gulcin, I., Oxidative stress and mRNA expression of acetylcholinesterase in the leukocytes of ischemic patients. *Biomed Pharmacother* **2017,** *87*, 561-567.

48. Kaur, C.; Rathnasamy, G.; Ling, E. A., Antioxidants and Neuroprotection in the Brain and Retina. *Front Med Chem* **2015,** *7*, 3-33.

49. Papapetrou, A.; Moris, D.; Patelis, N.; Kouvelos, G. N.; Bakogiannis, C.; Klonaris, C.; Georgopoulos, S., Oxidative Stress and Total Antioxidant Status During Internal Carotid Artery Clamping with or without Shunting: An Experimental Pilot Study. *Med Sci Monit Basic* **2015,** *21*, 200-205.

50. Imai, H.; Masayasu, H.; Dewar, D.; Graham, D. I.; Macrae, I. M., Ebselen protects both gray model of focal and white matter in a rodent cerebral ischemia. *Stroke* **2001,** *32* (9), 2149-2156.

51. Noor, J. I.; Ikeda, T.; Mishima, K.; Aoo, N.; Ohta, S.; Egashira, N.; Iwasaki, K.; Fujiwara, M.; Ikenoue, T., Short-term administration of a new free radical scavenger, edaravone, is more effective than its long-term administration for the treatment of neonatal hypoxic-ischemic encephalopathy. *Stroke* **2005,** *36* (11), 2468-2474.

52. Schmid-Elsaesser, R.; Zausinger, S.; Hungerhuber, E.; Baethmann, A.; Reulen, H. J., Neuroprotective effects of combination therapy with tirilazad and magnesium in rats subjected to reversible focal cerebral ischemia. *Neurosurgery* **1999,** *44* (1), 163-171.

53. Maples, K. R.; Ma, F.; Zhang, Y. K., Comparison of the radical trapping ability of PBN, S-PBN and NXY-059. *Free Radical Res* **2001,** *34* (4), 417-426.

54. Green, A. R.; Shuaib, A., Therapeutic strategies for the treatment of stroke. *Drug Discov Today* **2006,** *11* (15-16), 681-693.

55. Jin, Q.; Cai, Y.; Li, S.; Liu, H. R.; Zhou, X. Y.; Lu, C. Q.; Gao, X. H.; Qian, J.; Zhang, J.; Ju, S. H.; Li, C., Edaravone-Encapsulated Agonistic Micelles Rescue Ischemic Brain Tissue by Tuning Blood-Brain Barrier Permeability. *Theranostics* **2017,** *7* (4), 884-898.

56. Ju, R. K.; Wen, Y. J.; Gou, R. B.; Wang, Y.; Xu, Q. Y., The Experimental Therapy on Brain Ischemia by Improvement of Local Angiogenesis With Tissue Engineering in the Mouse. *Cell Transplant* **2014,** *23*, S83-S95.

57. Wang, Z.; Wang, J.; Jin, Y.; Luo, Z.; Yang, W.; Xie, H. J.; Huang, K.; Wang, L., A Neuroprotective Sericin Hydrogel As an Effective Neuronal Cell Carrier for the Repair of Ischemic Stroke. *Acs Appl Mater Inter* **2015,** *7* (44), 24629-24640.

58. Lampe, K. J.; Heilshorn, S. C., Building stem cell niches from the molecule up through engineered peptide materials. *Neuroscience Letters* **2012,** *519* (2), 138-146.

59. Mura, C.; McAnany, C. E., An introduction to biomolecular simulations and docking. *Mol Simulat* **2014,** *40* (10-11), 732-764.

60. Chang, D. K.; Urry, D. W., Molecular-Dynamics Calculations on Relaxed and Extended States of the Polypentapeptide of Elastin. *Chem Phys Lett* **1988,** *147* (4), 395-400.

61. Leech, J.; Prins, J. F.; Hermans, J., SMD: Visual steering of molecular dynamics for protein design. *Ieee Comput Sci Eng* **1996,** *3* (4), 38-45.

62. MacKerell, A. D.; Bashford, D.; Bellott, M.; Dunbrack, R. L.; Evanseck, J. D.; Field, M. J.; Fischer, S.; Gao, J.; Guo, H.; Ha, S.; Joseph-McCarthy, D.; Kuchnir, L.; Kuczera, K.; Lau, F. T. K.; Mattos, C.; Michnick, S.; Ngo, T.; Nguyen, D. T.; Prodhom, B.; Reiher, W. E.; Roux, B.; Schlenkrich, M.; Smith, J. C.; Stote, R.; Straub, J.; Watanabe, M.; Wiorkiewicz-Kuczera, J.; Yin, D.; Karplus, M., All-atom empirical potential for molecular modeling and dynamics studies of proteins. *J Phys Chem B* **1998,** *102* (18), 3586-3616.

63. Sreerama, N.; Woody, R. W., Molecular dynamics simulations of polypeptide conformations in water: A comparison of alpha, beta, and poly(Pro)II conformations. *Proteins* **1999,** *36* (4), 400-406.

64. Phillips, J. C.; Braun, R.; Wang, W.; Gumbart, J.; Tajkhorshid, E.; Villa, E.; Chipot, C.; Skeel, R. D.; Kale, L.; Schulten, K., Scalable molecular dynamics with NAMD. *J Comput Chem* **2005,** *26* (16), 1781-1802.

65. Popovych, N.; Sun, S.; Ebright, R. H.; Kalodimos, C. G., Dynamically driven protein allostery. *Nature Structural & Molecular Biology* **2006,** *13* (9), 831-838.

66. Zhao, Y.; Kormos, B. L.; Beveridge, D. L.; Baranger, A. M., Molecular dynamics simulation studies of a protein-RNA complex with a selectively modified binding interface. *Biopolymers* **2006,** *81* (4), 256-269.

67. Frembgen-Kesner, T.; Elcock, A. H., Striking Effects of Hydrodynamic Interactions on the Simulated Diffusion and Folding of Proteins. *J Chem Theory Comput* **2009,** *5* (2), 242-256.
68. Li, N. K.; Quiroz, F. G.; Hall, C. K.; Chilkoti, A.; Yingling, Y. G., Molecular Description of the LCST Behavior of an Elastin-Like Polypeptide. *Biomacromolecules* **2014,** *15* (10), 3522-3530.
69. Li, B.; Alonso, D. O. V.; Daggett, V., The molecular basis for the inverse temperature transition of elastin. *J Mol Biol* **2001,** *305* (3), 581-592.
70. Rousseau, R.; Schreiner, E.; Kohlmeyer, A.; Marx, D., Temperature-dependent conformational transitions and hydrogen-bond dynamics of the elastin-like octapeptide GVG(VPGVG): A molecular-dynamics study. *Biophysical Journal* **2004,** *86* (3), 1393-1407.
71. Zhao, B. W.; Li, N. K.; Yingling, Y. G.; Hall, C. K., LCST Behavior is Manifested in a Single Molecule: Elastin-Like polypeptide (VPGVG)n. *Biomacromolecules* **2016,** *17* (1), 111-118.
72. Tarakanova, A.; Huang, W.; Weiss, A. S.; Kaplan, D. L.; Buehler, M. J., Computational smart polymer design based on elastin protein mutability. *Biomaterials* **2017,** *127*, 49-60.
73. Tang, J. D.; McAnany, C. E.; Mura, C.; Lampe, K. J., Toward a Designable Extracellular Matrix: Molecular Dynamics Simulations of an Engineered Laminin-Mimetic, Elastin-Like Fusion Protein. *Biomacromolecules* **2016,** *17* (10), 3222-3233.
74. Keten, S.; Xu, Z. P.; Ihle, B.; Buehler, M. J., Nanoconfinement controls stiffness, strength and mechanical toughness of beta-sheet crystals in silk. *Nat Mater* **2010,** *9* (4), 359-367.
75. Krishnaji, S. T.; Bratzel, G.; Kinahan, M. E.; Kluge, J. A.; Staii, C.; Wong, J. Y.; Buehler, M. J.; Kaplan, D. L., Sequence-Structure-Property Relationships of Recombinant Spider Silk Proteins: Integration of Biopolymer Design, Processing, and Modeling. *Adv Funct Mater* **2013,** *23* (2), 241-253.
76. Fu, I. W.; Markegard, C. B.; Nguyen, H. D., Solvent Effects on Kinetic Mechanisms of Self-Assembly by Peptide Amphiphiles via Molecular Dynamics Simulations. *Langmuir* **2015,** *31* (1), 315-324.
77. Lee, O. S.; Stupp, S. I.; Schatz, G. C., Atomistic Molecular Dynamics Simulations of Peptide Amphiphile Self-Assembly into Cylindrical Nanofibers. *J Am Chem Soc* **2011,** *133* (10), 3677-3683.
78. Tsonchev, S.; Troisi, A.; Schatz, G. C.; Ratner, M. A., All-atom numerical studies of self-assembly of Zwitterionic peptide amphiphiles. *J Phys Chem B* **2004,** *108* (39), 15278-15284.
79. Raspa, A.; Saracino, G. A. A.; Pugliese, R.; Silva, D.; Cigognini, D.; Vescovi, A.; Gelain, F., Complementary Co-assembling Peptides: From In Silico Studies to In Vivo Application. *Adv Funct Mater* **2014,** *24* (40), 6317-6328.
80. Marrink, S. J.; Tieleman, D. P.; Mark, A. E., Molecular dynamics simulation of the kinetics of spontaneous micelle formation. *J Phys Chem B* **2000,** *104* (51), 12165-12173.
81. Henriques, J.; Cragnell, C.; Skepö, M., Molecular Dynamics Simulations of Intrinsically Disordered Proteins: Force Field Evaluation and Comparison with Experiment. *J Chem Theory Comput* **2015,** *11* (7), 3420-3431.
82. Nguyen, H. D.; Hall, C. K., Molecular dynamics simulations of spontaneous fibril formation by random-coil peptides. *P Natl Acad Sci USA* **2004,** *101* (46), 16180-16185.
83. Bond, P. J.; Sansom, M. S. P., Molecular Dynamics simulations of spontaneous micelle formation around membrane proteins. *Biophysical Journal* **2005,** *88* (1), 356a-356a.
84. Saracino, G. A. A.; Gelain, F., Modelling and analysis of early aggregation events of BMHP1-derived self-assembling peptides. *J Biomol Struct Dyn* **2014,** *32* (5), 759-775.
85. Stanzione, F.; Jayaraman, A., Computational Design of Oligopeptide Containing Poly(ethylene glycol) Brushes for Stimuli-Responsive Drug Delivery. *J Phys Chem B* **2015,** *119* (42), 13309-13320.
86. McCullagh, M.; Prytkova, T.; Tonzani, S.; Winter, N. D.; Schatz, G. C., Modeling self-assembly processes driven by nonbonded interactions in soft materials. *J Phys Chem B* **2008,** *112* (34), 10388-10398.
87. Johnston, K.; Harmandaris, V., Hierarchical simulations of hybrid polymer-solid materials. *Soft Matter* **2013,** *9* (29), 6696-6710.
88. Frederix, P. W. J. M.; Scott, G. G.; Abul-Haija, Y. M.; Kalafatovic, D.; Pappas, C. G.; Javid, N.; Hunt, N. T.; Ulijn, R. V.; Tuttle, T., Exploring the sequence space for (tri-) peptide self-assembly to design and discover. *Nature Chemistry* **2015,** *7* (1), 30-37.
89. Dror, Y.; Ziv, T.; Makarov, V.; Wolf, H.; Admon, A.; Zussman, E., Nanofibers Made of Globular Proteins. *Biomacromolecules* **2008,** *9* (10), 2749-2754.
90. Zhang, Y. Z.; Wang, X.; Feng, Y.; Li, J.; Lim, C. T.; Ramakrishna, S., Coaxial electrospinning of (fluorescein isothiocyanate-conjugated bovine serum albumin)-encapsulated poly(epsilon-caprolactone) nanofibers for sustained release. *Biomacromolecules* **2006,** *7* (4), 1049-1057.
91. Dong, B.; Arnoult, O.; Smith, M. E.; Wnek, G. E., Electrospinning of Collagen Nanofiber Scaffolds from Benign Solvents. *Macromol Rapid Comm* **2009,** *30* (7), 539-542.
92. Fischer, R. L.; McCoy, M. G.; Grant, S. A., Electrospinning collagen and hyaluronic acid nanofiber meshes. *J Mater Sci-Mater M* **2012,** *23* (7), 1645-1654.
93. Rui, C.; Mo, X. M.; Ke, Q. F., Fabrication and characterization of thermoplastic polyurethane/collagen blend nanofiber by electrospinning method. *2007 International Forum on Biomedical Textile Materials, Proceedings* **2007**, 144-150.
94. Wnek, G. E.; Carr, M. E.; Simpson, D. G.; Bowlin, G. L., Electrospinning of nanofiber fibrinogen structures. *Nano Lett* **2003,** *3* (2), 213-216.
95. Carlisle, C. R.; Coulais, C.; Namboothiry, M.; Carroll, D. L.; Hantgan, R. R.; Guthold, M., The mechanical properties of individual, electrospun fibrinogen fibers. *Biomaterials* **2009,** *30* (6), 1205-1213.
96. Casper, C. L.; Yang, W. D.; Farach-Carson, M. C.; Rabolt, J. F., Coating electrospun collagen and gelatin fibers with perlecan domain I for increased growth factor binding. *Biomacromolecules* **2007,** *8* (4), 1116-1123.
97. Li, M. Y.; Guo, Y.; Wei, Y.; MacDiarmid, A. G.; Lelkes, P. I., Electrospinning polyaniline-contained gelatin nanofibers for tissue engineering applications. *Biomaterials* **2006,** *27* (13), 2705-2715.
98. Mascharak, S.; Benitez, P. L.; Proctor, A. C.; Madl, C. M.; Hu, K. H.; Dewi, R. E.; Butte, M. J.; Heilshorn, S. C., YAP-dependent mechanotransduction is required for proliferation and migration on native-like substrate topography. *Biomaterials* **2017,** *115*, 155-166.

99. Liu, Y.; Xu, Y. C.; Wang, Z. H.; Wen, D. Z.; Zhang, W. T.; Schmull, S.; Li, H. Y.; Chen, Y.; Xue, S., Electrospun nanofibrous sheets of collagen/elastin/polycaprolactone improve cardiac repair after myocardial infarction. *Am J Transl Res* **2016,** *8* (4), 1678-+.
100. McClure, M. J.; Sell, S. A.; Simpson, D. G.; Walpoth, B. H.; Bowlin, G. L., A three-layered electrospun matrix to mimic native arterial architecture using polycaprolactone, elastin, and collagen: A preliminary study. *Acta Biomaterialia* **2010,** *6* (7), 2422-2433.
101. Zhang, K. H.; Mo, X. M.; Huang, C.; He, C. L.; Wang, H. S., Electrospun scaffolds from silk fibroin and their cellular compatibility. *J Biomed Mater Res A* **2010,** *93a* (3), 976-983.
102. Kim, U. J.; Park, J.; Kim, H. J.; Wada, M.; Kaplan, D. L., Three-dimensional aqueous-derived biomaterial scaffolds from silk fibroin. *Biomaterials* **2005,** *26* (15), 2775-2785.
103. Zhang, H.; Wang, K. F.; Xing, Y. M.; Yu, Q. Z., Lysine-doped polypyrrole/spider silk protein/poly(L-lactic) acid containing nerve growth factor composite fibers for neural application. *Mat Sci Eng C-Mater* **2015,** *56*, 564-573.
104. Maleki, M.; Natalello, A.; Pugliese, R.; Gelain, F., Fabrication of nanofibrous electrospun scaffolds from a heterogeneous library of co- and self-assembling peptides. *Acta Biomaterialia* **2017,** *51*, 268-278.
105. Rho, K. S.; Jeong, L.; Lee, G.; Seo, B. M.; Park, Y. J.; Hong, S. D.; Roh, S.; Cho, J. J.; Park, W. H.; Min, B. M., Electrospinning of collagen nanofibers: Effects on the behavior of normal human keratinocytes and early-stage wound healing. *Biomaterials* **2006,** *27* (8), 1452-1461.
106. Lee, Y. S.; Arinzeh, T. L., Electrospun Nanofibrous Materials for Neural Tissue Engineering. *Polymers-Basel* **2011,** *3* (1), 413-426.
107. Jing, Z.; Xu, X. Y.; Chen, X. S.; Liang, Q. Z.; Bian, X. C.; Yang, L. X.; Jing, X. B., Biodegradable electrospun fibers for drug delivery. *J Control Release* **2003,** *92* (3), 227-231.
108. Sell, S. A.; McClure, M. J.; Garg, K.; Wolfe, P. S.; Bowlin, G. L., Electrospinning of collagen/biopolymers for regenerative medicine and cardiovascular tissue engineering. *Adv Drug Deliver Rev* **2009,** *61* (12), 1007-1019.
109. Abrigo, M.; McArthur, S. L.; Kingshott, P., Electrospun Nanofibers as Dressings for Chronic Wound Care: Advances, Challenges, and Future Prospects. *Macromol Biosci* **2014,** *14* (6), 772-792.
110. Liu, X.; Lin, T.; Fang, J. A.; Yao, G.; Zhao, H. Q.; Dodson, M.; Wang, X. G., In vivo wound healing and antibacterial performances of electrospun nanofibre membranes. *J Biomed Mater Res A* **2010,** *94a* (2), 499-508.
111. Ren, G. L.; Xu, X. H.; Liu, Q.; Cheng, J.; Yuan, X. Y.; Wu, L. L.; Wan, Y. Z., Electrospun poly(vinyl alcohol)/glucose oxidase biocomposite membranes for biosensor applications. *React Funct Polym* **2006,** *66* (12), 1559-1564.
112. El-Moghazy, A. Y.; Soliman, E. A.; Ibrahim, H. Z.; Marty, J. L.; Istamboulie, G.; Noguer, T., Biosensor based on electrospun blended chitosan-poly (vinyl alcohol) nanofibrous enzymatically sensitized membranes for pirimiphosmethyl detection in olive oil. *Talanta* **2016,** *155*, 258-264.
113. Chua, J. S.; Chng, C. P.; Moe, A. A. K.; Tann, J. Y.; Goh, E. L. K.; Chiam, K. H.; Yim, E. K. F., Extending neurites sense the depth of the underlying topography during neuronal differentiation and contact guidance. *Biomaterials* **2014,** *35* (27), 7750-7761.
114. Solanki, A.; Chueng, S. T. D.; Yin, P. T.; Kappera, R.; Chhowalla, M.; Lee, K. B., Axonal Alignment and Enhanced Neuronal Differentiation of Neural Stem Cells on Graphene-Nanoparticle Hybrid Structures. *Adv Mater* **2013,** *25* (38), 5477-5482.
115. Yang, K.; Jung, K.; Ko, E.; Kim, J.; Park, K. I.; Kim, J.; Cho, S. W., Nanotopographical Manipulation of Focal Adhesion Formation for Enhanced Differentiation of Human Neural Stem Cells. *Acs Appl Mater Inter* **2013,** *5* (21), 10529-10540.
116. Dalby, M. J.; Gadegaard, N.; Oreffo, R. O. C., Harnessing nanotopography and integrin-matrix interactions to influence stem cell fate. *Nat Mater* **2014,** *13* (6), 558-569.
117. Xu, T.; Jin, J.; Gregory, C.; Hickman, J. J.; Boland, T., Inkjet printing of viable mammalian cells. *Biomaterials* **2005,** *26* (1), 93-99.
118. Zopf, D. A.; Hollister, S. J.; Nelson, M. E.; Ohye, R. G.; Green, G. E., Bioresorbable Airway Splint Created with a Three-Dimensional Printer. *New Engl J Med* **2013,** *368* (21), 2043-2045.
119. Cui, X. F.; Breitenkamp, K.; Finn, M. G.; Lotz, M.; D'Lima, D. D., Direct Human Cartilage Repair Using Three-Dimensional Bioprinting Technology. *Tissue Eng Pt A* **2012,** *18* (11-12), 1304-1312.
120. Xu, T.; Zhao, W. X.; Zhu, J. M.; Albanna, M. Z.; Yoo, J. J.; Atala, A., Complex heterogeneous tissue constructs containing multiple cell types prepared by inkjet printing technology. *Biomaterials* **2013,** *34* (1), 130-139.
121. Highley, C. B.; Rodell, C. B.; Burdick, J. A., Direct 3D Printing of Shear-Thinning Hydrogels into Self-Healing Hydrogels. *Adv Mater* **2015,** *27* (34), 5075-+.
122. Hsieh, F. Y.; Lin, H. H.; Hsu, S. H., 3D bioprinting of neural stern cell-laden thermoresponsive biodegradable polyurethane hydrogel and potential in central nervous system repair. *Biomaterials* **2015,** *71*, 48-57.
123. Lozano, R.; Stevens, L.; Thompson, B. C.; Gilmore, K. J.; Gorkin, R.; Stewart, E. M.; Panhuis, M. I. H.; Romero-Ortega, M.; Wallace, G. G., 3D printing of layered brain-like structures using peptide modified gellan gum substrates. *Biomaterials* **2015,** *67*, 264-273.
124. Zhu, W.; Harris, B. T.; Zhang, L. J. G., Gelatin Methacrylamide Hydrogel with Graphene Nanoplatelets for Neural Cell-laden 3D Bioprinting. *Ieee Eng Med Bio* **2016**, 4185-4188.
125. DeForest, C. A.; Anseth, K. S., Photoreversible Patterning of Biomolecules within Click-Based Hydrogels. *Angew Chem Int Edit* **2012,** *51* (8), 1816-1819.
126. DeForest, C. A.; Tirrell, D. A., A photoreversible protein-patterning approach for guiding stem cell fate in three-dimensional gels. *Nat Mater* **2015,** *14* (5), 523-531.
127. Marklein, R. A.; Burdick, J. A., Spatially controlled hydrogel mechanics to modulate stem cell interactions. *Soft Matter* **2010,** *6* (1), 136-143.
128. Nichol, J. W.; Koshy, S. T.; Bae, H.; Hwang, C. M.; Yamanlar, S.; Khademhosseini, A., Cell-laden microengineered gelatin methacrylate hydrogels. *Biomaterials* **2010,** *31* (21), 5536-5544.
129. Timashev, P. S.; Vedunova, M. V.; Guseva, D.; Ponimaskin, E.; Deiwick, A.; Mishchenko, T. A.; Mitroshina, E. V.; Koroleva, A. V.; Pimashkin, A. S.; Mukhina, I. V.; Panchenko, V. Y.; Chichkov, B. N.; Bagratashvili, V. N., 3D in vitro platform produced by two-photon polymerization for the analysis of neural network formation and function. *Biomedical Physics & Engineering Express* **2016,** *2* (3), 035001.

130. Lutz, A. B.; Barres, B. A., Contrasting the Glial Response to Axon Injury in the Central and Peripheral Nervous Systems. *Dev Cell* **2014,** *28* (1), 7-17.
131. Lau, L. W.; Cua, R.; Keough, M. B.; Haylock-Jacobs, S.; Yong, V. W., OPINION Pathophysiology of the brain extracellular matrix: a new target for remyelination. *Nat Rev Neurosci* **2013,** *14* (10), 722-729.
132. Allen, N. J.; Barres, B. A., NEUROSCIENCE Glia - more than just brain glue. *Nature* **2009,** *457* (7230), 675-677.
133. Russell, L. N.; Lampe, K. J., Engineering Biomaterials to Influence Oligodendroglial Growth, Maturation, and Myelin Production. *Cells Tissues Organs* **2016,** *202* (1-2), 85-101.
134. Sofroniew, M. V.; Vinters, H. V., Astrocytes: biology and pathology. *Acta Neuropathol* **2010,** *119* (1), 7-35.
135. Zimmermann, D. R.; Dours-Zimmermann, M. T., Extracellular matrix of the central nervous system: from neglect to challenge. *Histochem Cell Biol* **2008,** *130* (4), 635-653.
136. Lampe, K. J.; Mooney, R. G.; Bjugstad, K. B.; Mahoney, M. J., Effect of macromer weight percent on neural cell growth in 2D and 3D nondegradable PEG hydrogel culture. *J Biomed Mater Res A* **2010,** *94a* (4), 1162-1171.
137. Freytes, D. O.; Godier-Furnemont, A.; Duan, Y.; O'Neill, J. D.; Vunjak-Novakovic, G., Biomaterial scaffolds for cardiac regeneration and repair derived from native heart matrix. *Woodh Publ Ser Biom* **2014,** *72*, 201-224.
138. Sirabella, D.; Cimetta, E.; Vunjak-Novakovic, G., "The state of the heart": Recent advances in engineering human cardiac tissue from pluripotent stem cells. *Exp Biol Med* **2015,** *240* (8), 1008-1018.
139. Ott, H. C.; Matthiesen, T. S.; Goh, S. K.; Black, L. D.; Kren, S. M.; Netoff, T. I.; Taylor, D. A., Perfusion-decellularized matrix: using nature's platform to engineer a bioartificial heart. *Nat Med* **2008,** *14* (2), 213-221.
140. Wainwright, J. M.; Czajka, C. A.; Patel, U. B.; Freytes, D. O.; Tobita, K.; Gilbert, T. W.; Badylak, S. F., Preparation of Cardiac Extracellular Matrix from an Intact Porcine Heart. *Tissue Eng Part C-Me* **2010,** *16* (3), 525-532.
141. Lee, J. W. S.; Doumouchtsis, S. K.; Fynes, M. M., A modified technique for the surgical correction of urethral diverticula using a porcine xenograft. *Int Urogynecol J* **2009,** *20* (1), 117-120.
142. Crapo, P. M.; Gilbert, T. W.; Badylak, S. F., An overview of tissue and whole organ decellularization processes. *Biomaterials* **2011,** *32* (12), 3233-3243.
143. Goh, S. K.; Bertera, S.; Olsen, P.; Candiello, J. E.; Halfter, W.; Uechi, G.; Balasubramani, M.; Johnson, S. A.; Sicari, B. M.; Kollar, E.; Badylak, S. F.; Banerjee, I., Perfusion-decellularized pancreas as a natural 3D scaffold for pancreatic tissue and whole organ engineering. *Biomaterials* **2013,** *34* (28), 6760-6772.
144. DeQuach, J. A.; Yuan, S. H.; Goldstein, L. S. B.; Christman, K. L., Decellularized Porcine Brain Matrix for Cell Culture and Tissue Engineering Scaffolds. *Tissue Eng Pt A* **2011,** *17* (21-22), 2583-2592.
145. Nagao, R. J.; Lundy, S.; Khaing, Z. Z.; Schmidt, C. E., Functional characterization of optimized acellular peripheral nerve graft in a rat sciatic nerve injury model. *Neurol Res* **2011,** *33* (6), 600-608.
146. Hudson, T. W.; Zawko, S.; Deister, C.; Lundy, S.; Hu, C. Y.; Lee, K.; Schmidt, C. E., Optimized acellular nerve graft is immunologically tolerated and supports regeneration. *Tissue Eng* **2004,** *10* (11-12), 1641-1651.
147. Oberwallner, B.; Brodarac, A.; Choi, Y. H.; Saric, T.; Anic, P.; Morawietz, L.; Stamm, C., Preparation of cardiac extracellular matrix scaffolds by decellularization of human myocardium. *J Biomed Mater Res A* **2014,** *102* (9), 3263-3272.
148. Uygun, B. E.; Soto-Gutierrez, A.; Yagi, H.; Izamis, M. L.; Guzzardi, M. A.; Shulman, C.; Milwid, J.; Kobayashi, N.; Tilles, A.; Berthiaume, F.; Hertl, M.; Nahmias, Y.; Yarmush, M. L.; Uygun, K., Organ reengineering through development of a transplantable recellularized liver graft using decellularized liver matrix. *Nat Med* **2010,** *16* (7), 814-U120.
149. Nakayama, K. H.; Batchelder, C. A.; Lee, C. I.; Tarantal, A. F., Decellularized Rhesus Monkey Kidney as a Three-Dimensional Scaffold for Renal Tissue Engineering. *Tissue Eng Pt A* **2010,** *16* (7), 2207-2216.
150. Nakayama, K. H.; Lee, C. C. I.; Batchelder, C. A.; Tarantal, A. F., Tissue Specificity of Decellularized Rhesus Monkey Kidney and Lung Scaffolds. *Plos One* **2013,** *8* (5).
151. Ott, H. C.; Clippinger, B.; Conrad, C.; Schuetz, C.; Pomerantseva, I.; Ikonomou, L.; Kotton, D.; Vacanti, J. P., Regeneration and orthotopic transplantation of a bioartificial lung. *Nat Med* **2010,** *16* (8), 927-U131.
152. Cortiella, J.; Niles, J.; Cantu, A.; Brettler, A.; Pham, A.; Vargas, G.; Winston, S.; Wang, J.; Walls, S.; Nichols, J. E., Influence of Acellular Natural Lung Matrix on Murine Embryonic Stem Cell Differentiation and Tissue Formation. *Tissue Eng Pt A* **2010,** *16* (8), 2565-2580.
153. Sood, D.; Chwalek, K.; Stuntz, E.; Pouli, D.; Du, C.; Tang-Schomer, M.; Georgakoudi, I.; Black, L. D.; Kaplan, D. L., Fetal Brain Extracellular Matrix Boosts Neuronal Network Formation in 3D Bioengineered Model of Cortical Brain Tissue. *Acs Biomater Sci Eng* **2016,** *2* (1), 131-140.
154. De Waele, J.; Reekmans, K.; Daans, J.; Berneman, Z.; Ponsaerts, P., 3d Culture of Murine Neural Stem Cells on Decellularized Mouse Brain Sections. *Neuro-Oncology* **2015,** *17*, 16-16.
155. Zhu, T. M.; Tang, Q. S.; Shen, Y. W.; Tang, H. L.; Chen, L. P.; Zhu, J. H., An acellular cerebellar biological scaffold: Preparation, characterization, biocompatibility and effects on neural stem cells. *Brain Res Bull* **2015,** *113*, 48-57.
156. Crapo, P. M.; Tottey, S.; Slivka, P. F.; Badylak, S. F., Effects of Biologic Scaffolds on Human Stem Cells and Implications for CNS Tissue Engineering. *Tissue Eng Pt A* **2014,** *20* (1-2), 313-323.
157. Lynch, K.; Pei, M., Age associated communication between cells and matrix: a potential impact on stem cell-based tissue regeneration strategies. *Organogenesis* **2014,** *10* (3), 289-298.
158. Conboy, I. M.; Rando, T. A., Aging, stem cells and tissue regeneration - Lessons from muscle. *Cell Cycle* **2005,** *4* (3), 407-410.
159. Fitzpatrick, L. E.; McDevitt, T. C., Cell-derived matrices for tissue engineering and regenerative medicine applications. *Biomater Sci* **2015,** *3* (1), 12-24.
160. Miller, M. E.; Miller, B. A.; Shuler, C. F., Comparison of Keratins Extracted from Fixed and Fresh Biopsy Specimens. *J Dent Res* **1990,** *69*, 198-198.
161. Cardamone, J. M., Investigating the microstructure of keratin extracted from wool: Peptide sequence (MALDI-TOF/TOF) and protein conformation (FTIR). *J Mol Struct* **2010,** *969* (1-3), 97-105.

162. Ayutthaya, S. I. N.; Tanpichai, S.; Wootthikanokkhan, J., Keratin Extracted from Chicken Feather Waste: Extraction, Preparation, and Structural Characterization of the Keratin and Keratin/Biopolymer Films and Electrospuns. *J Polym Environ* **2015,** *23* (4), 506-516.
163. Hill, P. S.; Apel, P. J.; Barnwell, J.; Smith, T.; Koman, L. A.; Atala, A.; Van Dyke, M., Repair of Peripheral Nerve Defects in Rabbits Using Keratin Hydrogel Scaffolds. *Tissue Eng Pt A* **2011,** *17* (11-12), 1499-1505.
164. Lin, Y. C.; Marra, K. G., Injectable systems and implantable conduits for peripheral nerve repair. *Biomed Mater* **2012,** *7* (2).
165. Pechter, P. M.; Gil, J.; Valdes, J.; Tomic-Canic, M.; Pastar, I.; Stojadinovic, O.; Kirsner, R. S.; Davis, S. C., Keratin dressings speed epithelialization of deep partial-thickness wounds. *Wound Repair Regen* **2012,** *20* (2), 236-242.
166. Loan, F.; Cassidy, S.; Marsh, C.; Simcock, J., Keratin-based products for effective wound care management in superficial and partial thickness burns injuries. *Burns* **2016,** *42* (3), 541-547.
167. Li, Q. M.; Zhu, L. J.; Liu, R. G.; Huang, D.; Jin, X.; Che, N.; Li, Z.; Qu, X. Z.; Kang, H. L.; Huang, Y., Biological stimuli responsive drug carriers based on keratin for triggerable drug delivery. *J Mater Chem* **2012,** *22* (37), 19964-19973.
168. Srinivasan, B.; Kumar, R.; Shanmugam, K.; Sivagnam, U. T.; Reddy, N. P.; Sehgal, P. K., Porous Keratin Scaffold-Promising Biomaterial for Tissue Engineering and Drug Delivery. *J Biomed Mater Res B* **2010,** *92b* (1), 5-12.
169. Kozlowska, J.; Sionkowska, A.; Skopinska-Wisniewska, J.; Piechowicz, K., Northern pike (Esox lucius) collagen: Extraction, characterization and potential application. *Int J Biol Macromol* **2015,** *81*, 220-227.
170. Cersoy, S.; Zazzo, A.; Lebon, M.; Rofes, J.; Zirah, S., Collagen Extraction and Stable Isotope Analysis of Small Vertebrate Bones: A Comparative Approach. *Radiocarbon* **2017,** *59* (3), 679-694.
171. Rodriguez, F.; Moran, L.; Gonzalez, G.; Troncoso, E.; Zuniga, R. N., Collagen extraction from mussel byssus: a new marine collagen source with physicochemical properties of industrial interest. *J Food Sci Tech Mys* **2017,** *54* (5), 1228-1238.
172. Watanabe, K.; Nakamura, M.; Okano, H.; Toyama, Y., Establishment of three-dimensional culture of neural stem/progenitor cells in collagen Type-1 Gel. *Restor Neurol Neuros* **2007,** *25* (2), 109-117.
173. Guggenberger, C.; Wolz, C.; Heesemann, J., Growth behavior and interaction of Staphylococcus aureus with neutrophils in a three-dimensional collagen gel as a tissue-like infection model. *Int J Med Microbiol* **2011,** *301*, 85-85.
174. Khan, S. Z.; Kokubu, E.; Matsuzaka, K.; Inoue, T., Behaviour of rat-cultured dental pulp cells in three-dimensional collagen type-1 gel in vitro and in vivo. *Aust Endod J* **2013,** *39* (3), 137-145.
175. Wei, S.; Chuang, C.; Chen, Y., Tuning Three-dimensional Collagen Gel Stiffness Independently Modulates Endothelial Cell Behavior. *Tissue Eng Pt A* **2015,** *21*, S12-S12.
176. Peterova, E.; Mrkvicova, A.; Podmolikova, L.; Rezacova, M.; Kanta, J., The Role of Cytokines TGF-beta 1 and FGF-1 in the Expression of Characteristic Markers of Rat Liver Myofibroblasts Cultured in Three-Dimensional Collagen Gel. *Physiol Res* **2016,** *65* (4), 661-672.
177. Ramshaw, J. A. M.; Peng, Y. Y.; Glattauer, V.; Werkmeister, J. A., Collagens as biomaterials. *J Mater Sci-Mater M* **2009,** *20*, 3-8.
178. Aigner, T.; Stove, J., Collagens - major component of the physiological cartilage matrix, major target of cartilage degeneration, major tool in cartilage repair. *Adv Drug Deliver Rev* **2003,** *55* (12), 1569-1593.
179. Verdu, E.; Labrador, R. O.; Rodriguez, F. J.; Ceballos, D.; Fores, J.; Navarro, X., Alignment of collagen and laminin-containing gels improve nerve regeneration within silicone tubes. *Restor Neurol Neuros* **2002,** *20* (5), 169-179.
180. Hamann, M. C. J.; Tator, C. H.; Shoichet, M. S., Injectable intrathecal delivery system for localized administration of EGF and FGF-2 to the injured rat spinal cord. *Exp Neurol* **2005,** *194* (1), 106-119.
181. Matsuse, D.; Kitada, M.; Ogura, F.; Wakao, S.; Kohama, M.; Kira, J.; Tabata, Y.; Dezawa, M., Combined Transplantation of Bone Marrow Stromal Cell-Derived Neural Progenitor Cells with a Collagen Sponge and Basic Fibroblast Growth Factor Releasing Microspheres Enhances Recovery After Cerebral Ischemia in Rats. *Tissue Eng Pt A* **2011,** *17* (15-16), 1993-2004.
182. Yu, H. W.; Cao, B.; Feng, M. Y.; Zhou, Q.; Sun, X. D.; Wu, S. L.; Jin, S. Z.; Liu, H. W.; Jin, L. H., Combinated Transplantation of Neural Stem Cells and Collagen Type I Promote Functional Recovery After Cerebral Ischemia in Rats. *Anat Rec* **2010,** *293* (5), 911-917.
183. Struzyna, L. A.; Wolf, J. A.; Mietus, C. J.; Adewole, D. O.; Chen, H. I.; Smith, D. H.; Cullen, D. K., Rebuilding Brain Circuitry with Living Micro-Tissue Engineered Neural Networks. *Tissue Eng Pt A* **2015,** *21* (21-22), 2744-2756.
184. Simionescua, D. T.; Lua, Q. J.; Song, Y.; Lee, J. S.; Rosenbalm, T. N.; Kelley, C.; Vyavahare, N. R., Biocompatibility and remodeling potential of pure arterial elastin and collagen scaffolds. *Biomaterials* **2006,** *27* (5), 702-713.
185. Jang, J.; Ko, J.; Cho, D. W.; Jun, M. B. G.; Kim, D. H., Elastin-sprayed tubular scaffolds with microstructures and nanotextures for vascular tissue engineering. *Proceedings of the Asme Summer Bioengineering Conference - 2013, Pt A* **2014**.
186. Chuang, T. H.; Stabler, C.; Simionescu, A.; Simionescu, D. T., Polyphenol-Stabilized Tubular Elastin Scaffolds for Tissue Engineered Vascular Grafts. *Tissue Eng Pt A* **2009,** *15* (10), 2837-2851.
187. Kurane, A.; Simionescu, D. T.; Vyavahare, N. R., In vivo cellular repopulation of tubular elastin scaffolds mediated by basic fibroblast growth factor. *Biomaterials* **2007,** *28* (18), 2830-2838.
188. Reddel, C. J.; Cultrone, D.; Rnjak-Kovacina, J.; Weiss, A. S.; Burgess, J. K., Tropoelastin modulates TGF-beta 1-induced expression of VEGF and CTGF in airway smooth muscle cells. *Matrix Biol* **2013,** *32* (7-8), 407-413.
189. Rodgers, U. R.; Weiss, A. S., Cellular interactions with elastin. *Pathol Biol (Paris)* **2005,** *53* (7), 390-8.
190. Hinek, A., Nature and the multiple functions of the 67-kD elastin-/laminin binding protein. *Cell Adhes Commun* **1994,** *2* (3), 185-93.
191. Mithieux, S. M.; Wise, S. G.; Raftery, M. J.; Starcher, B.; Weiss, A. S., A model two-component system for studying the architecture of elastin assembly in vitro. *J Struct Biol* **2005,** *149* (3), 282-9.
192. Mithieux, S. M.; Rasko, J. E.; Weiss, A. S., Synthetic elastin hydrogels derived from massive elastic assemblies of self-organized human protein monomers. *Biomaterials* **2004,** *25* (20), 4921-7.
193. Vepari, C.; Kaplan, D. L., Silk as a biomaterial. *Prog Polym Sci* **2007,** *32* (8-9), 991-1007.

194. Roloff, F.; Strauss, S.; Vogt, P. M.; Bicker, G.; Radtke, C., Spider Silk as Guiding Biomaterial for Human Model Neurons. *Biomed Res Int* **2014**.
195. Huang, W.; Begum, R.; Barber, T.; Ibba, V.; Tee, N. C. H.; Hussain, M.; Arastoo, M.; Yang, Q.; Robson, L. G.; Lesage, S.; Gheysens, T.; Skaer, N. J. V.; Knight, D. P.; Priestley, J. V., Regenerative potential of silk conduits in repair of peripheral nerve injury in adult rats. *Biomaterials* **2012,** *33* (1), 59-71.
196. Radtke, C.; Allmeling, C.; Waldmann, K. H.; Reimers, K.; Thies, K.; Schenk, H. C.; Hillmer, A.; Guggenheim, M.; Brandes, G.; Vogt, P. M., Spider Silk Constructs Enhance Axonal Regeneration and Remyelination in Long Nerve Defects in Sheep. *Plos One* **2011,** *6* (2).
197. Wittmer, C. R.; Claudepierre, T.; Reber, M.; Wiedemann, P.; Garlick, J. A.; Kaplan, D.; Egles, C., Multifunctionalized Electrospun Silk Fibers Promote Axon Regeneration in the Central Nervous System. *Adv Funct Mater* **2011,** *21* (22), 4232-4242.
198. Bai, S. M.; Zhang, W. M.; Lu, Q.; Ma, Q. H.; Kaplanad, D. L.; Zhu, H. S., Silk nanofiber hydrogels with tunable modulus to regulate nerve stem cell fate. *J Mater Chem B* **2014,** *2* (38), 6590-6600.
199. Tang-Schomer, M. D.; White, J. D.; Tien, L. W.; Schmitt, L. I.; Valentin, T. M.; Graziano, D. J.; Hopkins, A. M.; Omenetto, F. G.; Haydon, P. G.; Kaplan, D. L., Bioengineered functional brain-like cortical tissue. *P Natl Acad Sci USA* **2014,** *111* (38), 13811-13816.
200. Chwalek, K.; Tang-Schomer, M. D.; Omenetto, F. G.; Kaplan, D. L., In vitro bioengineered model of cortical brain tissue. *Nat Protoc* **2015,** *10* (9), 1362-1388.
201. Mosesson, M. W.; Siebenlist, K. R.; Meh, D. A., The structure and biological features of fibrinogen and fibrin. *Fibrinogen* **2001,** *936*, 11-30.
202. Sakiyama-Elbert, S. E.; Hubbell, J. A., Development of fibrin derivatives for controlled release of heparin-binding growth factors. *J Control Release* **2000,** *65* (3), 389-402.
203. Urech, L.; Bittermann, A. G.; Hubbell, J. A.; Hall, H., Mechanical properties, proteolytic degradability and biological modifications affect angiogenic process extension into native and modified fibrin matrices in vitro. *Biomaterials* **2005,** *26* (12), 1369-1379.
204. Bruns, H.; Kneser, U.; Holzhuter, S.; Roth, B.; Kluth, J.; Kaufmann, P. M.; Kluth, D.; Fiegel, H. C., Injectable liver: A novel approach using fibrin gel as a matrix for culture and intrahepatic transplantation of hepatocytes. *Tissue Eng* **2005,** *11* (11-12), 1718-1726.
205. Eyrich, D.; Brandl, F.; Appel, B.; Wiese, H.; Maier, G.; Wenzel, M.; Staudenmaier, R.; Goepferich, A.; Blunk, T., Long-term stable fibrin gels for cartilage engineering. *Biomaterials* **2007,** *28* (1), 55-65.
206. Chung, Y. I.; Ahn, K. M.; Jeon, S. H.; Lee, S. Y.; Lee, J. H.; Tae, G., Enhanced bone regeneration with BMP-2 loaded functional nanoparticle-hydrogel complex. *J Control Release* **2007,** *121* (1-2), 91-99.
207. Wood, M. D.; MacEwan, M. R.; French, A. R.; Moore, A. M.; Hunter, D. A.; Mackinnon, S. E.; Moran, D. W.; Borschel, G. H.; Sakiyama-Elbert, S. E., Fibrin Matrices With Affinity-Based Delivery Systems and Neurotrophic Factors Promote Functional Nerve Regeneration. *Biotechnol Bioeng* **2010,** *106* (6), 970-979.
208. Johnson, P. J.; Parker, S. R.; Sakiyama-Elbert, S. E., Fibrin-based tissue engineering scaffolds enhance neural fiber sprouting and delay the accumulation of reactive astrocytes at the lesion in a subacute model of spinal cord injury. *J Biomed Mater Res A* **2010,** *92a* (1), 152-163.
209. McCreedy, D. A.; Wilems, T. S.; Xu, H.; Butts, J. C.; Brown, C. R.; Smith, A. W.; Sakiyama-Elbert, S. E., Survival, differentiation, and migration of high-purity mouse embryonic stem cell-derived progenitor motor neurons in fibrin scaffolds after sub-acute spinal cord injury. *Biomater Sci-Uk* **2014,** *2* (11), 1672-1682.
210. Sakiyama, S. E.; Schense, J. C.; Hubbell, J. A., Incorporation of heparin-binding peptides into fibrin gels enhances neurite extension: an example of designer matrices in tissue engineering. *Faseb J* **1999,** *13* (15), 2214-2224.
211. Johnson, P. J.; Tatara, A.; Shiu, A.; Sakiyama-Elbert, S. E., Controlled Release of Neurotrophin-3 and Platelet-Derived Growth Factor From Fibrin Scaffolds Containing Neural Progenitor Cells Enhances Survival and Differentiation Into Neurons in a Subacute Model of SCI. *Cell Transplant* **2010,** *19* (1), 89-101.
212. Thomopoulos, S.; Kim, H. M.; Das, R.; Silva, M. J.; Sakiyama-Elbert, S.; Amiel, D.; Gelberman, R. H., The Effects of Exogenous Basic Fibroblast Growth Factor on Intrasynovial Flexor Tendon Healing in a Canine Model. *J Bone Joint Surg Am* **2010,** *92a* (13), 2285-2293.
213. Johnson, P. J.; Parker, S. R.; Sakiyama-Elbert, S. E., Controlled Release of Neurotrophin-3 From Fibrin-Based Tissue Engineering Scaffolds Enhances Neural Fiber Sprouting Following Subacute Spinal Cord Injury. *Biotechnol Bioeng* **2009,** *104* (6), 1207-1214.
214. Sharp, K. G.; Dickson, A. R.; Marchenko, S. A.; Yee, K. M.; Emery, P. N.; Laidmae, I.; Uibo, R.; Sawyer, E. S.; Steward, O.; Flanagan, L. A., Salmon fibrin treatment of spinal cord injury promotes functional recovery and density of serotonergic innervation. *Exp Neurol* **2012,** *235* (1), 345-56.
215. Ju, Y. E.; Janmey, P. A.; McCormick, M. E.; Sawyer, E. S.; Flanagan, L. A., Enhanced neurite growth from mammalian neurons in three-dimensional salmon fibrin gels. *Biomaterials* **2007,** *28* (12), 2097-2108.
216. Dandurand, J.; Samouillan, V.; Lacabanne, C.; Pepe, A.; Bochicchio, B., Water structure and elastin-like peptide aggregation A differential calorimetric approach. *J Therm Anal Calorim* **2015,** *120* (1), 419-426.
217. Li, B.; Alonso, D. O. V.; Bennion, B. J.; Daggett, V., Hydrophobic hydration is an important source of elasticity in elastin-based biopolymers. *J Am Chem Soc* **2001,** *123* (48), 11991-11998.
218. Urry, D. W., Physical chemistry of biological free energy transduction as demonstrated by elastic protein-based polymers. *J Phys Chem B* **1997,** *101* (51), 11007-11028.
219. Reguera, J.; Urry, D. W.; Parker, T. M.; McPherson, D. T.; Rodriguez-Cabello, J. C., Effect of NaCl on the exothermic and endothermic components of the inverse temperature transition of a model elastin-like polymer. *Biomacromolecules* **2007,** *8* (2), 354-358.
220. Straley, K. S.; Heilshorn, S. C., Design and adsorption of modular engineered proteins to prepare customized, neuron-compatible coatings. *Front Neuroengineering* **2009,** *2*, 1-10.
221. Straley, K. S.; Heilshorn, S. C., Independent tuning of multiple biomaterial properties using protein engineering. *Soft Matter* **2009,** *5* (1), 114-124.

222. Chung, C.; Lampe, K. J.; Heilshorn, S. C., Tetrakis(hydroxymethyl) Phosphonium Chloride as a Covalent Cross-Linking Agent for Cell Encapsulation within Protein-Based Hydrogels. *Biomacromolecules* **2012,** *13* (12), 3912-3916.
223. Lampe, K. J.; Antaris, A. L.; Heilshorn, S. C., Design of three-dimensional engineered protein hydrogels for tailored control of neurite growth. *Acta Biomaterialia* **2013,** *9* (3), 5590-5599.
224. Madl, C. M.; Katz, L. M.; Heilshorn, S. C., Bio-Orthogonally Crosslinked, Engineered Protein Hydrogels with Tunable Mechanics and Biochemistry for Cell Encapsulation. *Adv Funct Mater* **2016,** *26* (21), 3612-3620.
225. Johnson, T.; Koria, P., Expression and Purification of Neurotrophin-Elastin-Like Peptide Fusion Proteins for Neural Regeneration. *Biodrugs* **2016,** *30* (2), 117-127.
226. Hu, X.; Tang-Schomer, M. D.; Huang, W. W.; Xia, X. X.; Weiss, A. S.; Kaplan, D. L., Charge-Tunable Autoclaved Silk-Tropoelastin Protein Alloys That Control Neuron Cell Responses. *Adv Funct Mater* **2013,** *23* (31), 3875-3884.
227. Sun, W.; Incitti, T.; Migliaresi, C.; Quattrone, A.; Casarosa, S.; Motta, A., Viability and neuronal differentiation of neural stem cells encapsulated in silk fibroin hydrogel functionalized with an IKVAV peptide. *J Tissue Eng Regen M* **2017,** *11* (5), 1532-1541.
228. Banwell, E. F.; Abelardo, E. S.; Adams, D. J.; Birchall, M. A.; Corrigan, A.; Donald, A. M.; Kirkland, M.; Serpell, L. C.; Butler, M. F.; Woolfson, D. N., Rational design and application of responsive alpha-helical peptide hydrogels. *Nat Mater* **2009,** *8* (7), 596-600.
229. Fischer, S. E.; Liu, X. Y.; Mao, H. Q.; Harden, J. L., Controlling cell adhesion to surfaces via associating bioactive triblock proteins. *Biomaterials* **2007,** *28* (22), 3325-3337.
230. Foo, C. T. S. W. P.; Lee, J. S.; Mulyasasmita, W.; Parisi-Amon, A.; Heilshorn, S. C., Two-component protein-engineered physical hydrogels for cell encapsulation. *P Natl Acad Sci USA* **2009,** *106* (52), 22067-22072.
231. Merrifield, R. B., Solid Phase Peptide Synthesis. I. The Synthesis of a Tetrapeptide. *J Am Chem Soc* **1963,** *85* (14), 2149-2154.
232. Carpino, L. A.; Han, G. Y., 9-Fluorenylmethoxycarbonyl Function, a New Base-Sensitive Amino-Protecting Group. *J Am Chem Soc* **1970,** *92* (19), 5748-&.
233. Lutolf, M. P.; Lauer-Fields, J. L.; Schmoekel, H. G.; Metters, A. T.; Weber, F. E.; Fields, G. B.; Hubbell, J. A., Synthetic matrix metalloproteinase-sensitive hydrogels for the conduction of tissue regeneration: Engineering cell-invasion characteristics. *P Natl Acad Sci USA* **2003,** *100* (9), 5413-5418.
234. Patterson, J.; Hubbell, J. A., Enhanced proteolytic degradation of molecularly engineered PEG hydrogels in response to MMP-1 and MMP-2. *Biomaterials* **2010,** *31* (30), 7836-7845.
235. Tokatlian, T.; Shrum, C. T.; Kadoya, W. M.; Segura, T., Protease degradable tethers for controlled and cell-mediated release of nanoparticles in 2-and 3-dimensions. *Biomaterials* **2010,** *31* (31), 8072-8080.
236. Bellis, S. L., Advantages of RGD peptides for directing cell association with biomaterials. *Biomaterials* **2011,** *32* (18), 4205-4210.
237. Wang, A. Y.; Leong, S.; Liang, Y. C.; Huang, R. C. C.; Chen, C. S.; Yu, S. M., Immobilization of Growth Factors on Collagen Scaffolds Mediated by Polyanionic Collagen Mimetic Peptides and Its Effect on Endothelial Cell Morphogenesis. *Biomacromolecules* **2008,** *9* (10), 2929-2936.
238. Rothenfluh, D. A.; Bermudez, H.; O'Neil, C. P.; Hubbell, J. A., Biofunctional polymer nanoparticles for intra-articular targeting and retention in cartilage. *Nat Mater* **2008,** *7* (3), 248-254.
239. Chen, T. T.; Luque, A.; Lee, S.; Anderson, S. M.; Segura, T.; Iruela-Arispe, M. L., Anchorage of VEGF to the extracellular matrix conveys differential signaling responses to endothelial cells. *J Cell Biol* **2010,** *188* (4), 595-609.
240. Lesauteur, L.; Wei, L.; Gibbs, B. F.; Saragovi, H. U., Small Peptide Mimics of Nerve Growth-Factor Bind Trka Receptors and Affect Biological Responses. *J Biol Chem* **1995,** *270* (12), 6564-6569.
241. Martino, M. M.; Hubbell, J. A., The 12th-14th type III repeats of fibronectin function as a highly promiscuous growth factor-binding domain. *Faseb J* **2010,** *24* (12), 4711-4721.
242. Zhang, S. G.; Holmes, T.; Lockshin, C.; Rich, A., SPONTANEOUS ASSEMBLY OF A SELF-COMPLEMENTARY OLIGOPEPTIDE TO FORM A STABLE MACROSCOPIC MEMBRANE. *P Natl Acad Sci USA* **1993,** *90* (8), 3334-3338.
243. Schneider, J. P., Responsive hydrogels from the intramolecular folding and self-assembly of a designed peptide. *Abstr Pap Am Chem S* **2003,** *225*, U321-U321.
244. Rajagopal, K.; Ozbas, B.; Pochan, D. J.; Schneider, J. P., Self-assembly of beta hairpin peptides to hydrogels and tuning of material properties by design of turn sequence. *Abstr Pap Am Chem S* **2004,** *228*, U68-U68.
245. Ozbas, B.; Kretsinger, J.; Rajagopal, K.; Schneider, J. P.; Pochan, D. J., Salt-triggered peptide folding and consequent self-assembly into hydrogels with tunable modulus. *Macromolecules* **2004,** *37* (19), 7331-7337.
246. Dong, H.; Paramonov, S. E.; Aulisa, L.; Bakota, E. L.; Hartgerink, J. D., Self-assembly of multidomain peptides: Balancing molecular frustration controls conformation and nanostructure. *J Am Chem Soc* **2007,** *129* (41), 12468-12472.
247. Webber, M. J.; Tongers, J.; Newcomb, C. J.; Marquardt, K. T.; Bauersachs, J.; Losordo, D. W.; Stupp, S. I., Supramolecular nanostructures that mimic VEGF as a strategy for ischemic tissue repair. *P Natl Acad Sci USA* **2011,** *108* (33), 13438-13443.
248. Perez, C. M. R.; Stephanopoulos, N.; Sur, S.; Lee, S. S.; Newcomb, C.; Stupp, S. I., The Powerful Functions of Peptide-Based Bioactive Matrices for Regenerative Medicine. *Ann Biomed Eng* **2015,** *43* (3), 501-514.
249. Stephanopoulos, N.; Ortony, J. H.; Stupp, S. I., Self-assembly for the synthesis of functional biomaterials. *Acta Mater* **2013,** *61* (3), 912-930.
250. Tavakol, S.; Musavi, S. M. M.; Tavakol, B.; Hoveizi, E.; Ai, J.; Rezayat, S. M., Noggin Along with a Self-Assembling Peptide Nanofiber Containing Long Motif of Laminin Induces Tyrosine Hydroxylase Gene Expression. *Mol Neurobiol* **2017,** *54* (6), 4609-4616.
251. Holmes, T. C.; de Lacalle, S.; Su, X.; Liu, G. S.; Rich, A.; Zhang, S. G., Extensive neurite outgrowth and active synapse formation on self-assembling peptide scaffolds. *P Natl Acad Sci USA* **2000,** *97* (12), 6728-6733.
252. Koutsopoulos, S.; Zhang, S. G., Long-term three-dimensional neural tissue cultures in functionalized self-assembling peptide hydrogels, Matrigel and Collagen I. *Acta Biomaterialia* **2013,** *9* (2), 5162-5169.
253. Cheng, T. Y.; Chen, M. H.; Chang, W. H.; Huang, M. Y.; Wang, T. W., Neural stem cells encapsulated in a functionalized self-assembling peptide hydrogel for brain tissue engineering. *Biomaterials* **2013,** *34* (8), 2005-2016.

254. Liu, X.; Wang, X. M.; Horii, A.; Wang, X. J.; Qiao, L.; Zhang, S. G.; Cui, F. Z., In vivo studies on angiogenic activity of two designer self-assembling peptide scaffold hydrogels in the chicken embryo chorioallantoic membrane. *Nanoscale* **2012,** *4* (8), 2720-2727.
255. Silva, G. A.; Czeisler, C.; Niece, K. L.; Beniash, E.; Harrington, D. A.; Kessler, J. A.; Stupp, S. I., Selective differentiation of neural progenitor cells by high-epitope density nanofibers. *Science* **2004,** *303* (5662), 1352-1355.
256. Tysseling-Mattiace, V. M.; Sahni, V.; Niece, K. L.; Birch, D.; Czeisler, C.; Fehlings, M. G.; Stupp, S. I.; Kessler, J. A., Self-assembling nanofibers inhibit glial scar formation and promote axon elongation after spinal cord injury. *J Neurosci* **2008,** *28* (14), 3814-3823.
257. Tysseling, V. M.; Sahni, V.; Pashuck, E. T.; Birch, D.; Hebert, A.; Czeisler, C.; Stupp, S. I.; Kessler, J. A., Self-Assembling Peptide Amphiphile Promotes Plasticity of Serotonergic Fibers Following Spinal Cord Injury. *J Neurosci Res* **2010,** *88* (14), 3161-3170.
258. Yang, C. Y.; Song, B. B.; Ao, Y.; Nowak, A. P.; Abelowitz, R. B.; Korsak, R. A.; Havton, L. A.; Deming, T. J.; Sofroniew, M. V., Biocompatibility of amphiphilic diblock copolypeptide hydrogels in the central nervous system. *Biomaterials* **2009,** *30* (15), 2881-2898.
259. Das, S.; Zhou, K.; Ghosh, D.; Jha, N. N.; Singh, P. K.; Jacob, R. S.; Bernard, C. C.; Finkelstein, D. I.; Forsythe, J. S.; Maji, S. K., Implantable amyloid hydrogels for promoting stem cell differentiation to neurons. *Npg Asia Mater* **2016,** *8*.
260. Iwasaki, M.; Wilcox, J. T.; Nishimura, Y.; Zweckberger, K.; Suzuki, H.; Wang, J.; Liu, Y.; Karadimas, S. K.; Fehlings, M. G., Synergistic effects of self-assembling peptide and neural stem/progenitor cells to promote tissue repair and forelimb functional recovery in cervical spinal cord injury. *Biomaterials* **2014,** *35* (9), 2617-2629.
261. Veronese, F. M.; Mero, A., The impact of PEGylation on biological therapies. *Biodrugs* **2008,** *22* (5), 315-329.
262. Berkovitch, Y.; Yelin, D.; Seliktar, D., Photo-patterning PEG-based hydrogels for neuronal engineering. *Eur Polym J* **2015,** *72*, 473-483.
263. Sarig-Nadir, O.; Livnat, N.; Zajdman, R.; Shoham, S.; Seliktar, D., Laser Photoablation of Guidance Microchannels into Hydrogels Directs Cell Growth in Three Dimensions. *Biophysical Journal* **2009,** *96* (11), 4743-4752.
264. Freudenberg, U.; Hermann, A.; Welzel, P. B.; Stirl, K.; Schwarz, S. C.; Grimmer, M.; Zieris, A.; Panyanuwat, W.; Zschoche, S.; Meinhold, D.; Storch, A.; Werner, C., A star-PEG-heparin hydrogel platform to aid cell replacement therapies for neurodegenerative diseases. *Biomaterials* **2009,** *30* (28), 5049-5060.
265. Burdick, J. A.; Prestwich, G. D., Hyaluronic Acid Hydrogels for Biomedical Applications. *Adv Mater* **2011,** *23* (12), H41-H56.
266. Wang, Y. F.; Cooke, M. J.; Morshead, C. M.; Shoichet, M. S., Hydrogel delivery of erythropoietin to the brain for endogenous stem cell stimulation after stroke injury. *Biomaterials* **2012,** *33* (9), 2681-2692.
267. Lv, W.; Li, W. Y.; Xu, X. Y.; Jiang, H.; Bang, O. Y., Bone marrow mesenchymal stem cells transplantation promotes the release of endogenous erythropoietin after ischemic stroke. *Neural Regen Res* **2015,** *10* (8), 1265-1270.
268. Zhong, J.; Chan, A.; Morad, L.; Kornblum, H. I.; Fan, G. P.; Carmichael, S. T., Hydrogel Matrix to Support Stem Cell Survival After Brain Transplantation in Stroke. *Neurorehab Neural Re* **2010,** *24* (7), 636-644.
269. Moshayedi, P.; Nih, L. R.; Llorente, I. L.; Berg, A. R.; Cinkornpumin, J.; Lowry, W. E.; Segura, T.; Carmichael, S. T., Systematic optimization of an engineered hydrogel allows for selective control of human neural stem cell survival and differentiation after transplantation in the stroke brain. *Biomaterials* **2016,** *105*, 145-155.
270. Bible, E.; Qutachi, O.; Chau, D. Y. S.; Alexander, M. R.; Shakesheff, K. M.; Modo, M., Neo-vascularization of the stroke cavity by implantation of human neural stem cells on VEGF-releasing PLGA microparticles. *Biomaterials* **2012,** *33* (30), 7435-+.
271. Mdzinarishvili, A.; Sutariya, V.; Talasila, P. K.; Geldenhuys, W. J.; Sadana, P., Engineering triiodothyronine (T3) nanoparticle for use in ischemic brain stroke. *Drug Deliv Transl Re* **2013,** *3* (4), 309-317.
272. Klock, G.; Pfeffermann, A.; Ryser, C.; Grohn, P.; Kuttler, B.; Hahn, H. J.; Zimmermann, U., Biocompatibility of mannuronic acid-rich alginates. *Biomaterials* **1997,** *18* (10), 707-713.
273. Emerich, D. F.; Silva, E.; Ali, O.; Mooney, D.; Bell, W.; Yu, S. J.; Kaneko, Y.; Borlongan, C., Injectable VEGF Hydrogels Produce Near Complete Neurological and Anatomical Protection Following Cerebral Ischemia in Rats. *Cell Transplant* **2010,** *19* (9), 1063-1071.
274. Anderson, E. M.; Silva, E. A.; Hao, Y. B.; Martinick, K. D.; Vermillion, S. A.; Stafford, A. G.; Doherty, E. G.; Wang, L.; Doherty, E. J.; Grossman, P. M.; Mooney, D. J., VEGF and IGF Delivered from Alginate Hydrogels Promote Stable Perfusion Recovery in Ischemic Hind Limbs of Aged Mice and Young Rabbits. *J Vasc Res* **2017,** *54* (5), 288-298.
275. Yao, L.; Daly, W.; Newland, B.; Yao, S.; Wang, W.; Chen, B. K. K.; Madigan, N.; Windebank, A.; Pandit, A., Improved axonal regeneration of transected spinal cord mediated by multichannel collagen conduits functionalized with neurotrophin-3 gene. *Gene Ther* **2013,** *20* (12), 1149-1157.
276. Fan, C. X.; Li, X.; Xiao, Z. F.; Zhao, Y. N.; Liang, H.; Wang, B.; Han, S. F.; Li, X. R.; Xu, B.; Wang, N.; Liu, S. M.; Xue, W. W.; Dai, J. W., A modified collagen scaffold facilitates endogenous neurogenesis for acute spinal cord injury repair. *Acta Biomaterialia* **2017,** *51*, 304-316.
277. Masand, S. N.; Perron, I. J.; Schachner, M.; Shreiber, D. I., Neural cell type-specific responses to glycomimetic functionalized collagen. *Biomaterials* **2012,** *33* (3), 790-797.
278. Winter, C. C.; Katiyar, K. S.; Hernandez, N. S.; Song, Y. J.; Struzyna, L. A.; Harris, J. P.; Cullen, D. K., Transplantable living scaffolds comprised of micro-tissue engineered aligned astrocyte networks to facilitate central nervous system regeneration. *Acta Biomaterialia* **2016,** *38*, 44-58.
279. Welker, P.; MullerRover, S.; Tokura, Y.; Bolchkarev, V.; Paus, R., Topobiology of the hair follicle .2. Expression of cell-adhesion molecules during hair follicle cycling. *J Invest Dermatol* **1996,** *107* (3), 245-245.
280. Sierpinski, P.; Garrett, J.; Ma, J.; Apel, P.; Klorig, D.; Smith, T.; Koman, L. A.; Atala, A.; Van Dyke, M., The use of keratin biomaterials derived from human hair for the promotion of rapid regeneration of peripheral nerves. *Biomaterials* **2008,** *29* (1), 118-128.
281. Pace, L. A.; Plate, J. F.; Smith, T. L.; Van Dyke, M. E., The effect of human hair keratin hydrogel on early cellular response to sciatic nerve injury in a rat model. *Biomaterials* **2013,** *34* (24), 5907-5914.
282. Barros, D.; Amaral, I. F.; Pego, A. P., Biomimetic Synthetic Self-Assembled Hydrogels for Cell Transplantation. *Curr Top Med Chem* **2015,** *15* (13), 1209-1226.

283. Koutsopoulos, S.; Zhang, S. G., Two-layered injectable self-assembling peptide scaffold hydrogels for long-term sustained release of human antibodies. *J Control Release* **2012,** *160* (3), 451-458.
284. Kandalam, S.; Sindji, L.; Delcroix, G. J. R.; Violet, F.; Garric, X.; Andre, E. M.; Schiller, P. C.; Venier-Julienne, M. C.; des Rieux, A.; Guicheux, J.; Montero-Menei, C. N., Pharmacologically active microcarriers delivering BDNF within a hydrogel: Novel strategy for human bone marrow-derived stem cells neural neuronal differentiation guidance and therapeutic secretome enhancement. *Acta Biomaterialia* **2017,** *49*, 167-180.
285. Piscioneri, A.; Morelli, S.; Mele, M.; Canonaco, M.; Bilotta, E.; Pantano, P.; Drioli, E.; De Bartolo, L., Neuroprotective effect of human mesenchymal stem cells in a compartmentalized neuronal membrane system. *Acta Biomaterialia* **2015,** *24*, 297-308.
286. Yeng, C. H.; Chen, P. J.; Chang, H. K.; Lo, W. Y.; Wu, C. C.; Chang, C. Y.; Chou, C. H.; Chen, S. H., Attenuating spinal cord injury by conditioned medium from human umbilical cord blood-derived CD34(+) cells in rats. *Taiwan J Obstet Gyne* **2016,** *55* (1), 85-93.
287. Wen, J. H.; Vincent, L. G.; Fuhrmann, A.; Choi, Y. S.; Hribar, K. C.; Taylor-Weiner, H.; Chen, S. C.; Engler, A. J., Interplay of matrix stiffness and protein tethering in stem cell differentiation. *Nat Mater* **2014,** *13* (10), 979-987.
288. Ye, K.; Wang, X.; Cao, L. P.; Li, S. Y.; Li, Z. H.; Yu, L.; Ding, J. D., Matrix Stiffness and Nanoscale Spatial Organization of Cell-Adhesive Ligands Direct Stem Cell Fate. *Nano Lett* **2015,** *15* (7), 4720-4729.
289. Wallace, M.; Cardoso, A. Z.; Frith, W. J.; Iggo, J. A.; Adams, D. J., Magnetically Aligned Supramolecular Hydrogels. *Chem-Eur J* **2014,** *20* (50), 16484-16487.
290. Zhang, S. M.; Liu, X.; Barreto-Ortiz, S. F.; Yu, Y. X.; Ginn, B. P.; DeSantis, N. A.; Hutton, D. L.; Grayson, W. L.; Cui, F. Z.; Korgel, B. A.; Gerecht, S.; Mao, H. Q., Creating polymer hydrogel microfibres with internal alignment via electrical and mechanical stretching. *Biomaterials* **2014,** *35* (10), 3243-3251.
291. Nance, E.; Timbie, K.; Miller, G. W.; Song, J.; Louttit, C.; Klibanov, A. L.; Shih, T. Y.; Swaminathan, G.; Tamargo, R. J.; Woodworth, G. F.; Hanes, J.; Price, R. J., Non-invasive delivery of stealth, brain-penetrating nanoparticles across the blood - brain barrier using MRI-guided focused ultrasound. *J Control Release* **2014,** *189*, 123-132.
292. Nance, E. A.; Woodworth, G. F.; Sailor, K. A.; Shih, T. Y.; Xu, Q. G.; Swaminathan, G.; Xiang, D.; Eberhart, C.; Hanes, J., A Dense Poly(Ethylene Glycol) Coating Improves Penetration of Large Polymeric Nanoparticles Within Brain Tissue. *Sci Transl Med* **2012,** *4* (149).
293. Kaisar, M. A.; Sajja, R. K.; Prasad, S.; Abhyankar, V. V.; Liles, T.; Cucullo, L., New experimental models of the blood-brain barrier for CNS drug discovery. *Expert Opinion on Drug Discovery* **2017,** *12* (1), 89-103.
294. Lippmann, E. S.; Azarin, S. M.; Kay, J. E.; Nessler, R. A.; Wilson, H. K.; Al-Ahmad, A.; Palecek, S. P.; Shusta, E. V., Derivation of blood-brain barrier endothelial cells from human pluripotent stem cells. *Nat Biotechnol* **2012,** *30* (8), 783-91.
295. Mehdizadeh, H.; Sumo, S.; Bayrak, E. S.; Brey, E. M.; Cinar, A., Three-dimensional modeling of angiogenesis in porous biomaterial scaffolds. *Biomaterials* **2013,** *34* (12), 2875-2887.
296. Phelps, E. A.; Landazuri, N.; Thule, P. M.; Taylor, W. R.; Garcia, A. J., Bioartificial matrices for therapeutic vascularization. *P Natl Acad Sci USA* **2010,** *107* (8), 3323-3328.
297. Arulmoli, J.; Wright, H. J.; Phan, D. T. T.; Sheth, U.; Que, R. A.; Botten, G. A.; Keating, M.; Botvinick, E. L.; Pathak, M. M.; Zarembinski, T. I.; Yanni, D. S.; Razorenova, O. V.; Hughes, C. C. W.; Flanagan, L. A., Combination scaffolds of salmon fibrin, hyaluronic acid, and laminin for human neural stem cell and vascular tissue engineering. *Acta Biomaterialia* **2016,** *43*, 122-138.
298. Li, S. R.; Nih, L. R.; Bachman, H.; Fei, P.; Li, Y. L.; Nam, E.; Dimatteo, R.; Carmichael, S. T.; Barker, T. H.; Segura, T., Hydrogels with precisely controlled integrin activation dictate vascular patterning and permeability. *Nat Mater* **2017,** *16* (9), 953-+.

4 A stimuli-responsive, pentapeptide, nanofiber hydrogel for tissue engineering

Published as: JD Tang, C Mura, KJ Lampe, "A stimuli-responsive, pentapeptide, nanofiber hydrogel for tissue engineering," J. Am. Chem. Soc., 141: 4886-4899 (2019)

4.1 Abstract

Short peptides are uniquely versatile building blocks for self-assembly. Supramolecular peptide assemblies can be used to construct functional hydrogel biomaterials—an attractive approach for neural tissue engineering. Here, we report a new class of short, five-residue peptides that form hydrogels with nanofiber structures. Using rheology and spectroscopy, we describe how sequence variations, pH, and peptide concentration alter the mechanical properties of our pentapeptide hydrogels. We find that this class of seven unmodified peptides forms robust hydrogels from 0.2–20 kPa at low weight percent (less than 3 wt. %) in cell culture media, and undergoes shear-thinning and rapid self-healing. The peptides self-assemble into long fibrils with sequence-dependent fibrillar morphologies. These fibrils exhibit a unique twisted ribbon shape, as visualized by TEM and Cryo-EM imaging, with diameters in the low tens of nanometers and periodicities similar to amyloid fibrils. Experimental gelation behavior corroborates our molecular dynamics simulations, which demonstrate peptide assembly behavior, an increase in β-sheet content, and patterns of variation in solvent accessibility. Our Rapidly Assembling Pentapeptides for Injectable Delivery (RAPID) hydrogels are syringe-injectable and support cytocompatible encapsulation of oligodendrocyte progenitor cells (OPCs), as well as their proliferation and three-dimensional process extension. Furthermore, RAPID gels protect OPCs from mechanical membrane disruption and acute loss of viability when ejected from a syringe needle, highlighting the protective capability of the hydrogel as potential cell carriers for transplantation therapies. The tunable mechanical and structural properties of these supramolecular assemblies are shown to be permissive to cell expansion and remodeling, making this hydrogel system suitable as an injectable material for cell delivery and tissue engineering applications.

4.2 Introduction

An attractive approach to tissue regeneration relies on water-swollen polymeric networks known as hydrogels, which can mimic features of the native extracellular matrix (ECM) such as proteolytic remodeling, cell-adhesion and mechanical properties, while guiding stem/progenitor cell fate decisions. Tissue engineering using biologically relevant hydrogel culture systems may improve regeneration, as hydrogels have a broad range of structural flexibility, biological activity, and similar mechanical properties as native tissue; this, in turn, can yield more physiologically-relevant cellular behavior[1-4]. However, there continues to be a need to develop suitable microenvironments that retain relevant biological and structural functions. Further progress requires materials that 1) are simple and inexpensive to synthesize, 2) gel in response to cytocompatible stimuli, such as small shifts in pH or temperature, and 3) support and regulate cell function, as a substitute for their normal physiological microenvironment[4].

Transplanting stem cells may improve behavioral recovery following an injury or insult[5], or during chronic or degenerative diseases[6]. However, transplant cell viability is often poor[6-8], at least partly due to negative effects (cellular damage) that occur during injection, wherein cells undergo stresses such as non-physiological elongational flow and super-physiological shear forces[6]. Utilizing injectable and self-healing hydrogels as cell carriers could increase the surviving percentage of transplanted cells post-injection into damaged tissue for therapeutic repair[9].

Oligopeptides are versatile building blocks that can be engineered to create self-assembled supramolecular structures which build upon non-covalent, reversible bonds[10-14]. For example, peptide amphiphiles spontaneously self-assemble into hydrogels in aqueous solution, driven by a sequence's hydrophobic alkyl tail and a hydrophilic peptide domain[15]. Similarly, short amphiphilic peptides, such as LIVAGD[16], form robust hydrogels via β-sheet assembly. Several other β-sheet forming peptides feature aromatic interactions (π-π stacking) that drive fibril formation and gelation, e.g., NFGAIL[16-18] (a fragment of human islet amyloid polypeptide$_{22-27}$), DFNKF[19-20] (human calcitonin-derived peptide hCT$_{15-19}$), and KLVFFAE[21] (parts of amyloid β$_{16-22}$). Recently, the 8-residue FDFSFDFS[22] sequence and two pentapeptide analogs of an IDIDI[23] sequence were shown to self-assemble into hydrogels. Likewise, a $K_2(QL)_6K_2$ sequence also demonstrates self-assembly capabilities, where hydrogel formation is driven primarily by ionic screening of charges[13, 24]. Such self-assembling peptide materials can be designed to gel after injection, enabling

uniform encapsulation of cells in 3D, ex vivo, and minimally invasive injection into target tissue such as brain and spinal cord[25-26].

Several challenges limit the broader utility of these peptide systems in tissue engineering and

A

Sequence	pI
KYFIL	8.50
AYFIL	5.28
KYFAL	8.50
KYFIV	8.50
KYFIA	8.50
KAFIL	8.86
KYAIL	8.50

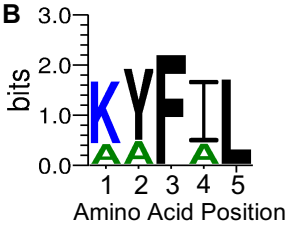

C

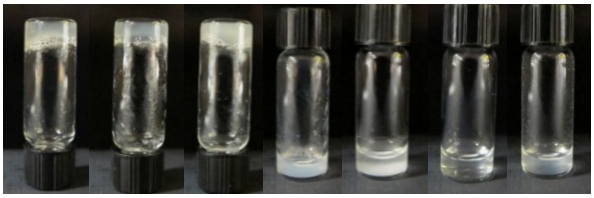

Figure 4-1. Sequences investigated in this study. A) Each sequence examined is listed, along with its theoretical isoelectric point (pI). All peptides are C-terminally amidated. B) A sequence logo highlights the order and predominance of amino acids within pentapeptide analogs that gel under any pH condition. The sequence profiling suggests that Phe (F) and Leu (L) must be conserved for gelation. C) When peptides are dissolved in PBS at pH 7.4 and 1.5 wt. %, the KYFIL, AYFIL and KYFAL pentapeptides form hydrogels, whereas other sequences do not gel under these conditions; note that KAFIL can gel at pH > 10.

regenerative medicine. First, protecting groups such as acetyl[27], *t*-butyloxycarbonyl[28], other large aromatic groups[29-30], or the incorporation of D-stereoisomers[31] are often required to induce gelation, thereby complicating synthetic processes and limiting scalability. Second, there are relatively few examples of short oligopeptides that exist beyond the derivation or analogs of the well-established diphenylalanine peptide sequence[32-33]. While these dipeptides form robust hydrogel systems, the hydrophobicity of the sequence limits their solubility and their range of potential applicability. Third, rather than having complete design freedom, many oligopeptides have been derived by sequence mapping onto relevant biological systems known to self-assemble into a variety of nanostructures. For example, designer peptide scaffolds have been based on an $(EAK)_{16}$ sequence derived from the DNA-binding protein zuotin[34].

We seek an approach to peptide-based hydrogel design that leverages the power of computation to guide peptide engineering efforts. Candidate peptides can be modeled in silico, using molecular dynamics (MD) simulations to interrogate, in atomic detail, the physicochemical properties of a given sequence[35-39]. Few examples exist of using computational approaches to design functional

peptide scaffolds for tissue regeneration applications. The complex interactions between polypeptides and their environments, which mediate their self-assembly into useful biomaterials, demand new tools for characterizing the structure and function of peptide ECMs. An integrated approach that leverages computational modeling to understand experimental peptide behavior can more rapidly (and affordably) examine assembly. Moreover, such an approach could even survey the suitability of an array of potential sequence constructs (i.e., a library) toward creation of a general-purpose hydrogel scaffold for tissue engineering applications.

Here, we use an integrated computational and experimental approach in the design, synthesis, and characterization of a pH-triggered, self-assembling pentapeptide suitable as a three-dimensional scaffold for cell culturing. We term these materials *Rapidly Assembling Pentapeptides for Injectable Delivery* (RAPID) hydrogels. To decipher the self-assembly mechanism, we analyzed the peptide sequence KYFIL, with the goal of identifying specific residues that play a key role in intermolecular association and self-assembly. We screened seven different sequences for their ability to form hydrogels, and analyzed their supramolecular assembly behavior using a host of methods: attenuated total reflectance–Fourier-transform infrared (ATR-FTIR) spectroscopy, cryogenic electron microscopy (cryo-EM) and transmission electron microscopy (TEM), rheometry, and molecular dynamics (MD) simulations. RAPID hydrogels were also evaluated as three-dimensional scaffolds for cell encapsulation, via cell culture–based biological assays, thus allowing us to determine their cytocompatibility under physiological conditions.

While demonstrating a wide range of stiffnesses suitable to emulate a variety of human tissues, we focused here on tailoring RAPID hydrogels to mimic the biomechanical properties of brain tissue (Young's moduli ranging 0.1–3.5 kPa[1, 40]). Encapsulation of oligodendrocyte progenitor cells (OPCs) enabled us to demonstrate the 3D cell culture matrix potential of RAPID hydrogels. We find that RAPID hydrogels can also mitigate the damaging effects of extensional flow experienced by cells during syringe injections.

4.3 **Results and Discussion**

We have designed pentapeptides, based on a KYFIL-NH_2 sequence (Figure 1) hereafter referred to simply as 'KYFIL,' that can self-assemble into β-sheet–forming nanofibers. The sequence

KYFIL was chosen based on previously published results on aromatic-rich tripeptides that could gel under certain experimental conditions[27, 30, 35, 41-42] (such as a change in pH or ionic strength). In particular, we chose Lys as the head-group to improve solubility in aqueous solution[24], while the overall sequence design was guided by the goal of increasing the hydrophobicity of amino acid residues so as to increase the amphiphilicity of the peptides . In initial screens, we assayed several peptide designs by performing an alanine scan. Displaying the results as a sequence logo[43-44] revealed that the central phenylalanine (F), as well as preservation of the amphiphilicity of the sequence, are two key elements that facilitate hydrogel formation (Figures 1 and 2). Interestingly, the carboxyl-terminated variant KYFIL-CO_2H (i.e., with 'natural' peptide end-chemistry) did not readily form hydrogels at pH 7.4. Because the carboxylic acid moiety is deprotonated at neutral pH, this finding suggests that an uncharged C-terminus is required for gelation of the peptide. By examining the peptide's secondary structural conformation via ATR-FTIR spectroscopy and MD simulations, we detected that structural transitions occur when a pentapeptide self-assembles under gelling conditions.

4.3.1 Secondary Structure Analysis via FTIR Spectroscopy

The secondary structural content of pentapeptide specimens was probed by ATR-FTIR spectroscopy. Samples of the pentapeptides of interest were generated via solid-phase peptide

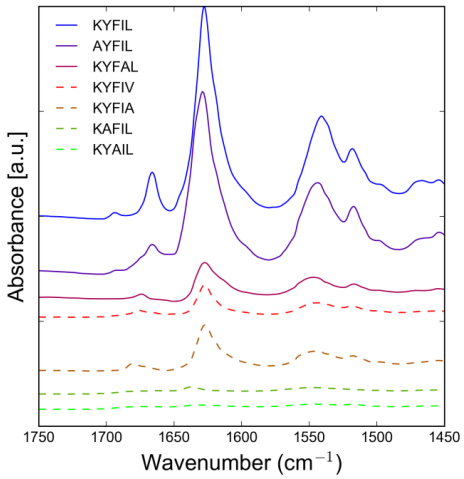

Figure 4-2. Peptides exhibit characteristic secondary structures via ATR-FTIR. Peptides dissolved at 3 wt.% in PBS and pH 7.4 were examined. All gelling peptides (solid lines) exhibit an Amide I absorbance at 1629 cm^{-1}, indicative of β-sheet hydrogen bonding. A peak near 1679 cm^{-1} to 1683 cm^{-1} suggests anti-parallel β-sheet conformation. Non-gelling peptides (dashed lines) exhibit much weaker, less intense peaks at the same wavenumbers. All spectra are baseline corrected, normalized, and vertically offset for clarity.

synthesis methods. An alanine (Ala) scan[45] of KYFIL was used to assess each AA's contribution to gelation, wherein individual amino acids (AAs) were sequentially exchanged with Ala or Val. Ala and Val were the substituted residues of choice, as they either eliminate a side-chain beyond the Cβ atom (Ala) or otherwise would be expected to minimally alter the main-chain conformation (Val). As uncharged and relatively compact residues, Ala and Val would not be expected to introduce (confounding) electrostatic or steric effects[46]. All pentapeptides were dissolved in phosphate-buffered saline (PBS) at a concentration of 3% (weight/volume) and adjusted to a pH of 7.4. Gelling peptides (solid lines, Figure 2) display a strong Amide I absorbance at ≈1629 cm^{-1}, arising from vibrational modes of the amide group; these vibrations, in the region of 1700→1600 cm^{-1}, correspond to stretching of the C=O and C–N bonds, as well as bending of the N–H[47-48]. This region of the IR spectrum is particularly sensitive to variations in secondary structural conformation and, in the case of our pentapeptide samples, is indicative of β-sheet hydrogen bonding[49-50] (Figure 2, Figure S2 and S3). A secondary peak near 1679 cm^{-1} to 1683 cm^{-1}, in some of the specimens, indicates that the β-sheet is anti-parallel[51]. We can infer this because the Amide I region of parallel β-sheets harbors a single predominant signature (near 1630 cm^{-1}), while antiparallel sheets generally feature a second (minor) peak near ≈ 1680-1690 cm^{-1}. Peptide variants which do not form gels at the same concentration and pH (dashed lines, Figure 2) exhibit less intense peaks, suggesting a lack of significantly structured hydrogen bonding networks in those solutions. By correlating our IR observations with variations in AA sequence, it appears that amphiphilicity and a capacity for π-system interactions (e.g., π···π stacking and π···cation interactions with the benzyl side-chain of the central Phe) play a key role in self-assembly and hydrogel formation (Figure 2).

4.3.2 Probing the Conformational Space and Interaction Events via MD Simulations

MD simulations were used to examine the atomically-detailed molecular interactions underlying peptide self-assembly processes. MD simulations offer a powerful approach to examine the

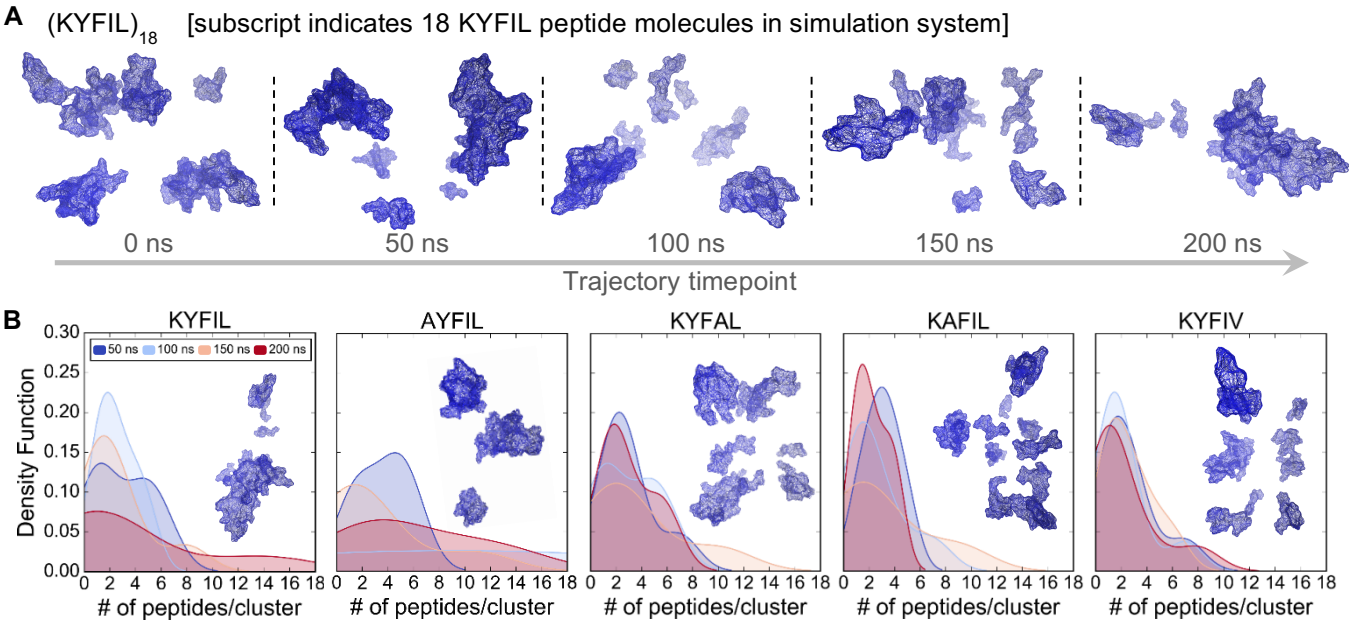

Figure 4-3. KYFIL peptide molecules simulated in explicit solvent assemble into multimeric structures. A) Representative structures of the simulated pentapeptide sequence, KYFIL. Spatiotemporal evolution of peptide assembly is demonstrated from the simulation trajectory of the peptides at 50 ns intervals as the molecules assemble into large clusters on the timescale of 200 ns. B) Density functions representing the clustering propensity of different pentapeptide systems over time. At the end of the 200 ns simulation, KYFIL has the least number of distinct clusters and largest number of peptides per cluster, versus other peptide sequences. Insets are representative snapshots of the peptides near 200 ns.

structural properties and conformational dynamics of engineered peptides and can yield experimentally-inaccessible insight about the dynamical basis of self-assembly[52-53]. Simulations can help guide adjustments to the peptide sequence in order to optimize the system's properties toward a target goal. Using MD simulations, one can study a peptide system's aggregation propensity by simulating multiple peptides together in a single system. While other work has focused on the diffusional association of protein molecules within a solvated system[39, 54] or detailed the biomolecular recognition events (i.e. conformational rearrangement and binding/unbinding events[55]), few examples exist of using computational approaches to design functional peptide scaffolds for tissue regeneration applications[56]. In this study, we used MD simulations to study the emergence of structural features in a peptide system and provide an atomistic view of the self-assembly process of nanostructures.

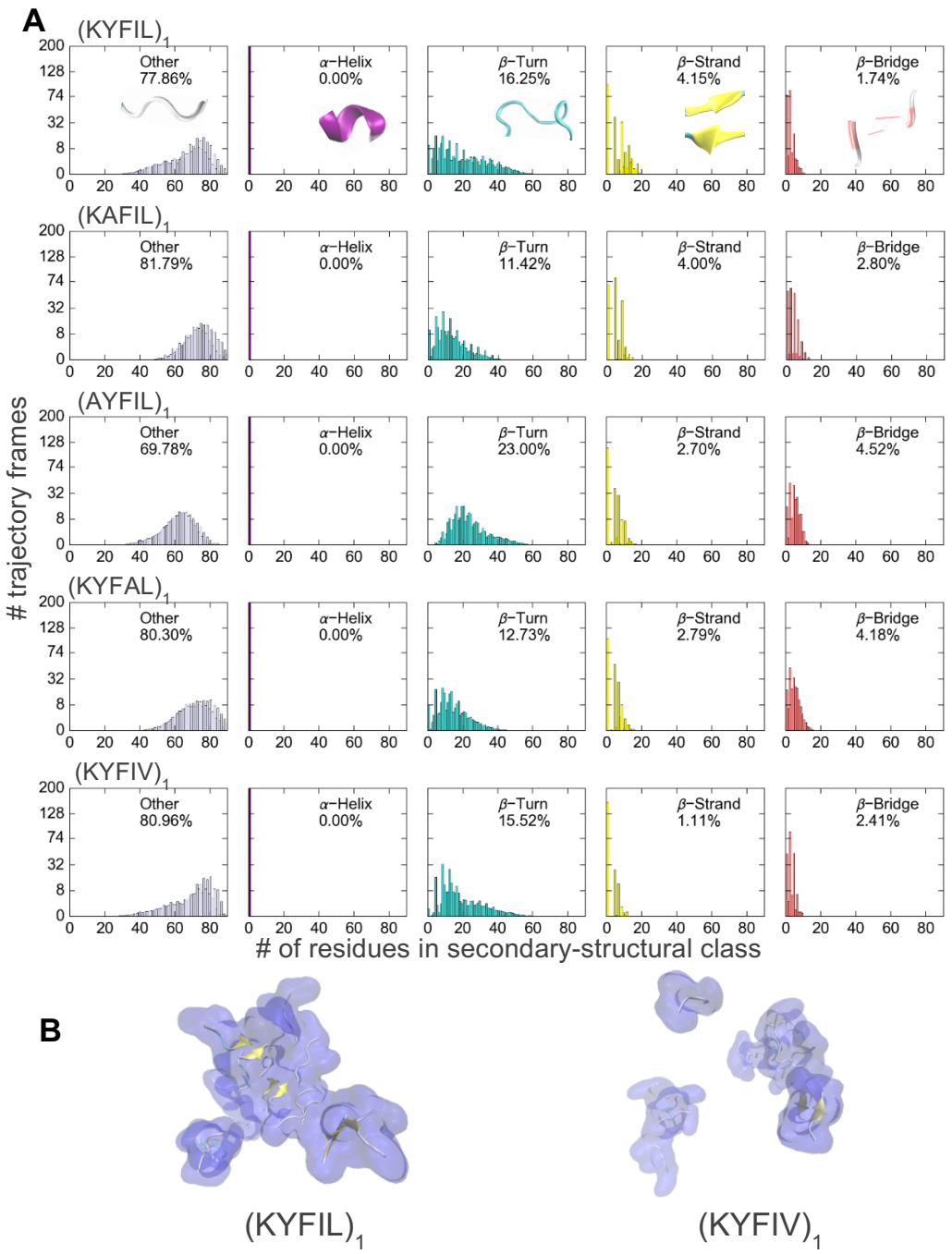

Figure 4-4. Secondary structural content of the simulated KYFIL, KAFIL, AYFIL, KYFAL, and KYFIV systems. Numbers within a plot represent the population of the secondary structure observed in the simulation over all possible secondary structure conformations. Secondary structure cartoon representations in the thumbnails displayed in the first row match the colors in the histogram. A) Histograms that depict the predominant conformations exhibited by the polypeptide are β-turns and 'other' structures. For all sequences, there is an absence of α-helical structures, consistent with our experimental results. In addition, β-turn structures are prevalent with β-strand and bridge structures. A significant shift from strand to bridge occurs in the character of the β structure in the non-gelling sequence, KYFIV. B) Representative snapshots taken at 180 ns and 177 ns for KYFIL and KYFIV, respectively, illustrating sequence-dependent conformational states of the pentapeptides. The peptides can be seen to be a mixture of helices and coils; the secondary structures are labelled in this view with α-helices colored purple, 3_{10} helices blue, β-strands yellow, the β-turn motif cyan and irregular coil regions white. These trajectory frames illustrate the formation of β-sheet regions within the two peptide systems, with more pronounced populations of β-sheet conformations present in KYFIL versus KYFIV.

established pentapeptide sequences that can assemble in aqueous media, we conducted MD simulations of select peptide candidates (Figure 3). These extended (200-ns), all-atom simulations were performed in explicit solvent using the CHARMM36 force-field. Such force-fields represent the physicochemical properties of each amino acid—including partial charges, atomic interaction (Lennard-Jones) potentials, and other parameters—via a classical, molecular mechanics–based approach, as described in various primers[52]. In practice, CHARMM36[57] is a state-of-the-art force-field that can be applied to many types of biomolecular systems, as illustrated for instance by the analysis of disordered regions of the protein desmoplakin[58]. Our simulations show that the assembly propensity of RAPID peptides correlates with the diffusional association of individual peptides. The peptides primarily adopt irregular conformations, with some transiently-stable β-turns 'flickering' into existence (Movie S1–S5). Within ≈50 nsec, individual KYFIL peptides assemble into six discrete groups of peptides, as can be seen by visual inspection of trajectories,

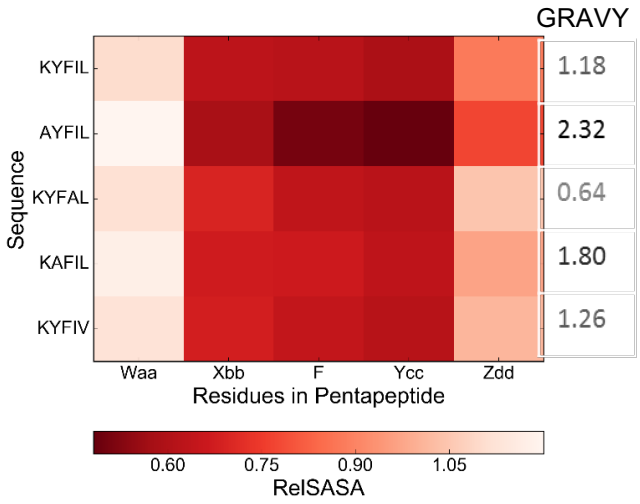

Figure 4-5. Sequence-dependent changes in relative solvent accessible surface areas (RelSASA) for individual residues in each pentapeptide simulation. The RelSASA quantifies the accessible surface area of each residue in the folded pentapeptide. A white color indicates that a residue is more solvent-exposed than average, while the intensity of a red scales with residue burial. Computed grand average hydropathicity (GRAVY) values, which are essentially Kyte-Doolittle (KD) hydrophobicity indices averaged over the amino acid sequence for each peptide, are given on the right; on the KD scale, the hydrophobic amino acids have positive values (the most hydrophobic is Ile, with a value of +4.5), while hydrophilic residues have negative values (the least hydrophobic is Arg, at -4.5, followed by Lys at -3.9). At least qualitatively, the MD-based results and general hydropathicity patterns are consistent: the most hydrophobic peptide, AYFIL (most positive GRAVY score), features the least solvent exposure over the course of its MD trajectory, while the most hydrophilic peptide, KYFAL (least positive GRAVY score), exhibits the largest RelSASA values.

with some β-sheet secondary structure (Figure S1 and Figure 3A). Extending the simulation further yields peptides that have assembled into two large clusters by ≈200 nsec (Figure 3A).

We used a discrete number-density function (a measure of the local concentration) to quantify the aggregation propensity of the four different peptides along their respective trajectories. Those sequences which were found to gel in experiments—KYFIL, AYFIL, KYFAL, and KAFIL at pH 10—exhibited a higher propensity to aggregate; those peptides which formed gels also tended to exhibit greater variation in the number of peptides per cluster at 200 ns, consistent with a higher propensity to assemble, even non-specifically into heterogeneous aggregates (Figure 3B). In addition, the time-evolution of the radius of gyration (R_g) of the peptide systems (R_g computed system wide across all peptides, not per-peptide) reveals a gross structural rearrangement—from mostly diffuse peptides to closely associated molecular interactions, as indicated by the net decrease in R_g for pentapeptide sequences (Figure S4) relative to the initial trajectory, except for KAFIL, KYFAL, and KYFIV. These data are consistent with the FTIR spectra (Figure 2), as KAFIL, KYFAL and KYFIV have lower β-sheet peak intensities, suggesting lower assembly propensity. For KYFIL, a detectable, and presumably hydrophobically-driven, 'collapse' of the system appears to be more kinetically allowed, versus other sequences; i.e. transitions between secondary structures occur frequently, implying relatively low activation barriers[59]. Visual inspection of trajectories shows a sharp structural reorganization early on (< 100 ns) in most of the simulations.

We also examined the structural transitions from the initial peptide system (post-equilibration) to the final conformational ensemble. For all simulated peptide sequences, there was a notable dearth of α-helicity (Figure 4A), consistent with the experimental FTIR data (Figure 2, Figure S3). All pentapeptides preferentially sampled β-type structures (Figure 4a), and the gelling peptide sequences (KYFIL, AYFIL, KYFAL, KAFIL) exhibited a nominally greater fraction of β-strand character over the course of the 200-ns trajectory, versus a non-gelling sequence, KYFIV (Figure 4B). The domain-swapping mode of β-rich association can be induced by intermolecular β···β-strand/bridge contacts, via directional hydrogen bonding between the backbones of aromatic residues and β-branched amino acids (e.g. isoleucine)[60-61]. Consequently, the structural rearrangement of peptides can reduce conformational strain, as the formation of such β-strand

structures are enthalpically favorable, driving the folding of β-sheets[62-63]. The torsion angles for each type of amino acid, barring the N- and C- termini (Figure S5), indicate significant structural heterogeneity for each peptide system. Our results suggest that, in general, the middle Phe in each pentapeptide often adopts a type-II β-turn conformation (ϕ = -60°, φ = 120°) or an antiparallel β-sheet structure (ϕ = -140°, φ = 135°); this is consistent with our aforementioned FTIR results. For the KYFAL and KAFIL sequences, the Ala preferentially samples a polyproline type-II helix (ϕ = -75°, φ = 145°), with a decreased β-sheet propensity. This result is unsurprising, as the peptide backbone near an Ala (versus Tyr) residue encounters less steric hindrance, given the absence of the phenol side-chain[64]. The most densely populated regions of conformational space for Ile, in all pentapeptide sequences (Figure S5), highlights this amino acid's propensity to adopt β-sheet conformations. In this context, Phe···Ile intermolecular interactions (steric occlusion, as well as London dispersion forces and other van der Waals forces) are particularly relevant, as they would facilitate the hydrophobic aggregation of these peptide regions and indirectly enable the formation of hydrogen-bond networks between the local backbones[65]; this model is also consistent with both MD simulations and FTIR spectroscopic data (Figure 2).

In addition to internal (intra-peptide) and external (inter-peptide) interactions, the conformational dynamics of a peptide system are governed by peptide···solvent interactions. By quantifying peptide···water contacts, we can discern hydrophobic side-chain contributions to the energetics of peptide assembly, and also study a peptide's solvation dynamics. Thus, we evaluated the solvent-accessible surface area (SASA) of individual residues in each pentapeptide, averaged over entire 200-ns trajectories. In computing the relative SASA of a peptide system (via Rost & Sander's method[66]), we consider the ordinary accessibility of a residue in a structure normalized by the maximal value possible for that residue type (i.e., that amino acid side-chain). Unsurprisingly, for each pentapeptide sequence the N-terminal Lys was the most solvent-exposed (Figure 5) and the central tripeptide (···Tyr/Ala–Phe–Ile/Ala···) was the most consistently buried throughout the simulation. The significant changes in relative accessibility of the C-terminal residue (position 5) indicate the system's structural rearrangement in the context of side-chain functional groups[67]. Our findings are consistent with patterns in Kyte-Doolittle hydropathicities[68] (GRAVY values in Figure 5) as well as prior experimental results regarding the hydration structure of ABA triblock copolymeric systems[13, 24, 69-70], wherein the termini were found to be exposed to aqueous solvent

molecules and dehydration of nonpolar side-chains biases the middle block of the amphiphilic pentapeptide to preferentially adopt compact 3D structures (β-strands, turns, etc.) that occlude solvent.

4.3.3 Hierarchical Self-Assembly: Evaluating Hydrogel Rheological Properties

The mechanical properties of 1.5 and 3 wt. % hydrogels were found to depend on the concentration, pH, and peptide sequence. Hydrogels formed *in situ*, in an epitube, within several seconds (Movie S6) and were then pipetted onto the rheometer platform for rheological measurements. RAPID hydrogel stiffnesses span two orders of magnitude, from approximately 50 – 17,000 Pa in shear storage moduli (G′) (Figure 6a). (For comparison, this would be similar to 520 – 44,200 Young's modulus, although this requires a potentially fraught assumption of a Poisson's ratio of 0.5.) KYFIL at 1.5 and 3 wt. % forms hydrogels of 8,000 and 17,000 Pa, respectively (Figure 6 and S6).

Peptide hydrogels can provide structural flexibility and mechanical properties that emulate native biological tissues[4, 71-72]. Bulk matrix stiffness and topography are well known biomechanical cues that can direct stem cell proliferation as well as differentiation[73-74]. In most tissues, such as the heart, muscle and bone, the extracellular matrix contributes to the biophysical microenvironment, e.g. a Young's modulus of 6.8 kPa for heart tissue and up to 103 kPa for bone[75-76]. However, tissues within the central nervous system (CNS), such as the brain and spinal cord, are some of the most compliant tissues in the body[77], with moduli of ~0.7 kPa to 3.5 kPa[78-80]. Such an extensive range of stiffness requires hydrogel biomaterials to have highly tunable biomechanical properties that can be catered to a wide range of applications, for numerous different tissue types throughout the body.

Our class of peptide sequences is unique in that the peptide lengths are quite short (5 amino-acid residues), and have a broad range of mechanical properties (~50 – 17,000 Pa) that can be fine-tuned via small changes in concentration or pH (Figure 6). The broad range and large magnitude of storage moduli we can attain is in contrast to other short, self-assembling oligopeptides. For example, $K_2(QL)_6K_2$, RADA16-I, $(FKFE)_2$[81], MAX1/8[82], and KLVFF[83] sequences yield gels with

much lower storage moduli and narrower ranges of mechanical properties (storage moduli of 50 - 1000 Pa).[13, 84-85]

The lower storage modulus of KYFAL can be reconciled with its weaker signature peak intensities for β-sheets in the FTIR spectra (Figure 2), implying less content of well-ordered β-sheet for KYFAL (Figure 4). Additionally, Lys did not seem to affect gelation, so long as the amphiphilicity of the sequence was maintained. Rather, the substitution of Lys → Ala affected the solubility of the peptide (Figure S8). Similarly, at 3 wt. %, KAFIL had a G′ of 200 Pa compared to KYFAL at 133 Pa. The additional bulky methyl group in the Ile–Leu C-terminus of KAFIL, relative to Ala–Leu (in KYFAL) or Ile–Ala and Ile–Val (in KYFIA and KYFIV, respectively) confers greater hydrophobicity, resulting in a self-assembly process driven mainly by increased hydrophobic interactions.

The apparent pKa shift following the substitution of Tyr to Ala increases the electrostatic repulsion between peptides[30], reducing the aggregation propensity. Increasing the pH, which alters the average degree of ionization, better neutralizes KAFIL and favors self-assembly of the peptide, by

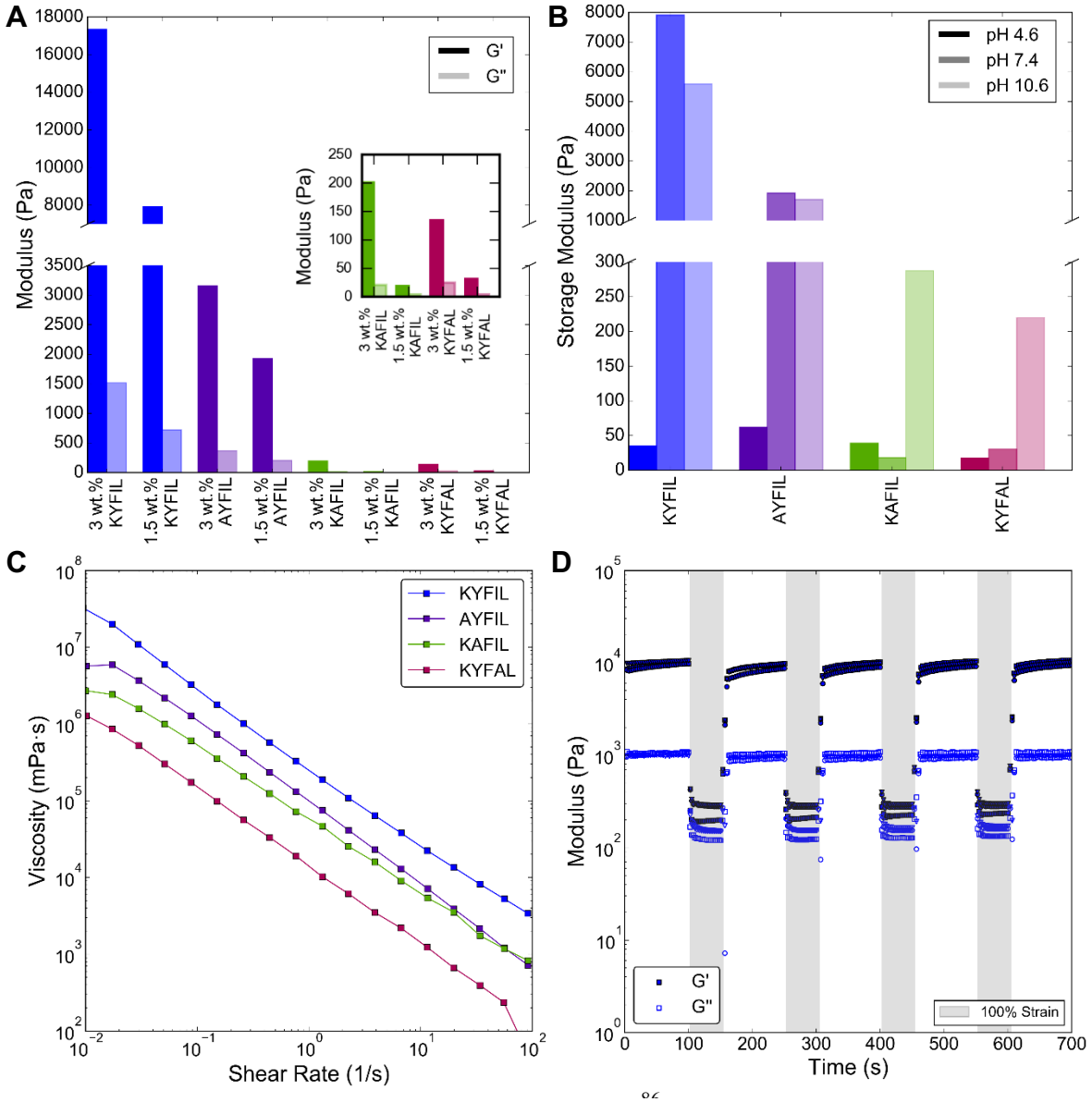

Figure 4-6. Rheological properties of self-assembling pentapeptides at different concentrations and pH conditions. a) Storage and loss moduli as determined from the linear viscoelastic region (LVE) taken from strain sweeps at a constant frequency of 1 hz of 1.5 wt. % and 3 wt. % hydrogels at pH 7.4. Hydrogels were formed in situ in an epitube and then pipetted onto the rheometer platform. Hydrogel stiffness can be tuned by concentration and peptide sequence variation. The inset is a magnification of the G' and G" for KAFIL and KYFAL hydrogels. b) Storage moduli taken from the LVE from strain sweeps at a constant frequency of 1 hz of 1.5 wt. % hydrogels at different pH conditions of 4.6, 7.4, and 10.6. The mechanical properties of the hydrogel are dependent on pH, where all peptide sequences are very weak gels (G' < 80 Pa) in acidic conditions, and form robust hydrogels at pH 7.4 and 10.6. c) Hydrogel forming sequences were evaluated under shear flow to determine their shear-thinning properties. The apparent viscosity of each sample decreased with increasing shear rate demonstrating that these hydrogels are capable of shear-thinning. d) 1.5 wt. % KYFIL hydrogels (n = 3) were subjected to five step strain sweeps of 100 % strain (50 s), followed by a 100 s recovery period (0.1 % strain). The hydrogel recovers 70-80% of its initial G' within several seconds. Even after multiple high strain cycles, the hydrogel is able to repeatedly retain its mechanical strength.

hydrogel-forming peptides indicates that Ile facilitates self-assembly[87]: we detect a higher population of β-sheet conformations for Phe–Ile–Leu versus Phe–Ala–Leu sequences.

In investigating the pH responsiveness of hydrogel-forming sequences, we found that all peptides exhibited lower storage moduli upon a decrease in pH. The three pHs were chosen (4.6, 7.4 and 10.6) to include the physiological pH of 7.4—particularly relevant for viable cell encapsulation—as well as acidic and basic pHs that bracket the pI of each sequence (Figure 1A). The G′ increases by several orders of magnitude as the pH of the solution increases toward neutrality (Figure 6B). Non-gelling sequences (KYFIV, KYFIA, KYAIL) also exhibit pH-responsive behavior: at low pH, the peptides were soluble, but precipitated as an off-white powder as the pH was raised (but never gelled). The storage (G′) and loss (G″) moduli of 1.5 and 3 wt. % hydrogels increased with increasing concentrations of the hydrogel and increasing pH conditions (Figure 6A, B, S7 and S8).

The apparent viscosity of all gelling sequences decreased linearly with increasing shear rate, demonstrating the shear-thinning capacity of these hydrogels (Figure 6C, Figure S10). Multiple high-strain (100%) sweep cycles, with 30 s recovery periods, demonstrated KYFIL's ability to self-heal following mechanical deformation, without any evidence of hysteresis (Figure 6d, Figure S11). Following a 100% strain, hydrogels repeatedly recovered gel behavior within 14 seconds (G' > G"). Within 1 minute, the gel recovered 82% of its initial G', and required 3.4 minutes to recover 90% and 7 minutes to recover 96% (Figure S11). Even after multiple high-strain cycles, the hydrogel rapidly and repeatedly recovers its mechanical strength—rendering these materials particularly ideal for biomedical applications that require injection. This enables uniform encapsulation of cells in 3D, *ex vivo*, and then injection via a minimally invasive technique. Similarly, we found that the hydrogels could re-gel, macroscopically, following a syringe ejection (Movie S7), suggesting that materials based upon these peptides could be well-suited to additive manufacturing applications like extrusion-based 3D printing.

The propensity of our RAPID peptides to adopt β-rich structures, alongside their capacity to form hydrogels (and the presence of fibrillar networks in such gels [see below]), bears a striking resemblance to the phenomenon of liquid phase condensation[88] as a means to form P-bodies, stress granules, and other types of intracellular protein gels or "membrane-less organelles". In such

liquid-liquid phase separated systems[89], a multivalent web of relatively weak (individually) molecular interactions leads to the mesoscopic assembly of a distinct, de-mixed liquid phase (e.g., the nucleolus) within the cell. Notably, these molecular interactions generally occur between low-complexity, conformationally pliable peptides, as in the recently characterized, hydrogel-forming "low-complexity aromatic-rich kinked segments (LARKS)"[90]. A possible direction for future work involves elucidating any similarities between the 'aromatic ladders' and other structural features of LARKS assemblies and, for instance, the conserved Phe in our RAPID peptide systems.

4.3.4 Electron Microscopy of Nanofiber Morphology: TEM and CryoEM

Fibrils, tubes, dendrimers and other ultrastructures often form via a hierarchical supramolecular arrangement of specific, noncovalent contacts[91-92]. TEM analysis revealed that our RAPID hydrogels are composed of nanofibers as well as dense regions of fibrous bundles. At low pH (i.e. non-gelling conditions), fibers do not form within the peptide solution; rather, amorphous aggregates are present (Figure 7A). At physiological pH, individual fibers bundle into hierarchical nanostructures with clearly twisted, ribbon-like morphologies (Figure 7B). The multi-stranded, twisted ribbons reported here are unique among nanofiber-forming, self-assembling peptide hydrogels[41, 93]. In at least some characterized systems, the helicity (and other geometric properties) of fibers are thought to depend on such atomic-level effects as the properties of steric packing between aromatic side-chains, such as for Tyr and Phe[94]; whether the general morphological properties that we find for RAPID peptides can be traced to such underlying factors is an appealing question for future structural modeling studies. In earlier work[87, 94], cooperative intermolecular hydrogen-bonding between the backbone N- and C-termini were found (by modeling) to enable stronger interactions (i.e. closer intermolecular packing), leading to the classical geometric features of twisted ribbons. Our peptides are C-terminally amidated, and it is more likely that RAPID fibrils assemble via anti-parallel stacking of pentapeptides, with details of the molecular packing predominantly stemming from apolar dispersion forces and other enthalpically favorable interactions among the Phe moiety and amphiphilic nature of the sequence[95-96].

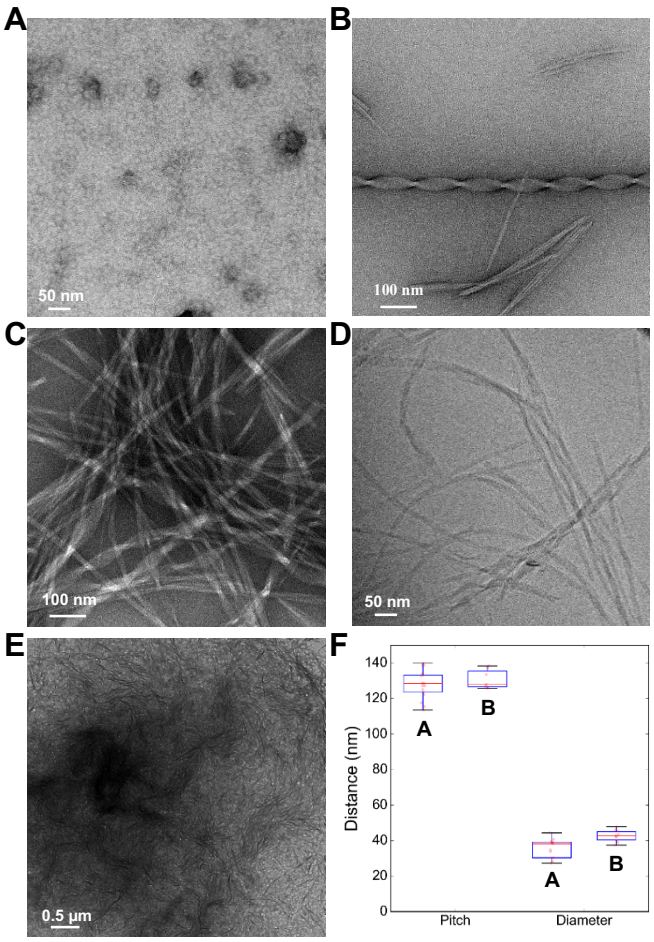

Figure 4-7. Representative EM images of 1.5 wt.% KYFIL hydrogels. A) Images of amorphous peptide aggregates in non-gelling conditions (pH 4.6). There is no distinct fiber formation within peptide solutions. B) Images of individual twisted ribbon molecular assemblies present within the hydrogel at pH 7.4. These twisted ribbons have ca. 40 nm width and ca. 132 nm pitch. C) TEM images of bulk fibres within the hydrogel. Both 'classical' fibrous bundles that are commonly observed in other reported self-assembling peptides and the twisted ribbon morphology are present within this hydrogel system. D) Cryo-EM images of 1.5 wt. % KYFIL hydrogel. Twisted ribbon morphologies are present within the hydrogel. E) Lower magnification of the KYFIL peptide, demonstrating that twisted ribbon morphologies are present in mass throughout the hydrogel volume. F) Quantification of the pitch and diameter of the twisted ribbons is consistent and reproducible. A and B refer to different synthetic batches.

Individual fibers can apparently entangle, yielding multi-stranded twisted ribbons (Figure 7C). Similar hierarchical 'bundling' of fibrils, interwound 'superhelices', and other higher-order assemblies have been seen in systems such as amyloid-related peptides[97-99]. In other previously characterized self-assembling peptide systems, ionic interactions, modulation by the solvent environment, and hydrogen bonds are thought to govern the formation of interconnected networks

of nano-fibrils[13, 15, 24, 27, 93, 100-101]. In addition—unlike other nanofiber-forming peptides—the pentapeptide sequences presented here are significantly shorter than many hitherto characterized systems (decapeptides and beyond). Furthermore, other self-assembling peptide hydrogels[13, 24, 85, 92] often lack distinct morphology within their nanofiber-forming sequences (instead being irregular and heterogeneous), whereas RAPID peptides form highly regular, twisted fibril nanostructures.

Cryo-TEM of our pentapeptide samples in vitreous ice reveals fibers that maintain twisted fiber morphologies, with finite fiber lengths up to ~100 μm (Figure 7D). At relatively low magnification, twisted ribbons appear to pervade the hydrogel network, suggesting that these particular morphologies are not isolated, localized or otherwise spurious instances of self-assembly (Figure 7E). As part of an unbiased experimental design, two different batches of the KYFIL pentapeptide were independently synthesized and evaluated under TEM in order to assess the robustness and reproducibility of fibril formation. The geometric features of the fibers (helical pitch, diameter) were consistent across the two separate batches (Figure 7F), demonstrating that these results are replicable and that there is low batch-to-batch variability as regards the peptide synthesis process, purification, and self-assembly. The periodicity of the fibrillar twist is ≈ 120 nm, as determined via visual analysis (Figure 7) and by calculation of the autocorrelation function of pixel intensity along individual fibrils (Figure S12).

Notably, both of these morphological features of our RAPID peptides—the presence of a fibrillar twist, and the ≈ 120 nm value of its pitch—are recapitulated in the structural features of many peptide-related systems, amyloidogenic and otherwise. One example is β-sheet fibrils and "periodically-twisted nanoribbons" formed by an Ac-NNFGAILSS peptide from the "amyloidogenic core" of islet amyloid polypeptide ($IAPP_{21-29}$)[97]. These peptides featured axial repeats of ≈ 85-100 nm. In a closely related system, an overlapping IAPP-derived peptide ($IAPP_{20-29}$) had AFM-characterized fibril periodicities of ≈ 203 nm[99]. Fibrils from disparate proteins (e.g., SH3-containing proteins, and lysozyme) can also be polymorphic. Based on AFM studies, two subpopulations of SH3 fibrils form helical repeats of ≈ 105 nm and ≈ 156 nm, while human lysozyme fibrils have an "axial crossover repeat" of ≈ 200 nm[102]. Perhaps most pertinent to our current study, systematic studies of a family of short peptides based on I_3K (including all stereoisomeric combinations of L- and D-amino acids), showed that these amphipathic peptides

form twisted fibrils with a helical pitch of ≈ 120 nm[103]. This is in remarkable agreement with our RAPID fibrils, which exhibit nearly the same pitch (Figure 7F). Though not identical to these previously characterized systems, the morphological properties of our RAPID peptide-based fibrils nevertheless are quite similar, suggesting that perhaps some unifying structural and energetic principles underlie the formation of these various supramolecular structures, amyloid-related and beyond. Most broadly, such commonalities could have overarching implications for peptide engineering and nanomaterials.

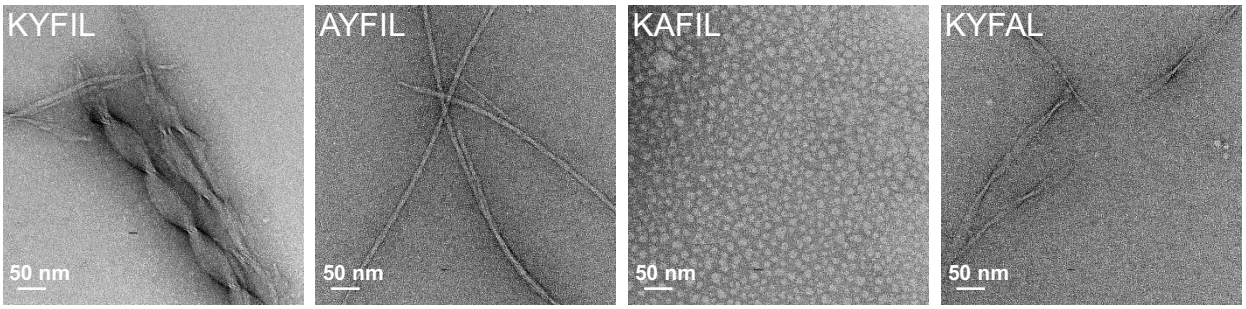

Figure 4-8. Representative TEM images of 1.5 wt. % pentapeptides in PBS at pH 7.4. KYFIL hydrogels exhibit twisted ribbon morphologies, while AYFIL hydrogels are comprised of twisted fibrils. KAFIL peptide solutions at pH 7.4 form spherical aggregates (non-gelling conditions), while KYFAL hydrogels also form twisted ribbon morphologies, with longer and more infrequent pitch than KYFIL peptides.

As expected, peptide sequence has a significant effect on the nanofiber morphology. More specifically, the self-assembly of hierarchical twisted 'macromolecular' structures can be altered by substituting any residue within the ···Phe–Ile–Leu··· moiety that detracts from the amphiphilicity of the sequence and π-system interactions. Similarly, any modification to the sequence also results in drastically different mechanical properties, as indicated in our rheology studies. We observe some twisting in nanofibers occurs within 1.5 wt. % AYFIL hydrogels at pH 7.4, but the typical diameters of these fibers (≈ 10 nm) are significantly smaller than those of KYFIL hydrogels (≈ 40 nm). Though impossible to assess without more detailed analyses, a possible molecular basis for this difference relates to the sterically smaller alanine enabling a tighter packing of individual peptides within fibers or protofibers (versus the more extended Lys side-chain). For the KAFIL system under the same conditions, there is no distinct fiber formation—only spherical aggregates are seen (Figure 8), though it should be noted that KAFIL peptides can form hydrogels at higher pH conditions. Interestingly, for KYFAL hydrogels, twisted ribbon morphologies still occur, though the persistence length of these fibers appears to be

significantly shorter (based on qualitative/visual analysis), and the twist periodicity (i.e., helical pitch) is more irregular. The change in fibrillar morphology, upon an Ile → Ala substitution, may ultimately stem from an alteration in the steric properties of side chain–mediated geometric packing of peptides. While there is a great difference in length-scale between an individual peptide on the nm-scale and a supramolecular assembly (such as a fibril), we do see correlations between hydrophobicity properties of the different pentapeptides and the patterns of relative solvent accessibility across the different peptides, as captured by MD simulations (Figure 5). An intriguing problem for future work is elucidation of the sequence correlates and stereochemical basis for fiber morphology (e.g., thicker ribbon diameters [≈40 nm] for KYFIL versus [≈10 nm] for KYFAL). Successfully addressing this goal will likely require an integrative, multidisciplinary and multiscale approach, such as was used to decipher the atomic structures of cross-β amyloid fibrils of a transthyretin-derived peptide[98].

4.3.5 Cell-Protection by RAPID Hydrogels during Syringe Ejection

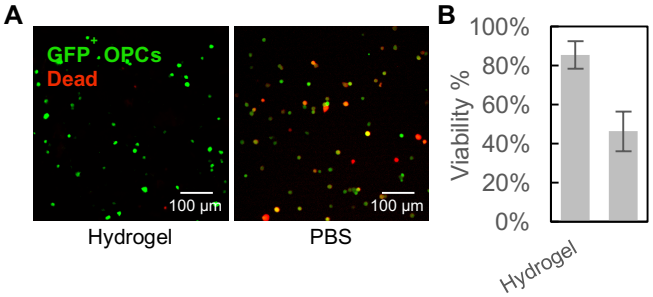

*Figure 4-9. Viability of OPCs immediately after syringe needle flow in PBS and AYFIL hydrogels. A) Live/Dead images of viable (green, GFP+) and membrane damaged (red, ethidium homodimer-1) cells postejection in PBS or 1.5 wt. % AYFIL hydrogels. Each sample of cells encapsulated in RAPID and PBS, respectively contained at least 140 total cells. B) Percent cell viability with injection in PBS or hydrogels. Error bars represent standard error of the mean (SEM) from three separate syringe ejections (n = 3), *p < 0.05.*

During syringe needle flow, cells can experience various types of mechanical forces that ultimately disrupt the cellular membrane: 1) extensional flow, where cells encounter stretching forces, 2) pressure drop across the cell, and 3) shear stresses, due to linear shear flow as the cell travels across the syringe[6]. In our present study, we experimentally tested the effects of syringe needle flow on the viability of oligodendrocyte precursor cells (OPCs) suspended in PBS or RAPID hydrogels as a cell carrier at a flow rate of 1000 µL/min. OPCs are therapeutically relevant, as OPC transplantation may help circumvent the inherent regenerative limitations within the

central nervous system (CNS).[104-105] Indeed, this OPC transplantation strategy is currently being pursued as a therapeutic intervention in human traumatic spinal cord injury patients[22]. When cells were ejected in PBS, OPC viability was significantly decreased compared to cells encapsulated in RAPID hydrogels and ejected ($p < 0.05$, Figure 9). This finding suggests that RAPID hydrogels could protect transplanted cells from the mechanical forces encountered during syringe needle flow and serve as valuable cell carriers in transplantation protocols.

4.3.6 Cytocompatibility and 3D Cell Culture Potential of RAPID Hydrogels

Mounting evidence now highlights the mechanosensitive nature of OPCs within the CNS. These lineage-restricted glial cells give rise to myelinating oligodendrocytes, and OPC proliferation and differentiation both correlate with the physical stiffness of underlying 2D[106] or surrounding 3D matrices[107].

The biophysical properties of hydrogels sharply influence the proliferation and differentiation of stem cells within a 3D environment[108-109]. For instance, neural stem cells (NSCs) proliferate significantly more in softer substrates[1, 110], and preferentially differentiate into neurons in hydrogels with low moduli[111-113]. Recent evidence indicates that OPCs are also sensitive to the biophysical stiffness of their surrounding microenvironment[114]. We encapsulated OPCs[115] in order to examine the effect of the RAPID hydrogels on viability and proliferation. OPCs survived and grew in 1.5 wt. % AYFIL hydrogels (1900 Pa), as determined by the increase in both ATP and DNA concentrations over time (Figure 10a and 10b, respectively). A 1.5 wt. % AYFIL hydrogel was used to investigate cytocompatibility and cell growth, as its mechanical properties (~1900 Pa) approximate CNS tissue stiffness[1, 116]. Cell encapsulations with 1.5 wt. % KYFIL hydrogels resulted in poor cell viability, likely due to the stiffness (~8000 Pa) being much greater than native CNS tissue.

Live/dead imaging indicated a high percentage of viable cells (Figure 10C). Others have previously shown that OPCs can extend processes within 3D poly(ethylene glycol) hydrogels after 7 days of culture, but only in the presence of laminin[107]. Here, we demonstrate that cells within an AYFIL hydrogel can extend processes within 2 days of culture without any bioactive cellular adhesion peptide sequences or incorporating native ECM proteins (Figure 10D, Movie S8-S10). This could be due to physical hydrogel peptide matrix being permissive of remodeling by the cells.

This finding highlights that the simplicity of our cell culture system is sufficient for growth of cells derived from the CNS, without the need for laminin-derived peptide sequences as has been demonstrated in other peptide hydrogel systems[15].

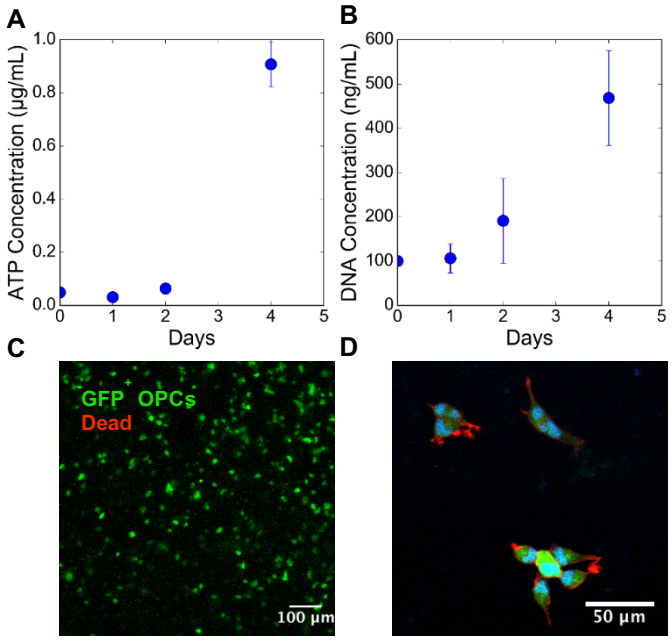

Figure 4-10. MADM OPC line encapsulated in 1.5 wt. % AYFIL hydrogels and cultured over 4 days. A) OPCs remained viable after encapsulation for at least 4 days, as determined by the increase of ATP over time (B). The increase in DNA concentration suggests that cells proliferate over the course of 4 days. Error bars represent standard error of the mean (SEM, n = 3). C) Live/Dead (green/red staining) images taken at Day 1 of the experiment demonstrate that the majority of cells remained viable following encapsulation. Image is a maximum projection of a 132 µm thick z-stack. D) Maximum projection (23 µm thick z-stack) of OPCs encapsulated in AYFIL hydrogels after 2 days of culture. Process extension of OPCs are observed, suggesting that these hydrogel systems are suitable for neural cell culture. GFP (green), Actin (red), DAPI (blue).

4.3.7 Conclusions

We have devised a new family of short, five amino acid, peptide sequences capable of self-assembling into robust hydrogels. We synthesized seven closely-related, stimuli-responsive pentapeptide sequences. Four of our RAPID sequences form robust hydrogels at concentrations down to at least 1.5 % (w/v). Physicochemical features of the sequence—in particular, amphiphilicity and inclusion of a central phenylalanine—influence the self-assembly and β-strand formation propensities of this class of peptides. MD simulations, aimed at examining the structural properties of these β-strand–forming peptides, reveal that hydration plays an integral role in the conformational dynamics of these peptides. Experiments reveal that our hydrogels exhibit shear-

thinning and self-healing properties—features that may stem, at least partly, from the facile formation of β-sheet structures (in accord with our MD simulations). These rheological properties suggest the suitability of our RAPID peptides for biomedical applications requiring injection. Additionally, we observe that at physiological pH, hierarchical nanostructures (i.e. individual fibers) bundle into clearly twisted, ribbon-like morphologies. The multi-stranded, twisted ribbons reported here are unique among nanofiber-forming, self-assembling peptide hydrogels. We demonstrate that these self-assembling hydrogels offer effective strategies for encapsulating OPCs within 3D matrices of tunable viscoelasticity. These scaffolds allow for cell growth and morphological process extension in OPCs. We also demonstrate that RAPID hydrogels can mitigate the damaging effects of extensional flow during syringe injections. The supramolecular assemblies formed by RAPID peptides represent injectable hydrogel systems that may offer new and translational approaches for cell delivery and tissue engineering applications.

4.3.8 ACKNOWLEDGMENT

The authors thank UVA's Molecular Electron Microscopy Core for EM imaging and UVA's W.M. Keck Center for Cellular Imaging for use of the Zeiss 510 and Zeiss 780 confocal/multiphoton microscopy systems. We acknowledge support from the UVA Center for Advanced Biomanufacturing for acquiring and supporting the peptide synthesis and rheometry equipment. We also thank Dr. Phil Bourne (UVA) for supporting these efforts, as well as Stephanie Guthrie and Dr. Gaurav Giri (UVA) for their assistance with FTIR characterization.

4.3.9 REFERENCES

1. Lampe, K. J.; Mooney, R. G.; Bjugstad, K. B.; Mahoney, M. J., Effect of macromer weight percent on neural cell growth in 2D and 3D nondegradable PEG hydrogel culture. *J Biomed Mater Res A* **2010,** *94a* (4), 1162-1171.
2. Asmani, M. N.; Ai, J.; Amoabediny, G.; Noroozi, A.; Azami, M.; Ebrahimi-Barough, S.; Navaei-Nigjeh, M.; Ai, A.; Jafarabadi, M., Three-dimensional culture of differentiated endometrial stromal cells to oligodendrocyte progenitor cells (OPCs) in fibrin hydrogel. *Cell Biol Int* **2013,** *37* (12), 1340-1349.
3. Annabi, N.; Tsang, K.; Mithieux, S. M.; Nikkhah, M.; Ameri, A.; Khademhosseini, A.; Weiss, A. S., Highly Elastic Micropatterned Hydrogel for Engineering Functional Cardiac Tissue. *Adv Funct Mater* **2013,** *23* (39), 4950-4959.
4. Tang, J. D.; Lampe, K. J., From de novo peptides to native proteins: advancements in biomaterial scaffolds for acute ischemic stroke repair. *Biomed Mater* **2018,** *13* (3).
5. Tam, R. Y.; Fuehrmann, T.; Mitrousis, N.; Shoichet, M. S., Regenerative Therapies for Central Nervous System Diseases: a Biomaterials Approach. *Neuropsychopharmacol* **2014,** *39* (1), 169-188.
6. Aguado, B. A.; Mulyasasmita, W.; Su, J.; Lampe, K. J.; Heilshorn, S. C., Improving Viability of Stem Cells During Syringe Needle Flow Through the Design of Hydrogel Cell Carriers. *Tissue Eng Pt A* **2012,** *18* (7-8), 806-815.
7. Cooke, M. J.; Zahir, T.; Phillips, S. R.; Shah, D. S. H.; Athey, D.; Lakey, J. H.; Shoichet, M. S.; Przyborski, S. A., Neural differentiation regulated by biomimetic surfaces presenting motifs of extracellular matrix proteins. *J Biomed Mater Res A* **2010,** *93a* (3), 824-832.

8. Kubinova, S.; Sykova, E., Nanotechnology for treatment of stroke and spinal cord injury. *Nanomedicine-Uk* **2010,** *5* (1), 99-108.
9. Sortwell, C. E., Strategies for the augmentation of grafted dopamine neuron survival. *Front Biosci* **2003,** *8*, S522-S532.
10. Raspa, A.; Saracino, G. A. A.; Pugliese, R.; Silva, D.; Cigognini, D.; Vescovi, A.; Gelain, F., Complementary Co-assembling Peptides: From In Silico Studies to In Vivo Application. *Adv Funct Mater* **2014,** *24* (40), 6317-6328.
11. Roberts, D.; Rochas, C.; Saiani, A.; Miller, A. F., Effect of Peptide and Guest Charge on the Structural, Mechanical and Release Properties of beta-Sheet Forming Peptides. *Langmuir* **2012,** *28* (46), 16196-16206.
12. Schneider, J. P.; Pochan, D. J.; Ozbas, B.; Rajagopal, K.; Pakstis, L.; Kretsinger, J., Responsive hydrogels from the intramolecular folding and self-assembly of a designed peptide. *J Am Chem Soc* **2002,** *124* (50), 15030-15037.
13. Aulisa, L.; Dong, H.; Hartgerink, J. D., Self-Assembly of Multidomain Peptides: Sequence Variation Allows Control over Cross-Linking and Viscoelasticity. *Biomacromolecules* **2009,** *10* (9), 2694-2698.
14. Foo, C. T. S. W. P.; Lee, J. S.; Mulyasasmita, W.; Parisi-Amon, A.; Heilshorn, S. C., Two-component protein-engineered physical hydrogels for cell encapsulation. *P Natl Acad Sci USA* **2009,** *106* (52), 22067-22072.
15. Silva, G. A.; Czeisler, C.; Niece, K. L.; Beniash, E.; Harrington, D. A.; Kessler, J. A.; Stupp, S. I., Selective differentiation of neural progenitor cells by high-epitope density nanofibers. *Science* **2004,** *303* (5662), 1352-1355.
16. Hauser, C. A. E.; Deng, R. S.; Mishra, A.; Loo, Y. H.; Khoe, U.; Zhuang, F. R.; Cheong, D. W.; Accardo, A.; Sullivan, M. B.; Riekel, C.; Ying, J. Y.; Hauser, U. A., Natural tri- to hexapeptides self-assemble in water to amyloid beta-type fiber aggregates by unexpected alpha-helical intermediate structures. *P Natl Acad Sci USA* **2011,** *108* (4), 1361-1366.
17. Tenidis, K.; Waldner, M.; Bernhagen, J.; Fischle, W.; Bergmann, M.; Weber, M.; Merkle, M. L.; Voelter, W.; Brunner, H.; Kapurniotu, A., Identification of a penta- and hexapeptide of islet amyloid polypeptide (IAPP) with amyloidogenic and cytotoxic properties. *J Mol Biol* **2000,** *295* (4), 1055-1071.
18. Doran, T. M.; Kamens, A. J.; Byrnes, N. K.; Nilsson, B. L., Role of amino acid hydrophobicity, aromaticity, and molecular volume on IAPP(20-29) amyloid self-assembly. *Proteins-Structure Function and Bioinformatics* **2012,** *80* (4), 1053-1065.
19. Bertolani, A.; Pirrie, L.; Stefan, L.; Houbenov, N.; Haataja, J. S.; Catalano, L.; Terraneo, G.; Giancane, G.; Valli, L.; Milani, R.; Ikkala, O.; Resnati, G.; Metrangolo, P., Supramolecular amplification of amyloid self-assembly by iodination. *Nat Commun* **2015,** *6*.
20. Reches, M.; Porat, Y.; Gazit, E., Amyloid fibril formation by pentapeptide and tetrapeptide fragments of human calcitonin. *J Biol Chem* **2002,** *277* (38), 35475-35480.
21. Thirumalai, D.; Klimov, D. K.; Dima, R. I., Emerging ideas on the molecular basis of protein and peptide aggregation. *Curr Opin Struc Biol* **2003,** *13* (2), 146-159.
22. Pappas, C. G.; Shafi, R.; Sasselli, I. R.; Siccardi, H.; Wang, T.; Narang, V.; Abzalimov, R.; Wijerathne, N.; Ulijn, R. V., Dynamic peptide libraries for the discovery of supramolecular nanomaterials. *Nat Nanotechnol* **2016,** *11* (11), 960-967.
23. Clarke, D. E.; Parmenter, C. D. J.; Scherman, O. A., Tunable Pentapeptide Self-Assembled beta-Sheet Hydrogels. *Angew Chem Int Edit* **2018,** *57* (26), 7709-7713.
24. Dong, H.; Paramonov, S. E.; Aulisa, L.; Bakota, E. L.; Hartgerink, J. D., Self-assembly of multidomain peptides: Balancing molecular frustration controls conformation and nanostructure. *J Am Chem Soc* **2007,** *129* (41), 12468-12472.
25. Stephanopoulos, N.; Ortony, J. H.; Stupp, S. I., Self-assembly for the synthesis of functional biomaterials. *Acta Mater* **2013,** *61* (3), 912-930.
26. Tysseling, V. M.; Sahni, V.; Pashuck, E. T.; Birch, D.; Hebert, A.; Czeisler, C.; Stupp, S. I.; Kessler, J. A., Self-Assembling Peptide Amphiphile Promotes Plasticity of Serotonergic Fibers Following Spinal Cord Injury. *J Neurosci Res* **2010,** *88* (14), 3161-3170.
27. Qin, S. Y.; Pei, Y.; Liu, X. J.; Zhuo, R. X.; Zhang, X. Z., Hierarchical self-assembly of a beta-amyloid peptide derivative. *J Mater Chem B* **2013,** *1* (5), 668-675.
28. Subbalakshmi, C.; Manorama, S. V.; Nagaraj, R., Self-assembly of short peptides composed of only aliphatic amino acids and a combination of aromatic and aliphatic amino acids. *J Pept Sci* **2012,** *18* (5), 283-292.
29. Debnath, S.; Shome, A.; Das, D.; Das, P. K., Hydrogelation Through Self-Assembly of Fmoc-Peptide Functionalized Cationic Amphiphiles: Potent Antibacterial Agent. *J Phys Chem B* **2010,** *114* (13), 4407-4415.
30. Tang, C.; Smith, A. M.; Collins, R. F.; Ulijn, R. V.; Saiani, A., Fmoc-Diphenylalanine Self-Assembly Mechanism Induces Apparent pK(a) Shifts. *Langmuir* **2009,** *25* (16), 9447-9453.
31. Melchionna, M.; Styan, K. E.; Marchesan, S., The Unexpected Advantages of Using D-Amino Acids for Peptide Self-Assembly into Nanostructured Hydrogels for Medicine. *Curr Top Med Chem* **2016,** *16* (18), 2009-2018.
32. Reches, M.; Gazit, E., Casting metal nanowires within discrete self-assembled peptide nanotubes. *Science* **2003,** *300* (5619), 625-627.
33. Zhou, M.; Smith, A. M.; Das, A. K.; Hodson, N. W.; Collins, R. F.; Ulijn, R. V.; Gough, J. E., Self-assembled peptide-based hydrogels as scaffolds for anchorage-dependent cells. *Biomaterials* **2009,** *30* (13), 2523-2530.
34. Zhang, S. G.; Holmes, T.; Lockshin, C.; Rich, A., SPONTANEOUS ASSEMBLY OF A SELF-COMPLEMENTARY OLIGOPEPTIDE TO FORM A STABLE MACROSCOPIC MEMBRANE. *P Natl Acad Sci USA* **1993,** *90* (8), 3334-3338.
35. Frederix, P. W. J. M.; Scott, G. G.; Abul-Haija, Y. M.; Kalafatovic, D.; Pappas, C. G.; Javid, N.; Hunt, N. T.; Ulijn, R. V.; Tuttle, T., Exploring the sequence space for (tri-) peptide self-assembly to design and discover. *Nature Chemistry* **2015,** *7* (1), 30-37.
36. Ogata, S.; Igarashi, T., Concurrent coupling of electronic-density-functional, molecular dynamics, and coarse-grained particles schemes for multiscale simulation of nanostructured materials. *New Frontiers of Processing and Engineering in Advanced Materials* **2005,** *502*, 33-38.
37. Head, D. A.; Tronci, G.; Russell, S. J.; Wood, D. J., In Silico Modeling of the Rheological Properties of Covalently Cross-Linked Collagen Triple Helices. *Acs Biomater Sci Eng* **2016,** *2* (8), 1224-1233.
38. Zhao, B. W.; Li, N. K.; Yingling, Y. G.; Hall, C. K., LCST Behavior is Manifested in a Single Molecule: Elastin-Like polypeptide (VPGVG)n. *Biomacromolecules* **2016,** *17* (1), 111-118.
39. Li, N. K.; Quiroz, F. G.; Hall, C. K.; Chilkoti, A.; Yingling, Y. G., Molecular Description of the LCST Behavior of an Elastin-Like Polypeptide. *Biomacromolecules* **2014,** *15* (10), 3522-3530.

40. Aurand, E. R.; Lampe, K. J.; Bjugstad, K. B., Defining and designing polymers and hydrogels for neural tissue engineering. *Neuroscience Research* **2012,** *72* (3), 199-213.
41. Lampel, A.; McPhee, S. A.; Park, H. A.; Scott, G. G.; Humagain, S.; Hekstra, D. R.; Yoo, B.; Frederix, P. W. J. M.; Li, T. D.; Abzalimov, R. R.; Greenbaum, S. G.; Tuttle, T.; Hu, C. H.; Bettinger, C. J.; Ulijn, R. V., Polymeric peptide pigments with sequence-encoded properties. *Science* **2017,** *356* (6342), 1064-1068.
42. Fleming, S.; Ulijn, R. V., Design of nanostructures based on aromatic peptide amphiphiles. *Chem Soc Rev* **2014,** *43* (23), 8150-8177.
43. Schneider, T. D.; Stephens, R. M., Sequence Logos - a New Way to Display Consensus Sequences. *Nucleic Acids Res* **1990,** *18* (20), 6097-6100.
44. Crooks, G. E.; Hon, G.; Chandonia, J. M.; Brenner, S. E., WebLogo: A sequence logo generator. *Genome Res* **2004,** *14* (6), 1188-1190.
45. Weiss, G. A.; Watanabe, C. K.; Zhong, A.; Goddard, A.; Sidhu, S. S., Rapid mapping of protein functional epitopes by combinatorial alanine scanning. *P Natl Acad Sci USA* **2000,** *97* (16), 8950-8954.
46. Cunningham, B. C.; Wells, J. A., High-Resolution Epitope Mapping of Hgh-Receptor Interactions by Alanine-Scanning Mutagenesis. *Science* **1989,** *244* (4908), 1081-1085.
47. Yang, H. Y.; Yang, S. N.; Kong, J. L.; Dong, A. C.; Yu, S. N., Obtaining information about protein secondary structures in aqueous solution using Fourier transform IR spectroscopy. *Nat Protoc* **2015,** *10* (3).
48. Byler, D. M.; Susi, H., Examination of the Secondary Structure of Proteins by Deconvolved Ftir Spectra. *Biopolymers* **1986,** *25* (3), 469-487.
49. Shivu, B.; Seshadri, S.; Li, J.; Oberg, K. A.; Uversky, V. N.; Fink, A. L., Distinct beta-Sheet Structure in Protein Aggregates Determined by ATR-FTIR Spectroscopy. *Biochemistry-Us* **2013,** *52* (31), 5176-5183.
50. Arluison, W.; Mura, C.; Guzman, M. R.; Liquier, J.; Pellegrini, O.; Gingery, M.; Regnier, P.; Marco, S., Three-dimensional structures of fibrillar Sm proteins: Hfq and other Sm-like proteins. *J Mol Biol* **2006,** *356* (1), 86-96.
51. Zandomeneghi, G.; Krebs, M. R. H.; Mccammon, M. G.; Fandrich, M., FTIR reveals structural differences between native beta-sheet proteins and amyloid fibrils. *Protein Sci* **2004,** *13* (12), 3314-3321.
52. Mura, C.; McAnany, C. E., An introduction to biomolecular simulations and docking. *Mol Simulat* **2014,** *40* (10-11), 732-764.
53. Tang, J. D.; McAnany, C. E.; Mura, C.; Lampe, K. J., Toward a Designable Extracellular Matrix: Molecular Dynamics Simulations of an Engineered Laminin-Mimetic, Elastin-Like Fusion Protein. *Biomacromolecules* **2016,** *17* (10), 3222-3233.
54. Crosby, K. C.; Postma, M.; Hink, M. A.; Zeelenberg, C. H. C.; Adjobo-Hermans, M. J. W.; Gadella, T. W. J., Quantitative Analysis of Self-Association and Mobility of Annexin A4 at the Plasma Membrane. *Biophysical Journal* **2013,** *104* (9), 1875-1885.
55. Popovych, N.; Sun, S.; Ebright, R. H.; Kalodimos, C. G., Dynamically driven protein allostery. *Nature Structural & Molecular Biology* **2006,** *13* (9), 831-838.
56. Melchels, F. P. W.; Barradas, A. M. C.; van Blitterswijk, C. A.; de Boer, J.; Feijen, J.; Grijpma, D. W., Effects of the architecture of tissue engineering scaffolds on cell seeding and culturing. *Acta Biomaterialia* **2010,** *6* (11), 4208-4217.
57. Huang, J.; MacKerell, A. D., CHARMM36 all-atom additive protein force field: Validation based on comparison to NMR data. *J Comput Chem* **2013,** *34* (25), 2135-2145.
58. McAnany, C. E.; Mura, C., Claws, Disorder, and Conformational Dynamics of the C-Terminal Region of Human Desmoplakin. *J Phys Chem B* **2016,** *120* (33), 8654-8667.
59. Papoian, G. A.; Wolynes, P. G., The physics and bioinformatics of binding and folding—an energy landscape perspective. *Biopolymers* **2003,** *68* (3), 333-349.
60. Das, P.; King, J. A.; Zhou, R. H., Aggregation of gamma-crystallins associated with human cataracts via domain swapping at the C-terminal beta-strands. *P Natl Acad Sci USA* **2011,** *108* (26), 10514-10519.
61. Rousseau, F.; Schymkowitz, J.; Itzhaki, L. S., Implications of 3d Domain Swapping for Protein Folding, Misfolding and Function. *Adv Exp Med Biol* **2012,** *747*, 137-152.
62. Nguyen, H. D.; Hall, C. K., Molecular dynamics simulations of spontaneous fibril formation by random-coil peptides. *P Natl Acad Sci USA* **2004,** *101* (46), 16180-16185.
63. Kozer, N.; Kuttner, Y. Y.; Haran, G.; Schreiber, G., Protein-protein association in polymer solutions: From dilute to semidilute to concentrated. *Biophysical Journal* **2007,** *92* (6), 2139-2149.
64. Pappu, R. V.; Rose, G. D., A simple model for polyproline II structure in unfolded states of alanine-based peptides. *Protein Sci* **2002,** *11* (10), 2437-2455.
65. de Groot, N. S.; Parella, T.; Aviles, F. X.; Vendrell, J.; Ventura, S., Ile-Phe dipeptide self-assembly: Clues to amyloid formation. *Biophysical Journal* **2007,** *92* (5), 1732-1741.
66. Rost, B.; Sander, C., Conservation and Prediction of Solvent Accessibility in Protein Families. *Proteins* **1994,** *20* (3), 216-226.
67. Saraboji, K.; Gromiha, M. M.; Ponnuswamy, M. N., Relative importance of secondary structure and solvent accessibility to the stability of protein mutants. A case study with amino acid properties and energetics on T4 and human lysozymes. *Comput Biol Chem* **2005,** *29* (1), 25-35.
68. Kyte, J.; Doolittle, R. F., A Simple Method for Displaying the Hydropathic Character of a Protein. *J Mol Biol* **1982,** *157* (1), 105-132.
69. Izzo, D.; Marques, C. M., Formation of Micelles of Diblock and Triblock Copolymers in a Selective Solvent. *Macromolecules* **1993,** *26* (26), 7189-7194.
70. Krogstad, D. V.; Lynd, N. A.; Miyajima, D.; Gopez, J.; Hawker, C. J.; Kramer, E. J.; Tirrell, M. V., Structural Evolution of Polyelectrolyte Complex Core Micelles and Ordered-Phase Bulk Materials. *Macromolecules* **2014,** *47* (22), 8026-8032.
71. Barros, D.; Amaral, I. F.; Pego, A. P., Biomimetic Synthetic Self-Assembled Hydrogels for Cell Transplantation. *Curr Top Med Chem* **2015,** *15* (13), 1209-1226.
72. Cai, L.; Heilshorn, S. C., Designing ECM-mimetic materials using protein engineering. *Acta Biomaterialia* **2014,** *10* (4), 1751-1760.

73. Wen, J. H.; Vincent, L. G.; Fuhrmann, A.; Choi, Y. S.; Hribar, K. C.; Taylor-Weiner, H.; Chen, S. C.; Engler, A. J., Interplay of matrix stiffness and protein tethering in stem cell differentiation. *Nat Mater* **2014,** *13* (10), 979-987.
74. Ye, K.; Wang, X.; Cao, L. P.; Li, S. Y.; Li, Z. H.; Yu, L.; Ding, J. D., Matrix Stiffness and Nanoscale Spatial Organization of Cell-Adhesive Ligands Direct Stem Cell Fate. *Nano Lett* **2015,** *15* (7), 4720-4729.
75. Janmey, P. A.; Miller, R. T., Mechanisms of mechanical signaling in development and disease. *Journal of Cell Science* **2011,** *124* (1), 9-18.
76. Discher, D. E.; Janmey, P.; Wang, Y. L., Tissue cells feel and respond to the stiffness of their substrate. *Science* **2005,** *310* (5751), 1139-1143.
77. Macaya, D.; Spector, M., Injectable hydrogel materials for spinal cord regeneration: a review. *Biomed Mater* **2012,** *7* (1).
78. Budday, S.; Nay, R.; de Rooij, R.; Steinmann, P.; Wyrobek, T.; Ovaert, T. C.; Kuhl, E., Mechanical properties of gray and white matter brain tissue by indentation. *J Mech Behav Biomed* **2015,** *46*, 318-330.
79. van Dommelen, J. A. W.; van der Sande, T. P. J.; Hrapko, M.; Peters, G. W. M., Mechanical properties of brain tissue by indentation: Interregional variation. *J Mech Behav Biomed* **2010,** *3* (2), 158-166.
80. Bjugstad, K. B.; Redmond, D. E.; Lampe, K. J.; Kern, D. S.; Sladek, J. R.; Mahoney, M. J., Biocompatibility of PEG-based hydrogels in primate brain. *Cell Transplant* **2008,** *17* (4), 409-415.
81. Bowerman, C. J.; Liyanage, W.; Federation, A. J.; Nilsson, B. L., Tuning beta-Sheet Peptide Self-Assembly and Hydrogelation Behavior by Modification of Sequence Hydrophobicity and Aromaticity. *Biomacromolecules* **2011,** *12* (7), 2735-2745.
82. Haines-Butterick, L. A.; Rajagopal, K.; Lamm, M.; Pochan, D. J.; Schnieder, J. P., Controlling hydrogelation kinetics via peptide design for three-dimensional encapsulation and injectable delivery of cells. *Biopolymers* **2007,** *88* (4), 518-518.
83. Krysmann, M. J.; Castelletto, V.; Kelarakis, A.; Hamley, I. W.; Hule, R. A.; Pochan, D. J., Self-assembly and hydrogelation of an amyloid peptide fragment. *Biochemistry-Us* **2008,** *47* (16), 4597-4605.
84. Zhang, Z. X.; Zheng, Q. X.; Wu, Y. C.; Hao, D. J., Compatibility of Neural Stem Cells with Functionalized Self-assembling Peptide Scaffold In vitro. *Biotechnol Bioproc E* **2010,** *15* (4), 545-551.
85. Yokoi, H.; Kinoshita, T.; Zhang, S. G., Dynamic reassembly of peptide RADA16 nanofiber scaffold. *P Natl Acad Sci USA* **2005,** *102* (24), 8414-8419.
86. Wang, H. M.; Yang, Z. M.; Adams, D. J., Controlling peptide-based hydrogelation. *Mater Today* **2012,** *15* (11), 500-507.
87. Dagdas, Y. S.; Tombuloglu, A.; Tekinay, A. B.; Dana, A.; Guler, M. O., Interfiber interactions alter the stiffness of gels formed by supramolecular self-assembled nanofibers. *Soft Matter* **2011,** *7* (7), 3524-3532.
88. Shin, Y.; Brangwynne, C. P., Liquid phase condensation in cell physiology and disease. *Science* **2017,** *357* (6357).
89. Boeynaems, S.; Alberti, S.; Fawzi, N. L.; Mittag, T.; Polymenidou, M.; Rousseau, F.; Schymkowitz, J.; Shorter, J.; Wolozin, B.; Van Den Bosch, L.; Tompa, P.; Fuxreiter, M., Protein Phase Separation: A New Phase in Cell Biology. *Trends Cell Biol* **2018,** *28* (6), 420-435.
90. Hughes, M. P.; Sawaya, M. R.; Boyer, D. R.; Goldschmidt, L.; Rodriguez, J. A.; Cascio, D.; Chong, L.; Gonen, T.; Eisenberg, D. S., Atomic structures of low-complexity protein segments reveal kinked beta sheets that assemble networks. *Science* **2018,** *359* (6376), 698-701.
91. Moore, A. N.; Hartgerink, J. D., Self-Assembling Multidomain Peptide Nanofibers for Delivery of Bioactive Molecules and Tissue Regeneration. *Accounts Chem Res* **2017,** *50* (4), 714-722.
92. Tian, Y. F.; Hudalla, G. A.; Han, H. F.; Collier, J. H., Controllably degradable beta-sheet nanofibers and gels from self-assembling depsipeptides. *Biomater Sci-Uk* **2013,** *1* (10), 1037-1045.
93. Clarke, D. E.; Parmenter, C. D. J.; Scherman, O. A., Tunable Pentapeptide Self-Assembled beta-Sheet Hydrogels. *Angew Chem Int Ed Engl* **2018**.
94. Aggeli, A.; Nyrkova, I. A.; Bell, M.; Harding, R.; Carrick, L.; McLeish, T. C. B.; Semenov, A. N.; Boden, N., Hierarchical self-assembly of chiral rod-like molecules as a model for peptide beta-sheet tapes, ribbons, fibrils, and fibers. *P Natl Acad Sci USA* **2001,** *98* (21), 11857-11862.
95. Uesaka, A.; Ueda, M.; Makino, A.; Imai, T.; Sugiyama, J.; Kimura, S., Morphology Control between Twisted Ribbon, Helical Ribbon, and Nanotube Self-Assemblies with His-Containing Helical Peptides in Response to pH Change. *Langmuir* **2014,** *30* (4), 1022-1028.
96. Fishwick, C. W. G.; Beevers, A. J.; Carrick, L. M.; Whitehouse, C. D.; Aggeli, A.; Boden, N., Structures of helical beta-tapes and twisted ribbons: The role of side-chain interactions on twist and bend behavior. *Nano Lett* **2003,** *3* (11), 1475-1479.
97. Wang, S. T.; Lin, Y.; Spencer, R. K.; Thomas, M. R.; Nguyen, A. I.; Amdursky, N.; Pashuck, E. T.; Skaalure, S. C.; Song, C. Y.; Parmar, P. A.; Morgan, R. M.; Ercius, P.; Aloni, S.; Zuckermann, R. N.; Stevens, M. M., Sequence-Dependent Self-Assembly and Structural Diversity of Islet Amyloid Polypeptide-Derived beta-Sheet Fibrils. *Acs Nano* **2017,** *11* (9), 8579-8589.
98. Fitzpatrick, A. W.; Debelouchina, G. T.; Bayro, M. J.; Clare, D. K.; Caporini, M. A.; Bajaj, V. S.; Jaroniec, C. P.; Wang, L.; Ladizhansky, V.; Muller, S. A.; MacPhee, C. E.; Waudby, C. A.; Mott, H. R.; De Simone, A.; Knowles, T. P.; Saibil, H. R.; Vendruscolo, M.; Orlova, E. V.; Griffin, R. G.; Dobson, C. M., Atomic structure and hierarchical assembly of a cross-beta amyloid fibril. *P Natl Acad Sci USA* **2013,** *110* (14), 5468-73.
99. Zhang, S.; Andreasen, M.; Nielsen, J. T.; Liu, L.; Nielsen, E. H.; Song, J.; Ji, G.; Sun, F.; Skrydstrup, T.; Besenbacher, F.; Nielsen, N. C.; Otzen, D. E.; Dong, M. D., Coexistence of ribbon and helical fibrils originating from hIAPP(20-29) revealed by quantitative nanomechanical atomic force microscopy. *P Natl Acad Sci USA* **2013,** *110* (8), 2798-2803.
100. Toksoz, S.; Guler, M. O., Self-assembled peptidic nanostructures. *Nano Today* **2009,** *4* (6), 458-469.
101. Chen, L.; Revel, S.; Morris, K.; Serpell, L. C.; Adams, D. J., Effect of Molecular Structure on the Properties of Naphthalene-Dipeptide Hydrogelators. *Langmuir* **2010,** *26* (16), 13466-13471.
102. Chamberlain, A. K.; MacPhee, C. E.; Zurdo, J.; Morozova-Roche, L. A.; Hill, H. A.; Dobson, C. M.; Davis, J. J., Ultrastructural organization of amyloid fibrils by atomic force microscopy. *Biophysical Journal* **2000,** *79* (6), 3282-93.
103. Wang, M.; Zhou, P.; Wang, J.; Zhao, Y.; Ma, H.; Lu, J. R.; Xu, H., Left or Right: How Does Amino Acid Chirality Affect the Handedness of Nanostructures Self-Assembled from Short Amphiphilic Peptides? *J Am Chem Soc* **2017,** *139* (11), 4185-4194.

104. Kocsis, J. D.; Sasaki, M.; Lankford, K. L.; Priest, C.; Wirth, E. D., Cell fate of human embryonic stem cell-derived oligodendrocyte progenitors (GRNOPC1) transplanted into the demyelinated nonhuman primate spinal cord. *Mult Scler J* **2011,** *17*, S46-S46.

105. Keirstead, H. S.; Nistor, G.; Bernal, G.; Totoiu, M.; Cloutier, F.; Sharp, K.; Steward, O., Human embryonic stem cell-derived oligodendrocyte progenitor cell transplants remyelinate and restore locomotion after spinal cord injury. *J Neurosci* **2005,** *25* (19), 4694-4705.

106. Urbanski, M. M.; Kingsbury, L.; Moussouros, D.; Kassim, I.; Mehjabeen, S.; Paknejad, N.; Melendez-Vasquez, C. V., Myelinating glia differentiation is regulated by extracellular matrix elasticity. *Sci Rep-Uk* **2016,** *6*.

107. Russell, L. N.; Lampe, K. J., Oligodendrocyte Precursor Cell Viability, Proliferation, and Morphology is Dependent on Mesh Size and Storage Modulus in 3D Poly(ethylene glycol)-Based Hydrogels. *Acs Biomater Sci Eng* **2017,** *3* (12), 3459-3468.

108. Tibbitt, M. W.; Anseth, K. S., Hydrogels as Extracellular Matrix Mimics for 3D Cell Culture. *Biotechnol Bioeng* **2009,** *103* (4), 655-663.

109. Haines-Butterick, L.; Rajagopal, K.; Branco, M.; Salick, D.; Rughani, R.; Pilarz, M.; Lamm, M. S.; Pochan, D. J.; Schneider, J. P., Controlling hydrogelation kinetics by peptide design for three-dimensional encapsulation and injectable delivery of cells. *P Natl Acad Sci USA* **2007,** *104* (19), 7791-7796.

110. Amer, M. H.; Rose, F. R. A. J.; Shakesheff, K. M.; White, L. J., A biomaterials approach to influence stem cell fate in injectable cell-based therapies. *Stem Cell Res Ther* **2018,** *9*.

111. Banerjee, A.; Arha, M.; Choudhary, S.; Ashton, R. S.; Bhatia, S. R.; Schaffer, D. V.; Kane, R. S., The influence of hydrogel modulus on the proliferation and differentiation of encapsulated neural stem cells. *Biomaterials* **2009,** *30* (27), 4695-4699.

112. Gao, M. Y.; Tao, H. Y.; Wang, T.; Wei, A. L.; He, B., Functionalized self-assembly polypeptide hydrogel scaffold applied in modulation of neural progenitor cell behavior. *J Bioact Compat Pol* **2017,** *32* (1), 45-60.

113. Cooke, M. J.; Wang, Y. F.; Morshead, C. M.; Shoichet, M. S., Controlled epi-cortical delivery of epidermal growth factor for the stimulation of endogenous neural stem cell proliferation in stroke-injured brain. *Biomaterials* **2011,** *32* (24), 5688-5697.

114. Lourenco, T.; Graos, M., Modulation of Oligodendrocyte Differentiation by Mechanotransduction. *Front Cell Neurosci* **2016,** *10*.

115. Liu, C.; Sage, J. C.; Miller, M. R.; Verhaak, R. G. W.; Hippenmeyer, S.; Vogel, H.; Foreman, O.; Bronson, R. T.; Nishiyama, A.; Luo, L. Q.; Zong, H., Mosaic Analysis with Double Markers Reveals Tumor Cell of Origin in Glioma. *Cell* **2011,** *146* (2), 209-221.

116. Massensini, A. R.; Ghuman, H.; Saldin, L. T.; Medberry, C. J.; Keane, T. J.; Nicholls, F. J.; Velankar, S. S.; Badylak, S. F.; Modo, M., Concentration-dependent rheological properties of ECM hydrogel for intracerebral delivery to a stroke cavity. *Acta Biomaterialia* **2015,** *27*, 116-130.

5 Rapidly Assembling Pentapeptides for Injectable Delivery (RAPID) Hydrogels as Cytoprotective Cell Carriers

Published as JD Tang, Roloson EB, Amelung CD, KJ Lampe, "Rapidly Assembling Pentapeptides for Injectable Delivery (RAPID) Hydrogels as Cytoprotective Cell Carriers," ACS Biomater. Sci. Eng. 5: 2117-2121 (2019)

5.1 Abstract

Low cell survival after syringe injection hampers the success of preclinical and clinical cell transplantation trials. During syringe injection, cells experience mechanical forces that lead to cell-membrane disruption and decreased viability. To improve cell survival, we designed Rapidly Assembling Pentapeptides for Injectable Delivery (RAPID) hydrogels that shear-thin, protect cells from extensional flow, form fibers, and provide mechanical properties similar to native tissue. We found that 1.5 wt % RAPID hydrogels mitigate the damaging effects of extensional flow resulting in significantly greater cell viability (of common laboratory cell lines, primary cells, and human cells) than cells injected in PBS.

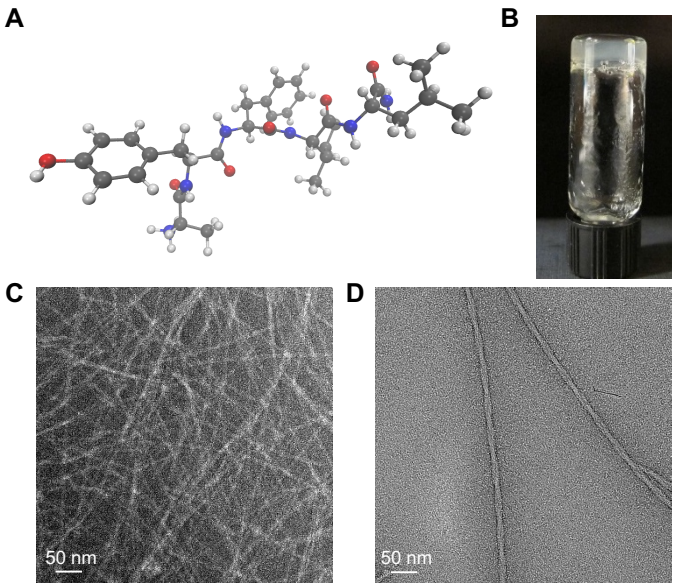

Figure 5-1. RAPID hydrogels here are formed from the AYFIL pentapeptide sequence. A) A ball-and-stick model of the peptide sequence with C'-terminal amidation displays the peptide backbone and side chains of residues (carbon in gray, hydrogen in silver, oxygen in red, and nitrogen in blue). B) 1.5 wt. % RAPID peptides undergo physical crosslinking and rapid gel formation upon mixing with PBS (pH 7.4). C) Representative EM images of 1.5 wt.% RAPID hydrogels show bulk fibers within the hydrogel. D) Individual fiber molecular assemblies within the pH 7.4 hydrogel exhibit twisted fibrillar morphology.

Recently, interest has grown in transplanting stem cells to restore tissue and organ function following an acute injury or debilitating disease, including stroke[1-3], tissue fibrosis[4-5], cardiac diseases[6-8], and Alzheimer's disease[9-11]. However, cell transplantation strategies suffer from poor cell survival (often with viabilities as low as 1% - 32% post-transplantation[12-13]) due, in part, to the harsh microenvironment and acute immune response at the injury site[14-15]. Stem cell therapeutics often require the use of syringe-based devices to deliver cells in a minimally invasive manner. Where accessibility is limited, delivery may be restricted to the usage of small-gauge needles, and the actual injection process itself may negatively affect the viability of cells during their passage through the needle[16].

Suspending cells in microenvironments conducive to cell survival through manipulation of their biomechanical properties can protect transplanted cells during and after delivery and support cell survival and growth[17-19]. Hydrogels are suitable for cell encapsulation because they can provide biophysical support for cells. Hydrogels that undergo reversible shear-induced thinning and self-healing could protect cells both during and after injection. Hydrogels can be easily modified with biological moieties[20-22], such as the attachment of cell-adhesive ligands[23-24], and growth factors[25]

[26], that support cellular proliferation and/or differentiation. However, in order to initiate a sol-gel phase transition, these hydrogels require either 1) covalent crosslinks either formed in vivo, which could potentially be cytotoxic[27-28], or formed *ex vivo,* creating preformed gels or 2) physical crosslinks formed via non-covalent and reversible bonds. Many physically crosslinked hydrogels are preferred for biomedical applications due to their cytocompatible properties, with some exhibiting shear-thinning and injectable capabilities[29-31]. However, these systems often require a substantial change to their environment, such as changes in pH[32-33], temperature[34-35], or ionic strength[36-37] in order to induce a gel phase transition. Consequently, cells encapsulated within these materials are often subject to non-physiological conditions that could lead to undesirable decreases in cell viability[38]. To address these challenges, we developed a new class of self-assembling pentapeptides capable of forming robust hydrogels upon mixing under physiological conditions[39]. These supramolecular assembly-based cell delivery vehicles are cost effective and simple to synthesize. Here, we demonstrate that this rapidly assembling pentapeptides for injectable delivery (RAPID) hydrogel can mitigate the damaging effects of extensional flow during syringe injections.

In this study, we report the design, synthesis, and characterization of a self-assembling pentapeptide hydrogel that can serve as a cell carrier for cell transplantation (Figure 1A). Our designer AYFIL-NH_2 sequence (hereafter referred to simply as 'AYFIL') self-assembles into β-sheet–forming nanofiber hydrogels. These hydrogels were examined via transmission electron microscopy (TEM) and were found to be uniformly composed of twisted nanofibers (Figure 1C, D). AYFIL morphologies included long fibers with a mean diameter of 10.18 ± 1.81 nm with twisted fibrillar morphology as determined via visual analysis. In comparison to previously reported pentapeptide sequences in the RAPID family[39], AYFIL fibers do not exhibit distinct ribbon-like morphology and the typical diameters of AYFIL fibers (≈ 10 nm) are significantly smaller than those of related KYFIL peptide sequence hydrogel fibers (≈ 40 nm)[39]. The smaller size of the AYFIL fibers is likely related to the fact that AYFIL hydrogels have a lower shear moduli than KYFIL hydrogels, perhaps indicating less robust or organized fiber assembly. AYFIL hydrogels also have a lower loss moduli (viscous component of shear modulus) and demonstrate a slightly lower viscosity as a function of shear (Figure 2D)[39], which could potentially make them easier to inject.

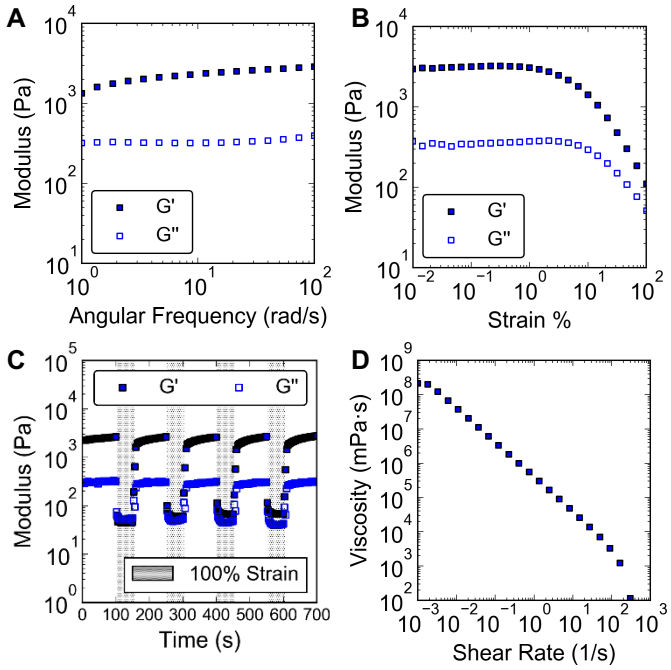

Figure 5-2. Rheological properties of 1.5 wt. % RAPID hydrogels at pH 7.4 (n = 1 for all samples). A) Angular frequency sweep of AYFIL pentapeptide sequence at constant strain of 0.1%. G' is an order of magnitude greaten than G" indicating hydrogelation has occurred. B) Strain sweep of gelling pentapeptide sequences at constant angular frequency of 10 rad/s. Above the critical strain at 5%, the material becomes progressively more fluid-like, where G' starts to increase and G" begins to decrease. C) Five step strain sweeps of 0.1 % (100 s) and 100 % strain (50 s), followed by a 100 s recovery period, were performed on RAPID hydrogels. The hydrogel recovered 90% of its initial G' within several seconds. The hydrogel repeatedly recovered its mechanical strength following multiple high strain cycles. D) The apparent viscosity decreased linearly with increasing shear rate demonstrating that these hydrogels are capable of shear-thinning.

RAPID samples had higher storage moduli (*G′*) than loss moduli (*G″),* verifying that a hydrogel was indeed formed (Figure 2A, B). Multiple high strain (100%) sweep cycles with 30 s recovery periods demonstrated the AYFIL hydrogel's ability to self-heal following mechanical deformation (Figure 2C). 1.5 wt. % AYFIL hydrogels recovered 90% of their initial *G′* after the first cycle within 10 s, and up to 98% in the following cycles, with no further decrease in *G′* observed in subsequent large-amplitude oscillatory shear cycles. After multiple high strain cycles, the hydrogel's ability to rapidly and repeatedly recover its mechanical strength indicates that these materials can withstand mechanical deformation from exogenous strains. Additionally, the apparent viscosity decreases linearly as a function of increasing shear rate, emulating the behavior of similar KYFIL pentapeptides[39], demonstrating the hydrogel's shear-thinning capability (Figure 2D).

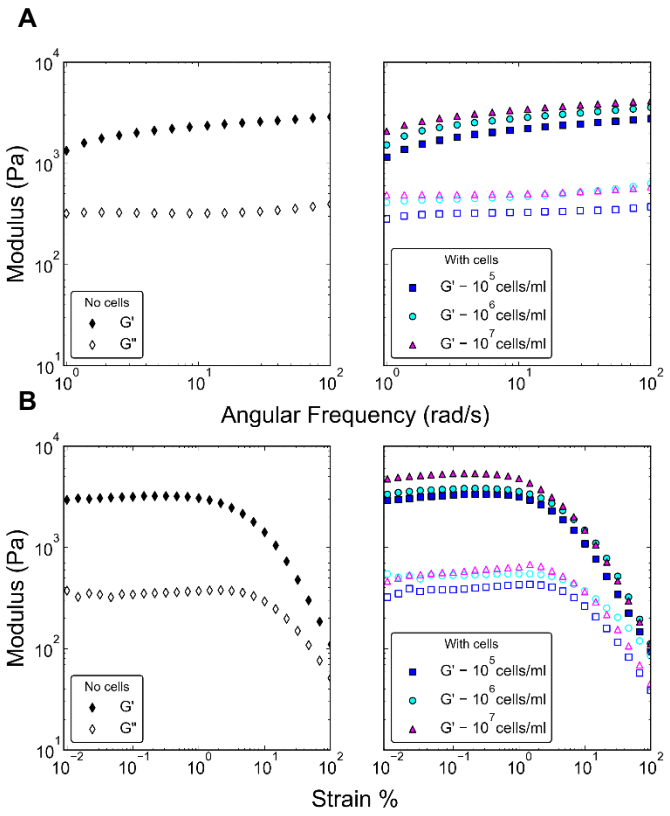

Figure 5-3. Rheological properties of 1.5 wt. % RAPID hydrogels with and without encapsulated cells. (n = 1 for all samples). A) Angular frequency sweep of gelling pentapeptide sequences at constant 0.1% strain with and without encapsulated cells (10^5 cells/ml in blue squares, 10^6 cells/ml in cyan circles, 10^7 cells/ml in purple triangles; no cells in black diamonds). G' is an order of magnitude greaten than G" indicating hydrogelation has occurred for all samples. B) Strain sweep of gelling pentapeptide sequences at constant frequency of 1 hz (10^5 cells/ml in blue squares, 10^6 cells/ml in cyan circles, 10^7 cells/ml in magenta triangles; no cells in black diamonds). Above the critical strain at 5%, the material becomes progressively more fluid-like, where G' starts to increase and G" begins to decrease. The storage modulus (G') is indicated by filled-in shapes, and the loss modulus (G") is indicated by empty shapes.

We hypothesized that the shear-thinning and rapid self-healing nature of hydrogels would make them useful as injectable cell carriers. Studies have previously shown that cell damage occurs during the ejection process due to the mechanical disruption of cell membranes[16]. During syringe needle flow, cells can experience various types of mechanical forces that ultimately disrupt the cellular membrane: 1) extensional flow, where cells encounter stretching forces, 2) pressure drop across the cell, and 3) shear stresses, due to linear shear flow as the cell travels down the syringe[16]. Cross-linked alginate hydrogels with the lowest storage modulus (29.6 Pa) significantly improve the viability of ejected cells to 88.9 ± 4.9% versus uncross-linked alginate (58.7 ± 8.1%)[16]. While

this is a markedly improved result compared to Newtonian fluids, a high concentration of calcium ions involved in the crosslinking process could have a detrimental effect on cell survival and proliferation immediately following the injection process[38, 40].

We sought to address these challenges using RAPID hydrogels that rapidly form in PBS solution. Before the syringe injection process, we examined the effect of cell density on hydrogel mechanical properties as the addition of cells into the hydrogel matrix could significantly alter their mechanical properties[41-42]. One of the many advantages of physically crosslinked hydrogels (such as RAPID) versus covalently crosslinked hydrogels is that cell mobility (i.e. through contractile and adhesive forces exerted by the cell) is often not hindered since fibers within physically crosslinked hydrogels are compliant enough to allow for cellular-based remodeling induced by cellular contractile forces[43-44]. We then investigated three different cell concentrations (1×10^5, 1×10^6, and 1×10^7 cells/mL) to determine whether increasing cell concentrations would drastically alter the hydrogel's mechanical properties, and subsequently the injectability of these constructs.

First, we examined the mechanical properties of cell-free hydrogels. G' was determined to be 3.1 ± 0.13 kPa as indicated by the linear viscoelastic regime. We next determined the effects of adding oligodendrocyte precursor cells (OPCs) to the hydrogel precursor solution. Once cells were encapsulated within the hydrogel and incubated for 10 minutes, the combined solution was pipetted unto the rheometer platform for further mechanical characterization (please refer to the supplementary material where more experimental detail is provided). G' increased with cell density and decreased with increasing shear strain (Figure 3). The increase in cell density results in an increase of G' upwards of 30% compared to hydrogels with no cells. For comparison, cells typically exert strains of up to 3 – 4% in 2D culture[45] and up to 20 – 30% in 3D culture[46-47]. The increase in G' is subsequently reflected in increasing cell density and increased mechanical strength[48] of the hydrogel, most likely as a result of the contributing strain forces exerted by encapsulated cells. Similarly, culture time can also affect the stiffness and viscoelastic characteristics of hydrogels owing to differences in matrix accumulation[49]. Our results are in agreement with other physical hydrogels such as alginate hydrogels[40], and they illustrate the positive relationship between increasing cell density and mechanical strength of our RAPID hydrogels. Others observe a decrease in the compressive modulus in covalently crosslinked

hydrogels with higher encapsulated cell concentration[50]. The decrease in modulus in such a system could be attributed to cell-mediated quenching of photoinitiated radicals, thus inhibiting polymerization[51]. Alternatively, cells may perturb covalent hydrogel networks by introducing defects that prevent higher-order crosslinking within the precursor solutions[52].

Finally, we experimentally tested the effects of syringe needle flow (1000 μL/min[53]) on cell viability for several cell types: oligodendrocyte precursor cells (OPC), mouse myoblasts (C2C12), primary human mesenchymal stem cells (hMSC), and primary mouse lung fibroblasts (MLF) (n = 3 to 5 replicates). We chose these mammalian cells, including common laboratory cell lines, primary cells, and human cells, to robustly show that the gel could protect a variety of cell types from damage occurring during syringe injection. All cell samples experienced a significant decrease in cell viability during syringe needle flow when delivered in PBS alone ($*p < 0.05$, Figure 4A, B). For primary MLFs, the cells incurred significantly more damage to their membranes, as indicated by the colocalization of the calcein AM and ethidium homodimer-1 stains. For OPCs specifically, the viability was 86.8% for cells injected with RAPID hydrogels, and 48.8% in PBS. This agrees well with the previously reported viability of ejected OPCs, 85.2% and 46.2% for cells in hydrogels and PBS, respectively[54], suggesting the reproducibility of our experiments. RAPID hydrogels with G' = 3.1 kPa were able to mitigate the damaging effects of extensional flow for all tested cell types, resulting in significantly greater cell viability than cells injected in PBS.

In summary, we synthesized an AYFIL peptide sequence capable of self-assembling into a hydrogel in physiological conditions. The rheological properties indicate the suitability of RAPID hydrogels for biomedical applications requiring injection. At physiological pH, hierarchical nanostructures (i.e. individual fibrils) bundle into twisted nanofiber morphologies to form the gel.

We show that these RAPID hydrogels exhibit shear-thinning and self-healing properties. Increasing cell density leads to a trend toward increasing hydrogel modulus. Importantly, we observe higher overall cell viability after syringe flow in hydrogels compared to cells ejected in

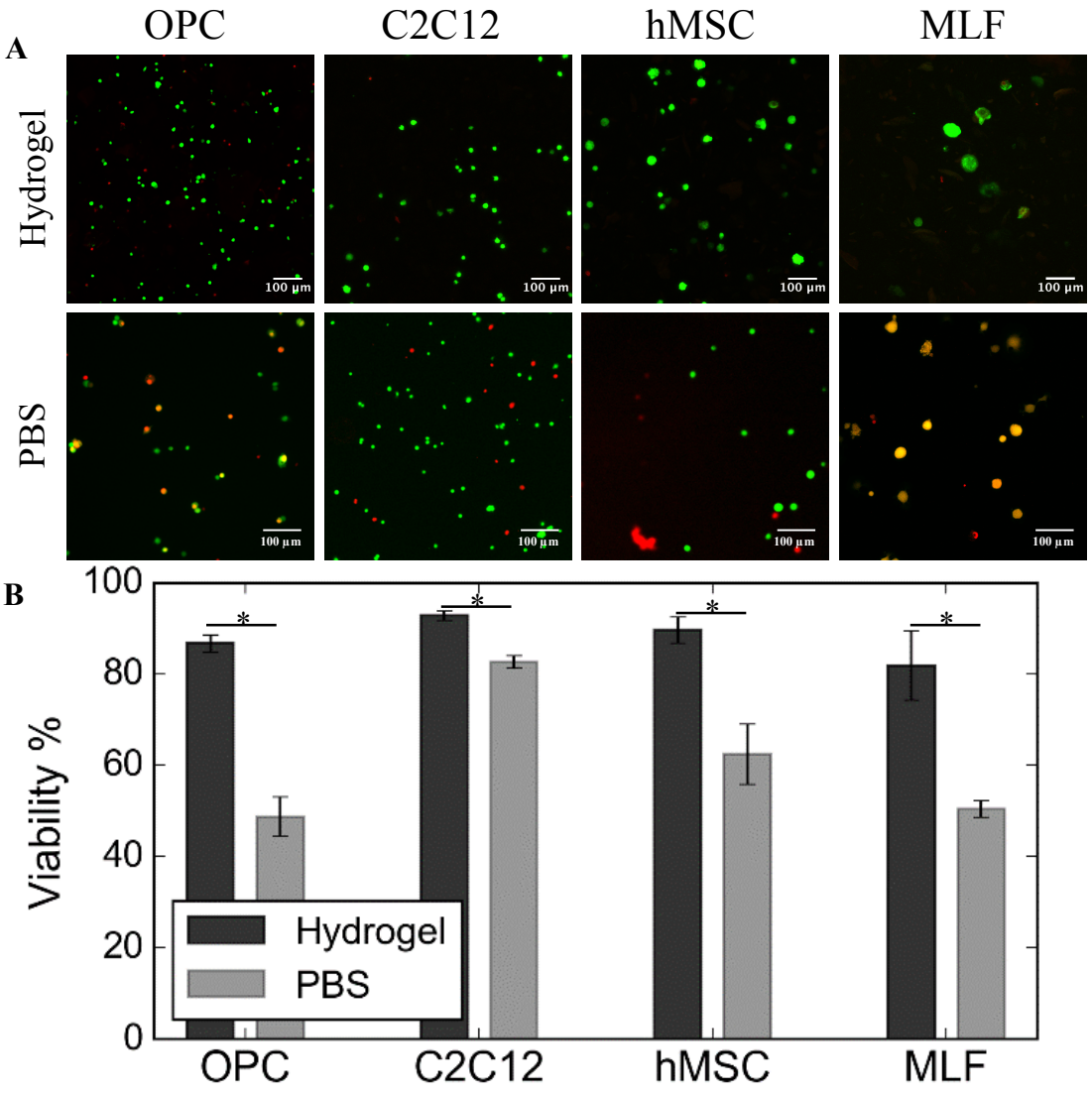

*Figure 5-4. Short-term viability of oligodendrocyte precursor cells (OPC), mouse myoblast (C2C12), human mesenchymal stem cells (hMSC), and primary mouse lung fibroblasts (MLF) after syringe needle flow in 1.5 wt. % RAPID hydrogels and PBS. A) Live/Dead images of viable (green) and membrane damaged (red) cells one hour post-ejection show that cell membranes are significantly comprised when PBS is used as an ejection vehicle. Viability is rescued when RAPID hydrogels were used as an ejection vehicle. B) When cells were ejected in PBS, cell viability was significantly decreased compared to cells encapsulated in RAPID hydrogels and ejected. Error bars represent standard error of the mean (SEM) from three separate ejections (n = 3), *p < 0.05. Total cell numbers reported for OPCs, C2C12s, hMSCs, and MLFs in hydrogels are 222, 38, 40, and 40 respectively, and 167, 476, 61, and 32 in PBS, respectively.*

PBS. These self-assembling hydrogels offer effective strategies for encapsulating various cell types within 3D matrices, including sensitive primary and human cells, and for protecting them from syringe-needle flow during the injection process. We used several different cell types in the experiment to test the universal protective capabilities of RAPID hydrogels, and demonstrate that cell protection applies across different cell types. All cell types that were encapsulated within RAPID hydrogels displayed significantly higher viability compared to cells ejected with PBS. Encapsulating these cells within RAPID hydrogels may shield them from deformation by extensional flow and shear by linear flow and could potentially improve the therapeutic outcomes of stem-cell based therapies. Furthermore, this material could be used for a variety of cell culture and 3D printing applications, or to inject therapeutic cells and localize them to a potential injury site, given the injectability and self-recovery capabilities of the RAPID hydrogel.

5.2 **Acknowledgements**

The authors thank Stephanie Guthrie and Dr. Gaurav Giri (University of Virginia) for the usage of their syringe pump (Harvard Apparatus PHD 2000). Cells were kind gifts from Steven R. Caliari (C2C12, hMSC), UVA Chemical Engineering; and Thomas H. Barker (MLF), UVA Biomedical Engineering.

5.3 References

1. Chau, M. J.; Deveau, T. C.; Song, M. K.; Gu, X. H.; Chen, D. D.; Wei, L., iPSC Transplantation Increases Regeneration and Functional Recovery After Ischemic Stroke in Neonatal Rats. *Stem Cells* **2014,** *32* (12), 3075-3087.
2. Wechsler, L.; Steindler, D.; Borlongan, C.; Chopp, M.; Savitz, S.; Deans, R.; Caplan, L.; Hess, D.; Mays, R. W.; Participants, S., Stem Cell Therapies as an Emerging Paradigm in Stroke (STEPS) Bridging Basic and Clinical Science for Cellular and Neurogenic Factor Therapy in Treating Stroke. *Stroke* **2009,** *40* (2), 510-515.
3. Wong, F. S. Y.; Chan, B. P.; Lo, A. C. Y., Carriers in Cell-Based Therapies for Neurological Disorders. *Int J Mol Sci* **2014,** *15* (6), 10669-10723.
4. Prockop, D. J., Inflammation, fibrosis, and modulation of the process by mesenchymal stem/stromal cells. *Matrix Biol* **2016,** *51*, 7-13.
5. Oakland, M.; Sinn, P. L.; McCray, P. B., Advances in Cell and Gene-based Therapies for Cystic Fibrosis Lung Disease. *Mol Ther* **2012,** *20* (6), 1108-1115.
6. Annabi, N.; Tsang, K.; Mithieux, S. M.; Nikkhah, M.; Ameri, A.; Khademhosseini, A.; Weiss, A. S., Highly Elastic Micropatterned Hydrogel for Engineering Functional Cardiac Tissue. *Adv Funct Mater* **2013,** *23* (39), 4950-4959.
7. Chen, H. J.; Chen, C. H.; Chang, M. Y.; Tsai, D. C.; Baum, E. Z.; Hariri, R.; Herzberg, U.; Hsteh, P. C. H., Human Placenta-Derived Adherent Cells Improve Cardiac Performance in Mice With Chronic Heart Failure. *Stem Cell Transl Med* **2015,** *4* (3), 269-275.
8. Sirabella, D.; Cimetta, E.; Vunjak-Novakovic, G., "The state of the heart": Recent advances in engineering human cardiac tissue from pluripotent stem cells. *Exp Biol Med* **2015,** *240* (8), 1008-1018.
9. Bali, P.; Lahiri, D. K.; Banik, A.; Nehru, B.; Anand, A., Potential for Stem Cells Therapy in Alzheimer's Disease: Do Neurotrophic Factors Play Critical Role? *Curr Alzheimer Res* **2017,** *14* (2), 208-220.
10. Li, X. Y.; Bao, X. J.; Wang, R. Z., Potential of neural stem cell-based therapies for Alzheimer's disease. *J Neurosci Res* **2015,** *93* (9), 1313-1324.
11. Raman, D.; Choudhary, M.; Cleary, J. P.; Punzalan, R. R.; Sharma, C. V.; Sharma, M. V.; Balmiki, R.; Chopra, N.; Lahiri, D. K.; Sharma, J. P., Potential of neuronal progenitor stem cell therapy for Alzheimer's disease. *Mol Biol Cell* **2011,** *22*.
12. Zhang, M.; Methot, D.; Poppa, V.; Fujio, Y.; Walsh, K.; Murry, C. E., Cardiomyocyte grafting for cardiac repair: Graft cell death and anti-death strategies. *J Mol Cell Cardiol* **2001,** *33* (5), 907-921.

13. Allan, D. S.; Keeney, M.; Howson-Jan, K.; Bhatia, M.; Sutherland, D. R.; Chin-Yee, I., Number of viable CD34+cells reinfused predicts engraftment in autologous hematopoietic stem cell transplantation. *Blood* **2000,** *96* (11), 381a-381a.
14. Cooke, M. J.; Zahir, T.; Phillips, S. R.; Shah, D. S. H.; Athey, D.; Lakey, J. H.; Shoichet, M. S.; Przyborski, S. A., Neural differentiation regulated by biomimetic surfaces presenting motifs of extracellular matrix proteins. *J Biomed Mater Res A* **2010,** *93a* (3), 824-832.
15. Kubinova, S.; Sykova, E., Nanotechnology for treatment of stroke and spinal cord injury. *Nanomedicine-Uk* **2010,** *5* (1), 99-108.
16. Aguado, B. A.; Mulyasasmita, W.; Su, J.; Lampe, K. J.; Heilshorn, S. C., Improving Viability of Stem Cells During Syringe Needle Flow Through the Design of Hydrogel Cell Carriers. *Tissue Eng Pt A* **2012,** *18* (7-8), 806-815.
17. Amer, M. H.; Rose, F. R. A. J.; Shakesheff, K. M.; Modo, M.; White, L. J., Translational considerations in injectable cell-based therapeutics for neurological applications: concepts, progress and challenges. *Npj Regen Med* **2017,** *2*.
18. Abbott, R. D.; Kimmerling, E. P.; Cairns, D. M.; Kaplan, D. L., Silk as a Biomaterial to Support Long-Term Three-Dimensional Tissue Cultures. *Acs Appl Mater Inter* **2016,** *8* (34), 21861-21868.
19. Weber, L. M.; Hayda, K. N.; Haskins, K.; Anseth, K. S., The effects of cell-matrix interactions on encapsulated beta-cell function within hydrogels functionalized with matrix-derived adhesive peptides. *Biomaterials* **2007,** *28* (19), 3004-11.
20. Lampe, K. J.; Heilshorn, S. C., Building stem cell niches from the molecule up through engineered peptide materials. *Neurosci Lett* **2012,** *519* (2), 138-146.
21. Galler, K. M.; Aulisa, L.; Regan, K. R.; D'Souza, R. N.; Hartgerink, J. D., Self-Assembling Multidomain Peptide Hydrogels: Designed Susceptibility to Enzymatic Cleavage Allows Enhanced Cell Migration and Spreading. *J Am Chem Soc* **2010,** *132* (9), 3217-3223.
22. Cai, L.; Heilshorn, S. C., Designing ECM-mimetic materials using protein engineering. *Acta Biomaterialia* **2014,** *10* (4), 1751-1760.
23. Bellis, S. L., Advantages of RGD peptides for directing cell association with biomaterials. *Biomaterials* **2011,** *32* (18), 4205-4210.
24. Ye, K.; Wang, X.; Cao, L. P.; Li, S. Y.; Li, Z. H.; Yu, L.; Ding, J. D., Matrix Stiffness and Nanoscale Spatial Organization of Cell-Adhesive Ligands Direct Stem Cell Fate. *Nano Lett* **2015,** *15* (7), 4720-4729.
25. Anderson, E. M.; Silva, E. A.; Hao, Y. B.; Martinick, K. D.; Vermillion, S. A.; Stafford, A. G.; Doherty, E. G.; Wang, L.; Doherty, E. J.; Grossman, P. M.; Mooney, D. J., VEGF and IGF Delivered from Alginate Hydrogels Promote Stable Perfusion Recovery in Ischemic Hind Limbs of Aged Mice and Young Rabbits. *J Vasc Res* **2017,** *54* (5), 288-298.
26. Nih, L. R.; Gojgini, S.; Carmichael, S. T.; Segura, T., Dual-function injectable angiogenic biomaterial for the repair of brain tissue following stroke. *Nat Mater* **2018,** *17* (7), 642-+.
27. Lampe, K. J.; Namba, R. M.; Silverman, T. R.; Bjugstad, K. B.; Mahoney, M. J., Impact of Lactic Acid on Cell Proliferation and Free Radical-Induced Cell Death in Monolayer Cultures of Neural Precursor Cells. *Biotechnol Bioeng* **2009,** *103* (6), 1214-1223.
28. Lampe, K. J.; Mooney, R. G.; Bjugstad, K. B.; Mahoney, M. J., Effect of macromer weight percent on neural cell growth in 2D and 3D nondegradable PEG hydrogel culture. *J Biomed Mater Res A* **2010,** *94a* (4), 1162-1171.
29. Ding, X. C.; Gao, J.; Wang, Z. G.; Awada, H.; Wang, Y. D., A shear-thinning hydrogel that extends in vivo bioactivity of FGF2. *Biomaterials* **2016,** *111*, 80-89.
30. Highley, C. B.; Rodell, C. B.; Burdick, J. A., Direct 3D Printing of Shear-Thinning Hydrogels into Self-Healing Hydrogels. *Adv Mater* **2015,** *27* (34), 5075-+.
31. Sing, M. K.; Glassman, M. J.; Vronay-Ruggles, X. T.; Burghardt, W. R.; Olsen, B. D., Structure and rheology of dual-associative protein hydrogels under nonlinear shear flow. *Soft Matter* **2017,** *13* (45), 8511-8524.
32. Clarke, D. E.; Parmenter, C. D. J.; Scherman, O. A., Tunable Pentapeptide Self-Assembled beta-Sheet Hydrogels. *Angew Chem Int Ed Engl* **2018**.
33. Cheng, T. Y.; Chen, M. H.; Chang, W. H.; Huang, M. Y.; Wang, T. W., Neural stem cells encapsulated in a functionalized self-assembling peptide hydrogel for brain tissue engineering. *Biomaterials* **2013,** *34* (8), 2005-2016.
34. Araujo, A.; Olsen, B. D.; Machado, A. V., Engineering Elastin-Like Polypeptide-Poly(ethylene glycol) Multiblock Physical Networks. *Biomacromolecules* **2018,** *19* (2), 329-339.
35. Stabenfeldt, S. E.; Garcia, A. J.; LaPlaca, M. C., Thermoreversible laminin-functionalized hydrogel for neural tissue engineering. *J Biomed Mater Res A* **2006,** *77a* (4), 718-725.
36. Ozbas, B.; Kretsinger, J.; Rajagopal, K.; Schneider, J. P.; Pochan, D. J., Salt-triggered peptide folding and consequent self-assembly into hydrogels with tunable modulus. *Macromolecules* **2004,** *37* (19), 7331-7337.
37. Wang, H. M.; Yang, Z. M.; Adams, D. J., Controlling peptide-based hydrogelation. *Mater Today* **2012,** *15* (11), 500-507.
38. Bohari, S. P. M.; Hukins, D. W. L.; Grover, L. M., Effect of calcium alginate concentration on viability and proliferation of encapsulated fibroblasts. *Bio-Med Mater Eng* **2011,** *21* (3), 159-170.
39. Tang, J. D.; Mura, C.; Lampe, K. J., Stimuli-Responsive, Pentapeptide, Nanofiber Hydrogel for Tissue Engineering. *J Am Chem Soc* **2019,** *141* (12), 4886-4899.
40. Cao, N.; Chen, X. B.; Schreyer, D. J., Influence of Calcium Ions on Cell Survival and Proliferation in the Context of an Alginate Hydrogel. *ISRN Chemical Engineering* **2012,** *2012*, 9.
41. Buckley, C. T.; Thorpe, S. D.; O'Brien, F. J.; Robinson, A. J.; Kelly, D. J., The effect of concentration, thermal history and cell seeding density on the initial mechanical properties of agarose hydrogels. *J Mech Behav Biomed* **2009,** *2* (5), 512-521.
42. Payne, C.; Dolan, E. B.; O'Sullivan, J.; Cryan, S. A.; Kelly, H. M., A methylcellulose and collagen based temperature responsive hydrogel promotes encapsulated stem cell viability and proliferation in vitro. *Drug Deliv Transl Re* **2017,** *7* (1), 132-146.
43. Wakatsuki, T.; Elson, E. L., Reciprocal interactions between cells and extracellular matrix during remodeling of tissue constructs. *Biophys Chem* **2003,** *100* (1-3), 593-605.
44. Brown, R. A.; Prajapati, R.; McGrouther, D. A.; Yannas, I. V.; Eastwood, M., Tensional homeostasis in dermal fibroblasts: Mechanical responses to mechanical loading in three-dimensional substrates. *J Cell Physiol* **1998,** *175* (3), 323-332.

45. Discher, D. E.; Janmey, P.; Wang, Y. L., Tissue cells feel and respond to the stiffness of their substrate. *Science* **2005,** *310* (5751), 1139-1143.
46. Legant, W. R.; Miller, J. S.; Blakely, B. L.; Cohen, D. M.; Genin, G. M.; Chen, C. S., Measurement of mechanical tractions exerted by cells in three-dimensional matrices. *Nat Methods* **2010,** *7* (12), 969-U113.
47. Chaudhuri, O.; Gu, L.; Klumpers, D.; Darnell, M.; Bencherif, S. A.; Weaver, J. C.; Huebsch, N.; Lee, H. P.; Lippens, E.; Duda, G. N.; Mooney, D. J., Hydrogels with tunable stress relaxation regulate stem cell fate and activity. *Nat Mater* **2016,** *15* (3), 326-+.
48. Williams, G. M.; Klein, T. J.; Sah, R. L., Cell density alters matrix accumulation in two distinct fractions and the mechanical integrity of alginate-chondrocyte constructs. *Acta Biomaterialia* **2005,** *1* (6), 625-633.
49. Wan, L. Q.; Jiang, J.; Miller, D. E.; Guo, X. E.; Mow, V. C.; Lu, H. H., Matrix Deposition Modulates the Viscoelastic Shear Properties of Hydrogel-Based Cartilage Grafts. *Tissue Eng Pt A* **2011,** *17* (7-8), 1111-1122.
50. Schneider, M. C.; Chu, S.; Sridhar, S. L.; de Roucy, G.; Vernerey, F. J.; Bryant, S. J., Local Heterogeneities Improve Matrix Connectivity in Degradable and Photoclickable Poly(ethylene glycol) Hydrogels for Applications in Tissue Engineering. *Acs Biomater Sci Eng* **2017,** *3* (10), 2480-2492.
51. Farnsworth, N.; Bensard, C.; Bryant, S. J., The role of the PCM in reducing oxidative stress induced by radical initiated photoencapsulation of chondrocytes in poly(ethylene glycol) hydrogels. *Osteoarthr Cartilage* **2012,** *20* (11), 1326-1335.
52. Lange, F.; Schwenke, K.; Kurakazu, M.; Akagi, Y.; Chung, U. I.; Lang, M.; Sommer, J. U.; Sakai, T.; Saalwachter, K., Connectivity and Structural Defects in Model Hydrogels: A Combined Proton NMR and Monte Carlo Simulation Study. *Macromolecules* **2011,** *44* (24), 9666-9674.
53. Tol, M.; Akar, A. R.; Durdu, S.; Ayyildiz, E.; Ilhan, O., Comparison of different needle diameters and flow rates on bone marrow mononuclear stem cell viability: an ex vivo experimental study. *Cytotherapy* **2008,** *10* (1), 98-99.
54. Tang, J. D.; Mura, C.; Lampe, K. J., A stimuli-responsive, pentapeptide, nanofiber hydrogel for tissue engineering. *J Am Chem Soc* **2019**.

6 Conclusions

This thesis focused on developing supramolecular biomaterials for applications in neural tissue regeneration. We employed a multifaceted approach that employs computational modeling of peptides and proteins to design and synthesize multi-domain assemblies similar to those found within the CNS. We have thus employed MD simulations in the design of a new class of self-assembling pentapeptide hydrogels (RAPID) in combination with experimental approaches. By simulating our systems at physiological temperature and for significant durations (>100 nsec per system), we developed an atomic-resolution, quantitative understanding of the 3D structure and conformational dynamics of our design. In this way, we were able to assess the suitability of our construct as a general-purpose scaffold for our longer-term goals (hydrogels to mimic ECMs of neural tissues). In the work presented, we report a self-assembling pentapeptide sequence that does not require any protection groups such as acetyl[1-4], t-butyloxycarbonyl[5], or other large aromatic groups[6-7], which simplifies the synthesis process and greatly reduces the cost of materials. We created and modeled several peptides that gel under physiological conditions and recapitulates the biomechanical properties of the native brain extracellular matrix (ECM). This combinatorial strategy provides 1) an important molecular model and mechanistic understanding of peptide assembly, 2) rheological behavior conducive to injectable delivery, and 3) hydrogel properties favorable to neural cell growth and development.

In the last three decades, most short self-assembling peptides have been discovered by mapping onto sequence design principles derived from biological systems, or synthesized based on the conformational heterogeneity of amyloid fibers[8-10]. However, descriptions of the thermodynamics in the folding pathway are often plagued by ill-informed design principles that fail to predict the structural diversity of highly ordered structures. While the principles are generally able to make clear the biomolecular function to which these structures are associated with, they are not readily interpretable at an atomic or molecular level. Currently, we are limited by our understanding of how specific sequences of amino acids spontaneously fold into higher-order structural units. How can we capture this highly dynamical process that involves the formation and dissociation of molecular interactions that vary greatly in the type (e.g. long-range electrostatic interactions, hydrophobic effect, hydrogen bonding etc.), number, and duration?[11] For this work, we found that MD simulations serve as a versatile toolbox that allows us to dissect the

conformational dynamics of our peptide system, namely, we were able to show that the assembly propensity of the peptides is correlated with the diffusional association of individual peptides in the presence of long-range forces. Additionally, these MD simulations, aimed at examining the structural properties of these β-strand–forming peptides, reveal that hydration plays an integral role in the conformational dynamics of these peptides. We also find that self-assembly is primarily driven by π-π stacking interactions and the amphiphilicity of the peptide sequence, resulting in stacked β-sheet conformations, as confirmed by FTIR studies.

For our experimental studies, we synthesized seven closely-related, stimuli-responsive pentapeptide sequences. Four of these pentapeptide sequences form robust hydrogels at concentrations down to at least 1.5 % (w/v). Physicochemical features of the sequence—in particular, amphiphilicity and inclusion of a central phenylalanine—influence the self-assembly and β-strand formation propensities of this class of peptides. Experiments reveal that our hydrogels exhibit shear-thinning and self-healing properties—features that may stem, at least partly, from the facile formation of β-sheet structures (in accord with our MD simulations). We observe that at physiological pH, hierarchical nanostructures (i.e. individual fibers) bundle into clearly twisted, ribbon-like morphologies. The multi-stranded, twisted ribbons reported here are unique among nanofiber-forming, self-assembling peptide hydrogels. The supramolecular assemblies formed by RAPID peptides represent injectable hydrogel systems that may offer new and translational approaches for cell delivery and tissue engineering applications.

Additionally, we also demonstrate that the rheological properties of RAPID hydrogels render them suitable for biomedical applications requiring injection. This is important because low cell survival after syringe injection hampers the success of preclinical and clinical cell transplantation trials. During syringe injection, cells experience mechanical forces that lead to cell-membrane disruption and decreased viability. To improve cell survival, these RAPID hydrogels were designed to shear-thin, protect cells from extensional flow, form fibers, and provide mechanical properties similar to native tissue. In our syringe experiments, we found that 1.5 wt % RAPID hydrogels mitigate the damaging effects of extensional flow resulting in significantly greater cell viability (of common laboratory cell lines, primary cells, and human cells) than cells injected in PBS. Increasing cell density of encapsulated cells leads to a trend toward increasing hydrogel modulus. Importantly, we observe higher overall cell viability after syringe flow in hydrogels compared to cells ejected in PBS. These self-assembling hydrogels offer effective

strategies for encapsulating various cell types within 3D matrices, including sensitive primary and human cells, and for protecting them from syringe-needle flow during the injection process. We used several different cell types in the experiment to test the universal protective capabilities of RAPID hydrogels, and demonstrate that cell protection applies across different cell types. Encapsulating these cells within RAPID hydrogels may shield them from deformation by extensional flow and shear by linear flow and could potentially improve the therapeutic outcomes of stem-cell based therapies. Furthermore, this material could be used for a variety of cell culture and 3D printing applications, or to inject therapeutic cells and localize them to a potential injury site, given the injectability and self-recovery capabilities of the RAPID hydrogel.

Finally, we demonstrated that the presence of cell-adhesive epitopes influences the growth and process extension of OPCs. Nonfunctionalized RAPID hydrogels alone saw limited changes in OPC morphology compared to gels that incorporated cell-adhesive ligands. IKVAV, RGD, and YIGSR functionalized hydrogels had similar material mechanics, and increased levels of cell metabolic activity compared to non-functionalized hydrogel controls. The hydrogel system presented here allows for independent adjusting of the concentration of multiple cell-adhesive ligands without any changes to the mechanical properties of the hydrogel. The facile preparation of functionalized RAPID hydrogels should be widely applicable to other studies at understanding the effects of matrix-bound ligands involving 3D hydrogel encapsulation studies.

7 Future Perspectives

While it has been demonstrated that cell transplantation strategies using biomaterial scaffolds can potentially improve the neurologic outcome and reduce infarct size, many questions still remain, and the precise cellular and biochemical mechanisms of cell-induced repair remain to be elucidated. For example, are necrotic cells being replaced, or do transplanted cells produce neurotrophic factors that stimulate endogenous repair? What cell type(s) should be used that would promote neurogenesis and/or vasculogenesis? What are the specific cues that initiate cell propagation or differentiation within biomaterials? What intracellular signaling pathways should be considered (i.e. conjugation of growth factors and ECM proteins to biomaterials) that would have the most impact on cell-matrix interactions? What is the optimum therapeutic time window

for such biomaterials-based therapy? What key mechanical properties (e.g. topography, matrix stiffness, porosity) of hydrogel biomaterials are most important in improving regeneration? And, most importantly, what types of biomaterials, or combinations thereof, will yield the most therapeutic benefit?

Additionally, biomaterials development should consider cell-matrix interactions that influence trophic support and differentiation potentials. This includes incorporating degradable sites in the biomaterial to allow for cell secreted protease-induced remodeling of the matrix. Additional molecules from the secretome (i.e. cytokines, chemokines produced through paracrine signaling, and trophic factors) derived from stem cells also play a large role in improving post-stroke angiogenesis and functional recovery[12-14]. Furthermore, stroke therapies should also consider the delivery of neuroprotective compounds that suppress the deleterious effects of inflammation and prevent cellular degeneration. Unfortunately, most of these drugs are inactive following systemic administration due to the low permeability of the blood-brain barrier (BBB)[15]. From a biological standpoint, nano-scale delivery systems that can mediate cell-cell and cell surface receptors-ligand levels that can reliably permeate through the BBB have yet to be developed. Subsequently, in order to effectively develop drugs that can cross the BBB, a refined understanding of the crosstalk between endothelial cells and associated astrocytes, as well as the selectivity of the tight junctions from between the two is required. Even after the delivery vehicle is able to penetrate into the brain tissue, the surface of the vehicle must be tailored with site-specific ligands to localize the bioavailability to only the affected areas of the brain (i.e. infarct cavity).

Incorporation of vasculature within biomaterial scaffolds, especially in the context of neural regeneration in stroke injury models, still remains a significant challenge in the field. Mimicking the endogenous expansion of blood vessels into vast networks during neurogenesis and concomitantly remodeling of the neovasculature is a highly unexplored area. NSCs and oligodendrocyte progenitor cells are frequently found, and migrate along, small blood vessels. Ultimately, most in the field have opted for developing models that can establish tight junctions between endothelial cells and contacts with pericytes and astrocyte endfeet using induced pluripotent stem cell (iPSC)-derived sources[16-17], however, these models insufficiently describe the vascular tree and cerebral arterial hierarchy inherently present in the CNS. Understanding the

cross-talk between neural and vascular cells and signaling pathways will reveal how a dysfunctional neurovascular unit is remodeled upon injury. The challenge of decoupling the synergistic effects of vascular development and brain development, however, remain to be addressed[18-19].

Finally, it is important to consider modulating the immune system in response to ischemia-induced inflammation. Ideally, a reduced inflammatory response from biomaterials engraftment is a favorable outcome. However, it has become exceedingly clear that activated microglial and perivascular macrophages play an integral role in reestablishing tissue homeostasis in the brain and remodeling of the neurovascular unit. In early stages of recovery, chronically activated microglial produce pro-inflammatory cytokines, toxic amounts of ROS, and MMPs that degrade the BBB. At later stages, phagocytosis of cellular debris along with the production of anti-inflammatory cytokines by the same microglia occurs, consequently attenuating the deleterious effects of inflammation and inhibition of tissue regeneration. Because of the Janus-faced nature of these reactive glia that could play both a destructive and protective role at different time points, therapeutics targeting inflammation in cerebral ischemia should be mindful of temporal considerations that can block deleterious effects within the penumbra and foster post-ischemic anti-inflammation mediators that can contribute to tissue repair. Ultimately transplanted biomaterials will likely serve as a provisional matrix, influencing the injury environment and directing any transplanted cell behavior, until the integrating transplant or host cells can establish de novo tissue. Modulating both the injury, and the immune reaction to it, are underexplored areas ripe for new strategies in CNS regeneration.

7.1 References

1. Lakshmanan, A.; Zhang, S. G.; Hauser, C. A. E., Short self-assembling peptides as building blocks for modern nanodevices. *Trends Biotechnol* **2012,** *30* (3), 155-165.
2. Hauser, C. A. E.; Deng, R. S.; Mishra, A.; Loo, Y. H.; Khoe, U.; Zhuang, F. R.; Cheong, D. W.; Accardo, A.; Sullivan, M. B.; Riekel, C.; Ying, J. Y.; Hauser, U. A., Natural tri- to hexapeptides self-assemble in water to amyloid beta-type fiber aggregates by unexpected alpha-helical intermediate structures. *P Natl Acad Sci USA* **2011,** *108* (4), 1361-1366.
3. Mishra, A.; Loo, Y. H.; Deng, R. H.; Chuah, Y. J.; Hee, H. T.; Ying, J. Y.; Hauser, C. A. E., Ultrasmall natural peptides self-assemble to strong temperature-resistant helical fibers in scaffolds suitable for tissue engineering. *Nano Today* **2011,** *6* (3), 232-239.
4. Aulisa, L.; Dong, H.; Hartgerink, J. D., Self-Assembly of Multidomain Peptides: Sequence Variation Allows Control over Cross-Linking and Viscoelasticity. *Biomacromolecules* **2009,** *10* (9), 2694-2698.
5. Subbalakshmi, C.; Manorama, S. V.; Nagaraj, R., Self-assembly of short peptides composed of only aliphatic amino acids and a combination of aromatic and aliphatic amino acids. *J Pept Sci* **2012,** *18* (5), 283-292.
6. Fleming, S.; Ulijn, R. V., Design of nanostructures based on aromatic peptide amphiphiles. *Chem Soc Rev* **2014,** *43* (23), 8150-8177.
7. Chen, L.; Revel, S.; Morris, K.; Serpell, L. C.; Adams, D. J., Effect of Molecular Structure on the Properties of Naphthalene-Dipeptide Hydrogelators. *Langmuir* **2010,** *26* (16), 13466-13471.
8. Ridgley, D. M.; Freedman, B. G.; Lee, P. W.; Barone, J. R., Genetically encoded self-assembly of large amyloid fibers. *Biomater Sci-Uk* **2014,** *2* (4), 560-566.
9. Qin, S. Y.; Pei, Y.; Liu, X. J.; Zhuo, R. X.; Zhang, X. Z., Hierarchical self-assembly of a beta-amyloid peptide derivative. *J Mater Chem B* **2013,** *1* (5), 668-675.
10. Tamamis, P.; Archontis, G., Amyloid-like self-assembly of a dodecapeptide sequence from the adenovirus fiber shaft: Perspectives from molecular dynamics simulations. *J Non-Cryst Solids* **2011,** *357* (2), 717-722.
11. Mura, C.; McAnany, C. E., An introduction to biomolecular simulations and docking. *Mol Simulat* **2014,** *40* (10-11), 732-764.
12. Kandalam, S.; Sindji, L.; Delcroix, G. J. R.; Violet, F.; Garric, X.; Andre, E. M.; Schiller, P. C.; Venier-Julienne, M. C.; des Rieux, A.; Guicheux, J.; Montero-Menei, C. N., Pharmacologically active microcarriers delivering BDNF within a hydrogel: Novel strategy for human bone marrow-derived stem cells neural neuronal differentiation guidance and therapeutic secretome enhancement. *Acta Biomaterialia* **2017,** *49*, 167-180.
13. Piscioneri, A.; Morelli, S.; Mele, M.; Canonaco, M.; Bilotta, E.; Pantano, P.; Drioli, E.; De Bartolo, L., Neuroprotective effect of human mesenchymal stem cells in a compartmentalized neuronal membrane system. *Acta Biomaterialia* **2015,** *24*, 297-308.
14. Yeng, C. H.; Chen, P. J.; Chang, H. K.; Lo, W. Y.; Wu, C. C.; Chang, C. Y.; Chou, C. H.; Chen, S. H., Attenuating spinal cord injury by conditioned medium from human umbilical cord blood-derived CD34(+) cells in rats. *Taiwan J Obstet Gyne* **2016,** *55* (1), 85-93.
15. Nance, E.; Timbie, K.; Miller, G. W.; Song, J.; Louttit, C.; Klibanov, A. L.; Shih, T. Y.; Swaminathan, G.; Tamargo, R. J.; Woodworth, G. F.; Hanes, J.; Price, R. J., Non-invasive delivery of stealth, brain-penetrating nanoparticles across the blood - brain barrier using MRI-guided focused ultrasound. *J Control Release* **2014,** *189*, 123-132.
16. Kaisar, M. A.; Sajja, R. K.; Prasad, S.; Abhyankar, V. V.; Liles, T.; Cucullo, L., New experimental models of the blood-brain barrier for CNS drug discovery. *Expert Opinion on Drug Discovery* **2017,** *12* (1), 89-103.
17. Lippmann, E. S.; Azarin, S. M.; Kay, J. E.; Nessler, R. A.; Wilson, H. K.; Al-Ahmad, A.; Palecek, S. P.; Shusta, E. V., Derivation of blood-brain barrier endothelial cells from human pluripotent stem cells. *Nat Biotechnol* **2012,** *30* (8), 783-91.
18. Mehdizadeh, H.; Sumo, S.; Bayrak, E. S.; Brey, E. M.; Cinar, A., Three-dimensional modeling of angiogenesis in porous biomaterial scaffolds. *Biomaterials* **2013,** *34* (12), 2875-2887.
19. Phelps, E. A.; Landazuri, N.; Thule, P. M.; Taylor, W. R.; Garcia, A. J., Bioartificial matrices for therapeutic vascularization. *P Natl Acad Sci USA* **2010,** *107* (8), 3323-3328.

8 Bibliography

1. Lutz, A. B.; Barres, B. A., Contrasting the Glial Response to Axon Injury in the Central and Peripheral Nervous Systems. *Dev Cell* **2014,** *28* (1), 7-17.
2. Lau, L. W.; Cua, R.; Keough, M. B.; Haylock-Jacobs, S.; Yong, V. W., OPINION Pathophysiology of the brain extracellular matrix: a new target for remyelination. *Nat Rev Neurosci* **2013,** *14* (10), 722-729.
3. Allen, N. J.; Barres, B. A., NEUROSCIENCE Glia - more than just brain glue. *Nature* **2009,** *457* (7230), 675-677.
4. Russell, L. N.; Lampe, K. J., Engineering Biomaterials to Influence Oligodendroglial Growth, Maturation, and Myelin Production. *Cells Tissues Organs* **2016,** *202* (1-2), 85-101.
5. Sofroniew, M. V.; Vinters, H. V., Astrocytes: biology and pathology. *Acta Neuropathol* **2010,** *119* (1), 7-35.
6. Zimmermann, D. R.; Dours-Zimmermann, M. T., Extracellular matrix of the central nervous system: from neglect to challenge. *Histochem Cell Biol* **2008,** *130* (4), 635-653.
7. World Health Organization, Global Health Estimates 2015: Deaths by Cause, Age, Sex, by Country and by Region, 2000-2015. **2016**.
8. Murray, C. J. L.; Vos, T.; Lozano, R., Disability-adjusted life years (DALYs) for 291 diseases and injuries in 21 regions, 1990-2010: a systematic analysis for the Global Burden of Disease Study 2010 (vol 380, pg 2197, 2012). *Lancet* **2014,** *384* (9943), 582-582.
9. Krishnamurthi, R. V.; deVeber, G.; Feigin, V. L.; Barker-Collo, S.; Fullerton, H.; Mackay, M. T.; O'Callahan, F.; Lindsay, M. P.; Kolk, A.; Lo, W.; Shah, P.; Linds, A.; Jones, K.; Parmar, P.; Taylor, S.; Norrving, B.; Mensah, G. A.; Moran, A. E.; Naghavi, M.; Forouzanfar, M. H.; Nguyen, G.; Johnson, C. O.; Vos, T.; Murray, C. J. L.; Roth, G. A.; Grp, G. S. P. E., Stroke Prevalence, Mortality and Disability-Adjusted Life Years in Children and Youth Aged 0-19 Years: Data from the Global and Regional Burden of Stroke 2013. *Neuroepidemiology* **2015,** *45* (3), 177-189.
10. Feigin, V. L.; Forouzanfar, M. H.; Krishnamurthi, R.; Mensah, G. A.; Connor, M.; Bennett, D. A.; Moran, A. E.; Sacco, R. L.; Anderson, L.; Truelsen, T.; O'Donnell, M.; Venketasubramanian, N.; Barker-Collo, S.; Lawes, C. M. M.; Wang, W. Z.; Shinohara, Y.; Witt, E.; Ezzati, M.; Naghavi, M.; Murray, C.; Fa, G. B. D. I. R.; Grp, G. S. E., Global and regional burden of stroke during 1990-2010: findings from the Global Burden of Disease Study 2010. *Lancet* **2014,** *383* (9913), 245-255.
11. Moskowitz, M. A.; Lo, E. H.; Iadecola, C., The Science of Stroke: Mechanisms in Search of Treatments. *Neuron* **2010,** *67* (2), 181-198.
12. Mitsios, N.; Gaffney, J.; Kumar, P.; Krupinski, J.; Kumar, S.; Slevin, M., Pathophysiology of acute ischaemic stroke: An analysis of common signalling mechanisms and identification of new molecular targets. *Pathobiology* **2006,** *73* (4), 159-175.
13. Zhang, L.; Chopp, M.; Liu, X. S.; Teng, H.; Tang, T.; Kassis, H.; Zhang, Z. G., Combination Therapy With VELCADE and Tissue Plasminogen Activator Is Neuroprotective in Aged Rats After Stroke and Targets MicroRNA-146a and the Toll-Like Receptor Signaling Pathway. *Arterioscl Throm Vas* **2012,** *32* (8), 1856-U336.
14. Peerschke, E. I.; Yin, W.; Ghebrehiwet, B., Complement activation on platelets: Implications for vascular inflammation and thrombosis. *Mol Immunol* **2010,** *47* (13), 2170-2175.

15. Wechsler, L. R.; Jovin, T. G., Intravenous Recombinant Tissue-Type Plasminogen Activator in the Extended Time Window and the US Food and Drug Administration Confused About the Time. *Stroke* **2012,** *43* (9), 2517-2519.
16. Wechsler, L.; Steindler, D.; Borlongan, C.; Chopp, M.; Savitz, S.; Deans, R.; Caplan, L.; Hess, D.; Mays, R. W.; Participants, S., Stem Cell Therapies as an Emerging Paradigm in Stroke (STEPS) Bridging Basic and Clinical Science for Cellular and Neurogenic Factor Therapy in Treating Stroke. *Stroke* **2009,** *40* (2), 510-515.
17. Savitz, S. I.; Chopp, M.; Deans, R.; Carmichael, S. T.; Phinney, D.; Wechsler, L., Stem Cell Therapy as an Emerging Paradigm for Stroke (STEPS) II. *Stroke* **2011,** *42* (3), 825-829.
18. Cooke, M. J.; Zahir, T.; Phillips, S. R.; Shah, D. S. H.; Athey, D.; Lakey, J. H.; Shoichet, M. S.; Przyborski, S. A., Neural differentiation regulated by biomimetic surfaces presenting motifs of extracellular matrix proteins. *J Biomed Mater Res A* **2010,** *93a* (3), 824-832.
19. Kubinova, S.; Sykova, E., Nanotechnology for treatment of stroke and spinal cord injury. *Nanomedicine-Uk* **2010,** *5* (1), 99-108.
20. Sharp, K. G.; Dickson, A. R.; Marchenko, S. A.; Yee, K. M.; Emery, P. N.; Laidmae, I.; Uibo, R.; Sawyer, E. S.; Steward, O.; Flanagan, L. A., Salmon fibrin treatment of spinal cord injury promotes functional recovery and density of serotonergic innervation. *Exp Neurol* **2012,** *235* (1), 345-56.
21. Hamann, M. C. J.; Tator, C. H.; Shoichet, M. S., Injectable intrathecal delivery system for localized administration of EGF and FGF-2 to the injured rat spinal cord. *Exp Neurol* **2005,** *194* (1), 106-119.
22. Matsuse, D.; Kitada, M.; Ogura, F.; Wakao, S.; Kohama, M.; Kira, J.; Tabata, Y.; Dezawa, M., Combined Transplantation of Bone Marrow Stromal Cell-Derived Neural Progenitor Cells with a Collagen Sponge and Basic Fibroblast Growth Factor Releasing Microspheres Enhances Recovery After Cerebral Ischemia in Rats. *Tissue Eng Pt A* **2011,** *17* (15-16), 1993-2004.
23. Ajioka, I.; Jinnou, H.; Okada, K.; Sawada, M.; Saitoh, S.; Sawamoto, K., Enhancement of Neuroblast Migration into the Injured Cerebral Cortex Using Laminin-Containing Porous Sponge. *Tissue Eng Pt A* **2015,** *21* (1-2), 193-201.
24. Oshikawa, M.; Okada, K.; Kaneko, N.; Sawamoto, K.; Ajioka, I., Affinity-Immobilization of VEGF on Laminin Porous Sponge Enhances Angiogenesis in the Ischemic Brain. *Adv Healthc Mater* **2017,** *6* (11).
25. Hess, D. C.; Auchus, A. P.; Uchino, K.; Sila, C.; Clark, W. M.; Chiu, D.; Wechsler, L. R.; Mays, R. W.; Investigators, B.-. Final Results of the B01-02 Phase 2 Trial Testing the Safety and Efficacy of MultiStem(R) in Treatment of Ischemic Stroke. *Stroke* **2016,** *47*.
26. Friedrich, M. A. G.; Martins, M. P.; Araujo, M. D.; Klamt, C.; Vedolin, L.; Garicochea, B.; Raupp, E. F.; El Ammar, J. S.; Machado, D. C.; da Costa, J. C.; Nogueira, R. G.; Rosado-de-Castro, P. H.; Mendez-Otero, R.; de Freitas, G. R., Intra-Arterial Infusion of Autologous Bone Marrow Mononuclear Cells in Patients With Moderate to Severe Middle Cerebral Artery Acute Ischemic Stroke. *Cell Transplant* **2012,** *21*, S13-S21.
27. Bang, O. Y., Clinical Trials of Adult Stem Cell Therapy in Patients with Ischemic Stroke. *J Clin Neurol* **2016,** *12* (1), 14-20.
28. Burnstock, G., Purinergic signalling and disorders of the central nervous system. *Nat Rev Drug Discov* **2008,** *7* (7), 575-590.
29. Broughton, B. R. S.; Reutens, D. C.; Sobey, C. G., Apoptotic Mechanisms After Cerebral Ischemia. *Stroke* **2009,** *40* (5), E331-E339.

30. Unal-Cevik, I.; Kilinc, M.; Can, A.; Gursoy-Ozdemir, Y.; Dalkara, T., Apoptotic and necrotic death mechanisms are concomitantly activated in the same cell after cerebral ischemia. *Stroke* **2004,** *35* (9), 2189-2194.
31. Fabricius, M.; Fuhr, S.; Bhatia, R.; Boutelle, M.; Hashemi, P.; Strong, A. J.; Lauritzen, M., Cortical spreading depression and peri-infarct depolarization in acutely injured human cerebral cortex. *Brain* **2006,** *129*, 778-790.
32. Mattson, M. P.; Culmsee, C.; Yu, Z. F., Apoptotic and antiapoptotic mechanisms in stroke. *Cell Tissue Res* **2000,** *301* (1), 173-187.
33. Chukanova, E. I.; Khozhamzharov, B. E.; Chukanova, A. S., Current possibilities of the correction of oxidative stress in acute brain ischemia. *Zh Nevrol Psikhiatr* **2012,** *112* (11), 79-82.
34. Dobrotvorskaya, I. S.; Fedorova, T. N.; Dobrota, D.; Berezov, T. T., Characteristics of Oxidative Stress in Experimental Rat Brain Ischemia Aggravated by Homocysteic Acid. *Neurochem J+* **2011,** *5* (1), 42-46.
35. Dirnagl, U.; Iadecola, C.; Moskowitz, M. A., Pathobiology of ischaemic stroke: an integrated view. *Trends Neurosci* **1999,** *22* (9), 391-397.
36. Sims, N. R.; Anderson, M. F., Mitochondrial contributions to tissue damage in stroke. *Neurochem Int* **2002,** *40* (6), 511-526.
37. Lakhan, S. E.; Kirchgessner, A.; Tepper, D.; Leonard, A., Matrix metalloproteinases and blood-brain barrier disruption in acute ischemic stroke. *Front Neurol* **2013,** *4*.
38. Iadecola, C.; Anrather, J., The immunology of stroke: from mechanisms to translation. *Nat Med* **2011,** *17* (7), 796-808.
39. Hyman, M. C.; Petrovic-Djergovic, D.; Visovatti, S. H.; Liao, H.; Yanamadala, S.; Bouis, D.; Su, E. M. J.; Lawrence, D. A.; Broekman, M. J.; Marcus, A. J.; Pinsky, D. J., Self-regulation of inflammatory cell trafficking in mice by the leukocyte surface apyrase CD39. *J Clin Invest* **2009,** *119* (5), 1136-1149.
40. Zhang, R. L.; Chopp, M.; Zhang, Z. G.; Jiang, N.; Powers, C., The expression of P- and E-selectins in three models of middle cerebral artery occlusion. *Brain Res* **1998,** *785* (2), 207-214.
41. Stephan, A. H.; Barres, B. A.; Stevens, B., The Complement System: An Unexpected Role in Synaptic Pruning During Development and Disease. *Annual Review of Neuroscience, Vol 35* **2012,** *35*, 369-389.
42. Rosenberg, G. A., Extracellular matrix inflammation in vascular cognitive impairment and dementia. *Clin Sci* **2017,** *131* (6), 425-437.
43. Cekanaviciute, E.; Fathali, N.; Doyle, K. P.; Williams, A. M.; Han, J.; Buckwalter, M. S., Astrocytic Transforming Growth Factor-Beta Signaling Reduces Subacute Neuroinflammation After Stroke in Mice. *Glia* **2014,** *62* (8), 1227-1240.
44. Arnold, L.; Henry, A.; Poron, F.; Baba-Amer, Y.; van Rooijen, N.; Plonquet, A.; Gherardi, R. K.; Chazaud, B., Inflammatory monocytes recruited after skeletal muscle injury switch into antiinflammatory macrophages to support myogenesis. *J Exp Med* **2007,** *204* (5), 1057-1069.
45. Nathan, C.; Ding, A. H., Nonresolving Inflammation. *Cell* **2010,** *140* (6), 871-882.
46. Liesz, A.; Suri-Payer, E.; Veltkamp, C.; Doerr, H.; Sommer, C.; Rivest, S.; Giese, T.; Veltkamp, R., Regulatory T cells are key cerebroprotective immunomodulators in acute experimental stroke. *Nat Med* **2009,** *15* (2), 192-199.
47. Veltkamp, R.; Suri-Payer, E.; Veltkamp, C.; Sommer, C.; Rivest, S.; Liesz, A., Endogenous immunomodulation after experimental focal ischemia: multitargeted cerebroprotection by regulatory T cells is the key. *J Cerebr Blood F Met* **2009,** *29*, S508-S509.

48. Gliem, M.; Krammes, K.; Liaw, L.; van Rooijen, N.; Hartung, H. P.; Jander, S., Macrophage-Derived Osteopontin Induces Reactive Astrocyte Polarization and Promotes Re-Establishment of the Blood Brain Barrier After Ischemic Stroke. *Glia* **2015,** *63* (12), 2198-2207.
49. Wiese, S.; Karus, M.; Faissner, A., Astrocytes as a source for extracellular matrix molecules and cytokines. *Front Pharmacol* **2012,** *3*.
50. Marler, J. R.; Brott, T.; Broderick, J.; Kothari, R.; Odonoghue, M.; Barsan, W.; Tomsick, T.; Spilker, J.; Miller, R.; Sauerbeck, L.; Jarrell, J.; Kelly, J.; Perkins, T.; Mcdonald, T.; Rorick, M.; Hickey, C.; Armitage, J.; Perry, C.; Thalinger, K.; Rhude, R.; Schill, J.; Becker, P. S.; Heath, R. S.; Adams, D.; Reed, R.; Klei, M.; Hughes, S.; Anthony, J.; Baudendistel, D.; Zadicoff, C.; Rymer, M.; Bettinger, I.; Laubinger, P.; Schmerler, M.; Meirose, G.; Lyden, P.; Rapp, K.; Babcock, T.; Daum, P.; Persona, D.; Brody, M.; Jackson, C.; Lewis, S.; Liss, J.; Mahdavi, Z.; Rothrock, J.; Tom, T.; Zweifler, R.; Dunford, J.; Zivin, J.; Kobayashi, R.; Kunin, J.; Licht, J.; Rowen, R.; Stein, D.; Grisolia, J.; Martin, F.; Chaplin, E.; Kaplitz, N.; Nelson, J.; Neuren, A.; Silver, D.; Chippendale, T.; Diamond, E.; Lobatz, M.; Murphy, D.; Rosenberg, D.; Ruel, T.; Sadoff, M.; Schim, J.; Schleimer, J.; Atkinson, R.; Wentworth, D.; Cummings, R.; Frink, R.; Heublein, P.; Grotta, J. C.; Degraba, T.; Fisher, M.; Ramirez, A.; Hanson, S.; Morgenstern, L.; Sills, C.; Pasteur, W.; Yatsu, F.; Andrews, K.; Villarcordova, C.; Pepe, P.; Bratina, P.; Greenberg, L.; Rozek, S.; Simmons, K.; Kwiatkowski, T. G.; Horowitz, S. H.; Libman, R.; Kanner, R.; Silverman, R.; Lamantia, J.; Mealie, C.; Duarte, R.; Donnarumma, R.; Okola, M.; Cullin, V.; Mitchell, E.; Levine, S. R.; Lewandowski, C. A.; Tokarski, G.; Ramadan, N. M.; Mitsias, P.; Gorman, M.; Zarowitz, B.; Kokkinos, J.; Dayno, J.; Verro, P.; Gymnopoulos, C.; Dafer, R.; Dolhaberriague, L.; Sawaya, K.; Daley, S.; Mitchell, M.; Frankel, M.; Mackay, B.; Barch, C.; Braimah, J.; Faherty, B.; Macdonald, J.; Sailor, S.; Cook, A.; Karp, H.; Nguyen, B.; Washington, J.; Weissman, J.; Williams, M.; Williamson, T.; Kozinn, M.; Hellwick, L.; Haley, E. C.; Bleck, T. P.; Cail, W. S.; Lindbeck, G. H.; Granner, M. A.; Wolf, S. S.; Gwynn, M. W.; Mettetal, R. W.; Chang, C. W. J.; Solenski, N. J.; Brock, D. G.; Ford, G. F.; Kongable, G. L.; Parks, K. N.; Wilkinson, S. S.; Davis, M. K.; Sheppard, G. L.; Zontine, D. W.; Gustin, K. H.; Crowe, N. M.; Massey, S. L.; Meyer, M.; Gaines, K.; Payne, A.; Bales, C.; Malcolm, J.; Barlow, R.; Wilson, M.; Cape, C.; Bertorini, T.; Misulis, K.; Paulsen, W.; Shepard, D.; Tilley, B. C.; Welch, K. M. A.; Fagan, S. C.; Lu, M.; Patel, S.; Masha, E.; Verter, J.; Boura, J.; Main, J.; Gordon, L.; Maddy, N.; Chociemski, T.; Windham, J.; Zadeh, H. S.; Alves, W.; Keller, M. F.; Wenzel, J. R.; Raman, N.; Cantwell, L.; Warren, A.; Smith, K.; Bailey, E.; Welch, K. M. A.; Tilley, B. C.; Froehlich, J.; Breed, J.; Easton, J. D.; Hallenbeck, J. F.; Lan, G.; Marsh, J. D.; Walker, M. D., Tissue-Plasminogen Activator for Acute Ischemic Stroke. *New Engl J Med* **1995,** *333* (24), 1581-1587.
51. Frey, J. L., Recombinant tissue plasminogen activator (rtPA) for stroke - The perspective at 8 years. *Neurologist* **2005,** *11* (2), 123-133.
52. Heo, J. H.; Kim, S. H.; Lee, K. Y.; Kim, E. H.; Chu, C. K.; Nam, J. M., Increase in plasma matrix metalloproteinase-9 in acute stroke patients with thrombolysis failure. *Stroke* **2003,** *34* (6), E48-E50.
53. Zhu, J. X.; Xiao, Y. L.; Li, Z. M.; Han, F. B.; Xiao, T. W.; Zhang, Z. T.; Geng, F. Y., Efficacy of Surgery Combined with Autologous Bone Marrow Stromal Cell Transplantation for Treatment of Intracerebral Hemorrhage. *Stem Cells Int* **2015**.
54. Yoo, J.; Seo, J. J.; Eom, J. H.; Hwang, D. Y., Enhanced Recovery From Chronic Ischemic Injury by Bone Marrow Cells in a Rat Model of Ischemic Stroke. *Cell Transplant* **2015,** *24* (2), 167-182.

55. Chen, J. L.; Ye, X. C.; Yan, T.; Zhang, C. L.; Yang, X. P.; Cui, X.; Cui, Y. S.; Zacharek, A.; Roberts, C.; Liu, X. F.; Dai, X. G.; Lu, M.; Chopp, M., Adverse Effects of Bone Marrow Stromal Cell Treatment of Stroke in Diabetic Rats. *Stroke* **2011,** *42* (12), 3551-3558.
56. Efimenko, A. Y.; Kochegura, T. N.; Akopyan, Z. A.; Parfyonova, Y. V., Autologous Stem Cell Therapy: How Aging and Chronic Diseases Affect Stem and Progenitor Cells. *Bioresearch Open Acc* **2015,** *4* (1), 26-38.
57. Davis, S. M.; Pennypacker, K. R., Targeting antioxidant enzyme expression as a therapeutic strategy for ischemic stroke. *Neurochem Int* **2017,** *107*, 23-32.
58. Ghezzi, P.; Jaquet, V.; Marcucci, F.; Schmidt, H. H. H. W., The oxidative stress theory of disease: levels of evidence and epistemological aspects. *Brit J Pharmacol* **2017,** *174* (12), 1784-1796.
59. Petro, M.; Jaffer, H.; Yang, J.; Kabu, S.; Morris, V. B.; Labhasetwar, V., Tissue plasminogen activator followed by antioxidant-loaded nanoparticle delivery promotes activation/mobilization of progenitor cells in infarcted rat brain. *Biomaterials* **2016,** *81*, 169-180.
60. Isik, M.; Beydemir, S.; Yilmaz, A.; Naldan, M. E.; Aslan, H. E.; Gulcin, I., Oxidative stress and mRNA expression of acetylcholinesterase in the leukocytes of ischemic patients. *Biomed Pharmacother* **2017,** *87*, 561-567.
61. Kaur, C.; Rathnasamy, G.; Ling, E. A., Antioxidants and Neuroprotection in the Brain and Retina. *Front Med Chem* **2015,** *7*, 3-33.
62. Papapetrou, A.; Moris, D.; Patelis, N.; Kouvelos, G. N.; Bakogiannis, C.; Klonaris, C.; Georgopoulos, S., Oxidative Stress and Total Antioxidant Status During Internal Carotid Artery Clamping with or without Shunting: An Experimental Pilot Study. *Med Sci Monit Basic* **2015,** *21*, 200-205.
63. Imai, H.; Masayasu, H.; Dewar, D.; Graham, D. I.; Macrae, I. M., Ebselen protects both gray model of focal and white matter in a rodent cerebral ischemia. *Stroke* **2001,** *32* (9), 2149-2156.
64. Noor, J. I.; Ikeda, T.; Mishima, K.; Aoo, N.; Ohta, S.; Egashira, N.; Iwasaki, K.; Fujiwara, M.; Ikenoue, T., Short-term administration of a new free radical scavenger, edaravone, is more effective than its long-term administration for the treatment of neonatal hypoxic-ischemic encephalopathy. *Stroke* **2005,** *36* (11), 2468-2474.
65. Schmid-Elsaesser, R.; Zausinger, S.; Hungerhuber, E.; Baethmann, A.; Reulen, H. J., Neuroprotective effects of combination therapy with tirilazad and magnesium in rats subjected to reversible focal cerebral ischemia. *Neurosurgery* **1999,** *44* (1), 163-171.
66. Maples, K. R.; Ma, F.; Zhang, Y. K., Comparison of the radical trapping ability of PBN, S-PBN and NXY-059. *Free Radical Res* **2001,** *34* (4), 417-426.
67. Green, A. R.; Shuaib, A., Therapeutic strategies for the treatment of stroke. *Drug Discov Today* **2006,** *11* (15-16), 681-693.
68. Jin, Q.; Cai, Y.; Li, S.; Liu, H. R.; Zhou, X. Y.; Lu, C. Q.; Gao, X. H.; Qian, J.; Zhang, J.; Ju, S. H.; Li, C., Edaravone-Encapsulated Agonistic Micelles Rescue Ischemic Brain Tissue by Tuning Blood-Brain Barrier Permeability. *Theranostics* **2017,** *7* (4), 884-898.
69. Zheng, S. Y.; Bai, Y. Y.; Liu, Y. K.; Gao, X. H.; Li, Y.; Changyi, Y. Z.; Wang, Y. C.; Chang, D.; Ju, S. H.; Li, C., Salvaging brain ischemia by increasing neuroprotectant uptake via nanoagonist mediated blood brain barrier permeability enhancement. *Biomaterials* **2015,** *66*, 9-20.
70. Massensini, A. R.; Ghuman, H.; Saldin, L. T.; Medberry, C. J.; Keane, T. J.; Nicholls, F. J.; Velankar, S. S.; Badylak, S. F.; Modo, M., Concentration-dependent rheological properties of ECM hydrogel for intracerebral delivery to a stroke cavity. *Acta Biomaterialia* **2015,** *27*, 116-130.

71. Boisserand, L. S. B.; Kodama, T.; Papassin, J.; Auzely, R.; Moisan, A.; Rome, C.; Detante, O., Biomaterial Applications in Cell-Based Therapy in Experimental Stroke. *Stem Cells Int* **2016**.
72. Wang, Z.; Wang, J.; Jin, Y.; Luo, Z.; Yang, W.; Xie, H. J.; Huang, K.; Wang, L., A Neuroprotective Sericin Hydrogel As an Effective Neuronal Cell Carrier for the Repair of Ischemic Stroke. *Acs Appl Mater Inter* **2015,** *7* (44), 24629-24640.
73. Lampe, K. J.; Heilshorn, S. C., Building stem cell niches from the molecule up through engineered peptide materials. *Neurosci Lett* **2012,** *519* (2), 138-146.
74. Harris, J. P.; Struzyna, L. A.; Murphy, P. L.; Adewole, D. O.; Kuo, E.; Cullen, D. K., Advanced biomaterial strategies to transplant preformed micro-tissue engineered neural networks into the brain. *J Neural Eng* **2016,** *13* (1).
75. Mehdizadeh, H.; Bayrak, E. S.; Lu, C.; Somo, S. I.; Akar, B.; Brey, E. M.; Cinar, A., Agent-based modeling of porous scaffold degradation and vascularization: Optimal scaffold design based on architecture and degradation dynamics. *Acta Biomaterialia* **2015,** *27*, 167-178.
76. Manning, C. N.; Schwartz, A. G.; Liu, W.; Xie, J.; Havlioglu, N.; Sakiyama-Elbert, S. E.; Silva, M. J.; Xia, Y.; Gelberman, R. H.; Thomopoulos, S., Controlled delivery of mesenchymal stem cells and growth factors using a nanofiber scaffold for tendon repair. *Acta Biomaterialia* **2013,** *9* (6), 6905-6914.
77. Ju, R. K.; Wen, Y. J.; Gou, R. B.; Wang, Y.; Xu, Q. Y., The Experimental Therapy on Brain Ischemia by Improvement of Local Angiogenesis With Tissue Engineering in the Mouse. *Cell Transplant* **2014,** *23*, S83-S95.
78. Pace, L. A.; Plate, J. F.; Smith, T. L.; Van Dyke, M. E., The effect of human hair keratin hydrogel on early cellular response to sciatic nerve injury in a rat model. *Biomaterials* **2013,** *34* (24), 5907-5914.
79. Merrifield, R. B., Solid Phase Peptide Synthesis. I. The Synthesis of a Tetrapeptide. *J Am Chem Soc* **1963,** *85* (14), 2149-2154.
80. Carpino, L. A.; Han, G. Y., 9-Fluorenylmethoxycarbonyl Function, a New Base-Sensitive Amino-Protecting Group. *J Am Chem Soc* **1970,** *92* (19), 5748-&.
81. Lutolf, M. P.; Lauer-Fields, J. L.; Schmoekel, H. G.; Metters, A. T.; Weber, F. E.; Fields, G. B.; Hubbell, J. A., Synthetic matrix metalloproteinase-sensitive hydrogels for the conduction of tissue regeneration: Engineering cell-invasion characteristics. *P Natl Acad Sci USA* **2003,** *100* (9), 5413-5418.
82. Patterson, J.; Hubbell, J. A., Enhanced proteolytic degradation of molecularly engineered PEG hydrogels in response to MMP-1 and MMP-2. *Biomaterials* **2010,** *31* (30), 7836-7845.
83. Tokatlian, T.; Shrum, C. T.; Kadoya, W. M.; Segura, T., Protease degradable tethers for controlled and cell-mediated release of nanoparticles in 2-and 3-dimensions. *Biomaterials* **2010,** *31* (31), 8072-8080.
84. Bellis, S. L., Advantages of RGD peptides for directing cell association with biomaterials. *Biomaterials* **2011,** *32* (18), 4205-4210.
85. Wang, A. Y.; Leong, S.; Liang, Y. C.; Huang, R. C. C.; Chen, C. S.; Yu, S. M., Immobilization of Growth Factors on Collagen Scaffolds Mediated by Polyanionic Collagen Mimetic Peptides and Its Effect on Endothelial Cell Morphogenesis. *Biomacromolecules* **2008,** *9* (10), 2929-2936.
86. Rothenfluh, D. A.; Bermudez, H.; O'Neil, C. P.; Hubbell, J. A., Biofunctional polymer nanoparticles for intra-articular targeting and retention in cartilage. *Nat Mater* **2008,** *7* (3), 248-254.

87. Chen, T. T.; Luque, A.; Lee, S.; Anderson, S. M.; Segura, T.; Iruela-Arispe, M. L., Anchorage of VEGF to the extracellular matrix conveys differential signaling responses to endothelial cells. *J Cell Biol* **2010,** *188* (4), 595-609.
88. Lesauteur, L.; Wei, L.; Gibbs, B. F.; Saragovi, H. U., Small Peptide Mimics of Nerve Growth-Factor Bind Trka Receptors and Affect Biological Responses. *J Biol Chem* **1995,** *270* (12), 6564-6569.
89. Martino, M. M.; Hubbell, J. A., The 12th-14th type III repeats of fibronectin function as a highly promiscuous growth factor-binding domain. *Faseb J* **2010,** *24* (12), 4711-4721.
90. Zhang, S. G.; Holmes, T.; Lockshin, C.; Rich, A., SPONTANEOUS ASSEMBLY OF A SELF-COMPLEMENTARY OLIGOPEPTIDE TO FORM A STABLE MACROSCOPIC MEMBRANE. *P Natl Acad Sci USA* **1993,** *90* (8), 3334-3338.
91. Schneider, J. P., Responsive hydrogels from the intramolecular folding and self-assembly of a designed peptide. *Abstr Pap Am Chem S* **2003,** *225*, U321-U321.
92. Rajagopal, K.; Ozbas, B.; Pochan, D. J.; Schneider, J. P., Self-assembly of beta hairpin peptides to hydrogels and tuning of material properties by design of turn sequence. *Abstr Pap Am Chem S* **2004,** *228*, U68-U68.
93. Ozbas, B.; Kretsinger, J.; Rajagopal, K.; Schneider, J. P.; Pochan, D. J., Salt-triggered peptide folding and consequent self-assembly into hydrogels with tunable modulus. *Macromolecules* **2004,** *37* (19), 7331-7337.
94. Dong, H.; Paramonov, S. E.; Aulisa, L.; Bakota, E. L.; Hartgerink, J. D., Self-assembly of multidomain peptides: Balancing molecular frustration controls conformation and nanostructure. *J Am Chem Soc* **2007,** *129* (41), 12468-12472.
95. Webber, M. J.; Tongers, J.; Newcomb, C. J.; Marquardt, K. T.; Bauersachs, J.; Losordo, D. W.; Stupp, S. I., Supramolecular nanostructures that mimic VEGF as a strategy for ischemic tissue repair. *P Natl Acad Sci USA* **2011,** *108* (33), 13438-13443.
96. Perez, C. M. R.; Stephanopoulos, N.; Sur, S.; Lee, S. S.; Newcomb, C.; Stupp, S. I., The Powerful Functions of Peptide-Based Bioactive Matrices for Regenerative Medicine. *Ann Biomed Eng* **2015,** *43* (3), 501-514.
97. Stephanopoulos, N.; Ortony, J. H.; Stupp, S. I., Self-assembly for the synthesis of functional biomaterials. *Acta Mater* **2013,** *61* (3), 912-930.
98. Tavakol, S.; Musavi, S. M. M.; Tavakol, B.; Hoveizi, E.; Ai, J.; Rezayat, S. M., Noggin Along with a Self-Assembling Peptide Nanofiber Containing Long Motif of Laminin Induces Tyrosine Hydroxylase Gene Expression. *Mol Neurobiol* **2017,** *54* (6), 4609-4616.
99. Fleming, S.; Ulijn, R. V., Design of nanostructures based on aromatic peptide amphiphiles. *Chem Soc Rev* **2014,** *43* (23), 8150-8177.
100. Pappas, C. G.; Shafi, R.; Sasselli, I. R.; Siccardi, H.; Wang, T.; Narang, V.; Abzalimov, R.; Wijerathne, N.; Ulijn, R. V., Dynamic peptide libraries for the discovery of supramolecular nanomaterials. *Nat Nanotechnol* **2016,** *11* (11), 960-967.
101. Zhou, J.; Li, J.; Du, X. W.; Xu, B., Supramolecular biofunctional materials. *Biomaterials* **2017,** *129*, 1-27.
102. Webber, M. J.; Appel, E. A.; Meijer, E. W.; Langer, R., Supramolecular biomaterials. *Nat Mater* **2016,** *15* (1), 13-26.
103. Mura, C.; McAnany, C. E., An introduction to biomolecular simulations and docking. *Mol Simulat* **2014,** *40* (10-11), 732-764.
104. Chang, D. K.; Urry, D. W., Molecular-Dynamics Calculations on Relaxed and Extended States of the Polypentapeptide of Elastin. *Chem Phys Lett* **1988,** *147* (4), 395-400.

105. Leech, J.; Prins, J. F.; Hermans, J., SMD: Visual steering of molecular dynamics for protein design. *Ieee Comput Sci Eng* **1996,** *3* (4), 38-45.
106. MacKerell, A. D.; Bashford, D.; Bellott, M.; Dunbrack, R. L.; Evanseck, J. D.; Field, M. J.; Fischer, S.; Gao, J.; Guo, H.; Ha, S.; Joseph-McCarthy, D.; Kuchnir, L.; Kuczera, K.; Lau, F. T. K.; Mattos, C.; Michnick, S.; Ngo, T.; Nguyen, D. T.; Prodhom, B.; Reiher, W. E.; Roux, B.; Schlenkrich, M.; Smith, J. C.; Stote, R.; Straub, J.; Watanabe, M.; Wiorkiewicz-Kuczera, J.; Yin, D.; Karplus, M., All-atom empirical potential for molecular modeling and dynamics studies of proteins. *J Phys Chem B* **1998,** *102* (18), 3586-3616.
107. Sreerama, N.; Woody, R. W., Molecular dynamics simulations of polypeptide conformations in water: A comparison of alpha, beta, and poly(Pro)II conformations. *Proteins* **1999,** *36* (4), 400-406.
108. Phillips, J. C.; Braun, R.; Wang, W.; Gumbart, J.; Tajkhorshid, E.; Villa, E.; Chipot, C.; Skeel, R. D.; Kale, L.; Schulten, K., Scalable molecular dynamics with NAMD. *J Comput Chem* **2005,** *26* (16), 1781-1802.
109. Popovych, N.; Sun, S.; Ebright, R. H.; Kalodimos, C. G., Dynamically driven protein allostery. *Nature Structural & Molecular Biology* **2006,** *13* (9), 831-838.
110. Zhao, Y.; Kormos, B. L.; Beveridge, D. L.; Baranger, A. M., Molecular dynamics simulation studies of a protein-RNA complex with a selectively modified binding interface. *Biopolymers* **2006,** *81* (4), 256-269.
111. Frembgen-Kesner, T.; Elcock, A. H., Striking Effects of Hydrodynamic Interactions on the Simulated Diffusion and Folding of Proteins. *J Chem Theory Comput* **2009,** *5* (2), 242-256.
112. Li, N. K.; Quiroz, F. G.; Hall, C. K.; Chilkoti, A.; Yingling, Y. G., Molecular Description of the LCST Behavior of an Elastin-Like Polypeptide. *Biomacromolecules* **2014,** *15* (10), 3522-3530.
113. Li, B.; Alonso, D. O. V.; Daggett, V., The molecular basis for the inverse temperature transition of elastin. *J Mol Biol* **2001,** *305* (3), 581-592.
114. Rousseau, R.; Schreiner, E.; Kohlmeyer, A.; Marx, D., Temperature-dependent conformational transitions and hydrogen-bond dynamics of the elastin-like octapeptide GVG(VPGVG): A molecular-dynamics study. *Biophysical Journal* **2004,** *86* (3), 1393-1407.
115. Zhao, B. W.; Li, N. K.; Yingling, Y. G.; Hall, C. K., LCST Behavior is Manifested in a Single Molecule: Elastin-Like polypeptide (VPGVG)n. *Biomacromolecules* **2016,** *17* (1), 111-118.
116. Tarakanova, A.; Huang, W.; Weiss, A. S.; Kaplan, D. L.; Buehler, M. J., Computational smart polymer design based on elastin protein mutability. *Biomaterials* **2017,** *127*, 49-60.
117. Tang, J. D.; McAnany, C. E.; Mura, C.; Lampe, K. J., Toward a Designable Extracellular Matrix: Molecular Dynamics Simulations of an Engineered Laminin-Mimetic, Elastin-Like Fusion Protein. *Biomacromolecules* **2016,** *17* (10), 3222-3233.
118. Keten, S.; Xu, Z. P.; Ihle, B.; Buehler, M. J., Nanoconfinement controls stiffness, strength and mechanical toughness of beta-sheet crystals in silk. *Nat Mater* **2010,** *9* (4), 359-367.
119. Krishnaji, S. T.; Bratzel, G.; Kinahan, M. E.; Kluge, J. A.; Staii, C.; Wong, J. Y.; Buehler, M. J.; Kaplan, D. L., Sequence-Structure-Property Relationships of Recombinant Spider Silk Proteins: Integration of Biopolymer Design, Processing, and Modeling. *Adv Funct Mater* **2013,** *23* (2), 241-253.
120. Fu, I. W.; Markegard, C. B.; Nguyen, H. D., Solvent Effects on Kinetic Mechanisms of Self-Assembly by Peptide Amphiphiles via Molecular Dynamics Simulations. *Langmuir* **2015,** *31* (1), 315-324.

121. Lee, O. S.; Stupp, S. I.; Schatz, G. C., Atomistic Molecular Dynamics Simulations of Peptide Amphiphile Self-Assembly into Cylindrical Nanofibers. *J Am Chem Soc* **2011,** *133* (10), 3677-3683.
122. Tsonchev, S.; Troisi, A.; Schatz, G. C.; Ratner, M. A., All-atom numerical studies of self-assembly of Zwitterionic peptide amphiphiles. *J Phys Chem B* **2004,** *108* (39), 15278-15284.
123. Raspa, A.; Saracino, G. A. A.; Pugliese, R.; Silva, D.; Cigognini, D.; Vescovi, A.; Gelain, F., Complementary Co-assembling Peptides: From In Silico Studies to In Vivo Application. *Adv Funct Mater* **2014,** *24* (40), 6317-6328.
124. Marrink, S. J.; Tieleman, D. P.; Mark, A. E., Molecular dynamics simulation of the kinetics of spontaneous micelle formation. *J Phys Chem B* **2000,** *104* (51), 12165-12173.
125. Henriques, J.; Cragnell, C.; Skepö, M., Molecular Dynamics Simulations of Intrinsically Disordered Proteins: Force Field Evaluation and Comparison with Experiment. *J Chem Theory Comput* **2015,** *11* (7), 3420-3431.
126. Nguyen, H. D.; Hall, C. K., Molecular dynamics simulations of spontaneous fibril formation by random-coil peptides. *P Natl Acad Sci USA* **2004,** *101* (46), 16180-16185.
127. Bond, P. J.; Sansom, M. S. P., Molecular Dynamics simulations of spontaneous micelle formation around membrane proteins. *Biophysical Journal* **2005,** *88* (1), 356a-356a.
128. Saracino, G. A. A.; Gelain, F., Modelling and analysis of early aggregation events of BMHP1-derived self-assembling peptides. *J Biomol Struct Dyn* **2014,** *32* (5), 759-775.
129. Darden, T.; York, D.; Pedersen, L., Particle Mesh Ewald - an N.Log(N) Method for Ewald Sums in Large Systems. *J Chem Phys* **1993,** *98* (12), 10089-10092.
130. Andersen, H. C., Molecular-Dynamics Simulations at Constant Pressure and-or Temperature. *J Chem Phys* **1980,** *72* (4), 2384-2393.
131. Sborgi, L.; Verma, A.; Piana, S.; Lindorff-Larsen, K.; Cerminara, M.; Santiveri, C. M.; Shaw, D. E.; de Alba, E.; Munoz, V., Interaction Networks in Protein Folding via Atomic-Resolution Experiments and Long-Time-Scale Molecular Dynamics Simulations. *J Am Chem Soc* **2015,** *137* (20), 6506-6516.
132. Bouvignies, G.; Bernado, P.; Meier, S.; Cho, K.; Grzesiek, S.; Bruschweiler, R.; Blackledge, M., Identification of slow correlated motions in proteins using residual dipolar and hydrogen-bond scalar couplings. *P Natl Acad Sci USA* **2005,** *102* (39), 13885-13890.
133. Stanzione, F.; Jayaraman, A., Computational Design of Oligopeptide Containing Poly(ethylene glycol) Brushes for Stimuli-Responsive Drug Delivery. *J Phys Chem B* **2015,** *119* (42), 13309-13320.
134. McCullagh, M.; Prytkova, T.; Tonzani, S.; Winter, N. D.; Schatz, G. C., Modeling self-assembly processes driven by nonbonded interactions in soft materials. *J Phys Chem B* **2008,** *112* (34), 10388-10398.
135. Johnston, K.; Harmandaris, V., Hierarchical simulations of hybrid polymer-solid materials. *Soft Matter* **2013,** *9* (29), 6696-6710.
136. Frederix, P. W. J. M.; Scott, G. G.; Abul-Haija, Y. M.; Kalafatovic, D.; Pappas, C. G.; Javid, N.; Hunt, N. T.; Ulijn, R. V.; Tuttle, T., Exploring the sequence space for (tri-) peptide self-assembly to design and discover. *Nature Chemistry* **2015,** *7* (1), 30-37.
137. Pham, Q. P.; Sharma, U.; Mikos, A. G., Electrospinning of polymeric nanofibers for tissue engineering applications: A review. *Tissue Eng* **2006,** *12* (5), 1197-1211.
138. Abrigo, M.; McArthur, S. L.; Kingshott, P., Electrospun Nanofibers as Dressings for Chronic Wound Care: Advances, Challenges, and Future Prospects. *Macromol Biosci* **2014,** *14* (6), 772-792.

139. Dror, Y.; Ziv, T.; Makarov, V.; Wolf, H.; Admon, A.; Zussman, E., Nanofibers Made of Globular Proteins. *Biomacromolecules* **2008,** *9* (10), 2749-2754.
140. Zhang, Y. Z.; Wang, X.; Feng, Y.; Li, J.; Lim, C. T.; Ramakrishna, S., Coaxial electrospinning of (fluorescein isothiocyanate-conjugated bovine serum albumin)-encapsulated poly(epsilon-caprolactone) nanofibers for sustained release. *Biomacromolecules* **2006,** *7* (4), 1049-1057.
141. Dong, B.; Arnoult, O.; Smith, M. E.; Wnek, G. E., Electrospinning of Collagen Nanofiber Scaffolds from Benign Solvents. *Macromol Rapid Comm* **2009,** *30* (7), 539-542.
142. Fischer, R. L.; McCoy, M. G.; Grant, S. A., Electrospinning collagen and hyaluronic acid nanofiber meshes. *J Mater Sci-Mater M* **2012,** *23* (7), 1645-1654.
143. Rui, C.; Mo, X. M.; Ke, Q. F., Fabrication and characterization of thermoplastic polyurethane/collagen blend nanofiber by electrospinning method. *2007 International Forum on Biomedical Textile Materials, Proceedings* **2007**, 144-150.
144. Wnek, G. E.; Carr, M. E.; Simpson, D. G.; Bowlin, G. L., Electrospinning of nanofiber fibrinogen structures. *Nano Lett* **2003,** *3* (2), 213-216.
145. Carlisle, C. R.; Coulais, C.; Namboothiry, M.; Carroll, D. L.; Hantgan, R. R.; Guthold, M., The mechanical properties of individual, electrospun fibrinogen fibers. *Biomaterials* **2009,** *30* (6), 1205-1213.
146. Casper, C. L.; Yang, W. D.; Farach-Carson, M. C.; Rabolt, J. F., Coating electrospun collagen and gelatin fibers with perlecan domain I for increased growth factor binding. *Biomacromolecules* **2007,** *8* (4), 1116-1123.
147. Li, M. Y.; Guo, Y.; Wei, Y.; MacDiarmid, A. G.; Lelkes, P. I., Electrospinning polyaniline-contained gelatin nanofibers for tissue engineering applications. *Biomaterials* **2006,** *27* (13), 2705-2715.
148. Mascharak, S.; Benitez, P. L.; Proctor, A. C.; Madl, C. M.; Hu, K. H.; Dewi, R. E.; Butte, M. J.; Heilshorn, S. C., YAP-dependent mechanotransduction is required for proliferation and migration on native-like substrate topography. *Biomaterials* **2017,** *115*, 155-166.
149. Liu, Y.; Xu, Y. C.; Wang, Z. H.; Wen, D. Z.; Zhang, W. T.; Schmull, S.; Li, H. Y.; Chen, Y.; Xue, S., Electrospun nanofibrous sheets of collagen/elastin/polycaprolactone improve cardiac repair after myocardial infarction. *Am J Transl Res* **2016,** *8* (4), 1678-+.
150. McClure, M. J.; Sell, S. A.; Simpson, D. G.; Walpoth, B. H.; Bowlin, G. L., A three-layered electrospun matrix to mimic native arterial architecture using polycaprolactone, elastin, and collagen: A preliminary study. *Acta Biomaterialia* **2010,** *6* (7), 2422-2433.
151. Zhang, K. H.; Mo, X. M.; Huang, C.; He, C. L.; Wang, H. S., Electrospun scaffolds from silk fibroin and their cellular compatibility. *J Biomed Mater Res A* **2010,** *93a* (3), 976-983.
152. Kim, U. J.; Park, J.; Kim, H. J.; Wada, M.; Kaplan, D. L., Three-dimensional aqueous-derived biomaterial scaffolds from silk fibroin. *Biomaterials* **2005,** *26* (15), 2775-2785.
153. Zhang, H.; Wang, K. F.; Xing, Y. M.; Yu, Q. Z., Lysine-doped polypyrrole/spider silk protein/poly(L-lactic) acid containing nerve growth factor composite fibers for neural application. *Mat Sci Eng C-Mater* **2015,** *56*, 564-573.
154. Maleki, M.; Natalello, A.; Pugliese, R.; Gelain, F., Fabrication of nanofibrous electrospun scaffolds from a heterogeneous library of co- and self-assembling peptides. *Acta Biomaterialia* **2017,** *51*, 268-278.
155. Rho, K. S.; Jeong, L.; Lee, G.; Seo, B. M.; Park, Y. J.; Hong, S. D.; Roh, S.; Cho, J. J.; Park, W. H.; Min, B. M., Electrospinning of collagen nanofibers: Effects on the behavior of normal human keratinocytes and early-stage wound healing. *Biomaterials* **2006,** *27* (8), 1452-1461.

156. Lee, Y. S.; Arinzeh, T. L., Electrospun Nanofibrous Materials for Neural Tissue Engineering. *Polymers-Basel* **2011,** *3* (1), 413-426.
157. Jing, Z.; Xu, X. Y.; Chen, X. S.; Liang, Q. Z.; Bian, X. C.; Yang, L. X.; Jing, X. B., Biodegradable electrospun fibers for drug delivery. *J Control Release* **2003,** *92* (3), 227-231.
158. Sell, S. A.; McClure, M. J.; Garg, K.; Wolfe, P. S.; Bowlin, G. L., Electrospinning of collagen/biopolymers for regenerative medicine and cardiovascular tissue engineering. *Adv Drug Deliver Rev* **2009,** *61* (12), 1007-1019.
159. Liu, X.; Lin, T.; Fang, J. A.; Yao, G.; Zhao, H. Q.; Dodson, M.; Wang, X. G., In vivo wound healing and antibacterial performances of electrospun nanofibre membranes. *J Biomed Mater Res A* **2010,** *94a* (2), 499-508.
160. Ren, G. L.; Xu, X. H.; Liu, Q.; Cheng, J.; Yuan, X. Y.; Wu, L. L.; Wan, Y. Z., Electrospun poly(vinyl alcohol)/glucose oxidase biocomposite membranes for biosensor applications. *React Funct Polym* **2006,** *66* (12), 1559-1564.
161. El-Moghazy, A. Y.; Soliman, E. A.; Ibrahim, H. Z.; Marty, J. L.; Istamboulie, G.; Noguer, T., Biosensor based on electrospun blended chitosan-poly (vinyl alcohol) nanofibrous enzymatically sensitized membranes for pirimiphosmethyl detection in olive oil. *Talanta* **2016,** *155*, 258-264.
162. Chua, J. S.; Chng, C. P.; Moe, A. A. K.; Tann, J. Y.; Goh, E. L. K.; Chiam, K. H.; Yim, E. K. F., Extending neurites sense the depth of the underlying topography during neuronal differentiation and contact guidance. *Biomaterials* **2014,** *35* (27), 7750-7761.
163. Solanki, A.; Chueng, S. T. D.; Yin, P. T.; Kappera, R.; Chhowalla, M.; Lee, K. B., Axonal Alignment and Enhanced Neuronal Differentiation of Neural Stem Cells on Graphene-Nanoparticle Hybrid Structures. *Adv Mater* **2013,** *25* (38), 5477-5482.
164. Yang, K.; Jung, K.; Ko, E.; Kim, J.; Park, K. I.; Kim, J.; Cho, S. W., Nanotopographical Manipulation of Focal Adhesion Formation for Enhanced Differentiation of Human Neural Stem Cells. *Acs Appl Mater Inter* **2013,** *5* (21), 10529-10540.
165. Dalby, M. J.; Gadegaard, N.; Oreffo, R. O. C., Harnessing nanotopography and integrin-matrix interactions to influence stem cell fate. *Nat Mater* **2014,** *13* (6), 558-569.
166. Xu, T.; Jin, J.; Gregory, C.; Hickman, J. J.; Boland, T., Inkjet printing of viable mammalian cells. *Biomaterials* **2005,** *26* (1), 93-99.
167. Zopf, D. A.; Hollister, S. J.; Nelson, M. E.; Ohye, R. G.; Green, G. E., Bioresorbable Airway Splint Created with a Three-Dimensional Printer. *New Engl J Med* **2013,** *368* (21), 2043-2045.
168. Cui, X. F.; Breitenkamp, K.; Finn, M. G.; Lotz, M.; D'Lima, D. D., Direct Human Cartilage Repair Using Three-Dimensional Bioprinting Technology. *Tissue Eng Pt A* **2012,** *18* (11-12), 1304-1312.
169. Xu, T.; Zhao, W. X.; Zhu, J. M.; Albanna, M. Z.; Yoo, J. J.; Atala, A., Complex heterogeneous tissue constructs containing multiple cell types prepared by inkjet printing technology. *Biomaterials* **2013,** *34* (1), 130-139.
170. Highley, C. B.; Rodell, C. B.; Burdick, J. A., Direct 3D Printing of Shear-Thinning Hydrogels into Self-Healing Hydrogels. *Adv Mater* **2015,** *27* (34), 5075-+.
171. Hsieh, F. Y.; Lin, H. H.; Hsu, S. H., 3D bioprinting of neural stern cell-laden thermoresponsive biodegradable polyurethane hydrogel and potential in central nervous system repair. *Biomaterials* **2015,** *71*, 48-57.

172. Lozano, R.; Stevens, L.; Thompson, B. C.; Gilmore, K. J.; Gorkin, R.; Stewart, E. M.; Panhuis, M. I. H.; Romero-Ortega, M.; Wallace, G. G., 3D printing of layered brain-like structures using peptide modified gellan gum substrates. *Biomaterials* **2015,** *67*, 264-273.
173. Zhu, W.; Harris, B. T.; Zhang, L. J. G., Gelatin Methacrylamide Hydrogel with Graphene Nanoplatelets for Neural Cell-laden 3D Bioprinting. *Ieee Eng Med Bio* **2016**, 4185-4188.
174. DeForest, C. A.; Anseth, K. S., Photoreversible Patterning of Biomolecules within Click-Based Hydrogels. *Angew Chem Int Edit* **2012,** *51* (8), 1816-1819.
175. DeForest, C. A.; Tirrell, D. A., A photoreversible protein-patterning approach for guiding stem cell fate in three-dimensional gels. *Nat Mater* **2015,** *14* (5), 523-531.
176. Marklein, R. A.; Burdick, J. A., Spatially controlled hydrogel mechanics to modulate stem cell interactions. *Soft Matter* **2010,** *6* (1), 136-143.
177. Nichol, J. W.; Koshy, S. T.; Bae, H.; Hwang, C. M.; Yamanlar, S.; Khademhosseini, A., Cell-laden microengineered gelatin methacrylate hydrogels. *Biomaterials* **2010,** *31* (21), 5536-5544.
178. Timashev, P. S.; Vedunova, M. V.; Guseva, D.; Ponimaskin, E.; Deiwick, A.; Mishchenko, T. A.; Mitroshina, E. V.; Koroleva, A. V.; Pimashkin, A. S.; Mukhina, I. V.; Panchenko, V. Y.; Chichkov, B. N.; Bagratashvili, V. N., 3D in vitro platform produced by two-photon polymerization for the analysis of neural network formation and function. *Biomedical Physics & Engineering Express* **2016,** *2* (3), 035001.
179. Dandurand, J.; Samouillan, V.; Lacabanne, C.; Pepe, A.; Bochicchio, B., Water structure and elastin-like peptide aggregation A differential calorimetric approach. *J Therm Anal Calorim* **2015,** *120* (1), 419-426.
180. Li, B.; Alonso, D. O. V.; Bennion, B. J.; Daggett, V., Hydrophobic hydration is an important source of elasticity in elastin-based biopolymers. *J Am Chem Soc* **2001,** *123* (48), 11991-11998.
181. Urry, D. W., Physical chemistry of biological free energy transduction as demonstrated by elastic protein-based polymers. *J Phys Chem B* **1997,** *101* (51), 11007-11028.
182. Reguera, J.; Urry, D. W.; Parker, T. M.; McPherson, D. T.; Rodriguez-Cabello, J. C., Effect of NaCl on the exothermic and endothermic components of the inverse temperature transition of a model elastin-like polymer. *Biomacromolecules* **2007,** *8* (2), 354-358.
183. Straley, K. S.; Heilshorn, S. C., Design and adsorption of modular engineered proteins to prepare customized, neuron-compatible coatings. *Front Neuroengineering* **2009,** *2*, 1-10.
184. Straley, K. S.; Heilshorn, S. C., Independent tuning of multiple biomaterial properties using protein engineering. *Soft Matter* **2009,** *5* (1), 114-124.
185. Chung, C.; Lampe, K. J.; Heilshorn, S. C., Tetrakis(hydroxymethyl) Phosphonium Chloride as a Covalent Cross-Linking Agent for Cell Encapsulation within Protein-Based Hydrogels. *Biomacromolecules* **2012,** *13* (12), 3912-3916.
186. Lampe, K. J.; Antaris, A. L.; Heilshorn, S. C., Design of three-dimensional engineered protein hydrogels for tailored control of neurite growth. *Acta Biomaterialia* **2013,** *9* (3), 5590-5599.
187. Madl, C. M.; Katz, L. M.; Heilshorn, S. C., Bio-Orthogonally Crosslinked, Engineered Protein Hydrogels with Tunable Mechanics and Biochemistry for Cell Encapsulation. *Adv Funct Mater* **2016,** *26* (21), 3612-3620.
188. Johnson, T.; Koria, P., Expression and Purification of Neurotrophin-Elastin-Like Peptide Fusion Proteins for Neural Regeneration. *Biodrugs* **2016,** *30* (2), 117-127.

189. Hu, X.; Tang-Schomer, M. D.; Huang, W. W.; Xia, X. X.; Weiss, A. S.; Kaplan, D. L., Charge-Tunable Autoclaved Silk-Tropoelastin Protein Alloys That Control Neuron Cell Responses. *Adv Funct Mater* **2013,** *23* (31), 3875-3884.
190. Sun, W.; Incitti, T.; Migliaresi, C.; Quattrone, A.; Casarosa, S.; Motta, A., Viability and neuronal differentiation of neural stem cells encapsulated in silk fibroin hydrogel functionalized with an IKVAV peptide. *J Tissue Eng Regen M* **2017,** *11* (5), 1532-1541.
191. Banwell, E. F.; Abelardo, E. S.; Adams, D. J.; Birchall, M. A.; Corrigan, A.; Donald, A. M.; Kirkland, M.; Serpell, L. C.; Butler, M. F.; Woolfson, D. N., Rational design and application of responsive alpha-helical peptide hydrogels. *Nat Mater* **2009,** *8* (7), 596-600.
192. Fischer, S. E.; Liu, X. Y.; Mao, H. Q.; Harden, J. L., Controlling cell adhesion to surfaces via associating bioactive triblock proteins. *Biomaterials* **2007,** *28* (22), 3325-3337.
193. Foo, C. T. S. W. P.; Lee, J. S.; Mulyasasmita, W.; Parisi-Amon, A.; Heilshorn, S. C., Two-component protein-engineered physical hydrogels for cell encapsulation. *P Natl Acad Sci USA* **2009,** *106* (52), 22067-22072.
194. Holmes, T. C.; de Lacalle, S.; Su, X.; Liu, G. S.; Rich, A.; Zhang, S. G., Extensive neurite outgrowth and active synapse formation on self-assembling peptide scaffolds. *P Natl Acad Sci USA* **2000,** *97* (12), 6728-6733.
195. Koutsopoulos, S.; Zhang, S. G., Long-term three-dimensional neural tissue cultures in functionalized self-assembling peptide hydrogels, Matrigel and Collagen I. *Acta Biomaterialia* **2013,** *9* (2), 5162-5169.
196. Cheng, T. Y.; Chen, M. H.; Chang, W. H.; Huang, M. Y.; Wang, T. W., Neural stem cells encapsulated in a functionalized self-assembling peptide hydrogel for brain tissue engineering. *Biomaterials* **2013,** *34* (8), 2005-2016.
197. Liu, X.; Wang, X. M.; Horii, A.; Wang, X. J.; Qiao, L.; Zhang, S. G.; Cui, F. Z., In vivo studies on angiogenic activity of two designer self-assembling peptide scaffold hydrogels in the chicken embryo chorioallantoic membrane. *Nanoscale* **2012,** *4* (8), 2720-2727.
198. Silva, G. A.; Czeisler, C.; Niece, K. L.; Beniash, E.; Harrington, D. A.; Kessler, J. A.; Stupp, S. I., Selective differentiation of neural progenitor cells by high-epitope density nanofibers. *Science* **2004,** *303* (5662), 1352-1355.
199. Tysseling-Mattiace, V. M.; Sahni, V.; Niece, K. L.; Birch, D.; Czeisler, C.; Fehlings, M. G.; Stupp, S. I.; Kessler, J. A., Self-assembling nanofibers inhibit glial scar formation and promote axon elongation after spinal cord injury. *J Neurosci* **2008,** *28* (14), 3814-3823.
200. Tysseling, V. M.; Sahni, V.; Pashuck, E. T.; Birch, D.; Hebert, A.; Czeisler, C.; Stupp, S. I.; Kessler, J. A., Self-Assembling Peptide Amphiphile Promotes Plasticity of Serotonergic Fibers Following Spinal Cord Injury. *J Neurosci Res* **2010,** *88* (14), 3161-3170.
201. Yang, C. Y.; Song, B. B.; Ao, Y.; Nowak, A. P.; Abelowitz, R. B.; Korsak, R. A.; Havton, L. A.; Deming, T. J.; Sofroniew, M. V., Biocompatibility of amphiphilic diblock copolypeptide hydrogels in the central nervous system. *Biomaterials* **2009,** *30* (15), 2881-2898.
202. Das, S.; Zhou, K.; Ghosh, D.; Jha, N. N.; Singh, P. K.; Jacob, R. S.; Bernard, C. C.; Finkelstein, D. I.; Forsythe, J. S.; Maji, S. K., Implantable amyloid hydrogels for promoting stem cell differentiation to neurons. *Npg Asia Mater* **2016,** *8*.
203. Iwasaki, M.; Wilcox, J. T.; Nishimura, Y.; Zweckberger, K.; Suzuki, H.; Wang, J.; Liu, Y.; Karadimas, S. K.; Fehlings, M. G., Synergistic effects of self-assembling peptide and neural stem/progenitor cells to promote tissue repair and forelimb functional recovery in cervical spinal cord injury. *Biomaterials* **2014,** *35* (9), 2617-2629.

204. Lampe, K. J.; Mooney, R. G.; Bjugstad, K. B.; Mahoney, M. J., Effect of macromer weight percent on neural cell growth in 2D and 3D nondegradable PEG hydrogel culture. *J Biomed Mater Res A* **2010,** *94a* (4), 1162-1171.
205. Freytes, D. O.; Godier-Furnemont, A.; Duan, Y.; O'Neill, J. D.; Vunjak-Novakovic, G., Biomaterial scaffolds for cardiac regeneration and repair derived from native heart matrix. *Woodh Publ Ser Biom* **2014,** *72*, 201-224.
206. Sirabella, D.; Cimetta, E.; Vunjak-Novakovic, G., "The state of the heart": Recent advances in engineering human cardiac tissue from pluripotent stem cells. *Exp Biol Med* **2015,** *240* (8), 1008-1018.
207. Ott, H. C.; Matthiesen, T. S.; Goh, S. K.; Black, L. D.; Kren, S. M.; Netoff, T. I.; Taylor, D. A., Perfusion-decellularized matrix: using nature's platform to engineer a bioartificial heart. *Nat Med* **2008,** *14* (2), 213-221.
208. Wainwright, J. M.; Czajka, C. A.; Patel, U. B.; Freytes, D. O.; Tobita, K.; Gilbert, T. W.; Badylak, S. F., Preparation of Cardiac Extracellular Matrix from an Intact Porcine Heart. *Tissue Eng Part C-Me* **2010,** *16* (3), 525-532.
209. Lee, J. W. S.; Doumouchtsis, S. K.; Fynes, M. M., A modified technique for the surgical correction of urethral diverticula using a porcine xenograft. *Int Urogynecol J* **2009,** *20* (1), 117-120.
210. Crapo, P. M.; Gilbert, T. W.; Badylak, S. F., An overview of tissue and whole organ decellularization processes. *Biomaterials* **2011,** *32* (12), 3233-3243.
211. Goh, S. K.; Bertera, S.; Olsen, P.; Candiello, J. E.; Halfter, W.; Uechi, G.; Balasubramani, M.; Johnson, S. A.; Sicari, B. M.; Kollar, E.; Badylak, S. F.; Banerjee, I., Perfusion-decellularized pancreas as a natural 3D scaffold for pancreatic tissue and whole organ engineering. *Biomaterials* **2013,** *34* (28), 6760-6772.
212. DeQuach, J. A.; Yuan, S. H.; Goldstein, L. S. B.; Christman, K. L., Decellularized Porcine Brain Matrix for Cell Culture and Tissue Engineering Scaffolds. *Tissue Eng Pt A* **2011,** *17* (21-22), 2583-2592.
213. Nagao, R. J.; Lundy, S.; Khaing, Z. Z.; Schmidt, C. E., Functional characterization of optimized acellular peripheral nerve graft in a rat sciatic nerve injury model. *Neurol Res* **2011,** *33* (6), 600-608.
214. Hudson, T. W.; Zawko, S.; Deister, C.; Lundy, S.; Hu, C. Y.; Lee, K.; Schmidt, C. E., Optimized acellular nerve graft is immunologically tolerated and supports regeneration. *Tissue Eng* **2004,** *10* (11-12), 1641-1651.
215. Oberwallner, B.; Brodarac, A.; Choi, Y. H.; Saric, T.; Anic, P.; Morawietz, L.; Stamm, C., Preparation of cardiac extracellular matrix scaffolds by decellularization of human myocardium. *J Biomed Mater Res A* **2014,** *102* (9), 3263-3272.
216. Uygun, B. E.; Soto-Gutierrez, A.; Yagi, H.; Izamis, M. L.; Guzzardi, M. A.; Shulman, C.; Milwid, J.; Kobayashi, N.; Tilles, A.; Berthiaume, F.; Hertl, M.; Nahmias, Y.; Yarmush, M. L.; Uygun, K., Organ reengineering through development of a transplantable recellularized liver graft using decellularized liver matrix. *Nat Med* **2010,** *16* (7), 814-U120.
217. Nakayama, K. H.; Batchelder, C. A.; Lee, C. I.; Tarantal, A. F., Decellularized Rhesus Monkey Kidney as a Three-Dimensional Scaffold for Renal Tissue Engineering. *Tissue Eng Pt A* **2010,** *16* (7), 2207-2216.
218. Nakayama, K. H.; Lee, C. C. I.; Batchelder, C. A.; Tarantal, A. F., Tissue Specificity of Decellularized Rhesus Monkey Kidney and Lung Scaffolds. *Plos One* **2013,** *8* (5).

219. Ott, H. C.; Clippinger, B.; Conrad, C.; Schuetz, C.; Pomerantseva, I.; Ikonomou, L.; Kotton, D.; Vacanti, J. P., Regeneration and orthotopic transplantation of a bioartificial lung. *Nat Med* **2010,** *16* (8), 927-U131.
220. Cortiella, J.; Niles, J.; Cantu, A.; Brettler, A.; Pham, A.; Vargas, G.; Winston, S.; Wang, J.; Walls, S.; Nichols, J. E., Influence of Acellular Natural Lung Matrix on Murine Embryonic Stem Cell Differentiation and Tissue Formation. *Tissue Eng Pt A* **2010,** *16* (8), 2565-2580.
221. Sood, D.; Chwalek, K.; Stuntz, E.; Pouli, D.; Du, C.; Tang-Schomer, M.; Georgakoudi, I.; Black, L. D.; Kaplan, D. L., Fetal Brain Extracellular Matrix Boosts Neuronal Network Formation in 3D Bioengineered Model of Cortical Brain Tissue. *Acs Biomater Sci Eng* **2016,** *2* (1), 131-140.
222. De Waele, J.; Reekmans, K.; Daans, J.; Berneman, Z.; Ponsaerts, P., 3d Culture of Murine Neural Stem Cells on Decellularized Mouse Brain Sections. *Neuro-Oncology* **2015,** *17*, 16-16.
223. Zhu, T. M.; Tang, Q. S.; Shen, Y. W.; Tang, H. L.; Chen, L. P.; Zhu, J. H., An acellular cerebellar biological scaffold: Preparation, characterization, biocompatibility and effects on neural stem cells. *Brain Res Bull* **2015,** *113*, 48-57.
224. Crapo, P. M.; Tottey, S.; Slivka, P. F.; Badylak, S. F., Effects of Biologic Scaffolds on Human Stem Cells and Implications for CNS Tissue Engineering. *Tissue Eng Pt A* **2014,** *20* (1-2), 313-323.
225. Lynch, K.; Pei, M., Age associated communication between cells and matrix: a potential impact on stem cell-based tissue regeneration strategies. *Organogenesis* **2014,** *10* (3), 289-298.
226. Conboy, I. M.; Rando, T. A., Aging, stem cells and tissue regeneration - Lessons from muscle. *Cell Cycle* **2005,** *4* (3), 407-410.
227. Fitzpatrick, L. E.; McDevitt, T. C., Cell-derived matrices for tissue engineering and regenerative medicine applications. *Biomater Sci* **2015,** *3* (1), 12-24.
228. Miller, M. E.; Miller, B. A.; Shuler, C. F., Comparison of Keratins Extracted from Fixed and Fresh Biopsy Specimens. *J Dent Res* **1990,** *69*, 198-198.
229. Cardamone, J. M., Investigating the microstructure of keratin extracted from wool: Peptide sequence (MALDI-TOF/TOF) and protein conformation (FTIR). *J Mol Struct* **2010,** *969* (1-3), 97-105.
230. Ayutthaya, S. I. N.; Tanpichai, S.; Wootthikanokkhan, J., Keratin Extracted from Chicken Feather Waste: Extraction, Preparation, and Structural Characterization of the Keratin and Keratin/Biopolymer Films and Electrospuns. *J Polym Environ* **2015,** *23* (4), 506-516.
231. Hill, P. S.; Apel, P. J.; Barnwell, J.; Smith, T.; Koman, L. A.; Atala, A.; Van Dyke, M., Repair of Peripheral Nerve Defects in Rabbits Using Keratin Hydrogel Scaffolds. *Tissue Eng Pt A* **2011,** *17* (11-12), 1499-1505.
232. Lin, Y. C.; Marra, K. G., Injectable systems and implantable conduits for peripheral nerve repair. *Biomed Mater* **2012,** *7* (2).
233. Pechter, P. M.; Gil, J.; Valdes, J.; Tomic-Canic, M.; Pastar, I.; Stojadinovic, O.; Kirsner, R. S.; Davis, S. C., Keratin dressings speed epithelialization of deep partial-thickness wounds. *Wound Repair Regen* **2012,** *20* (2), 236-242.
234. Loan, F.; Cassidy, S.; Marsh, C.; Simcock, J., Keratin-based products for effective wound care management in superficial and partial thickness burns injuries. *Burns* **2016,** *42* (3), 541-547.
235. Li, Q. M.; Zhu, L. J.; Liu, R. G.; Huang, D.; Jin, X.; Che, N.; Li, Z.; Qu, X. Z.; Kang, H. L.; Huang, Y., Biological stimuli responsive drug carriers based on keratin for triggerable drug delivery. *J Mater Chem* **2012,** *22* (37), 19964-19973.

236. Srinivasan, B.; Kumar, R.; Shanmugam, K.; Sivagnam, U. T.; Reddy, N. P.; Sehgal, P. K., Porous Keratin Scaffold-Promising Biomaterial for Tissue Engineering and Drug Delivery. *J Biomed Mater Res B* **2010,** *92b* (1), 5-12.
237. Kozlowska, J.; Sionkowska, A.; Skopinska-Wisniewska, J.; Piechowicz, K., Northern pike (Esox lucius) collagen: Extraction, characterization and potential application. *Int J Biol Macromol* **2015,** *81*, 220-227.
238. Cersoy, S.; Zazzo, A.; Lebon, M.; Rofes, J.; Zirah, S., Collagen Extraction and Stable Isotope Analysis of Small Vertebrate Bones: A Comparative Approach. *Radiocarbon* **2017,** *59* (3), 679-694.
239. Rodriguez, F.; Moran, L.; Gonzalez, G.; Troncoso, E.; Zuniga, R. N., Collagen extraction from mussel byssus: a new marine collagen source with physicochemical properties of industrial interest. *J Food Sci Tech Mys* **2017,** *54* (5), 1228-1238.
240. Watanabe, K.; Nakamura, M.; Okano, H.; Toyama, Y., Establishment of three-dimensional culture of neural stem/progenitor cells in collagen Type-1 Gel. *Restor Neurol Neuros* **2007,** *25* (2), 109-117.
241. Guggenberger, C.; Wolz, C.; Heesemann, J., Growth behavior and interaction of Staphylococcus aureus with neutrophils in a three-dimensional collagen gel as a tissue-like infection model. *Int J Med Microbiol* **2011,** *301*, 85-85.
242. Khan, S. Z.; Kokubu, E.; Matsuzaka, K.; Inoue, T., Behaviour of rat-cultured dental pulp cells in three-dimensional collagen type-1 gel in vitro and in vivo. *Aust Endod J* **2013,** *39* (3), 137-145.
243. Wei, S.; Chuang, C.; Chen, Y., Tuning Three-dimensional Collagen Gel Stiffness Independently Modulates Endothelial Cell Behavior. *Tissue Eng Pt A* **2015,** *21*, S12-S12.
244. Peterova, E.; Mrkvicova, A.; Podmolikova, L.; Rezacova, M.; Kanta, J., The Role of Cytokines TGF-beta 1 and FGF-1 in the Expression of Characteristic Markers of Rat Liver Myofibroblasts Cultured in Three-Dimensional Collagen Gel. *Physiol Res* **2016,** *65* (4), 661-672.
245. Ramshaw, J. A. M.; Peng, Y. Y.; Glattauer, V.; Werkmeister, J. A., Collagens as biomaterials. *J Mater Sci-Mater M* **2009,** *20*, 3-8.
246. Aigner, T.; Stove, J., Collagens - major component of the physiological cartilage matrix, major target of cartilage degeneration, major tool in cartilage repair. *Adv Drug Deliver Rev* **2003,** *55* (12), 1569-1593.
247. Verdu, E.; Labrador, R. O.; Rodriguez, F. J.; Ceballos, D.; Fores, J.; Navarro, X., Alignment of collagen and laminin-containing gels improve nerve regeneration within silicone tubes. *Restor Neurol Neuros* **2002,** *20* (5), 169-179.
248. Yu, H. W.; Cao, B.; Feng, M. Y.; Zhou, Q.; Sun, X. D.; Wu, S. L.; Jin, S. Z.; Liu, H. W.; Jin, L. H., Combinated Transplantation of Neural Stem Cells and Collagen Type I Promote Functional Recovery After Cerebral Ischemia in Rats. *Anat Rec* **2010,** *293* (5), 911-917.
249. Struzyna, L. A.; Wolf, J. A.; Mietus, C. J.; Adewole, D. O.; Chen, H. I.; Smith, D. H.; Cullen, D. K., Rebuilding Brain Circuitry with Living Micro-Tissue Engineered Neural Networks. *Tissue Eng Pt A* **2015,** *21* (21-22), 2744-2756.
250. Simionescua, D. T.; Lua, Q. J.; Song, Y.; Lee, J. S.; Rosenbalm, T. N.; Kelley, C.; Vyavahare, N. R., Biocompatibility and remodeling potential of pure arterial elastin and collagen scaffolds. *Biomaterials* **2006,** *27* (5), 702-713.
251. Jang, J.; Ko, J.; Cho, D. W.; Jun, M. B. G.; Kim, D. H., Elastin-sprayed tubular scaffolds with microstructures and nanotextures for vascular tissue engineering. *Proceedings of the Asme Summer Bioengineering Conference - 2013, Pt A* **2014**.

252. Chuang, T. H.; Stabler, C.; Simionescu, A.; Simionescu, D. T., Polyphenol-Stabilized Tubular Elastin Scaffolds for Tissue Engineered Vascular Grafts. *Tissue Eng Pt A* **2009,** *15* (10), 2837-2851.
253. Kurane, A.; Simionescu, D. T.; Vyavahare, N. R., In vivo cellular repopulation of tubular elastin scaffolds mediated by basic fibroblast growth factor. *Biomaterials* **2007,** *28* (18), 2830-2838.
254. Reddel, C. J.; Cultrone, D.; Rnjak-Kovacina, J.; Weiss, A. S.; Burgess, J. K., Tropoelastin modulates TGF-beta 1-induced expression of VEGF and CTGF in airway smooth muscle cells. *Matrix Biol* **2013,** *32* (7-8), 407-413.
255. Rodgers, U. R.; Weiss, A. S., Cellular interactions with elastin. *Pathol Biol (Paris)* **2005,** *53* (7), 390-8.
256. Hinek, A., Nature and the multiple functions of the 67-kD elastin-/laminin binding protein. *Cell Adhes Commun* **1994,** *2* (3), 185-93.
257. Mithieux, S. M.; Wise, S. G.; Raftery, M. J.; Starcher, B.; Weiss, A. S., A model two-component system for studying the architecture of elastin assembly in vitro. *J Struct Biol* **2005,** *149* (3), 282-9.
258. Mithieux, S. M.; Rasko, J. E.; Weiss, A. S., Synthetic elastin hydrogels derived from massive elastic assemblies of self-organized human protein monomers. *Biomaterials* **2004,** *25* (20), 4921-7.
259. Vepari, C.; Kaplan, D. L., Silk as a biomaterial. *Prog Polym Sci* **2007,** *32* (8-9), 991-1007.
260. Roloff, F.; Strauss, S.; Vogt, P. M.; Bicker, G.; Radtke, C., Spider Silk as Guiding Biomaterial for Human Model Neurons. *Biomed Res Int* **2014**.
261. Huang, W.; Begum, R.; Barber, T.; Ibba, V.; Tee, N. C. H.; Hussain, M.; Arastoo, M.; Yang, Q.; Robson, L. G.; Lesage, S.; Gheysens, T.; Skaer, N. J. V.; Knight, D. P.; Priestley, J. V., Regenerative potential of silk conduits in repair of peripheral nerve injury in adult rats. *Biomaterials* **2012,** *33* (1), 59-71.
262. Radtke, C.; Allmeling, C.; Waldmann, K. H.; Reimers, K.; Thies, K.; Schenk, H. C.; Hillmer, A.; Guggenheim, M.; Brandes, G.; Vogt, P. M., Spider Silk Constructs Enhance Axonal Regeneration and Remyelination in Long Nerve Defects in Sheep. *Plos One* **2011,** *6* (2).
263. Wittmer, C. R.; Claudepierre, T.; Reber, M.; Wiedemann, P.; Garlick, J. A.; Kaplan, D.; Egles, C., Multifunctionalized Electrospun Silk Fibers Promote Axon Regeneration in the Central Nervous System. *Adv Funct Mater* **2011,** *21* (22), 4232-4242.
264. Bai, S. M.; Zhang, W. M.; Lu, Q.; Ma, Q. H.; Kaplanad, D. L.; Zhu, H. S., Silk nanofiber hydrogels with tunable modulus to regulate nerve stem cell fate. *J Mater Chem B* **2014,** *2* (38), 6590-6600.
265. Tang-Schomer, M. D.; White, J. D.; Tien, L. W.; Schmitt, L. I.; Valentin, T. M.; Graziano, D. J.; Hopkins, A. M.; Omenetto, F. G.; Haydon, P. G.; Kaplan, D. L., Bioengineered functional brain-like cortical tissue. *P Natl Acad Sci USA* **2014,** *111* (38), 13811-13816.
266. Chwalek, K.; Tang-Schomer, M. D.; Omenetto, F. G.; Kaplan, D. L., In vitro bioengineered model of cortical brain tissue. *Nat Protoc* **2015,** *10* (9), 1362-1388.
267. Mosesson, M. W.; Siebenlist, K. R.; Meh, D. A., The structure and biological features of fibrinogen and fibrin. *Fibrinogen* **2001,** *936*, 11-30.
268. Sakiyama-Elbert, S. E.; Hubbell, J. A., Development of fibrin derivatives for controlled release of heparin-binding growth factors. *J Control Release* **2000,** *65* (3), 389-402.

269. Urech, L.; Bittermann, A. G.; Hubbell, J. A.; Hall, H., Mechanical properties, proteolytic degradability and biological modifications affect angiogenic process extension into native and modified fibrin matrices in vitro. *Biomaterials* **2005,** *26* (12), 1369-1379.
270. Bruns, H.; Kneser, U.; Holzhuter, S.; Roth, B.; Kluth, J.; Kaufmann, P. M.; Kluth, D.; Fiegel, H. C., Injectable liver: A novel approach using fibrin gel as a matrix for culture and intrahepatic transplantation of hepatocytes. *Tissue Eng* **2005,** *11* (11-12), 1718-1726.
271. Eyrich, D.; Brandl, F.; Appel, B.; Wiese, H.; Maier, G.; Wenzel, M.; Staudenmaier, R.; Goepferich, A.; Blunk, T., Long-term stable fibrin gels for cartilage engineering. *Biomaterials* **2007,** *28* (1), 55-65.
272. Chung, Y. I.; Ahn, K. M.; Jeon, S. H.; Lee, S. Y.; Lee, J. H.; Tae, G., Enhanced bone regeneration with BMP-2 loaded functional nanoparticle-hydrogel complex. *J Control Release* **2007,** *121* (1-2), 91-99.
273. Wood, M. D.; MacEwan, M. R.; French, A. R.; Moore, A. M.; Hunter, D. A.; Mackinnon, S. E.; Moran, D. W.; Borschel, G. H.; Sakiyama-Elbert, S. E., Fibrin Matrices With Affinity-Based Delivery Systems and Neurotrophic Factors Promote Functional Nerve Regeneration. *Biotechnol Bioeng* **2010,** *106* (6), 970-979.
274. Johnson, P. J.; Parker, S. R.; Sakiyama-Elbert, S. E., Fibrin-based tissue engineering scaffolds enhance neural fiber sprouting and delay the accumulation of reactive astrocytes at the lesion in a subacute model of spinal cord injury. *J Biomed Mater Res A* **2010,** *92a* (1), 152-163.
275. McCreedy, D. A.; Wilems, T. S.; Xu, H.; Butts, J. C.; Brown, C. R.; Smith, A. W.; Sakiyama-Elbert, S. E., Survival, differentiation, and migration of high-purity mouse embryonic stem cell-derived progenitor motor neurons in fibrin scaffolds after sub-acute spinal cord injury. *Biomater Sci-Uk* **2014,** *2* (11), 1672-1682.
276. Sakiyama, S. E.; Schense, J. C.; Hubbell, J. A., Incorporation of heparin-binding peptides into fibrin gels enhances neurite extension: an example of designer matrices in tissue engineering. *Faseb J* **1999,** *13* (15), 2214-2224.
277. Johnson, P. J.; Tatara, A.; Shiu, A.; Sakiyama-Elbert, S. E., Controlled Release of Neurotrophin-3 and Platelet-Derived Growth Factor From Fibrin Scaffolds Containing Neural Progenitor Cells Enhances Survival and Differentiation Into Neurons in a Subacute Model of SCI. *Cell Transplant* **2010,** *19* (1), 89-101.
278. Thomopoulos, S.; Kim, H. M.; Das, R.; Silva, M. J.; Sakiyama-Elbert, S.; Amiel, D.; Gelberman, R. H., The Effects of Exogenous Basic Fibroblast Growth Factor on Intrasynovial Flexor Tendon Healing in a Canine Model. *J Bone Joint Surg Am* **2010,** *92a* (13), 2285-2293.
279. Johnson, P. J.; Parker, S. R.; Sakiyama-Elbert, S. E., Controlled Release of Neurotrophin-3 From Fibrin-Based Tissue Engineering Scaffolds Enhances Neural Fiber Sprouting Following Subacute Spinal Cord Injury. *Biotechnol Bioeng* **2009,** *104* (6), 1207-1214.
280. Ju, Y. E.; Janmey, P. A.; McCormick, M. E.; Sawyer, E. S.; Flanagan, L. A., Enhanced neurite growth from mammalian neurons in three-dimensional salmon fibrin gels. *Biomaterials* **2007,** *28* (12), 2097-2108.
281. Veronese, F. M.; Mero, A., The impact of PEGylation on biological therapies. *Biodrugs* **2008,** *22* (5), 315-329.
282. Berkovitch, Y.; Yelin, D.; Seliktar, D., Photo-patterning PEG-based hydrogels for neuronal engineering. *Eur Polym J* **2015,** *72*, 473-483.
283. Sarig-Nadir, O.; Livnat, N.; Zajdman, R.; Shoham, S.; Seliktar, D., Laser Photoablation of Guidance Microchannels into Hydrogels Directs Cell Growth in Three Dimensions. *Biophysical Journal* **2009,** *96* (11), 4743-4752.

284. Freudenberg, U.; Hermann, A.; Welzel, P. B.; Stirl, K.; Schwarz, S. C.; Grimmer, M.; Zieris, A.; Panyanuwat, W.; Zschoche, S.; Meinhold, D.; Storch, A.; Werner, C., A star-PEG-heparin hydrogel platform to aid cell replacement therapies for neurodegenerative diseases. *Biomaterials* **2009,** *30* (28), 5049-5060.
285. Burdick, J. A.; Prestwich, G. D., Hyaluronic Acid Hydrogels for Biomedical Applications. *Adv Mater* **2011,** *23* (12), H41-H56.
286. Wang, Y. F.; Cooke, M. J.; Morshead, C. M.; Shoichet, M. S., Hydrogel delivery of erythropoietin to the brain for endogenous stem cell stimulation after stroke injury. *Biomaterials* **2012,** *33* (9), 2681-2692.
287. Lv, W.; Li, W. Y.; Xu, X. Y.; Jiang, H.; Bang, O. Y., Bone marrow mesenchymal stem cells transplantation promotes the release of endogenous erythropoietin after ischemic stroke. *Neural Regen Res* **2015,** *10* (8), 1265-1270.
288. Zhong, J.; Chan, A.; Morad, L.; Kornblum, H. I.; Fan, G. P.; Carmichael, S. T., Hydrogel Matrix to Support Stem Cell Survival After Brain Transplantation in Stroke. *Neurorehab Neural Re* **2010,** *24* (7), 636-644.
289. Moshayedi, P.; Nih, L. R.; Llorente, I. L.; Berg, A. R.; Cinkornpumin, J.; Lowry, W. E.; Segura, T.; Carmichael, S. T., Systematic optimization of an engineered hydrogel allows for selective control of human neural stem cell survival and differentiation after transplantation in the stroke brain. *Biomaterials* **2016,** *105*, 145-155.
290. Bible, E.; Qutachi, O.; Chau, D. Y. S.; Alexander, M. R.; Shakesheff, K. M.; Modo, M., Neo-vascularization of the stroke cavity by implantation of human neural stem cells on VEGF-releasing PLGA microparticles. *Biomaterials* **2012,** *33* (30), 7435-+.
291. Mdzinarishvili, A.; Sutariya, V.; Talasila, P. K.; Geldenhuys, W. J.; Sadana, P., Engineering triiodothyronine (T3) nanoparticle for use in ischemic brain stroke. *Drug Deliv Transl Re* **2013,** *3* (4), 309-317.
292. Klock, G.; Pfeffermann, A.; Ryser, C.; Grohn, P.; Kuttler, B.; Hahn, H. J.; Zimmermann, U., Biocompatibility of mannuronic acid-rich alginates. *Biomaterials* **1997,** *18* (10), 707-713.
293. Emerich, D. F.; Silva, E.; Ali, O.; Mooney, D.; Bell, W.; Yu, S. J.; Kaneko, Y.; Borlongan, C., Injectable VEGF Hydrogels Produce Near Complete Neurological and Anatomical Protection Following Cerebral Ischemia in Rats. *Cell Transplant* **2010,** *19* (9), 1063-1071.
294. Anderson, E. M.; Silva, E. A.; Hao, Y. B.; Martinick, K. D.; Vermillion, S. A.; Stafford, A. G.; Doherty, E. G.; Wang, L.; Doherty, E. J.; Grossman, P. M.; Mooney, D. J., VEGF and IGF Delivered from Alginate Hydrogels Promote Stable Perfusion Recovery in Ischemic Hind Limbs of Aged Mice and Young Rabbits. *J Vasc Res* **2017,** *54* (5), 288-298.
295. Yao, L.; Daly, W.; Newland, B.; Yao, S.; Wang, W.; Chen, B. K. K.; Madigan, N.; Windebank, A.; Pandit, A., Improved axonal regeneration of transected spinal cord mediated by multichannel collagen conduits functionalized with neurotrophin-3 gene. *Gene Ther* **2013,** *20* (12), 1149-1157.
296. Fan, C. X.; Li, X.; Xiao, Z. F.; Zhao, Y. N.; Liang, H.; Wang, B.; Han, S. F.; Li, X. R.; Xu, B.; Wang, N.; Liu, S. M.; Xue, W. W.; Dai, J. W., A modified collagen scaffold facilitates endogenous neurogenesis for acute spinal cord injury repair. *Acta Biomaterialia* **2017,** *51*, 304-316.
297. Masand, S. N.; Perron, I. J.; Schachner, M.; Shreiber, D. I., Neural cell type-specific responses to glycomimetic functionalized collagen. *Biomaterials* **2012,** *33* (3), 790-797.
298. Winter, C. C.; Katiyar, K. S.; Hernandez, N. S.; Song, Y. J.; Struzyna, L. A.; Harris, J. P.; Cullen, D. K., Transplantable living scaffolds comprised of micro-tissue engineered aligned

astrocyte networks to facilitate central nervous system regeneration. *Acta Biomaterialia* **2016,** *38*, 44-58.
299. Welker, P.; MullerRover, S.; Tokura, Y.; Bolchkarev, V.; Paus, R., Topobiology of the hair follicle .2. Expression of cell-adhesion molecules during hair follicle cycling. *J Invest Dermatol* **1996,** *107* (3), 245-245.
300. Sierpinski, P.; Garrett, J.; Ma, J.; Apel, P.; Klorig, D.; Smith, T.; Koman, L. A.; Atala, A.; Van Dyke, M., The use of keratin biomaterials derived from human hair for the promotion of rapid regeneration of peripheral nerves. *Biomaterials* **2008,** *29* (1), 118-128.
301. Barros, D.; Amaral, I. F.; Pego, A. P., Biomimetic Synthetic Self-Assembled Hydrogels for Cell Transplantation. *Curr Top Med Chem* **2015,** *15* (13), 1209-1226.
302. Koutsopoulos, S.; Zhang, S. G., Two-layered injectable self-assembling peptide scaffold hydrogels for long-term sustained release of human antibodies. *J Control Release* **2012,** *160* (3), 451-458.
303. Kandalam, S.; Sindji, L.; Delcroix, G. J. R.; Violet, F.; Garric, X.; Andre, E. M.; Schiller, P. C.; Venier-Julienne, M. C.; des Rieux, A.; Guicheux, J.; Montero-Menei, C. N., Pharmacologically active microcarriers delivering BDNF within a hydrogel: Novel strategy for human bone marrow-derived stem cells neural neuronal differentiation guidance and therapeutic secretome enhancement. *Acta Biomaterialia* **2017,** *49*, 167-180.
304. Piscioneri, A.; Morelli, S.; Mele, M.; Canonaco, M.; Bilotta, E.; Pantano, P.; Drioli, E.; De Bartolo, L., Neuroprotective effect of human mesenchymal stem cells in a compartmentalized neuronal membrane system. *Acta Biomaterialia* **2015,** *24*, 297-308.
305. Yeng, C. H.; Chen, P. J.; Chang, H. K.; Lo, W. Y.; Wu, C. C.; Chang, C. Y.; Chou, C. H.; Chen, S. H., Attenuating spinal cord injury by conditioned medium from human umbilical cord blood-derived CD34(+) cells in rats. *Taiwan J Obstet Gyne* **2016,** *55* (1), 85-93.
306. Wen, J. H.; Vincent, L. G.; Fuhrmann, A.; Choi, Y. S.; Hribar, K. C.; Taylor-Weiner, H.; Chen, S. C.; Engler, A. J., Interplay of matrix stiffness and protein tethering in stem cell differentiation. *Nat Mater* **2014,** *13* (10), 979-987.
307. Ye, K.; Wang, X.; Cao, L. P.; Li, S. Y.; Li, Z. H.; Yu, L.; Ding, J. D., Matrix Stiffness and Nanoscale Spatial Organization of Cell-Adhesive Ligands Direct Stem Cell Fate. *Nano Lett* **2015,** *15* (7), 4720-4729.
308. Wallace, M.; Cardoso, A. Z.; Frith, W. J.; Iggo, J. A.; Adams, D. J., Magnetically Aligned Supramolecular Hydrogels. *Chem-Eur J* **2014,** *20* (50), 16484-16487.
309. Zhang, S. M.; Liu, X.; Barreto-Ortiz, S. F.; Yu, Y. X.; Ginn, B. P.; DeSantis, N. A.; Hutton, D. L.; Grayson, W. L.; Cui, F. Z.; Korgel, B. A.; Gerecht, S.; Mao, H. Q., Creating polymer hydrogel microfibres with internal alignment via electrical and mechanical stretching. *Biomaterials* **2014,** *35* (10), 3243-3251.
310. Nance, E.; Timbie, K.; Miller, G. W.; Song, J.; Louttit, C.; Klibanov, A. L.; Shih, T. Y.; Swaminathan, G.; Tamargo, R. J.; Woodworth, G. F.; Hanes, J.; Price, R. J., Non-invasive delivery of stealth, brain-penetrating nanoparticles across the blood - brain barrier using MRI-guided focused ultrasound. *J Control Release* **2014,** *189*, 123-132.
311. Nance, E. A.; Woodworth, G. F.; Sailor, K. A.; Shih, T. Y.; Xu, Q. G.; Swaminathan, G.; Xiang, D.; Eberhart, C.; Hanes, J., A Dense Poly(Ethylene Glycol) Coating Improves Penetration of Large Polymeric Nanoparticles Within Brain Tissue. *Sci Transl Med* **2012,** *4* (149).
312. Kaisar, M. A.; Sajja, R. K.; Prasad, S.; Abhyankar, V. V.; Liles, T.; Cucullo, L., New experimental models of the blood-brain barrier for CNS drug discovery. *Expert Opinion on Drug Discovery* **2017,** *12* (1), 89-103.

313. Lippmann, E. S.; Azarin, S. M.; Kay, J. E.; Nessler, R. A.; Wilson, H. K.; Al-Ahmad, A.; Palecek, S. P.; Shusta, E. V., Derivation of blood-brain barrier endothelial cells from human pluripotent stem cells. *Nat Biotechnol* **2012,** *30* (8), 783-91.
314. Mehdizadeh, H.; Sumo, S.; Bayrak, E. S.; Brey, E. M.; Cinar, A., Three-dimensional modeling of angiogenesis in porous biomaterial scaffolds. *Biomaterials* **2013,** *34* (12), 2875-2887.
315. Phelps, E. A.; Landazuri, N.; Thule, P. M.; Taylor, W. R.; Garcia, A. J., Bioartificial matrices for therapeutic vascularization. *P Natl Acad Sci USA* **2010,** *107* (8), 3323-3328.
316. Arulmoli, J.; Wright, H. J.; Phan, D. T. T.; Sheth, U.; Que, R. A.; Botten, G. A.; Keating, M.; Botvinick, E. L.; Pathak, M. M.; Zarembinski, T. I.; Yanni, D. S.; Razorenova, O. V.; Hughes, C. C. W.; Flanagan, L. A., Combination scaffolds of salmon fibrin, hyaluronic acid, and laminin for human neural stem cell and vascular tissue engineering. *Acta Biomaterialia* **2016,** *43*, 122-138.
317. Li, S. R.; Nih, L. R.; Bachman, H.; Fei, P.; Li, Y. L.; Nam, E.; Dimatteo, R.; Carmichael, S. T.; Barker, T. H.; Segura, T., Hydrogels with precisely controlled integrin activation dictate vascular patterning and permeability. *Nat Mater* **2017,** *16* (9), 953-+.
318. Asmani, M. N.; Ai, J.; Amoabediny, G.; Noroozi, A.; Azami, M.; Ebrahimi-Barough, S.; Navaei-Nigjeh, M.; Ai, A.; Jafarabadi, M., Three-dimensional culture of differentiated endometrial stromal cells to oligodendrocyte progenitor cells (OPCs) in fibrin hydrogel. *Cell Biology International* **2013,** *37* (12), 1340-1349.
319. Annabi, N.; Tsang, K.; Mithieux, S. M.; Nikkhah, M.; Ameri, A.; Khademhosseini, A.; Weiss, A. S., Highly Elastic Micropatterned Hydrogel for Engineering Functional Cardiac Tissue. *Adv Funct Mater* **2013,** *23* (39), 4950-4959.
320. Tang, J. D.; Lampe, K. J., From de novo peptides to native proteins: advancements in biomaterial scaffolds for acute ischemic stroke repair. *Biomed Mater* **2018,** *13* (3).
321. Tam, R. Y.; Fuehrmann, T.; Mitrousis, N.; Shoichet, M. S., Regenerative Therapies for Central Nervous System Diseases: a Biomaterials Approach. *Neuropsychopharmacol* **2014,** *39* (1), 169-188.
322. Aguado, B. A.; Mulyasasmita, W.; Su, J.; Lampe, K. J.; Heilshorn, S. C., Improving Viability of Stem Cells During Syringe Needle Flow Through the Design of Hydrogel Cell Carriers. *Tissue Eng Pt A* **2012,** *18* (7-8), 806-815.
323. Sortwell, C. E., Strategies for the augmentation of grafted dopamine neuron survival. *Front Biosci* **2003,** *8*, S522-S532.
324. Roberts, D.; Rochas, C.; Saiani, A.; Miller, A. F., Effect of Peptide and Guest Charge on the Structural, Mechanical and Release Properties of beta-Sheet Forming Peptides. *Langmuir* **2012,** *28* (46), 16196-16206.
325. Schneider, J. P.; Pochan, D. J.; Ozbas, B.; Rajagopal, K.; Pakstis, L.; Kretsinger, J., Responsive hydrogels from the intramolecular folding and self-assembly of a designed peptide. *J Am Chem Soc* **2002,** *124* (50), 15030-15037.
326. Aulisa, L.; Dong, H.; Hartgerink, J. D., Self-Assembly of Multidomain Peptides: Sequence Variation Allows Control over Cross-Linking and Viscoelasticity. *Biomacromolecules* **2009,** *10* (9), 2694-2698.
327. Hauser, C. A. E.; Deng, R. S.; Mishra, A.; Loo, Y. H.; Khoe, U.; Zhuang, F. R.; Cheong, D. W.; Accardo, A.; Sullivan, M. B.; Riekel, C.; Ying, J. Y.; Hauser, U. A., Natural tri- to hexapeptides self-assemble in water to amyloid beta-type fiber aggregates by unexpected alpha-helical intermediate structures. *P Natl Acad Sci USA* **2011,** *108* (4), 1361-1366.
328. Tenidis, K.; Waldner, M.; Bernhagen, J.; Fischle, W.; Bergmann, M.; Weber, M.; Merkle, M. L.; Voelter, W.; Brunner, H.; Kapurniotu, A., Identification of a penta- and hexapeptide of islet

amyloid polypeptide (IAPP) with amyloidogenic and cytotoxic properties. *J Mol Biol* **2000,** *295* (4), 1055-1071.
329. Doran, T. M.; Kamens, A. J.; Byrnes, N. K.; Nilsson, B. L., Role of amino acid hydrophobicity, aromaticity, and molecular volume on IAPP(20-29) amyloid self-assembly. *Proteins-Structure Function and Bioinformatics* **2012,** *80* (4), 1053-1065.
330. Bertolani, A.; Pirrie, L.; Stefan, L.; Houbenov, N.; Haataja, J. S.; Catalano, L.; Terraneo, G.; Giancane, G.; Valli, L.; Milani, R.; Ikkala, O.; Resnati, G.; Metrangolo, P., Supramolecular amplification of amyloid self-assembly by iodination. *Nat Commun* **2015,** *6*.
331. Reches, M.; Porat, Y.; Gazit, E., Amyloid fibril formation by pentapeptide and tetrapeptide fragments of human calcitonin. *J Biol Chem* **2002,** *277* (38), 35475-35480.
332. Thirumalai, D.; Klimov, D. K.; Dima, R. I., Emerging ideas on the molecular basis of protein and peptide aggregation. *Curr Opin Struc Biol* **2003,** *13* (2), 146-159.
333. Clarke, D. E.; Parmenter, C. D. J.; Scherman, O. A., Tunable Pentapeptide Self-Assembled beta-Sheet Hydrogels. *Angew Chem Int Edit* **2018,** *57* (26), 7709-7713.
334. Qin, S. Y.; Pei, Y.; Liu, X. J.; Zhuo, R. X.; Zhang, X. Z., Hierarchical self-assembly of a beta-amyloid peptide derivative. *J Mater Chem B* **2013,** *1* (5), 668-675.
335. Subbalakshmi, C.; Manorama, S. V.; Nagaraj, R., Self-assembly of short peptides composed of only aliphatic amino acids and a combination of aromatic and aliphatic amino acids. *J Pept Sci* **2012,** *18* (5), 283-292.
336. Debnath, S.; Shome, A.; Das, D.; Das, P. K., Hydrogelation Through Self-Assembly of Fmoc-Peptide Functionalized Cationic Amphiphiles: Potent Antibacterial Agent. *J Phys Chem B* **2010,** *114* (13), 4407-4415.
337. Tang, C.; Smith, A. M.; Collins, R. F.; Ulijn, R. V.; Saiani, A., Fmoc-Diphenylalanine Self-Assembly Mechanism Induces Apparent pK(a) Shifts. *Langmuir* **2009,** *25* (16), 9447-9453.
338. Melchionna, M.; Styan, K. E.; Marchesan, S., The Unexpected Advantages of Using D-Amino Acids for Peptide Self-Assembly into Nanostructured Hydrogels for Medicine. *Curr Top Med Chem* **2016,** *16* (18), 2009-2018.
339. Reches, M.; Gazit, E., Casting metal nanowires within discrete self-assembled peptide nanotubes. *Science* **2003,** *300* (5619), 625-627.
340. Zhou, M.; Smith, A. M.; Das, A. K.; Hodson, N. W.; Collins, R. F.; Ulijn, R. V.; Gough, J. E., Self-assembled peptide-based hydrogels as scaffolds for anchorage-dependent cells. *Biomaterials* **2009,** *30* (13), 2523-2530.
341. Ogata, S.; Igarashi, T., Concurrent coupling of electronic-density-functional, molecular dynamics, and coarse-grained particles schemes for multiscale simulation of nanostructured materials. *New Frontiers of Processing and Engineering in Advanced Materials* **2005,** *502*, 33-38.
342. Head, D. A.; Tronci, G.; Russell, S. J.; Wood, D. J., In Silico Modeling of the Rheological Properties of Covalently Cross-Linked Collagen Triple Helices. *Acs Biomater Sci Eng* **2016,** *2* (8), 1224-1233.
343. Aurand, E. R.; Lampe, K. J.; Bjugstad, K. B., Defining and designing polymers and hydrogels for neural tissue engineering. *Neuroscience Research* **2012,** *72* (3), 199-213.
344. Lampel, A.; McPhee, S. A.; Park, H. A.; Scott, G. G.; Humagain, S.; Hekstra, D. R.; Yoo, B.; Frederix, P. W. J. M.; Li, T. D.; Abzalimov, R. R.; Greenbaum, S. G.; Tuttle, T.; Hu, C. H.; Bettinger, C. J.; Ulijn, R. V., Polymeric peptide pigments with sequence-encoded properties. *Science* **2017,** *356* (6342), 1064-1068.
345. Schneider, T. D.; Stephens, R. M., Sequence Logos - a New Way to Display Consensus Sequences. *Nucleic Acids Res* **1990,** *18* (20), 6097-6100.

346. Crooks, G. E.; Hon, G.; Chandonia, J. M.; Brenner, S. E., WebLogo: A sequence logo generator. *Genome Res* **2004,** *14* (6), 1188-1190.
347. Weiss, G. A.; Watanabe, C. K.; Zhong, A.; Goddard, A.; Sidhu, S. S., Rapid mapping of protein functional epitopes by combinatorial alanine scanning. *P Natl Acad Sci USA* **2000,** *97* (16), 8950-8954.
348. Cunningham, B. C.; Wells, J. A., High-Resolution Epitope Mapping of Hgh-Receptor Interactions by Alanine-Scanning Mutagenesis. *Science* **1989,** *244* (4908), 1081-1085.
349. Yang, H. Y.; Yang, S. N.; Kong, J. L.; Dong, A. C.; Yu, S. N., Obtaining information about protein secondary structures in aqueous solution using Fourier transform IR spectroscopy. *Nat Protoc* **2015,** *10* (3).
350. Byler, D. M.; Susi, H., Examination of the Secondary Structure of Proteins by Deconvolved Ftir Spectra. *Biopolymers* **1986,** *25* (3), 469-487.
351. Shivu, B.; Seshadri, S.; Li, J.; Oberg, K. A.; Uversky, V. N.; Fink, A. L., Distinct beta-Sheet Structure in Protein Aggregates Determined by ATR-FTIR Spectroscopy. *Biochemistry-Us* **2013,** *52* (31), 5176-5183.
352. Arluison, W.; Mura, C.; Guzman, M. R.; Liquier, J.; Pellegrini, O.; Gingery, M.; Regnier, P.; Marco, S., Three-dimensional structures of fibrillar Sm proteins: Hfq and other Sm-like proteins. *J Mol Biol* **2006,** *356* (1), 86-96.
353. Zandomeneghi, G.; Krebs, M. R. H.; Mccammon, M. G.; Fandrich, M., FTIR reveals structural differences between native beta-sheet proteins and amyloid fibrils. *Protein Sci* **2004,** *13* (12), 3314-3321.
354. Crosby, K. C.; Postma, M.; Hink, M. A.; Zeelenberg, C. H. C.; Adjobo-Hermans, M. J. W.; Gadella, T. W. J., Quantitative Analysis of Self-Association and Mobility of Annexin A4 at the Plasma Membrane. *Biophysical Journal* **2013,** *104* (9), 1875-1885.
355. Melchels, F. P. W.; Barradas, A. M. C.; van Blitterswijk, C. A.; de Boer, J.; Feijen, J.; Grijpma, D. W., Effects of the architecture of tissue engineering scaffolds on cell seeding and culturing. *Acta Biomaterialia* **2010,** *6* (11), 4208-4217.
356. Huang, J.; MacKerell, A. D., CHARMM36 all-atom additive protein force field: Validation based on comparison to NMR data. *J Comput Chem* **2013,** *34* (25), 2135-2145.
357. McAnany, C. E.; Mura, C., Claws, Disorder, and Conformational Dynamics of the C-Terminal Region of Human Desmoplakin. *J Phys Chem B* **2016,** *120* (33), 8654-8667.
358. Papoian, G. A.; Wolynes, P. G., The physics and bioinformatics of binding and folding—an energy landscape perspective. *Biopolymers* **2003,** *68* (3), 333-349.
359. Das, P.; King, J. A.; Zhou, R. H., Aggregation of gamma-crystallins associated with human cataracts via domain swapping at the C-terminal beta-strands. *P Natl Acad Sci USA* **2011,** *108* (26), 10514-10519.
360. Rousseau, F.; Schymkowitz, J.; Itzhaki, L. S., Implications of 3d Domain Swapping for Protein Folding, Misfolding and Function. *Adv Exp Med Biol* **2012,** *747*, 137-152.
361. Kozer, N.; Kuttner, Y. Y.; Haran, G.; Schreiber, G., Protein-protein association in polymer solutions: From dilute to semidilute to concentrated. *Biophysical Journal* **2007,** *92* (6), 2139-2149.
362. Pappu, R. V.; Rose, G. D., A simple model for polyproline II structure in unfolded states of alanine-based peptides. *Protein Sci* **2002,** *11* (10), 2437-2455.
363. de Groot, N. S.; Parella, T.; Aviles, F. X.; Vendrell, J.; Ventura, S., Ile-Phe dipeptide self-assembly: Clues to amyloid formation. *Biophysical Journal* **2007,** *92* (5), 1732-1741.
364. Rost, B.; Sander, C., Conservation and Prediction of Solvent Accessibility in Protein Families. *Proteins* **1994,** *20* (3), 216-226.

365. Saraboji, K.; Gromiha, M. M.; Ponnuswamy, M. N., Relative importance of secondary structure and solvent accessibility to the stability of protein mutants. A case study with amino acid properties and energetics on T4 and human lysozymes. *Comput Biol Chem* **2005,** *29* (1), 25-35.
366. Kyte, J.; Doolittle, R. F., A Simple Method for Displaying the Hydropathic Character of a Protein. *J Mol Biol* **1982,** *157* (1), 105-132.
367. Izzo, D.; Marques, C. M., Formation of Micelles of Diblock and Triblock Copolymers in a Selective Solvent. *Macromolecules* **1993,** *26* (26), 7189-7194.
368. Krogstad, D. V.; Lynd, N. A.; Miyajima, D.; Gopez, J.; Hawker, C. J.; Kramer, E. J.; Tirrell, M. V., Structural Evolution of Polyelectrolyte Complex Core Micelles and Ordered-Phase Bulk Materials. *Macromolecules* **2014,** *47* (22), 8026-8032.
369. Cai, L.; Heilshorn, S. C., Designing ECM-mimetic materials using protein engineering. *Acta Biomaterialia* **2014,** *10* (4), 1751-1760.
370. Janmey, P. A.; Miller, R. T., Mechanisms of mechanical signaling in development and disease. *Journal of Cell Science* **2011,** *124* (1), 9-18.
371. Discher, D. E.; Janmey, P.; Wang, Y. L., Tissue cells feel and respond to the stiffness of their substrate. *Science* **2005,** *310* (5751), 1139-1143.
372. Macaya, D.; Spector, M., Injectable hydrogel materials for spinal cord regeneration: a review. *Biomed Mater* **2012,** *7* (1).
373. Budday, S.; Nay, R.; de Rooij, R.; Steinmann, P.; Wyrobek, T.; Ovaert, T. C.; Kuhl, E., Mechanical properties of gray and white matter brain tissue by indentation. *J Mech Behav Biomed* **2015,** *46*, 318-330.
374. van Dommelen, J. A. W.; van der Sande, T. P. J.; Hrapko, M.; Peters, G. W. M., Mechanical properties of brain tissue by indentation: Interregional variation. *J Mech Behav Biomed* **2010,** *3* (2), 158-166.
375. Bjugstad, K. B.; Redmond, D. E.; Lampe, K. J.; Kern, D. S.; Sladek, J. R.; Mahoney, M. J., Biocompatibility of PEG-based hydrogels in primate brain. *Cell Transplant* **2008,** *17* (4), 409-415.
376. Bowerman, C. J.; Liyanage, W.; Federation, A. J.; Nilsson, B. L., Tuning beta-Sheet Peptide Self-Assembly and Hydrogelation Behavior by Modification of Sequence Hydrophobicity and Aromaticity. *Biomacromolecules* **2011,** *12* (7), 2735-2745.
377. Haines-Butterick, L. A.; Rajagopal, K.; Lamm, M.; Pochan, D. J.; Schnieder, J. P., Controlling hydrogelation kinetics via peptide design for three-dimensional encapsulation and injectable delivery of cells. *Biopolymers* **2007,** *88* (4), 518-518.
378. Krysmann, M. J.; Castelletto, V.; Kelarakis, A.; Hamley, I. W.; Hule, R. A.; Pochan, D. J., Self-assembly and hydrogelation of an amyloid peptide fragment. *Biochemistry-Us* **2008,** *47* (16), 4597-4605.
379. Zhang, Z. X.; Zheng, Q. X.; Wu, Y. C.; Hao, D. J., Compatibility of Neural Stem Cells with Functionalized Self-assembling Peptide Scaffold In vitro. *Biotechnol Bioproc E* **2010,** *15* (4), 545-551.
380. Yokoi, H.; Kinoshita, T.; Zhang, S. G., Dynamic reassembly of peptide RADA16 nanofiber scaffold. *P Natl Acad Sci USA* **2005,** *102* (24), 8414-8419.
381. Wang, H. M.; Yang, Z. M.; Adams, D. J., Controlling peptide-based hydrogelation. *Mater Today* **2012,** *15* (11), 500-507.
382. Dagdas, Y. S.; Tombuloglu, A.; Tekinay, A. B.; Dana, A.; Guler, M. O., Interfiber interactions alter the stiffness of gels formed by supramolecular self-assembled nanofibers. *Soft Matter* **2011,** *7* (7), 3524-3532.

383. Shin, Y.; Brangwynne, C. P., Liquid phase condensation in cell physiology and disease. *Science* **2017,** *357* (6357).
384. Boeynaems, S.; Alberti, S.; Fawzi, N. L.; Mittag, T.; Polymenidou, M.; Rousseau, F.; Schymkowitz, J.; Shorter, J.; Wolozin, B.; Van Den Bosch, L.; Tompa, P.; Fuxreiter, M., Protein Phase Separation: A New Phase in Cell Biology. *Trends Cell Biol* **2018,** *28* (6), 420-435.
385. Hughes, M. P.; Sawaya, M. R.; Boyer, D. R.; Goldschmidt, L.; Rodriguez, J. A.; Cascio, D.; Chong, L.; Gonen, T.; Eisenberg, D. S., Atomic structures of low-complexity protein segments reveal kinked beta sheets that assemble networks. *Science* **2018,** *359* (6376), 698-701.
386. Moore, A. N.; Hartgerink, J. D., Self-Assembling Multidomain Peptide Nanofibers for Delivery of Bioactive Molecules and Tissue Regeneration. *Accounts Chem Res* **2017,** *50* (4), 714-722.
387. Tian, Y. F.; Hudalla, G. A.; Han, H. F.; Collier, J. H., Controllably degradable beta-sheet nanofibers and gels from self-assembling depsipeptides. *Biomater Sci-Uk* **2013,** *1* (10), 1037-1045.
388. Clarke, D. E.; Parmenter, C. D. J.; Scherman, O. A., Tunable Pentapeptide Self-Assembled beta-Sheet Hydrogels. *Angew Chem Int Ed Engl* **2018**.
389. Aggeli, A.; Nyrkova, I. A.; Bell, M.; Harding, R.; Carrick, L.; McLeish, T. C. B.; Semenov, A. N.; Boden, N., Hierarchical self-assembly of chiral rod-like molecules as a model for peptide beta-sheet tapes, ribbons, fibrils, and fibers. *P Natl Acad Sci USA* **2001,** *98* (21), 11857-11862.
390. Uesaka, A.; Ueda, M.; Makino, A.; Imai, T.; Sugiyama, J.; Kimura, S., Morphology Control between Twisted Ribbon, Helical Ribbon, and Nanotube Self-Assemblies with His-Containing Helical Peptides in Response to pH Change. *Langmuir* **2014,** *30* (4), 1022-1028.
391. Fishwick, C. W. G.; Beevers, A. J.; Carrick, L. M.; Whitehouse, C. D.; Aggeli, A.; Boden, N., Structures of helical beta-tapes and twisted ribbons: The role of side-chain interactions on twist and bend behavior. *Nano Lett* **2003,** *3* (11), 1475-1479.
392. Wang, S. T.; Lin, Y.; Spencer, R. K.; Thomas, M. R.; Nguyen, A. I.; Amdursky, N.; Pashuck, E. T.; Skaalure, S. C.; Song, C. Y.; Parmar, P. A.; Morgan, R. M.; Ercius, P.; Aloni, S.; Zuckermann, R. N.; Stevens, M. M., Sequence-Dependent Self-Assembly and Structural Diversity of Islet Amyloid Polypeptide-Derived beta-Sheet Fibrils. *Acs Nano* **2017,** *11* (9), 8579-8589.
393. Fitzpatrick, A. W.; Debelouchina, G. T.; Bayro, M. J.; Clare, D. K.; Caporini, M. A.; Bajaj, V. S.; Jaroniec, C. P.; Wang, L.; Ladizhansky, V.; Muller, S. A.; MacPhee, C. E.; Waudby, C. A.; Mott, H. R.; De Simone, A.; Knowles, T. P.; Saibil, H. R.; Vendruscolo, M.; Orlova, E. V.; Griffin, R. G.; Dobson, C. M., Atomic structure and hierarchical assembly of a cross-beta amyloid fibril. *P Natl Acad Sci USA* **2013,** *110* (14), 5468-73.
394. Zhang, S.; Andreasen, M.; Nielsen, J. T.; Liu, L.; Nielsen, E. H.; Song, J.; Ji, G.; Sun, F.; Skrydstrup, T.; Besenbacher, F.; Nielsen, N. C.; Otzen, D. E.; Dong, M. D., Coexistence of ribbon and helical fibrils originating from hIAPP(20-29) revealed by quantitative nanomechanical atomic force microscopy. *P Natl Acad Sci USA* **2013,** *110* (8), 2798-2803.
395. Toksoz, S.; Guler, M. O., Self-assembled peptidic nanostructures. *Nano Today* **2009,** *4* (6), 458-469.
396. Chen, L.; Revel, S.; Morris, K.; Serpell, L. C.; Adams, D. J., Effect of Molecular Structure on the Properties of Naphthalene-Dipeptide Hydrogelators. *Langmuir* **2010,** *26* (16), 13466-13471.
397. Chamberlain, A. K.; MacPhee, C. E.; Zurdo, J.; Morozova-Roche, L. A.; Hill, H. A.; Dobson, C. M.; Davis, J. J., Ultrastructural organization of amyloid fibrils by atomic force microscopy. *Biophysical Journal* **2000,** *79* (6), 3282-93.

398. Wang, M.; Zhou, P.; Wang, J.; Zhao, Y.; Ma, H.; Lu, J. R.; Xu, H., Left or Right: How Does Amino Acid Chirality Affect the Handedness of Nanostructures Self-Assembled from Short Amphiphilic Peptides? *J Am Chem Soc* **2017,** *139* (11), 4185-4194.
399. Kocsis, J. D.; Sasaki, M.; Lankford, K. L.; Priest, C.; Wirth, E. D., Cell fate of human embryonic stem cell-derived oligodendrocyte progenitors (GRNOPC1) transplanted into the demyelinated nonhuman primate spinal cord. *Mult Scler J* **2011,** *17*, S46-S46.
400. Keirstead, H. S.; Nistor, G.; Bernal, G.; Totoiu, M.; Cloutier, F.; Sharp, K.; Steward, O., Human embryonic stem cell-derived oligodendrocyte progenitor cell transplants remyelinate and restore locomotion after spinal cord injury. *J Neurosci* **2005,** *25* (19), 4694-4705.
401. Urbanski, M. M.; Kingsbury, L.; Moussouros, D.; Kassim, I.; Mehjabeen, S.; Paknejad, N.; Melendez-Vasquez, C. V., Myelinating glia differentiation is regulated by extracellular matrix elasticity. *Sci Rep-Uk* **2016,** *6*.
402. Russell, L. N.; Lampe, K. J., Oligodendrocyte Precursor Cell Viability, Proliferation, and Morphology is Dependent on Mesh Size and Storage Modulus in 3D Poly(ethylene glycol)-Based Hydrogels. *Acs Biomater Sci Eng* **2017,** *3* (12), 3459-3468.
403. Tibbitt, M. W.; Anseth, K. S., Hydrogels as Extracellular Matrix Mimics for 3D Cell Culture. *Biotechnol Bioeng* **2009,** *103* (4), 655-663.
404. Haines-Butterick, L.; Rajagopal, K.; Branco, M.; Salick, D.; Rughani, R.; Pilarz, M.; Lamm, M. S.; Pochan, D. J.; Schneider, J. P., Controlling hydrogelation kinetics by peptide design for three-dimensional encapsulation and injectable delivery of cells. *P Natl Acad Sci USA* **2007,** *104* (19), 7791-7796.
405. Amer, M. H.; Rose, F. R. A. J.; Shakesheff, K. M.; White, L. J., A biomaterials approach to influence stem cell fate in injectable cell-based therapies. *Stem Cell Res Ther* **2018,** *9*.
406. Banerjee, A.; Arha, M.; Choudhary, S.; Ashton, R. S.; Bhatia, S. R.; Schaffer, D. V.; Kane, R. S., The influence of hydrogel modulus on the proliferation and differentiation of encapsulated neural stem cells. *Biomaterials* **2009,** *30* (27), 4695-4699.
407. Gao, M. Y.; Tao, H. Y.; Wang, T.; Wei, A. L.; He, B., Functionalized self-assembly polypeptide hydrogel scaffold applied in modulation of neural progenitor cell behavior. *J Bioact Compat Pol* **2017,** *32* (1), 45-60.
408. Cooke, M. J.; Wang, Y. F.; Morshead, C. M.; Shoichet, M. S., Controlled epi-cortical delivery of epidermal growth factor for the stimulation of endogenous neural stem cell proliferation in stroke-injured brain. *Biomaterials* **2011,** *32* (24), 5688-5697.
409. Lourenco, T.; Graos, M., Modulation of Oligodendrocyte Differentiation by Mechanotransduction. *Front Cell Neurosci* **2016,** *10*.
410. Liu, C.; Sage, J. C.; Miller, M. R.; Verhaak, R. G. W.; Hippenmeyer, S.; Vogel, H.; Foreman, O.; Bronson, R. T.; Nishiyama, A.; Luo, L. Q.; Zong, H., Mosaic Analysis with Double Markers Reveals Tumor Cell of Origin in Glioma. *Cell* **2011,** *146* (2), 209-221.
411. Chau, M. J.; Deveau, T. C.; Song, M. K.; Gu, X. H.; Chen, D. D.; Wei, L., iPSC Transplantation Increases Regeneration and Functional Recovery After Ischemic Stroke in Neonatal Rats. *Stem Cells* **2014,** *32* (12), 3075-3087.
412. Wong, F. S. Y.; Chan, B. P.; Lo, A. C. Y., Carriers in Cell-Based Therapies for Neurological Disorders. *Int J Mol Sci* **2014,** *15* (6), 10669-10723.
413. Prockop, D. J., Inflammation, fibrosis, and modulation of the process by mesenchymal stem/stromal cells. *Matrix Biol* **2016,** *51*, 7-13.
414. Oakland, M.; Sinn, P. L.; McCray, P. B., Advances in Cell and Gene-based Therapies for Cystic Fibrosis Lung Disease. *Mol Ther* **2012,** *20* (6), 1108-1115.

415. Chen, H. J.; Chen, C. H.; Chang, M. Y.; Tsai, D. C.; Baum, E. Z.; Hariri, R.; Herzberg, U.; Hsteh, P. C. H., Human Placenta-Derived Adherent Cells Improve Cardiac Performance in Mice With Chronic Heart Failure. *Stem Cell Transl Med* **2015,** *4* (3), 269-275.
416. Bali, P.; Lahiri, D. K.; Banik, A.; Nehru, B.; Anand, A., Potential for Stem Cells Therapy in Alzheimer's Disease: Do Neurotrophic Factors Play Critical Role? *Curr Alzheimer Res* **2017,** *14* (2), 208-220.
417. Li, X. Y.; Bao, X. J.; Wang, R. Z., Potential of neural stem cell-based therapies for Alzheimer's disease. *J Neurosci Res* **2015,** *93* (9), 1313-1324.
418. Raman, D.; Choudhary, M.; Cleary, J. P.; Punzalan, R. R.; Sharma, C. V.; Sharma, M. V.; Balmiki, R.; Chopra, N.; Lahiri, D. K.; Sharma, J. P., Potential of neuronal progenitor stem cell therapy for Alzheimer's disease. *Mol Biol Cell* **2011,** *22*.
419. Zhang, M.; Methot, D.; Poppa, V.; Fujio, Y.; Walsh, K.; Murry, C. E., Cardiomyocyte grafting for cardiac repair: Graft cell death and anti-death strategies. *J Mol Cell Cardiol* **2001,** *33* (5), 907-921.
420. Allan, D. S.; Keeney, M.; Howson-Jan, K.; Bhatia, M.; Sutherland, D. R.; Chin-Yee, I., Number of viable CD34+cells reinfused predicts engraftment in autologous hematopoietic stem cell transplantation. *Blood* **2000,** *96* (11), 381a-381a.
421. Amer, M. H.; Rose, F. R. A. J.; Shakesheff, K. M.; Modo, M.; White, L. J., Translational considerations in injectable cell-based therapeutics for neurological applications: concepts, progress and challenges. *Npj Regen Med* **2017,** *2*.
422. Abbott, R. D.; Kimmerling, E. P.; Cairns, D. M.; Kaplan, D. L., Silk as a Biomaterial to Support Long-Term Three-Dimensional Tissue Cultures. *Acs Appl Mater Inter* **2016,** *8* (34), 21861-21868.
423. Weber, L. M.; Hayda, K. N.; Haskins, K.; Anseth, K. S., The effects of cell-matrix interactions on encapsulated beta-cell function within hydrogels functionalized with matrix-derived adhesive peptides. *Biomaterials* **2007,** *28* (19), 3004-11.
424. Galler, K. M.; Aulisa, L.; Regan, K. R.; D'Souza, R. N.; Hartgerink, J. D., Self-Assembling Multidomain Peptide Hydrogels: Designed Susceptibility to Enzymatic Cleavage Allows Enhanced Cell Migration and Spreading. *J Am Chem Soc* **2010,** *132* (9), 3217-3223.
425. Nih, L. R.; Gojgini, S.; Carmichael, S. T.; Segura, T., Dual-function injectable angiogenic biomaterial for the repair of brain tissue following stroke. *Nat Mater* **2018,** *17* (7), 642-+.
426. Lampe, K. J.; Namba, R. M.; Silverman, T. R.; Bjugstad, K. B.; Mahoney, M. J., Impact of Lactic Acid on Cell Proliferation and Free Radical-Induced Cell Death in Monolayer Cultures of Neural Precursor Cells. *Biotechnol Bioeng* **2009,** *103* (6), 1214-1223.
427. Ding, X. C.; Gao, J.; Wang, Z. G.; Awada, H.; Wang, Y. D., A shear-thinning hydrogel that extends in vivo bioactivity of FGF2. *Biomaterials* **2016,** *111*, 80-89.
428. Sing, M. K.; Glassman, M. J.; Vronay-Ruggles, X. T.; Burghardt, W. R.; Olsen, B. D., Structure and rheology of dual-associative protein hydrogels under nonlinear shear flow. *Soft Matter* **2017,** *13* (45), 8511-8524.
429. Araujo, A.; Olsen, B. D.; Machado, A. V., Engineering Elastin-Like Polypeptide-Poly(ethylene glycol) Multiblock Physical Networks. *Biomacromolecules* **2018,** *19* (2), 329-339.
430. Stabenfeldt, S. E.; Garcia, A. J.; LaPlaca, M. C., Thermoreversible laminin-functionalized hydrogel for neural tissue engineering. *J Biomed Mater Res A* **2006,** *77a* (4), 718-725.
431. Bohari, S. P. M.; Hukins, D. W. L.; Grover, L. M., Effect of calcium alginate concentration on viability and proliferation of encapsulated fibroblasts. *Bio-Med Mater Eng* **2011,** *21* (3), 159-170.

432. Tang, J. D.; Mura, C.; Lampe, K. J., Stimuli-Responsive, Pentapeptide, Nanofiber Hydrogel for Tissue Engineering. *J Am Chem Soc* **2019,** *141* (12), 4886-4899.
433. Cao, N.; Chen, X. B.; Schreyer, D. J., Influence of Calcium Ions on Cell Survival and Proliferation in the Context of an Alginate Hydrogel. *ISRN Chemical Engineering* **2012,** *2012*, 9.
434. Buckley, C. T.; Thorpe, S. D.; O'Brien, F. J.; Robinson, A. J.; Kelly, D. J., The effect of concentration, thermal history and cell seeding density on the initial mechanical properties of agarose hydrogels. *J Mech Behav Biomed* **2009,** *2* (5), 512-521.
435. Payne, C.; Dolan, E. B.; O'Sullivan, J.; Cryan, S. A.; Kelly, H. M., A methylcellulose and collagen based temperature responsive hydrogel promotes encapsulated stem cell viability and proliferation in vitro. *Drug Deliv Transl Re* **2017,** *7* (1), 132-146.
436. Wakatsuki, T.; Elson, E. L., Reciprocal interactions between cells and extracellular matrix during remodeling of tissue constructs. *Biophys Chem* **2003,** *100* (1-3), 593-605.
437. Brown, R. A.; Prajapati, R.; McGrouther, D. A.; Yannas, I. V.; Eastwood, M., Tensional homeostasis in dermal fibroblasts: Mechanical responses to mechanical loading in three-dimensional substrates. *J Cell Physiol* **1998,** *175* (3), 323-332.
438. Legant, W. R.; Miller, J. S.; Blakely, B. L.; Cohen, D. M.; Genin, G. M.; Chen, C. S., Measurement of mechanical tractions exerted by cells in three-dimensional matrices. *Nat Methods* **2010,** *7* (12), 969-U113.
439. Chaudhuri, O.; Gu, L.; Klumpers, D.; Darnell, M.; Bencherif, S. A.; Weaver, J. C.; Huebsch, N.; Lee, H. P.; Lippens, E.; Duda, G. N.; Mooney, D. J., Hydrogels with tunable stress relaxation regulate stem cell fate and activity. *Nat Mater* **2016,** *15* (3), 326-+.
440. Williams, G. M.; Klein, T. J.; Sah, R. L., Cell density alters matrix accumulation in two distinct fractions and the mechanical integrity of alginate-chondrocyte constructs. *Acta Biomaterialia* **2005,** *1* (6), 625-633.
441. Wan, L. Q.; Jiang, J.; Miller, D. E.; Guo, X. E.; Mow, V. C.; Lu, H. H., Matrix Deposition Modulates the Viscoelastic Shear Properties of Hydrogel-Based Cartilage Grafts. *Tissue Eng Pt A* **2011,** *17* (7-8), 1111-1122.
442. Schneider, M. C.; Chu, S.; Sridhar, S. L.; de Roucy, G.; Vernerey, F. J.; Bryant, S. J., Local Heterogeneities Improve Matrix Connectivity in Degradable and Photoclickable Poly(ethylene glycol) Hydrogels for Applications in Tissue Engineering. *Acs Biomater Sci Eng* **2017,** *3* (10), 2480-2492.
443. Farnsworth, N.; Bensard, C.; Bryant, S. J., The role of the PCM in reducing oxidative stress induced by radical initiated photoencapsulation of chondrocytes in poly(ethylene glycol) hydrogels. *Osteoarthr Cartilage* **2012,** *20* (11), 1326-1335.
444. Lange, F.; Schwenke, K.; Kurakazu, M.; Akagi, Y.; Chung, U. I.; Lang, M.; Sommer, J. U.; Sakai, T.; Saalwachter, K., Connectivity and Structural Defects in Model Hydrogels: A Combined Proton NMR and Monte Carlo Simulation Study. *Macromolecules* **2011,** *44* (24), 9666-9674.
445. Tol, M.; Akar, A. R.; Durdu, S.; Ayyildiz, E.; Ilhan, O., Comparison of different needle diameters and flow rates on bone marrow mononuclear stem cell viability: an ex vivo experimental study. *Cytotherapy* **2008,** *10* (1), 98-99.
446. Tang, J. D.; Mura, C.; Lampe, K. J., A stimuli-responsive, pentapeptide, nanofiber hydrogel for tissue engineering. *J Am Chem Soc* **2019**.
447. Lakshmanan, A.; Zhang, S. G.; Hauser, C. A. E., Short self-assembling peptides as building blocks for modern nanodevices. *Trends Biotechnol* **2012,** *30* (3), 155-165.

448. Mishra, A.; Loo, Y. H.; Deng, R. H.; Chuah, Y. J.; Hee, H. T.; Ying, J. Y.; Hauser, C. A. E., Ultrasmall natural peptides self-assemble to strong temperature-resistant helical fibers in scaffolds suitable for tissue engineering. *Nano Today* **2011,** *6* (3), 232-239.
449. Ridgley, D. M.; Freedman, B. G.; Lee, P. W.; Barone, J. R., Genetically encoded self-assembly of large amyloid fibers. *Biomater Sci-Uk* **2014,** *2* (4), 560-566.
450. Tamamis, P.; Archontis, G., Amyloid-like self-assembly of a dodecapeptide sequence from the adenovirus fiber shaft: Perspectives from molecular dynamics simulations. *J Non-Cryst Solids* **2011,** *357* (2), 717-722.
451. Hanwell, M. D.; Curtis, D. E.; Lonie, D. C.; Vandermeersch, T.; Zurek, E.; Hutchison, G. R., Avogadro: an advanced semantic chemical editor, visualization, and analysis platform. *J Cheminformatics* **2012,** *4*.
452. Humphrey, W.; Dalke, A.; Schulten, K., VMD: Visual molecular dynamics. *J Mol Graph Model* **1996,** *14* (1), 33-38.
453. Rossum, G. *Python reference manual*; CWI (Centre for Mathematics and Computer Science): 1995.
454. Bright, W., The D programming language. *Dr Dobbs J* **2002,** *27* (2), 36-40.
455. Frishman, D.; Argos, P., Knowledge-based protein secondary structure assignment. *Proteins* **1995,** *23* (4), 566-579.
456. Heinig, M.; Frishman, D., STRIDE: a web server for secondary structure assignment from known atomic coordinates of proteins. *Nucleic Acids Res* **2004,** *32*, W500-W502.
457. Schindelin, J.; Arganda-Carreras, I.; Frise, E.; Kaynig, V.; Longair, M.; Pietzsch, T.; Preibisch, S.; Rueden, C.; Saalfeld, S.; Schmid, B.; Tinevez, J. Y.; White, D. J.; Hartenstein, V.; Eliceiri, K.; Tomancak, P.; Cardona, A., Fiji: an open-source platform for biological-image analysis. *Nat Methods* **2012,** *9* (7), 676-682.
458. Usov, I.; Mezzenga, R., FiberApp: An Open-Source Software for Tracking and Analyzing Polymers, Filaments, Biomacromolecules, and Fibrous Objects. *Macromolecules* **2015,** *48* (5), 1269-1280.
459. Nolles, A.; Westphal, A. H.; de Hoop, J. A.; Fokkink, R. G.; Kleijn, J. M.; van Berkel, W. J. H.; Borst, J. W., Encapsulation of GFP in Complex Coacervate Core Micelles. *Biomacromolecules* **2015,** *16* (5), 1542-1549.
460. Srivastava, S.; Tirrell, M. V., Polyelectrolyte Complexation. *Adv Chem Phys* **2016,** *161*, 499-544.
461. Vieregg, J. R.; Tang, T. Y. D., Polynucleotides in cellular mimics: Coacervates and lipid vesicles. *Curr Opin Colloid In* **2016,** *26*, 50-57.
462. Capito, R. M.; Azevedo, H. S.; Velichko, Y. S.; Mata, A.; Stupp, S. I., Self-assembly of large and small molecules into hierarchically ordered sacs and membranes. *Science* **2008,** *319* (5871), 1812-1816.
463. Meka, V. S.; Singe, M. K. G.; Pichika, M. R.; Nali, S. R.; Kolapaili, V. R. M.; Kesharwani, P., A comprehensive review on polyelectrolyte complexes. *Drug Discov Today* **2017,** *22* (11), 1697-1706.
464. Le Cerf, D.; Pepin, A. S.; Niang, P. M.; Cristea, M.; Karakasyan-Dia, C.; Picton, L., Formation of polyelectrolyte complexes with diethylaminoethyl dextran: Charge ratio and molar mass effect. *Carbohyd Polym* **2014,** *113*, 217-224.
465. Lemmers, M.; Spruijt, E.; Beun, L.; Fokkink, R.; Leermakers, F.; Portale, G.; Stuart, M. A. C.; van der Gucht, J., The influence of charge ratio on transient networks of polyelectrolyte complex micelles. *Soft Matter* **2012,** *8* (1), 104-117.

466. Priftis, D.; Tirrell, M., Phase behaviour and complex coacervation of aqueous polypeptide solutions. *Soft Matter* **2012,** *8* (36), 9396-9405.
467. Chollakup, R.; Beck, J. B.; Dirnberger, K.; Tirrell, M.; Eisenbach, C. D., Polyelectrolyte Molecular Weight and Salt Effects on the Phase Behavior and Coacervation of Aqueous Solutions of Poly(acrylic acid) Sodium Salt and Poly(allylamine) Hydrochloride. *Macromolecules* **2013,** *46* (6), 2376-2390.
468. Park, W. M.; Champion, J. A., Two-Step Protein Self-Assembly in the Extracellular Matrix. *Angew Chem Int Edit* **2013,** *52* (31), 8098-8101.
469. Johnson, N. R.; Wang, Y. D., Coacervate delivery systems for proteins and small molecule drugs. *Expert Opin Drug Del* **2014,** *11* (12), 1829-1832.
470. Vignesh, S.; Sivashanmugam, A.; Mohandas, A.; Janarthanan, R.; Iyer, S.; Nair, S. V.; Jayakumar, R., Injectable deferoxamine nanoparticles loaded chitosan-hyaluronic acid coacervate hydrogel for therapeutic angiogenesis. *Colloid Surface B* **2018,** *161*, 129-138.
471. Jin, K. M.; Kim, Y. H., Injectable, thermo-reversible and complex coacervate combination gels for protein drug delivery. *J Control Release* **2008,** *127* (3), 249-256.
472. Gao, X. Q.; Cheng, H. Z.; Amra, S.; Tang, Y.; Sun, X. Y.; Awada, H.; Lu, A. P.; Deng, Z. H.; Wang, B.; Wang, Y. D.; Huard, J., A Comparison of BMP2 Delivery by Gene Therapy and Coacervate for Promoting Human Muscle-Derived Stem Cell-Mediated Cartilage Repair. *Mol Ther* **2017,** *25* (5), 160-160.
473. Haile, M.; Sarwar, O.; Henderson, R.; Smith, R.; Grunlan, J. C., Polyelectrolyte Coacervates Deposited as High Gas Barrier Thin Films. *Macromol Rapid Comm* **2017,** *38* (1).
474. Hwang, D. S.; Zeng, H. B.; Srivastava, A.; Krogstad, D. V.; Tirrell, M.; Israelachvili, J. N.; Waite, J. H., Viscosity and interfacial properties in a mussel-inspired adhesive coacervate. *Soft Matter* **2010,** *6* (14), 3232-3236.
475. Kelly, K. D.; Schlenoff, J. B., Spin-Coated Polyelectrolyte Coacervate Films. *Acs Appl Mater Inter* **2015,** *7* (25), 13980-13986.
476. Aberkane, L.; Jasniewski, J.; Gaiani, C.; Hussain, R.; Scher, J.; Sanchez, C., Structuration mechanism of beta-lactoglobulin - acacia gum assemblies in presence of quercetin. *Food Hydrocolloid* **2012,** *29* (1), 9-20.
477. Croguennec, T.; Tavares, G. M.; Bouhallab, S., Heteroprotein complex coacervation: A generic process. *Adv Colloid Interfac* **2017,** *239*, 115-126.
478. de Souza, G. I. D. H.; Santamarina, A. B.; de Santana, A. A.; Lira, F. S.; de Laquila, R.; Moreno, M. F.; Ribeiro, E. B.; do Nascimento, C. M. D. O.; Rodrigues, B.; Esposito, E.; Oyama, L. M., Preventive Effects of Chitosan Coacervate Whey Protein on Body Composition and Immunometabolic Aspect in Obese Mice. *Mediat Inflamm* **2014**.
479. Evdokimov, I. A.; Alieva, L. R.; Varlamov, V. P.; Kharitonov, V. D.; Butkevich, T. V.; Kurchenko, V. P., Usage of Chitosan in Dairy Products Production. *Food Raw Mater* **2015,** *3* (2), 29-39.
480. Souza, C. J. F.; da Costa, A. R.; Souza, C. F.; Tosin, F. F. S.; Garcia-Rojas, E. E., Complex coacervation between lysozyme and pectin: Effect of pH, salt, and biopolymer ratio. *Int J Biol Macromol* **2018,** *107*, 1253-1260.
481. Liu, H. J.; Wise, S. G.; Rnjak-Kovacina, J.; Kaplan, D. L.; Bilek, M. M. M.; Weiss, A. S.; Fei, J.; Bao, S. S., Biocompatibility of silk-tropoelastin protein polymers. *Biomaterials* **2014,** *35* (19), 5138-5147.
482. Thompson, R. E.; Pardieck, J.; Smith, L.; Kenny, P.; Crawford, L.; Shoichet, M.; Sakiyama-Elbert, S., Effect of hyaluronic acid hydrogels containing astrocyte-derived

extracellular matrix and/or V2a interneurons on histologic outcomes following spinal cord injury. *Biomaterials* **2018,** *162*, 208-223.
483. White, J. D.; Wang, S. R.; Weiss, A. S.; Kaplan, D. L., Silk-tropoelastin protein films for nerve guidance. *Acta Biomaterialia* **2015,** *14*, 1-10.
484. Meyer, D. E.; Chilkoti, A., Purification of recombinant proteins by fusion with thermally-responsive polypeptides. *Nat Biotechnol* **1999,** *17* (11), 1112-1115.
485. Long, M. M.; Urry, D. W.; Cox, B. A.; Ohnishi, T.; Jacobs, M., Coacervation of Repeat Sequences of Elastin. *Biophysical Journal* **1975,** *15* (2), A71-A71.
486. Trabbic-Carlson, K.; Meyer, D. E.; Liu, L.; Piervincenzi, R.; Nath, N.; LaBean, T.; Chilkoti, A., Effect of protein fusion on the transition temperature of an environmentally responsive elastin-like polypeptide: a role for surface hydrophobicity? *Protein Eng Des Sel* **2004,** *17* (1), 57-66.
487. Inostroza-Brito, K. E.; Collin, E.; Siton-Mendelson, O.; Smith, K. H.; Monge-Marcet, A.; Ferreira, D. S.; Rodriguez, R. P.; Alonso, M.; Rodriguez-Cabello, J. C.; Reis, R. L.; Sagues, F.; Botto, L.; Bitton, R.; Azevedo, H. S.; Mata, A., Co-assembly, spatiotemporal control and morphogenesis of a hybrid protein-peptide system. *Nat Chem* **2015,** *7* (11), 897-904.
488. Mills, C. E.; Michaud, Z.; Olsen, B. D., Elastin-like Polypeptide (ELP) Charge Influences Self-Assembly of ELP–mCherry Fusion Proteins. *Biomacromolecules* **2018,** *19* (7), 2517-2525.
489. Christensen, T.; Hassouneh, W.; Trabbic-Carlson, K.; Chilkoti, A., Predicting Transition Temperatures of Elastin-Like Polypeptide Fusion Proteins. *Biomacromolecules* **2013,** *14* (5), 1514-1519.
490. Trabbic-Carlson, K.; Liu, L.; Kim, B.; Chilkoti, A., Expression and purification of recombinant proteins from Escherichia coli: Comparison of an elastin-like polypeptide fusion with an oligohistidine fusion. *Protein Sci* **2004,** *13* (12), 3274-84.
491. Choi, S. K.; Park, J. K.; Lee, K. M.; Lee, S. K.; Jeon, W. B., Improved neural progenitor cell proliferation and differentiation on poly(lactide-co-glycolide) scaffolds coated with elastin-like polypeptide. *J Biomed Mater Res B* **2013,** *101* (8), 1329-1339.
492. Ozaki, C.; Somamoto, S.; Kawabata, S.; Tabata, Y., Effect of an artificial silk elastin-like protein on the migration and collagen production of mouse fibroblasts. *J Biomat Sci-Polym E* **2014,** *25* (12), 1266-1277.
493. Xia, X. X.; Wang, M.; Lin, Y. A.; Xu, Q. B.; Kaplan, D. L., Hydrophobic Drug-Triggered Self-Assembly of Nanoparticles from Silk-Elastin-Like Protein Polymers for Drug Delivery. *Biomacromolecules* **2014,** *15* (3), 908-914.
494. Hassouneh, W.; Zhulina, E. B.; Chilkoti, A.; Rubinstein, M., Elastin-like Polypeptide Diblock Copolymers Self-Assemble into Weak Micelles. *Macromolecules* **2015,** *48* (12), 4183-4195.
495. Toole, B. P., Hyaluronan: from extracellular glue to cell signaling cue. *Int J Exp Pathol* **2009,** *90* (2), A96-A96.
496. Toole, B. P., Hyaluronan in morphogenesis. *J Intern Med* **1997,** *242* (1), 35-40.
497. Blancas, A. A.; Acosta, F. M.; Grande-Allen, K. J., Not just skin deep: cosmetic and medical applications of injectable hyaluronan and fibrin. *Mater Technol* **2015,** *30* (B4), B206-B210.
498. D'Este, M.; Sprecher, C. M.; Milz, S.; Nehrbass, D.; Dresing, I.; Zeiter, S.; Alini, M.; Eglin, D., Evaluation of an injectable thermoresponsive hyaluronan hydrogel in a rabbit osteochondral defect model. *J Biomed Mater Res A* **2016,** *104* (6), 1469-1478.

499. Sabbieti, M. G.; Dubbini, A.; Laus, F.; Paggi, E.; Marchegiani, A.; Capitani, M.; Marchetti, L.; Dini, F.; Vermonden, T.; Di Martino, P.; Agas, D.; Censi, R., In vivo biocompatibility of p(HPMAm-lac)-PEG hydrogels hybridized with hyaluronan. *J Tissue Eng Regen M* **2017,** *11* (11), 3056-3067.
500. Lee, S. B.; Lee, Y. M.; Song, K. W.; Park, M. H., Preparation and properties of polyelectrolyte complex sponges composed of hyaluronic acid and chitosan and their biological behaviors. *J Appl Polym Sci* **2003,** *90* (4), 925-932.
501. Kim, S. J.; Shin, S. R.; Lee, K. B.; Park, Y. D.; Kim, S. I., Synthesis and characteristics of polyelectrolyte complexes composed of chitosan and hyaluronic acid. *J Appl Polym Sci* **2004,** *91* (5), 2908-2913.
502. Kim, S. J.; Lee, C. K.; Lee, Y. M.; Kim, I. Y.; Kim, S. I., Electrical/pH-sensitive swelling behavior of polyelectrolyte hydrogels prepared with hyaluronic acid-poly(vinyl alcohol) interpenetrating polymer networks. *React Funct Polym* **2003,** *55* (3), 291-298.
503. Hahn, S. K.; Hoffman, A. S., Characterization of biocompatible polyelectrolyte complex multilayer of hyaluronic acid and poly-L-lysine. *Biotechnol Bioproc E* **2004,** *9* (3), 179-183.
504. Hahn, S. K.; Hoffman, A. S., Preparation and characterization of biocompatible polyelectrolyte complex multilayer of hyaluronic acid and poly-L-lysine. *Int J Biol Macromol* **2005,** *37* (5), 227-231.
505. Yamanlar, S.; Sant, S.; Boudou, T.; Picart, C.; Khademhosseini, A., Surface functionalization of hyaluronic acid hydrogels by polyelectrolyte multilayer films. *Biomaterials* **2011,** *32* (24), 5590-5599.
506. Castelletto, V.; Kaur, A.; Hamley, I. W.; Barnes, R. H.; Karatzas, K. A.; Hermida-Merino, D.; Swioklo, S.; Connon, C. J.; Stasiak, J.; Reza, M.; Ruokolainen, J., Hybrid membrane biomaterials from self-assembly in polysaccharide and peptide amphiphile mixtures: controllable structural and mechanical properties and antimicrobial activity. *Rsc Adv* **2017,** *7* (14), 8366-8375.
507. Zha, R. H.; Velichko, Y. S.; Bitton, R.; Stupp, S. I., Molecular design for growth of supramolecular membranes with hierarchical structure. *Soft Matter* **2016,** *12* (5), 1401-1410.
508. Matson, J. B.; Navon, Y.; Bitton, R.; Stupp, S. I., Light-Controlled Hierarchical Self-Assembly of Polyelectrolytes and Supramolecular Polymers. *Acs Macro Letters* **2015,** *4* (1), 43-47.
509. Zha, R. H.; Sur, S.; Stupp, S. I., Self-assembly of Cytotoxic Peptide Amphiphiles into Supramolecular Membranes for Cancer Therapy. *Adv Healthc Mater* **2013,** *2* (1), 126-133.
510. Artimo, P.; Jonnalagedda, M.; Arnold, K.; Baratin, D.; Csardi, G.; de Castro, E.; Duvaud, S.; Flegel, V.; Fortier, A.; Gasteiger, E.; Grosdidier, A.; Hernandez, C.; Ioannidis, V.; Kuznetsov, D.; Liechti, R.; Moretti, S.; Mostaguir, K.; Redaschi, N.; Rossier, G.; Xenarios, I.; Stockinger, H., ExPASy: SIB bioinformatics resource portal. *Nucleic Acids Res* **2012,** *40* (W1), W597-W603.
511. Mero, A.; Campisi, M., Hyaluronic Acid Bioconjugates for the Delivery of Bioactive Molecules. *Polymers-Basel* **2014,** *6* (2), 346-369.
512. Kayitmazer, A. B.; Bohidar, H. B.; Mattison, K. W.; Bose, A.; Sarkar, J.; Hashidzume, A.; Russo, P. S.; Jaeger, W.; Dubin, P. L., Mesophase separation and probe dynamics in protein-polyelectrolyte coacervates. *Soft Matter* **2007,** *3* (8), 1064-1076.
513. Harmon, T. S.; Roberts, S.; Chilkoti, A.; Pappu, R. V., A Model for Hysteresis Observed in Phase Transitions of Thermally Responsive Intrinsically Disordered Protein Polymers. *Biophysical Journal* **2017,** *112* (3), 207a-207a.
514. Roberts, S.; Dzuricky, M.; Chilkoti, A., Elastin-like polypeptides as models of intrinsically disordered proteins. *Febs Lett* **2015,** *589* (19), 2477-2486.

515. Zhang, Y. J.; Trabbic-Carlson, K.; Albertorio, F.; Chilkoti, A.; Cremer, P. S., Aqueous two-phase system formation kinetics for elastin-like polypeptides of varying chain length. *Biomacromolecules* **2006,** *7* (7), 2192-2199.
516. Meyer, D. E.; Chilkoti, A., Quantification of the effects of chain length and concentration on the thermal behavior of elastin-like polypeptides. *Biomacromolecules* **2004,** *5* (3), 846-851.
517. Hait, S. K.; Moulik, S. P.; Palepu, R., Refined method of assessment of parameters of micellization of surfactants and percolation of w/o microemulsions. *Langmuir* **2002,** *18* (7), 2471-2476.
518. Ray, G. B.; Chakraborty, I.; Moulik, S. P., Pyrene absorption can be a convenient method for probing critical micellar concentration (cmc) and indexing micellar polarity. *J Colloid Interf Sci* **2006,** *294* (1), 248-254.
519. Mi, Y.; Liu, Y. T.; Feng, S. S., Formulation of Docetaxel by folic acid-conjugated D-alpha-tocopheryl polyethylene glycol succinate 2000 (Vitamin E TPGS(2k)) micelles for targeted and synergistic chemotherapy. *Biomaterials* **2011,** *32* (16), 4058-4066.
520. Bales, B. L.; Almgren, M., Fluorescence Quenching of Pyrene by Copper(Ii) in Sodium Dodecyl-Sulfate Micelles - Effect of Micelle Size as Controlled by Surfactant Concentration. *J Phys Chem-Us* **1995,** *99* (41), 15153-15162.
521. Yekta, A.; Duhamel, J.; Brochard, P.; Adiwidjaja, H.; Winnik, M. A., A Fluorescent-Probe Study of Micelle-Like Cluster Formation in Aqueous-Solutions of Hydrophobically Modified Poly(Ethylene Oxide). *Macromolecules* **1993,** *26* (8), 1829-1836.
522. Berezney, J. P.; Saleh, O. A., Electrostatic Effects on the Conformation and Elasticity of Hyaluronic Acid, a Moderately Flexible Polyelectrolyte. *Macromolecules* **2017,** *50* (3), 1085-1089.
523. Kim, S.; Huang, J.; Lee, Y.; Dutta, S.; Yoo, H. Y.; Jung, Y. M.; Jho, Y.; Zeng, H. B.; Hwang, D. S., Complexation and coacervation of like-charged polyelectrolytes inspired by mussels. *P Natl Acad Sci USA* **2016,** *113* (7), E847-E853.
524. Wang, Q. F.; Schlenoff, J. B., The Polyelectrolyte Complex/Coacervate Continuum. *Macromolecules* **2014,** *47* (9), 3108-3116.
525. Ding, Y. W.; Zhang, G. Z., Folding of a single polymer chain and phase transition. *Chinese Sci Bull* **2009,** *54* (11), 1908-1911.
526. LunaBarcenas, G.; Gromov, D. G.; Meredith, J. C.; Sanchez, I. C.; dePablo, J. J.; Johnston, K. P., Polymer chain collapse near the lower critical solution temperature. *Chem Phys Lett* **1997,** *278* (4-6), 302-306.
527. Karle, I. L.; Urry, D. W., Crystal structure of cyclic (APGVGV)(2,) an analog of elastin, and a suggested mechanism for elongation/contraction of the molecule. *Biopolymers* **2005,** *77* (4), 198-204.
528. Bhattacharjee, S. M.; Giacometti, A.; Maritan, A., Flory theory for polymers. *J Phys-Condens Mat* **2013,** *25* (50).
529. Favre, E.; Nguyen, Q. T.; Sacco, D.; Moncuy, A.; Clement, R., Multicomponent polymer/solvents equilibria: An evaluation of Flory-Huggins theory for crosslinked PDMS networks swelled by binary mixtures. *Chem Eng Commun* **1996,** *140*, 193-205.
530. Priftis, D.; Laugel, N.; Tirrell, M., Thermodynamic Characterization of Polypeptide Complex Coacervation. *Langmuir* **2012,** *28* (45), 15947-15957.
531. Xia, J. L.; Zhang, H. W.; Rigsbee, D. R.; Dubin, P. L.; Shaikh, T., Structural Elucidation of Soluble Polyelectrolyte-Micelle Complexes - Intrapolymer Vs Interpolymer Association. *Macromolecules* **1993,** *26* (11), 2759-2766.

532. Gribbon, P.; Heng, B. C.; Hardingham, T. E., The molecular basis of the solution properties of hyaluronan investigated by confocal fluorescence recovery after photobleaching. *Biophysical Journal* **1999,** *77* (4), 2210-2216.
533. Krukau, A.; Brovchenko, I.; Geiger, A., Temperature-induced conformational transition of a model elastin-like peptide GVG(VPGVG)(3) in water. *Biomacromolecules* **2007,** *8* (7), 2196-2202.
534. Urry, D. W.; Trapane, T. L.; Prasad, K. U., Phase-Structure Transitions of the Elastin Polypentapeptide Water-System within the Framework of Composition Temperature Studies. *Biopolymers* **1985,** *24* (12), 2345-2356.
535. Ohgo, K.; Ashida, J.; Kumashiro, K. K.; Asakura, T., Structural determination of an elastin-mimetic model peptide, (Val-Pro-Gly-Val-Gly)(6), studied by C-13 CP/MAS NMR chemical shifts, two-dimensional off magic angle spinning spin-diffusion NMR, rotational echo double resonance, and statistical distribution of torsion angles from protein data bank. *Macromolecules* **2005,** *38* (14), 6038-6047.
536. Rapaka, R. S.; Okamoto, K.; Urry, D. W., Coacervation Properties in Sequential Polypeptide Models of Elastin - Synthesis of H-(Ala-Pro-Gly-Gly)N-Val-Ome and H-(Ala-Pro-Gly-Val-Gly)N-Val-Ome. *Int J Pept Prot Res* **1978,** *12* (2), 81-92.
537. Doss, S. S.; Bhatt, N. P.; Jayaraman, G., Improving the accuracy of hyaluronic acid molecular weight estimation by conventional size exclusion chromatography. *J Chromatogr B* **2017,** *1060*, 255-261.
538. Yu, L. P.; Masi, L.; Burns, J. W., Size Exclusion Chromatography and Multi Angle Laser-Light Scattering for Molecular-Weight Analysis of Hyaluronic-Acid. *Abstr Pap Am Chem S* **1989,** *198*, 81-Poly.
539. Yu, J.; Mao, J.; Yuan, G. C.; Satija, S.; Jiang, Z.; Chen, W.; Tirrell, M., Structure of Polyelectrolyte Brushes in the Presence of Multivalent Counterions. *Macromolecules* **2016,** *49* (15), 5609-5617.
540. Perry, S. L.; Li, Y.; Priftis, D.; Leon, L.; Tirrell, M., The Effect of Salt on the Complex Coacervation of Vinyl Polyelectrolytes. *Polymers-Basel* **2014,** *6* (6), 1756-1772.
541. Lalevee, G.; Sudre, G.; Montembault, A.; Meadows, J.; Malaise, S.; Crepet, A.; David, L.; Delair, T., Polyelectrolyte complexes via desalting mixtures of hyaluronic acid and chitosan-Physicochemical study and structural analysis. *Carbohyd Polym* **2016,** *154*, 86-95.
542. Dreher, M. R.; Simnick, A. J.; Fischer, K.; Smith, R. J.; Patel, A.; Schmidt, M.; Chilkoti, A., Temperature triggered self-assembly of polypeptides into multivalent spherical micelles. *J Am Chem Soc* **2008,** *130* (2), 687-694.
543. Astafieva, I.; Zhong, X. F.; Eisenberg, A., Critical Micellization Phenomena in Block Polyelectrolyte Solutions. *Macromolecules* **1993,** *26* (26), 7339-7352.
544. Johnson, A. E., Fluorescence approaches for determining protein conformations, interactions and mechanisms at membranes. *Traffic* **2005,** *6* (12), 1078-1092.
545. Goudsmits, J. M. H.; Slotboom, D. J.; van Oijen, A. M., Single-molecule visualization of conformational changes and substrate transport in the vitamin B-12 ABC importer BtuCD-F. *Nat Commun* **2017,** *8*.
546. Yu, L. L.; Tan, M. Y.; Ho, B.; Ding, J. L.; Wohland, T., Determination of critical micelle concentrations and aggregation numbers by fluorescence correlation spectroscopy: Aggregation of a lipopolysaccharide. *Anal Chim Acta* **2006,** *556* (1), 216-225.
547. Liaw, J.; Aoyagi, T.; Kataoka, K.; Sakurai, Y.; Okano, T., Permeation of PEO-PBLA-FITC polymeric micelles in aortic endothelial cells. *Pharm Res-Dord* **1999,** *16* (2), 213-220.

548. Hugerth, A.; Caram-Lelham, N.; Sundelof, L. O., The effect of charge density and conformation on the polyelectrolyte complex formation between carrageenan and chitosan. *Carbohyd Polym* **1997,** *34* (3), 149-156.
549. Ishii, Y.; Lehrer, S. S., Intramolecular Excimer Fluorescence of Pyrene Maleimide-Labeled Dithiothreitol (P-Dtt). *Biophysical Journal* **1987,** *51* (2), A276-A276.
550. Kalyanasundaram, K.; Thomas, J. K., Environmental Effects on Vibronic Band Intensities in Pyrene Monomer Fluorescence and Their Application in Studies of Micellar Systems. *J Am Chem Soc* **1977,** *99* (7), 2039-2044.
551. Bertoncini, C. W.; Celej, M. S., Small Molecule Fluorescent Probes for the Detection of Amyloid Self-Assembly In Vitro and In Vivo. *Curr Protein Pept Sc* **2011,** *12* (3), 206-220.
552. Bains, G.; Patel, A. B.; Narayanaswami, V., Pyrene: A Probe to Study Protein Conformation and Conformational Changes. *Molecules* **2011,** *16* (9), 7909-7935.
553. Ribeiro, A.; Arias, F. J.; Reguera, J.; Alonso, M.; Rodriguez-Cabello, J. C., Influence of the Amino-Acid Sequence on the Inverse Temperature Transition of Elastin-Like Polymers. *Biophysical Journal* **2009,** *97* (1), 312-320.
554. Geddes, C. D., Optical halide sensing using fluorescence quenching: theory, simulations and applications - a review. *Meas Sci Technol* **2001,** *12* (9), R53-R88.
555. Teale, F. W. J., Principles of Fluorescence Spectroscopy - Lakowicz,Jr. *Nature* **1984,** *307* (5950), 486-486.
556. Limpouchova, Z.; Prochazka, K., Theoretical Principles of Fluorescence Spectroscopy. *Springer Ser Fluores* **2016,** *16*, 91-149.
557. Jiang, H.; Zhao, X. Y.; Schanze, K. S., Amplified fluorescence quenching of a conjugated polyelectrolyte mediated by Ca2+. *Langmuir* **2006,** *22* (13), 5541-5543.
558. George, W. N.; Giles, M.; McCulloch, I.; de Mello, J. C.; Steinke, J. H. G., Amplified fluorescence quenching in high ionic strength media. *Soft Matter* **2007,** *3* (11), 1381-1387.
559. Graceffa, P.; Lehrer, S. S., The Excimer Fluorescence of Pyrene-Labeled Tropomyosin - a Probe of Conformational Dynamics. *J Biol Chem* **1980,** *255* (23), 1296-1300.
560. Rodrigues, G. M. C.; Gaj, T.; Adil, M. M.; Wahba, J.; Rao, A. T.; Lorbeer, F. K.; Kulkarni, R. U.; Diogo, M. M.; Cabral, J. M. S.; Miller, E. W.; Hockemeyer, D.; Schaffer, D. V., Defined and Scalable Differentiation of Human Oligodendrocyte Precursors from Pluripotent Stem Cells in a 3D Culture System. *Stem Cell Rep* **2017,** *8* (6), 1770-1783.
561. Lee, S.; Leach, M. K.; Redmond, S. A.; Chong, S. Y. C.; Mellon, S. H.; Tuck, S. J.; Feng, Z. Q.; Corey, J. M.; Chan, J. R., A culture system to study oligodendrocyte myelination processes using engineered nanofibers. *Nature Methods* **2012,** *9* (9), 917-+.
562. Diao, H. J.; Low, W. C.; Milbreta, U.; Lu, Q. R.; Chew, S. Y., Nanofiber-mediated microRNA delivery to enhance differentiation and maturation of oligodendroglial precursor cells. *J Control Release* **2015,** *208*, 85-92.
563. Veiga, S.; Ly, J.; Chan, P. H.; Bresnahan, J. C.; Beattie, M. S., SOD1 overexpression improves features of the oligodendrocyte precursor response in vitro. *Neurosci Lett* **2011,** *503* (1), 10-4.
564. Larsen, P. H.; Yong, V. W., The expression of matrix metalloproteinase-12 by oligodendrocytes regulates their maturation and morphological differentiation. *J Neurosci* **2004,** *24* (35), 7597-603.
565. Miller, J. S.; Shen, C. J.; Legant, W. R.; Baranski, J. D.; Blakely, B. L.; Chen, C. S., Bioactive hydrogels made from step-growth derived PEG-peptide macromers. *Biomaterials* **2010,** *31* (13), 3736-3743.

566. Thompson, H. L.; Burbelo, P. D.; Yamada, Y.; Kleinman, H. K.; Metcalfe, D. D., Identification of an Amino-Acid-Sequence in the Laminin a-Chain Mediating Mast-Cell Attachment and Spreading. *Immunology* **1991,** *72* (1), 144-149.
567. Grant, D. S.; Kinsella, J. L.; Fridman, R.; Auerbach, R.; Piasecki, B. A.; Yamada, Y.; Zain, M.; Kleinman, H. K., Interaction of Endothelial-Cells with a Laminin-a Chain Peptide (Sikvav) Invitro and Induction of Angiogenic Behavior Invivo. *J Cell Physiol* **1992,** *153* (3), 614-625.
568. Nakamura, M.; Mie, M.; Mihara, H.; Nakamura, M.; Kobatake, E., Construction of a Multi-Functional Extracellular Matrix Protein That Increases Number of N1E-115 Neuroblast Cells Having Neurites. *J Biomed Mater Res B* **2009,** *91b* (1), 425-432.
569. Grant, D. S.; Zukowska, Z., Revascularization of ischemic tissues with SIKVAV and neuropeptide Y (NPY). *Angiogenesis: From the Molecular to Integrative Pharmacology* **2000,** *476*, 139-154.
570. Yu, X. J.; Dillon, G. P.; Bellamkonda, R. V., A laminin and nerve growth factor-laden three-dimensional scaffold for enhanced neurite extension. *Tissue Eng* **1999,** *5* (4), 291-304.
571. Cui, G. H.; Shao, S. J.; Yang, J. J.; Liu, J. R.; Guo, H. D., Designer Self-Assemble Peptides Maximize the Therapeutic Benefits of Neural Stem Cell Transplantation for Alzheimer's Disease via Enhancing Neuron Differentiation and Paracrine Action. *Mol Neurobiol* **2016,** *53* (2), 1108-1123.
572. Tang, J. D.; Roloson, E. B.; Amelung, C. D.; Lampe, K. J., Rapidly Assembling Pentapeptides for Injectable Delivery (RAPID) Hydrogels as Cytoprotective Cell Carriers. *Acs Biomater Sci Eng* **2019,** *5* (5), 2117-2121.
573. Jung, J. P.; Moyano, J. V.; Collier, J. H., Multifactorial optimization of endothelial cell growth using modular synthetic extracellular matrices. *Integr Biol-Uk* **2011,** *3* (3), 185-196.
574. Heilshorn, S. C.; Liu, J. C.; Tirrell, D. A., Cell-binding domain context affects cell behavior on engineered proteins. *Biomacromolecules* **2005,** *6* (1), 318-323.
575. Farrukh, A.; Ortega, F.; Fan, W. Q.; Marichal, N.; Paez, J. I.; Berninger, B.; del Campo, A.; Salierno, M. J., Bifunctional Hydrogels Containing the Laminin Motif IKVAV Promote Neurogenesis. *Stem Cell Rep* **2017,** *9* (5), 1432-1440.
576. Li, X. W.; Liu, X. Y.; Josey, B.; Chou, C. J.; Tan, Y.; Zhang, N.; Wen, X. J., Short Laminin Peptide for Improved Neural Stem Cell Growth. *Stem Cell Transl Med* **2014,** *3* (5), 662-670.

9 Appendices

9.1 Appendix 1: Materials and Methods for Tang et al. J. Am. Chem. Soc., 141: 4886-4899 (2019)

9.1.1 Peptide Synthesis.

All peptides were synthesized by solid-phase chemistry in 0.1 mmol batches on a Tribute peptide synthesizer (Gyros Protein Technologies, AZ). A TentaGel R Rink Amide Resin was used which results in a C-terminal amide. Solvents and Fmoc (fluorenylmethoxycarbonyl)–protected AAs were purchased from Gyros Protein Technologies. Reagents were made with 5 equiv. moles of amino acid and 5 equiv. moles of HBTU (2-(1*H*-benzotriazol-1-yl)-1,1,3,3-tetramethyluronium hexafluorophosphate), and subsequently dissolved in DMF (dimethylformamide). Amino acid coupling cycles were 60 min in length. Protecting groups were removed with treatments of 20/80 v/v piperidine/DMF for 10 minutes. After the coupling reaction was complete, the resin was washed three times with DCM (dichloromethane) before running the cleavage step. Cleavage of the peptides were accomplished by shaking the resin with 10 mL of TFA (trifluoroacetic acid)/triisopropylsilane/H_2O (95:2.5:2.5 volume ratios) for 2 h at room temperature. The peptide solution was collected, and the peptide precipitated by the addition of cold diethyl ether followed by two washes with cold ether after centrifugation. The peptides were dried overnight, redissolved in deionized water and dialyzed with 10 water exchanges over 5 days using molecular weight cutoff of 100-500 Da (Spectra/Por, Spectrum Laboratories Inc., Rancho Dominguez, CA). Lyophilized peptides were stored at -20 °C and protected from light. MALDI-TOF (matrix assisted laser desorption ionization time-of-flight) analysis was used to characterize the mass of the final products. See Supporting Information for spectra (Figure S7-S13).

9.1.2 Attenuated Total Reflection–Fourier Transform Infrared Spectroscopy (ATR-FTIR).

IR measurements were obtained for 3 wt. % peptides in PBS on a PerkinElmer 400 FT-IR spectrometer equipped with an ATR accessory. Aliquots of the peptide were deposited on a “Golden Gate” diamond ATR (PerkinElmer, USA). PBS was used as a background spectrum. Collected spectra were normalized by dividing all the absorbance values in the spectrum within

the Amide I band by the largest absorbance value[1], baseline corrected, and vertically offset for ease of comparison.

9.1.3 Molecular Dynamics Simulations of Pentapeptides.

KYFIL, KYFAL, KAFIL and KYFIV peptides were constructed using the peptide builder tool in the program *Avogadro*[2]. A custom Tcl script was used to amidate the C-termini in VMD[3] using the CHARMM36 forcefield[4]. Eighteen individual pentapeptides were solvated in a cube of explicit TIP3P water molecules, using VMD's solvation box extension; a 4-Å padding between the solute and nearest box face was used along with periodic boundary conditions. The pentapeptides were staggered 8 Å apart (as measured by their geometric centers) and rotated randomly so as to prevent orientational bias in the starting structures. The final simulation cell contains approximately 15,000 atoms (and varies with peptide sequences) with a rectangular parallelepiped box of water measuring 67 Å x 71 Å x 49 Å. Physiological concentrations (150 mM) of Na^+ ions, including sufficient Cl^- ions to neutralize the solute's charge, were added to the solvated system using VMD's *ionize* plugin. The internal energy was minimized for 10,000 steps, and the system was then equilibrated for 10 ns (with a 2-fs integration step) in the isothermal–isobaric ensemble (NPT) ensemble. Temperature (300 K) and pressure (1 atm) were regulated via Langevin dynamics for all non-hydrogen atoms and a hybrid Nosé–Hoover Langevin piston. Simulations were performed in NAMD 2.10[5], with final production trajectories extended to 200 ns. Trajectories were processed and further analyzed using in-house scripts written in the Python[6] and D[7] programming languages, as well as VMD. Secondary structures were assigned using STRIDE[8-9]. Peptide structures were characterized via the SURF calculation (surface areas), with the solvent probe radius set to 1.4-Å and applied to all peptides; in this way, clusters were then defined as any peptides that have overlapping molecular surfaces, within 1.4-Å of each other. Density function plots were determined using a univariate kernel density estimate from the Python Seaborn package. Table S1 summarizes our peptide MD simulation systems. Grand average hydropathicity (GRAVY) values are computed from Kyte-Doolittle (KD) hydrophobicity[10] indices averaged over the amino acid sequence for each peptide.

9.1.4 Hydrogel Formation and Rheological Properties.

Lyophilized peptides were dissolved in PBS to a final concentration of 1.5 or 3 wt. %. The pH of the peptide solutions was adjusted by drop-wise addition of minute amounts of HCl or NaOH.

Rheological tests were performed on 50 μL hydrogels 30 minutes after induction of gelation (Anton Par, P25S 25 mm parallel steel plates) with a measuring gap of 250 μm. Storage (G') and loss (G'') moduli were measured as a function of strain (%) ranging from 0.01 to 100% with a constant frequency of 10 rad/s. Frequency sweeps were performed at angular frequencies ranging from 1 to 100 rad/s at 0.1% strain. For recovery experiments, a step-time procedure was utilized with a series of applied strains at a fixed oscillation frequency of 10 rad/s. Initially, samples were applied with 0.01% strain for 100 s followed immediately by a 100% strain for 50 s, and cycled 5 times.

9.1.5 Transmission Electron Microscopy.

3.5 μL of peptide hydrogel was placed on a holey carbon grid (Protochips, Inc.). Three washes of deionized water, and three washes of 2% uranyl acetate staining solutions with 2 s blotting between each step was performed. Samples were analyzed on a Tecnai F20 equipped with a 4k x 4k UltraScan CCD camera. Pitch and length were determined using Fiji[11], and the FiberApp software package[12] was used to compute autocorrelation functions of intensity profiles.

9.1.6 Cell Culture.

GFP^+ MADM OPC lines[13] were expanded *in vitro* on T75 tissue culture plates treated with poly-ornithine. OPCs were cultured in DMEM with high glucose, 4 mM L-glutamine, 1 mM sodium pyruvate (Life Technologies) with N2 and B27 supplement (Life Technologies), 1% penicillin-streptomycin (Life Technologies), 10 ng/mL mouse PDGFA-AA (eBioscience), and 50 ng/mL human NT3 (Peprotech). Cell media was changed every 2 days, and cells were grown to 90% confluency and passaged using 0.25% trypsin in Dulbecco's phosphate buffered saline (PBS). Cells were cultured in 5% CO_2 atmosphere, and 21% O_2 at 37 °C.

9.1.7 Hydrogel Cell Encapsulation and Analysis.

Hydrogels for cell encapsulation were made using 1.5 wt% AYFIL peptide in PBS. 25 uL hydrogels with 5×10^6 cells/mL were made by mixing cells and peptides and then transferred to a cell incubator for 10 minutes at 37 °C at 100% humidity. OPC proliferation media was then added to the hydrogels, and changed every 2 days. Hydrogels were stored at −80 °C in lysis buffer before running ATP or DNA quantification assays. For quantification, gels were homogenized in lysis buffer using a hand grinder and were measured using the CellTiter-Glo luminescent Cell Viability

Assay (Promega, United States) and the Quant-iT PicoGreen dsDNA assay (ThermoFisher) according to manufacturer protocols.

9.1.8 Syringe Needle Flow Viability Assay.

OPCs were resuspended at a cell density of 1×10^5 cells/mL in either PBS or 1.5 wt.% AYFIL hydrogels, and loaded into a 1-mL syringe with an 18-gauge needle, mounted onto the syringe pump, and ejected onto a 24 well plate at a constant volumetric flow rate of 1000 μL/min. Cell viability was assessed with a dead stain assay (Invitrogen). Briefly, hydrogels were rinsed for 10 minutes in PBS plus glucose (PBSG), and stained with 4 μM ethidium homodimer-1 for 40 minutes in PBSG, and rinsed in PBSG prior to imaging. GFP^+/dead images were collected using a Zeiss LSM 510 confocal microscope. 150 μm z-stack images were collected with a frame distance of 1 μm. For image analysis, channels for live cells in the green channel and dead cells in the red channel were split and analyzed separately, and converted to 8-bit to allow for thresholding based on the intensity. The Find Maxima plugin was used for each channel to count the number of dead or live cells. Using the point selection tool, the Noise Tolerance values were adjusted by increments of 5 until background staining was excluded (the Noise Tolerance value was 50 for all images). The number of points for each channel were recorded, and were used to calculate the percentage of live and dead cells. Total cell count was between 146 and 287 for each image (n = 3 samples per condition). Statistical significance was determined using the Student's t-test with $p < 0.05$.

9.1.9 Immunostaining.

After 2 days of culture, gels were fixed in 4% paraformaldehyde for 20 minutes at 4 °C and rinsed with PBS before permeabilizing overnight with 0.3% triton-X in PBS. Hydrogels were rinsed in PBS, and then incubated with 10 μg/mL stock solution of Alexa Fluor 568 Phalloidin (ThermoFisher) in 1% BSA in PBS overnight. 4′,6-diamidino-2-phenylindole (DAPI) was added to stain cell nuclei during the last 20 minutes of incubation. Gels were then washed 4 × 20 min in PBS and imaged with a Zeiss LSM 780 confocal microscope. 100 μm z-stack images were collected with a z-spacing distance of 1 μm.

9.1.10 References

1. Yang, H. Y.; Yang, S. N.; Kong, J. L.; Dong, A. C.; Yu, S. N., Obtaining information about protein secondary structures in aqueous solution using Fourier transform IR spectroscopy. *Nat Protoc* **2015,** *10* (3).
2. Hanwell, M. D.; Curtis, D. E.; Lonie, D. C.; Vandermeersch, T.; Zurek, E.; Hutchison, G. R., Avogadro: an advanced semantic chemical editor, visualization, and analysis platform. *J Cheminformatics* **2012,** *4*.
3. Humphrey, W.; Dalke, A.; Schulten, K., VMD: Visual molecular dynamics. *J Mol Graph Model* **1996,** *14* (1), 33-38.
4. MacKerell, A. D.; Bashford, D.; Bellott, M.; Dunbrack, R. L.; Evanseck, J. D.; Field, M. J.; Fischer, S.; Gao, J.; Guo, H.; Ha, S.; Joseph-McCarthy, D.; Kuchnir, L.; Kuczera, K.; Lau, F. T. K.; Mattos, C.; Michnick, S.; Ngo, T.; Nguyen, D. T.; Prodhom, B.; Reiher, W. E.; Roux, B.; Schlenkrich, M.; Smith, J. C.; Stote, R.; Straub, J.; Watanabe, M.; Wiorkiewicz-Kuczera, J.; Yin, D.; Karplus, M., All-atom empirical potential for molecular modeling and dynamics studies of proteins. *J Phys Chem B* **1998,** *102* (18), 3586-3616.
5. Phillips, J. C.; Braun, R.; Wang, W.; Gumbart, J.; Tajkhorshid, E.; Villa, E.; Chipot, C.; Skeel, R. D.; Kale, L.; Schulten, K., Scalable molecular dynamics with NAMD. *J Comput Chem* **2005,** *26* (16), 1781-1802.
6. Rossum, G. *Python reference manual*; CWI (Centre for Mathematics and Computer Science): 1995.
7. Bright, W., The D programming language. *Dr Dobbs J* **2002,** *27* (2), 36-40.
8. Frishman, D.; Argos, P., Knowledge-based protein secondary structure assignment. *Proteins* **1995,** *23* (4), 566-579.
9. Heinig, M.; Frishman, D., STRIDE: a web server for secondary structure assignment from known atomic coordinates of proteins. *Nucleic Acids Res* **2004,** *32*, W500-W502.
10. Kyte, J.; Doolittle, R. F., A Simple Method for Displaying the Hydropathic Character of a Protein. *J Mol Biol* **1982,** *157* (1), 105-132.
11. Schindelin, J.; Arganda-Carreras, I.; Frise, E.; Kaynig, V.; Longair, M.; Pietzsch, T.; Preibisch, S.; Rueden, C.; Saalfeld, S.; Schmid, B.; Tinevez, J. Y.; White, D. J.; Hartenstein, V.; Eliceiri, K.; Tomancak, P.; Cardona, A., Fiji: an open-source platform for biological-image analysis. *Nat Methods* **2012,** *9* (7), 676-682.
12. Usov, I.; Mezzenga, R., FiberApp: An Open-Source Software for Tracking and Analyzing Polymers, Filaments, Biomacromolecules, and Fibrous Objects. *Macromolecules* **2015,** *48* (5), 1269-1280.
13. Liu, C.; Sage, J. C.; Miller, M. R.; Verhaak, R. G. W.; Hippenmeyer, S.; Vogel, H.; Foreman, O.; Bronson, R. T.; Nishiyama, A.; Luo, L. Q.; Zong, H., Mosaic Analysis with Double Markers Reveals Tumor Cell of Origin in Glioma. *Cell* **2011,** *146* (2), 209-221.

9.2 Supplemental information for Tang et al. J. Am. Chem. Soc., 141: 4886-4899 (2019)

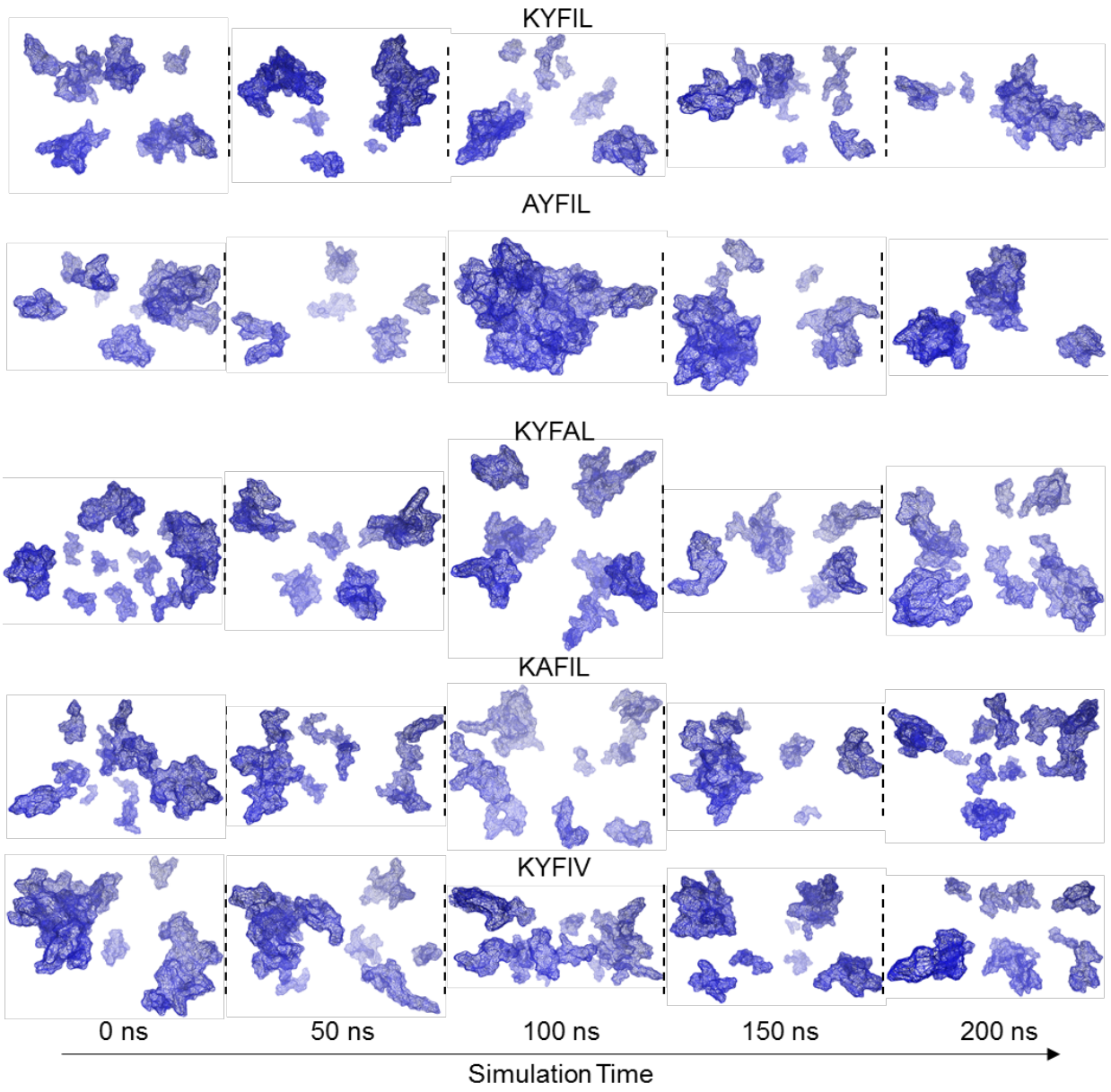

Figure 9-1. Representative snapshots of KYFIL, KYFAL, KAFIL, and KYFIV peptide systems at increasing time points following minimization and equilibration. Snapshots were taken after minimization for 10,000 steps, and equilibration for 10 ns. MD simulations were conducted for 200 ns, and peptide systems were simulated with an explicit water solvent (TIP3 solvent model). For experimentally-determined gelling peptides (KYFIL, AYFIL, KYFAL, KAFIL) the number of peptide clusters decreases as the simulation progresses, highlighting their aggregation propensity.

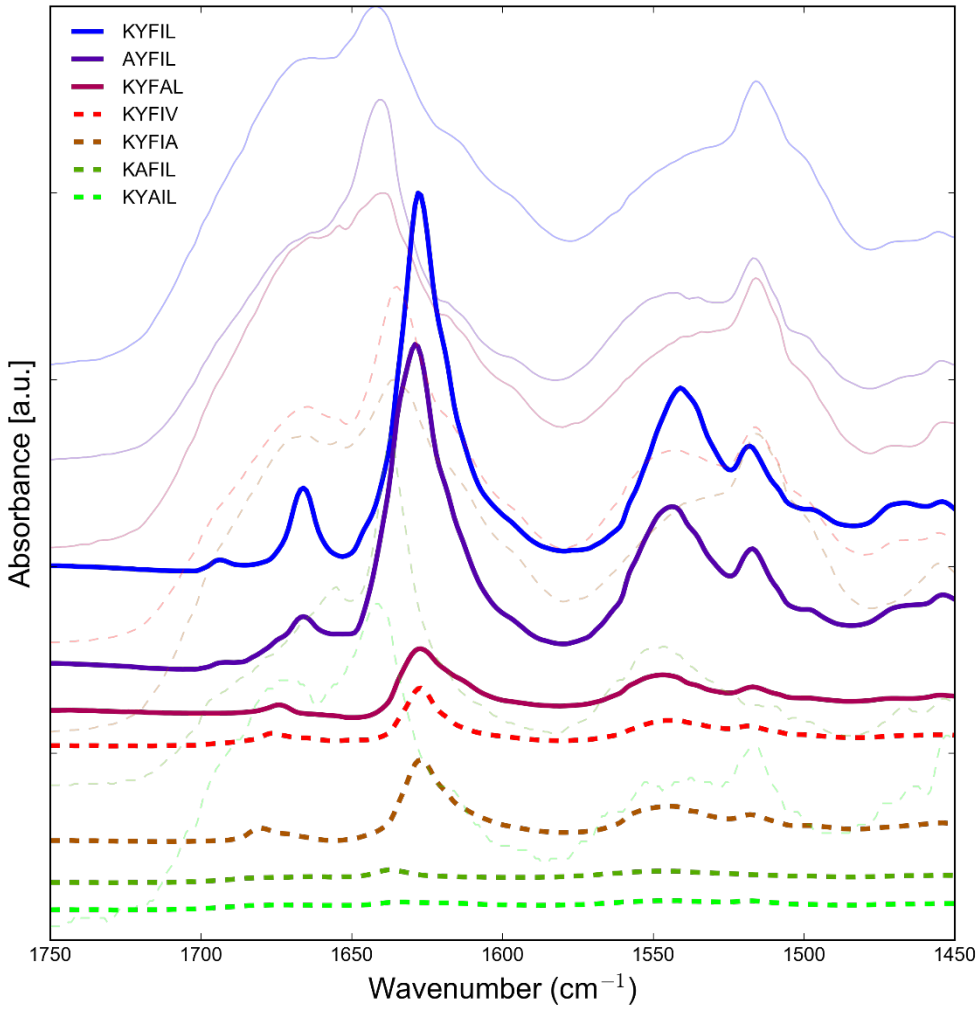

Figure 9-2. ATR-FTIR spectrum of peptides in PBS (thick lines) and freeze-dried peptides (thin, transparent lines). All peptides that are able to gel at pH 7.4 (solid lines) exhibit an Amide I absorbance at 1629-1645 cm-1, indicative of β-sheet hydrogen bonding. Non-gelling peptides in the same conditions (dashed lines) exhibit much weaker, less intense peaks at the same wavenumbers. All spectra are baseline corrected, normalized, and offset for clarity.

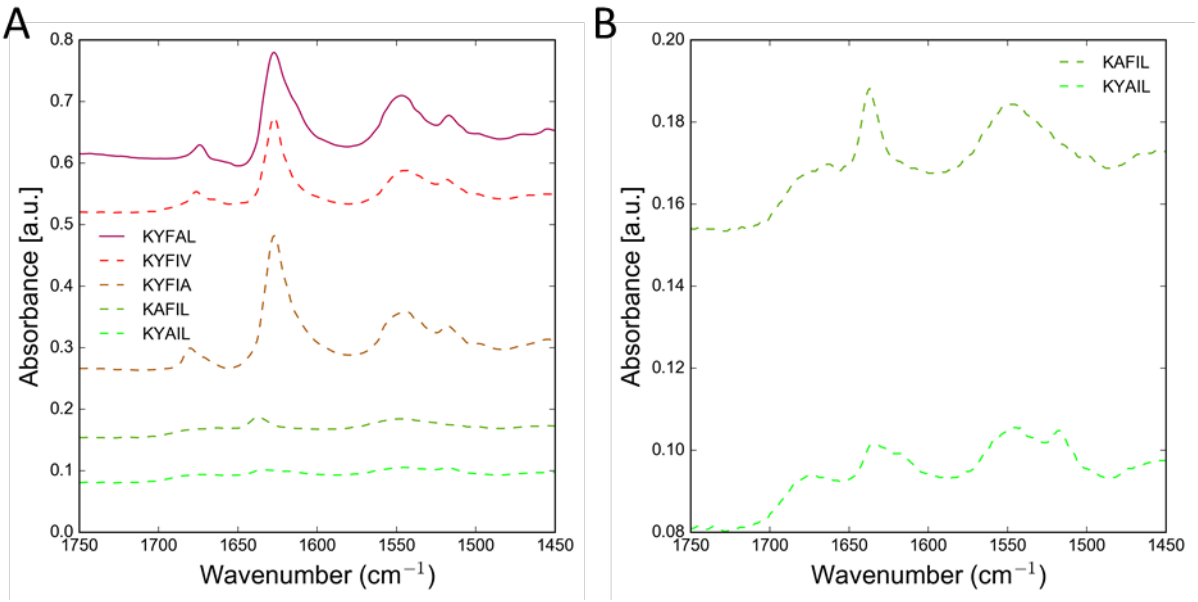

Figure 9-3. A) A magnified view of the ATR-FTIR spectrum of peptides dissolved at 3 wt.% in PBS and pH 7.4. All gelling peptides (solid lines) exhibit an Amide I absorbance at 1629 cm-1, indicative of β-sheet hydrogen bonding. A peak at 1679 cm-1 to 1683 cm-1 indicates that the β-sheet is in anti-parallel conformation. B) Non-gelling peptides (dashed lines) exhibit much weaker, less intense peaks at the same wavenumbers. All spectra are baseline corrected, normalized, and offset for clarity.

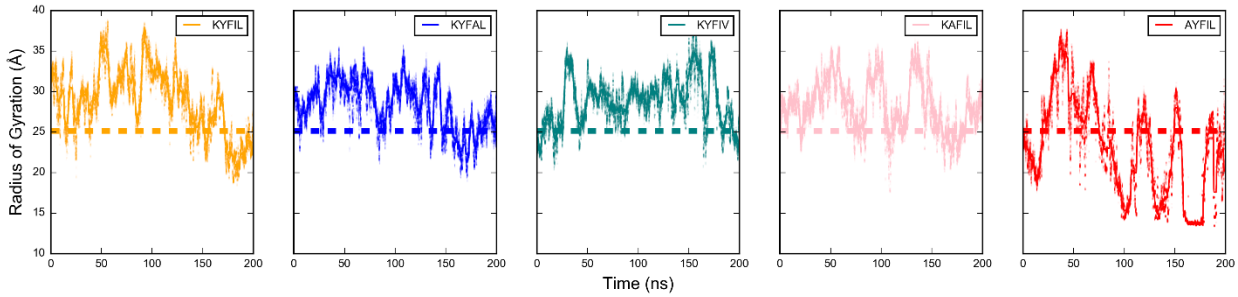

Figure 9-4. Sequence dependence of the radius of gyration (R_g). The R_g was measured for an ensemble of 18 peptides of different sequences (KYFIL, KYFAL, KYFIV, KAFIL, and AYFIL) after equilibration of 10 ns. All peptides incur hydrophobically-driven collapse (relative to initial starting structure). Dashed line indicates initial R_g before equilibration. Towards the end of the simulation, the R_g for KYFIL and AYFIL decreases relative to the beginning of the trajectory, highlighting their aggregation propensity.

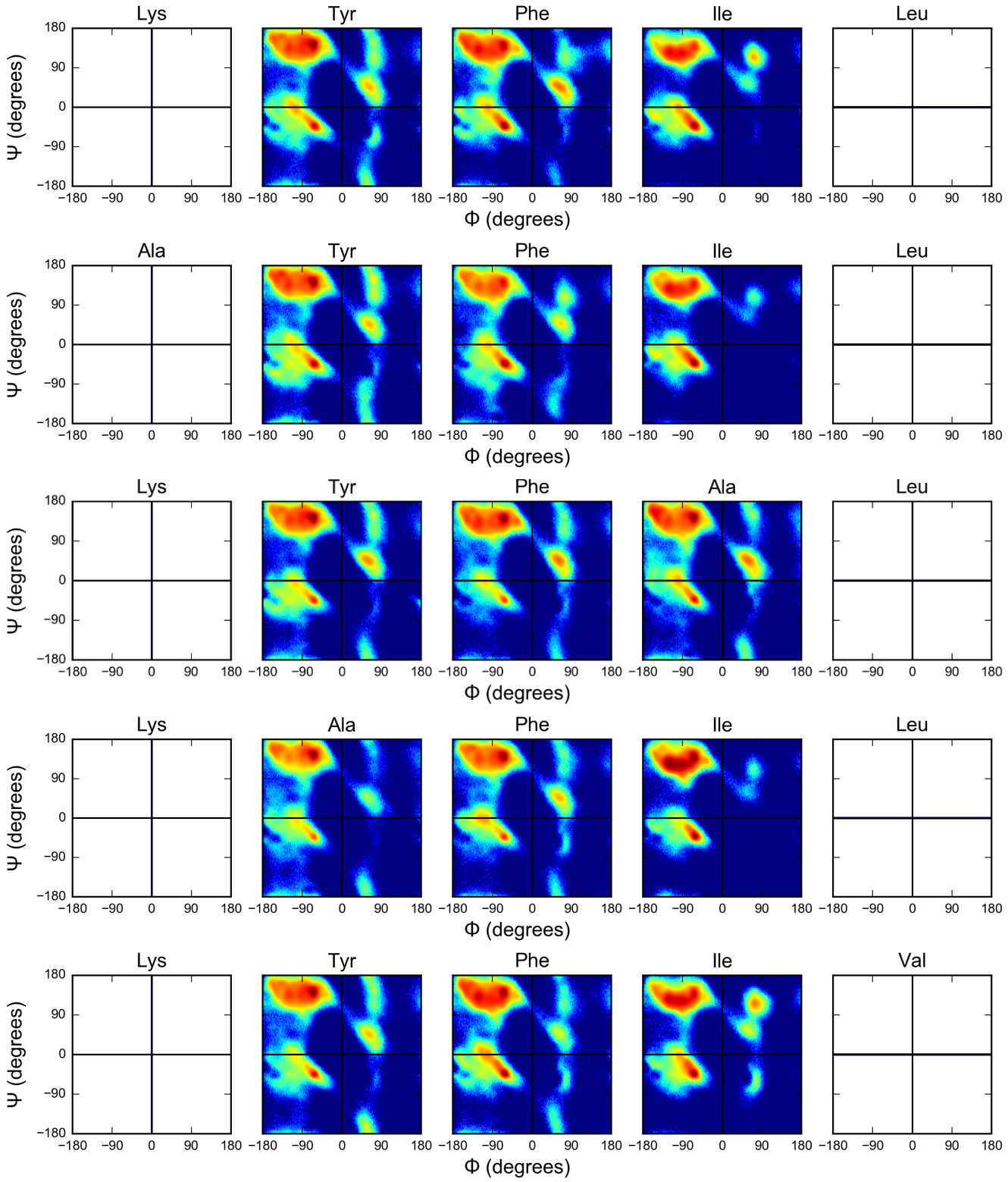

Figure 9-5. Ramachandran plot (φ, ψ distributions) for each residue in a pentapeptide sequence. The torsion angles for each type of amino acid, barring the N- and C- termini indicate significant structural heterogeneity within the peptide systems. The Phe for all pentapeptide analogs, adopts higher populations of β-turn type-II (φ = -60, ψ = 120) and antiparallel β-sheet structures (φ = -140, ψ = 135). For both the KYFAL and KAFIL sequence, the Ala preferentially adopts a polyproline type-II helix (φ = -75, ψ = 145) and decreased propensity for β-sheet structures. Note that the residue at the N- and C-terminus does not have a Phi or Psi angle since the dihedral angle requires a plane comprised of C'-N-Cα-C' and N-Cα-C'-N for Phi and Psi angles, respectively.

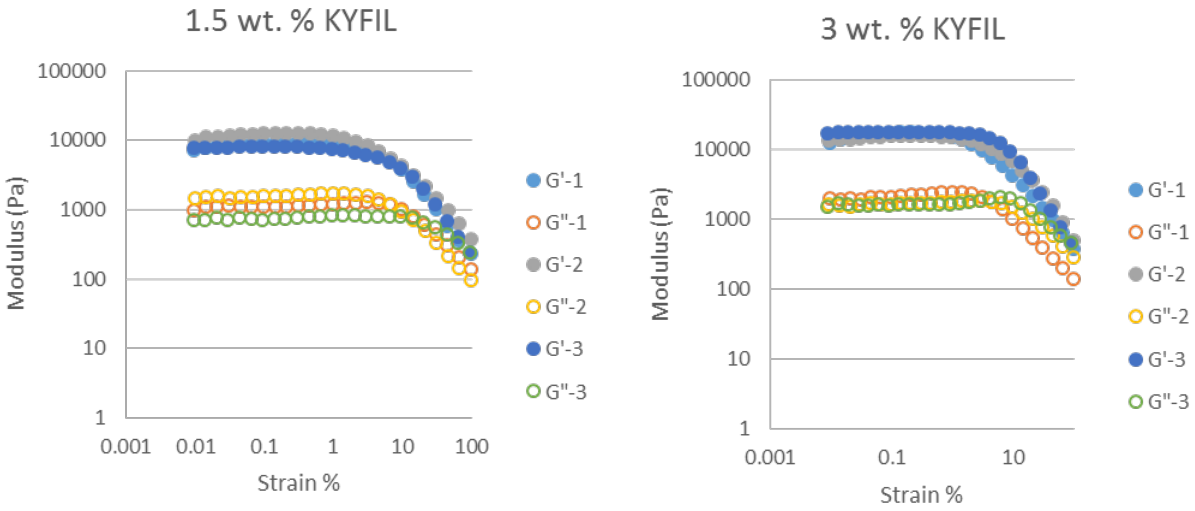

Figure 9-6. Strain sweep of gelling KYFIL sequences at constant frequency of 1 hz. Measurements are carried out at 3 wt.% and 1.5 wt %. For all sequences, G' decreases significantly in acidic conditions. Higher concentrations of peptides exhibit increased G'. Legend indicates 3 sample replicates.

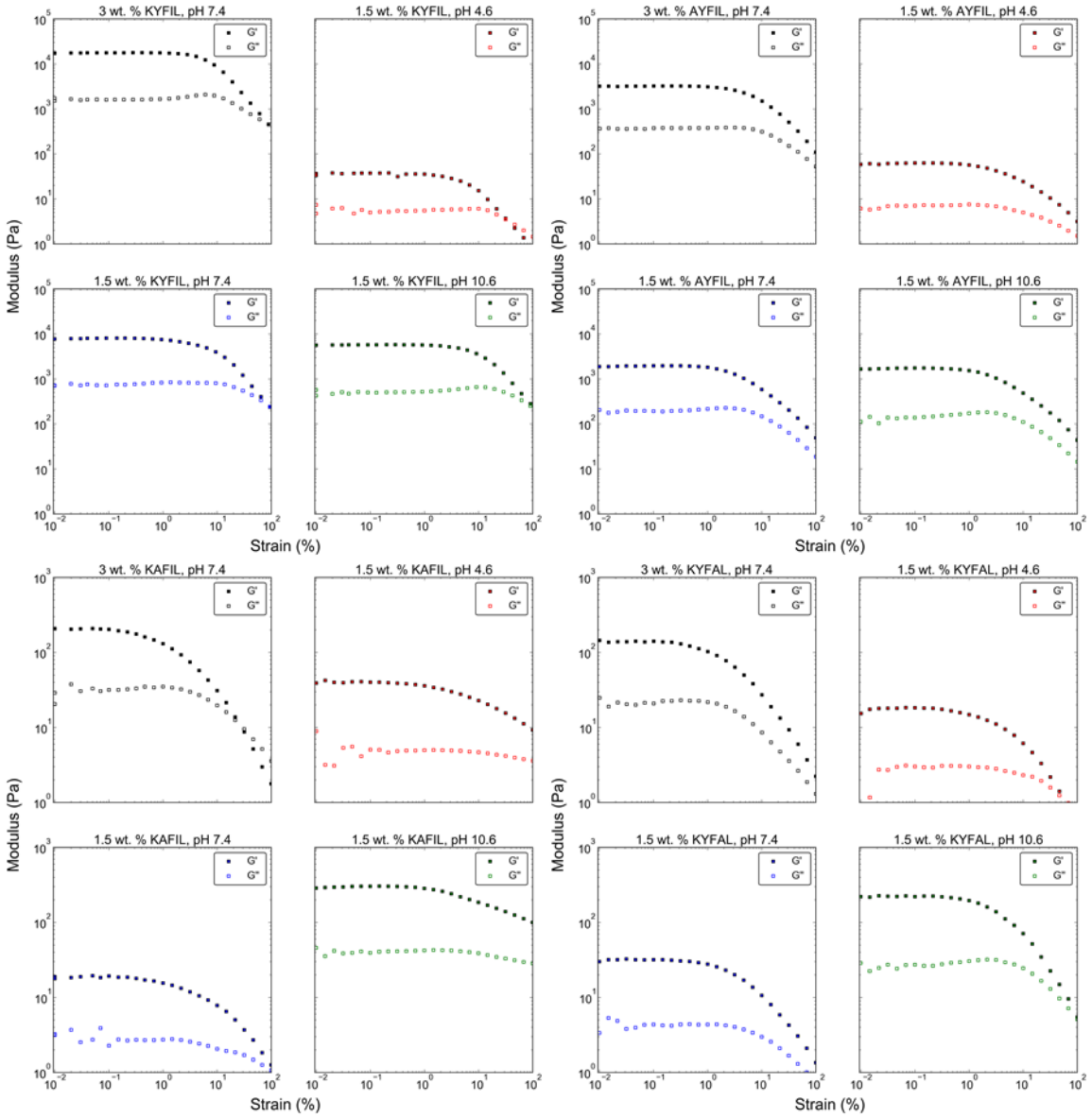

Figure 9-7. Strain sweep of gelling pentapeptide sequences at constant frequency of 1 hz. Measurements are carried out at 3 wt.% and 1.5 wt.%, and different pH conditions (4.6, 7.4, 10.6). For all sequences, G' decreases significantly in acidic conditions. Higher concentrations of peptides exhibit increased G'. For KAFIL hydrogels, the G' increases significantly in basic conditions.

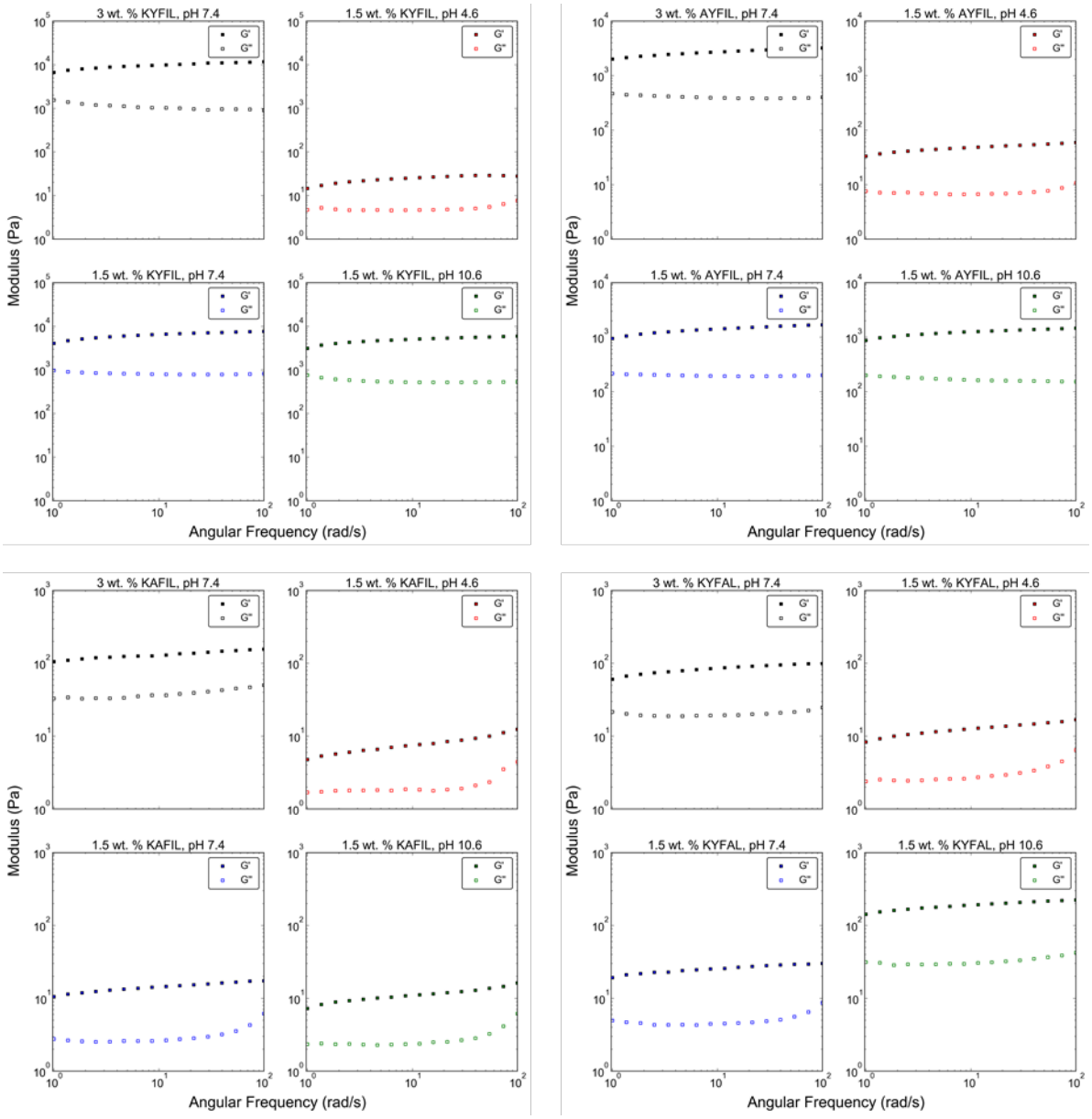

Figure 9-8. Frequency sweep of gelling pentapeptide sequences at constant strain at 0.1%. Measurements are carried out at 3 wt.% and 1.5 wt.%, and different pH conditions (4.6, 7.4, 10.6). For all sequences, G' decreases significantly in acidic conditions. Higher concentrations of peptides exhibit increased G'. For KAFIL hydrogels, the G' increases significantly in basic conditions.

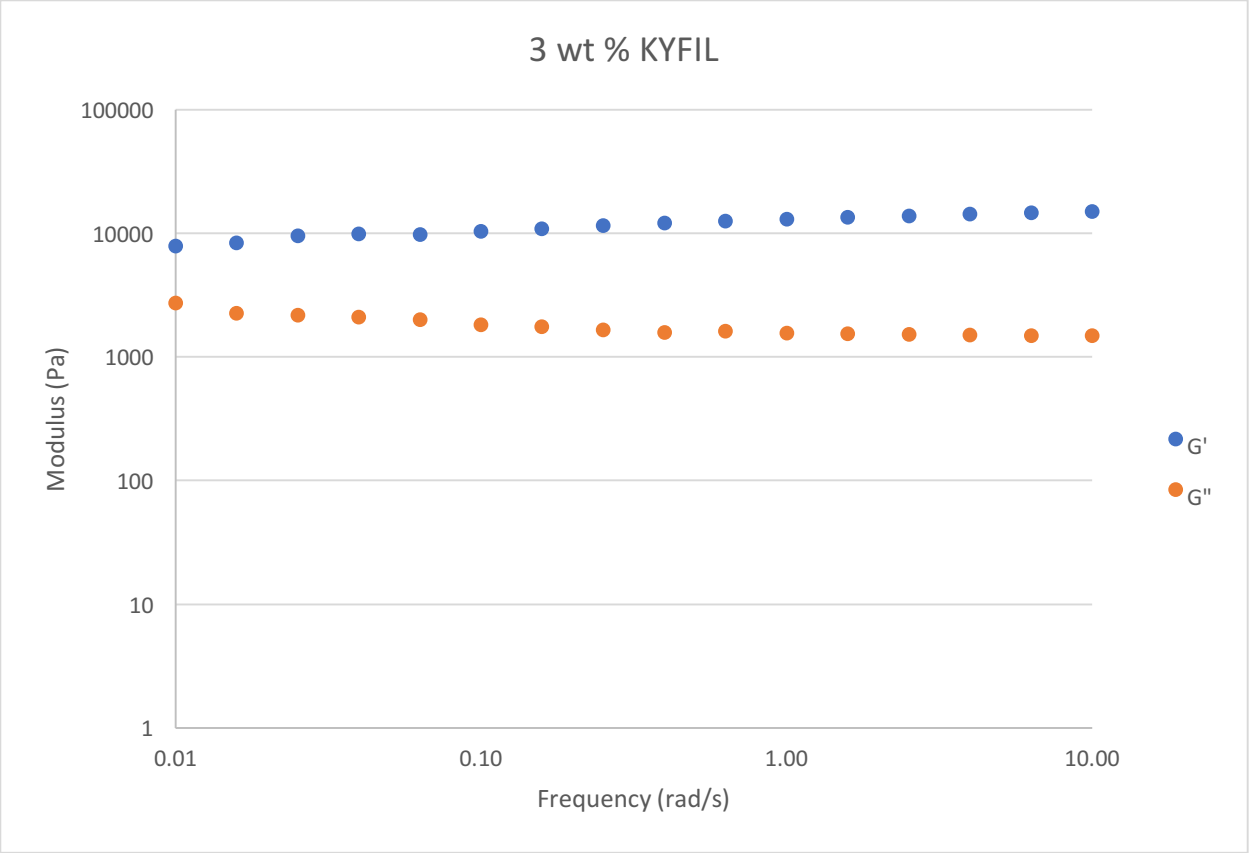

Figure 9-9. Frequency sweep of gelling pentapeptide sequence KYFIL at constant strain at 0.1%. Measurements are carried out at 3 wt.% from 0.01 to 10 rad/s to investigate the inherent dynamics of the hydrogel network.

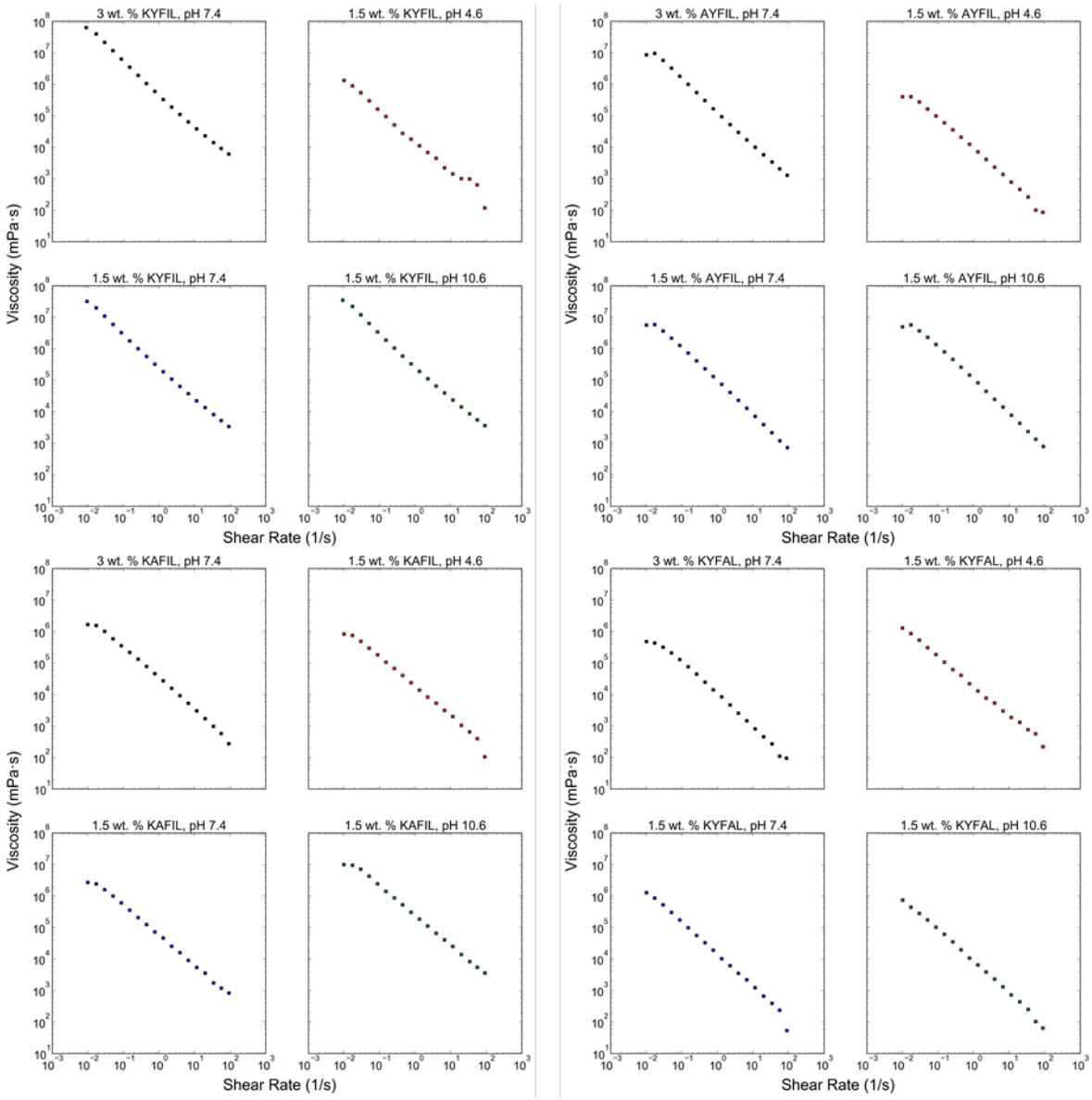

Figure 9-10. Apparent viscosity versus shear rate measurements of gelling peptide sequences at different wt.% and pH conditions. All hydrogels displayed shear-thinning behavior, in which the viscosity of each sample decreases with increasing shear rate.

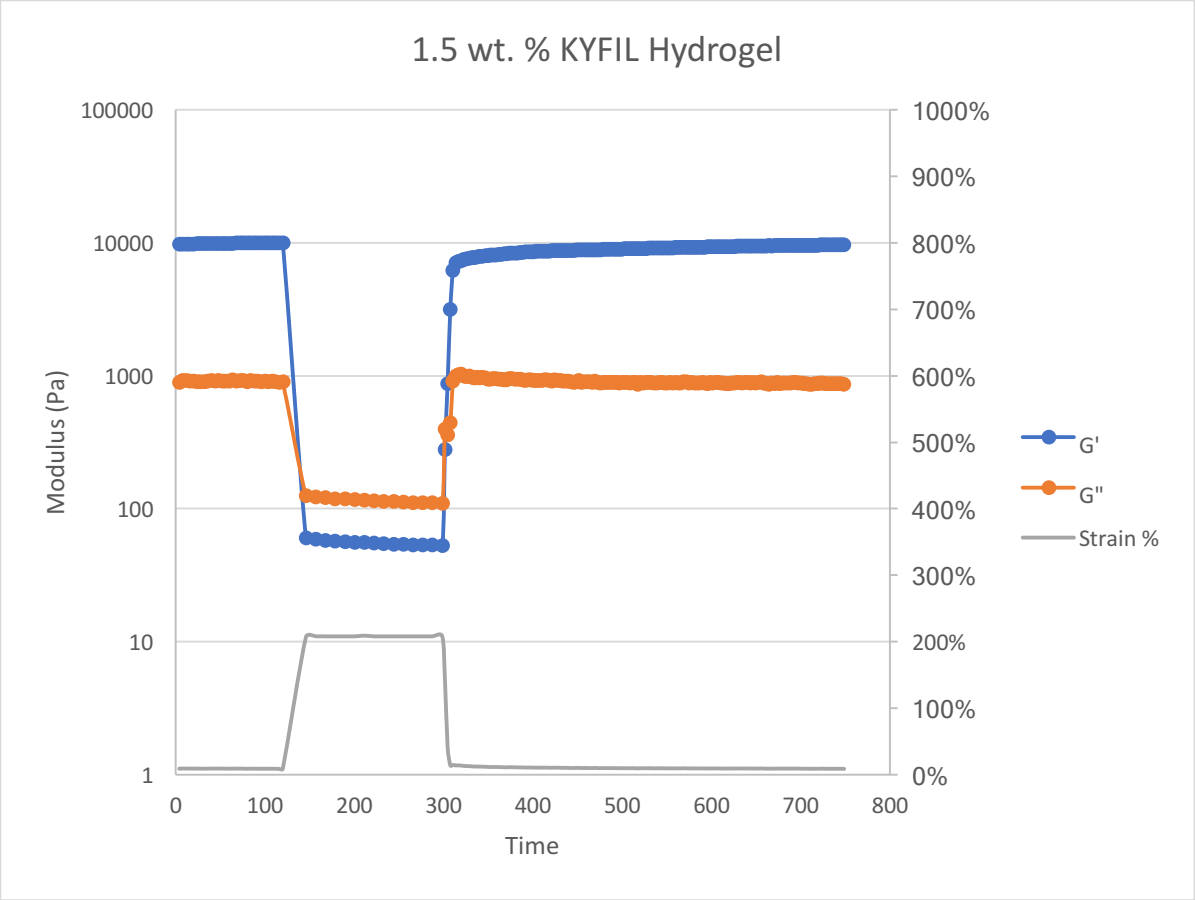

Figure 9-11. A thixotropy test was performed for 1.5 wt. % KYFIL hydrogels. A strain sweep of 0.1 % (100 s) followed by a 200 % strain (200 s), followed by a 400 s recovery period. The hydrogel is able to recover 90% of its initial G' in 3.5 minutes, and 7 minutes to recover 96%.

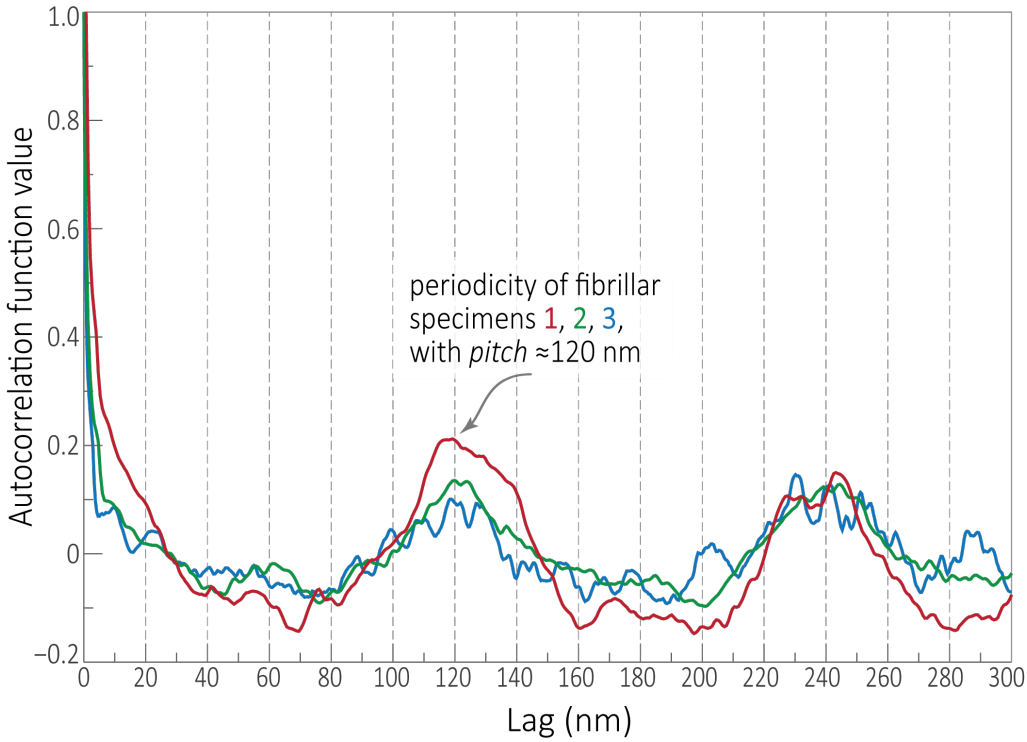

Figure 9-12. Periodicity of the fibrillar twist, as quantified by the intensity autocorrelation function (ACF). The ACF was computed for the height intensity of fibrils found in micrograph images of three independent TEM specimens (red, green and blue traces); the fundamental frequency can be seen to correspond to a distance (lag) of ≈120 nm.

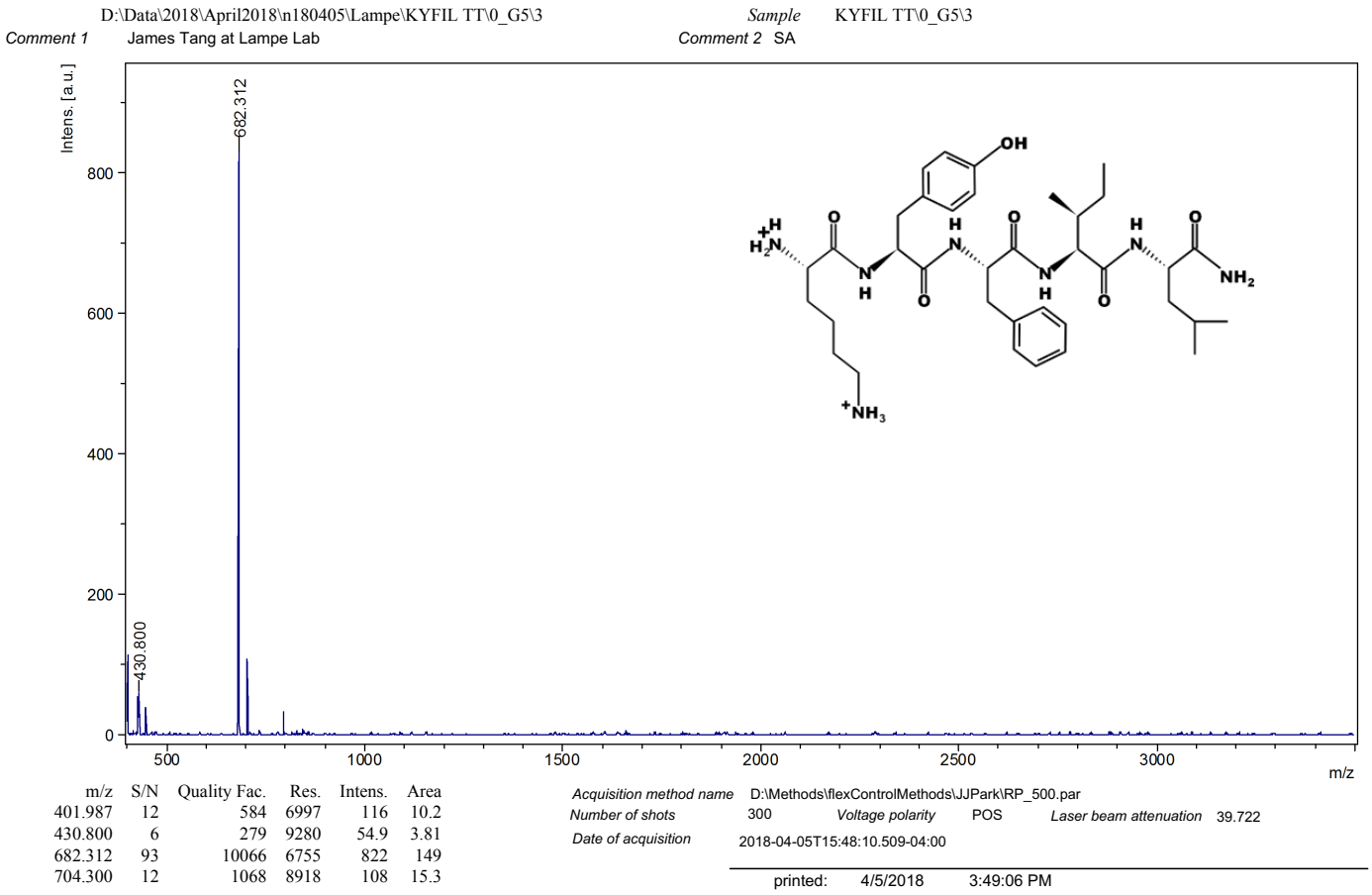

Figure 9-13. MALDI-TOF MS of KYFIL peptide. Expected mass $[M+H^+]^+$ = 682.87, observed mass = 682.312.

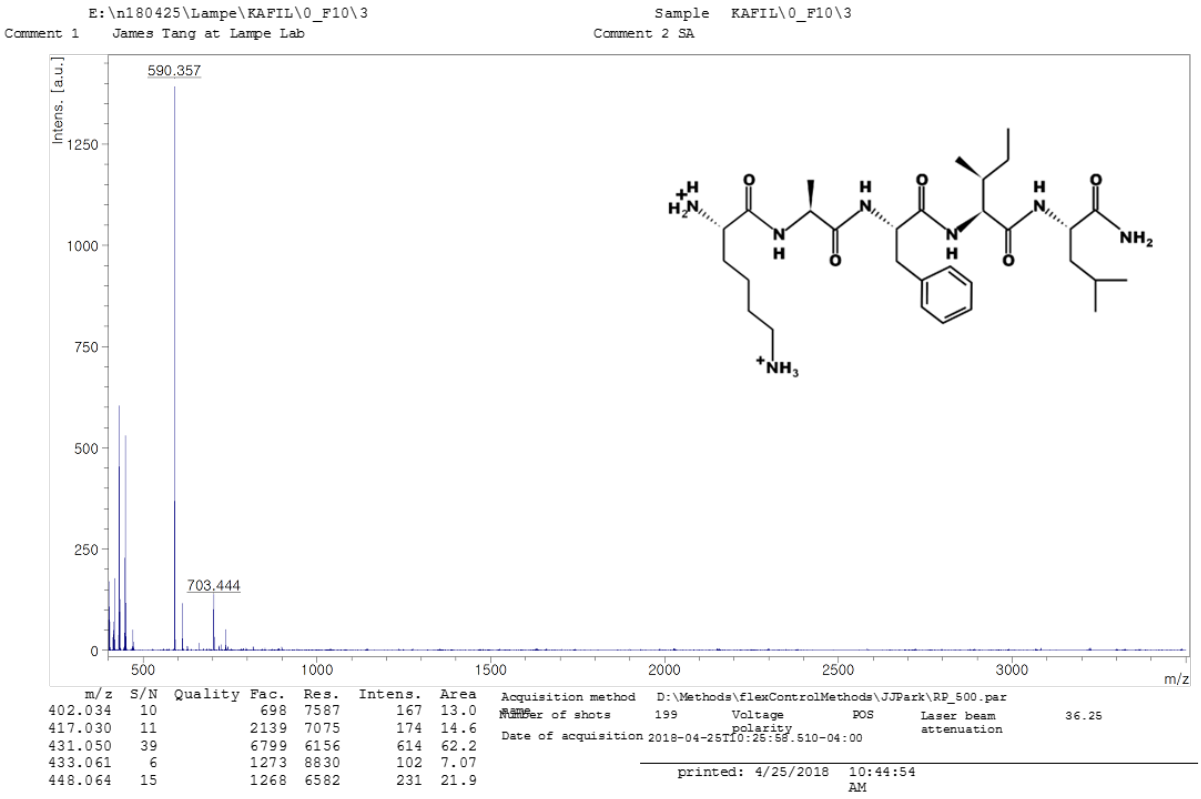

Figure 9-14. MALDI-TOF MS of KAFIL peptide. Expected mass $[M+H^+]^+$ = 589.77, observed mass = 590.357

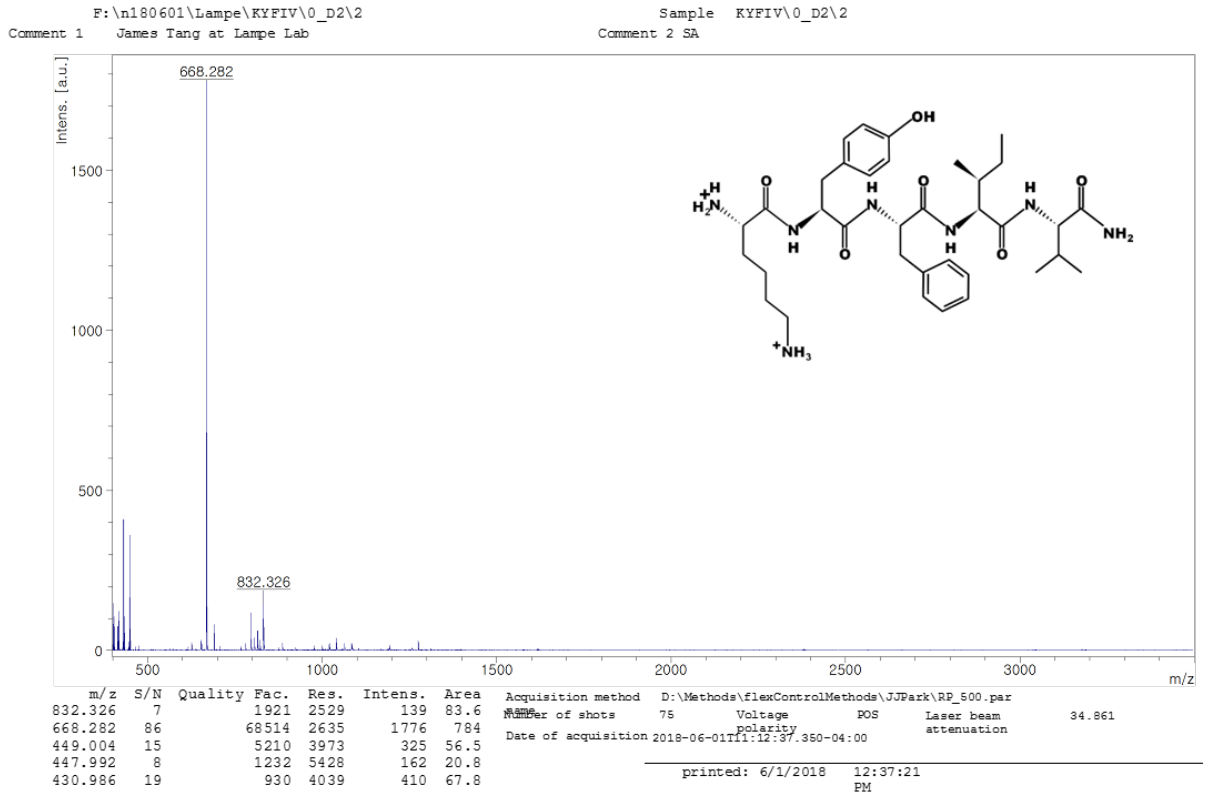

Figure 9-15. MALDI-TOF MS of KYFIV peptide. Expected mass $[M+H^+]^+$ = 667.84, observed mass = 668.282

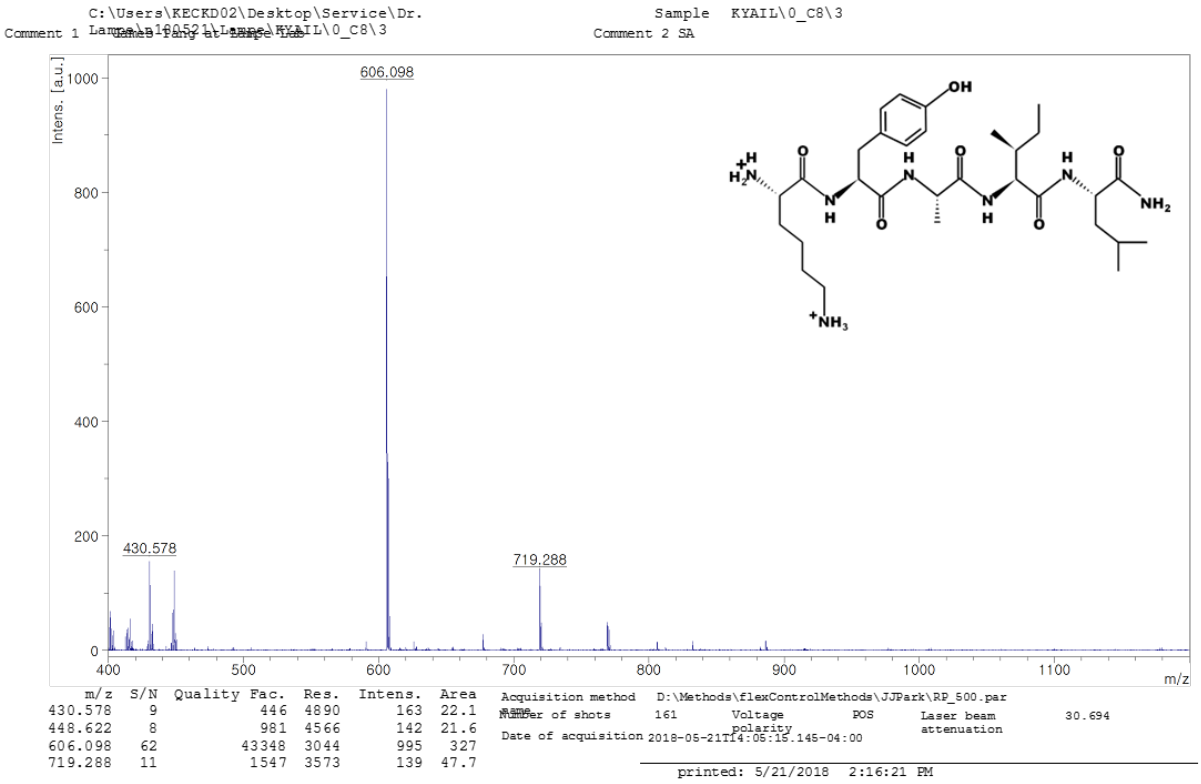

Figure 9-16. MALDI-TOF MS of KYAIL peptide. Expected mass $[M+H^+]^+$ = 605.77, observed mass = 606.098

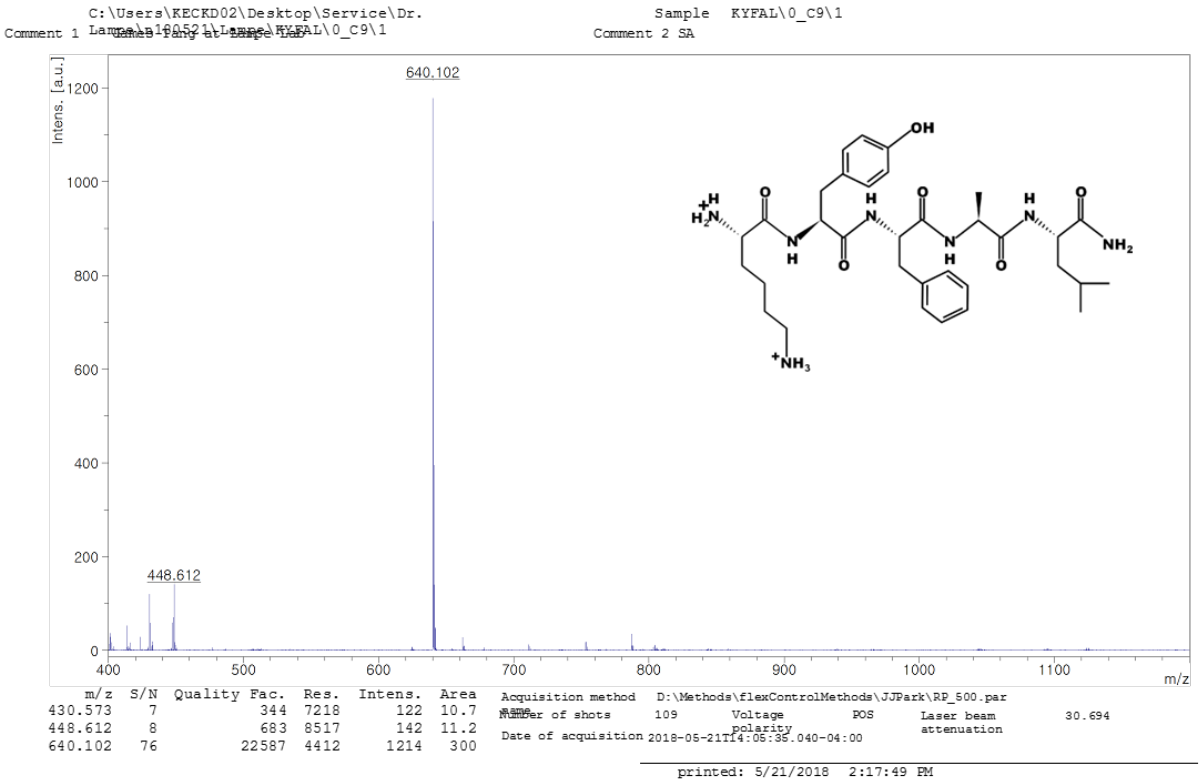

Figure 9-17. MALDI-TOF MS of KYFAL peptide. Expected mass $[M+H^+]^+$ = 639.79, observed mass = 640.102

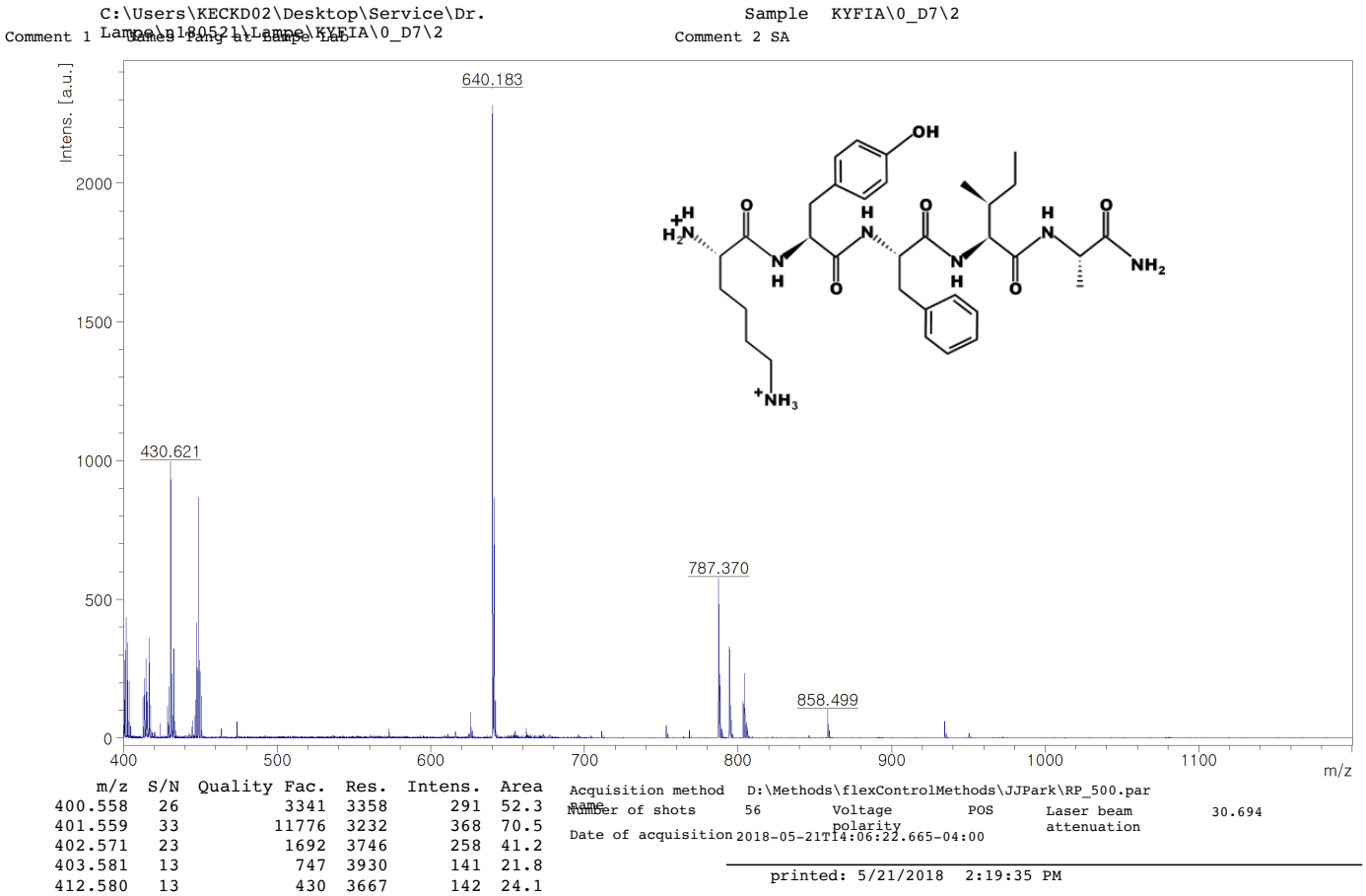

Figure 9-18. MALDI-TOF MS of KYFIA peptide. Expected mass [M+H+]+ = 639.79, observed mass = 640.183

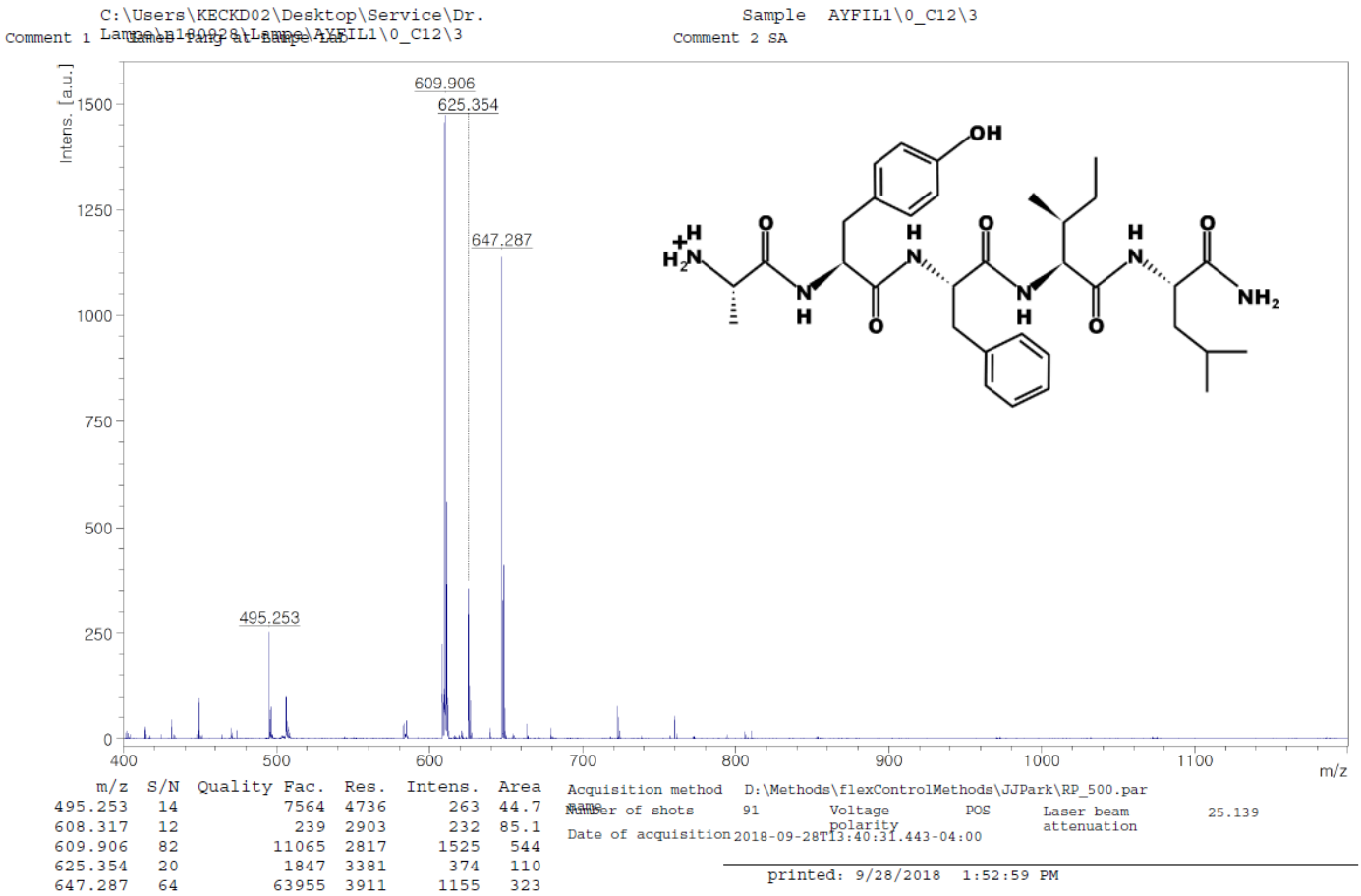

Figure 9-19. MALDI-TOF MS of AYFIL peptide. Expected mass [M+H+]+ = 624.77, observed mass = 625.354.

10 Appendix 2: Toward a Designable Extracellular Matrix: Molecular Dynamics Simulations of an Engineered Laminin-mimetic, Elastin-like Fusion Protein

Published as: JD Tang, CE McAnany, C Mura, KJ Lampe, " Toward a Designable Extracellular Matrix: Molecular Dynamics Simulations of an Engineered Laminin-Mimetic, Elastin-Like Fusion Protein," Biomacromolecules, 17: 3222–3233 (2016)

10.1 ABSTRACT:

Native extracellular matrices (ECMs) exhibit networks of molecular interactions between specific matrix proteins and other tissue components. Guided by these naturally self-assembling supramolecular systems, we have designed a matrix-derived protein chimera that contains a laminin globular–like (LG) domain fused to an elastin–like polypeptide (ELP). This bipartite design offers a flexible protein engineering platform: (i) laminin is a key multifunctional component of the ECM in human brains and other neural tissues, making it an ideal bioactive component of our fusion, and (ii) ELPs, known to be well-tolerated *in vivo*, provide a self-assembly scaffold with tunable physicochemical (viscoelastic, thermoresponsive) properties. Experimental characterization of novel proteins is resource-intensive, and examining many conceivable designs would be a formidable challenge in the laboratory. Computational approaches offer a way forward: molecular dynamics (MD) simulations can be used to analyze the structural/physical behavior of candidate LG-ELP fusion proteins, particularly in terms of conformational properties salient to our design goals, such as assembly propensity in a temperature range spanning the inverse temperature transition. As a first step in examining the physical characteristics of a model LG-ELP fusion protein, including its temperature-dependent structural behavior, we simulated the protein over a range of physiologically-relevant temperatures (290-320 K). We find that the ELP region, built upon the archetypal $(VPGXG)_5$ scaffold, is quite flexible, and has a propensity for β-rich secondary structures near physiological (310-315 K) temperatures. Our trajectories indicate that the temperature-dependent burial of hydrophobic patches in the ELP region, coupled to the

local water structure dynamics and mediated by intramolecular contacts between aliphatic side-chains, correlates with the temperature-dependent structural transitions in known ELP polymers. Because of the link between compaction of ELP segments into β-rich structures and differential solvation properties of this region, we posit that future variation of ELP sequence and composition can be used to systematically alter the phase transition profiles, and thus the general functionality, of our LG-ELP fusion protein system.

10.2 Introduction

A major challenge in neural tissue engineering and regenerative medicine is one of tissue construction: what biomaterial, in terms of chemical composition and physical properties, might best mimic the native extracellular matrix (ECM) that houses neural stem cells (NSCs), neurons, glia, and other cells? Engineered proteins afford an opportunity to systematically control both biological functionality and the structural/mechanical properties of the resulting ECM mimetic, thus enabling one to guide the behavior of encapsulated cells.[1, 2] For instance, neural cells encapsulated in engineered protein or peptide materials extend neurites hundreds of microns into the surrounding 3D matrix.[3] These materials permit cellular remodeling and bioresorption via cell-controlled proteolytic degradation, and inherently behave in a more physiologically native manner than do other biomimetics (e.g. commonly-used synthetic hydrogels). Tissue engineering can benefit immensely from artificial ECMs designed from naturally-occurring protein sequences: such polymers promote native cellular interactions and elicit desired regenerative behaviors *in vivo*[4, 5] while enabling control over bioactive and structural properties (porosity, proteolytic remodeling, cellular adhesion, stiffness, etc.). In short, biologically-based ECM mimetics provide a suitable matrix for the controlled organization of viable cells into physiologically-relevant tissues.[6, 7]

The ECM in neural tissue is a hierarchically structured composite material, consisting of proteoglycans and the large (typically >400 kDa) structural proteins collagen, fibronectin, and laminin. In the central nervous system (CNS), laminin is a particularly vital component of the ECM.[8, 9] Following a neural tissue injury, temporal regulation of laminin expression is critical in the production of potential neurotrophic and neurite-promoting factors by reactive astrocytes.[10] Laminin also plays an important role in axonal growth in the developing mammalian CNS and in concurrent mechanotransduction events, such as in astrocyte cell adhesion and spreading.[8, 11]

Laminins are glycoproteins that provide a key linkage between cells and the broader ECM scaffold. Human laminin is an immense (900 kDa), disulfide-linked heterotrimer that consists of many globular domains and α–, *β*–, ϒ–rod-like chains; together, these entities assemble into a four-armed cruciform shape.[12] Several adhesion peptides have been identified within the laminin amino acid sequence; in particular, the ^{1124}RGD, ^{925}YIGSR and ^{2101}IKVAV segments are known recognition sites for as many as 20 integrins,[13] the 67 kDa laminin-1 receptor[14] and the 110-kDa laminin-binding protein,[15] respectively. These recognition sequences have been used to functionalize non-adhesive polymeric scaffolds, such as in hydrogels based on polyethylene glycol or hyaluronic acid.[16-18] However, these short ECM-derived peptide fragments are often imperfect in mediating cell-signaling events in neural tissue (cell attachment, axonal growth, etc.), likely because of (i) insufficient binding with cell-surface receptors and (ii) failure to initiate anchoring for assembly of basement membrane scaffolds.[19-23]

The fifth globular domain from the C-terminal region of the laminin α2 chain, denoted 'LG5', plays a key role as a binding site for integrins, heparin, and α-dystroglycan (α-DG).[24-27] Heparin is a highly anionic, polysulfated glycosaminoglycan (GAG) that binds exogenous growth factors and thereby helps regulate and maintain neural stem cell (NSC) differentiation.[28, 29] In neural cells, the α-DG glycoprotein complex plays a fundamental role in facilitating new laminin polymerization at the cell surface and in supporting cellular adhesion.[30, 31] LG5 also contains a region that binds integrin *β*1,[25, 27] which is part of an integrin adhesive complex that links the cytoskeleton and the ECM. Past work has focused on engineering hydrogels that contain only the short integrin-binding peptides from LG modules. A more effective biomimicry strategy might incorporate longer laminin sequences, enabling multifunctional biomaterials with native-like cell-binding capacities and targeted selectivity for growth factors (which, in turn, initiate stem cell self-renewal and differentiation programs). There is a precedent for engineering proteins functionalized with the LG5 domain to mediate cellular behavior.[32, 33] A yet further design criterion for ECM-mimetic fusion proteins is that they contain regions that enable assembly into higher-order structures, via either noncovalent (self-assembly) or covalent (chemical crosslinking) mechanisms. Elastin-like polypeptides (ELP) have generated much interest in the tissue engineering field, as the hierarchical self-assembly of these relatively ordered (via local interactions) peptides provides structural support in ECM materials, as well as the ability to control viscoelastic properties. The ability to tune the physical properties of ELP-containing regions offers a versatile way to modulate protein-

mediated interactions between cells and the ECM—interactions that are critical in cellular adhesion, spreading, and migration.

ELPs undergo thermally-triggered first-order phase transitions,[34] characterized by a system-specific transition temperature known as the 'lower critical solution temperature' (LCST). This behavior is also termed an 'inverse temperature transition' as the polymer becomes *more* structured upon reaching the LCST, and separates into polymer-rich and water-rich phases. The solution behavior at/near the LCST depends on both (i) intrinsic factors, such as the amino acid composition[35, 36] and the number of $(VPGXG)_n$ pentapeptide repeats ('X' denotes a 'guest' residue, which can vary from one repeat to another), as well as (ii) extrinsic parameters, such as the concentration, pH, ionic strength, and other bulk solution properties.[37-42] Both sets of factors are useful in the context of protein design and engineering, as they are entirely manipulable: various ELP regions can be fused to a target protein and combined with systematic perturbation of experimental conditions to modulate protein/solution properties at and near the LCST. The assembly behavior at the LCST has been introduced into otherwise soluble polypeptides by fusing them to ELP regions.[43, 44] The thermoresponsive behavior of recombinant ELP fusions then allows simple purification via inverse transition cycling,[37] thus obviating expensive chromatographic resins and enabling large-scale production. Also, biocompatibility of ELP fusion proteins with biomechano-responsive properties has recently been demonstrated in animals.[45]

Fundamental progress in biomaterials discovery has been limited by a lack of high-resolution data about the structural dynamics of the underlying polymeric network. The properties of any material ultimately stem from the three-dimensional (3D) structures and dynamics of its molecular constituents—from the level of individual proteins to their higher–order assembly into matrices. These structural and dynamical properties, in turn, are deeply linked to the patterns of intra- and inter-molecular interactions that are thermodynamically accessible (and substantially populated) under a given set of experimental conditions. The structural and thermodynamic properties of a fusion protein design can be quantitatively characterized via experimental means (e.g., X-ray scattering), but systematically doing so on the scale of many dozens or even hundreds of designs would be prohibitively laborious and resource-intensive. Moreover, such approaches do not, in general, provide the atomic-resolution information on structure and dynamics that we need in order to iteratively refine and systematically improve our designs.

The thermodynamic properties and structural dynamics of various ELPs, above and below their LCSTs, have been studied by experimental and computational means.[46-50] However, a universally accepted, atomically-detailed description of the physicochemical and structural basis of this phase transition remains elusive;[48, 51, 52] also, past studies have generally examined short ELP regions in isolation, not fused to other protein domains. Deeper knowledge of the phase behavior and interfacial properties of ELPs would expand their general utility in biomaterial applications, and would mitigate the costs of producing and characterizing what end up being poorly structured (or otherwise undesirable) ECM candidates. Here, we have designed and simulated a multifunctional fusion construct, with the ultimate goal of driving neural differentiation via an engineered ECM that assembles under cyto-compatible conditions. We use the LG5 domain to supply crucial cell-protein-matrix interactions, while the ELP component of our modular design provides control over desired micro- and nanostructures. Being able to control the properties of our fusion goes in tandem with the architecture and physical properties of these matrices being stimuli-responsive, so environmental parameters such as temperature must be able to modulate the individual protein structures that compose such a matrix.

Using classical, all-atom MD simulations[53] we have examined the behavior of our LG-ELP design near its putative phase transition, as well as the temperature-dependent conformational and structural dynamics leading up to the LCST. These simulations supply picosecond-resolved, atomically-detailed information on discrete structural and functional states for our protein, on the overall timescale of ca. 100 ns. Thus, we can both analyze the molecular events near the presumed LCST transition of our fusion protein and also obtain an *a priori* view of the structural properties of our design, before dedicating experimental resources to the synthesis and characterization of a novel biopolymer with unknown (and otherwise unpredictable) LCST behavior.

10.3 Methods of Procedure

LG-ELP fusion protein design methodology. We designed an LG5–ELP fusion protein with the intention that it be able to undergo a temperature-induced structural transition, leading to formation of a functional ECM suitable for CNS tissue regeneration. Four design criteria were applied: (i) The fusion protein should be thermodynamically stable (i.e. retain native structure) under physiological conditions (temperature, pH, ionic strength). (ii) The fusion protein should feature bioactive sites along the LG portion of the peptide chain, and the ELP must not interact with the LG portion in a manner that occludes these bioactive sites (proteolytic sites, cell-binding

domains, binding sites for other ECM molecules or growth factors, etc.). (iii) The fusion protein should be capable of self-assembly via noncovalent interactions. (iv) The self-assembly properties should be readily controllable by altering the assembly-driving sequence element (ELP, in our case).

ELPs consist of a pentapeptide repeat, $(VPGXG)_n$, where X is any guest residue other than proline. ELPs are described using the notation "ELP$[W_iY_jZ_k]_n$", where *W*, *Y*, and *Z* are the single-letter codes for the amino acids at X, the subscripts *i*, *j* and *k* indicate the number of pentamers featuring that guest residue, and *n* is the total number of repeats. From our estimates using the T_t-based hydrophobicity scale of amino acids, [50, 54, 55] and the LCST behavior of various other engineered ELP fusions,[44, 56] we designed an ELP with the sequence ELP$[K_2L_2I_2K_2]_1$. We predict that this motif will satisfy the aforementioned design criteria. The repeated Gly-Leu and Gly-Ile dipeptides serve as cleavage sites for type IV collagenase (gelatinase),[57] rendering the hydrogel susceptible to enzymatic cleavage and thereby allowing cell spreading and migration. In addition, the primary amine functionality of the lysine side-chain (ε-NH_3^+) enables site-specific coupling or crosslinking reactions.[58]

MD simulations of LG-ELP. Our LG-ELP design fuses the LG5 domain, known to adopt an antiparallel β-sandwich fold, to a C′-terminal ELP tail (Figure 1). Our starting 3D model for the LG5 domain was drawn from the crystal structure of the mouse homolog of the laminin α2 chain (PDB 1DYK),[19] which contains residues 2934–3117 of that particular laminin chain. An initial 3D structure for the 42-residue ELP-$[K_2L_2I_2K_2]_1$ sequence, (GVG)(VPG<u>K</u>G)$_2$(VPG<u>L</u>G)$_2$(VPG<u>I</u>G)$_2$(VPG<u>K</u>G-VPG<u>K</u>), was built using the peptide builder tool in the program Avogadro;[46] the N′-terminal GVG in the above sequence is a linker from the C′-terminus of the LG5 domain. The ELP starting structure was modeled as a canonical α-helix, with backbone torsion angles of $\varphi = -60°$, $\psi = -40°$ (Figure S1). ELPs are likely only loosely structured in solution,[59] so the helical starting structure was not anticipated to bias the equilibrium structural ensemble (at least not if given sufficient sampling). Atomistic MD simulations were performed in NAMD, under the CHARMM36 force-field for proteins.[60, 61]

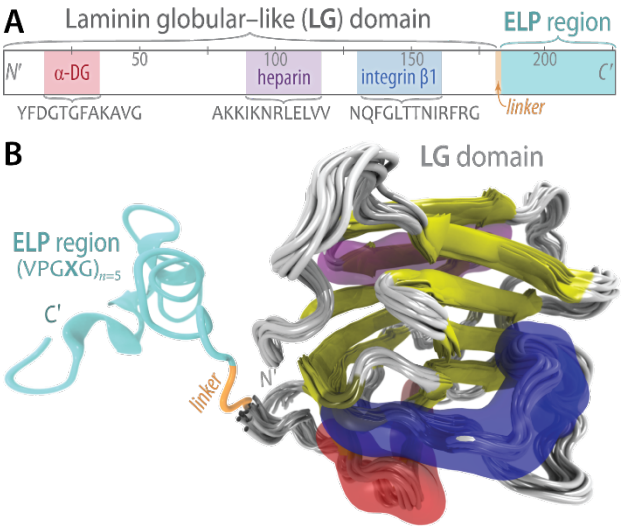

Figure 10-1. The proposed LG–ELP fusion protein. This schematic of our protein engineering design shows a laminin globular-like (LG) domain fused to a C'-terminal elastin-like polypeptide (ELP). (A) The biologically active segments25, 27 in the LG domain function as recognition/binding sites for α-DG (red), heparin (purple), and integrin-β1 (blue). Our ELP repeat region (cyan), consisting of 42 residues of the ELP pentapeptide repeat motif and a three-residue linker (orange), comprises the C'-terminal tail of our fusion construct; this ELP region is intended to act as a self-assembly module. (B) A 3D structural rendition of the fusion protein (ribbon representation) shows the LG domain as an overlay of multiple snapshots from the 100-ns simulation. The LG domain folds as a β-sandwich, with two sheets (one with six strands and the other with seven strands) stacked atop one another; the colored regions correspond to the recognition sequences in (A). The ELP tail is indicated (cyan), with the specific structure shown here drawn from the 315 K trajectory at t = 1 ns (i.e., after energy minimization and initial trajectory equilibration).

To prepare for simulations under periodic boundary conditions, the initial 3D model of LG-ELP was solvated in a cube of explicit TIP3P water molecules, using the 'solvation box' extension in VMD[62]; a 15-Å padding of solvent, between the solute and nearest box face, was used to mitigate interactions between the protein and its periodic images. Physiological concentrations (150 mM) of Na^+ ions, including sufficient Cl^- ions to neutralize the solute's charge, were then added to the solvated system using VMD's 'ionize' plugin. The final simulation cell contained 166,137 atoms, with a cubic box of water measuring 120 Å/edge. The internal energy was minimized for 10,000 steps, and the system was then equilibrated for 10 ns (with a 2-fs integration step) in the NPT ensemble (Figure 2, initial pose). Simulations were conducted over a range of seven temperatures: 290, 295, 300, 305, 310, 315, and 320 K. In each case, temperature and pressure (1 atm) were maintained using a Langevin thermostat and piston. NAMD 2.9 was used for all simulations,[63] with each trajectory extended to a final production time of at least 100 ns. To assess whether trajectory-derived quantities were consistent across our various final (production) runs—and not

merely consequences of insufficient/limited sampling—we performed extended simulations. Using the final structure (trajectory frame) from the 310 K simulation (effectively providing a negative control) we computed the corresponding structural quantities of 100-140 ns trajectories at 290, 300, and 320 K. Moreover, we extended the 310 K simulation to 200 ns, as interesting transitions occur near this temperature.

Trajectories were processed and further analyzed using in-house scripts written in the Python[64] and D[65] programming languages, as well as VMD. Root-mean-square deviations (RMSD) for C^{α} atoms were computed with VMD's RMSD extension toolbox. Secondary structures in the ELP region were assigned using STRIDE.[66, 67] Table S1 summarizes all of our LG-ELP–related simulations. All simulation configuration files and analysis scripts are available upon request.

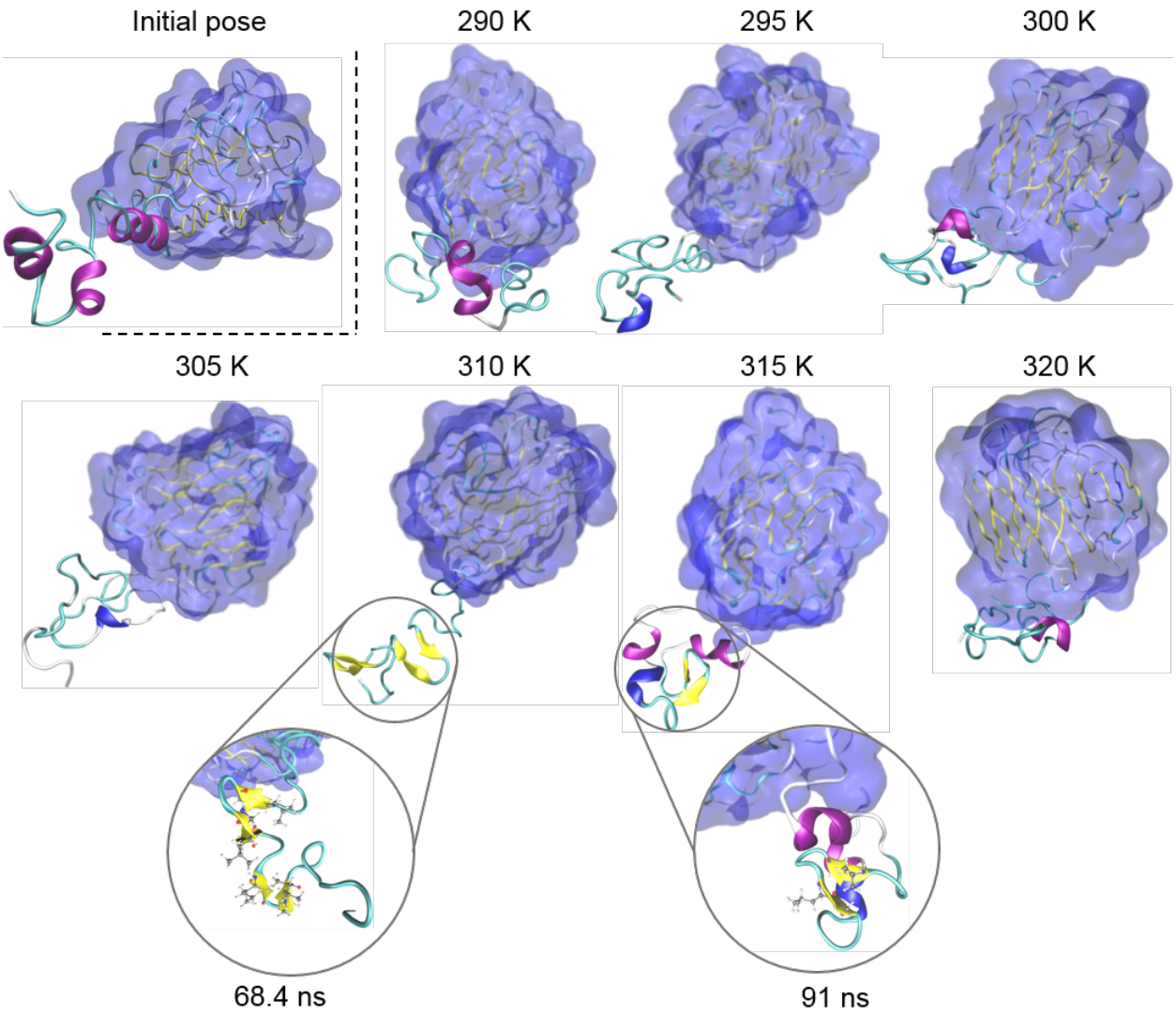

Figure 10-2. Representative structures, illustrating temperature-dependent conformational states of the LG-ELP fusion protein. In the initial pose, the LG-ELP protein is shown immediately after minimization and equilibration of the simulation system, with the LG domain (ribbon diagrams) enclosed by a semi-transparent blue surface. This initial pose was the starting model for simulations at each temperature. The ELP region (ribbons) in this starting state can be seen to be a mixture of helices and coils; the C'-terminus is labelled in this view with α-helices colored purple, 310 helices blue, β-strands yellow, the β-turn motif cyan and irregular coil regions white. LG-ELP structures are shown from each of the 290–320 K trajectories, with each temperature indicated and each structural snapshot taken at 100.0 ns. Insets are representative snapshots at 310 K and 315 K, taken from the 68.4 ns and 91 ns timepoints, respectively; the side-chains that contact one another to mediate β-sheet formation are depicted as ball-and-stick representations (gray carbons, blue nitrogens, red oxygens, and silver hydrogens). These trajectory frames illustrate the formation of β-sheet regions within the ELP tail.

Analysis of relative solvent-accessible surface area. Solvent-accessible surface areas (SASA) were calculated with the SASA tool in VMD, using a standard water probe radius of 1.4 Å. Rost

& Sander's method[68] was used to determine the relative solvent accessibility, $RelAcc_i$, of each residue i in the ELP region; this relative accessibility is simply the ordinary accessibility of a residue in a 3D structure (Acc_i) normalized by the maximal value possible for that residue type ($RelAcc_i = \frac{Acc_i}{maxAcc_i}$). In our analyses, $RelAcc_i$ values were computed over the entirety of the production trajectories for each simulation temperature.

Hydrogen-bonding analysis. Hydrogen bonds were computed using VMD's geometric criteria: namely, a distance cutoff of 3.5 Å and a D-H-A angle cutoff of 30°. Hydrogen bonds between two water molecules were excluded from our calculations. The number of water molecules surrounding the ELP backbone was determined by counting the number of waters within 3.15 Å of the peptide, as previously described.[52] This distance corresponds to the first minimum in the radial distribution function between the oxygen atoms of water molecules and atoms in the peptide backbone (Figure S2).

Statistical data analysis. Output data from our Tcl/Tk scripts (used with VMD's Tcl API) were analyzed using tools from the NumPy and SciPy Python packages. Note that all simulations, and subsequent trajectory and data analyses, were of the *full-length* (225–amino acid) LG-ELP protein. In many cases, we show only the ELP region in certain sections of our analyses; this is purely for the sake of clarity and simplicity. Spearman rank-order correlation coefficients, and associated *p*-values, for trajectory-derived data (taken from the beginning to the end of the trajectory)—such as intramolecular hydrogen bonding statistics, the number of neighboring water molecules, etc.—were calculated using SciPy's statistical modules.

10.4 Results and Discussion

Temperature-dependent structural transitions of the LG-ELP fusion construct. To explore the structural properties and conformational dynamics of our model LG-ELP fusion protein (Figure 1) at various temperatures, and illuminate its phase transition behavior, we performed all-atom MD simulations of the protein immersed in a bath of explicit solvent. This system was simulated at temperatures ranging from 290 K to 320 K, with each trajectory extended to at least 100-ns duration. Representative structures from the trajectories show that the ELP region in the initial pose is a mixture of helices and coils, and this region forms more structured β-strands near 310–315 K (Figure 2). This finding agrees with other studies of the assembly propensity of similar ELP segments (albeit in isolation, not as a fusion partner).[69, 70] We find that the ELP does not

associate with the LG domain, and thus the LG domain remains accessible in solution, for binding of bioactive agents such as integrins, heparin, and α-DG. The structural stability and general rigidity of the N′-terminal LG domain is largely maintained throughout each simulation, with the RMSD never exceeding 5 Å (data not shown), as opposed to the far more flexible ELP region (Figure 3).

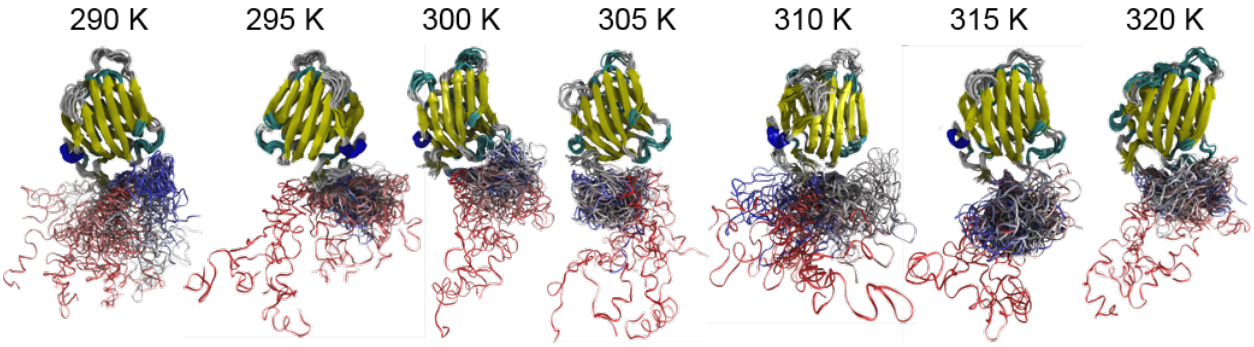

Figure 10-3. Representative structures of the LG-ELP fusion protein simulated at different temperatures. Spatiotemporal evolution of the LG-ELP fusion protein is demonstrated by superimposing frames, taken at 10-ns intervals, from the simulation of the entire fusion protein. The ELP region is colored so as to convey the simulation time, graded from early (red) to middle (gray) to late (blue) timesteps along the MD trajectory. Note the structural rigidity of the LG domain and the conformational flexibility of the ELP region.

As shown by the overlaid structural snapshots in Figure 3, the LG domain's initial structure is largely preserved throughout each simulation. The 'frayed' appearance of the ELP region highlights the structural disorder/flexibility inherent to native elastin-based sequences. At temperatures below 305 K, we see a collapse of the ELP from its initial conformation. A hydrophobic cluster within ELP, towards the end of the 100 ns trajectory, is present for all temperatures except 310 K, where the ELP region becomes extended; this point can also be seen in each contact map (Figure 4). Contact maps are matrices that show, for each residue in a 3D structure, the pairwise distance to all other residues. These symmetric matrices compactly represent the pattern of intramolecular contacts, and in our case reveal a lack of interatomic contacts between the LG and ELP regions (Figure 4). At 310 K, a transient—but noticeable—extension of the ELP occurred, starting at ~75 ns and highlighted by the loss of intra-strand hydrogen bonds (data not shown). This thermally-induced rearrangement of the ELP region may well correspond to the sampling of conformations that would favor higher-order (intermolecular) assembly, and we do not see this structural extension at 315 K (though, as for any simulation, absence of an observation could reflect limited sampling).

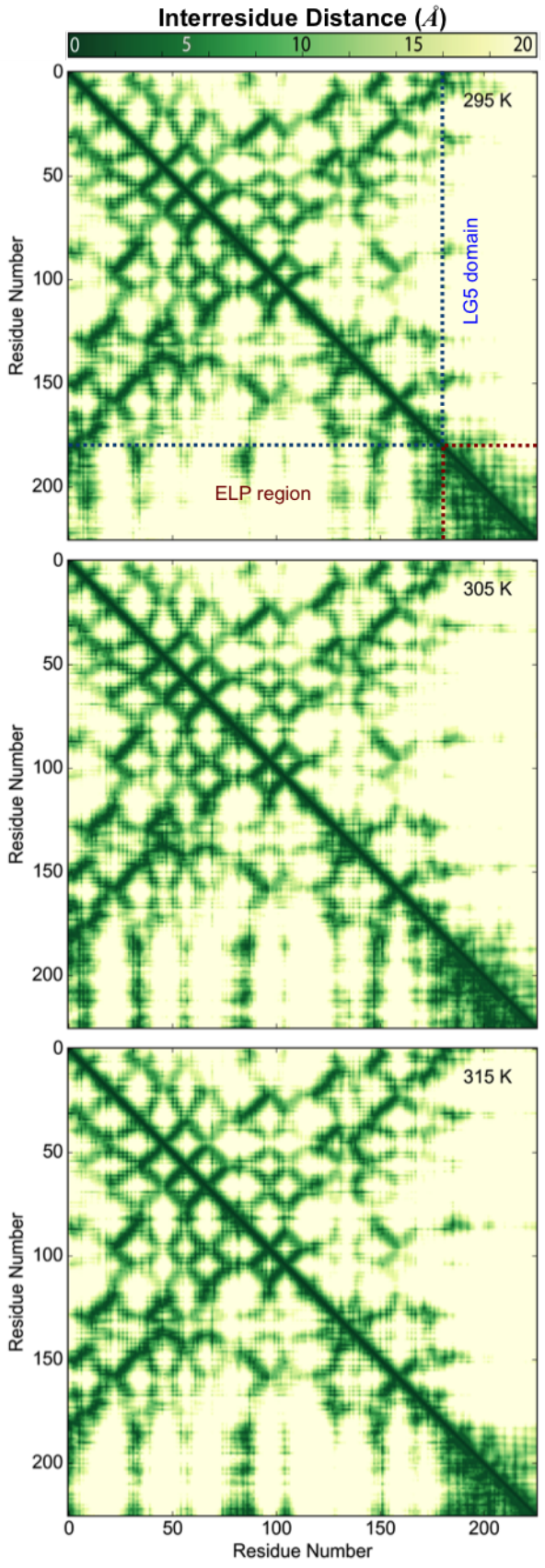

Figure 10-4. Contact maps of the dynamical interactions in our LG-ELP design reveal a lack of persistent LG···ELP interactions, independent of temperature. Contact maps are shown for the full length LG-ELP fusion at the indicated simulation temperatures, with colors graded by the pairwise distance (scale bar) between the two side-chains under consideration. The two discrete structural units in our fusion, i.e. the LG domain and ELP region, are demarcated by blue and red lines, respectively (for clarity, this is drawn only in the 295 K map). The classic crisscross patterns, highlighted by stripes of contacts perpendicular to the main diagonal, are indicative of the β-sheet core of the LG domain. Because an ordinary (symmetric) contact map contains two-fold redundant information, here we show (i) the minimum inter-residue distance in the lower triangular matrix, and (ii) the mean inter-residue distance, averaged over an entire trajectory, in the upper triangle. At all simulation temperatures, no stably persistent intra-molecular contacts (short distances) are found between the LG and ELP regions, as illustrated by (i) the high-intensity (short-distance) square submatrices at the lower-right of each map, indicating that most ELP residues interact with other ELP residues (not LG residues), and (ii) the vertical white stripes toward the right of each matrix, indicating a dearth of LG···ELP contacts. Thus, the ELP polypeptide does not engage in spurious/unwanted interactions with the LG region in solution, at least not on the 100-ns timescale of these simulations. (Contact maps for all simulated temperatures can be found in Figure S8.)

Secondary structure composition and its dependence on temperature. We examined the structural transitions from the initial starting peptide structure to the final conformational ensemble, focusing on the ELP region of the LG-ELP fusion. At all temperatures, the ELP region exhibits a significant amount of unstructured character (*β*-turn and 'other' in STRIDE), with these two classes accounting for most of the secondary structures in the ELP (Figures 5, S3, and S4). These findings are consistent with solid-state NMR data[59, 71] and CD spectroscopy[72, 73] of similar ELP sequences, where residues within the pentapeptide repeat preferentially adopt *β*-turn structures. We found that the ELP region accrues *β*-strand character over the course of a 100-ns trajectory at physiologically-relevant temperatures, and we posit that this *β*-strand enrichment can serve as a useful structural property for achieving temperature-triggered LG-ELP assembly; such assembly can occur via intermolecular *β*···*β*-strand contacts, e.g. by the domain swapping mode of *β*-rich protein association.[74, 75]

In simulations at 305 K, there is a sharp reduction of α-helicity, followed by a complete loss of helical structure after 74 ns (Figure S3 and S5). The secondary structure distribution at 305 K also shows a bimodal distribution in *β*-turn and 'other' motifs (Figure 5), indicating the preferential sampling of these two discrete conformational states. At 310 and 315 K, there is an increase in *β*-sheet character. The occurrence of *β*-sheet–like structures at temperatures above the phase transition has been experimentally detected in similar, single-molecule ELP systems.[46, 52, 73, 76, 77] The drastic change in secondary structural content found in our trajectories suggests that heating the system potentially destabilizes polyproline-induced α-helix conformations, perhaps by selectively decreasing the stability of water solvation effects[78, 79]. Such a disruption in helical propensity is consistent with the findings of Li et al.[46] and Ohgo et al.,[59] where, at higher temperatures, the proline in (VPGXG) adopts torsion angles similar to type-I and type-II *β*-turns. This shift in secondary structure in our LG-ELP system is especially prominent at 320 K, where there is a complete loss of *β*-sheet character, and the reduction of *β*-bridges with respect to 310 K and 315 K is associated with the increase in *β*-turns within the system. At lower temperatures, the composition favors more α-helical and 'other' secondary structures (3_{10} helices, π-helices, random coils, etc.). The pattern of sampling that we find in secondary structure formation, as a function of temperature, suggests that 310 K is near the target temperature at which macromolecular ordering of the LG-ELP fusion may occur.

This phenomenon associated with the structural changes accompanied by the phase transition is further demonstrated by the distribution of secondary structural content in the 200-ns trajectory. The time evolution of the secondary structure profile in the extended simulation at 310 K showed four distinct regions of persistent β-sheet like conformations, Leu4-Gly5$_{200\text{-}201}$ - Leu4-Gly5$_{205\text{-}206}$ and Ile4-Gly5$_{210\text{-}211}$ - Ile4-Gly5$_{214\text{-}215}$ (Fig. S6) with reduced conformational flexibility. Using the final trajectory frame of 310 K as a starting structure, we extended the simulation from 100 ns to 140 ns at 290 K, to assess the potential artefacts of limited sampling of structural classes. Reassuringly, we found that the β-sheet state does not persist, and in fact it disappears within 5 ns (Fig. S4, S7). Similarly, a transition from the 310 K trajectory to 320 K corresponds to a decrease of β-sheet content. At 300 K, however, the temperature shift resulted in a seemingly stable, extended β conformation of the peptide backbone in the Gly5$_{201}$-Leu4$_{205}$ region from 100-140 ns (Fig. S4 and S6). This result indicates that the intramolecular contacts between these nonpolar side-chains might be attributable to a population of pre-existing conformations from the previous structural ensemble at 310 K, as these are precisely the same β-sheet forming residues from the initial 100-ns trajectory.

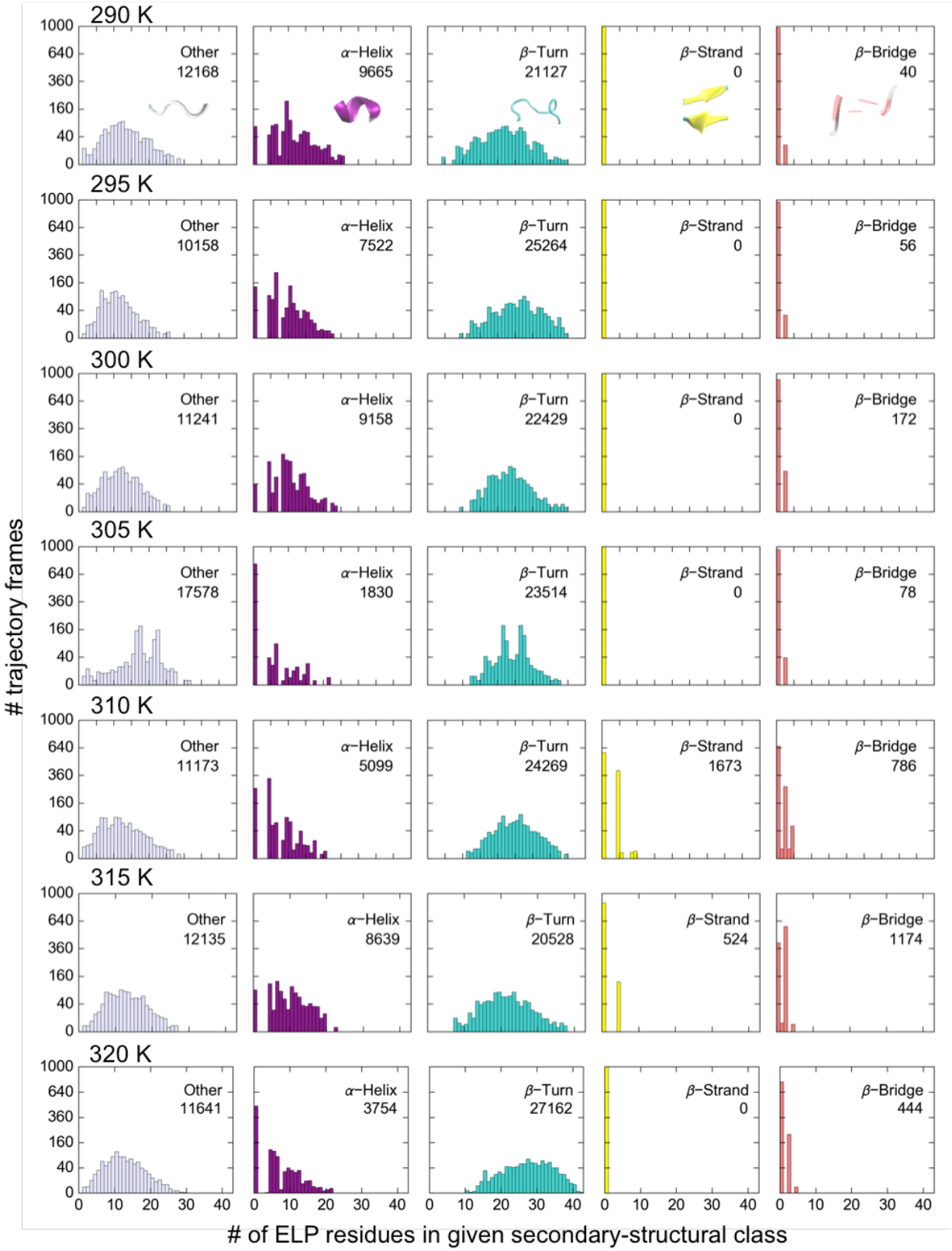

Figure 10-5. Secondary structural content of the ELP region as a function of temperature across the 290–320 K series. For simplicity, these trajectory analysis results are shown only

for the ELP region, instead of the full-length LG-ELP fusion; there are no noticeable changes in the structural content of the LG domain in all of our simulations. These secondary structure analyses show that the average conformational behavior of a single ELP monomer strongly depends on simulation temperature. Numbers written as insets within each panel give the total number of times that the secondary structure was detected in the simulation. Cartoon representations, shown as secondary structure thumbnail schematics in the first row, match the colors in the histogram. The predominant conformations exhibited by the ELP are β*-turns and 'other' structures. At low temperatures,* α*-helical and* β*-turn structures are prevalent, with minimal* β*-strand and bridge structures. However, states with greater* β*-sheet structural content occur as the temperature goes from 305 K to 310 K, indicating a possible order/disorder phase transition. Additionally, a significant shift in the character of the* β *structure, from strand to bridge, occurs at 315 K. The complete lack of* β*-strand structure at 320 K and subsequent rise in* β*-turns corresponds to an increased flexibility of the ELP backbone at higher temperatures.*

Relative solvent accessible surface area and visualization of association interactions. Conformational transitions can be analyzed via dynamical correlation functions, which provide information on how a molecule can interact with the surrounding solvent. We evaluated the solvent accessible surface area (SASA) of the ELP region in order to characterize the local ordering and solvation dynamics of the system. The SASA can help quantify protein surface–water contacts, and it is a parameter that has long been associated with the thermodynamics of protein structure, as related to the hydrophobic effect and folding.[80]

We find no strong trend in solvent exposure properties for residues in the ELP region (Figure 6). For all residues, a linear regression of SASA against temperature yields fits with R^2 values less than 0.5 (data not shown). This result suggests that the structural transitions of ELP regions do not strongly correlate with the SASA of any specific residue, representing a notable departure from previous models of ELP phase transitions.[69, 81] There is also a striking lack of correlation between $RelAcc_i$ and temperature. Linear regression gives R^2 values less than 0.35 for each residue, again suggesting that any ELP phase transition in this temperature regime is not accompanied by gross structural rearrangements. While the hydrophobic regions of ELP have been thought to become more exposed at elevated temperatures (at least for isolated ELP segments, unfused to other proteins),[82] our simulations do not reveal any such correlation. Though the *RelAcc* of our ELP residues is uncorrelated with temperature, the values do fluctuate (Figure 6), and no single residue is consistently buried or consistently exposed. The ELP phase transition, therefore, seems to be marked most strongly by the formation of *β*-sheet secondary structures, without any concomitant gross structural rearrangements (at least in terms of SASA).

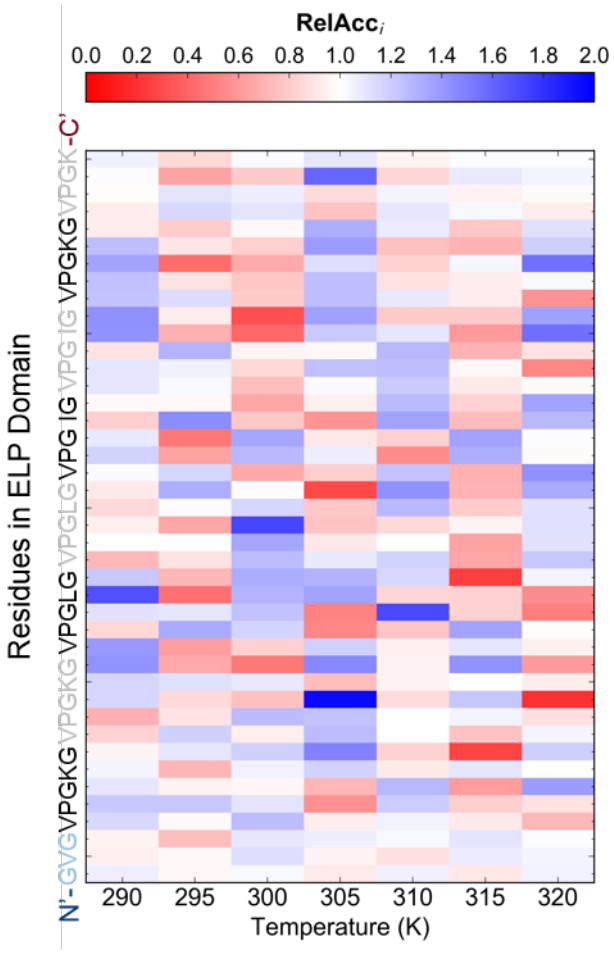

Figure 10-6. Temperature-dependent changes in relative SASAs of individual residues in the ELP region. The relative solvent accessibility, RelAcc_i*, represents the accessible surface area of a residue in the context of a (potentially folded) polypeptide. Blue colors indicate that a residue is more solvent-exposed than average, while red indicates that a residue is more buried than it otherwise would be (outside the context of the peptide).*

A close examination of the intramolecular contacts, i.e. within the fusion protein, reveals that the formation of β-sheets by ELP residues is not occluded or otherwise hindered by interatomic contacts between the ELP region and the LG domain (Figures 4, 5, and S8). From a protein design perspective, this is most reassuring: our simulations suggest that the ELP region will be accessible in solution, free of significant interactions with the nearby LG domain. Similarly, the LG domain's function should not be abrogated by the presence of ELP, and we expect putative ELP···ELP interactions to mirror those found in previous studies of ELP aggregation.[69, 73]

The role of hydration in compact conformations. We investigated the time-dependent hydration properties of our fusion's ELP region by examining the intramolecular hydrogen

bonding (within ELP) and the number of water molecules hydrogen-bonded with the ELP. The number of surrounding water molecules decreases and the number of intra-peptide hydrogen bonds increases, with increasing temperature from 305 to 315 K, and then a dip occurs at 320 K (Figure 7). There is a slow decrease, with time, in the number of solvating water molecules at all simulated temperatures (Figure S9A). The 310 K trajectory features an intriguingly abrupt dip in the number of water molecules at 64 ns and at 82 ns. The displacement of water molecules with higher temperatures is consistent with a model wherein desolvation (e.g., of nonpolar side-chains) biases specific (e.g., polar) segments of the amphipathic ELP chain into more compact conformations, such as β-turns and strand-like conformations. Helical structures are often unfavorable at elevated temperatures for entropic reasons, such as a greater loss, upon folding, of orientational and other conformational degrees of freedom[83, 84]. Thus, higher temperatures may indirectly, via effects on solvation structure, enhance the stability of β-sheet formation in relatively disordered conformational ensembles, such as that of ELP. Changes in hydration density exhibit a correlation with β-sheet propensity along all trajectories (Figures S5 and S9B). A Spearman's rank-order correlation coefficient of –0.83 (p = 0.04, for 100 ns) indicates a moderately strong negative correlation between intramolecular hydrogen bonding and surrounding water molecules with increasing temperature. This quantity captures the fact that, at elevated temperatures, the ELP region preferentially contacts itself rather than water—indicative of a phase transition[59]. The increased number of hydrogen bonds above 305 K suggests a coil-to-globule transition.[76] A possible model is that, at high temperatures, insufficient conformational order exists to allow for formation of a single, well-defined structural state. As such, at lower temperatures the increased rigidity of the system would not facilitate the formation of intramolecular peptide···peptide hydrogen bonds, which would, instead, be replaced by inter-molecular hydrogen bonds with the surrounding water structure.

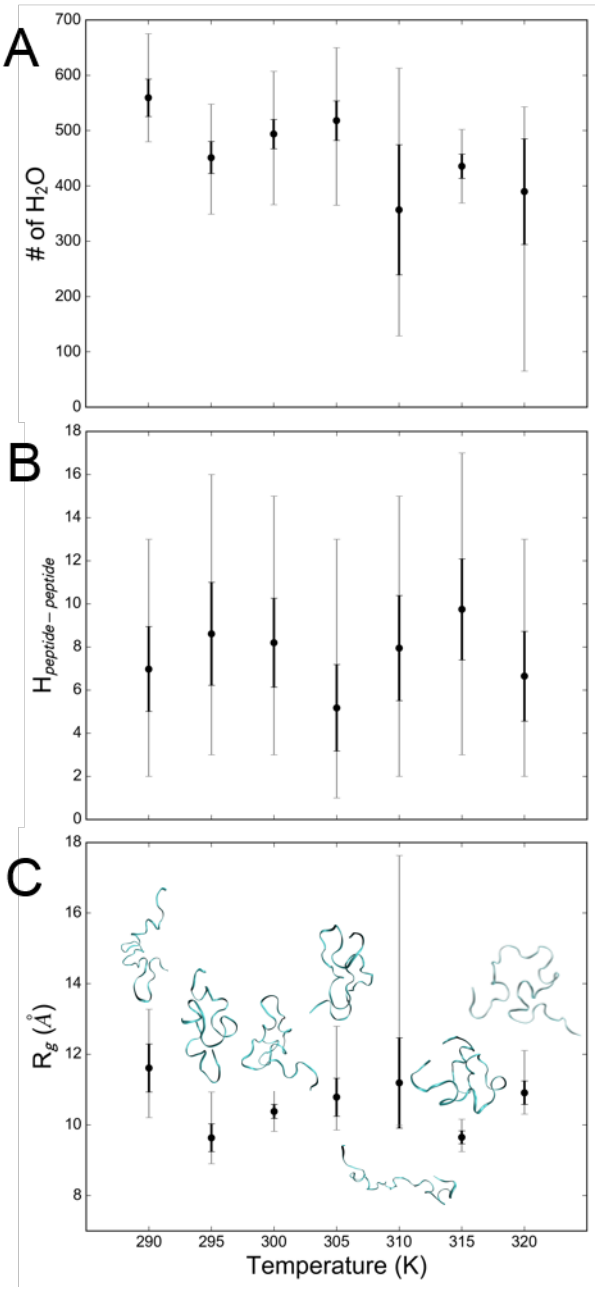

Figure 10-7. Changes in degree of hydration, hydrogen-bonding, and overall structure of the ELP region. (A) The number of water molecules is counted within 3.15 Å of the ELP, with varying temperature. An abrupt decrease in the number of surrounding water molecules suggests that this change is associated with the formation of β-sheets at 310 K in the ELP region. (B) The number of intramolecular peptide···peptide hydrogen bonds ($H_{peptide\text{-}peptide}$). The formation of intramolecular hydrogen bonding has been observed for many peptide aggregates that exhibit LCST behavior; however, the large number of disordered conformational states of our ELP hinders us from discerning any trend as regards a temperature that might be indicative of a phase transition. (C) Temperature dependence of the radius of gyration (R_g). Proteins in all simulated temperatures exhibit temperature-induced collapse (relative to the initial starting structure). Only 310 K and 320 K show a slight expansion of the polypeptide chain, while all other proteins exhibit compaction—reminiscent of the 'hydrophobic collapse' in typical (water-soluble) globular proteins. In all panels, black error bars represent standard deviations and gray error bars show min/max values. Only the last 40 ns of the trajectories at each temperature are included in the analysis shown here.

Coupled protein···solvent interactions are a key element of a system's structural properties and dynamical behavior in any order/disorder transition (e.g., protein folding), but time-resolved experimental data on such interactions are not easily obtained, at least at high spatial resolution. Atomistic simulations can provide information about literally each inter-atomic contact, including the dynamical networks of (i) apolar interactions within a protein, (ii) protein···solvent contacts, and (iii) solvent···solvent contacts, all of which are important factors in macromolecular folding and binding. The compactness of a biomolecular 3D structure—and, by inference, the degree of formation of a hydrophobic 'core'—can be measured as the radius of gyration, R_g. The time-evolution of R_g for the ELP region alone (Figures 7C, S10, and S11) does not clearly reveal a sharp phase transition, unlike many biopolymers that exhibit LCST behavior.[43, 77, 85] Though R_g data are, in principle, experimentally accessible via solution-state measurements, e.g. Guinier analysis of small-angle X-ray scattering data,[86] such approaches to extracting R_g values are confounded by phase changes in going from a soluble to insoluble state, as is common with many polymers that demonstrate LCST behavior. Our simulations reveal that the ELP portion of our fusion protein adopts β-strand secondary structures at high temperatures, implying that this region can undergo structural changes, akin to order/disorder phase transitions, and form ordered complexes. Intriguingly, the drastic solute re-structuring that is often associated with LCST behavior[82] does not appear to be a feature in our system's transition. At higher temperatures, the unfolding or 'elongation' of the polypeptide (Figure S10 and S11) is primarily entropically driven, but at a critical temperature (near 315 K in our system), the chain collapses because the loss of configurational entropy of the side-chains and backbone is counterbalanced by entropic changes in the network of solvent···{solvent, protein} interactions.[87, 88] To assess whether our findings were consistent with our results from the first 100-ns trajectories, we performed additional simulations at 290 K, 300 K, 310 K, and 320 K using the final (100 ns) frame from the 310 K simulation as the starting structure for each different temperature. These extended trajectory data support the argument of a structural transition near 310 K, where it is represented by a gross structural rearrangement of the polypeptide backbone. This transient state is characterized by a 'two-state' equilibrium between the collapsed and extended conformation (Fig. S11) within the ELP region. At low temperatures, i.e. 290 K and 300 K, we continue to observe a collapsed state, which is stabilized by the relatively strong peptide···peptide and peptide···water interactions, compared to the extended conformation at 310 K.

As a final step of analysis, we considered the 'end–to–end' distance, taken as the simple Euclidean distance between the N′- and C′-termini of a given polypeptide segment, as another geometric measure of peptide compactness. Monitoring the dynamics of the end–to–end distance for the ELP region (Figure S12) revealed that this part of our fusion design can explore a substantial region of conformational space without altering its global shape (as indicated by a relatively constant R_g value). Note that this behavior differs from that of larger, 'ordinary' globular proteins, where the detailed 3D structural changes that correspond to transitions between nearby local minima on the energy landscape effectively act as barriers to the rapid sampling of conformational space, thereby decreasing kinetic rates of transitions.[89-91]

10.5 **Conclusions**

Classical, all-atom MD simulations were used to examine the structural properties and conformational dynamics of an engineered, laminin–mimetic elastin–like fusion protein, referred to here as LG-ELP. Analyses of the temperature-dependent conformational changes in full-length LG-ELP—in terms of secondary structural content, solvent accessible surface area, hydrogen bonding, and hydration properties—illuminate the phase transition behavior of this fusion protein. The increased structuring of the protein, and the opportunity that that presents for engineering noncovalent interactions, provide a platform for the rational design of macroscopic material properties[92]. The secondary structural elements in a peptide are known to correlate with the compliance, stiffness, density, and other mechanical properties of hydrogels built upon the given peptide.[93, 94] In this work, we computed atomically-detailed MD trajectories of an engineered LG-ELP protein design at several temperatures thereby providing us with an *a priori* view of the phase behavior of our design as a function of temperature in the physiological range; reassuringly, we found that the ELP region of our fusion protein did not engage in spurious interactions with the LG domain. This type of information is invaluable in guiding the design of new fusion protein sequences and motifs with desired biological functionalities. Ultimately, our strategy can be used to simulate multiple fusion protein designs, rank-order them, and synthesize those candidates that exhibit the desired phase transition behavior. Because our strategy of using simulations is physics-based, our approach also illuminates the secondary and tertiary structural properties of our LG-ELP fusion, as well as physicochemical properties such as the coupled dynamics of the solvation environment and its influence on the phase transition behavior of our design.

Simulations are enjoying increased use in the analysis of protein structure and function, but to our knowledge an MD-based simulation methodology has not been used in the manner reported here: namely, to help guide the design and iterative refinement of novel fusion proteins that can act as stimuli-responsive cellular matrix materials. There exist relatively few examples of long-time, all-atom simulations of polypeptide-based materials. The simulations reported here elucidate the relationships between solvation, hydrophobicity, structural dynamics and other atomically-detailed properties, for a novel biomolecular system, and our strategy offers a robust and extensible platform to guide future design and syntheses of protein biomaterials. In particular, our general computational approach can be readily applied in the rational design of engineered extracellular matrix proteins for constructing stimuli-responsive and biocompatible materials for applications in drug delivery, tissue engineering, and regenerative medicine.

10.6 References

1. Lampe, K. J.; Heilshorn, S. C., Building stem cell niches from the molecule up through engineered peptide materials. *Neurosci Lett* **2012,** 519, (2), 138-146.
2. Straley, K. S.; Heilshorn, S. C., Independent tuning of multiple biomaterial properties using protein engineering. *Soft Matter* **2009,** 5, (1), 114-124.
3. Lampe, K. J.; Antaris, A. L.; Heilshorn, S. C., Design of three-dimensional engineered protein hydrogels for tailored control of neurite growth. *Acta Biomaterialia* **2013,** 9, (3), 5590-5599.
4. Webber, M. J.; Tongers, J.; Newcomb, C. J.; Marquardt, K. T.; Bauersachs, J.; Losordo, D. W.; Stupp, S. I., Supramolecular nanostructures that mimic VEGF as a strategy for ischemic tissue repair (vol 108, pg 13438, 2011). *P Natl Acad Sci USA* **2012,** 109, (23), 9220-9220.
5. Fagerholm, P.; Lagali, N. S.; Carlsson, D. J.; Merrett, K.; Griffith, M., Corneal Regeneration Following Implantation of a Biomimetic Tissue-Engineered Substitute. *Cts-Clin Transl Sci* **2009,** 2, (2), 162-164.
6. Cai, L.; Heilshorn, S. C., Designing ECM-mimetic materials using protein engineering. *Acta Biomaterialia* **2014,** 10, (4), 1751-1760.
7. Khaing, Z. Z.; Thomas, R. C.; Geissler, S. A.; Schmidt, C. E., Advanced biomaterials for repairing the nervous system: what can hydrogels do for the brain? *Mater Today* **2014,** 17, (7), 332-340.
8. Hallmann, R.; Horn, N.; Selg, M.; Wendler, O.; Pausch, F.; Sorokin, L. M., Expression and function of laminins in the embryonic and mature vasculature. *Physiol Rev* **2005,** 85, (3), 979-1000.
9. Beck, K.; Hunter, I.; Engel, J., Structure and Function of Laminin - Anatomy of a Multidomain Glycoprotein. *Faseb J* **1990,** 4, (2), 148-160.
10. Jucker, M.; Bialobok, P.; Kleinman, H. K.; Walker, L. C.; Hagg, T.; Ingram, D. K., Laminin-Like and Laminin-Binding Protein-Like Immunoreactive Astrocytes in Rat Hippocampus after Transient Ischemia - Antibody to Laminin-Binding Protein Is a Sensitive Marker of Neural Injury and Degeneration. *Ann Ny Acad Sci* **1993,** 679, 245-252.
11. Mckee, K. K.; Capizzi, S.; Yurchenco, P. D., Scaffold-forming and Adhesive Contributions of Synthetic Laminin-binding Proteins to Basement Membrane Assembly. *Journal of Biological Chemistry* **2009,** 284, (13), 8984-8994.
12. Yurchenco, P. D.; Quan, Y.; Colognato, H.; Mathus, T.; Harrison, D.; Yamada, Y.; Orear, J. J., The alpha chain of laminin-1 is independently secreted and drives secretion of its beta- and gamma-chain partners. *Proceedings of the National Academy of Sciences of the United States of America* **1997,** 94, (19), 10189-10194.
13. Pierschbacher, M. D.; Ruoslahti, E., Cell Attachment Activity of Fibronectin Can Be Duplicated by Small Synthetic Fragments of the Molecule. *Nature* **1984,** 309, (5963), 30-33.
14. Graf, J.; Iwamoto, Y.; Sasaki, M.; Martin, G. R.; Kleinman, H. K.; Robey, F. A.; Yamada, Y., Identification of an Amino-Acid-Sequence in Laminin Mediating Cell Attachment, Chemotaxis, and Receptor-Binding. *Cell* **1987,** 48, (6), 989-996.
15. Tashiro, K.; Sephel, G. C.; Weeks, B.; Sasaki, M.; Martin, G. R.; Kleinman, H. K.; Yamada, Y., A Synthetic Peptide Containing the Ikvav Sequence from the a-Chain of Laminin Mediates Cell Attachment, Migration, and Neurite Outgrowth. *J Biol Chem* **1989,** 264, (27), 16174-16182.
16. Miller, J. S.; Shen, C. J.; Legant, W. R.; Baranski, J. D.; Blakely, B. L.; Chen, C. S., Bioactive hydrogels made from step-growth derived PEG-peptide macromers. *Biomaterials* **2010,** 31, (13), 3736-3743.
17. Wang, L. S.; Lee, F.; Lim, J.; Du, C.; Chwee, A.; Wan, A.; Lee, S. S.; Kurisawa, M., Enzymatic conjugation of a bioactive peptide into an injectable hyaluronic acid-tyramine hydrogel system to promote the formation of functional vasculature. *Abstr Pap Am Chem S* **2014,** 248.

18. Sanborn, T. J.; Messersmith, P. B.; Barron, A. E., In situ crosslinking of a biomimetic peptide-PEG hydrogel via thermally triggered activation of factor XIII. *Biomaterials* **2002,** 23, (13), 2703-2710.
19. Timpl, R.; Tisi, D.; Talts, J. F.; Andac, Z.; Sasaki, T.; Hohenester, E., Structure and function of laminin LG modules. *Matrix Biol* **2000,** 19, (4), 309-317.
20. Tisi, D.; Talts, J. F.; Timpl, R.; Hohenester, E., Structure of the C-terminal laminin G-like domain pair of the laminin alpha 2 chain harbouring binding sites for alpha-dystroglycan and heparin. *Embo J* **2000,** 19, (7), 1432-1440.
21. Wizemann, H.; Garbe, J. H. O.; Friedrich, M. V. K.; Timpl, R.; Sasaki, T.; Hohenester, E., Distinct requirements for heparin and alpha-dystroglycan binding revealed by structure-based mutagenesis of the laminin alpha 2 LG4-LG5 domain pair. *J Mol Biol* **2003,** 332, (3), 635-642.
22. Tsiper, M. V.; Yurchenco, P. D., Laminin assembles into separate basement membrane and fibrillar matrices in Schwann cells. *Journal of Cell Science* **2002,** 115, (5), 1005-1015.
23. Li, S. H.; Liquari, P.; McKee, K. K.; Harrison, D.; Patel, R.; Lee, S.; Yurchenco, P. D., Laminin-sulfatide binding initiates basement membrane assembly and enables receptor signaling in Schwann cells and fibroblasts. *J Cell Biol* **2005,** 169, (1), 179-189.
24. Colognato, H.; Winkelmann, D. A.; Yurchenco, P. D., Laminin polymerization induces a receptor-cytoskeleton network. *J Cell Biol* **1999,** 145, (3), 619-631.
25. Urushibata, S.; Hozumi, K.; Ishikawa, M.; Katagiri, F.; Kikkawa, Y.; Nomizu, M., Identification of biologically active sequences in the laminin alpha 2 chain G domain. *Arch Biochem Biophys* **2010,** 497, (1-2), 43-54.
26. Jung, S. Y.; Kim, J. M.; Kang, H. K.; Jang, D. H.; Min, B. M., A Biologically Active Sequence of the Laminin alpha 2 Large Globular 1 Domain Promotes Cell Adhesion through Syndecan-1 by Inducing Phosphorylation and Membrane Localization of Protein Kinase C delta. *J Biol Chem* **2009,** 284, (46), 31764-31775.
27. Suzuki, N.; Hozumi, K.; Urushibata, S.; Yoshimura, T.; Kikkawa, Y.; Gumerson, J. D.; Michele, D. E.; Hoffman, M. P.; Yamada, Y.; Nomizu, M., Identification of alpha-dystroglycan binding sequences in the laminin alpha 2 chain LG4-5 module. *Matrix Biol* **2010,** 29, (2), 143-151.
28. Fromm, J. R.; Hileman, R. E.; Weiler, J. M.; Linhardt, R. J., Interaction of fibroblast growth factor-1 and related peptides with heparan sulfate and its oligosaccharides. *Arch Biochem Biophys* **1997,** 346, (2), 252-262.
29. Nugent, M. A.; Iozzo, R. V., Fibroblast growth factor-2. *Int J Biochem Cell B* **2000,** 32, (2), 115-120.
30. Michele, D. E.; Campbell, K. P., Dystrophin-glycoprotein complex: Post-translational processing and dystroglycan function. *J Biol Chem* **2003,** 278, (18), 15457-15460.
31. Muntoni, F.; Torelli, S.; Brockington, M., Muscular dystrophies due to glycosylation defects. *Neurotherapeutics* **2008,** 5, (4), 627-632.
32. Crosson, S.; Mckee, K.; Ruegg, M.; Yurchenco, P., Restoring laminin polymerization by transgenic expression of alpha LNNd in skeletal muscle improves muscle integrity of laminin-alpha 2-deficient mice. *Glycobiology* **2012,** 22, (11), 1536-1536.
33. Hozumi, K.; Otagiri, D.; Yamada, Y.; Sasaki, A.; Fujimori, C.; Wakai, Y.; Uchida, T.; Katagiri, F.; Kikkawa, Y.; Nomizu, M., Cell surface receptor-specific scaffold requirements for adhesion to laminin-derived peptide-chitosan membranes. *Biomaterials* **2010,** 31, (12), 3237-3243.
34. Urry, D. W., Physical chemistry of biological free energy transduction as demonstrated by elastic protein-based polymers. *J Phys Chem B* **1997,** 101, (51), 11007-11028.
35. Girotti, A.; Reguera, J.; Arias, F. J.; Alonso, M.; Testera, A. M.; Rodriguez-Cabello, J. C., Influence of the molecular weight on the inverse temperature transition of a model genetically engineered elastin-like pH-responsive polymer. *Macromolecules* **2004,** 37, (9), 3396-3400.
36. Ribeiro, A.; Arias, F. J.; Reguera, J.; Alonso, M.; Rodriguez-Cabello, J. C., Influence of the Amino-Acid Sequence on the Inverse Temperature Transition of Elastin-Like Polymers. *Biophysical Journal* **2009,** 97, (1), 312-320.
37. Meyer, D. E.; Chilkoti, A., Purification of recombinant proteins by fusion with thermally-responsive polypeptides. *Nat Biotechnol* **1999,** 17, (11), 1112-1115.
38. MacKay, J. A.; Callahan, D. J.; FitzGerald, K. N.; Chilkoti, A., Quantitative Model of the Phase Behavior of Recombinant pH-Responsive Elastin-Like Polypeptides. *Biomacromolecules* **2010,** 11, (11), 2873-2879.
39. Cho, Y. H.; Zhang, Y. J.; Christensen, T.; Sagle, L. B.; Chilkoti, A.; Cremer, P. S., Effects of Hofmeister Anions on the Phase Transition Temperature of Elastin-like Polypeptides. *Journal of Physical Chemistry B* **2008,** 112, (44), 13765-13771.
40. Long, M. M.; Urry, D. W.; Cox, B. A.; Ohnishi, T.; Jacobs, M., Coacervation of Repeat Sequences of Elastin. *Biophysical Journal* **1975,** 15, (2), A71-A71.
41. Meyer, D. E.; Chilkoti, A., Quantification of the effects of chain length and concentration on the thermal behavior of elastin-like polypeptides. *Biomacromolecules* **2004,** 5, (3), 846-851.
42. Trabbic-Carlson, K.; Meyer, D. E.; Liu, L.; Piervincenzi, R.; Nath, N.; LaBean, T.; Chilkoti, A., Effect of protein fusion on the transition temperature of an environmentally responsive elastin-like polypeptide: a role for surface hydrophobicity? *Protein Eng Des Sel* **2004,** 17, (1), 57-66.
43. Christensen, T.; Hassouneh, W.; Trabbic-Carlson, K.; Chilkoti, A., Predicting Transition Temperatures of Elastin-Like Polypeptide Fusion Proteins. *Biomacromolecules* **2013,** 14, (5), 1514-1519.
44. Qin, G. K.; Glassman, M. J.; Lam, C. N.; Chang, D.; Schaible, E.; Hexemer, A.; Olsen, B. D., Topological Effects on Globular Protein-ELP Fusion Block Copolymer Self-Assembly. *Advanced Functional Materials* **2015,** 25, (5), 729-738.
45. Liu, H. J.; Wise, S. G.; Rnjak-Kovacina, J.; Kaplan, D. L.; Bilek, M. M. M.; Weiss, A. S.; Fei, J.; Bao, S. S., Biocompatibility of silk-tropoelastin protein polymers. *Biomaterials* **2014,** 35, (19), 5138-5147.
46. Li, N. K.; Quiroz, F. G.; Hall, C. K.; Chilkoti, A.; Yingling, Y. G., Molecular Description of the LCST Behavior of an Elastin-Like Polypeptide. *Biomacromolecules* **2014,** 15, (10), 3522-3530.
47. Zhang, Y. J.; Trabbic-Carlson, K.; Albertorio, F.; Chilkoti, A.; Cremer, P. S., Aqueous two-phase system formation kinetics for elastin-like polypeptides of varying chain length. *Biomacromolecules* **2006,** 7, (7), 2192-2199.

48. Chen, Y. L.; Guan, Z. B., Bioinspired Modular Synthesis of Elastin-Mimic Polymers To Probe the Mechanism of Elastin Elasticity. *J Am Chem Soc* **2010,** 132, (13), 4577-+.
49. Li, B.; Alonso, D. O. V.; Daggett, V., The molecular basis for the inverse temperature transition of elastin. *J Mol Biol* **2001,** 305, (3), 581-592.
50. Urry, D. W.; Trapane, T. L.; Prasad, K. U., Phase-Structure Transitions of the Elastin Polypentapeptide Water-System within the Framework of Composition Temperature Studies. *Biopolymers* **1985,** 24, (12), 2345-2356.
51. Amiram, M.; Quiroz, F. G.; Callahan, D. J.; Chilkoti, A., A highly parallel method for synthesizing DNA repeats enables the discovery of 'smart' protein polymers. *Nat Mater* **2011,** 10, (2), 141-148.
52. Zhao, B. W.; Li, N. K.; Yingling, Y. G.; Hall, C. K., LCST Behavior is Manifested in a Single Molecule: Elastin-Like polypeptide (VPGVG)n. *Biomacromolecules* **2016,** 17, (1), 111-118.
53. Mura, C.; McAnany, C. E., An introduction to biomolecular simulations and docking. *Mol Simulat* **2014,** 40, (10-11), 732-764.
54. Urry, D. W., A New Hydrophobicity Scale for Proteins and Its Relevance to Interactions at Interfaces. *Abstr Pap Am Chem S* **1994,** 207, 220-Coll.
55. Urry, D. W.; Gowda, D. C.; Parker, T. M.; Luan, C. H.; Reid, M. C.; Harris, C. M.; Pattanaik, A.; Harris, R. D., Hydrophobicity Scale for Proteins Based on Inverse Temperature Transitions. *Biopolymers* **1992,** 32, (9), 1243-1250.
56. Hassouneh, W.; Zhulina, E. B.; Chilkoti, A.; Rubinstein, M., Elastin-like Polypeptide Diblock Copolymers Self-Assemble into Weak Micelles. *Macromolecules* **2015,** 48, (12), 4183-4195.
57. Seltzer, J. L.; Weingarten, H.; Akers, K. T.; Eschbach, M. L.; Grant, G. A.; Eisen, A. Z., Cleavage Specificity of Type-Iv Collagenase (Gelatinase) from Human-Skin - Use of Synthetic Peptides as Model Substrates. *J Biol Chem* **1989,** 264, (33), 19583-19586.
58. Chung, C.; Lampe, K. J.; Heilshorn, S. C., Tetrakis(hydroxymethyl) Phosphonium Chloride as a Covalent Cross-Linking Agent for Cell Encapsulation within Protein-Based Hydrogels. *Biomacromolecules* **2012,** 13, (12), 3912-3916.
59. Ohgo, K.; Ashida, J.; Kumashiro, K. K.; Asakura, T., Structural determination of an elastin-mimetic model peptide, (Val-Pro-Gly-Val-Gly)(6), studied by C-13 CP/MAS NMR chemical shifts, two-dimensional off magic angle spinning spin-diffusion NMR, rotational echo double resonance, and statistical distribution of torsion angles from protein data bank. *Macromolecules* **2005,** 38, (14), 6038-6047.
60. Denning, E. J.; Priyakumar, U. D.; Nilsson, L.; Mackerell, A. D., Impact of 2 '-Hydroxyl Sampling on the Conformational Properties of RNA: Update of the CHARMM All-Atom Additive Force Field for RNA. *J Comput Chem* **2011,** 32, (9), 1929-1943.
61. MacKerell, A. D.; Bashford, D.; Bellott, M.; Dunbrack, R. L.; Evanseck, J. D.; Field, M. J.; Fischer, S.; Gao, J.; Guo, H.; Ha, S.; Joseph-McCarthy, D.; Kuchnir, L.; Kuczera, K.; Lau, F. T. K.; Mattos, C.; Michnick, S.; Ngo, T.; Nguyen, D. T.; Prodhom, B.; Reiher, W. E.; Roux, B.; Schlenkrich, M.; Smith, J. C.; Stote, R.; Straub, J.; Watanabe, M.; Wiorkiewicz-Kuczera, J.; Yin, D.; Karplus, M., All-atom empirical potential for molecular modeling and dynamics studies of proteins. *J Phys Chem B* **1998,** 102, (18), 3586-3616.
62. Humphrey, W.; Dalke, A.; Schulten, K., VMD: Visual molecular dynamics. *J Mol Graph Model* **1996,** 14, (1), 33-38.
63. Phillips, J. C.; Braun, R.; Wang, W.; Gumbart, J.; Tajkhorshid, E.; Villa, E.; Chipot, C.; Skeel, R. D.; Kale, L.; Schulten, K., Scalable molecular dynamics with NAMD. *Journal of Computational Chemistry* **2005,** 26, (16), 1781-1802.
64. Rossum, G. *Python reference manual*; CWI (Centre for Mathematics and Computer Science): 1995.
65. Bright, W., The D programming language. *Dr Dobbs J* **2002,** 27, (2), 36-40.
66. Frishman, D.; Argos, P., Knowledge-based protein secondary structure assignment. *Proteins-Structure Function and Genetics* **1995,** 23, (4), 566-579.
67. Heinig, M.; Frishman, D., STRIDE: a web server for secondary structure assignment from known atomic coordinates of proteins. *Nucleic Acids Research* **2004,** 32, W500-W502.
68. Rost, B.; Sander, C., Conservation and Prediction of Solvent Accessibility in Protein Families. *Proteins* **1994,** 20, (3), 216-226.
69. Salvi, A. M.; Moscarelli, P.; Bochicchio, B.; Lanza, G.; Castle, J. E., Combined effects of solvation and aggregation propensity on the final supramolecular structures adopted by hydrophobic, glycine-rich, elastin-like polypeptides. *Biopolymers* **2013,** 99, (5), 292-313.
70. Flamia, R.; Lanza, G.; Salvi, A. M.; Castle, J. E.; Tamburro, A. M., Conformational study and hydrogen bonds detection on elastin-related polypeptides using X-ray photoelectron spectroscopy. *Biomacromolecules* **2005,** 6, (3), 1299-1309.
71. Kumashiro, K. K.; Kurano, T. L.; Niemczura, W. P.; Martino, M.; Tamburro, A. M., C-13 CPMAS NMR studies of the elastin-like polypeptide (LGGVG)(n). *Biopolymers* **2003,** 70, (2), 221-226.
72. Reiersen, H.; Clarke, A. R.; Rees, A. R., Short elastin-like peptides exhibit the same temperature-induced structural transitions as elastin polymers: Implications for protein engineering. *J Mol Biol* **1998,** 283, (1), 255-264.
73. Moscarelli, P.; Boraldi, F.; Bochicchio, B.; Pepe, A.; Salvi, A. M.; Quaglino, D., Structural characterization and biological properties of the amyloidogenic elastin-like peptide (VGGVG)(3). *Matrix Biol* **2014,** 36, 15-27.
74. Rousseau, F.; Schymkowitz, J.; Itzhaki, L. S., Implications of 3d Domain Swapping for Protein Folding, Misfolding and Function. *Adv Exp Med Biol* **2012,** 747, 137-152.
75. Das, P.; King, J. A.; Zhou, R. H., Aggregation of gamma-crystallins associated with human cataracts via domain swapping at the C-terminal beta-strands. *P Natl Acad Sci USA* **2011,** 108, (26), 10514-10519.
76. Nuhn, H.; Klok, H. A., Secondary Structure Formation and LCST Behavior of Short Elastin-Like Peptides. *Biomacromolecules* **2008,** 9, (10), 2755-2763.
77. Dandurand, J.; Samouillan, V.; Lacabanne, C.; Pepe, A.; Bochicchio, B., Water structure and elastin-like peptide aggregation A differential calorimetric approach. *J Therm Anal Calorim* **2015,** 120, (1), 419-426.
78. Creamer, T. P.; Campbell, M. N., Determinants of the polyproline II helix from modeling studies. *Adv Protein Chem* **2002,** 62, 263-282.
79. Sreerama, N.; Woody, R. W., Molecular dynamics simulations of polypeptide conformations in water: A comparison of alpha, beta, and poly(Pro)II conformations. *Proteins* **1999,** 36, (4), 400-406.
80. Chothia, C., Hydrophobic Bonding and Accessible Surface-Area in Proteins. *Nature* **1974,** 248, (5446), 338-339.

81. Huang, J. X.; Sun, C.; Mitchell, O.; Ng, N.; Wang, Z. N.; Boutisa, G. S., On the inverse temperature transition and development of an entropic elastomeric force of the elastin mimetic peptide [LGGVG](3,7). *J Chem Phys* **2012,** 136, (8).
82. Karle, I. L.; Urry, D. W., Crystal structure of cyclic (APGVGV)(2,) an analog of elastin, and a suggested mechanism for elongation/contraction of the molecule. *Biopolymers* **2005,** 77, (4), 198-204.
83. Kjaergaard, M.; Norholm, A. B.; Hendus-Altenburger, R.; Pedersen, S. F.; Poulsen, F. M.; Kragelund, B. B., Temperature-dependent structural changes in intrinsically disordered proteins: Formation of alpha-helices or loss of polyproline II? *Protein Sci* **2010,** 19, (8), 1555-1564.
84. Creamer, T. P.; Rose, G. D., Alpha-Helix-Forming Propensities in Peptides and Proteins. *Proteins* **1994,** 19, (2), 85-97.
85. Krukau, A.; Brovchenko, I.; Geiger, A., Temperature-induced conformational transition of a model elastin-like peptide GVG(VPGVG)(3) in water. *Biomacromolecules* **2007,** 8, (7), 2196-2202.
86. Receveur-Brechot, V.; Durand, D., How Random are Intrinsically Disordered Proteins? A Small Angle Scattering Perspective. *Curr Protein Pept Sc* **2012,** 13, (1), 55-75.
87. Wuttke, R.; Hofmann, H.; Nettels, D.; Borgia, M. B.; Mittal, J.; Best, R. B.; Schuler, B., Temperature-dependent solvation modulates the dimensions of disordered proteins. *P Natl Acad Sci USA* **2014,** 111, (14), 5213-5218.
88. Robertson, A. D.; Murphy, K. P., Protein structure and the energetics of protein stability. *Chem Rev* **1997,** 97, (5), 1251-1267.
89. Henriques, J.; Cragnell, C.; Skepö, M., Molecular Dynamics Simulations of Intrinsically Disordered Proteins: Force Field Evaluation and Comparison with Experiment. *Journal of Chemical Theory and Computation* **2015,** 11, (7), 3420-3431.
90. Lindorff-Larsen, K.; Piana, S.; Dror, R. O.; Shaw, D. E., How Fast-Folding Proteins Fold. *Science* **2011,** 334, (6055), 517-520.
91. Papoian, G. A.; Wolynes, P. G., The physics and bioinformatics of binding and folding—an energy landscape perspective. *Biopolymers* **2003,** 68, (3), 333-349.
92. Stephanopoulos, N.; Ortony, J. H.; Stupp, S. I., Self-assembly for the synthesis of functional biomaterials. *Acta Mater* **2013,** 61, (3), 912-930.
93. Dagdas, Y. S.; Tombuloglu, A.; Tekinay, A. B.; Dana, A.; Guler, M. O., Interfiber interactions alter the stiffness of gels formed by supramolecular self-assembled nanofibers. *Soft Matter* **2011,** 7, (7), 3524-3532.
94. Rajagopal, K.; Ozbas, B.; Pochan, D. J.; Schneider, J. P., Self-assembly of beta hairpin peptides to hydrogels and tuning of material properties by design of turn sequence. *Abstr Pap Am Chem S* **2004,** 228, U68-U68.

10.7 Supplemental Information

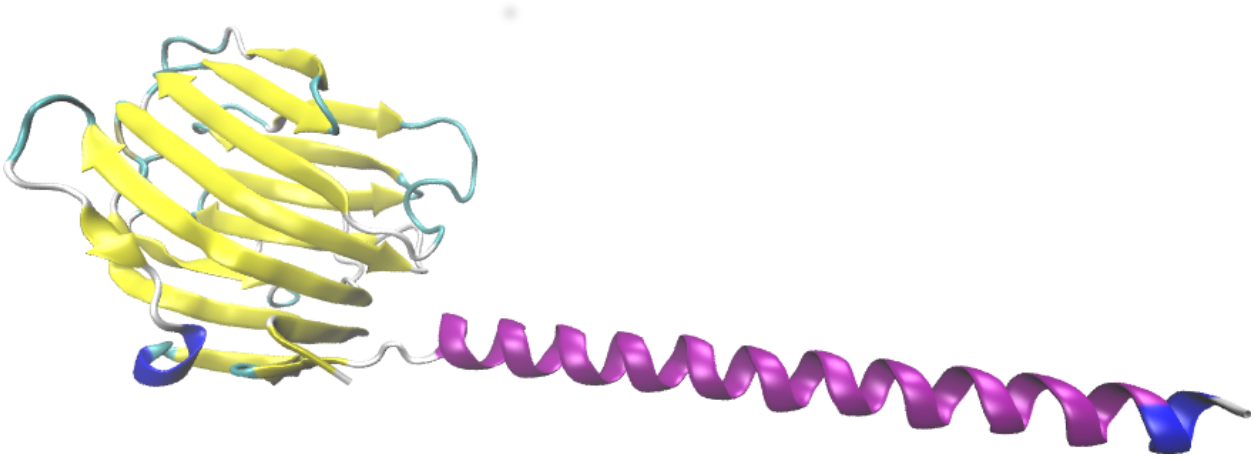

Figure 10-8. Initial starting structure of the LG-ELP protein. The LG5 domain was drawn from the crystal structure of the mouse homolog of the laminin α2 chain (1DYK), while the ELP domain was built using Avogadro's peptide builder, and was modelled as a canonical α-helix starting structure, with backbone torsion angles φ = –60°, ψ= –40.

Table 1. Summary of MD simulation systems of the engineered LG-ELP fusion protein. Atomistic MD simulations were performed using the NAMD 2.9 code and the CHARMM36 force-field for the protein system. The protein was solvated in explicit water with periodic boundary conditions and simulated as described in the Methods section.

System name	**Trajectory Duration (ns)**
LG5-ELP[K2L2I2K2]	Solvation, Minimization
LG5-ELP[K2L2I2K2]	Equilibration 10ns
LG5-ELP[K2L2I2K2] 290K	100
LG5-ELP[K2L2I2K2] 295K	100
LG5-ELP[K2L2I2K2] 300K	100
LG5-ELP[K2L2I2K2] 310K	100
LG5-ELP[K2L2I2K2] 315K	100
LG5-ELP[K2L2I2K2] 305K	100
LG5-ELP[K2L2I2K2] 320K	100
LG5-ELP[K2L2I2K2] 310K final trajectory to 290 K	40
LG5-ELP[K2L2I2K2] 310K final trajectory to 300 K	40
LG5-ELP[K2L2I2K2] 310K final trajectory to 320 K	40
LG5-ELP[K2L2I2K2] 310K trajectory extension to 200 ns	100

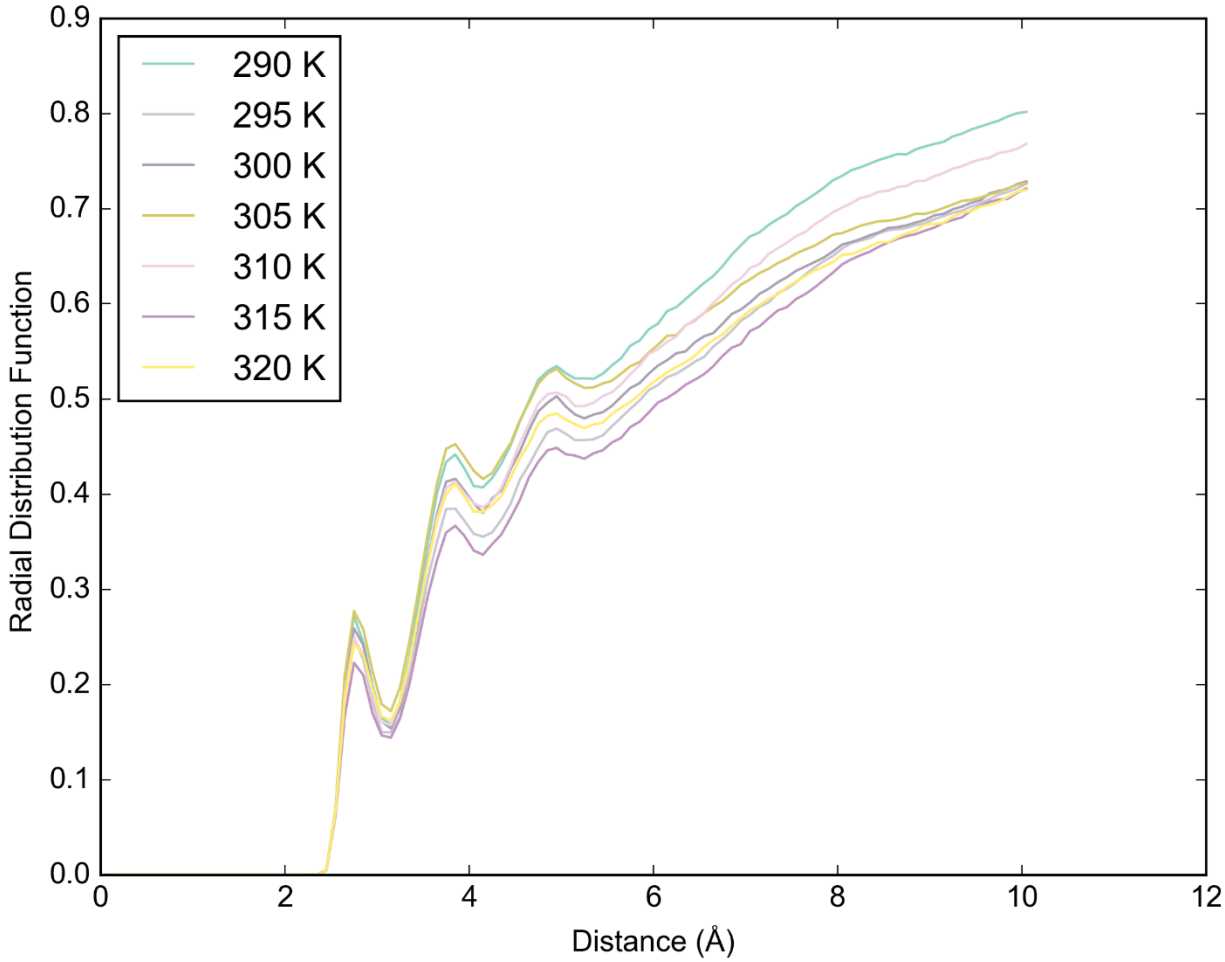

Figure 10-9. Radial distribution function (RDF) of oxygen atoms around the elastin-like polypeptide (ELP) backbone. The RDF is plotted as a function of temperature, and the first hydration shell was chosen to be the minimum for subsequent analysis in determining the number of surrounding water molecules (Figure 6a).

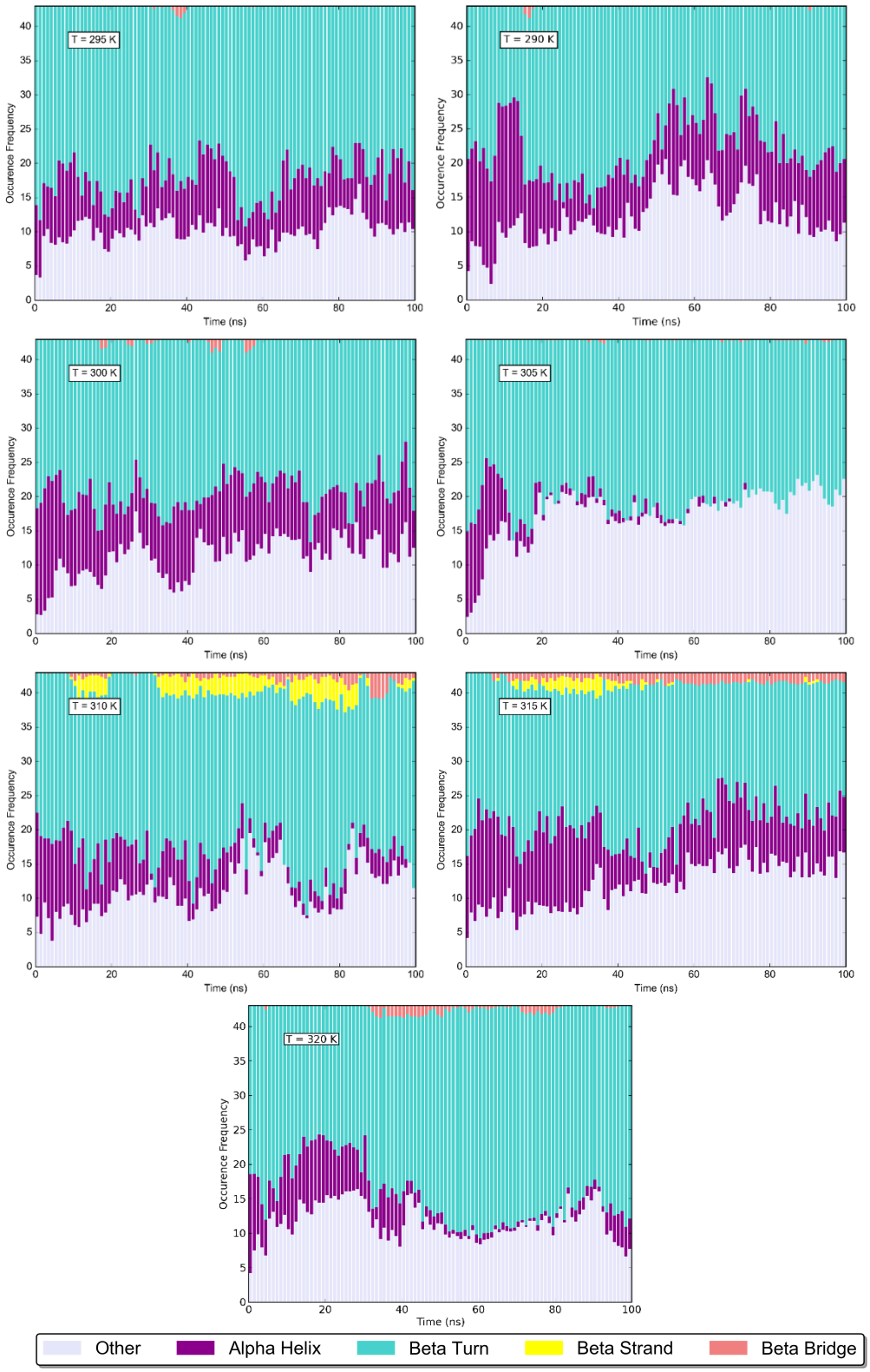

Figure 10-10. Secondary structural content across a range of temperatures as a function of time. Simulated systems were sampled at different temperatures (five degree increments from 290 K to 315 K).

A)

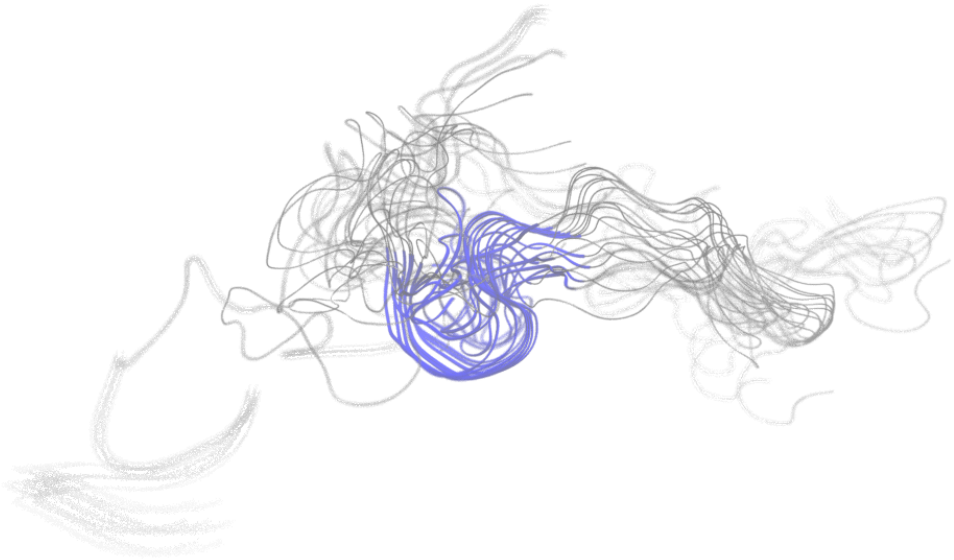

B)

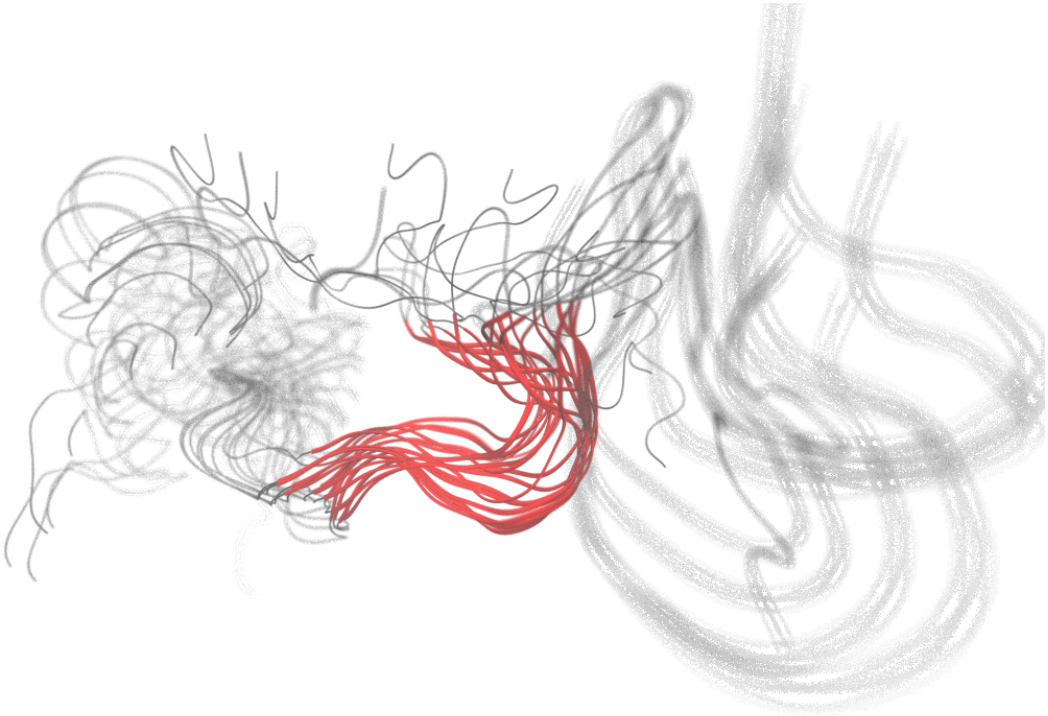

Figure 10-11. The time evolution of the secondary structure profile in the extended simulation at 310 K showed four distinct regions of persistent β-sheet like conformations, (a) Leu4-Gly5$_{200-201}$ - Leu4-Gly5$_{205-206}$ (highlighted by the blue ribbons) and (b) Ile4-Gly5$_{210-211}$ - Ile4-Gly5$_{214-215}$ (red ribbons) with reduced conformational flexibility. The trajectory was captured by overlaying multiple frames at 10 ns intervals.

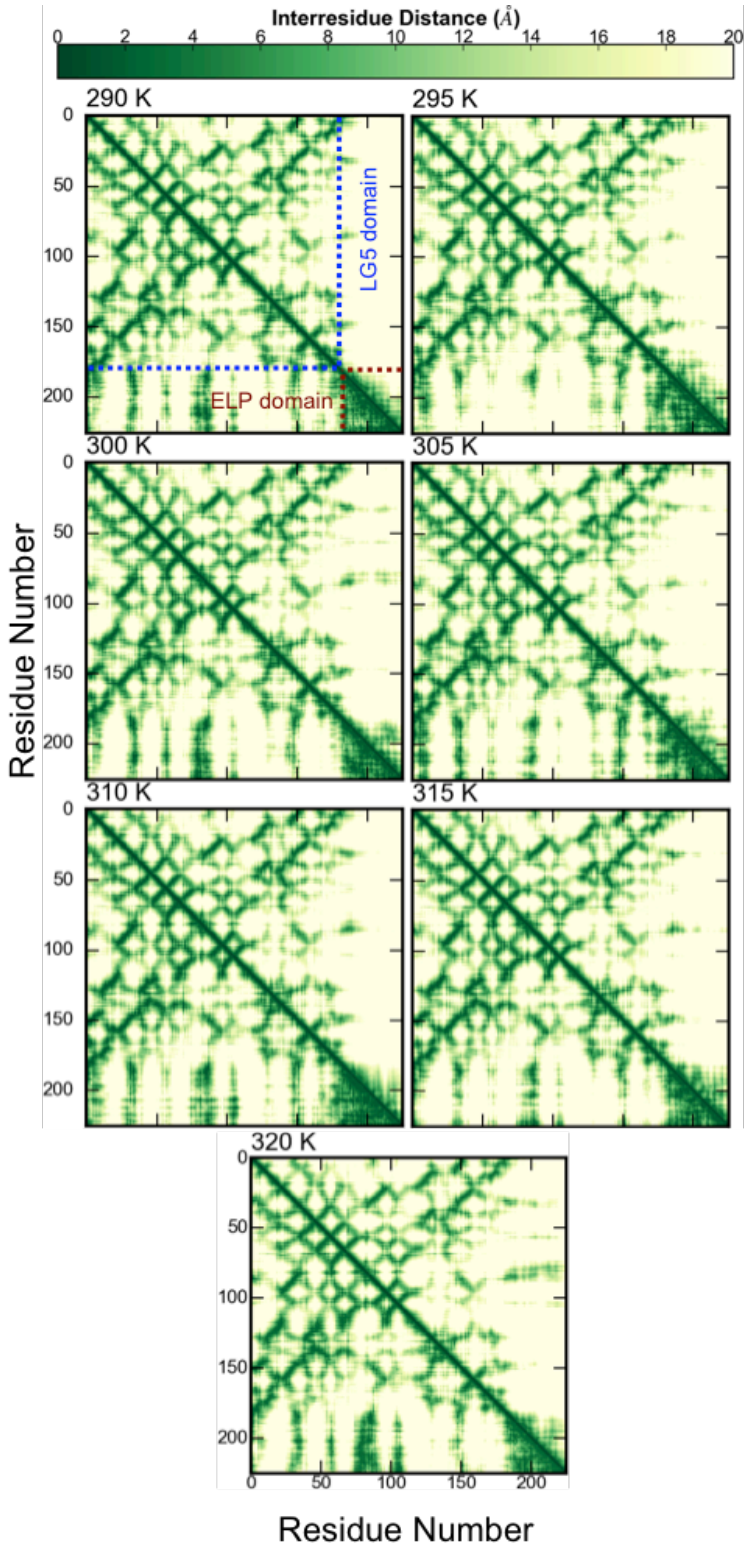

Figure 10-12. Protein contact maps of the dynamical interactions in the designed fusion suggest a lack of persistent LG···ELP interactions (for 290 K – 320 K).

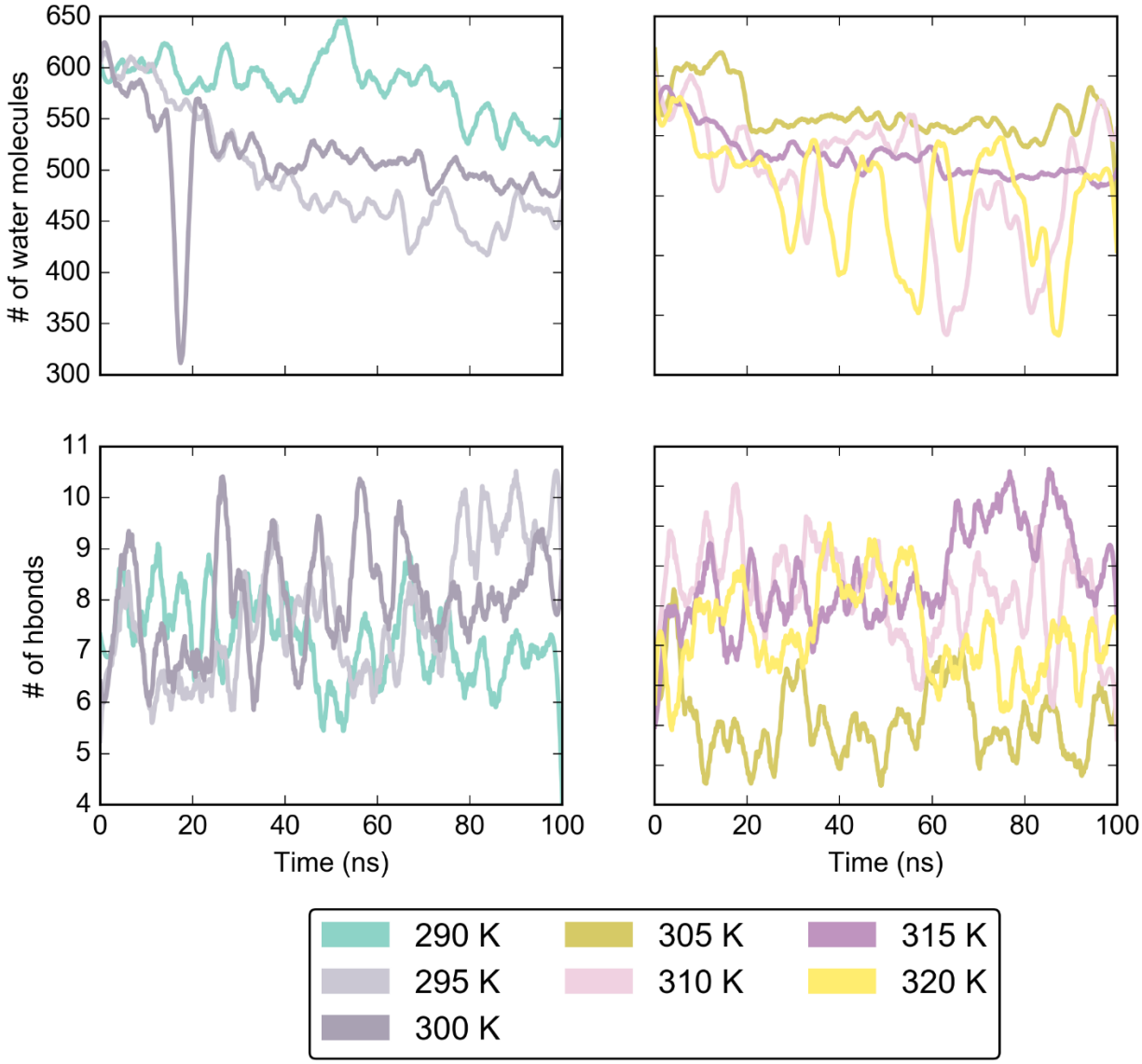

Figure 10-13. (A) Number of water molecules surrounding the ELP domain as a function of time. The abrupt drop in water molecules at 64 ns and 82 ns for 310 K corresponds to the formation of β-sheets. (B) Number of intramolecular hydrogen bonds as a function of time. All data was smoothed using a Savzky-Golay filter with a window size of 51 and 3rd order polynomial.

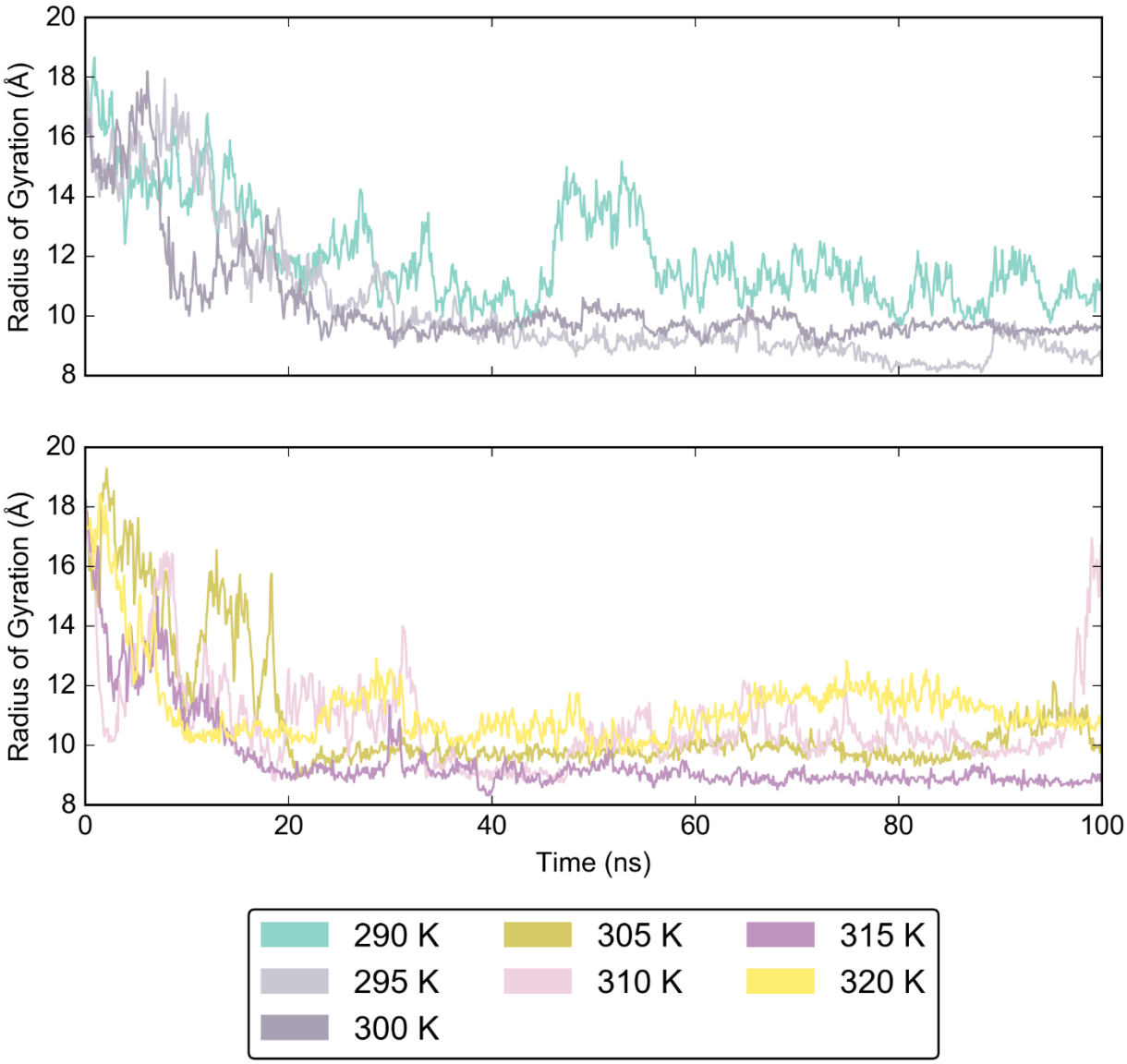

Figure 10-14. Time evolution of the radius of gyration simulated at different temperatures.

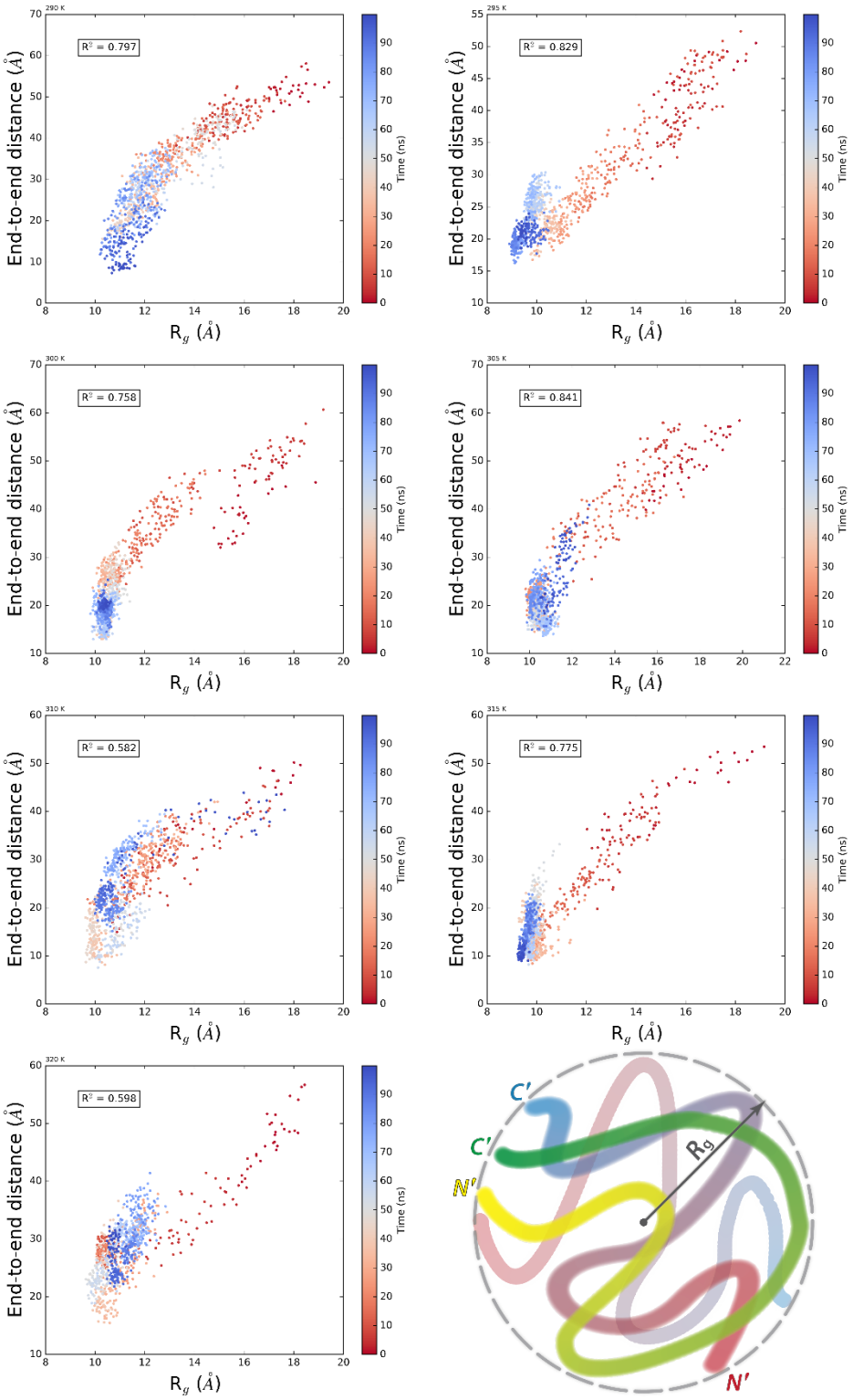

Figure 10-15. Correlation between the radius of gyration and end-to-end distance of the ELP domain. We computed a least-squares regression using SciPy's stats function. R2 is the coefficient of determination. Colors correspond to the time steps in the simulation (red indicates first time step, blue is the last time step of the MD simulation). The following schematic represents the differences between the end-to-end distance (Euclidean distance between N'- and C'- termini) and radius of gyration (Rg) of a random coil.

11 Appendix 3: Temperature-dependent complex coacervation of engineered elastin-like polypeptide and hyaluronic acid polyelectrolytes

Published as: JD Tang, SR Caliari, KJ Lampe, "Temperature-dependent complex coacervation of engineered elastin-like polypeptide and hyaluronic acid polyelectrolytes," *Biomacromolecules*, 19: 3925-3935 (2018)

11.1 ABSTRACT

Coacervates have enormous potential due to their diverse functional properties supporting a wide number of applications in personal care products, pharmaceuticals, and food processing. Normally, separation of coacervate phases is induced by changes in pH, ionic strength, and/or polyelectrolyte concentration. This study investigates the microphase separation and coacervate complex formation of two natural polyelectrolytes, elastin-like polypeptides (ELPs) and hyaluronic acid (HA), as simple models for biological coacervates. These complex coacervates are formed over a wide range of stoichiometric molar charge ratios without the presence of salt or changes in pH, and are primarily induced by changes in temperature. Unlike pure ELP solutions, the ELP/HA coascervates result in well-formed spherical particles after the temperature-induced phase transition. We also note that the formation of these complex coacervates is reversible, with low hysteresis. We have demonstrated via fluorescent imaging and dynamic light scattering that high positive/negative charge ratios at elevated temperatures produced 400-600 nm particles with relatively low polydispersity indices (PDIs) of ~0.1. Furthermore, dynamic light scattering, fluorescence microscopy, and optical microscopy revealed that the ratio of the two polyions strongly influenced the size and structure of these ELP/HA complex coacervates. Finally, we showed that the ELP/HA coacervates were able to sequester the hydrophobic fluorescent molecule pyrene, highlighting their potential for use as delivery vehicles for hydrophobic payloads.

11.2 Introduction

Polyelectrolyte complex (PEC) coacervates are a unique class of hybrid materials that can self-assemble into a variety of structures such as micellar-like particles,[1-2] vesicles,[3] and hydrogels[4] via

changes in solution pH or ionic strength. The formation of these coacervates is primarily driven by electrostatic interactions between oppositely charged polymers, and can lead to phase separation of aqueous solutions and complex coacervate particles[5]. Similarly, biopolymers often have additional driving forces that direct the association of PECs, such as hydrogen bonding and hydrophobic forces. The stoichiometric mixture of charge densities[6-7] as controlled by solution concentrations[8] and chain lengths,[9] determines the extent of attractive forces between the two polymers[10]. The importance of PECs is evident in numerous applications such as drug[3, 11-12] and gene delivery,[13-14] thin film coatings,[15-17] or processed food.[18-22] Coacervate usage is wide ranging, and warrants a broader understanding of the properties of these PEC coacervates, and individual parameters that drive phase separation and coacervate complexation. In this study, we employed the use of naturally-derived elastin-like polypeptides and hyaluronic acid, as their biodegradability and biocompatibility make them suitable for biomedical applications[23-25].

Elastin-like polypeptides (ELPs) exhibit a thermally-triggered first-order phase transition behavior in which they separate into polymer-rich and water-rich phases[26], where this behavior is characterized by a phase separation process at what is known as the lower critical solution temperature (LCST). The phase transition behavior at the LCST depends on both (i) intrinsic factors, such as the amino acid composition and the number of $(VPGXG)_n$ pentapeptide repeats ('X' denotes a 'guest' residue, which can vary from one repeat to another), as well as (ii) extrinsic parameters, such as the pH, ionic strength, and other bulk solution properties.[27-29] Likewise, the inherent, heterogeneous secondary conformations present in ELPs are highly system-specific, i.e. the temperature transitions can be modulated by variations in the polypeptide sequence, as well as the addition of biological complexes, such as peptide amphiphiles[30] or positively/negatively charged biomolecules[31].

ELPs above the LCST form aggregates and a highly collapsed protein conformation in aqueous environments. Variations in the amino acid composition allow for the control of the particular LCST where this phase transition occurs[32-33]. Polyelectrolyte coacervate formation using ELPs is advantageous due to their remarkably temperature-sensitive phase separation properties.[27, 32, 34] In our engineered ELP, with the guest 'X' residues being isoleucine (I) or lysine (K), the distinct hydrophobic (I) and positively-charged hydrophilic blocks (K) can be tuned to adjust the phase separation temperature of the polypeptide.[35] Additionally, the biocompatibility of ELPs and the

ability to tune their mechanical properties to influence cell behavior[35-36] are especially useful in tissue engineering[37-38] and drug delivery applications.[39-40]

Hyaluronic acid (HA) is a negatively charged, linear polysaccharide containing repeating units of N-acetylglucosamine and glucuronic acid. *In vivo,* HA is a hydrophilic polyanionic macromolecule that is an essential component of the extracellular matrix.[41-42] HA and its modified forms have a wide range of applications as medical products due to their biocompatibility, mechanical properties, and lack of immunogenicity[43-45]. Additionally, a class of HA-based hybrid polyelectrolyte biomaterials examined in early pioneering studies combine HA with chitosan,[46-47] poly(vinyl alcohol),[48] poly(L-lysine),[49-51] and more recently peptide amphiphiles,[4, 52-55] highlighting the versatility of HA to complex with a diverse set of cationic polymers.

While the ionic strength dependency of PEC assembly has been studied extensively in the field, the effect of temperature on polyelectrolyte complexation has attracted relatively little attention. Generally, coacervate complexation occurs via electrostatic charge-screening within the polyelectrolyte solution. Here we examine the ionic complexation of positively-charged ELP and negatively-charged HA with a mechanism of complexation that relies on temperature perturbation of the polyelectrolyte solutions. We document the formation of self-assembled coacervate particles as a result of the electrostatic associative interactions between ELPs and HA. Combining ELP and HA solutions led to a distinct microphase separation process, and the formation of spherical particles, as solution temperature increased. We examined the structural properties of the particles using scattering and microscopy techniques, and find evidence that coacervate formation was dependent on molar charge ratios of ELP and HA composites at elevated temperatures. Fluorescent analysis of TRITC-labeled ELP polymers and HA coacervates demonstrated that a critical coacervation concentration between 0.2 wt. % and 0.3 wt. % of total polymer concentration is required for the formation of coacervates at elevated temperatures. The polymer concentration required to achieve coacervation also increased with increasing charge ratio.

11.3 **Materials & Methods**

2.1 Elastin-like polypeptide synthesis and purification

Recombinant ELPs were synthesized and purified as previously reported.[35-36] Briefly, BL21 (DE3) *Escherichia coli* transformed with a pET15b plasmid incorporating our ELP sequence, $LQ[LDAS-TVYAVTGRGDSPASSAA-SA((VPGIG)_2VPGKG(VPGIG)_2)_3VP]_4LE$, were cultured to

an OD_{600} of 0.8. Protein expression was induced with 1 mM isopropyl β-D-1-thiogalactopyranoside (IPTG) for 6-8 h. Cell pellets were collected and resuspended in TEN buffer (0.1 M NaCl, 0.01 M Tris Hydrochloride, 0.001 M ethylenediaminetetraacetic acid (EDTA), pH 8), and underwent three freeze-thaw cycles, with 1 mM phenylmethanesulfonyl fluoride (PMSF) in isopropanol (IPA) and a few micrograms of deoxyribonuclease added after the first freeze/thaw cycle. After the last thaw cycle, the ELP was then subjected to three iterative temperature cycling and centrifugation steps at 4 °C in H_2O (pH 9) where the protein was in solution, and 37 °C where ELP precipitated in the presence of 1 M NaCl. Purified ELP was dialyzed against diH_2O using a cellulose ester membrane with a 500-1000 Dalton cut off (Spectrum Laboratories, Inc.) and lyophilized. Purity was confirmed by SDS-PAGE, with a molecular weight of 35.1 kDa. The theoretical pI of this ELP is calculated to be 9.89[56], indicating that all lysine residues within the engineered ELP sequence are protonated and positively charged. In some cases, ELP was labeled with tetramethylrhodamine-5-(and 6)-isothiocyanate (TRITC) (Life Technologies) following manufacturer's protocol and utilized for experiments noted below (ELP_{TRITC}). Briefly, synthesized ELP was dissolved in a 100 mM conjugate buffer (8.4 mg/ml $NaHCO_3$, 28.62 mg/ml $CH_{20}Na_2O_{13}$, mixed in a 9:1 volumetric ratio, respectively, adjust to pH 9) at 5 wt. %. TRITC was then added to the ELP solution at a 1:250 isothiocyanate to primary amine ratio, and shaken overnight at 4 °C. Unreacted fluorophore was removed using a Zeba™ desalting column (7,000 MWCO) (Thermo Fisher Scientific), and the final solution was lyophilized.

2.2 Preparation of Hyaluronic Acid/ELP coacervates

350 kDa HA (estimated 800 negatively charged carboxylic groups on a per molecule basis) was obtained (Lifecore Biomedical). The pKa of HA carboxyl groups is 3-4; at pH = 7, suggesting that these groups are ionized.[57] Lyophilized ELP (with 17 available positively charged groups on a per molecule basis) and HA were solubilized in diH_2O and mixed at different charge ratios, $f^{+/-}$:

$$f^{+/-} = \frac{[NH_3{}^+]}{\left([NH_3{}^+] + [COO^-]\right)} \quad (1)$$

where a $f^{+/-} = 0$ or $f^{+/-} = 1$ indicates solutions of ELP or HA alone, respectively. The pH was adjusted to 7 and the ELP/HA solution was heated to 37°C for 10 minutes. TRITC-modified ELP (ELP_{TRITC}) was used at a 1:20 molar ratio of ELP_{TRITC} to non-labeled ELP for all fluorescent

experiments, unless otherwise noted. Solutions of ELP_{TRITC}/HA were prepared at total polymer concentrations of 0.1 mg/ml to 10 mg/ml for each charge ratio to calculate the critical coacervation concentration. The formation of ELP_{TRITC}/HA coacervate particles was probed using a Zeiss LSM 510 confocal laser scanning microscope (Thornwood, New York) equipped with a stage-top incubator for temperature control. Temperature was increased using a ramp of 1°C/min alternating with an equilibration time of 10 minutes at each degree to allow for sufficient time for observing particle formation and imaging. Fiji[58] was used for particle analysis of fluorescent images taken with the confocal microscope. Auto-thresholding was used to sample pixel intensities, and the 'analyze particles' plug-in was used with the following parameters: size (μm^2) of 0-999 with a circularity of 0.00-1.00. "Large" particle formation refers to objects with a cross-sectional area greater than or equal to 1 μm^2.

2.3 Lower critical solution temperature analysis

Solutions of ELP/HA at a total polymer concentration of 5 mg/ml in water were heated with ramp-stamp function using a temperature ramp of 1°C/min and holding at that temperature for 2 min at each step for equilibration. This particular concentration was chosen as to not bias protein aggregation, which occurs at high protein concentrations,[59] and to minimize structural heterogeneity incurred from ELP unimer (non-interacting) collapsed structures that would otherwise influence the complexation with HA[60-63]. Solution turbidity at 350 nm was monitored as a function of temperature using a CLARIOstar® plate reader (BMG Labtech). The sample plate was agitated for 30 s before each reading. The transition temperature (T_t) was defined as the temperature at which the OD reaches the inflection point of the transition-induced change.

2.4 Determination of the critical coacervate concentration (CCC) of ELP/HA coacervate complexation

The fluorescence emission spectrum of ELP_{TRITC}/HA was obtained at an excitation wavelength of 475 and emission was recorded between 500 and 700 nm, using a CLARIOstar® plate reader. Fluorescence emission of TRITC was examined in ELP/HA solutions from 0.1 mg/ml to 10 mg/ml. Both excitation and emission slits were set to a bandwidth of 10 nm. All fluorescent experiments were carried out at 37°C. The corresponding fluorescent peaks at 575 nm for all

concentrations can be adequately described by a decreasing sigmoid curve. Briefly, the Sigmoidal-Boltzmann equation (2)[64-65] was employed to determine the CCC.

$$y_F = \frac{(a_i - a_f)}{1 + \exp\left[(x_{CCC} - x_0)/\Delta x\right]} + a_f$$

(2)

where y_F is the fluorescence intensity, a_i and a_f are the initial and final asymptotes of the sigmoid, respectively, x_0 is the center of the sigmoid, and Δx is the independent variable range. The CCC was analytically determined from the intersection of the tangent to the sigmoid passing through its center and the first asymptote.

2.5 Dynamic light scattering

Dynamic light scattering (DLS) experiments were performed on a DynaPro Nanostar instrument from Wyatt Technology (Santa Barbara, CVA, USA). A laser wavelength of 660 nm was used. The number of acquisitions was 10, with an acquisition time of 5 sec and an auto-attenuation time limit of 60 sec. The correlation function low and high cut-off was 1.5 µs and 107000 µs, respectively, and resulting hydrodynamic radii were determined based on the Stokes-Einstein relationship. Solutions of ELP/HA at a total polymer concentration of 5 mg/ml and 10 mg/ml in water were heated from 26 °C to 50 °C using a ramp-step function with at a ramp rate of 1°C/min and an equilibration time of 5 min at each step.

2.6 Pyrene loading and determination of excimer formation

Pyrene was prepared according to previously published methods.[66-68] Briefly, a stock solution of 5 x 10^{-7} M pyrene was prepared by adding ethanol into a known mass of the compound. 100 µl of the stock solution was allowed to evaporate overnight under ambient conditions and form a pyrene film. An equal volume of ELP and HA was then added to the pyrene film and incubated at 37°C for 30 min before measuring fluorescence via a CLARIOstar® plate reader. Excitation was performed at 328 nm (bandwidth of 8 nm) and emissions were recorded from 350 to 550 nm at 1 nm intervals (bandwidth of 10 nm).

11.4 **Results and Discussion**

In this work, temperature was used to modulate coacervate formation of ELP and HA PECs. Unlike other PEC systems, where the formation of these coacervates are induced by changes in pH or ionic strength of the solution, the microphase separation regime of the ELP/HA complex can simply be tuned by temperature. We demonstrated through optical density studies show that the solution becomes turbid upon warming. We also show that the charge ratio of the ELP/HA complex influences the size of the coacervate being formed. Additionally, temperature is used as a trigger to reversibly assemble monodisperse complex coacervates that are amenable to loading of hydrophobic payloads. The measurements carried out in this study refer to the nonequilibrated state, or 'discontinuous' phase, as indicated by the elevated temperatures of the solution. We report here results from dynamic light scattering and fluorescent microscopy techniques that support the notion that the structural dynamics of coacervation complexes are dominated by the charge density of the PECs, as well as changes in solution temperature.

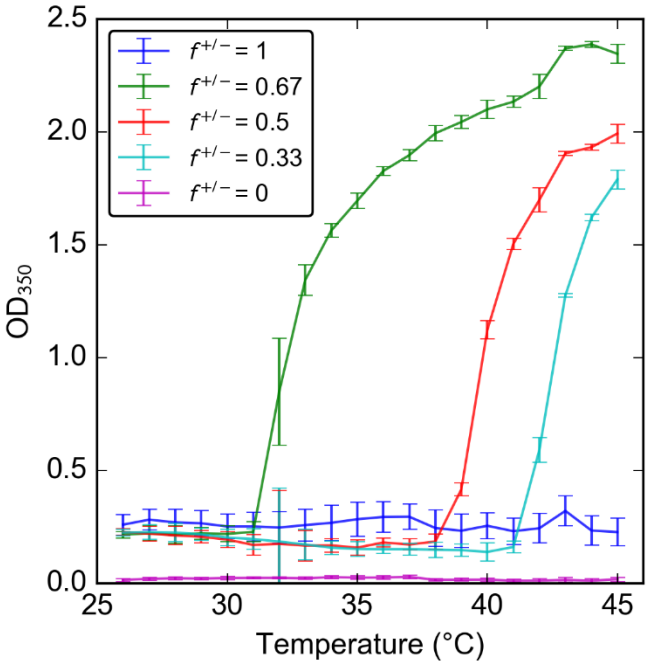

Figure 11-1. Turbidity profile versus temperature of ELP/HA mixtures. The rapid change in turbidity as the solution temperature increased indicates formation of complex coacervates. The inflection point of the sigmoidal curve is noted as the transition temperature (Tt), which is dependent on the charge ratios (f+/-), the stoichiometric ratios between the charged groups within cationic ELP monomers and all charged groups. Pure solutions (0.5 wt. %) of the two components (f+/- = 1 for ELP alone, f+/- = 0 for HA alone) do not exhibit a change in the optical density as a function of temperature at this concentration, highlighting the importance of electrostatic interactions within the

combination solution in order to propagate ionic complexation and coacervation. Charge ratios f+/- = 1 are represented by a blue line, 0.67 (green), 0.5 (red), 0.33 (cyan), and 0 (purple). Optical density of solutions was measured at 350 nm. All experiments were conducted at 0.5 wt. % of total polymer. Error bars represent standard deviation (3 replicates).

Turbidity profile of ELP/HA coacervate formation. We monitored the optical density of ELP/HA solutions upon heating from 26 to 45 °C. Changes in the measured light transmission depend on the size and composition of the coacervate being formed, thus turbidity reflects the extent of PEC coacervate formation[8]. Coacervation (liquid-liquid phase separation) of ELP with HA occurred and the phase transition temperature, T_t, was strongly dependent on charge ratio (Figure 1). As these experiments were conducted in the absence of salt, the particular driving force behind coacervate formation was that of temperature. The observed coalescence near the putative transition temperature is primarily driven by temperature-indcued ELP conformational transitions leading to the hydrophobic association of PECs. Increasing the charge ratio from 0.33 to 0.67 increased the turbidity of the 0.5 wt. % ELP/HA solution above the T_t (Figure 1). The 0.5 wt.% polymer concentration was chosen as to not bias inherent ELP polymer collapse, which would otherwise influence charge-charge interactions between the negatively charged repeating units of HA[69]. Additionally, we observed the same trends at 1 wt. % coacervates (Figure S1).

A plot of the binary solution phase behavior as a function of temperature of $f^{+/-} = 0.33$, 0.5, and 0.67 indicated that the T_t occurs at 42, 38, and 32°C, respectively. The rapid change in turbidity as the solution temperature increased indicates formation of complex coacervates.[8, 70-71] Interestingly, pure ELP solutions at 0.5 wt. % ($f^{+/-} = 1$) do not display a classical sigmoid curve under the same temperature conditions, as measured via OD. In dilute solutions, it is possible that the collapse and aggregation of individual ELP polymer chains kinetically arrests the formation of larger globules that result from the accumulation of individual chains. As such, we have shown that an LCST-like behavior can only occur through complexation of ELP with HA, whereas individual components at the measured temperature ranges do not exhibit such phase separation behavior. This coil-globule transition phenomenon has also been shown to occur in other polymers that exhibit LCST behavior.[72-74] The lack of intermolecular globule-formation behavior may also be attributed to the low diffusional association (i.e. diffusion-mediated encounters/collisions or association rates) of individual polymer chains (e.g. protein-protein interactions). As such, we expect that there are significantly less collisions occurring in order for attractive forces to have an effect.[75]

As the charge ratio increases, the sigmoidal phase transition curve shifts towards lower temperatures. This suggests that the water network around HA (as the HA concentration is increased) provides more resilience to the enthalpic dehydration of the hydrophobic backbone of the ELP. However, as water molecules are dehydrated from ELP, they also gain considerable translational entropy. Thus, both enthalpic and entropic interactions likely contribute to LCST behavior. Normally, the ELP phase transition in this temperature range is accompanied by gross structural rearrangements, highlighted by the solvent-exposed, hydrophobic regions of the ELP backbone at elevated temperatures.[76] However, the addition of HA seems to perturb the intra-protein interactions that would otherwise lead to desolvation of nonpolar side-chains within the ELP chain. Consequently, as the solution temperature reaches the T_t, this leads to fewer occurrences of a Flory coil-collapse globule transition of the ELP chain.[77-78] For this particular study, however, only combination solutions of HA and ELP together exhibited microphase separation at its nonequilibrated state, highlighting the importance of the additional polyanion to propagate ionic complexation and coacervation.[2, 79]

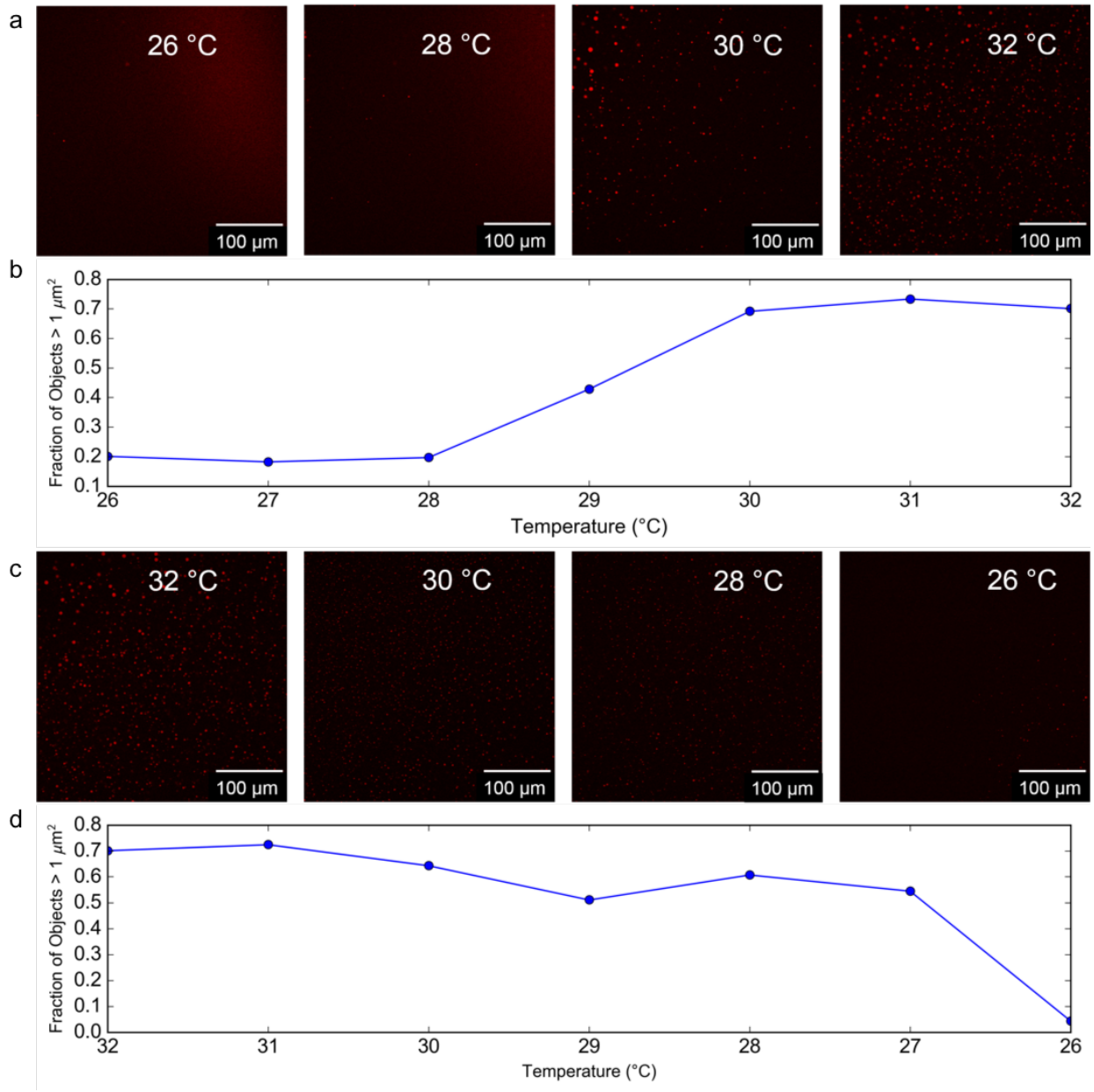

Figure 11-2. Visualization of reversible ELP/HA coacervation and particle formation as a function of temperature. As the temperature of the solution is increased, representative fluorescent confocal microscopy images of indicated microphase separation of 0.5 wt. % ELP/HA coacervates (at f+/- = 0.67) and an increase in particle size (a). Quantification of these images shows that the fraction of larger coascervate complexes/particles (above 1 µm2) increases as the temperature is increased (b). As the temperature decreases, the population of larger coacervate complexes decreases, highlighting the reversibility of the ELP/HA system (c), and the number of larger coacervate complexes (> 1 µm2) virtually disappear as the solution reaches room temperature (d).

Visualization of coacervate and solution phases. After showing that ELP/HA polyelectrolyte mixtures could form coacervate complexes through changes in turbidity, we used imaging of the

microphase separation induced by a temperature increase to probe the dynamics of the coacervate phase. At equilibrium (room temperature), the $f^{+/-}$ = 0.67 charge composition is seen as a well-mixed dispersed solution (Figure 2a). An $f^{+/-}$ = 0.67 was used because it had the lowest transition temperature at 34 ˚C (all other charge ratios were > 40 ˚C) and was therefore more physiologically relevant for our applications. A slight perturbation of the equilibration state by increasing the temperature results in a phase separation regime (i.e. phases that retain large amounts of water, and a phase with very high local polymer concentrations) where water molecules are dispersed (Figure 2a). This leads to increasing occurrences of electrostatic interactions between the positively charged $–NH_2$ groups in ELP and negatively charged –COOH groups of HA. Therefore, the intermolecular interactions between the two side chains primarily dictates the aggregation of the oppositely charged chains, as opposed to the intermolecular hydrogen bonding between the two chains that are held in place by the surrounding water network[80]. As the temperature increases, the droplets coalesce and a coacervate-solution boundary is slowly revealed at a new temperature equilibrium resulting in a number of spherical mesoscopic globules. DLS experiments indicate that these particles have monodisperse size distributions (Table 1). Pure HA ($f^{+/-}$ = 0) demonstrates multimodal behavior in DLS studies. It should be noted that at least two different peaks are present within HA solutions (Figure S4). The hydrodynamic radii for monomeric HA units are measured at 5 – 6 nm for both temperatures, and larger aggregates ranging from 1200 – 2000 nm, which is typical for HA in aqueous solutions[81]. The large HA peaks have different mean radii, 2060 and 1260 nm at 20 °C and 37 °C, respectively. However, these values are not statistically different, and therefore the temperature change is unlikely to strongly impact HA size/conformation.

Table 2. Summary of macromolecular characteristics of 0.5 wt. % ELP/HA coacervates as function of charge ratio ($f^{+/-}$) ($f^{+/-}$ = 0 for HA alone, $f^{+/-}$ = 1 for ELP alone). T_t is the transition temperature, as determined by the inflection point of the sigmoidal curve in the turbidity profile. CCC is the critical coacervate concentration derived from fluorescence experiments at 37°C and application of the Sigmoidal-Boltzmann equation. The hydrodynamic radius (R_H) and polydispersity index (PDI) were measured by dynamic light scattering.

$f^{+/-}$	T_t (°C)	CCC (mg/ml)	Hydrodynamic Radius (nm)			
			20°C	PDI	37°C	PDI
0	N/A	-	Monomer 5.09 Aggregate 2060	Multimodal	Monomer 6.16 Aggregate 1260	Multimodal
0.33	42	2.02	17.9 ± 5.9	Multimodal	1490 ± 230	0.11

0.50	38	2.07	12.5 ± 0.4	Multimodal	1050 ± 180	0.13
0.67	32	2.85	29.9 ± 1.4	0.28	456 ± 24	0.04
1	> 45	4.14	3.6 ± 0.1	0.18	470 ± 18	0.16

As the temperature was raised, the number of particles < 1 μm^2 rapidly decreased, while a steady increase in larger particles was seen (Figure 2b). Additionally, we see that the coacervate complexation is reversible, with low hysteresis, as the temperature decreases back to room temperature (Figure 2c). The larger particles begin to disappear, and the previously established phase separation is no longer observed. It is interesting to note that a greater fraction of larger particles persists to lower temperatures during the reverse temperature cycle (Figure 2d), although this does not appear to be a kinetic effect, since the phase separation upon heating was highly reproducible (Movie S1). Additionally, as the temperature increases, the number of smaller particles (< 1 μm^2) rapidly decreases, while the number of larger particles steadily increases (Figure S2). It is plausible that the perturbation of the ELP backbone induced by a temperature change results in a stable structural conformation.[82-83] This suggests that a population of preexisting conformations are maintained at lower temperatures, which has previously been demonstrated through molecular dynamics simulations.[74]

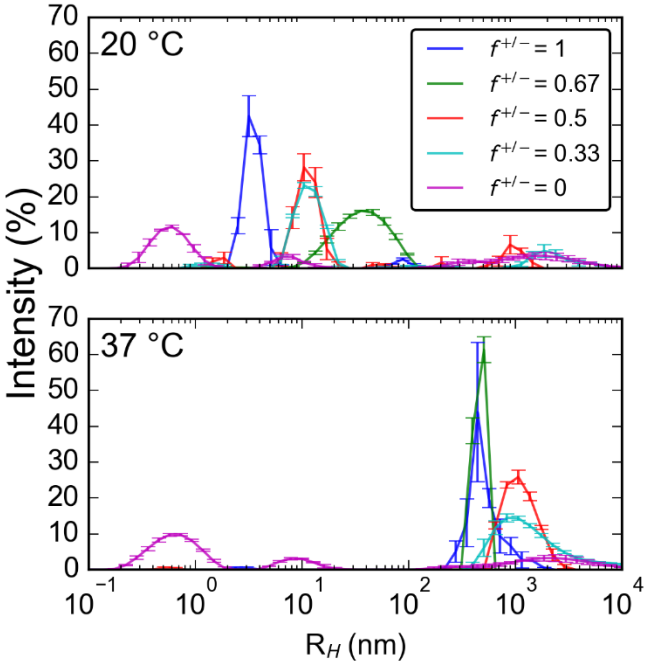

Figure 11-3. Dynamic light scattering size distribution profiles of different charge ratios for ELP/HA coacervation complexes at 20 °C and 37 °C ($f^{+/-}$ = 1 for ELP alone, $f^{+/-}$ = 0 for HA alone). All formulations of ELP/HA complexes exhibit polydisperse populations at 20 °C, but increase in size upon heating, and display a unimodal distribution at 37°C. The multiple intensity peaks of pure HA ($f^{+/-}$ = 0) at both temperature conditions demonstrate the exceedingly polydisperse properties of the HA polymer. However, peak distribution completely transitions to a monodisperse population once ELP is introduced, regardless of the charge density of the total polymer solution. Error bars represent standard error of the mean (3 replicates).

Particle size distribution of ELP/HA coacervates. To determine the influence of the charge density on the size and polydispersity of the PECs, we measured the particle size and distribution as a function of temperature using dynamic light scattering. Decreasing the charge ratio resulted in an increase of the hydrodynamic radius (R_H) of ELP/HA particles (Figure 3). Additionally, particle size also increased as the temperature of the solution increased, highlighting the aggregation propensity of the ELP/HA composition (Figure S3). The ELP/HA particle radius increased by approximately 500 nm for each stoichiometric addition of positively-charged HA (Table 1). Despite the potentially variable size distributions that are often incurred with aggregation-prone ELP chains[84-86] and heterogeneous size distributions of HA,[81, 87-88] it should not be surprising then that the polydispersity index (PDI) of the PECs displayed multimodal size distributions at 20°C.

A charge ratio of 0.67 showed a low intensity of scattered light at a R_H of 29.9 nm at 20°C highlighted by its broad peak, and a sharp and strong intensity of scattered light at 455 nm at 37°C (Figure 3). Small ~4 nm nano complexes were formed in the absence of HA with low PDI at nonequilibrium conditions; while at equilibrium, the relatively moderate PDI indicates that the samples are polydisperse. Previous studies have indicated that salt ions within the coacervate complex associates specifically with charges on weak polyelectrolytes[8-9, 89]. This equilibrium state demonstrates that the morphologies of the complexes are held together by polyelectrolyte/ion pairing[90]. However, our system is unique in that the instantaneous formation of coacervates is primarily driven by temperature perturbations of the PEC system. Compared to other studies involving the mixing of HA and other positively charged polymers[69, 91], the ELP/HA coacervate-solution boundary phase occurs in the absence of salt, highlighting the simplicity of our coacervate model.

The significant differences found in size distributions at the two temperatures suggests that ELP unimers are prone to intramolecular chain collapse[92] (i.e. self-association), as indicated by the high intensity peaks of 3.6 nm at 20 °C before an elevation of temperature induces a intermolecular

chain aggregation typical of LCST behavior at the T_t.[74, 84] The polydispersity index of ~0.1 indicates a homogenous size of coacervate complex particles (Table 1). Complexes of ELP with HA were greater than 400 nm in size for all charge ratios, with low PDI at nonequilibrated conditions, indicating monodisperse particle size distributions, irrespective of the molar ratio of positive and negative charges. While the total polymer concentration of the ELP/HA solution was held constant, the ratio of positive and negative charges was changed to achieve a desired charge density. Therefore the increase in particle size was due to the molar charge ratio of the ELP to HA polymers.

Interestingly, all ELP/HA complex mixtures increased in size upon heating, and display a unimodal distribution at 37°C. The multiple intensity peaks of HA at both temperature conditions demonstrate the exceedingly polydisperse properties of the HA polymer, but this peak distribution completely transitions to a monodisperse population once ELP is introduced, regardless of the charge ratio of the total polymer solution. This highlights the importance of the intermolecular interactions of the PECs, such that the complexation requires both polymers, and that the temperature-induced self-assembly plays an essential role in coacervation formation. Likewise, the accessibility of the positively charged lysine groups within ELP molecules have likely been more solvent exposed at the temperature transition. This also suggests that temperature is able to modulate the structural homogeneity and subsequently, coacervate formation in aqueous polypeptide-polysaccharide complexes.

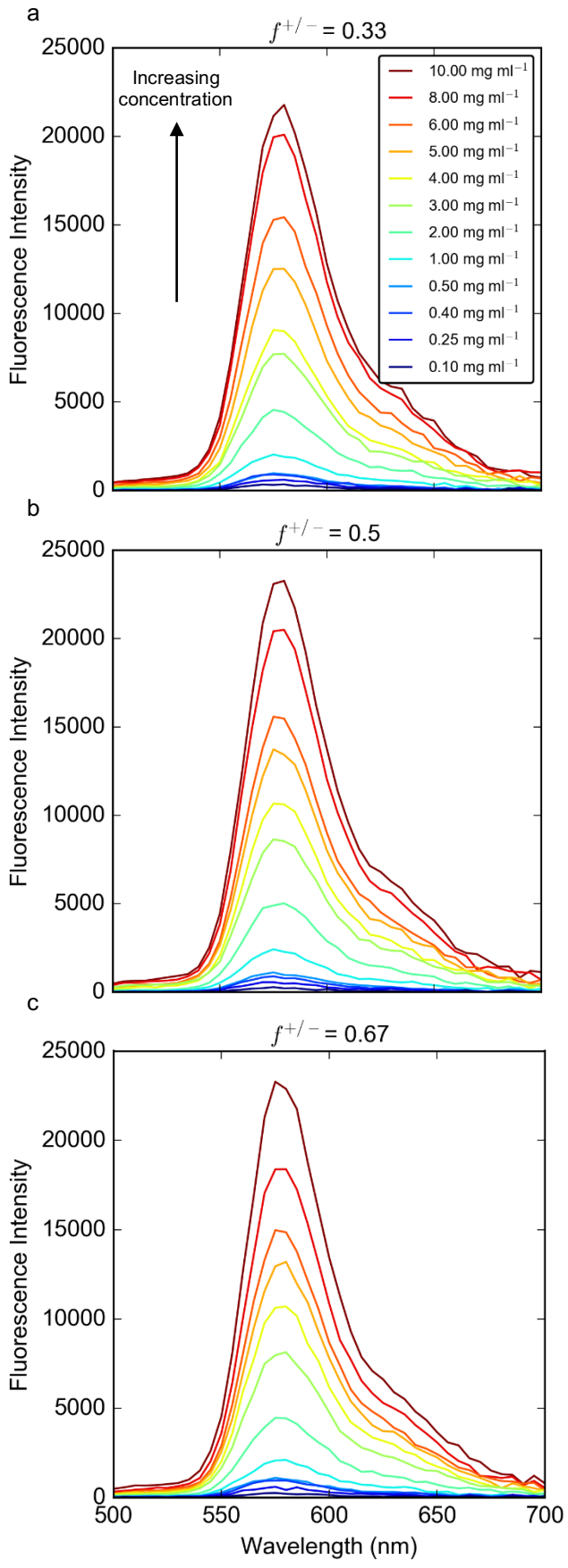
a
$f^{+/-}$ = 0.33
Increasing concentration
10.00 mg ml^{-1}
8.00 mg ml^{-1}
6.00 mg ml^{-1}
5.00 mg ml^{-1}
4.00 mg ml^{-1}
3.00 mg ml^{-1}
2.00 mg ml^{-1}
1.00 mg ml^{-1}
0.50 mg ml^{-1}
0.40 mg ml^{-1}
0.25 mg ml^{-1}
0.10 mg ml^{-1}
Fluorescence Intensity
b
$f^{+/-}$ = 0.5
Fluorescence Intensity
c
$f^{+/-}$ = 0.67
Fluorescence Intensity
0
5000
10000
15000
20000
25000
500
550
600
650
700
Wavelength (nm)

Figure 11-4. Fluorescence emission spectra (excitation at 475 nm) of HA and TRITC-labeled ELP coacervates at different charge ratios as a function of total polymer concentration. At low polymer concentrations of ELP/HA (below 1 mg/ml), blue colors), negligible changes in the fluorescence intensity were observed. As the concentration of ELP/HA increased, by concentrations around 2 mg/ml (green) the fluorescence intensity in the emission spectra increases. The differences in fluorescence intensity for the highest polymer concentrations (above 4 mg/ml) is more pronounced between f+/- = 0.67 and 0.33, where these polymer concentrations contribute disproportionally more to the fluorescence yield than would be expected from their stoichiometric charge ratios.

Determining the critical coacervation concentration. The relative monodispersity of these spherical globules prompted study of the concentration at which these coacervate complexes are formed in varying charge ratios. In this system, fluorescent particles can be readily detected, even at very low concentrations (μM range). This low concentration detection allows us to estimate the concentration at which these coacervate complexes form, similar to methods of determining the critical micelle concentration[1, 93]. As such, we were able to determine the critical "coacervation concentration" (CCC) of the composition at different charge ratios (Figure 4).

Unlike other PEC systems, where coacervate formation is dependent on factors such as pH, ionic strength, and concentration of the polymer, we can use temperature to modulate particle sizes and microphase separation. The fluorescence intensity of the ELP_{TRITC} molecule is dependent on the concentration of HA within the bulk mixture at 37°C. A likely explanation is that the addition of HA sequesters the positively charged lysine groups within ELP, resulting in conformational changes within the ELP backbone that leads to hydrophobic collapse of the polymer chain, and thus reduced accessibility of the fluorophore[94-95]. Incremental addition of HA solution to the ELP/HA composite resulted in stepwise changes in its fluorescence profile. The fluorescence profiles of the different charge ratios are sigmoidal in nature, and the Sigmoidal-Boltzmann equation (2)[64] was employed in determining the CCC (Figure 5).

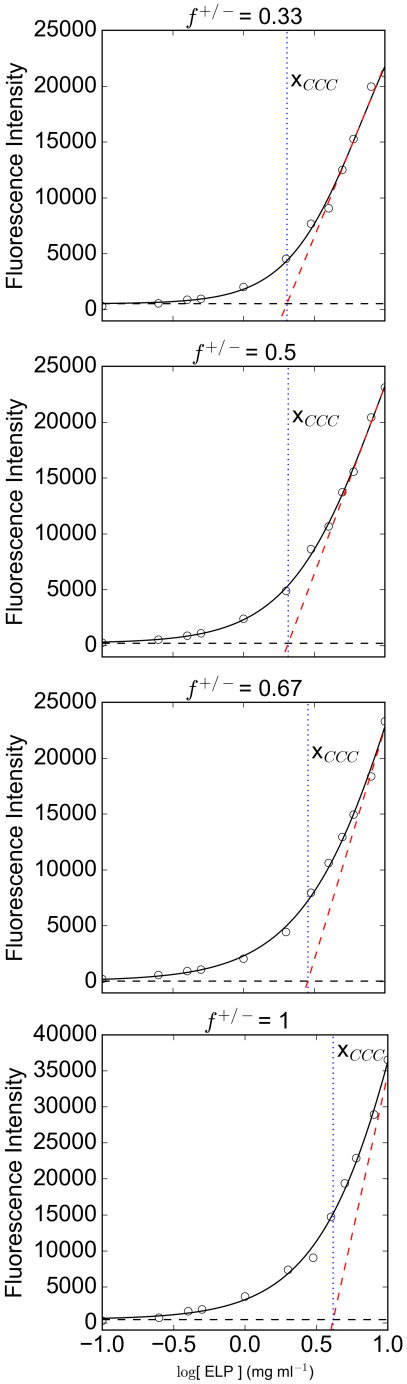

Figure 11-5. Fluorescence intensities at 575 nm as a function of ELPTRITC concentration (mg/ml) for ELPTRITC/HA coacervates, (f+/- = 0 for HA alone, f+/- = 1 for ELP alone). Symbols (○) denote experimental data points and lines represent the fitting of the Sigmoidal-Boltzmann function according to equation 2 (best fit parameters are listed in Table 2). As the concentration of ELP increases, the fluorescence intensity in the emission spectra increases dramatically in a sigmoidal manner. At low charge ratios (f+/- = 0.33), the critical coacervate concentration (xCCC) is lower than that of higher charge ratios (f+/- = 0.67), suggesting that the increase in positive charges, and therefore, increasing ELP···HA electrostatic interactions play a key role in coacervation formation.

The total fluorescence intensity as a function of the logarithm of ELP_{TRITC} concentration was measured to determine the critical coacervation concentration of our ELP/HA systems (Figure 5). The high fluorescent intensity of ELP_{TRITC} highlights its capabilities as a probe for the detection of structural changes[96-97]. At low polymer concentrations of ELP/HA (below 1 mg/ml), negligible changes in the fluorescence intensity were observed. As the concentration of ELP/HA increased, at certain concentrations (> 2 mg/ml) the fluorescence intensity in the emission spectra increased dramatically in a sigmoidal manner. The CCC and fit parameters are listed in Table 2.

The critical concentration appears to increase concurrently with the charge ratio of the composition, which is consistent with previously published results.[6, 98] Not surprisingly, the CCC of pure ELP ($f^{+/-} = 1$) was much greater than all other charge ratios. This is most likely due to the lack of contribution of electrostatic interactions via HA. The solvent environment and structural changes would be significantly different in pure ELP versus the conformational changes that would otherwise enable more pronounced hydrophobic collapse of the ELP backbone following complexation with HA. Thus ELP on its own would require a much higher concentration to undergo similar coacervation formation.

Table 3. Fitting parameters describing the critical coacervation concentrations as determined by the Sigmoidal-Boltzmann equation.

$f^{+/-}$	a_i	a_f	log [x_{CCC}] (mg ml^{-1})	x_0	Δx
0.33	532	39220	0.306	0.830	0.262
0.50	228	43710	0.316	0.961	0.322
0.67	68.6	60260	0.454	1.180	0.362
1	477	124518	0.617	1.310	0.346

Structural characterization of pyrene-doped ELP/HA coacervates. Finally, fluorescence spectroscopy was used to probe the structural formation of the coacervate complexes using pyrene, a fluorescent molecule that has served as a hydrophobic model drug for several decades[93, 99-100]. The aromatic complexes of pyrene molecules are extremely sensitive to their microenvironment, and have been used extensively to study the molecular conformations and intermolecular interactions of other systems.[65, 68, 101] The fluorescent spectrum of the pyrene-doped

ELP/HA coacervates exhibited a strong and broad excimer emission peak at 466 nm (with a red-shift in fluorescence as the charge ratio increases), whereas free pyrene solution prepared in the

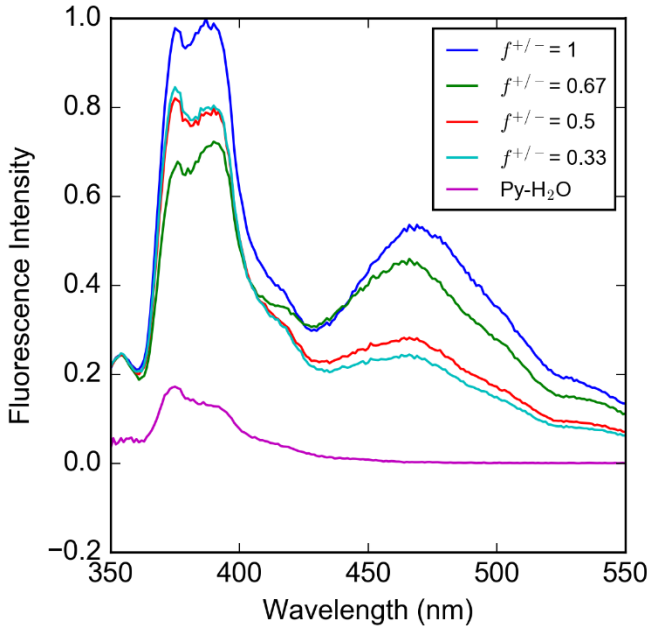

Figure 11-6. Fluorescence spectra (excitation at 328 nm) of pyrene in solutions of different ELP/HA charge ratios at 37 °C, (f+/- = 1 for ELP alone, f+/- = 0 for HA alone). Upon the addition of HA (or decreasing charge ratio, f+/-), the fluorescent peaks at 378 and 384 nm decreased in intensity, while the broad fluorescence peak at 460 nm (which indicates the formation of an excimer) showed a pronounced increase, highlighting the hydrophobically-driven tight packing of the polymer chains.

absence of the ELP/HA mixture did not exhibit an excimer peak in water (Figure 6). Upon the addition of HA, the fluorescent peaks at 378 and 384 nm decreased in intensity, while the broad fluorescence peak at 460 nm showed a pronounced increase, highlighting the aggregation propensity of the polymer chains. These observations indicate the close packing of pyrene molecules within a hydrophobic environment (when pyrene rings are ~10 Å apart from each other) as the formation of an excimer peak usually arises from an excited state dimer[102]. Interestingly, solutions of ELP ($f^{+/-}$ = 1) exhibited relatively higher excimer emission intensity, but this may be attributed ELP's well-studied collapsed conformational state and hydrophobic interior, where water molecules are usually excluded.[33, 103-104] The excimer emission of pyrene within the ELP/HA coacervate demonstrates a proof-of-concept that the ELP/HA PEC complexation can potentially serve as a drug delivery vehicle for hydrophobic molecules.

Finally, we observed that as HA is added to the PEC solution, the fluorescence intensity is reduced. A simplistic scheme of the fluorescence quenching is depicted below:

$$Py_G + Py_G \xrightarrow{hv_{exc}} Py_E \overset{\blacksquare}{\leftrightarrow} Py_{E\blacksquare}$$

(3)

where excitation of a ground state pyrene molecules (Py_g) reorient in solution to from the excimer (Py_E) and quenched via collisions from HA polymer chains (■). This quenching can be described using a modified Stern-Volmer equation, which considers both static and collisional quenching[105-106]:

$$\frac{F_0}{F} = (1 + K_{SV}[Q])(1 + K_a[Q])$$

(4)

$$\frac{F_0}{F} = (1 + K_{SV}[Q])$$

(5)

where F_0 and F are the fluorescence intensities that are observed in the absence and presence, respectively, of the quencher [Q]. For this study, the quencher [Q] is HA, K_{SV} is the Stern-Volmer quenching constant, and K_a is the association constant. Given the above quadratic equation, two solutions are expected, however, only one was found to be physically meaningful and therefore the value used in the discussions below (Equation 5).

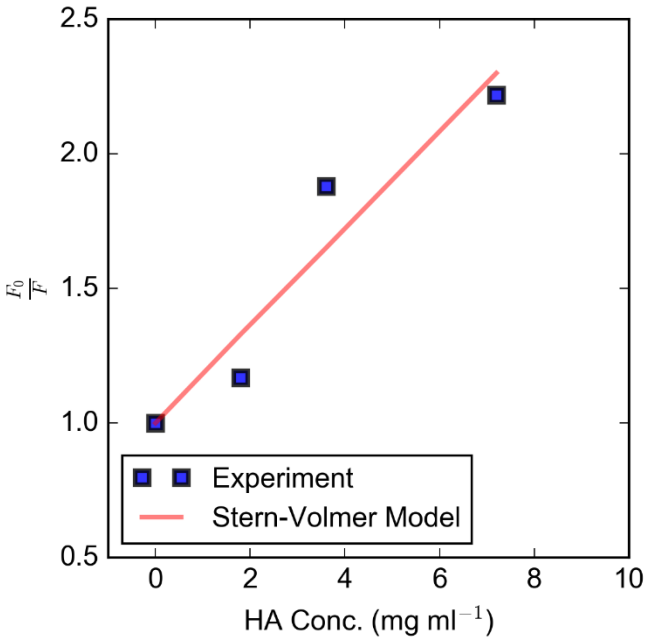

Figure 11-7. Fluorescence profile upon the addition of HA. This quenching can be described using a modified Stern-Volmer equation, highlighting the quenching of pyrene excimer formation during coacervate complexation as the concentration of HA is increased. The high linear correlation (r2 = 0.99) between the quencher concentration (HA) and the ratio

of F0 (measured fluorescence intensity without quencher present) and F (measured fluorescence intensity with quencher present) is in accordance with the Stern-Volmer equation.

The resulting plot in Figure 7 is linear with an upward curvature, showing a typical Stern-Volmer plot where collisional quenching occurs.[106-107] This fluorescence quenching is typical of other polyelectrolyte solutions.[108-109] The decrease of fluorescence intensity at the excimer peak upon the addition of HA is indicative of the quenching of excimer formation due to a reduced propensity for aggregation during coacervate complexation[-105]. We can hypothesize that the screening for electrostatic attractions between the HA backbone with the surrounding water network further reduces the potential number of binding sites for pyrene particles (i.e. the desolvated ELP chain).[45] The weaker intermolecular hydrogen bonding between the oppositely charged polymers results in a subsequent reduction in the number of pyrene dimer interactions.[100, 110]

11.5 **Conclusions**

We studied the effects of temperature and charge composition on the formation of polyelectrolyte coacervates consisting of ELP complexed with HA. Using DLS, sample turbidity, fluorescence microscopy and spectrometry to study the formation of these PECs, we found that the coacervation complexes can be formed over a range of charge ratios even without the presence of salt. We have also demonstrated that the T_t of PEC coacervates formation shifts to lower temperatures at higher charge ratios. Additionally, we have shown using DLS that the effect of temperature on particle size results in larger particles when the composite has a higher molar concentration of HA. More importantly, at temperatures above the T_t, we achieved monodisperse population of ELP/HA coacervate particles. Under these conditions the contribution of entangled or aggregated HA chains to light scattering is reduced due to the complexation of HA. However, at room temperature during the complexation process, not all of the HA has complexed with the ELP and free HA thus can still contribute to the scattering. When ELP alone undergoes a temperature-induced phase transition, only aggregation results, with no control of complex size or polydispersity.

For all charge densities, only a small concentration of negatively charged polymers were necessary for these composites to coacervate. These initial studies on the effect of charge ratios on temperature-responsive polypeptides and polysaccharide mixtures inform the future design of similar families of stimuli-responsive polypeptides (e.g. changes in pH and ionic strength). The

ability of these PECs to sequester hydrophobic molecules allows for their potential suitability in drug delivery applications. Also, incorporation of additional biological active molecules/moieties, through the modification of side chains in both HA and ELP polymers, could enable these coacervates to be applied to a wide-ranging suite of tissue engineering applications. Although coacervate formation has been shown from observations of self-assembly driven by microphase separation, the coacervation mechanism and the resultant macrostructure remains to be further explored.

11.6 References

1. Nolles, A.; Westphal, A. H.; de Hoop, J. A.; Fokkink, R. G.; Kleijn, J. M.; van Berkel, W. J. H.; Borst, J. W., Encapsulation of GFP in Complex Coacervate Core Micelles. *Biomacromolecules* **2015,** *16* (5), 1542-1549.
2. Srivastava, S.; Tirrell, M. V., Polyelectrolyte Complexation. *Adv Chem Phys* **2016,** *161*, 499-544.
3. Vieregg, J. R.; Tang, T. Y. D., Polynucleotides in cellular mimics: Coacervates and lipid vesicles. *Curr Opin Colloid In* **2016,** *26*, 50-57.
4. Capito, R. M.; Azevedo, H. S.; Velichko, Y. S.; Mata, A.; Stupp, S. I., Self-assembly of large and small molecules into hierarchically ordered sacs and membranes. *Science* **2008,** *319* (5871), 1812-1816.
5. Meka, V. S.; Singe, M. K. G.; Pichika, M. R.; Nali, S. R.; Kolapaili, V. R. M.; Kesharwani, P., A comprehensive review on polyelectrolyte complexes. *Drug Discov Today* **2017,** *22* (11), 1697-1706.
6. Le Cerf, D.; Pepin, A. S.; Niang, P. M.; Cristea, M.; Karakasyan-Dia, C.; Picton, L., Formation of polyelectrolyte complexes with diethylaminoethyl dextran: Charge ratio and molar mass effect. *Carbohyd Polym* **2014,** *113*, 217-224.
7. Lemmers, M.; Spruijt, E.; Beun, L.; Fokkink, R.; Leermakers, F.; Portale, G.; Stuart, M. A. C.; van der Gucht, J., The influence of charge ratio on transient networks of polyelectrolyte complex micelles. *Soft Matter* **2012,** *8* (1), 104-117.
8. Priftis, D.; Tirrell, M., Phase behaviour and complex coacervation of aqueous polypeptide solutions. *Soft Matter* **2012,** *8* (36), 9396-9405.
9. Chollakup, R.; Beck, J. B.; Dirnberger, K.; Tirrell, M.; Eisenbach, C. D., Polyelectrolyte Molecular Weight and Salt Effects on the Phase Behavior and Coacervation of Aqueous Solutions of Poly(acrylic acid) Sodium Salt and Poly(allylamine) Hydrochloride. *Macromolecules* **2013,** *46* (6), 2376-2390.
10. Park, W. M.; Champion, J. A., Two-Step Protein Self-Assembly in the Extracellular Matrix. *Angew Chem Int Edit* **2013,** *52* (31), 8098-8101.
11. Johnson, N. R.; Wang, Y. D., Coacervate delivery systems for proteins and small molecule drugs. *Expert Opin Drug Del* **2014,** *11* (12), 1829-1832.
12. Vignesh, S.; Sivashanmugam, A.; Mohandas, A.; Janarthanan, R.; Iyer, S.; Nair, S. V.; Jayakumar, R., Injectable deferoxamine nanoparticles loaded chitosan-hyaluronic acid coacervate hydrogel for therapeutic angiogenesis. *Colloid Surface B* **2018,** *161*, 129-138.
13. Jin, K. M.; Kim, Y. H., Injectable, thermo-reversible and complex coacervate combination gels for protein drug delivery. *J Control Release* **2008,** *127* (3), 249-256.
14. Gao, X. Q.; Cheng, H. Z.; Amra, S.; Tang, Y.; Sun, X. Y.; Awada, H.; Lu, A. P.; Deng, Z. H.; Wang, B.; Wang, Y. D.; Huard, J., A Comparison of BMP2 Delivery by Gene Therapy and Coacervate for Promoting Human Muscle-Derived Stem Cell-Mediated Cartilage Repair. *Mol Ther* **2017,** *25* (5), 160-160.
15. Haile, M.; Sarwar, O.; Henderson, R.; Smith, R.; Grunlan, J. C., Polyelectrolyte Coacervates Deposited as High Gas Barrier Thin Films. *Macromol Rapid Comm* **2017,** *38* (1).
16. Hwang, D. S.; Zeng, H. B.; Srivastava, A.; Krogstad, D. V.; Tirrell, M.; Israelachvili, J. N.; Waite, J. H., Viscosity and interfacial properties in a mussel-inspired adhesive coacervate. *Soft Matter* **2010,** *6* (14), 3232-3236.
17. Kelly, K. D.; Schlenoff, J. B., Spin-Coated Polyelectrolyte Coacervate Films. *Acs Appl Mater Inter* **2015,** *7* (25), 13980-13986.
18. Aberkane, L.; Jasniewski, J.; Gaiani, C.; Hussain, R.; Scher, J.; Sanchez, C., Structuration mechanism of beta-lactoglobulin - acacia gum assemblies in presence of quercetin. *Food Hydrocolloid* **2012,** *29* (1), 9-20.
19. Croguennec, T.; Tavares, G. M.; Bouhallab, S., Heteroprotein complex coacervation: A generic process. *Adv Colloid Interfac* **2017,** *239*, 115-126.
20. de Souza, G. I. D. H.; Santamarina, A. B.; de Santana, A. A.; Lira, F. S.; de Laquila, R.; Moreno, M. F.; Ribeiro, E. B.; do Nascimento, C. M. D. O.; Rodrigues, B.; Esposito, E.; Oyama, L. M., Preventive Effects of Chitosan Coacervate Whey Protein on Body Composition and Immunometabolic Aspect in Obese Mice. *Mediat Inflamm* **2014**.
21. Evdokimov, I. A.; Alieva, L. R.; Varlamov, V. P.; Kharitonov, V. D.; Butkevich, T. V.; Kurchenko, V. P., Usage of Chitosan in Dairy Products Production. *Food Raw Mater* **2015,** *3* (2), 29-39.
22. Souza, C. J. F.; da Costa, A. R.; Souza, C. F.; Tosin, F. F. S.; Garcia-Rojas, E. E., Complex coacervation between lysozyme and pectin: Effect of pH, salt, and biopolymer ratio. *Int J Biol Macromol* **2018,** *107*, 1253-1260.
23. Liu, H. J.; Wise, S. G.; Rnjak-Kovacina, J.; Kaplan, D. L.; Bilek, M. M. M.; Weiss, A. S.; Fei, J.; Bao, S. S., Biocompatibility of silk-tropoelastin protein polymers. *Biomaterials* **2014,** *35* (19), 5138-5147.

24. Thompson, R. E.; Pardieck, J.; Smith, L.; Kenny, P.; Crawford, L.; Shoichet, M.; Sakiyama-Elbert, S., Effect of hyaluronic acid hydrogels containing astrocyte-derived extracellular matrix and/or V2a interneurons on histologic outcomes following spinal cord injury. *Biomaterials* **2018,** *162*, 208-223.
25. White, J. D.; Wang, S. R.; Weiss, A. S.; Kaplan, D. L., Silk-tropoelastin protein films for nerve guidance. *Acta Biomaterialia* **2015,** *14*, 1-10.
26. Urry, D. W., Physical chemistry of biological free energy transduction as demonstrated by elastic protein-based polymers. *J Phys Chem B* **1997,** *101* (51), 11007-11028.
27. Meyer, D. E.; Chilkoti, A., Purification of recombinant proteins by fusion with thermally-responsive polypeptides. *Nature Biotechnology* **1999,** *17* (11), 1112-1115.
28. Long, M. M.; Urry, D. W.; Cox, B. A.; Ohnishi, T.; Jacobs, M., Coacervation of Repeat Sequences of Elastin. *Biophysical Journal* **1975,** *15* (2), A71-A71.
29. Trabbic-Carlson, K.; Meyer, D. E.; Liu, L.; Piervincenzi, R.; Nath, N.; LaBean, T.; Chilkoti, A., Effect of protein fusion on the transition temperature of an environmentally responsive elastin-like polypeptide: a role for surface hydrophobicity? *Protein Eng Des Sel* **2004,** *17* (1), 57-66.
30. Inostroza-Brito, K. E.; Collin, E.; Siton-Mendelson, O.; Smith, K. H.; Monge-Marcet, A.; Ferreira, D. S.; Rodriguez, R. P.; Alonso, M.; Rodriguez-Cabello, J. C.; Reis, R. L.; Sagues, F.; Botto, L.; Bitton, R.; Azevedo, H. S.; Mata, A., Co-assembly, spatiotemporal control and morphogenesis of a hybrid protein-peptide system. *Nat Chem* **2015,** *7* (11), 897-904.
31. Mills, C. E.; Michaud, Z.; Olsen, B. D., Elastin-like Polypeptide (ELP) Charge Influences Self-Assembly of ELP–mCherry Fusion Proteins. *Biomacromolecules* **2018,** *19* (7), 2517-2525.
32. Christensen, T.; Hassouneh, W.; Trabbic-Carlson, K.; Chilkoti, A., Predicting Transition Temperatures of Elastin-Like Polypeptide Fusion Proteins. *Biomacromolecules* **2013,** *14* (5), 1514-1519.
33. Dandurand, J.; Samouillan, V.; Lacabanne, C.; Pepe, A.; Bochicchio, B., Water structure and elastin-like peptide aggregation A differential calorimetric approach. *J Therm Anal Calorim* **2015,** *120* (1), 419-426.
34. Trabbic-Carlson, K.; Liu, L.; Kim, B.; Chilkoti, A., Expression and purification of recombinant proteins from Escherichia coli: Comparison of an elastin-like polypeptide fusion with an oligohistidine fusion. *Protein Sci* **2004,** *13* (12), 3274-84.
35. Straley, K. S.; Heilshorn, S. C., Independent tuning of multiple biomaterial properties using protein engineering. *Soft Matter* **2009,** *5* (1), 114-124.
36. Lampe, K. J.; Antaris, A. L.; Heilshorn, S. C., Design of three-dimensional engineered protein hydrogels for tailored control of neurite growth. *Acta Biomaterialia* **2013,** *9* (3), 5590-5599.
37. Choi, S. K.; Park, J. K.; Lee, K. M.; Lee, S. K.; Jeon, W. B., Improved neural progenitor cell proliferation and differentiation on poly(lactide-co-glycolide) scaffolds coated with elastin-like polypeptide. *J Biomed Mater Res B* **2013,** *101* (8), 1329-1339.
38. Ozaki, C.; Somamoto, S.; Kawabata, S.; Tabata, Y., Effect of an artificial silk elastin-like protein on the migration and collagen production of mouse fibroblasts. *J Biomat Sci-Polym E* **2014,** *25* (12), 1266-1277.
39. Xia, X. X.; Wang, M.; Lin, Y. A.; Xu, Q. B.; Kaplan, D. L., Hydrophobic Drug-Triggered Self-Assembly of Nanoparticles from Silk-Elastin-Like Protein Polymers for Drug Delivery. *Biomacromolecules* **2014,** *15* (3), 908-914.
40. Hassouneh, W.; Zhulina, E. B.; Chilkoti, A.; Rubinstein, M., Elastin-like Polypeptide Diblock Copolymers Self-Assemble into Weak Micelles. *Macromolecules* **2015,** *48* (12), 4183-4195.
41. Toole, B. P., Hyaluronan: from extracellular glue to cell signaling cue. *Int J Exp Pathol* **2009,** *90* (2), A96-A96.
42. Toole, B. P., Hyaluronan in morphogenesis. *J Intern Med* **1997,** *242* (1), 35-40.
43. Blancas, A. A.; Acosta, F. M.; Grande-Allen, K. J., Not just skin deep: cosmetic and medical applications of injectable hyaluronan and fibrin. *Mater Technol* **2015,** *30* (B4), B206-B210.
44. D'Este, M.; Sprecher, C. M.; Milz, S.; Nehrbass, D.; Dresing, I.; Zeiter, S.; Alini, M.; Eglin, D., Evaluation of an injectable thermoresponsive hyaluronan hydrogel in a rabbit osteochondral defect model. *J Biomed Mater Res A* **2016,** *104* (6), 1469-1478.
45. Sabbieti, M. G.; Dubbini, A.; Laus, F.; Paggi, E.; Marchegiani, A.; Capitani, M.; Marchetti, L.; Dini, F.; Vermonden, T.; Di Martino, P.; Agas, D.; Censi, R., In vivo biocompatibility of p(HPMAm-lac)-PEG hydrogels hybridized with hyaluronan. *J Tissue Eng Regen M* **2017,** *11* (11), 3056-3067.
46. Lee, S. B.; Lee, Y. M.; Song, K. W.; Park, M. H., Preparation and properties of polyelectrolyte complex sponges composed of hyaluronic acid and chitosan and their biological behaviors. *J Appl Polym Sci* **2003,** *90* (4), 925-932.
47. Kim, S. J.; Shin, S. R.; Lee, K. B.; Park, Y. D.; Kim, S. I., Synthesis and characteristics of polyelectrolyte complexes composed of chitosan and hyaluronic acid. *J Appl Polym Sci* **2004,** *91* (5), 2908-2913.
48. Kim, S. J.; Lee, C. K.; Lee, Y. M.; Kim, I. Y.; Kim, S. I., Electrical/pH-sensitive swelling behavior of polyelectrolyte hydrogels prepared with hyaluronic acid-poly(vinyl alcohol) interpenetrating polymer networks. *React Funct Polym* **2003,** *55* (3), 291-298.
49. Hahn, S. K.; Hoffman, A. S., Characterization of biocompatible polyelectrolyte complex multilayer of hyaluronic acid and poly-L-lysine. *Biotechnol Bioproc E* **2004,** *9* (3), 179-183.
50. Hahn, S. K.; Hoffman, A. S., Preparation and characterization of biocompatible polyelectrolyte complex multilayer of hyaluronic acid and poly-L-lysine. *Int J Biol Macromol* **2005,** *37* (5), 227-231.
51. Yamanlar, S.; Sant, S.; Boudou, T.; Picart, C.; Khademhosseini, A., Surface functionalization of hyaluronic acid hydrogels by polyelectrolyte multilayer films. *Biomaterials* **2011,** *32* (24), 5590-5599.
52. Castelletto, V.; Kaur, A.; Hamley, I. W.; Barnes, R. H.; Karatzas, K. A.; Hermida-Merino, D.; Swioklo, S.; Connon, C. J.; Stasiak, J.; Reza, M.; Ruokolainen, J., Hybrid membrane biomaterials from self-assembly in polysaccharide and peptide amphiphile mixtures: controllable structural and mechanical properties and antimicrobial activity. *Rsc Adv* **2017,** *7* (14), 8366-8375.
53. Zha, R. H.; Velichko, Y. S.; Bitton, R.; Stupp, S. I., Molecular design for growth of supramolecular membranes with hierarchical structure. *Soft Matter* **2016,** *12* (5), 1401-1410.
54. Matson, J. B.; Navon, Y.; Bitton, R.; Stupp, S. I., Light-Controlled Hierarchical Self-Assembly of Polyelectrolytes and Supramolecular Polymers. *Acs Macro Letters* **2015,** *4* (1), 43-47.

55. Zha, R. H.; Sur, S.; Stupp, S. I., Self-assembly of Cytotoxic Peptide Amphiphiles into Supramolecular Membranes for Cancer Therapy. *Adv Healthc Mater* **2013,** *2* (1), 126-133.
56. Artimo, P.; Jonnalagedda, M.; Arnold, K.; Baratin, D.; Csardi, G.; de Castro, E.; Duvaud, S.; Flegel, V.; Fortier, A.; Gasteiger, E.; Grosdidier, A.; Hernandez, C.; Ioannidis, V.; Kuznetsov, D.; Liechti, R.; Moretti, S.; Mostaguir, K.; Redaschi, N.; Rossier, G.; Xenarios, I.; Stockinger, H., ExPASy: SIB bioinformatics resource portal. *Nucleic Acids Res* **2012,** *40* (W1), W597-W603.
57. Mero, A.; Campisi, M., Hyaluronic Acid Bioconjugates for the Delivery of Bioactive Molecules. *Polymers-Basel* **2014,** *6* (2), 346-369.
58. Schindelin, J.; Arganda-Carreras, I.; Frise, E.; Kaynig, V.; Longair, M.; Pietzsch, T.; Preibisch, S.; Rueden, C.; Saalfeld, S.; Schmid, B.; Tinevez, J. Y.; White, D. J.; Hartenstein, V.; Eliceiri, K.; Tomancak, P.; Cardona, A., Fiji: an open-source platform for biological-image analysis. *Nat Methods* **2012,** *9* (7), 676-682.
59. Kayitmazer, A. B.; Bohidar, H. B.; Mattison, K. W.; Bose, A.; Sarkar, J.; Hashidzume, A.; Russo, P. S.; Jaeger, W.; Dubin, P. L., Mesophase separation and probe dynamics in protein-polyelectrolyte coacervates. *Soft Matter* **2007,** *3* (8), 1064-1076.
60. Harmon, T. S.; Roberts, S.; Chilkoti, A.; Pappu, R. V., A Model for Hysteresis Observed in Phase Transitions of Thermally Responsive Intrinsically Disordered Protein Polymers. *Biophysical Journal* **2017,** *112* (3), 207a-207a.
61. Roberts, S.; Dzuricky, M.; Chilkoti, A., Elastin-like polypeptides as models of intrinsically disordered proteins. *Febs Lett* **2015,** *589* (19), 2477-2486.
62. Zhang, Y. J.; Trabbic-Carlson, K.; Albertorio, F.; Chilkoti, A.; Cremer, P. S., Aqueous two-phase system formation kinetics for elastin-like polypeptides of varying chain length. *Biomacromolecules* **2006,** *7* (7), 2192-2199.
63. Meyer, D. E.; Chilkoti, A., Quantification of the effects of chain length and concentration on the thermal behavior of elastin-like polypeptides. *Biomacromolecules* **2004,** *5* (3), 846-851.
64. Hait, S. K.; Moulik, S. P.; Palepu, R., Refined method of assessment of parameters of micellization of surfactants and percolation of w/o microemulsions. *Langmuir* **2002,** *18* (7), 2471-2476.
65. Ray, G. B.; Chakraborty, I.; Moulik, S. P., Pyrene absorption can be a convenient method for probing critical micellar concentration (cmc) and indexing micellar polarity. *J Colloid Interf Sci* **2006,** *294* (1), 248-254.
66. Mi, Y.; Liu, Y. T.; Feng, S. S., Formulation of Docetaxel by folic acid-conjugated D-alpha-tocopheryl polyethylene glycol succinate 2000 (Vitamin E TPGS(2k)) micelles for targeted and synergistic chemotherapy. *Biomaterials* **2011,** *32* (16), 4058-4066.
67. Bales, B. L.; Almgren, M., Fluorescence Quenching of Pyrene by Copper(Ii) in Sodium Dodecyl-Sulfate Micelles - Effect of Micelle Size as Controlled by Surfactant Concentration. *J Phys Chem-Us* **1995,** *99* (41), 15153-15162.
68. Yekta, A.; Duhamel, J.; Brochard, P.; Adiwidjaja, H.; Winnik, M. A., A Fluorescent-Probe Study of Micelle-Like Cluster Formation in Aqueous-Solutions of Hydrophobically Modified Poly(Ethylene Oxide). *Macromolecules* **1993,** *26* (8), 1829-1836.
69. Berezney, J. P.; Saleh, O. A., Electrostatic Effects on the Conformation and Elasticity of Hyaluronic Acid, a Moderately Flexible Polyelectrolyte. *Macromolecules* **2017,** *50* (3), 1085-1089.
70. Kim, S.; Huang, J.; Lee, Y.; Dutta, S.; Yoo, H. Y.; Jung, Y. M.; Jho, Y.; Zeng, H. B.; Hwang, D. S., Complexation and coacervation of like-charged polyelectrolytes inspired by mussels. *P Natl Acad Sci USA* **2016,** *113* (7), E847-E853.
71. Wang, Q. F.; Schlenoff, J. B., The Polyelectrolyte Complex/Coacervate Continuum. *Macromolecules* **2014,** *47* (9), 3108-3116.
72. Ding, Y. W.; Zhang, G. Z., Folding of a single polymer chain and phase transition. *Chinese Sci Bull* **2009,** *54* (11), 1908-1911.
73. LunaBarcenas, G.; Gromov, D. G.; Meredith, J. C.; Sanchez, I. C.; dePablo, J. J.; Johnston, K. P., Polymer chain collapse near the lower critical solution temperature. *Chem Phys Lett* **1997,** *278* (4-6), 302-306.
74. Tang, J. D.; McAnany, C. E.; Mura, C.; Lampe, K. J., Toward a Designable Extracellular Matrix: Molecular Dynamics Simulations of an Engineered Laminin-Mimetic, Elastin-Like Fusion Protein. *Biomacromolecules* **2016,** *17* (10), 3222-3233.
75. Kozer, N.; Kuttner, Y. Y.; Haran, G.; Schreiber, G., Protein-protein association in polymer solutions: From dilute to semidilute to concentrated. *Biophysical Journal* **2007,** *92* (6), 2139-2149.
76. Karle, I. L.; Urry, D. W., Crystal structure of cyclic (APGVGV)(2,) an analog of elastin, and a suggested mechanism for elongation/contraction of the molecule. *Biopolymers* **2005,** *77* (4), 198-204.
77. Bhattacharjee, S. M.; Giacometti, A.; Maritan, A., Flory theory for polymers. *J Phys-Condens Mat* **2013,** *25* (50).
78. Favre, E.; Nguyen, Q. T.; Sacco, D.; Moncuy, A.; Clement, R., Multicomponent polymer/solvents equilibria: An evaluation of Flory-Huggins theory for crosslinked PDMS networks swelled by binary mixtures. *Chem Eng Commun* **1996,** *140*, 193-205.
79. Priftis, D.; Laugel, N.; Tirrell, M., Thermodynamic Characterization of Polypeptide Complex Coacervation. *Langmuir* **2012,** *28* (45), 15947-15957.
80. Xia, J. L.; Zhang, H. W.; Rigsbee, D. R.; Dubin, P. L.; Shaikh, T., Structural Elucidation of Soluble Polyelectrolyte-Micelle Complexes - Intrapolymer Vs Interpolymer Association. *Macromolecules* **1993,** *26* (11), 2759-2766.
81. Gribbon, P.; Heng, B. C.; Hardingham, T. E., The molecular basis of the solution properties of hyaluronan investigated by confocal fluorescence recovery after photobleaching. *Biophysical Journal* **1999,** *77* (4), 2210-2216.
82. Krukau, A.; Brovchenko, I.; Geiger, A., Temperature-induced conformational transition of a model elastin-like peptide GVG(VPGVG)(3) in water. *Biomacromolecules* **2007,** *8* (7), 2196-2202.
83. Urry, D. W.; Trapane, T. L.; Prasad, K. U., Phase-Structure Transitions of the Elastin Polypentapeptide Water-System within the Framework of Composition Temperature Studies. *Biopolymers* **1985,** *24* (12), 2345-2356.
84. Li, N. K.; Quiroz, F. G.; Hall, C. K.; Chilkoti, A.; Yingling, Y. G., Molecular Description of the LCST Behavior of an Elastin-Like Polypeptide. *Biomacromolecules* **2014,** *15* (10), 3522-3530.
85. Ohgo, K.; Ashida, J.; Kumashiro, K. K.; Asakura, T., Structural determination of an elastin-mimetic model peptide, (Val-Pro-Gly-Val-Gly)(6), studied by C-13 CP/MAS NMR chemical shifts, two-dimensional off magic angle spinning spin-diffusion NMR, rotational echo double resonance, and statistical distribution of torsion angles from protein data bank. *Macromolecules* **2005,** *38* (14), 6038-6047.
86. Rapaka, R. S.; Okamoto, K.; Urry, D. W., Coacervation Properties in Sequential Polypeptide Models of Elastin - Synthesis of H-(Ala-Pro-Gly-Gly)N-Val-Ome and H-(Ala-Pro-Gly-Val-Gly)N-Val-Ome. *Int J Pept Prot Res* **1978,** *12* (2), 81-92.

87. Doss, S. S.; Bhatt, N. P.; Jayaraman, G., Improving the accuracy of hyaluronic acid molecular weight estimation by conventional size exclusion chromatography. *J Chromatogr B* **2017,** *1060*, 255-261.
88. Yu, L. P.; Masi, L.; Burns, J. W., Size Exclusion Chromatography and Multi Angle Laser-Light Scattering for Molecular-Weight Analysis of Hyaluronic-Acid. *Abstr Pap Am Chem S* **1989,** *198*, 81-Poly.
89. Yu, J.; Mao, J.; Yuan, G. C.; Satija, S.; Jiang, Z.; Chen, W.; Tirrell, M., Structure of Polyelectrolyte Brushes in the Presence of Multivalent Counterions. *Macromolecules* **2016,** *49* (15), 5609-5617.
90. Perry, S. L.; Li, Y.; Priftis, D.; Leon, L.; Tirrell, M., The Effect of Salt on the Complex Coacervation of Vinyl Polyelectrolytes. *Polymers-Basel* **2014,** *6* (6), 1756-1772.
91. Lalevee, G.; Sudre, G.; Montembault, A.; Meadows, J.; Malaise, S.; Crepet, A.; David, L.; Delair, T., Polyelectrolyte complexes via desalting mixtures of hyaluronic acid and chitosan-Physicochemical study and structural analysis. *Carbohyd Polym* **2016,** *154*, 86-95.
92. Dreher, M. R.; Simnick, A. J.; Fischer, K.; Smith, R. J.; Patel, A.; Schmidt, M.; Chilkoti, A., Temperature triggered self-assembly of polypeptides into multivalent spherical micelles. *J Am Chem Soc* **2008,** *130* (2), 687-694.
93. Astafieva, I.; Zhong, X. F.; Eisenberg, A., Critical Micellization Phenomena in Block Polyelectrolyte Solutions. *Macromolecules* **1993,** *26* (26), 7339-7352.
94. Johnson, A. E., Fluorescence approaches for determining protein conformations, interactions and mechanisms at membranes. *Traffic* **2005,** *6* (12), 1078-1092.
95. Goudsmits, J. M. H.; Slotboom, D. J.; van Oijen, A. M., Single-molecule visualization of conformational changes and substrate transport in the vitamin B-12 ABC importer BtuCD-F. *Nat Commun* **2017,** *8*.
96. Yu, L. L.; Tan, M. Y.; Ho, B.; Ding, J. L.; Wohland, T., Determination of critical micelle concentrations and aggregation numbers by fluorescence correlation spectroscopy: Aggregation of a lipopolysaccharide. *Anal Chim Acta* **2006,** *556* (1), 216-225.
97. Liaw, J.; Aoyagi, T.; Kataoka, K.; Sakurai, Y.; Okano, T., Permeation of PEO-PBLA-FITC polymeric micelles in aortic endothelial cells. *Pharm Res-Dord* **1999,** *16* (2), 213-220.
98. Hugerth, A.; Caram-Lelham, N.; Sundelof, L. O., The effect of charge density and conformation on the polyelectrolyte complex formation between carrageenan and chitosan. *Carbohyd Polym* **1997,** *34* (3), 149-156.
99. Ishii, Y.; Lehrer, S. S., Intramolecular Excimer Fluorescence of Pyrene Maleimide-Labeled Dithiothreitol (P-Dtt). *Biophysical Journal* **1987,** *51* (2), A276-A276.
100. Kalyanasundaram, K.; Thomas, J. K., Environmental Effects on Vibronic Band Intensities in Pyrene Monomer Fluorescence and Their Application in Studies of Micellar Systems. *J Am Chem Soc* **1977,** *99* (7), 2039-2044.
101. Bertoncini, C. W.; Celej, M. S., Small Molecule Fluorescent Probes for the Detection of Amyloid Self-Assembly In Vitro and In Vivo. *Curr Protein Pept Sc* **2011,** *12* (3), 206-220.
102. Bains, G.; Patel, A. B.; Narayanaswami, V., Pyrene: A Probe to Study Protein Conformation and Conformational Changes. *Molecules* **2011,** *16* (9), 7909-7935.
103. Ribeiro, A.; Arias, F. J.; Reguera, J.; Alonso, M.; Rodriguez-Cabello, J. C., Influence of the Amino-Acid Sequence on the Inverse Temperature Transition of Elastin-Like Polymers. *Biophysical Journal* **2009,** *97* (1), 312-320.
104. Zhao, B. W.; Li, N. K.; Yingling, Y. G.; Hall, C. K., LCST Behavior is Manifested in a Single Molecule: Elastin-Like polypeptide (VPGVG)n. *Biomacromolecules* **2016,** *17* (1), 111-118.
105. Geddes, C. D., Optical halide sensing using fluorescence quenching: theory, simulations and applications - a review. *Meas Sci Technol* **2001,** *12* (9), R53-R88.
106. Teale, F. W. J., Principles of Fluorescence Spectroscopy - Lakowicz,Jr. *Nature* **1984,** *307* (5950), 486-486.
107. Limpouchova, Z.; Prochazka, K., Theoretical Principles of Fluorescence Spectroscopy. *Springer Ser Fluores* **2016,** *16*, 91-149.
108. Jiang, H.; Zhao, X. Y.; Schanze, K. S., Amplified fluorescence quenching of a conjugated polyelectrolyte mediated by Ca2+. *Langmuir* **2006,** *22* (13), 5541-5543.
109. George, W. N.; Giles, M.; McCulloch, I.; de Mello, J. C.; Steinke, J. H. G., Amplified fluorescence quenching in high ionic strength media. *Soft Matter* **2007,** *3* (11), 1381-1387.
110. Graceffa, P.; Lehrer, S. S., The Excimer Fluorescence of Pyrene-Labeled Tropomyosin - a Probe of Conformational Dynamics. *J Biol Chem* **1980,** *255* (23), 1296-1300.

12 Appendix 4: The effects of cell-adhesive peptide hydrogels on oligodendrocyte precursor cell morphology

12.1 Abstract

The extracellular matrix (ECM) is a complex, hierarchical, multicomponent material that contains multiple biomolecules assembled together. This complexity makes decoupling the effects of both biomechanical properties and cell-matrix interactions difficult, especially in studies of 3D encapsulations that involve the initiation and/or propagation of specific cellular processes. In this study, we developed a self-assembling pentapeptide hydrogel (RAPID) functionalized with multiple different matrix-derived cell adhesive ligands. RAPID can self-assemble with the addition of cell adhesive ligands into hydrogels with mechanical properties consistent with non-functionalized RAPID controls. This allows for the precise tuning of peptide ligand concentration, since the rheological properties of the RAPID hydrogels are not affected by the addition of cell-adhesive ligands. This permits us to study cell-matrix interactions of encapsulated oligodendrocyte precursor cells (OPCs) in the presence of laminin-derived peptide sequences, IKVAV, RGD, and YIGSR. Previous studies have utilized biomaterials to promote neuronal regeneration using neural stem cells, but little is known about how the encapsulation environments impact OPC growth or their differentiation into myelinating oligodendrocytes. We demonstrate that interactions with the sequences IKVAV, RGD, and YIGSR contribute to improved viability and process extension of OPCs versus non-functionalized RAPID controls. The results give evidence that cell adhesive peptide epitopes may promote OPC survival and morphological changes into more mature phenotypes.

12.2 Introduction

Remyelination is a limiting feature in any central nervous system (CNS) regeneration. Oligodendrocytes, which produce the insulating myelin sheaths around neuronal axons, have not been successfully cultured in a 3D *in vitro* system that permits growth and morphological changes indicative of oligodendrocyte maturation. Previous oligodendrocyte encapsulation studies have used bio-inert materials which provide very little cell-matrix support to encapsulated cells[1-2]. To address this issue, mimics of the CNS extracellular matrix (ECM) can be utilized that allow

physiologically relevant development of cell morphologies and interactions[3-7]. While cell-matrix interactions have been shown to influence the differentiation efficiency of oligodendrocyte precursor cells (OPCs)[8], a subtype of lineage-restricted glial cells that give rise to myelinating oligodendrocytes, there has been growing evidence of mechanosensitivity of where both proliferation and differentiation correlates with the mechanical stiffness of underlying substrata[1, 9]. Thus, in order to properly investigate cell-matrix interactions of OPCs and its surrounding microenvironment without the influence of biomechanically-related events (i.e. via mechanotransduction pathways), it is important to decouple these synergistic effects of both the hierarchical microstructures, biomechanical properties, and signaling cues that initiate and/or propagate specific cellular processes within the ECM.

Covalent immobilization of adhesive peptide sequences as well as cell-secreted matrix molecules in synthetic 3D hydrogels can modulate cell-matrix interactions[10-13]. Interactions between cells and these peptides and proteins are primarily mediated by integrins expressed on the cell surface. The most extensively studied adhesive recognition is the tripeptide, Arg-Gly-Asp (RGD), derived from fibronectin, but also found in collagen type I, fibrinogen, laminin, and other matrix proteins[14]. RGD binding on hydrogels increase dorsal root ganglia neurite outgrowth[15]. Proliferation of NSCs can be modulated through control of RGD surface density[16], where it was demonstrated that higher RGD concentrations were correlated with increased NSC cell attachment and dendrite extension. In addition to RGD, laminin-derived adhesion sequences such as IKVAV in combination with NSCs saw significantly enhanced regeneration of neural tissue in a rat brain surgery model[17]. IKVAV is a peptide derived from the α-chain of laminin, and previously shown to induce endothelial cell adhesion and subsequent tubule formation[18]. In the presence of immobilized IKVAV on collagen type I hydrogels, there was increased cell migration, adhesion, and capillary network formation in vascular endothelial cells and stimulated neurite outgrowth in conditions of serum deprivatios[19]. Additionally, IKVAV has been shown to mediate revascularization of ischemic tissue.[20] The integrin receptor ligand YIGSR is found in the laminin β chain, which has been extensively investigated as a promotor of neuronal cell adhesion.[11, 21] Similarly, YIGSR-functionalized matrices have been found to promote neurite sprouting and regeneration.[22]

The goal of this study was to investigate the effects of cell-matrix interactions via self-assembling pentapeptide hydrogels (RAPID) functionalized with adhesive peptide sequences. While in native ECM (e.g. biologically sourced ECMs such as Matrigel), it is difficult to decouple the synergistic effects between the complex interconnectivity of cell-derived matrices and heterogonous mixture of growth factors and other ligands. However, RAPID hydrogels are an ideal system of choice because 1) their short pentapeptide sequence is easily synthesized and chemically defined, 2) their rheological properties are easily tunable via subtle changes in pH and peptide concentration, and 3) they have previously been demonstrated to be suitable for cytocompatible encapsulation of OPCs[23-24]. RAPID can co-assemble into hydrogels that present short peptide ligands with consistent mechanical properties, which allows for the precise tuning of peptide ligand concentration. The modularity of this peptidic system permits us to study cell-matrix interactions of encapsulated oligodendrocyte precursor cells (OPCs) in the presence of laminin-derived recognition sequences, IKVAV, RGD, and YIGSR. For our RAPID system, we can control both the biomechanical properties, as well as ligand presentation allowing for the independent adjustment of specific molecules. For this study, we present a hydrogel system that can be facilely prepared for the encapsulation of OPCs. We find that incorporation of cell-adhesive ligands promoted process extension and cell growth within RAPID hydrogels. These results indicate the potential of RAPID hydrogels in providing a suitable microenvironment for OPCs and directing cell fate in CNS regeneration applications.

12.3 **Methods and Materials**

12.3.1 Peptide Synthesis.

All peptides were synthesized by solid-phase chemistry on a Liberty Blue peptide synthesizer (CEM, NC). A TentaGel R Rink Amide Resin was used to generate a terminal amide. Solvents and Fmoc (fluorenylmethoxycarbonyl) protected amino acids were purchased from Gyros Protein Technologies. Reagents were made with 5 equiv. moles of amino acid and 5 equiv. moles of HBTU (2-(1H-benzotriazol-1-yl)-1,1,3,3 tetramethyluronium hexafluorophosphate), and subsequently dissolved in DMF (dimethylformamide). Amino acid coupling cycles were 60 min in length. Protecting groups were removed with treatments of 20/80

v/v piperidine/DMF for 10 minutes. After the coupling reaction was complete, the resin was washed three times with DCM (dichloromethane) before cleavage. Cleavage of the peptides was accomplished by shaking the resin with 10 mL of TFA (trifluoroacetic cid)/triisopropylsilane/H2O (95:2.5:2.5 volume ratios) for 2 h at room temperature. The peptide solution was collected, and the peptide precipitated by the addition of cold diethyl ether followed by two washes with cold ether after centrifugation. Peptides were dried overnight, redissolved in deionized water, and dialyzed in semipermeable cellulose ester membranes with a molecular weight cutoff of 100-500 Da (Spectra/Por, Spectrum Laboratories Inc., Rancho Dominguez, CA). The dialysis buffer (deionized water) was changed every 12 h for 2 days and the peptides were lyophilized.

12.4 Hydrogel Formation and Rheological Properties.

Lyophilized peptides were dissolved in PBS to a final concentration of 1.5 wt.%. To evaluate the viscoelastic properties of the hydrogel forming peptides, 25 μL aliquots of the hydrogel were pipetted into 5 mm molds on glass slips. Gels were removed from the molds and rheometry tests were performed 10 minutes after induction of gelation (Anton Par, P25S 25 mm parallel steel plates) with a measuring gap of 250 μm. Storage (G') and Loss (G") moduli were measured as a function of strain (%) ranging from 0.01 to 100% with a constant frequency of 10 rad/s. Frequency sweeps were performed at angular frequencies ranging from 1 to 100 rad/s at 0.1% strain. For recovery experiments, a step-time procedure was utilized with a series of applied strains. Initially, samples were applied with 0.01% strain for 100 s followed immediately by a 500% strain for 50 s, and cycled 5 times. All steps were performed at a fixed oscillation frequency of 10 rad/s.

12.4.1 Cell Culture.

GFP+ MADM OPC lines4 were expanded in vitro on T75 tissue culture plates treated with poly-ornithine. OPCs were cultured in DMEM with high glucose, 4 mM L-glutamine, 1 mM sodium pyruvate (Life Technologies) with N2 and B27 supplement (Life Technologies)[i],1% penicillin-streptomycin (Life Technologies), 10 ng/mL mouse PDGFA-AA (eBioscience), and 50 ng/mL human NT3 (Peprotech). Cell media was changed every 2 days, and cells were grown to 90% confluency and passaged using 0.25% trypsin in Dulbecco's phosphate buffered saline

(PBS). Cell media was changed every 2 days, and cells were grown to 90% confluency and passaged using 0.5% trypsin-EDTA. All cells were cultured in 5% CO2 atmosphere, and 19.95% O2 at 37 °C.

12.4.2 Hydrogel Cell Encapsulation and Analysis.

Hydrogels for cell encapsulation were made using 3 wt% KYFIL, 1:15 IKVAVKYFIL, 1:15 YIGSRKYFIL, and 1:15 RGDKYFIL peptide in PBS. 5mm molds (what are they made of) were placed on 1cm glass slides in a 24 well plate. 25 uL 1.5 wt% hydrogels with 1E6 cells/mL were made by mixing cells and peptides in the molds and then transferred to a cell incubator for 10 minutes at 37 °C. OPC proliferation media was then added to the hydrogels, and changed every 2 days. Hydrogels were stored at −80 °C before running ATP or DNA quantification assays. For quantification, gels were homogenized in lysis buffer using a pipette and were measured using the CellTiter-Glo luminescent Cell Viability Assay (Promega, United States) and the QuantiT PicoGreen dsDNA assay (ThermoFisher) according to manufacturer protocols. For image analysis, channels for live cells were merged and converted to a mask, and then converted to 8-bit to allow for thresholding based on the intensity. The skeletonize plugin was used, and the skeleton analysis tool was then employed, with a prune cycle method using the shortest branch. The number of branches per cell for each image were recorded (n = 3 samples per condition).

12.4.3 Immunostaining.

After 2 days of culture, gels were fixed in 4% paraformaldehyde for 20 minutes at 4 °C and rinsed with PBS before permeabilizing overnight with 0.3% triton-X in PBS. Hydrogels were rinsed in PBS, and then incubated with 10 μg/mL stock solution of Alexa Fluor 568 Phalloidin (ThermoFisher) in 1% BSA in PBS overnight. 4′,6-diamidino-2-phenylindole (DAPI) was added to stain cell nuclei during the last 20 minutes of incubation. Gels were then washed 4 × 20 min in PBS and imaged with a Zeiss LSM 780 confocal microscope. 100 μm z-stack images were collected with a z-spacing distance of 1 μm.

12.5 Results and Discussion

12.5.1 Hydrogel rheological characterization

We evaluated the mechanical properties of 1.5 wt. % hydrogels, and found that the incorporation

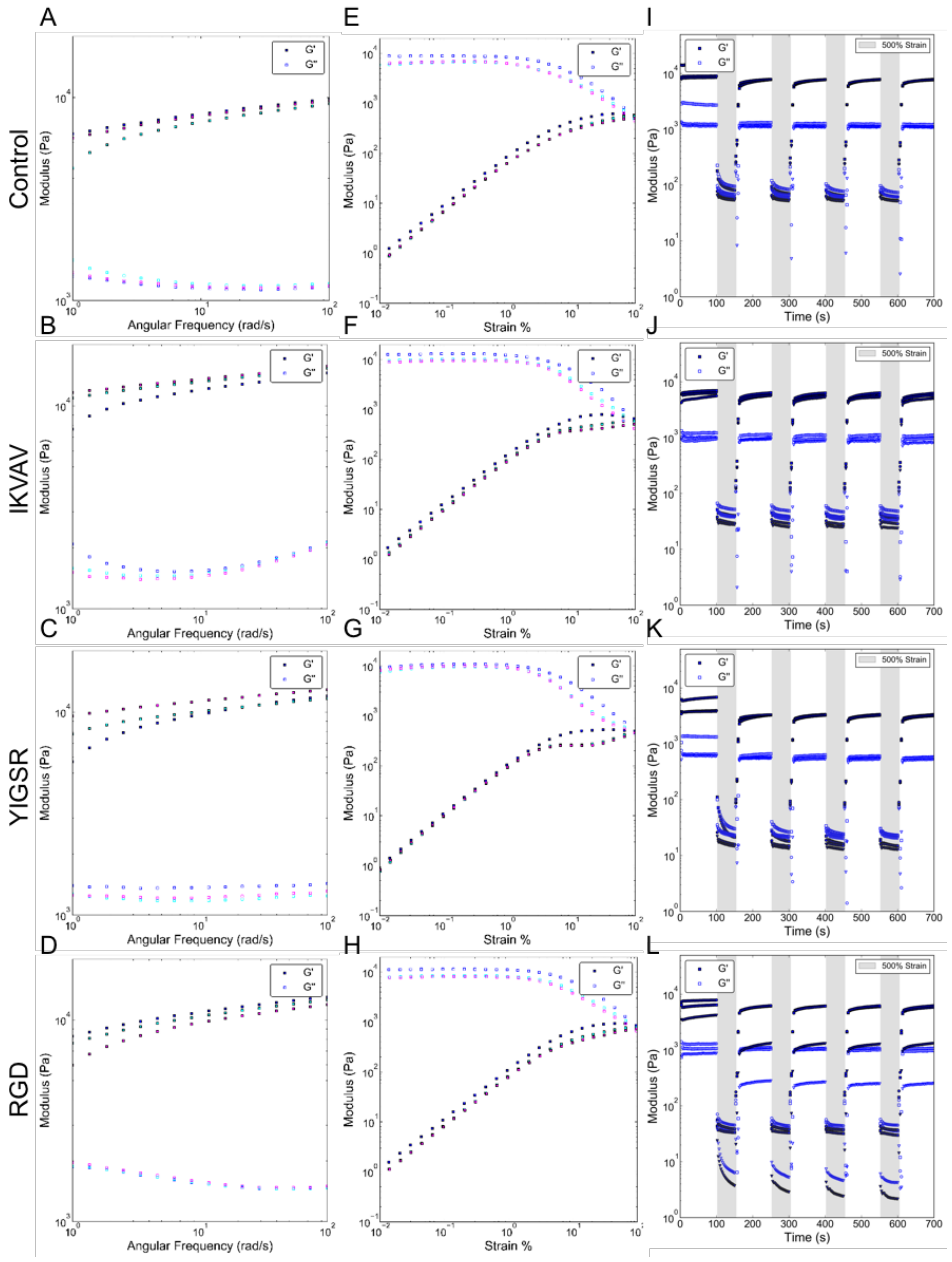

Figure 12-1. Rheological properties of 1.5 wt. % KYFIL hydrogels at pH 7.4 (n = 3 for all samples). A - D) Angular frequency sweep of control KYFIL, IKVAV-KYFIL, YIGSR-KYFIL, and RGD-KYFIL peptide sequences, respectively, at constant strain of 0.1%. G' is an order of magnitude greaten than G" indicating hydrogelation has occurred. E - H) Strain sweep of gelling control KYFIL, IKVAV-KYFIL, YIGSR-KYFIL, and RGD-KYFIL peptide sequences, respectively, at constant angular frequency of 10 rad/s. Above the critical strain at 5%, the material becomes progressively more fluid-like, where G' starts to increase and G" begins to decrease. I - L) Five step strain sweeps of 0.1 % (100 s) and 500 % strain (50 s), followed by a 100 s recovery period, were performed on control KYFIL, IKVAV-KYFIL, YIGSR-KYFIL, and RGD-KYFIL hydrogel peptide sequences, respectively. The hydrogel recovered 80% of its initial G' within several seconds. The hydrogel repeatedly recovered its mechanical strength following multiple high strain cycles.

of RGD, IKVAV, and YIGSR-modified peptides did not alter the storage modulus of RAPID hydrogels. Hydrogels were formed by mixing 22 mM of AYFIL or KYFIL peptides with 2 mM of the cell-adhesive ligands. This ligand concentration was based off multifactorial experiments to optimize endothelial cell growth as a function of individual cell-adhesive ligand incorporation, and demonstrated that there was significant cell growth for cells seeded on hydrogels with cell-adhesive ligand concentrations from 1.5 mM to 6 mM.[25] For all KYFIL and KYFIL-functionalized samples, the storage modulus (*G'*) was found to be 8.5 kPa (Figure 1) versus 3 kPa for AYFIL hydrogels (Figure 2). These stiffnesses are consistent with previously published results of RAPID hydrogel systems,[23-24] where it was reported that 1.5 wt % KYFIL hydrogels had a storage modulus ranging from 8 kPa, and 1.5 wt % AYFIL hydrogels had a stiffness of 3.2 kPa. This suggests we can reliably tune the mechanical properties of the hydrogel while maintaining a constant ligand concentration. Multiple high-strain (100%) sweep cycles, with 30 s recovery periods, were

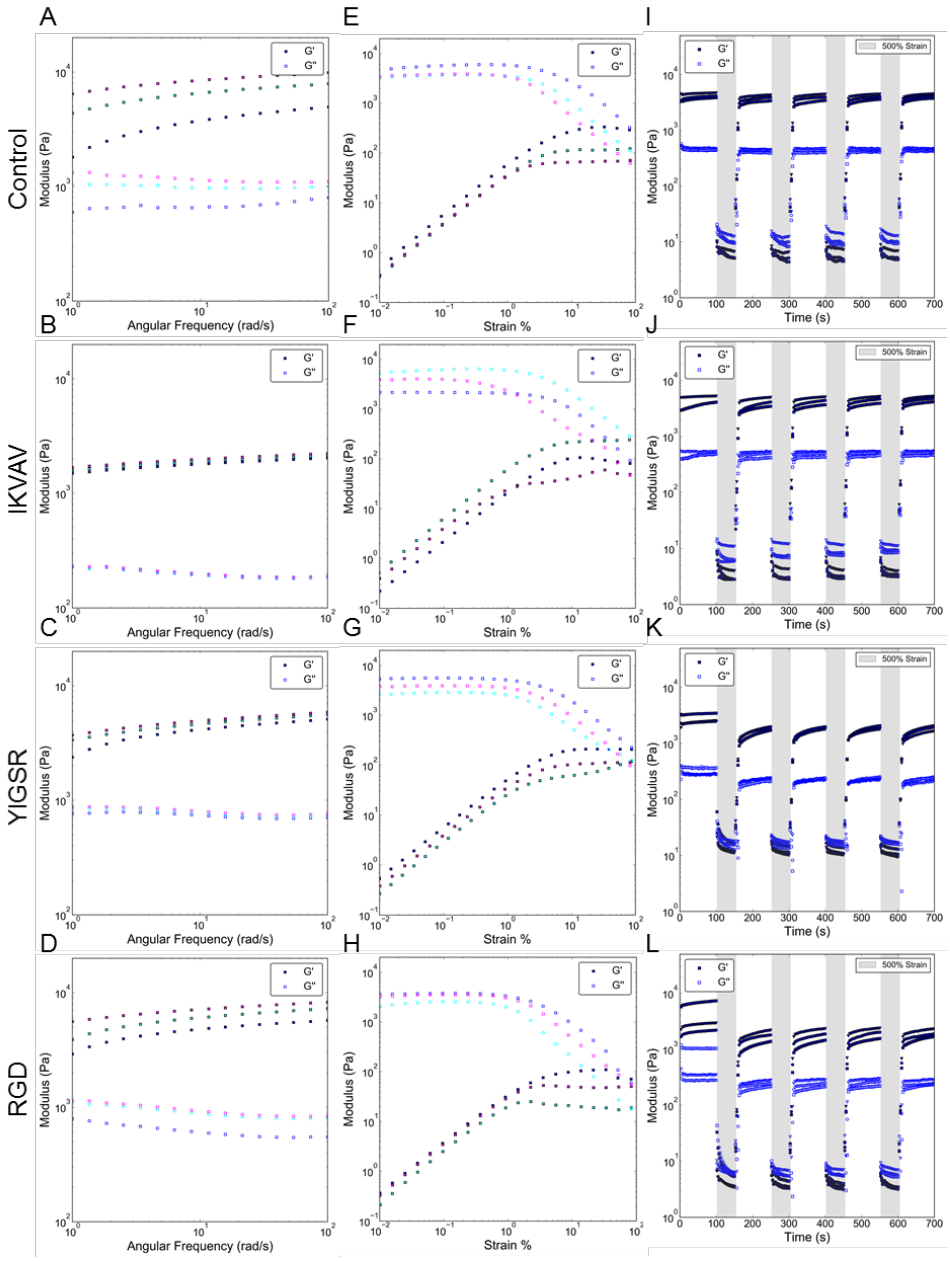

Figure 12-2. Rheological properties of 1.5 wt. % AYFIL hydrogels at pH 7.4 (n = 3 for all samples). A - D) Angular frequency sweep of control AYFIL, IKVAV-AYFIL, YIGSR-AYFIL, and RGD-AYFIL peptide sequences, respectively, at constant strain of 0.1%. G' is an order of magnitude greaten than G" indicating hydrogelation has occurred. E - H) Strain sweep of gelling control AYFIL, IKVAV-AYFIL, YIGSR-AYFIL, and RGD-AYFIL peptide sequences, respectively, at constant angular frequency of 10 rad/s. Above the critical strain at 5%, the material becomes progressively more fluid-like, where G' starts to increase and G" begins to decrease. I - L) Five step strain sweeps of 0.1 % (100 s) and 500 % strain (50 s), followed by a 100 s recovery period, were performed on control AYFIL, IKVAV-AYFIL, YIGSR-AYFIL, and RGD-AYFIL hydrogel peptide sequences, respectively. The hydrogel recovered 80% of its initial G' within several seconds. The hydrogel repeatedly recovered its mechanical strength following multiple high strain cycles.

performed to evaluate RAPID hydrogels' ability to self-heal following mechanical deformation.

All cell-adhesive motif functionalized RAPID hydrogels had similar recovery profiles compared to non-functionalized hydrogel controls (Figure 1I-L, Figure 2I-L). Following a 500% strain, KYFIL hydrogels repeatedly recovered gel behavior within 14 seconds. Within 1 minute, the gel recovered ~70% of its initial *G′*. For AYFIL hydrogels, following a 500% strain, hydrogels recovered 82% of its initial *G′* within a minute. Even after multiple high-strain cycles, the hydrogel rapidly and repeatedly recovers its mechanical strength—rendering these materials suitable for biomedical applications that require injection. This enables uniform encapsulation of cells in 3D, *ex vivo*, and then injection via a minimally invasive technique.

12.5.2 Effects of cell-matrix interactions on OPC growth and morphology

Previous studies have suggested that OPC proliferation and differentiation both correlate with the physical stiffness of underlying 2D[9] or surrounding 3D matrices in bio-inert materials[1]. While these studies of OPCs have primarily focused on 2D culture in poly-l-lysine or poly-l-ornithine coated tissue culture plates, few studies have examined the growth and metabolic activity of encapsulating these lineage-restricted cells in 3D matrices incorporated with cell-adhesive ligands. It has been shown that the biophysical properties of hydrogels sharply influence the proliferation and differentiation of stem cells within a 3D environment[10, 26]. Recent evidence indicates that OPCs are also sensitive to the biophysical stiffness of their surrounding microenvironment[23, 27]. We sought to encapsulate OPCs[28] in RAPID hydrogels, which are supportive of OPC cell growth

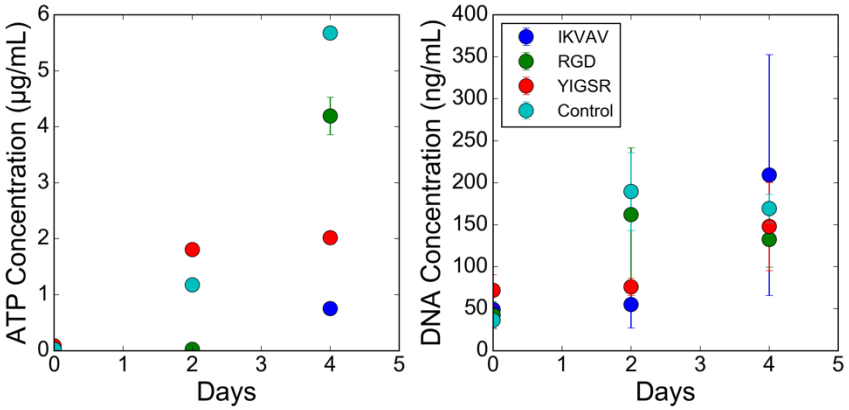

Figure 12-3. MADM OPC line encapsulated in 1.5 wt. % KYFIL hydrogels functionalized with cell-adhesive ligands IKVAV, RGD, or YIGSR and cultured over 4 days. A) OPCs remained viable after encapsulation for at least 4 days, as determined by the increase of ATP over time for all samples (B). The increase in DNA concentration suggests that cells

and survival[23-24]. Earlier published work primarily focused on the viability of cells encapsulated within RAPID hydrogels, while the present study investigates the effects on OPC proliferation and morphology when cell-adhesive ligands such as IKVAV, YIGSR, and RGD are introduced into the matrix formulation. The formulation of our hydrogels allows us to decouple the synergistic effects of cell-adhesive epitopes and biomechanical properties of the surrounding 3D microenvironment presented to these cells. This allows us to solely focus on the effect of individual ligands on cell growth and proliferation using ATP and DNA quantification assays. OPCs were encapsulated within these RAPID hydrogels, and their growth was measured at 0, 2, and 4 days using both an ATP and DNA quantification assay.

An approximate 5-fold increase for both ATP and DNA concentration was observed on Day 4 compared to Day 0 for all samples, suggesting that OPCs remained viable and proliferated over the course of the culture period for cells encapsulated within cell-adhesive functionalized KYFIL hydrogels. The presented data does not suggest there is a significant difference between individual motifs, so ongoing studies are currently in progress to replicate the experiment, as well as using AYFIL and functionalized AYFIL hydrogels.

12.5.3 Influence of cell-adhesive peptides on cell spreading and process extension

IKVAV, RGD, and YIGSR functionalized KYFIL hydrogels were capable of promoting cell growth and process extension of OPCs. Following hydrogel encapsulation, process extension was observed for all samples, however, non-functionalized hydrogel controls saw shorter processes.

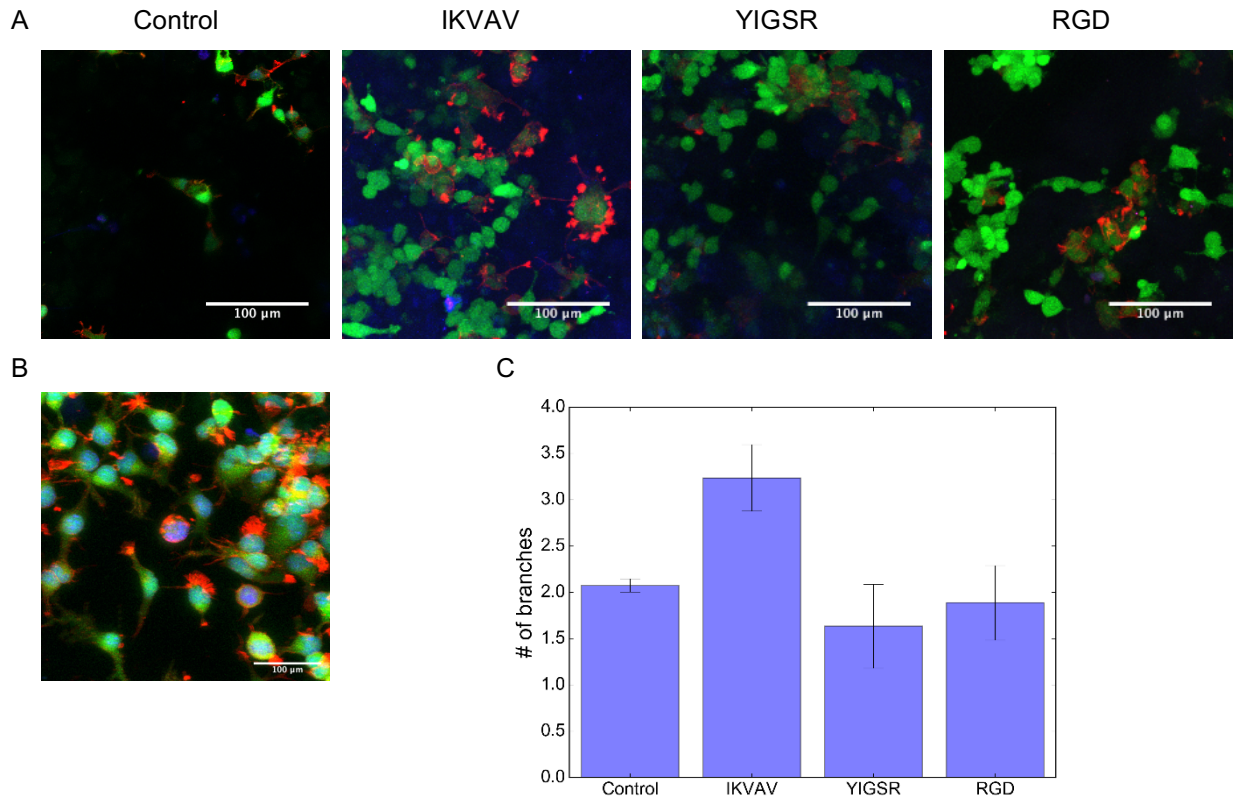

Figure 12-4. A) Maximum projection (78-136 µm thick z-stack) of OPCs encapsulated in KYFIL hydrogels functionalized with IKVAV, YIGSR, or RGD after 2 days of culture. Process extension of OPCs are observed for all samples. GFP (green), Actin (red), DAPI (blue). B) Inset of OPCs encapsulated in IKVAV functionalized hydrogels (63 µm thick z-stack). Magnification at 40x. C) Quantification of number of branches per cell. OPCs encapsulated in IKVAV-functionalized KYFIL hydrogels have the most branching. There was no significant increase in branching for YIGSR and RGD compared to control hydrogels. Error bars are SEM (n = 3 experiments).

For control (no cell-adhesive motifs), there were limited branching in encapsulated OPCs. Interestingly, YIGSR and RGD showed no influence on OPC process extension (Figure 1-4 A), despite the fact that YIGSR and RGD has previously been shown to facilitate cellular attachment and spreading.[11, 21] It is possible that the conformation of the YIGSR/RGD - KYFIL sequence and fibrillar conformation disrupted its cell-binding activity.[29] In this context, it would not be surprising if the YIGSR sequence was subject to intramolecular interactions via π-π stacking with the bound KYFIL sequence. IKVAV functionalized hydrogels saw the most branching of OPCs (Figure 1-4 B). In notable contrast to control hydrogels, the maximum length of processes were also observed in IKVAV hydrogels. This is consistent with other studies involving IKVAV

functionalized biomaterials for neuronal cells, where the most branching and longest process extension occurs.[17, 30-31]

12.6 Conclusions

We demonstrated that the presence of cell-adhesive epitopes influences the growth and process extension of OPCs. Nonfunctionalized RAPID hydrogels alone saw limited changes in OPC morphology compared to gels that incorporated cell-adhesive ligands. IKVAV, RGD, and YIGSR functionalized hydrogels had similar material mechanics, and increased levels of cell metabolic activity compared to non-functionalized hydrogel controls. The hydrogel system presented here allows for independent adjusting of the concentration of multiple cell-adhesive ligands without any changes to the mechanical properties of the hydrogel. The facile preparation of functionalized RAPID hydrogels should be widely applicable to other studies at understanding the effects of matrix-bound ligands involving 3D hydrogel encapsulation studies.

12.7 References

1. Russell, L. N.; Lampe, K. J., Oligodendrocyte Precursor Cell Viability, Proliferation, and Morphology is Dependent on Mesh Size and Storage Modulus in 3D Poly(ethylene glycol)-Based Hydrogels. *Acs Biomater Sci Eng* **2017,** *3* (12), 3459-3468.
2. Rodrigues, G. M. C.; Gaj, T.; Adil, M. M.; Wahba, J.; Rao, A. T.; Lorbeer, F. K.; Kulkarni, R. U.; Diogo, M. M.; Cabral, J. M. S.; Miller, E. W.; Hockemeyer, D.; Schaffer, D. V., Defined and Scalable Differentiation of Human Oligodendrocyte Precursors from Pluripotent Stem Cells in a 3D Culture System. *Stem Cell Rep* **2017,** *8* (6), 1770-1783.
3. Lee, S.; Leach, M. K.; Redmond, S. A.; Chong, S. Y. C.; Mellon, S. H.; Tuck, S. J.; Feng, Z. Q.; Corey, J. M.; Chan, J. R., A culture system to study oligodendrocyte myelination processes using engineered nanofibers. *Nature Methods* **2012,** *9* (9), 917-+.
4. Banerjee, A.; Arha, M.; Choudhary, S.; Ashton, R. S.; Bhatia, S. R.; Schaffer, D. V.; Kane, R. S., The influence of hydrogel modulus on the proliferation and differentiation of encapsulated neural stem cells. *Biomaterials* **2009,** *30* (27), 4695-4699.
5. Diao, H. J.; Low, W. C.; Milbreta, U.; Lu, Q. R.; Chew, S. Y., Nanofiber-mediated microRNA delivery to enhance differentiation and maturation of oligodendroglial precursor cells. *J Control Release* **2015,** *208*, 85-92.
6. Veiga, S.; Ly, J.; Chan, P. H.; Bresnahan, J. C.; Beattie, M. S., SOD1 overexpression improves features of the oligodendrocyte precursor response in vitro. *Neurosci Lett* **2011,** *503* (1), 10-4.
7. Larsen, P. H.; Yong, V. W., The expression of matrix metalloproteinase-12 by oligodendrocytes regulates their maturation and morphological differentiation. *J Neurosci* **2004,** *24* (35), 7597-603.
8. Asmani, M. N.; Ai, J.; Amoabediny, G.; Noroozi, A.; Azami, M.; Ebrahimi-Barough, S.; Navaei-Nigjeh, M.; Ai, A.; Jafarabadi, M., Three-dimensional culture of differentiated endometrial stromal cells to oligodendrocyte progenitor cells (OPCs) in fibrin hydrogel. *Cell Biology International* **2013,** *37* (12), 1340-1349.
9. Urbanski, M. M.; Kingsbury, L.; Moussouros, D.; Kassim, I.; Mehjabeen, S.; Paknejad, N.; Melendez-Vasquez, C. V., Myelinating glia differentiation is regulated by extracellular matrix elasticity. *Sci Rep-Uk* **2016,** *6*.
10. Tibbitt, M. W.; Anseth, K. S., Hydrogels as Extracellular Matrix Mimics for 3D Cell Culture. *Biotechnol Bioeng* **2009,** *103* (4), 655-663.
11. Weber, L. M.; Hayda, K. N.; Haskins, K.; Anseth, K. S., The effects of cell-matrix interactions on encapsulated beta-cell function within hydrogels functionalized with matrix-derived adhesive peptides. *Biomaterials* **2007,** *28* (19), 3004-11.
12. Madl, C. M.; Katz, L. M.; Heilshorn, S. C., Bio-Orthogonally Crosslinked, Engineered Protein Hydrogels with Tunable Mechanics and Biochemistry for Cell Encapsulation. *Adv Funct Mater* **2016,** *26* (21), 3612-3620.
13. Miller, J. S.; Shen, C. J.; Legant, W. R.; Baranski, J. D.; Blakely, B. L.; Chen, C. S., Bioactive hydrogels made from step-growth derived PEG-peptide macromers. *Biomaterials* **2010,** *31* (13), 3736-3743.
14. Thompson, H. L.; Burbelo, P. D.; Yamada, Y.; Kleinman, H. K.; Metcalfe, D. D., Identification of an Amino-Acid-Sequence in the Laminin a-Chain Mediating Mast-Cell Attachment and Spreading. *Immunology* **1991,** *72* (1), 144-149.
15. Lampe, K. J.; Antaris, A. L.; Heilshorn, S. C., Design of three-dimensional engineered protein hydrogels for tailored control of neurite growth. *Acta Biomaterialia* **2013,** *9* (3), 5590-5599.
16. Fischer, S. E.; Liu, X. Y.; Mao, H. Q.; Harden, J. L., Controlling cell adhesion to surfaces via associating bioactive triblock proteins. *Biomaterials* **2007,** *28* (22), 3325-3337.

17. Cheng, T. Y.; Chen, M. H.; Chang, W. H.; Huang, M. Y.; Wang, T. W., Neural stem cells encapsulated in a functionalized self-assembling peptide hydrogel for brain tissue engineering. *Biomaterials* **2013,** *34* (8), 2005-2016.
18. Grant, D. S.; Kinsella, J. L.; Fridman, R.; Auerbach, R.; Piasecki, B. A.; Yamada, Y.; Zain, M.; Kleinman, H. K., Interaction of Endothelial-Cells with a Laminin-a Chain Peptide (Sikvav) Invitro and Induction of Angiogenic Behavior Invivo. *J Cell Physiol* **1992,** *153* (3), 614-625.
19. Nakamura, M.; Mie, M.; Mihara, H.; Nakamura, M.; Kobatake, E., Construction of a Multi-Functional Extracellular Matrix Protein That Increases Number of N1E-115 Neuroblast Cells Having Neurites. *J Biomed Mater Res B* **2009,** *91b* (1), 425-432.
20. Grant, D. S.; Zukowska, Z., Revascularization of ischemic tissues with SIKVAV and neuropeptide Y (NPY). *Angiogenesis: From the Molecular to Integrative Pharmacology* **2000,** *476*, 139-154.
21. Yu, X. J.; Dillon, G. P.; Bellamkonda, R. V., A laminin and nerve growth factor-laden three-dimensional scaffold for enhanced neurite extension. *Tissue Eng* **1999,** *5* (4), 291-304.
22. Cui, G. H.; Shao, S. J.; Yang, J. J.; Liu, J. R.; Guo, H. D., Designer Self-Assemble Peptides Maximize the Therapeutic Benefits of Neural Stem Cell Transplantation for Alzheimer's Disease via Enhancing Neuron Differentiation and Paracrine Action. *Mol Neurobiol* **2016,** *53* (2), 1108-1123.
23. Tang, J. D.; Mura, C.; Lampe, K. J., Stimuli-Responsive, Pentapeptide, Nanofiber Hydrogel for Tissue Engineering. *J Am Chem Soc* **2019,** *141* (12), 4886-4899.
24. Tang, J. D.; Roloson, E. B.; Amelung, C. D.; Lampe, K. J., Rapidly Assembling Pentapeptides for Injectable Delivery (RAPID) Hydrogels as Cytoprotective Cell Carriers. *Acs Biomater Sci Eng* **2019,** *5* (5), 2117-2121.
25. Jung, J. P.; Moyano, J. V.; Collier, J. H., Multifactorial optimization of endothelial cell growth using modular synthetic extracellular matrices. *Integr Biol-Uk* **2011,** *3* (3), 185-196.
26. Haines-Butterick, L.; Rajagopal, K.; Branco, M.; Salick, D.; Rughani, R.; Pilarz, M.; Lamm, M. S.; Pochan, D. J.; Schneider, J. P., Controlling hydrogelation kinetics by peptide design for three-dimensional encapsulation and injectable delivery of cells. *P Natl Acad Sci USA* **2007,** *104* (19), 7791-7796.
27. Lourenco, T.; Graos, M., Modulation of Oligodendrocyte Differentiation by Mechanotransduction. *Front Cell Neurosci* **2016,** *10*.
28. Liu, C.; Sage, J. C.; Miller, M. R.; Verhaak, R. G. W.; Hippenmeyer, S.; Vogel, H.; Foreman, O.; Bronson, R. T.; Nishiyama, A.; Luo, L. Q.; Zong, H., Mosaic Analysis with Double Markers Reveals Tumor Cell of Origin in Glioma. *Cell* **2011,** *146* (2), 209-221.
29. Heilshorn, S. C.; Liu, J. C.; Tirrell, D. A., Cell-binding domain context affects cell behavior on engineered proteins. *Biomacromolecules* **2005,** *6* (1), 318-323.
30. Farrukh, A.; Ortega, F.; Fan, W. Q.; Marichal, N.; Paez, J. I.; Berninger, B.; del Campo, A.; Salierno, M. J., Bifunctional Hydrogels Containing the Laminin Motif IKVAV Promote Neurogenesis. *Stem Cell Rep* **2017,** *9* (5), 1432-1440.
31. Li, X. W.; Liu, X. Y.; Josey, B.; Chou, C. J.; Tan, Y.; Zhang, N.; Wen, X. J., Short Laminin Peptide for Improved Neural Stem Cell Growth. *Stem Cell Transl Med* **2014,** *3* (5), 662-670.